THE RELATIONSHIP BETWEEN LATE DEVONIAN MAFIC INTRUSIONS AND PERALUMINOUS GRANITOID GENERATION IN THE MEGUMA LITHOTECTONIC ZONE, NOVA SCOTIA, CANADA

by

Marcus C. Tate

Submitted in partial fulfillment of the requirements

for the degree of Doctor of Philosophy

at

Dalhousie University,

Halifax, Nova Scotia

February, 1995

ISBN 0-612-05234-6

Name MARCUS TATE

Dissertation Abstracts International is arranged by broad, general subject categories. Please select the one subject which most nearly describes the content of your dissertation. Enter the corresponding four-digit code in the spaces provided.

GEOLOGY — SUBJECT TERM

0372 — SUBJECT CODE

U·M·I

Subject Categories

THE HUMANITIES AND SOCIAL SCIENCES

COMMUNICATIONS AND THE ARTS
Architecture 0729
Art History 0377
Cinema 0900
Dance 0378
Fine Arts 0357
Information Science 0723
Journalism 0391
Library Science 0399
Mass Communications 0708
Music 0413
Speech Communication 0459
Theater 0465

EDUCATION
General 0515
Administration 0514
Adult and Continuing 0516
Agricultural 0517
Art 0273
Bilingual and Multicultural 0282
Business 0688
Community College 0275
Curriculum and Instruction 0727
Early Childhood 0518
Elementary 0524
Finance 0277
Guidance and Counseling 0519
Health 0680
Higher 0745
History of 0520
Home Economics 0278
Industrial 0521
Language and Literature 0279
Mathematics 0280
Music 0522
Philosophy of 0998
Physical 0523
Psychology 0525
Reading 0535
Religious 0527
Sciences 0714
Secondary 0533
Social Sciences 0534
Sociology of 0340
Special 0529
Teacher Training 0530
Technology 0710
Tests and Measurements 0288
Vocational 0747

LANGUAGE, LITERATURE AND LINGUISTICS
Language
- General 0679
- Ancient 0289
- Linguistics 0290
- Modern 0291

Literature
- General 0401
- Classical 0294
- Comparative 0295
- Medieval 0297
- Modern 0298
- African 0316
- American 0591
- Asian 0305
- Canadian (English) 0352
- Canadian (French) 0355
- English 0593
- Germanic 0311
- Latin American 0312
- Middle Eastern 0315
- Romance 0313
- Slavic and East European 0314

PHILOSOPHY, RELIGION AND THEOLOGY
Philosophy 0422
Religion
- General 0318
- Biblical Studies 0321
- Clergy 0319
- History of 0320
- Philosophy of 0322

Theology 0469

SOCIAL SCIENCES
American Studies 0323
Anthropology
- Archaeology 0324
- Cultural 0326
- Physical 0327

Business Administration
- General 0310
- Accounting 0272
- Banking 0770
- Management 0454
- Marketing 0338

Canadian Studies 0385
Economics
- General 0501
- Agricultural 0503
- Commerce-Business 0505
- Finance 0508
- History 0509
- Labor 0510
- Theory 0511

Folklore 0358
Geography 0366
Gerontology 0351
History
- General 0578
- Ancient 0579
- Medieval 0581
- Modern 0582
- Black 0328
- African 0331
- Asia, Australia and Oceania 0332
- Canadian 0334
- European 0335
- Latin American 0336
- Middle Eastern 0333
- United States 0337

History of Science 0585
Law 0398
Political Science
- General 0615
- International Law and Relations 0616
- Public Administration 0617

Recreation 0814
Social Work 0452
Sociology
- General 0626
- Criminology and Penology 0627
- Demography 0938
- Ethnic and Racial Studies 0631
- Individual and Family Studies 0628
- Industrial and Labor Relations 0629
- Public and Social Welfare 0630
- Social Structure and Development 0700
- Theory and Methods 0344

Transportation 0709
Urban and Regional Planning 0999
Women's Studies 0453

THE SCIENCES AND ENGINEERING

BIOLOGICAL SCIENCES
Agriculture
- General 0473
- Agronomy 0285
- Animal Culture and Nutrition 0475
- Animal Pathology 0476
- Food Science and Technology 0359
- Forestry and Wildlife 0478
- Plant Culture 0479
- Plant Pathology 0480
- Plant Physiology 0817
- Range Management 0777
- Wood Technology 0746

Biology
- General 0306
- Anatomy 0287
- Biostatistics 0308
- Botany 0309
- Cell 0379
- Ecology 0329
- Entomology 0353
- Genetics 0369
- Limnology 0793
- Microbiology 0410
- Molecular 0307
- Neuroscience 0317
- Oceanography 0416
- Physiology 0433
- Radiation 0821
- Veterinary Science 0778
- Zoology 0472

Biophysics
- General 0786
- Medical 0760

EARTH SCIENCES
Biogeochemistry 0425
Geochemistry 0996
Geodesy 0370
Geology 0372
Geophysics 0373
Hydrology 0388
Mineralogy 0411
Paleobotany 0345
Paleoecology 0426
Paleontology 0418
Paleozoology 0985
Palynology 0427
Physical Geography 0368
Physical Oceanography 0415

HEALTH AND ENVIRONMENTAL SCIENCES
Environmental Sciences 0768
Health Sciences
- General 0566
- Audiology 0300
- Chemotherapy 0992
- Dentistry 0567
- Education 0350
- Hospital Management 0769
- Human Development 0758
- Immunology 0982
- Medicine and Surgery 0564
- Mental Health 0347
- Nursing 0569
- Nutrition 0570
- Obstetrics and Gynecology 0380
- Occupational Health and Therapy 0354
- Ophthalmology 0381
- Pathology 0571
- Pharmacology 0419
- Pharmacy 0572
- Physical Therapy 0382
- Public Health 0573
- Radiology 0574
- Recreation 0575
- Speech Pathology 0460
- Toxicology 0383

Home Economics 0386

PHYSICAL SCIENCES
Pure Sciences

Chemistry
- General 0485
- Agricultural 0749
- Analytical 0486
- Biochemistry 0487
- Inorganic 0488
- Nuclear 0738
- Organic 0490
- Pharmaceutical 0491
- Physical 0494
- Polymer 0495
- Radiation 0754

Mathematics 0405
Physics
- General 0605
- Acoustics 0986
- Astronomy and Astrophysics 0606
- Atmospheric Science 0608
- Atomic 0748
- Electronics and Electricity 0607
- Elementary Particles and High Energy 0798
- Fluid and Plasma 0759
- Molecular 0609
- Nuclear 0610
- Optics 0752
- Radiation 0756
- Solid State 0611

Statistics 0463

Applied Sciences

Applied Mechanics 0346
Computer Science 0984
Engineering
- General 0537
- Aerospace 0538
- Agricultural 0539
- Automotive 0540
- Biomedical 0541
- Chemical 0542
- Civil 0543
- Electronics and Electrical 0544
- Heat and Thermodynamics 0348
- Hydraulic 0545
- Industrial 0546
- Marine 0547
- Materials Science 0794
- Mechanical 0548
- Metallurgy 0743
- Mining 0551
- Nuclear 0552
- Packaging 0549
- Petroleum 0765
- Sanitary and Municipal 0554
- System Science 0790

Geotechnology 0428
Operations Research 0796
Plastics Technology 0795
Textile Technology 0994

PSYCHOLOGY
General 0621
Behavioral 0384
Clinical 0622
Developmental 0620
Experimental 0623
Industrial 0624
Personality 0625
Physiological 0989
Psychobiology 0349
Psychometrics 0632
Social 0451

DEDICATION

To Dr. D.J. Gobbett (Solihull, U.K.) who brought "geology to life", and to Dr. N. Pearce (UCW, Aberystwyth, U.K.) who steered my geological course from palaeontology towards petrology.

"... there has been exerted an extreme degree of heat below the strata formed at the bottom of the sea; and this is precisely the action of a power required for the elevation of those heated bodies into a higher place."

James Hutton (1795) in the Theory of the Earth with proofs and illustrations, Volume I, p. 123

Oprostite mi na zarezima izmedu imenica i glagola

TABLE OF CONTENTS

Appendix F - THEORETICAL HEAT FLOW MODELLING PROCEDURES AND PROGRAMMING FOR CHAPTER 6

LIST OF FIGURES

Chapter 3

Chapter 4

Chapter 5

Appendix E

Appendix F

LIST OF TABLES

Chapter 5

Chapter 6

Chapter 7

Appendix B

Appendix C

Appendix D

Appendix E

Appendix F

ABSTRACT

Current theories for the generation of voluminous granitoid intrusions state that mafic magmas can provide a localized, external source of heat for crustal melting. Regardless of their age or tectonic setting, many alkaline, metaluminous, and peraluminous granitoid bodies occur with contemporaneous satellite mafic intrusions and show spatial relationships with mafic magmas in the form of synplutonic mafic bodies and mafic igneous enclaves. Physical juxtaposition of the intruded mafic magmas and resulting anatectic granitoid melts also allows for the transfer of chemical components to produce hybridized lithologies by mechanical interaction and/or chemical diffusion. In this multidisciplinary study, identification of all these established criteria for mafic-granitoid genetic relationships, in combination with one-dimensional thermal models of mafic intraplating, allows the assessment of a role for intruded mafic magma as a source of chemical components and, ultimately, heat in a suite of granitoid rocks.

Late Devonian (385-372 Ma) peraluminous granitoid plutons and batholiths in the Meguma Zone of southwestern Nova Scotia crop out with 14 volumetrically minor mafic dykes and plugs that have contemporaneous ages (380-370 Ma $^{40}Ar/^{39}Ar$; 376 Ma U-Pb). Four of these mafic bodies are synplutonic intrusions into the Barrington Passage, Shelburne, and Port Mouton plutons, where they formed mingled and commingled mafic pillows at their contacts or produced hybrid tonalites with metaluminous tendencies by chemical diffusion of mobile elements (alkalies, Rb, Ba, Sr) and exchange of Ti, Fe, Ca, and V in plagioclase and ferromagnesian phenocrysts. No granitoids contain enclaves with microtextures resembling the known mafic intrusions or hybrids, but the Barrington Passage, Shelburne, Port Mouton, and Canso plutons have enrichments of Ti, Fe, Ca, Cr, and V, coupled with low values for $\delta^{18}O$ (8.3-10.4‰), $\delta^{34}S$ (0-5‰), and $^{87}Sr/^{86}Sr_{t=380-370}$ (0.705-0.710) that suggest mantle chemical input.

These small granitoid intrusions peripheral to the South Mountain Batholith, therefore, show all of the required evidence to support a temporal and spatial genetic relationship between mafic and granitoid magmas, except enclaves. Poor exposure (<2%), and the epizonal exhumation of the Meguma Zone, probably explain the small number of mafic intrusions at the current exposure level. Emplacement of the synplutonic mafic bodies after the cessation of active granitoid convection may account for the lack of enclaves. Numerical models of heat advection above mafic sills intruded into the sub-Meguma basement allow heating from intruded mafic magmas in the protoliths for granitoid plutons occupying peripheral onshore areas of the MZ between circa 385 Ma and 372 Ma, and perhaps also to a lesser extent in centrally located intrusions at circa 372 Ma. Mafic magmatism possibly augmented heat produced by a variety of tectonic processes after the onset of Acadian terrane accretion.

LIST OF ABBREVIATIONS

The following abbreviations and acronyms appear frequently in the main text of this thesis. More specific short-forms used in the figures and tables are explained in the appropriate caption.

ANP	Average of northern plutons
BPP	Barrington Passage Pluton
CCF	Cobequid-Chedabucto Fault
CHUR	Chondrite uniform reservoir
CIPW	Cross-Iddings-Pirrson-Washington
CP	Canso pluton(s)
CZT	Contact Zone Transect
HFSE	High field strength elements
HREE	Heavy rare-earth elements
IRS	Incompatible elements, radiogenic isotopes, silica
LC	Liscomb Complex
LDMI	Late Devonian mafic intrusion
LILE	Large-ion lithophile elements
LOI	Loss on ignition
LREE	Light rare-earth elements
MB	Musquodoboit Batholith
MIM	"mafic intrusion model"
MORB	Mid-ocean ridge basalt
MREE	Middle rare-earth elements
MZ	Meguma Zone
PMP	Port Mouton Pluton
PPL	Plane-polarized light
QAP	Quartz, alkali feldspar, plagioclase
REE	Rare-earth elements
SMB	South Mountain Batholith
SP	Shelburne Pluton
TNT	Tantalum, niobium, titanium
XPL	Cross-polarized light

ACKNOWLEDGMENTS

I would initially like to thank my supervisor, Dr. Barrie Clarke, for illustrating the importance of this project, and for his substantial support, input, and enthusiasm from the beginning to the end of this study. In addition, my committee members, Drs. N.G. Culshaw and P.H. Reynolds (Dalhousie University), Mr. A. Ruffman (Geomarine Associates Ltd), and Dr. J.D. Hill (Technical University of Nova Scotia) provided many stimulating discussions and kept my mind focused. Peter Reynolds improved my understanding of argon systematics considerably, and particularly entertaining structural discussions with Nick Culshaw significantly advanced my knowledge of orogenic processes and their possible applications to the Meguma Zone. Alan Ruffman and Geoff Gallant contributed towards two very enjoyable field seasons during the summers of 1991 and 1992, when they provided assistance over and above the call of duty. Bob McKay provided much invaluable knowledge regarding the use of the electron microprobe/image analysis system, and Keith Taylor helped with the $^{40}Ar/^{39}Ar$ analyses. Dr. Larry Heaman graciously collaborated in the production of U-Pb ages and provided expert supervision during my stay at the Royal Ontario Museum (ROM); Dr. Chris Beaumont kindly critiqued the heat flow modelling presented in Chapter 6.

Thanks also to Mike Marks and Raivo Tähista (ROM) for helping with the preparation of my U-Pb samples, and to Mike MacDonald and other staff members at the Nova Scotia Department of Natural Resources for fruitful discussions of the South Mountain Batholith. Dr. Paul Robinson provided unlimited access to his scanner and optical character recognition software, which made the compilation of geochemical data painless. Rory Kempster, Linda Richard, and Stephanie Douma granted permission for the use of their unpublished analyses in this study, and both Tom Duffett and Charlie Walls provided invaluable technical support. Andrew Henry helped to prepare final copies of the figures and tables and loaned his computer to help with the production of the formatted document. Special thanks also to John and Judy Adams (Seaview Bed and Breakfast, Port Mouton) who provided the most comfortable field camp during 1991 and 1992! Last, but not least, I extend appreciation and gratitude to my friends and colleagues Kevin Desroches, Robbie Hicks, John Ketchum, Doug Merrett, Ana Putar, Yi Ding, and Mei-Fu Zhou, for providing many welcome distractions over the last four years. Financial support for this work was provided in the form of a Dalhousie University Graduate Fellowship for the period 1990-1994, and through Natural Sciences and Engineering Research Council of Canada (NSERC) research grants awarded to D.B. Clarke.

Chapter 1

INTRODUCTION, GEOLOGICAL SETTING, AND PURPOSE

1-1. The Generation of Granitoid Batholiths

The processes resulting in batholith formation were extensively debated after the initial suggestion of a magmatic origin for granitoid rocks by Hutton (1795). Early documentation of spatial associations between mafic and granitoid intrusions between 1930 and 1940 suggested that granitoids formed as fractionates from mantle-derived mafic magmas. However, Holmes (1931) recognized the inability of small mafic intrusions to evolve more voluminous granitoid batholiths, and subsequent hypotheses invoked regional infracrustal anatexis, either through the depression of metasedimentary rocks into deep geosynclines, or in response to the elevation of hot lower crust to shallower crustal levels (Read, 1948). More recent theoretical and experimental studies of crustal thickening by thrusting suggest that the generation of large granitoid intrusions must involve extraordinarily high heat inputs (Clemens and Vielzeuf, 1987; Bergantz, 1989), which might only occur in continental regions with exceptionally steep geothermal gradients produced by thick crust and/or long incubation periods (Molnar et al., 1983; Pitcher, 1987; Wyllie, 1984; Pitcher, 1987; Sandiford et al., 1992). The inferred geological histories of many areas are commonly at variance with such high temperature histories (Pitcher, 1979a; Pitcher, 1979b; Reid et al., 1983; Zen, 1990) and current opinion suggests that a localized and/or external thermal influence may be at least partially responsible for generating large granitoid intrusions (e.g. Jaupart and Provost, 1985; Williamson et al., 1992).

Such local thermal effects may include frictional heating in the vicinity of major fault zones (Strong and Hanmer, 1981), ultrametamorphism (Brown and Fyfe, 1970; White and Chappell, 1977), fluid influxes from the lower crust or mantle (Chamberlain and Rumble, 1989; Litvinovsky and Podladchikov, 1993), anomalously radioactive crust (Huppert and Sparks, 1988a; Lathrop et al., 1994), and thermal focusing (Jaupart and Provost, 1985). However, current models for intense heating once again recognize the importance of mafic intrusions associated with granitoid rocks (Younker and Vogel, 1976; Cantagrel et al., 1984; Huppert and Sparks, 1988a; preface to Brown and Chappell, 1992). The increasingly widespread recognition of bimodal magmatism in granitoid provinces ranging in age from Archean to Recent (e.g. Gupta and Sutcliffe, 1990; Lindberg and Eklund, 1988; Reid et al., 1983; Michael, 1991; Bacon and Metz, 1984), and with both orogenic calc-alkaline and anorogenic alkaline granitoids (Pitcher, 1987; Clemens et al., 1986), reinforces the original suggestion of a fundamental mafic-granitoid genetic relationship in many tectonic environments throughout geological time (Table 1.1). Although current opinions preclude fractionation relationships outside alkaline granitoid complexes (e.g. Mitchell et al., 1983), Blake et al. (1965; p. 41-2) suggested that "the presence of basic magma may...be essential to the uprise (and perhaps even the generation) of acid magma". Quantifying the degree to which the mantle contributes to anatectic processes is an important problem in granitoid petrology (DePaolo et al., 1992) and the focus for this thesis.

1-2. An Overview of Mafic-Granitoid Magma Relationships

Intraplated mafic magmas can provide an efficient source of heat for the formation of granitoids in bimodal complexes (Hyndman and Foster, 1988; Figure 1.1). Theoretical heat flow simulations imply an approximate 2:1 relationship between the volume of mafic magma emplaced and the volume of anatectic granitoid produced over short periods of geological time (100-5000 years), given standard geothermal gradients, lithostatic pressures, and fluid-absent conditions (Huppert and Sparks, 1988b; Bergantz, 1989). After mafic intraplating and anatexis, however, pronounced rheological and thermal contrasts exist between the juxtaposed mafic and granitoid melts (Cantagrel et al., 1984; Frost and Mahood, 1987), and the developing low density, superheated granitoid melt layer traps the subjacent mafic material (Biggi and Hodge, 1982; Michael, 1991; Figure 1.1a, b). Consequently, the concurrent availability of mantle-derived mafic and crust-derived anatectic magmas also allows for mechanical interaction and chemical

Table 1.1. Previously published studies documenting mafic-granitic bimodal magmatism in continental environments.

Era	Batholith/ Complex	Pluton	Location	Peralk.	Metalum.	Peralum.	Tect. Assoc.	Age (Ma)	MIM evidence	Scale of evidence	% of mafic material	Ref.
Cenozoic	Punzo Complex	-	Chile	-	-	-	Su	Holocene	Enc	cm-m	-	1
Cenozoic	Monts Dore volcanic domain	Sancy volcano	France, Massif Central	-	-	-	-	Quaternary (0.85)	Hyb, Enc	cm-km	-	2
Cenozoic	Coso volcanic field	-	Southern California	Y	-	-	-	0.4-0.004	Enc, Hyb	cm-km	-	3
Cenozoic	Niijina Volcano	-	Japan	-	-	-	Su	0.5-0	Enc	cm-m	-	4
Cenozoic	-	Wilson Ridge	Arizona	-	Y	Y	Ri	13.5	Maf, Enc	cm-m	70	5
Cenozoic	-	Red Mountains	Colorado	-	-	-	Ri	34	Syn, Com	m	-	6
Cenozoic	-	Climax	Colorado	-	-	-	Ri	34	Syn, Com	m	-	6
Cenozoic	-	Egan Range	Nevada	Y	-	-	Ri	Tertiary	Pil	cm-m	-	7
Cenozoic	British Tertiary Province	St. Kilda		-	-	-	Ri	Tertiary	Pil	cm-m	-	8
Cenozoic	British Tertiary Province	St. Kilda	Scotland	-	Y	-	Ri	Tertiary	Hyb	km	-	9
Cenozoic	British Tertiary Province	Ardnamurchan	Scotland	-	Y	-	Ri	Tertiary	Hyb	km	-	10
Cenozoic	British Tertiary Province	Slieve Gullion	Ireland	-	Y	-	Ri	Tertiary	Syn	cm-m	-	11
Cenozoic	British Tertiary Province	Coire Uaigneich	Skye, Scotland	-	Y	-	Ri	Late Tertiary	Che	-	50	12
Cenozoic	Adamello massif	-	Italian Alps	-	-	Y	Cc	Tertiary	Syn, Hyb, Enc	cm-m	-	13
Cenozoic	Patagonian	Cordillera del Paine	Southern Chile	-	Y	-	Su	Miocene	Syn, Hyb, Pil	cm-km	-	14
Cenozoic	Monte Caponne	-	Elba Isle, Italy	-	-	Y	Su	Late Miocene	Enc	cm-m	-	15
Cenozoic	Kallithea Complex	-	Samos, Greece	-	Y	-	-	Miocene	Com, Hyb, Maf	cm-m	-	16
Cenozoic	Hoyazo		Spanish Cordillera	-	-	-	Ri	Neogene (13-7)	Enc	cm-m	-	17

Table 1.1. (Continued) Previously published studies documenting mafic-granitic bimodal magmatism in continental environments.

Era	Batholith/ Complex	Pluton	Location	Peralk.	Metalum.	Peralum.	Tect. Assoc.	Age (Ma)	MIM evidence	Scale of evidence	% of mafic material	Ref.
Mesozoic	Boulder	-	Montana	-	-	-	-	Cretaceous (78-68)	Syn, Che	m-km	-	18
Mesozoic	Sierra Nevada	Eagle Peak	Yosemite, California	-	Y	Y	Ri/Su	Mesozoic	Syn, Pil	cm-m	2	19
Mesozoic	Sierra Nevada	Lamarck	California	-	Y	Y	Su	89.6	Enc, Syn, Hyb	cm-km	-	20
Mesozoic	Sierra Nevada	-	California	-	Y	Y	-	-	Enc	cm-m	-	21
Mesozoic	Sierra Nevada	Smartville Complex	Northern California	-	Y	Y	Ri	Jurassic (160)	Enc, Maf, Syn	cm-m	-	22
Mesozoic	Sierra Nevada	Dinkey Creek	California	-	Y	-	-	100	Enc	cm-km	-	23
Mesozoic	Sierra Nevada	-	California	-	Y	Y	Si	-	Enc	cm	-	24, 25
Mesozoic	Coastal Batholith, Peru	-	South America	-	Y	-	Ia	-	Maf, Syn	m	20	26, 27, 28
Mesozoic	Coastal Batholith, Peru	-	South America	-	-	-	-	104-34	Enc	cm-m	-	29
Mesozoic	Idaho	Bitteroot Lobe		-	-	Y	Su	110-100	Hyb, Syn, Com, Enc	cm-km	52	30, 31
Mesozoic	Peninsular Ranges	-	Baja, California	-	Y	Y	Ia	-	Maf, Che, Enc	cm-km	-	32
Mesozoic	Snake Creek	-	Nevada	-	-	Y	-	Jurassic	Che	km	-	33
Mesozoic	Querigut Complex	-	French Pyrenees	-	Y	Y	-	Hercynian	Hyb	km	-	34, 2
Mesozoic	Coast Mountains	-	British Columbia	-	-	-	-	-	Syn	m	-	35
Mesozoic	Anglem Complex	The Neck	New Zealand	-	Y	-	-	Cretaceous	Enc, Syn, Pil	cm-m	-	36
Palaeozoic		Ploumanac'h	Brittany, France	-	Y	-	Cc	300	Maf, Enc	cm-km	-	37, 2
Palaeozoic	Velay	-	France, Massif Central	-	Y	-	Cc	304	Enc, Che	cm-km	-	38

Table 1.1. (Continued) Previously published studies documenting mafic-granitic bimodal magmatism in continental environments.

Era	Batholith/ Complex	Pluton	Location	Peralk.	Metalum.	Peralum.	Tect. Assoc.	Age (Ma)	MIM evidence	Scale of evidence	% of mafic material	Ref.
Palaeozoic	Velay	Rocies	France, Massif Central	-	-	-	-	308	Enc	m	-	39
Palaeozoic	Velay	Moyet, St Gervais, St Julien	France, Massif Central	-	-	Y	Cc	328	Enc	cm-m	-	40
Palaeozoic	Braga Massif	-	Portugal	-	Y	Y	Cc	310	Maf, Enc, Hyb	cm-km		41
Palaeozoic	-	Sierra de Paiman	Argentina	-	-	-	-	350	Enc, Maf, Hyb	cm-m	-	42
Palaeozoic	-	SP, BPP, PMP	Nova Scotia, Canada	-	-	Y	Su	370	Maf	cm-m	-	43, 44
Palaeozoic	-	Liscomb Complex	Nova Scotia, Canada	-	-	Y	Su	372	Maf	cm-m	5	45
Palaeozoic	Northeast Kingdom	-	Vermont	-	Y	Y	Su	ca. 380	Maf, Hyb	m-km	-	46
Palaeozoic	Newer Granites	Strontian, Criffell	Scotland	-	Y	Y	Ia	430-395	Enc, Maf	m-km	-	47, 48
Palaeozoic	Coastal Maine Magmatic Province	-	Maine	-	Y	Y	Su/Ri	436-380	Maf, Enc, Hyb, Com, Syn	cm-km	20	49
Palaeozoic	Coastal Maine Magmatic Province	Cadillac Mountain	Mount Desert Island, Maine	-	-	-	Ri	-	Syn, Com, Maf	m-km	-	50
Palaeozoic	Coastal Maine Magmatic Province	-	Mount Desert Island, Maine	Y	Y	-	-	-	Pil, Com, Syn, Maf	m	-	51
Palaeozoic	Coastal Maine Magmatic Province	Cadillac Mountain, Somesville	Mount Desert Island, Maine	-	-	-	-	-	Enc	cm-m	-	52, 53
Palaeozoic	Coastal Maine Magmatic Province	Pleasant Bay	Mount Desert Island, Maine	-	Y	Y	-	-	Maf, Syn, Com, Hyb	m	-	54
Palaeozoic	Topsails Igneous terrane		Newfoundland Canada	Y	Y	-	Su	470-460	Com, Hyb	cm-m	-	55
Palaeozoic	Older Granites		Scotland			Y	Ia	> 480				

Table 1.1. (Concluded) Previously published studies documenting mafic-granitic bimodal magmatism in continental environments.

Era	Batholith/ Complex	Pluton	Location	Peralk.	Metalum.	Peralum.	Tect. Assoc.	Age (Ma)	MIM evidence	Scale of evidence	% of mafic material	Ref.
Palaeozoic	Carres, Erisa, Abellara Complexes	-	Corsica, France	Y	-	-	An	Permian	Enc, Syn	cm-m	-	56
Palaeozoic		Burgos, Emauru, Budduso,	Northern Sardinia	-	-	-	Cc	Carboniferous	Enc, Hyb	cm-km	-	57
Palaeozoic	Berridale, Cooma Complex, Murrumbidgee, Kosciusko, Moruya	Lachlan Fold Belt	Southern Australia	-	Y	Y	-	-	Enc, Che	cm, km	-	58
Palaeozoic			Iberia	-	Y	Y	-	-	Enc, Che	cm-km	-	59
Palaeozoic	Swifts Creek	-	Southeastern Australia	-	-	-	-	Early Devonian	Enc	cm-m	-	60
Proterozoic	Finnish G's	Püngo	Svecofennia	-	Y	-	An	Proterozoic	Hyb	km	-	61
Proterozoic	Pikes Peak		Colorado	Y	-	-	An	1,040	Hyb	km	-	62
Proterozoic	San Isabel		Colorado	-	Y	Y	An	Proterozoic (1441)	Pil, Syn	cm-m	-	63
Proterozoic	Coldwell Complex	-	Ontario, Canada	Y	-	-		1,044	Maf, Enc	cm-km	-	64
Proterozoic	Rapakivi	-	scuth Greenland	Y	-	-	An	Proterozoic (1740)	Maf	m	-	65
Proterozoic	Nain		Labrador	-	-	-	An	Proterozoic	Maf, Enc, Hyb	cm-km	-	66
Archean	Lac des Isles		Ontario, Canada				Su	Archean	Pil, Syn, Hyb	cm-km	-	67
Archean	Bushveld		South Africa	Y	-	-	An	2,050	-	km	-	68
Unknown age or affiliation		Um-mara	Eilat, Sinaï	-	-	-	-	-	Syn	m	-	69

Su = subduction, Ri = rift, Cc = continent-continent collision, Ia = island arc, An = anorogenic; Enc = mafic igneous enclaves, Hyb = hybrid granitoid lithologies, Maf = contemporaneous mafic intrusions, Pil = pillowed synplutonic mafic intrusions, Syn = synplutonic mafic intrusions, Com = synplutonic composite dykes, Che = granitoid Sr, Nd, or O isotope chemistry. 1 = Davidson et al. (1990), 2 = Cantagrel et al. (1984), 3 = Bacon and Metz (1984), 4 = Koyagouchi (1992), 5 = Larsen and Smith (1990), 6 = Shannon (1984), 7 = Feeley and Grunder (1990), 8 = Wager and Bailey (1955), 9 = Sparks and Marshall (1986), 10 = Vogel (1982), 11 = Gamble (1979), 12 = Dickin and Exley (1981), 13 = Blundy and Sparks (1992), 14 = Michael (1991), 15 = Bussy (1992), 16 = Mezger et al. (1985), 17 = Zeck (1992), 18 = Tilling (1973), 19 = Ried et al. (1983), 20 = Frost and Mahood (1987), 21 = Dodge and Kistler (1988), 22 = Beard and Day (1988), 23 = Dorais et al. (1989), 24 = Barbarin (1992), 25 = Holden et al. (1987), 26 = Brown et al. (1984), 27 = Pitcher (1987), 28 = Pitcher (1992), 29 = Bussell (1992), 30 = Foster and Hyndman (1990), 31 = Hyndman and Foster (1988), 32 = Silver and Chappell (1988), 33 = Lee and Christiensen (1983), 34 = Fourcade and Allegre (1981), 35 = Roddick and Armstrong (1959), 36 = Cook (1988), 37 = Albarede et al. (1980), 38 = Williamson et al. (1992), 39 = Sabatier (1991), 40 = Pin et al. (1990), 41 = Dias and Leterrier (1994), 42 = Lorenc (1990), 43 = de Albuquerque (1977), 44 = de Albuquerque (1979), 45 = Clarke et al. (1993a), 46 = Ayuso and Arth (1992), 47 = Fowler (1988), 48 = Stephens et al. (1992), 49 = Hogan and Sinha (1989), 50 = Chapman (1961), 51 = Taylor et al. (1980), 52 = Seaman (1990), 53 = Seaman and Powers (1991), 54 = Wiebe (1993), 55 = Whalen and Currie (1984), 56 = Platevoet and Bonin (1992), 57 = Zorpi et al. (1989), 58 = Gray (1984), 59 = Eberz and Nicholls (1988), 60 = Lindberg and Eklund (1988), 61 = Barker et al. (1975), 62 = Barker et al. (1975), 63 = Noblett and Staub (1990), 64 = Mitchell et al. (1983), 65 = Brown et al. 1992, 66 = Wiebe (1980), 67 = Sutcliffe et al. (1990), 68 = Kleemann and Twist (1989), 69 = Eyal (1980).

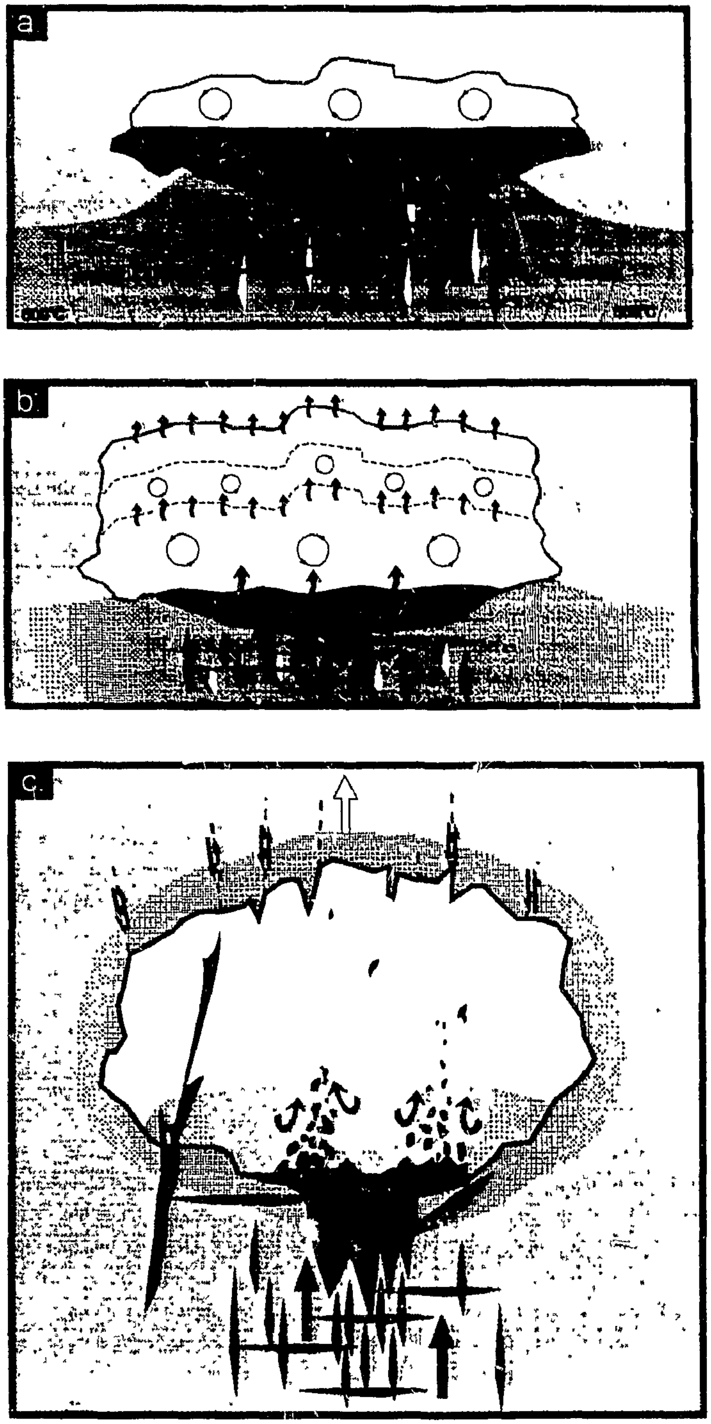

Figure 1.1. Graphical summary of anatectic melt generation and magmatic interaction resulting from mafic intraplating. See the text for a discussion.

mass transfer between the contrasting magma types, either in the anatectic source region, or during the movement of granitoid melts to shallower crustal levels (Castro et al., 1990; Barbarin and Didier, 1992a).

Initially, minor mafic dykes, sills, and plugs of mafic material intersecting the supersolidus granitoid mingle and form an immiscible emulsion of mafic "pillows" in response to the marked thermal and viscosity contrasts (Kouchi and Sunagawa, 1985; Furman and Spera, 1985). Larger mafic synplutonic dykes with cuspate and crenulate margins may be preserved at the site of intrusion if rapid cooling occurs under relatively tranquil conditions in the host granitoid (Hyndman and Foster, 1988; Noblett and Staub, 1990). However, convection in the granitoid may disrupt the mafic incursion, and redistribute its material as enclaves and inclusion trains (Furman and Spera, 1985; Chen et al., 1990). Given sufficiently voluminous incursions of mafic magma into the crystallizing granitoid magma chamber, open system magma mixing may produce intermediate lithologies when the relative temperatures and viscosities of the end-members become similar (Campbell and Turner, 1985; Figure 1.1c). Hybridism generally produces composite dykes (Chapman, 1961) and localized hybrid patches (Reid et al., 1983; Huppert and Sparks, 1983b), but it may also induce extreme compositional variation in the granitoid magma chamber (Zorpi et al., 1989). Fractionation of the mafic material to produce a variety of evolved granitoid compositions can occur on a minor scale in exceptionally hot or insulating crust (cf. Stern and Hanson, 1991).

1-3. The "Mafic Intrusion Model"

Table 1.1 summarizes important published investigations of granitoids supposedly influenced by these chemical and thermal contributions from mafic intrusions. Regardless of the tectonic environment or the chemical classification of the granitoid, all previous studies rely on the recognition of close temporal and spatial associations between mafic and granitoid rocks in outcrop (Lee and Christiansen, 1983; Hogan and Sinha, 1989; Rock, 1990). In bimodal complexes, the mafic rocks invariably occur as independent precursor intrusions, penecontemporaneous cross-cutting bodies, synplutonic intrusions, and/or as mafic igneous enclaves (Furman and Spera, 1985). Where mafic intrusions do not crop out, regional gravity or seismic studies commonly suggest their presence at depth (Lynn et al. 1981; Gupta and Sutcliffe, 1990), and/or metaluminous granitoid compositions argue strongly for mafic-granitoid magma mixing (Hogan and Sinha, 1989). Many recently published studies of mafic-granitoid relationships recognize the significance of these features and use them to suggest the importance of contemporaneous mafic magmas as suppliers of chemical components and, therefore, also as a source of heat (Hogan and Sinha, 1989; Michael, 1991; Dias and Leterrier, 1994), especially if the inferred geological history of a region necessitates a thermal supplement (Feeley and Grunder, 1990; Williamson et al., 1992).

In this study, combination of all the criteria for mafic-granitoid genetic relationships with the results of heat flow modelling allows the construction of a test for granitoid generation by mafic intraplating, hereafter named the "mafic intrusion model" (MIM). The MIM requires that granitoid rocks crop out with age-equivalent mafic intrusions and that they show evidence for mafic-felsic magmatic interaction in the form of synplutonic intrusions, hybrid granitoid lithologies, and/or mafic igneous enclaves. In areas with the deepest erosion, the number of preserved MIM criteria probably reflects the importance of mafic material during granitoid petrogenesis, but in areas with shallower exhumation, direct evidence for mafic involvement may be less obvious or absent (Hyndman and Foster, 1988). The evaluation of a MIM for any granitoid suite must, therefore, recognize the crustal depth represented by the current level of exposure, and it must rely on indirect constraints applied by geochronology, and on the physical and geochemical characteristics of both the mafic and granitoid end-members. This study provides the first investigation of a MIM for the peraluminous granitoids of the Meguma lithotectonic zone in the northern Appalachians.

1-4. Geological History of the Meguma Zone

The Canadian segment of the Appalachian Orogen contains five distinct lithotectonic zones (Figure 1.2). From northwest to southeast, the Humber Zone represents the ancient North American continental margin of the Iapetus Ocean (Keppie, 1985; Williams et al., 1988), the Dunnage Zone contains parautochthonous ophiolites and olistostromes, and the Gander Zone consists of allochthonous siliclastic and volcanic rocks with conjectural provenance in Iapetus (Keppie, 1982; Williams and Hatcher, 1982). The Avalon Zone represents a composite of microcontinental fragments (Zen and Palmer, 1981) and current interpretations suggest that it may mark the conjugate southeastern margin of Iapetus (Keppie, 1985; Keppie, 1989; Keppie et al., 1992). The Meguma Zone (MZ) forms the fifth and outermost Appalachian zone, and it occupies an onshore area in excess of 125,000 km^2 in southwestern Nova Scotia. Regional gravity and magnetic fingerprinting implies that the MZ extends 200 km out to the shelf edge, and it may also be present offshore southwest of Cape Breton and Newfoundland (Pe-Piper and Loncarevic, 1989; Figure 1.2). The Cobequid-Chedabucto fault system separates the MZ from the adjacent Avalon Zone and represents the terrane boundary (Williams and Hatcher, 1983; Figure 1.2). Distinct metallogenic, faunal, plutonic, and tectonic characteristics suggest that an ocean lay between the MZ and North America until the Devonian (Schenk, 1975; Schenk, 1981; Keppie, 1977; Piqué and Skehan, 1992).

Figures 1.3 and 1.4 summarize the stratigraphic succession and the chronology of Palaeozoic geological events in the MZ. The Meguma Group is the oldest exposed lithologic unit, and it forms a circa 14 km thick sequence of Cambrian and Lower Ordovician texturally and compositionally mature metapelites and metagreywackes (Schenk, 1970; Schenk, 1981; Schenk, 1983; Figure 1.3). The lowermost Goldenville Formation contains fine-grained psammitic turbidites with subordinate slate interbeds (Krogh and Keppie, 1990), whereas the overlying Halifax Formation consists of predominantly pelitic Bouma sequences (Schenk, 1983). Schenk (1975) and Schenk (1991) interpreted the Meguma Group as a deep-sea fan complex that

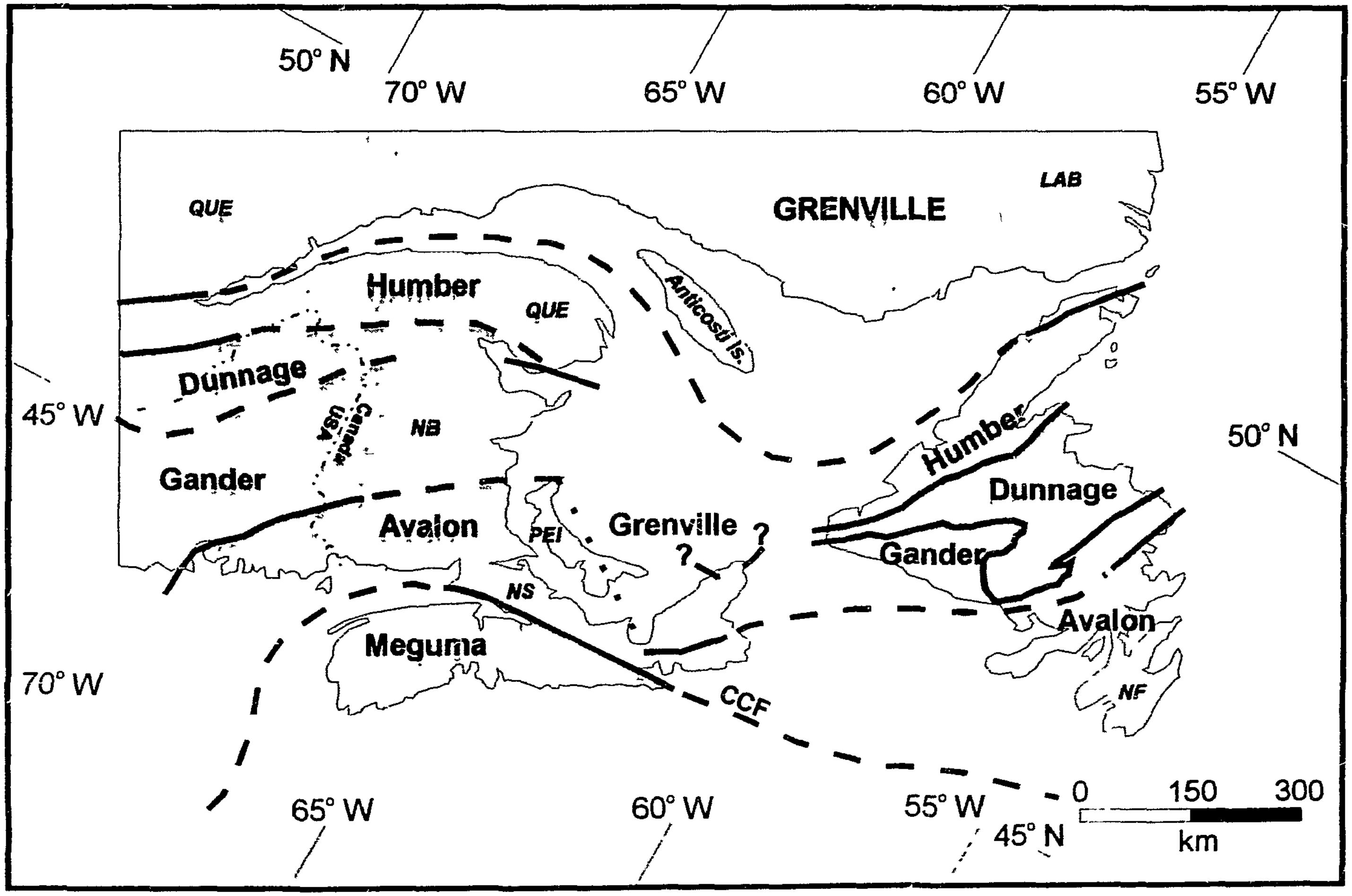

Figure 1.2. Simplified terrane map of the Canadian Appalachian segment. Lithotectonic subdivisions after *Stockmal et al. (1990) and the* offshore extent of the Meguma Zone after Pe-Piper and Loncarevic (1989). NS = Nova Scotia, NB = New Brunswick, PEI = Prince Edward Island, NF = Newfoundland, QUE = Quebec, LAB = Labrador, CCF = Cobequid-Chedabucto Fault.

developed on the northern passive margin of Gondwana during the closure of the Theic Ocean. Samarium-neodymium isotope systematics (T_{CHUR} = 1358±104 Ma), and detrital zircon ages between 0.5 and 3.0 Ga, dictate the provenance of Meguma sediments from Archean and Pan-African metasedimentary and meta-igneous protoliths in either present-day Morocco or Colombia during the Cambro-Ordovician (Clarke and Halliday, 1985; Krogh and Keppie, 1990).

Upper Ordovician glacio-eustatic regression produced a 3 km thick conformable shelf succession known as the Annapolis Supergroup above the Meguma Group before the Mid-Devonian (Schenk, 1978). The Upper Ordovician White Rock Formation rests directly on the Meguma Group, and it consists of a glacial diamictite overlain by massive orthoquartzites, greywackes, and tholeiitic-alkaline volcanics deposited in a neritic environment (Lane, 1975a). Volcanic rocks and associated hypabyssal dykes, sills, and plugs suggest either within-plate hot-spot volcanism or a subduction-related island arc environment with thick continental crust, during the progressive transport of the Meguma terrane towards the North American continental margin (Sarkar, 1978; Barr et al., 1983). Shallowing of the Theic Ocean allowed the development of near-shore siltstones, graptolitic slates, quartzites, and overlying fossiliferous and volcaniclastic strata belonging to the Kentville, Torbrook, and New Canaan Formations (Smitheringdale, 1973; Lane, 1975b; Schenk, 1981; Figure 1.4).

Polyphase regional deformation and metamorphism of the Acadian Orogeny occurred between 410 and 375 Ma (Keppie and Dallmeyer, 1987; Figure 1.4), initially penecontemporaneous with the deposition of the super-Meguma strata. Probable Avalonian basement xenoliths within the Popes Harbour dyke (Eberz et al., 1991) suggest that the Acadian event represents the northwesterly obduction and progressive dextral rotation of the Meguma terrane onto the Avalon Zone along the Cobequid-Chedabucto fault system (Keppie, 1982; Williams and Hatcher, 1982; Mawer and White, 1987; Eberz et al., 1991). The earliest deformation occurred between 410 and 385 Ma (Dallmeyer and Keppie, 1986) and it produced open, upright, northeast-trending regional folds and thrusts within the Meguma Group (Fyson,

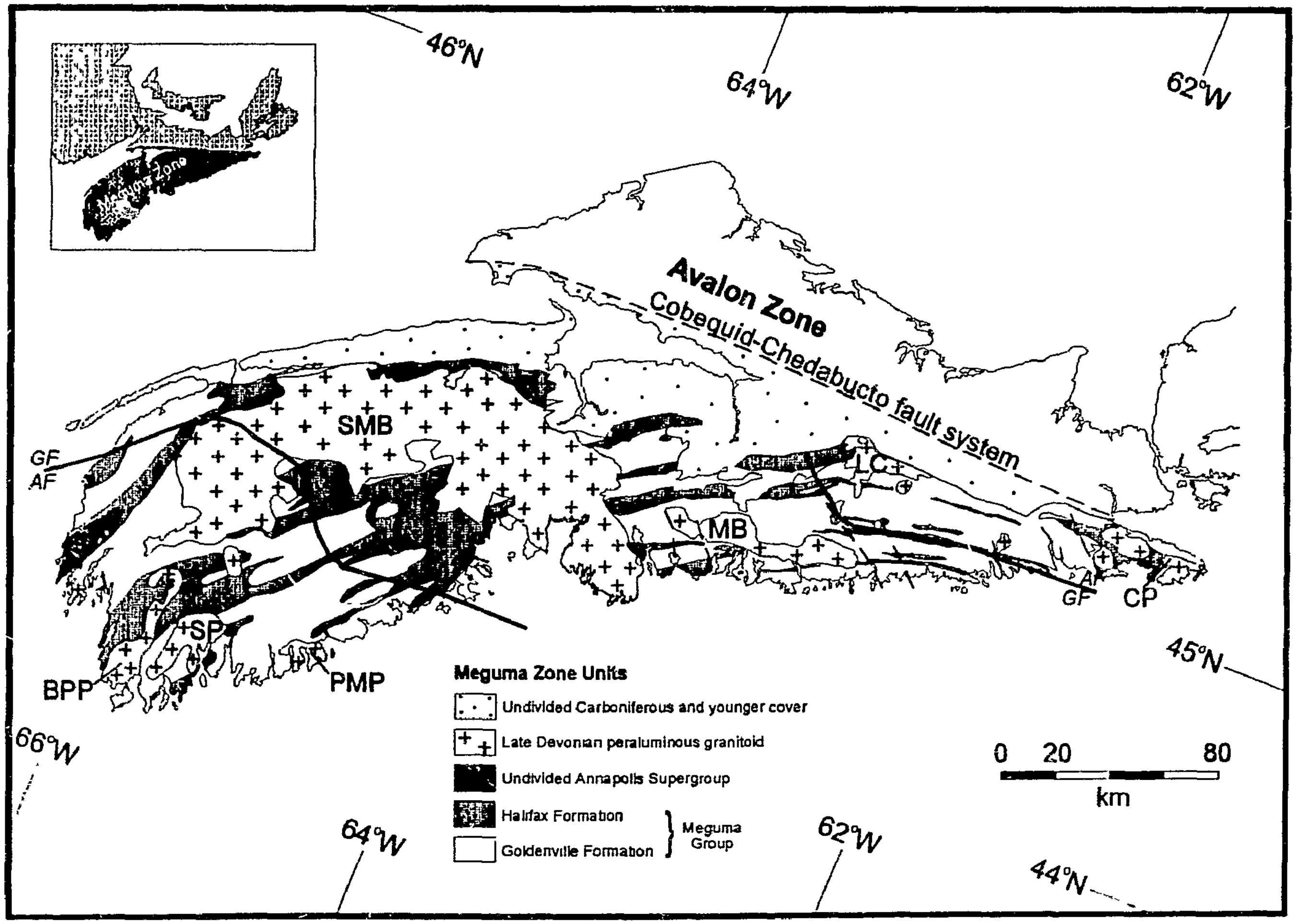

Figure 1.3. Geological map of the Meguma Zone in southwestern Nova Scotia. BPP = Barrington Passage Pluton, CP = Canso plutons, SP = Shelburne Pluton, PMP = Port Mouton Pluton, SMB = South Mountain Batholith, MB = Musquobuboit Batholith, LC = Liscomb Complex. Modified after Donahoe and Grantham (1989). The solid lines approximately represent the limits of metamorphic culminations in the Meguma Group (after Douma, 1988). AF = amphibolite facies, GF = greenschist facies.

1966; Schenk, 1975; N. Culshaw, pers. comm., 1993). Contemporaneous regional greenschist facies metamorphism occurred at less than 500°C and 350 MPa (Raeside et al., 1988) and it probably results from crustal thickening during terrane emplacement (Keppie and Dallmeyer, 1987); lower amphibolite grade metamorphic culminations also exist in southwestern and northeastern areas of the MZ (Figure 1.3; Elias, 1986; Raeside et al., 1988). Satellite crossfolds and micro-scale crenulations formed on northeasterly oriented structures during terrane rotation between 385 and 375 Ma (Fyson, 1966; Keppie and Dallmeyer, 1986) and they formed with northwest-trending sinistral, dextral, and transcurrent faults and shear joints (Eisbacher, 1969; O'Brien, 1983) that probably record the onset of tectonic uplift.

A suite of predominantly peraluminous granitoid plutons intruded the Meguma crust in the Late Devonian. The most primitive tonalites and granodiorites crop out as small plutons in the extreme southwest and northeast of the MZ (de Albuquerque, 1977; Hill, 1988; Figure 1.3). Magmatic hornblende from the Barrington Passage Pluton and zircon from the Canso plutons suggest syntectonic tonalite crystallization at 385-378 Ma (Reynolds et al., 1987; Hill et al., 1990). In contrast, the South Mountain Batholith (SMB) represents a 7,500 km^2 polyintrusive complex of more evolved granodiorite, monzogranite, and leucomonzogranite lithologies (Horne et al., 1989). The SMB forms the largest granitoid intrusion in the Appalachian Orogen and it consists of 13 identified plutons that intruded simultaneously at circa 372 Ma (Clarke and Muecke, 1985; Reynolds et al., 1987; Clarke et al., 1993b; Figures 1.3 and 1.4). Elongation of the SMB parallel to regional fold trends, the presence of a cordierite foliation within the marginal granodiorite, the occurrence of syn-intrusion faults (Horne et al., 1988), and a contact aureole that locally overprints regional metamorphic assemblages, all suggest its syn-tectonic to late-tectonic emplacement (Raeside et al., 1988). All granitoid bodies have miarolitic cavities and show the abundant pegmatites of epizonal granitoids; they probably represent diapirs that intruded by both stoping and forceful emplacement (Clarke and Muecke, 1985; Douma, 1988; Ham, 1988; Hill, 1991). AFM mineral and two-feldspar palaeobarometry suggest the

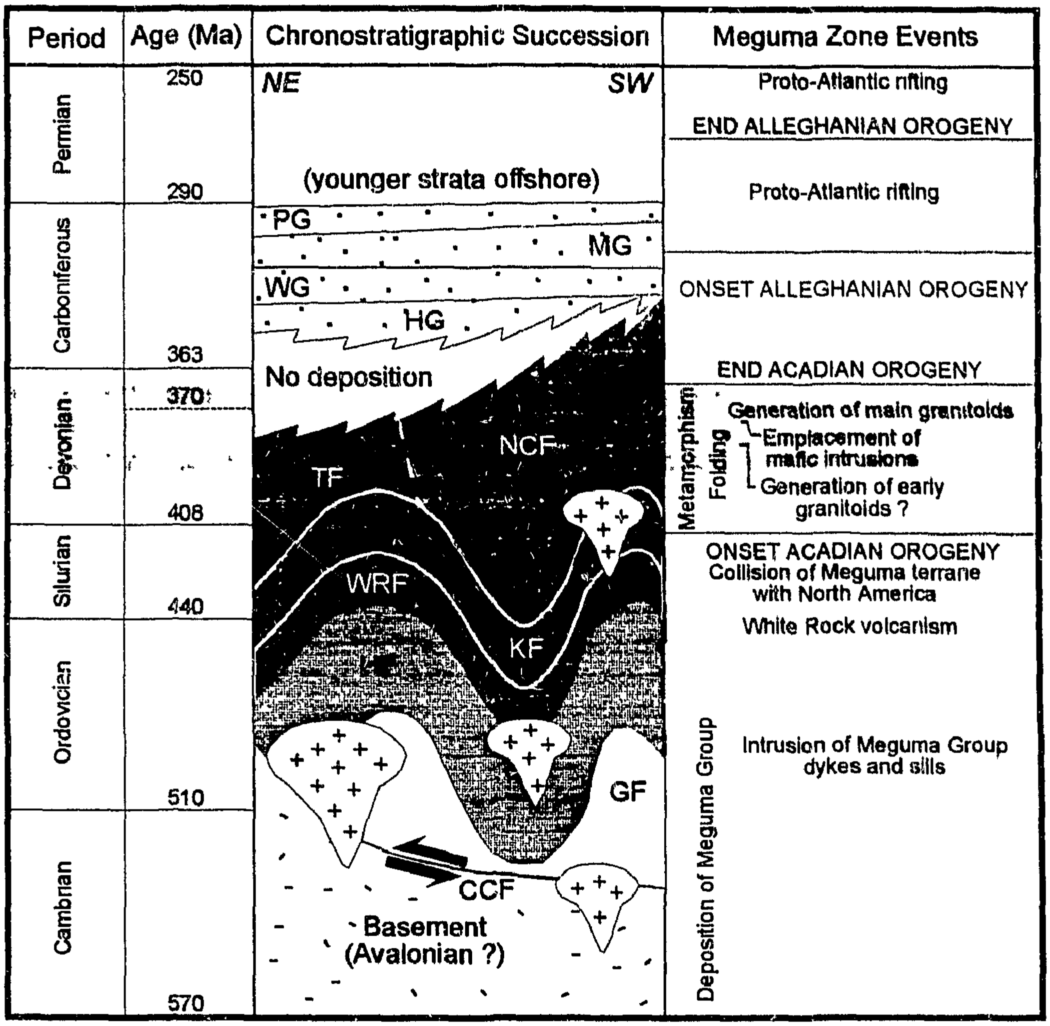

Figure 1.4. Summary of the chronostratigraphic succession of Nova Scotia, emphasizing the Palaeozoic geological events in the Meguma Zone. The shaded area represents the time period considered by this thesis. Geological timescale after Harland et al. (1989) with Carboniferous chronolithologic information after Gibling (in press). Ornament as in Figure 1.3; CCF = Cobequid-Chedabucto Fault, GF = Goldenville Formation, HF = Halifax Formation, WRF = White Rock Formation, KF = Kentville Formation, TF = Torbrook Formation, NCF = New Canaan Formation, HG = Horton Group, WG = Windsor Group, MG = Mabou Group, PG = Pictou Group, NMB = North Mountain Basalt.

emplacement of most bodies at approximately 10-14 km depth in the middle to lower epizone (e.g. Ham, 1988), and metamorphic assemblages in the Meguma Group support this depth range (Raeside et al., 1988).

Following Meguma-Avalon collision, what is now Atlantic Canada became the locus of dextral transtension prior to and during the Upper Carboniferous-Lower Permian Alleghanian (=Hercynian) Orogeny between 375 and 260 Ma (Keppie, 1977; Scotese et al., 1984; Mawer and Williams, 1986; Piqué and Skehan, 1992; Figure 1.4). Penetrative foliations developed in granitoid plutons close to the Cobequid-Chedabucto fault system at Canso (Hill, 1986; Hill and Raeside, 1987; Hill, 1988; Figure 1.3), and uplift exposed the SMB to erosion 5-15 Ma after emplacement (Horne, 1988; Martel et al., 1993). Localized shearing, retrograde metamorphism, and hydrothermal mineralization occurred most intensely in southwestern and northeastern areas of the MZ, where it partially reset $^{40}Ar/^{39}Ar$ geochronometers (Reynolds et al., 1987; Muecke et al., 1988). Throughout the Carboniferous and Permian, immature fluvial and lacustrine siliclastic molasse and coal accumulated in the fault-bounded Fundy rift and Magdalen Basin (Martel and Gibling, 1991; Keppie, 1989; Figure 1.4) to form the earliest overlap assemblages common to both the Meguma and Avalon terranes (Williams and Hatcher, 1982). The culmination of rifting in the Triassic led to the opening of the Atlantic Ocean and the isolation of the MZ in its present position against the North American continental margin (Schenk, 1981).

1-5. Previous Studies of Granitoid Petrogenesis in the Meguma Zone

Late Devonian granitoids in the MZ range in composition from subordinate hornblende- and biotite-tonalite and biotite-granodiorite, dominant two-mica monzogranites (Rogers, 1984; Clarke and Muecke, 1985; Douma, 1988; MacDonald et al., 1989) to leucomonzogranites and leucogranites. Most lithologies have peraluminous compositions (A/CNK >1) (Clarke et al., 1993b) and they, therefore, contain accessory muscovite, cordierite, garnet, andalusite, or topaz (Clarke and Muecke, 1985 and references therein). Within the South Mountain Batholith (SMB), geochemical variation largely results from modal phenocryst and accessory mineral fractionation, from late-magmatic fluid-rock interaction (Muecke and Clarke, 1981; Clarke and Chatterjee, 1988), and probably also from Meguma Group contamination (Clarke et al., 1988; MacDonald et al., 1990). Epsilon neodymium values are variable (-5.2 to -1.4) but higher than those for the Meguma Group (Clarke et al., 1988), and they suggest the derivation of SMB magmas from sub-Meguma basement sources composed of metagreywackes and possibly a minor component of altered volcanic rocks. Ortho- and paragneisses exposed at two localities in the MZ have Sr-Nd isotopic compositions appropriate for the formation of peraluminous partial melts similar to the SMB granitoids (Eberz et al., 1991; Clarke et al., 1993a).

Keppie and Dallmeyer (1987) suggested that the generation of anatectic granitoid melts occurred in response to the slow rise of isotherms in the lower crust during terrane accretion, but Clarke et al. (1988) recognized that considerable overthrusting would be required to produce temperatures sufficient for the generation of the voluminous SMB and Culshaw (pers. comm., 1993) noted that the open, upright morphologies of kilometric folds within the Meguma Group do not suggest extreme thickening. Hill (1991) proposed that the presence of tonalites requires high temperatures in the sub-Meguma basement source, and that the existence of amphibolite metamorphic culminations at the northeastern and southwestern extents of the MZ also indicate steep geothermal gradients of >40°C km^{-1} in parts of the Meguma Group. Both Owen et al. (1988) and Eberz et al. (1991) document sub-Meguma basement that records much lower temperatures (<760°C at circa 25 km depth) than this steep gradient predicts, and crustal thickening alone may not explain these features. Although the degree of thickening associated with Meguma Group accretion is not known, current interpretations favour a localized and external source of heat to explain both metamorphic and petrologic features in the MZ.

De Albuquerque (1979) initially discovered that the emplacement of MZ granitoids occurred synchronously with a suite of volumetrically minor mafic intrusions. Two of these intrusions crop out within tonalites of the Barrington Passage and Shelburne plutons (Rogers, 1984). Douma (1988) later documented synplutonic lamprophyre intrusions within the Port Mouton Pluton, and $^{40}Ar/^{39}Ar$ dating by Reynolds et al. (1987) and Kempster et al. (1989) confirmed contemporaneous (circa 370 Ma) ages for mafic bodies intruding the Meguma Group. Most recently, Hill (1991) and Clarke et al. (1993a) suggested the thermal significance of Late Devonian mafic intrusions (LDMIs) during their study of the Liscomb Complex and Canso plutons. Given that crustal thickening may not adequately explain petrological and metamorphic features in the MZ, and that temporally and spatially intimate mafic intrusions apparently exist, models for granitoid petrogenesis must consider the importance of the much smaller mafic bodies.

1-6. Purpose, Objectives, and Organization

This project describes and accounts for the nature and characteristics of the LDMIs, and it investigates the importance of mafic material as a source of both chemical components and, therefore, heat in the entire MZ during the Acadian Orogeny. To fully explore the MIM hypothesis, this work adopts an integrated, multidisciplinary approach with the following objectives:

(1) recognize all of the Late Devonian mafic intrusions and investigate their intrusion age(s), evolutionary processes, magma source(s), and regional tectonic significance;

(2) examine the evidence for interaction between mafic and peraluminous granitoid material (synplutonic mafic intrusions and enclaves) and evaluate the elements transferred;

(3) test a compiled granitoid geochemical database for indications of interaction between mafic and granitoid melts, based on the physical and chemical evidence outlined above; and

(4) model the feasibility of the LDMIs as anatectic heat sources using theoretical simulations constrained by Acadian metamorphic conditions in the crust of the MZ.

The characteristics and petrogenesis of the mafic intrusions appears in Chapter 2, and Chapter 3 evaluates the evidence for mafic-granitoid magmatic interaction at the synplutonic intrusion sites. These sections provide the foundation for examining mafic-granitoid genetic relationships in the MZ. Chapter 4 studies the enclaves preserved in four MZ granitoids, whereas Chapter 5 applies the results of the field studies to the geochemical characteristics of all granitoid intrusions in the MZ and searches for mantle-derived chemical components. Finally, Chapter 6 tests the thermal capabilities of the LDMIs with theoretical heat flow models. The discussion in Chapter 7 evaluates the applicability of a MIM to the peraluminous granitoids in the MZ, and suggests the imposition of a modified petrogenetic model that advocates mafic intraplating as a petrogenetic process. This study also considers other possible sources for localized and/or external heating, and discusses the assumptions and limitations intrinsic to the MIM.

Chapter 2

THE CHARACTERISTICS AND PETROGENESIS OF LATE DEVONIAN MAFIC INTRUSIONS

2-1. Introduction

The Meguma Zone (MZ) contains four suites of minor mafic intrusions defined on the basis of relative age (Figure 2.1).

(1) *Ordovician (?).* Diabase dykes and sills intrude the Meguma Group and White Rock Formations in the vicinity of Wolfville, Nictaux-Torbrook, and Bear River (Barr et al., 1983). Most bodies have thicknesses less than 2 m and they show characteristic vesicular textures. Thin sections reveal a saussuritized mineralogy dominated by chlorite, sericite, albite, and plagioclase. Folding of the sills with their host sediments indicates pre-Acadian intrusion, and soft-sediment deformation at their contacts with the Meguma Group implies an Ordovician age, although no bodies contain primary magmatic geochronometers (S. M. Barr pers. comm., 1992). These rocks show the geochemical characteristics of ocean tholeiites (Barr et al., 1983).

(2) *Early Silurian.* Deformed and metamorphosed gabbroic plugs, diabase dykes, and metabasites intrude the Halifax and White Rock Formations in the vicinity of Yarmouth (Sarkar, 1978; Calder and Barr, 1982). The physical characteristics and mineralogy of these rocks resemble those of the Ordovician dykes and sills, but their discordant contact relations with the White Rock Formation instead suggest an Early Silurian age (Keppie and Dostal, 1991) despite Alleghanian tectonothermal resetting of $^{40}Ar/^{39}Ar$ (amphibole) geochronometers (Elias, 1986; Muecke et al., 1988). The geochemistry of these bodies reflects continental or island arc tholeiitic magmatism (Calder and Barr, 1982).

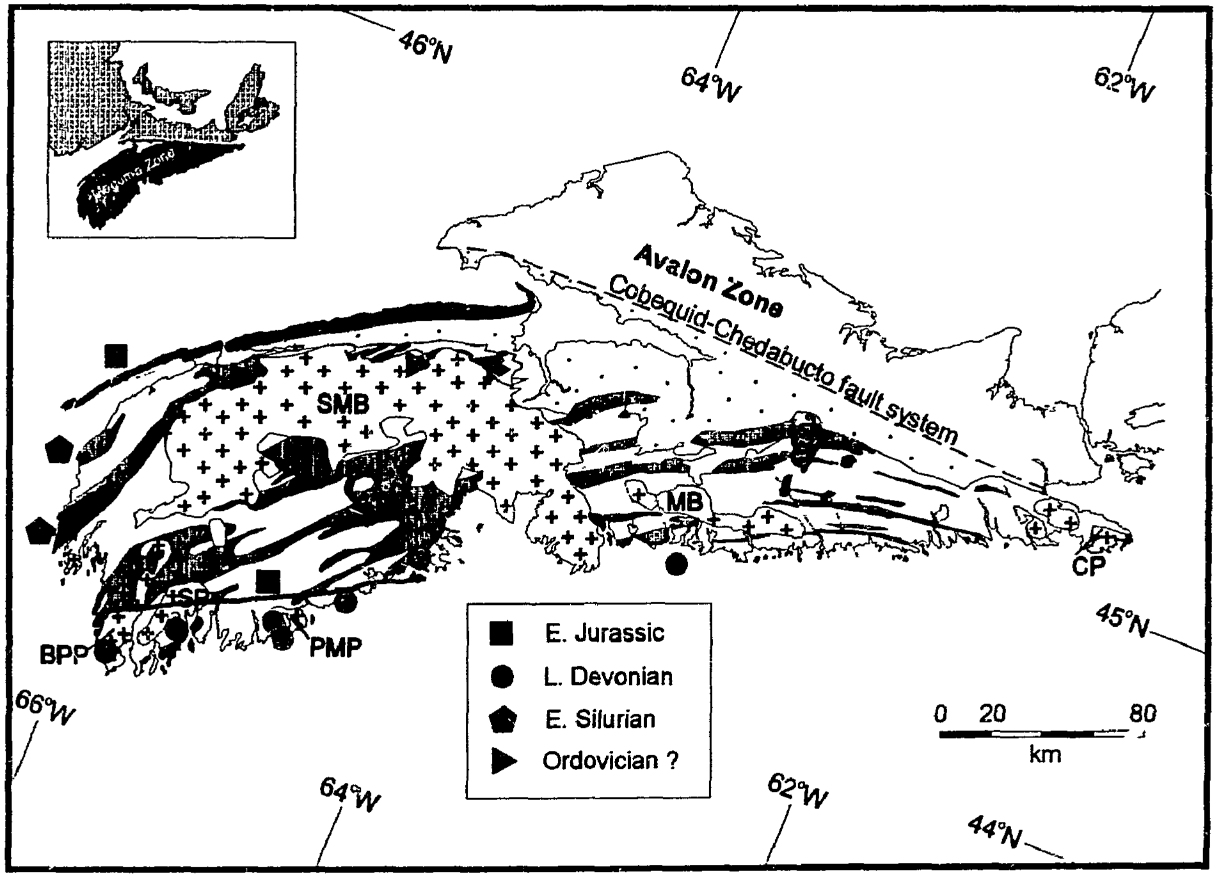

Figure 2.1. Geological map of the Meguma Zone showing the locations and ages of currently identified mafic intrusions. Ordovician mafic intrusions: 1 = Wolfville area dykes and sills, 2 = Nictaux-Torbrook dykes and sills, 3 = Bear River area dykes and sills. Early Silurian mafic intrusions: 1= Yarmouth area White Rock dykes, sills, and lavas, 2 = Mavillette diabase plug. Late Devonian mafic intrusions: 1 = Attwoods Brook gabbronorite plug, 2 = Birchtown diorite sheet(?), 3 = Forbes Point lamprophyre dyke, 4 = Mcleods Cove lamprophyre sheet, 5 = Mersey Point picrite plug, 6 = Ovens altered diorite dykes, 7 = Weekend dyke lamprophyre dykes, 8 = Liscomb Complex gabbro-diorite plugs. Early Jurassic mafic intrusions: 1 = North Mountain basalt lavas, 2 = Shelburne diabase dyke. Abbreviations and ornament as in Figure 1.3 in Chapter 1. Modified after Donohoe and Grantham (1989).

(3) *Late Devonian.* Volumetrically minor plugs, synplutonic bodies, and dykes crop out along the southern and eastern shores of Nova Scotia (de Albuquerque, 1979; Kempster et al., 1989). Eleven bodies occur within the Meguma Group, four mafic intrusions crop out as synplutonic intrusions within granitoid bodies (Rogers, 1984; Douma, 1988; Gallant, 1991), and two mafic-intermediate bodies crop out within high-grade ortho- and paragneisses in close proximity to the granitoid bodies of the Liscomb Complex (Clarke et al., 1993a). These rocks have hydrous ferromagnesian mineral assemblages.

(4) *Triassic-Early Jurassic.* Tholeiitic "olivine-lamprophyre" dykes of Mesozoic age intrude the Wedgeport Pluton (Cullen, 1983), and the Shelburne diabase dyke cuts the Meguma Group and crops out discontinuously from Pubnico to LaHave (Papezic and Barr, 1981). These dykes have diabasic textures and they consist of olivine, clinopyroxene, and plagioclase microphenocrysts that are partially altered to chlorite and epidote. They form part of a swarm of northeasterly trending tholeiites in Eastern North America associated with proto-Atlantic rifting (McHone, 1992), and may be genetically related to the mineralogically similar North Mountain basalts (Dostal and Greenough, 1992).

This chapter documents the field relations, petrography, ages, and geochemical characteristics of the predominantly mafic third suite, hereafter known as the Late Devonian mafic intrusions (LDMIs) despite the inclusion of two intermediate intrusions. It develops a petrogenetic model for their magmatic evolution, mantle source(s), and their tectonic environment, and it provides criteria for the recognition of Late Devonian mafic material. Figure 2.1 shows the locations of the currently recognized LDMIs. Detailed location maps, microprobe data, and geochemical analyses for each intrusion appear in Appendices B-1, B-2, and B-3, respectively.

2-2. Field Relations and Petrography of Late Devonian Mafic Intrusions

The LDMI suite consists of five isolated intrusions, an intrusive complex, and two small dyke "swarms". Table 2.1 summarizes their lithologic characteristics, modal mineralogy, and previously published documentation. A detailed synopsis for each body appears below; Appendix A-1 describes the microprobe operating conditions.

2-2.1. Hornblende-Gabbronorite at Attwoods Brook, Barrington Passage

Field relations

A black (ginger-brown weathering) massive body of medium to coarse-grained gabbronorite crops out along the shore and on three of the islands in Murray Cove near Attwoods Brook, entirely enclosed within the Barrington Passage Pluton (Figure 2.1). Although the contact relations with the host tonalite do not crop out, a ground magnetic survey (Appendix A-2) superimposed upon the outcrop pattern, suggests that it has an irregular morphology and probably thins to the northwest. Despite the current exposure of less than approximately 10% of the gabbronorite, interpolation between outcrops suggests that this body must extend for at least 600 m parallel to its longest axis. Fresh material exhibits a randomly oriented and equigranular intergrowth of black pyroxene and tabular plagioclase laths up to 2.5 mm, and it commonly hosts 1-20 cm scale coarse-grained gabbro-pegmatite veinlets containing pyroxene, amphibole, and plagioclase euhedra up to 1 cm. Altered gabbronorite has a greenish hue resulting from chloritization and it shows the development of randomly oriented biotite and amphibole grains up to 2.5 mm. Alteration commonly coincides with pervasive, anastomosing joints that dissect all recognized exposures (Figure 2.2). Along the shore and on one island in Murray Cove, granitic pegmatites emanating from the host tonalite brecciate the gabbronorite into angular fragments.

Table 2.1. Summary of the lithologies, intrusive type, macroscopic characteristics, and previous research for the Late Devonian mafic intrusions.

Fig. 2.1 No.	Location	No. of bodies	Lithology	Morphology	Length (m)	Width (m)	Strike (°)	Dip	Mode	n	Refs.
1	Attwoods Brook	1	Gabbronorite	plug (?)	~750	~250	-	-	$Pl_{63.26}$ $Cpx_{18.74}$ $Opx_{5.96}$ $Hbl_{5.88}$ $Bt_{1.03}$ $Qtz_{0.14}$ $Opq_{0.35}$ $Chl_{4.64}$	5	1, 2
2	Birchtown	1	Diorite (High-K diorite)	sheet (?)	>100	>100	-	-	$Pl_{18.72}$ $Kfs_{0.63}$ $Hbl_{45.04}$ $Bt_{23.27}$ $Qtz_{10.68}$ $Opq_{0.58}$ $Chl_{1.08}$	4	1, 2
3	Forbes Point	1	Spessartite	dyke	-	5	20	90	$Pl_{18.0}$ $Kfs_{2.1}$ $Hbl_{40.2}$ $Bt_{37.1}$ $Qtz_{2.5}$ $Opq_{0.1}$	1	3
4	Mcleods Cove	1	Kersantite/ spessartite	sheet	>80	0.1-1	40	45SW	$Pl_{11.5}$ $Kfs_{2.54}$ $Hbl_{33.85}$ $Bt_{48.26}$ $Qtz_{5.38}$ $Opq_{0.47}$	3	3
5	Mersey Point	1	Picrite	plug	~200	~300	-	-	$Ol_{30.98}$ $Pl_{23.47}$ $Cpx_{7.67}$ $Opx_{3.47}$ $Hbl_{26.51}$ $Phl_{5.92}$ $Qtz_{0.19}$ $Opq_{0.77}$ $Chl_{1.02}$	4	1, 4
6	Ovens	4	Diorite (altered)	dyke	>1000	0.75-3.2	220	85SE	$Pl_{8.0}$ $Kfs_{9.0}$ $Qtz_{<1.0}$ $Cal_{14.0}$	3	5
7	Weekend dykes	10	Spessartite	dyke	>1000	0.01-14.7	154	90	See Table 2.2	-	6, 7, 8
8	Liscomb complex	2	Gabbro-diorite	plug	2500-5000	2500-7000	-	-	Pl Cpx Hbl Bt Opq	-	9, 10

Modal percentages represent averages of between 3 and 5 thin sections per body (between 2500 and 3500 counts per thin section) using a Swift F415C point counting device. The results lie statistically ±2% with 95% confidence (Van der Plas and Tobi, 1965). Modal classifications after Streckeisen (1976, 1979). Mineral abbreviations after Kretz (1983); Opq (opaques) = Spl+Mag+Py. 1 = de Albuquerque (1979), 2 = Rogers (1984), 3 = Douma (1988), 4 = Elias (1986), 5 = Hall (1979), 6 = Greenough et al. (1988), 7 = Kempster (1988), 8 = Ruffman and Greenough (1990), 9 = Chatterjee et al. (1989), 10 = Clarke et al. (1993a).

Figure 2.2. A typical outcrop of gabbronorite at Attwoods Brook. Note the pervasive joint pattern. View to the northeast, notebook 20 cm long.

Petrography

The Attwoods Brook gabbronorite contains a panidiomorphic-hypidiomorphic intergrowth of plagioclase (60-63%), clinopyroxene (18-22%), orthopyroxene (4-9%), and amphibole (4-10%), with subordinate biotite (0.5-3%) and rare quartz (0.1-0.7%). The texture of this intrusion varies over the outcrops. Samples taken away from the presumed contacts show orthocumulate characteristics (Figure 2.3). They have flow-aligned, normally zoned plagioclase (1.0-5.5 mm; An_{58}-An_{44}) ophitically to subophitically enclosed by augite (2.5-5 mm; $Wo_{48-23}En_{44-60}Fs_{8-17}$) and subordinate hypersthene (2.5-3.5 mm; $En_{69}Fs_{31}$). Light brown magnesio-hornblende, tschermakitic hornblende, and actinolite (2.5-5 mm) occur as equant patches that crystallized interstitially with quartz. Chalcopyrite and chrome-spinel occur with accessory zircon and apatite as hypidiomorphic inclusions within all mineral phases. Close to joint planes, and towards the contacts with the Barrington Passage Pluton, the gabbronorite becomes progressively altered. Figure 2.3 illustrates the development of amphibole overgrowths on augite and hypersthene. Epidote and calcite commonly occur in these regions with sericitized plagioclase and locally abundant quartz.

Preliminary interpretations

De Albuquerque (1979) noted the preferential development of amphibole towards the presumed gabbronorite-tonalite contact and suggested the synplutonic intrusion of this body. Rogers (1984) instead considered the gabbronorite a large xenolith within the Barrington Passage Pluton, but Gallant (1991) demonstrated the re-orientation of tonalite magmatic foliations around the gabbronorite, perhaps in support of the synplutonic interpretation. Although poor exposure obscures the intrusive nature of the gabbronorite, its large size argues strongly against a xenolith origin unless the Barrington Passage Pluton enveloped the body *in situ*.

Amphibole compositions may support a synplutonic nature for the intrusion. If the euhedral and overgrowth amphiboles resulted from both magmatic recrystallization and

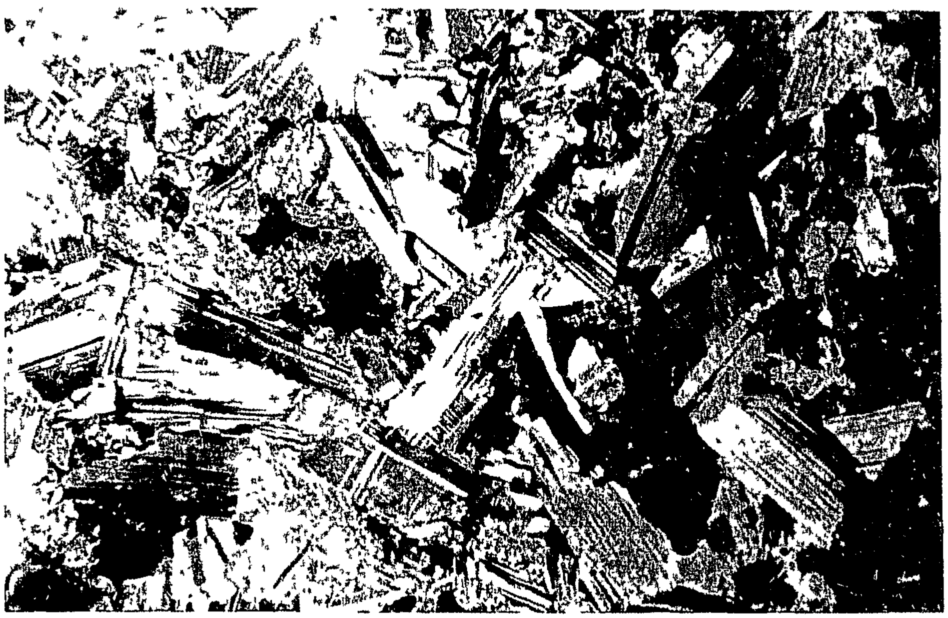

Figure 2.3. Photomicrograph of the plagioclase-orthocumulate texture in the Attwoods Brook gabbronorite. Note the weak flow alignment of plagioclase, and the intercumulus clinopyroxene, amphibole, biotite, and quartz. Amphibole also replaces clinopyroxene in the groundmass. Field of view 17 mm, XPL.

subsequent metamorphism or alteration, two different compositions should exist. Instead, Figure 2.4 shows the compositional continuum of amphiboles present within the Attwoods Brook gabbronorite. Amphibole crystals have Si (atomic) between 7.0 and 7.8 that suggest they formed under both subsolidus magmatic and hydrothermal conditions (Pe-Piper, 1988), but no clear chemical separation exists between the euhedral intercumulus (presumed late-magmatic) amphiboles, and the poikilitic overgrowths on clinopyroxene (presumed hydrothermal). The restriction of amphibole overgrowths close to the contacts with the Barrington Passage Pluton may implicate the thermal and chemical effects of the tonalite host on the crystallizing gabbronorite; perhaps the tonalite and gabbronorite coexisted in a magmatic state and transferred volatile constituents.

2-2.2. Diorite at Birchtown Quarry, Shelburne

Field relations

Birchtown Quarry exposes a massive and coarse-grained, grey-green diorite, completely enclosed within a granodiorite phase of the Shelburne Pluton (Figure 2.1). Poor exposure obscures the maximum extent of the diorite and a ground magnetic survey (Appendix A-2) failed to reveal its shape or size; the geographic separation of known outcrops in the quarry suggests that it must have a diameter greater than >100 m. Diorite typically shows an equigranular intergrowth of randomly oriented green amphibole, plagioclase, biotite, and pyrite up to 2 mm in diameter (Figure 2.5a, b). Considerable grain size variation occurs in the quarry. To the west (close to the contact with the Shelburne Pluton) the equigranular diorite coarsens and develops randomly oriented hexagonal biotite and tabular K-feldspar macrocrysts up to 1 cm in diameter. At one locality, the diorite contains a medium-grained psammitic enclave approximately 2 m long, surrounded by a 1 cm thick zone of chilled diorite (see Figure B1.3 in Appendix B). Randomly oriented granitic dykes and pegmatites from the Shelburne Pluton commonly intrude the diorite, and numerous irregular joints occur in both the diorite and its granitoid host.

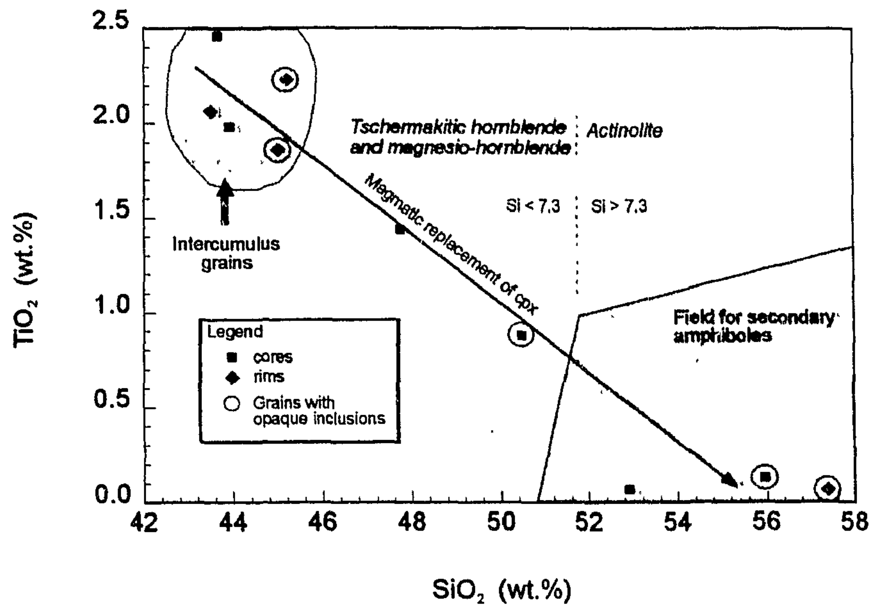

Figure 2.4. Plot of TiO_2-SiO_2 after Rock (1990) for Attwoods Brook gabbronorite amphiboles. Note the compositional continuum and the variable presence of opaque inclusions (circled data points) in crystals with different compositions. The titanian amphiboles (Si <7.3) probably represent magmatic compositions and/or deuteric reaction products derived from clinopyroxene breakdown, whereas crystals with Si >7.3 probably represent alteration products. Silica classification scheme after Pe-Piper (1988).

a

b

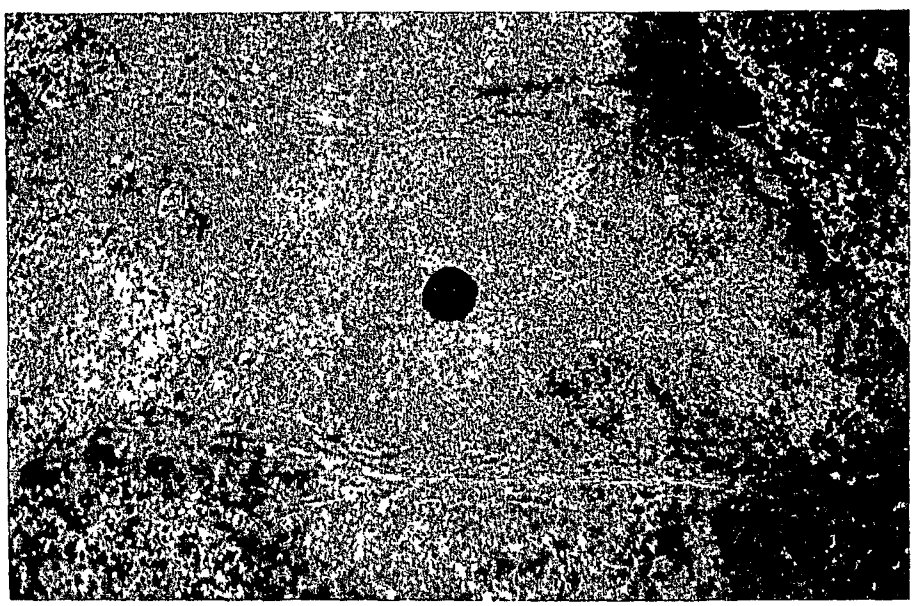

Figure 2.5. The field characteristics of Birchtown diorite. (a) A typical outcrop of diorite in the Birchtown Quarry. View to the southwest, building for scale; (b) A close-up view of the diorite showing the typical grey-green colouration imparted by amphibole, the irregularly distributed patches of feldspar, and the closely-spaced joints containing quartz-chlorite slickencrysts. Plan view, lens cap 7 cm diameter.

Quartz-chlorite slickencrysts indicate small amounts of relative movement along these weaknesses after diorite intrusion (Figure 2.5b).

Petrography

Amphibole (45-52%; magnesio-hornblende-actinolite), mildly pleochroic biotite (15-25%; [Mg/(Mg+Fe)] = 0.6-0.7), tabular labradorite-andesine (18-28%; An_{52}-An_{39}) and slightly strained quartz blebs (1-12%), form the main modal constituents of the diorite. Regardless of its grain size, all samples show inequigranular-subporphyritic textures and complex intergrowths between amphibole and biotite (Figure 2.6). Textural criteria define two biotite populations. Light brown (non-pleochroic) and dark brown (pleochroic) biotite euhedra occur as 0.1-1.5 mm inclusions in amphibole, as both isolated crystals at grain boundaries between amphibole and plagioclase, and as randomly oriented hexagonal sheaves (appearing as hexagonal macrocrysts in hand sample). Normally zoned amphiboles occur as panidiomorphic crystals up to 3 mm that may represent phenocrysts, or as subhedral intergrowths and allotriomorphic rims associated with the hexagonal biotite clusters. Normally zoned, hypidiomorphic plagioclase occurs interstitially with allotriomorphic blebs of slightly subgrained quartz and allotriomorphic K-feldspar (0.1-1%), except to the west where centimetric oikocrysts enclose biotite or amphibole and apparently represent late-magmatic growth products. Pyrite blebs occur as inclusions within amphibole and biotite and they locally reach modal abundances of 1%. Panidiomorphic sphene, apatite, and zircon inclusions up to 0.1 mm occur in all other mineral phases. Minor sericitization of plagioclase cores, and chloritization of amphibole and biotite may reflect deuteric rather than secondary alteration.

Preliminary interpretations

Rogers (1984) considered this body a large xenolith similar to the Attwoods Brook gabbronorite, but a recently exposed transitional contact with the Shelburne Pluton consists of

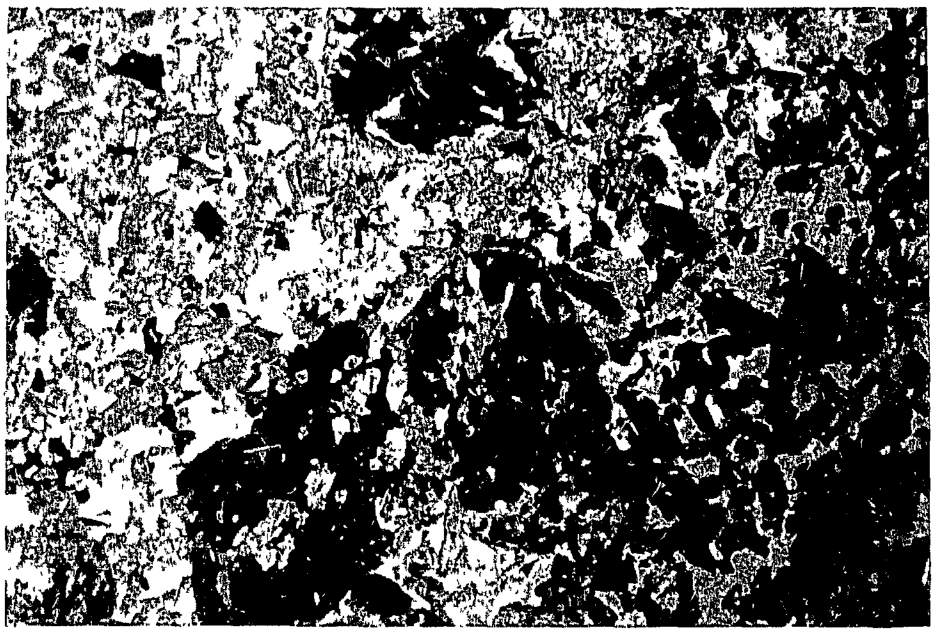

Figure 2.6. Photomicrograph showing the unusual texture of the Birchtown diorite. Note that amphibole occurs both as euhedral prismatic crystals, as crystalline aggregates, and as hypidiomorphic tangential rims on biotite. Biotite occurs as small, isolated single crystals and as polycrystalline, pseudohexagonal clusters. Plagioclase and quartz occur interstitially. Field of view 14 mm, PPL.

putative hybrid lithologies that confirm the synplutonic nature of this body (Chapter 3, Section 3.3). Diamond drilling in the 1940's penetrated granodiorite of the Shelburne pluton below the diorite at depths between 7 m and 23 m (Douglas, 1943), suggesting that the diorite has an irregular but sheet-like morphology (Rogers, 1984). Diorite also contains similar amphibole compositions to the Attwoods Brook gabbronorite; the amphiboles have Si (atomic) between 7.1 and 7.8 and span the magmatic-hydrothermal divide (Pe-Piper, 1988). Figure 2.7 chemically discriminates the clustered biotites from their single crystal counterparts. Clustered grains contain higher MgO and lower FeO relative to the single crystals. Three possibilities exist for the formation of these structures: (1) early crystallized (more primitive) glomeroporphyritic mats; (2) a magmatic reaction phenomenon resulting from the synplutonic intrusion of the diorite; or (3) pseudomorphs after a ferromagnesian precursor replaced during deuteric alteration. Chemical and textural criteria cannot distinguish between these hypotheses, although the hexagonal cluster morphology tentatively suggests a garnet precursor for them. Garnet occurs as a high pressure phenocryst in some exotic diorites (Green and Ringwood, 1968a).

2-2.3. Lamprophyre at Forbes Point, Port Mouton

Field relations

A coarse-grained, olive-green synplutonic lamprophyre dyke crops out in the Port Mouton Pluton at Forbes Point (Figure 2.1). The dyke ranges in thickness from 7 m at the base of the outcrop to 3 m at the top, and it has an arcuate attitude (Figure 2.8). Ground magnetic data (Appendix A-2) failed to trace the body along strike, suggesting that it is laterally discontinuous. Internally, the dyke consists of heterogeneous lamprophyre with variably coarse grain sizes up to 6 mm. Irregular pegmatitic veins, stringers, and patches, contain chaotically oriented amphibole and plagioclase phenocrysts up to 1 cm long situated in a matrix of intergrown amphibole and biotite up to 8 mm in diameter. These structures locally disrupt the chilled margins at the contact with the Port Mouton Pluton (Figure 2.9) and they appear to be

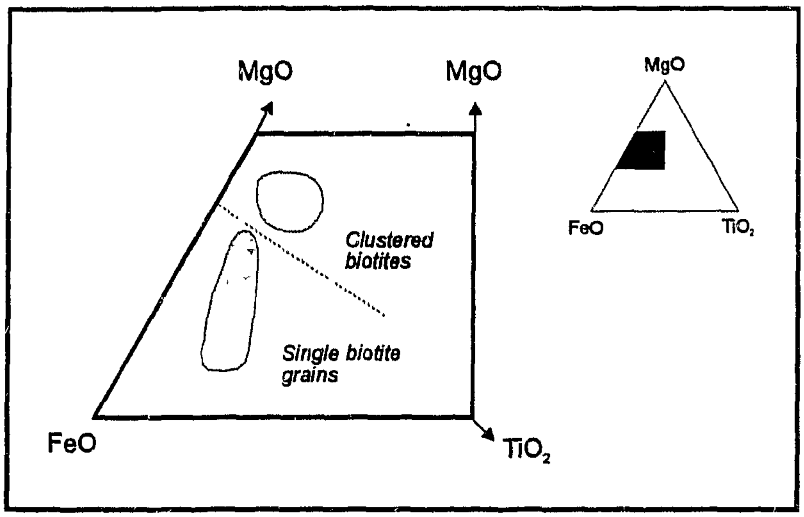

Figure 2.7. MgO-FeO-TiO_2 compositional discrimination of the single grain and clustered biotites in the Birchtown diorite. Clustered biotite crystals contain higher MgO and lower FeO than single grains and they, therefore, have more primitive compositions.

Figure 2.8. The Forbes Point dyke cropping out within the Port Mouton Pluton. Note the unusual arcuate attitude of the dyke and the enclave of feldspathic lamprophyre at its centre. View to the northwest, figure approximately 1.8 m tall.

late-stage fractionates. A 1.5 m diameter enclave of medium-grained, equigranular feldspathic lamprophyre has a sharp contact with the dyke, and it is emphasized by three aphyric chilled margins oriented concentric to the contact surface.

Petrography

Forbes Point lamprophyre has a seriate-subporphyritic texture and consists of hypidiomorphic green amphibole (40%; magnesio hastingsite-actinolite), weakly pleochroic and rutilated biotite (37%; [Mg/(Mg+Fe)] = 0.7), and hypidiomorphic, patchily zoned andesine (18%) up to 8 mm in diameter, with interstitial quartz blebs (3%), minor K-feldspar (2%), and accessory ilmenite and chalcopyrite (Figure 2.10). Pervasive alteration results in the internal aggregation of amphiboles and the replacement of primary textures by mats of chlorite, biotite, epidote, prehnite, and sericite. Coarse pegmatitic material contains randomly distributed actinolite, andesine, and minor quartz, with abundant sphene and apatite inclusions.

Preliminary interpretations

The melanocratic yet hydrous mineralogy (amphibole>biotite), the porphyritic characteristics, and the presence of modal quartz, identify the Forbes Point body as a spessartite lamprophyre (Streckeisen, 1979). Although it lacks the primary magmatic carbonates that commonly occur in lamprophyres (Rock, 1990), the predominantly hydrous mineral assemblage and the common pegmatitic segregations indicate the volatile-rich nature of the parent magma and suggest a deuteric origin for the alteration. The Forbes Point body exhibits strikingly similar mineral compositions and textural characteristics to the Birchtown diorite, and it also shares textural and modal similarities with the vaugnerites (synplutonic kersantites and spessartites) described by Sabatier (1991).

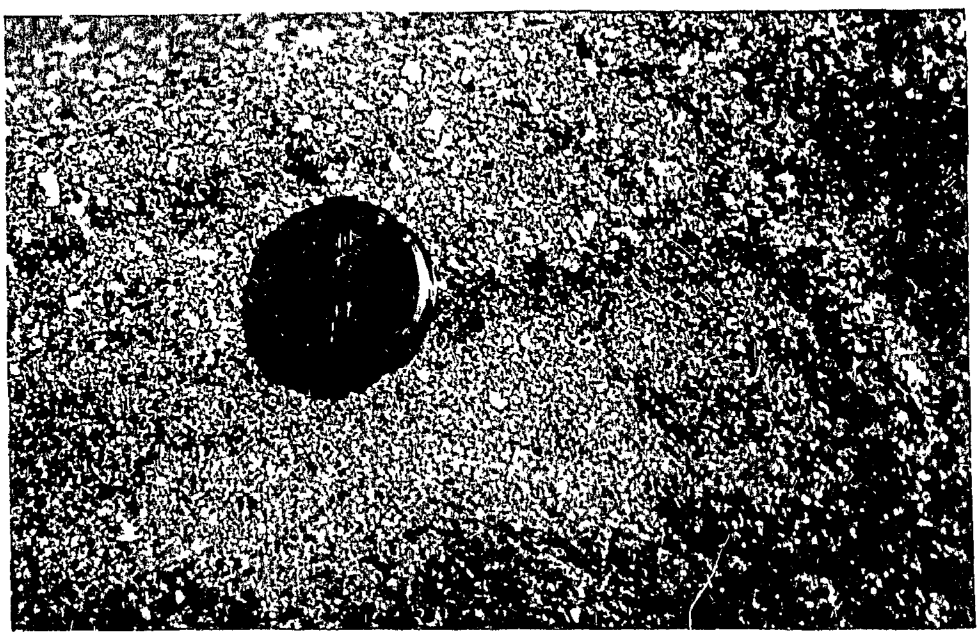

Figure 2.9. Late-magmatic lamprophyric pegmatite veins and stringers disrupting the lamprophyre-tonalite contact at Forbes Point. View to the northwest, lens cap 7 cm diameter.

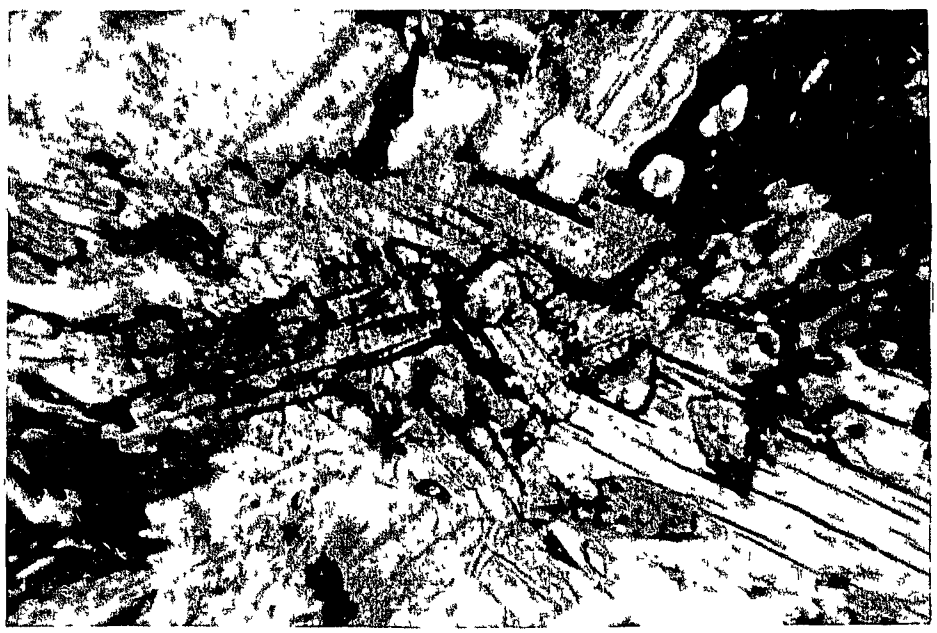

Figure 2.10. Photomicrograph of the coarse-grained and inequigranular intergrowth of amphibole and biotite in the Forbes Point lamprophyre. Biotite occurs as both light brown and orange brown crystals, and amphibole shows internal aggregation that results from partial deuteric alteration to prehnite and clays. Quartz and feldspar occur interstitially. Field of view 6 mm, XPL.

2-2.4. Lamprophyre at Mcleods Cove, Port Mouton

Field relations

A second synplutonic occurrence of olive-green lamprophyre crops out within the Port Mouton Pluton at Mcleods Cove (Figure 2.1). The Mcleods Cove body represents a medium-grained, subhorizontal sheet approximately 80 m long and at least 2 m thick (with an erosional upper surface). It dips to the southwest at approximately 45° (Figure 2.11). Metric "pillows" with lamprophyric compositions mark the lower contact of the sheet with the Port Mouton pluton. This body appears mineralogically identical to the occurrence at Forbes Point but it has finer grain size (Douma, 1988) and shows an equigranular texture. A steeply dipping foliation transects the contact with the granitoid host at a high angle, and it parallels the magmatic foliation in the host granitoid (Douma, 1988). Feldspathic patches and stringers with gradational contacts probably represent late-magmatic lamprophyre fractionates.

Petrography

Mcleods Cove lamprophyre contains an identical modal assemblage to the Forbes Point dyke. Panidiomorphic-hypidiomorphic (equant) green amphibole (29-40%; actinolitic hornblende-actinolite) is locally intergrown with both strongly aligned light brown biotite and dark brown biotite (41-52%; [Mg/(Mg+Fe)] = 0.6-0.7) to form a seriate and inequigranular framework with 1.2-3.0 mm grain size (Figure 2.12). Oligoclase-andesine (9-14%; An_{36}-An_{20}) up to 2.5 mm in diameter shows patchy zoning, and it occurs only interstitially between the mafic mineral phases with hypidiomorphic-allotriomorphic K-feldspar (3%) and quartz (3-7%). Accessory minerals include unusually high concentrations of equant sphene (up to 2%), with abundant apatite, ilmenite, rutile, zircon, and chalcopyrite inclusions in all mineral phases. Ilmenite at least partly results from biotite alteration, which probably occurred with deuteric albitization of the feldspars.

Figure 2.11. The Mcleods Cove synplutonic lamprophyre sheet in the Port Mouton Pluton. Note the erosional upper surface of the lamprophyre and the characteristic olive-green colouration. The basal surface (at the base of the notebook) consists of ovoid, metric "pillows" of lamprophyre in the tonalite. View to the north, notebook 20 cm long.

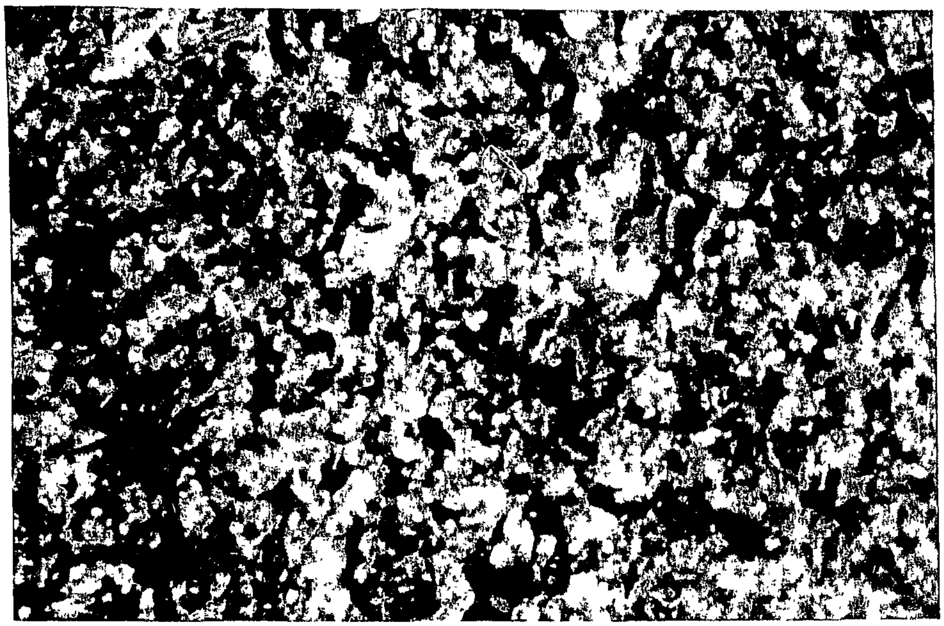

Figure 2.12. Photomicrograph of the equigranular texture of lamprophyre at Mcleods Cove. This lithology has a similar modal mineral assemblage to the Forbes Point body (Figure 2.10), but it has a finer grain size and contains more abundant feldspars and quartz. Field of view 7 mm, XPL.

Preliminary interpretations

The pillowed and crenulate contact with the host tonalite (considered in Section 3.2 of Chapter 3) and the magmatic foliation imparted by its host tonalite, constrain this body as a synplutonic intrusion. Compared to the Forbes Point dyke, lamprophyre at Mcleods Cove contains biotite as the most abundant modal constituent, and it, therefore, shows transitional kersantite-spessartite characteristics (Rock, 1987). Manifestations of alteration similar to those in the Forbes Point dyke (chlorite, sericite and muscovite after amphibole, biotite, and plagioclase) probably also occurred under deuteric conditions.

2-2.5. Picrite at Mersey Point, Liverpool

Field relations

A black (ginger-brown weathering) plug of massive, coarse-grained picrite approximately 300 m wide intrudes the Goldenville Formation along the coast south of Liverpool (Figure 2.1). Beach boulders obscure all intrusive contacts with the Meguma Group, but a ground magnetic survey indicates that it has steeply dipping contact surfaces that truncate regional fold trends in the Goldenville Formation. Aeromagnetic data (Geological Survey of Canada, 1986) suggest that the picrite has a plug-like nature. Known outcrops occur only at the centre of the body and they expose a horizontal section through the intrusion with little vertical relief. The picrite has poorly developed columnar cooling joints, and it consists of randomly-oriented olivine and pyroxene, with minor amphibole, plagioclase up to 5 mm, and euhedral macrocrysts of biotite up to 1 cm in diameter. Little grain size variation occurs horizontally over the outcrop, but vertical joint surfaces commonly display 1-3 cm thick rhythmic layers enriched in plagioclase (Figure 2.13). At least four subangular granitic and garnet-bearing metapelitic enclaves, between 3 and 8 cm in diameter, occur in the picrite and they have thin epidote haloes at their contacts that probably result from a magmatic reaction. A lithologically similar glacial erratic exposed on the

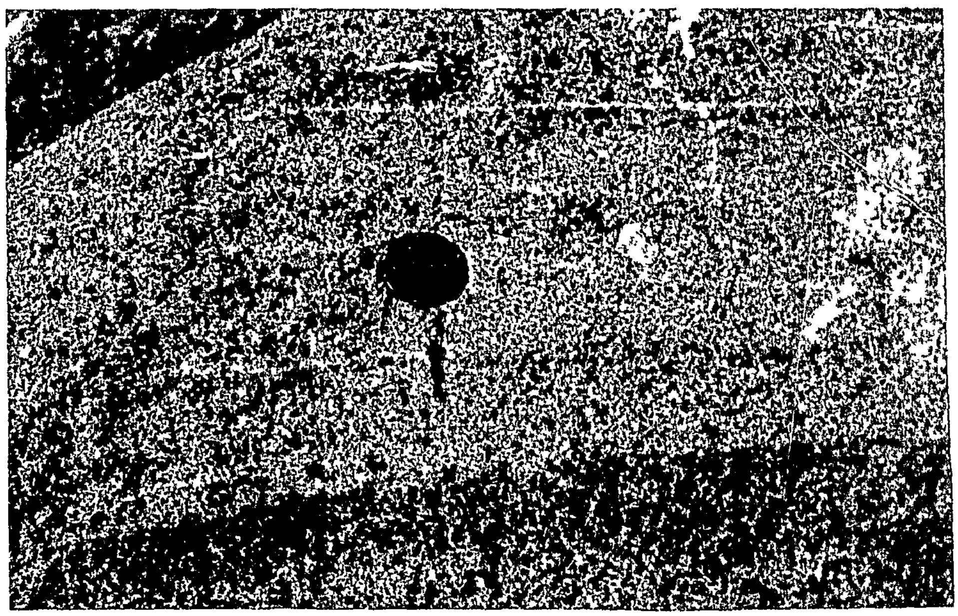

Figure 2.13. A typical vertical cross-section through the Mersey Point picrite showing subhorizontal, centimetric phase layering. Most layers have leucocratic colourations because they contain abundant cumulus plagioclase. Note the ginger-brown weathering characteristic that is typical of the LDMIs. View to the southeast, lens cap 7 cm diameter.

beach north of Moose Harbour (see Figure B1.5 in Appendix B) exhibits 10-20 cm thick pyroxene and plagioclase-rich and olivine-rich cumulate horizons with undulose and diffuse boundaries and distinct grain sizes (Figure 2.14).

Petrography

The Mersey Point picrite consists of an inequigranular intergrowth of randomly-oriented olivine, clino- and orthopyroxene, amphibole, plagioclase, biotite, and opaques that range in size from 0.1-10 mm (Figure 2.15). Hypidiomorphic magnesian olivine (Fo_{80}) ranges in size from 0.3-3.0 mm (25-34%) and it may show glomeroporphyritic tendencies. Hypidiomorphic-allotriomorphic augite (5-10%; $Wo_{44}En_{53}Fs_{3}$) and colourless hypidiomorphic hypersthene (3-4%; $En_{69}Fs_{31}$) occur either as small nuclei within olivine, or as ophitic crystals (0.4-3 mm in diameter) rimmed by light brown poikilitic amphibole subhedra (21-35%; magnesio-hastingsite to actinolite) and brown phlogopite (~8%; [Mg/(Fe+Mg)] = 0.8-0.9) oikocrysts up to 1 cm in diameter. Plagioclase (17-28%) occurs both as tabular phenocrysts (An_{81}) and as hypidomorphic interstitial pore fillings (An_{55}) between olivine and clinopyroxene. Pyrite, chalcopyrite, chrome-spinel, and accessory apatite (0.6-1.2%) occur both as inclusions within all anhydrous mineral phases, and as isolated groundmass constituents. Deuteric or secondary alteration manifests as minor serpentinization of olivine or sericitization of plagioclase, and as chlorite, epidote, or biotite rims developed on all ferromagnesian mineral phases (<0.1%).

Preliminary interpretations

Quaternary glaciation probably derived the isolated beach boulder at Moose Harbour from the Mersey Point picrite at some height above the current level of exposure. Although *in situ* material does not display such obvious cumulate characteristics, the lack of textural or modal variation along strike, and the weak centimetric phase layering, suggests that some modal

Figure 2.14. The glacial erratic boulder of Mersey Point picrite exposed on the beach at Moose Harbour (Figure B1.5 in Appendix B). Note the irregular but sharp contact between the lower dunitic and upper peridotitic layer. View to the north, lens cap 7 cm diameter.

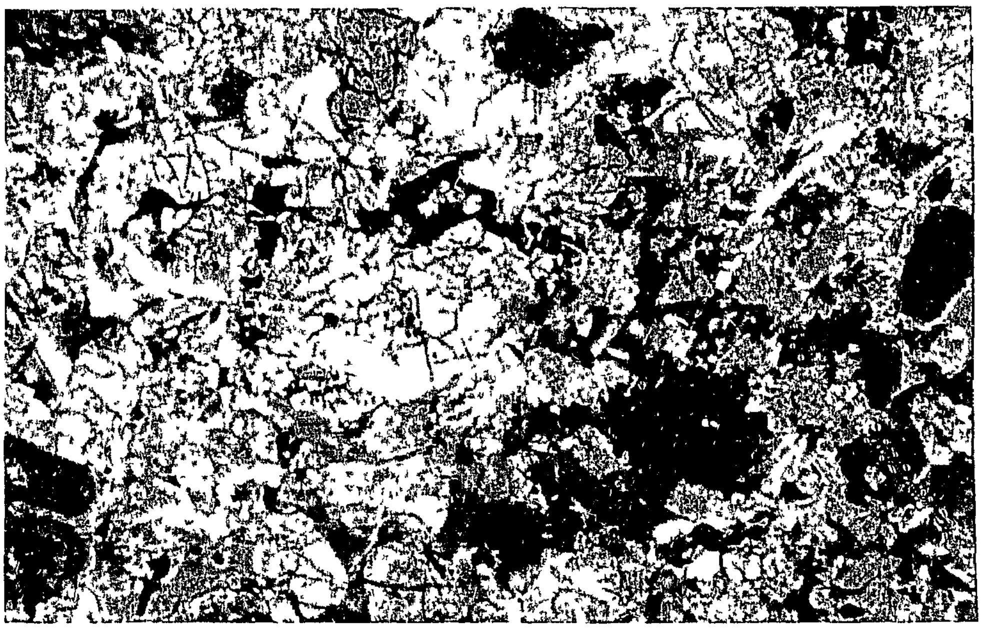

Figure 2.15. Photomicrograph showing the coarse-grained mesocumulate texture of the Mersey Point picrite. Cumulus olivine, orthopyroxene, and clinopyroxene sit in a groundmass of panidiomorphic clinopyroxene, plagioclase, and deuteric amphibole and phlogopite (extinct interstitial grains). Field of view 9 mm, XPL.

accumulation occurred. The weak mesocumulate texture in thin section indicates that early crystallized olivine, hypersthene, and minor plagioclase accumulated, although olivine alone never crystallized as an intercumulus phase. Oikocrystic and interstitial amphiboles and phlogopites probably formed late from trapped intercumulus magma, rather than during alteration as Elias (1986) suggested. Thermometry based on tetrahedral Al in amphibole suggests that they formed under late-magmatic conditions above 900°C (Page and Zientek, 1987), probably with phlogopite and deuteric chlorite and epidote. Both field and mineralogical information suggest that the Mersey Point picrite preserves a former magma chamber, and the presence of granitoid and high-grade metasedimentary xenoliths indicates that the mafic parent magma encountered and interacted with solid country rocks *en route* to the current emplacement level.

2-2.6. Altered Diorite Dykes at the Ovens Natural Park

Field relations

Four grey, fine-grained porphyritic dykes occur along the shore in the Ovens Natural Park, where they intrude the steeply plunging hinge of the Ovens anticline (Hall, 1979; Figure 2.1). All dykes range in width from 0.75 to 3.2 m and they strike northeast with vertical attitudes (Figure 2.16). Most bodies weather preferentially and consist of medium to coarse-grained, tabular plagioclase phenocrysts set in a fine-grained (1 mm) groundmass. The smallest dykes show weak alignments of elongate feldspar phenocrysts parallel to the dyke margins, they have weakly developed centimetric chilled margins, and they commonly finger out along strike. All dykes preserve well-developed cooling joints oriented perpendicular to the dyke margins, and a small fault offsets the largest dyke. Despite their superficial sill-like appearances, the dyke contacts locally cut across bedding in the Halifax Formation, and a traverse across the small peninsula in the park suggests that they discordantly intersect regional bedding at an acute angle (Hall, 1979).

Figure 2.16. A steeply dipping, leucocratic diorite dyke exposed at the Ovens. Below the figure, the body shows local discordance to regional fold trends in the Halifax Formation. The rusty colouration results from pyrite weathering. View to the southwest, figure 1.8 m tall.

Petrography

All Ovens dykes have similar textures and feldspar-phyric mineral assemblages that consist of 0.1-0.8 mm diameter panidiomorphic phenocrysts of randomly oriented-weakly aligned albite (8%; $An_{<10}$), K-feldspar (9%), and subsidiary sphene patches (6%) embedded in an altered felsitic groundmass consisting largely of randomly oriented plagioclase, euhedral pyrite, secondary chlorite, and quartz (Figure 2.17). The propylitic groundmass accounts for at least 60% of the total dyke volume, and no indications of internal deformation occur. Plagioclase and (rare) K-feldspar phenocrysts show random distribution and some examples show glomeroporphyritic tendencies and swallowtail terminations that indicate rapid crystallization. Calcite and sphene crystals (circa 0.5 mm) completely pseudomorph the former mafic phenocrysts, but they retain the original euhedral morphologies of amphibole and clinopyroxene (Figure 2.17). Calcite currently accounts for at least 14% of the rock by volume, and its presence precludes determination of the original mafic modes for these rocks.

Preliminary interpretations

Despite advanced propylitic alteration, the Ovens dykes preserve their original mafic igneous microtextures, although carbonates replaced the mafic phenocrysts and albite forms pseudomorphs of the original feldspars. Modal classification of these rocks is not feasible, but the original abundance of amphibole and clinopyroxene was probably greater than 25%; the dykes had more mafic compositions before alteration. Despite their porphyritic nature, no modal constituents occur both as groundmass and phenocryst phases, and these rocks have few lamprophyric characteristics (Streckeisen, 1979; Rock, 1987). Their discordant nature and lack of tectonic strain suggests that the dykes intruded after folding in the Halifax Formation, although regional fold trends apparently influenced the dyke intrusion trajectories. Carbonation and chloritization occurred after intrusion, probably in response to interaction of the hot dykes with circulating groundwaters. The abundance of syntectonic and post-tectonic auriferous quartz

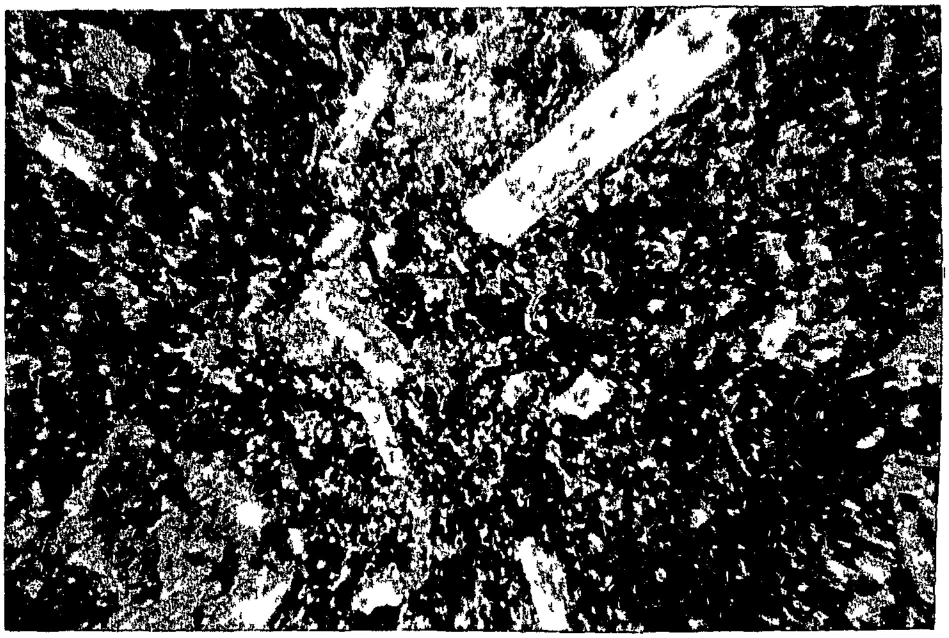

Figure 2.17. Photomicrograph showing the mafic microtextures preserved in the Ovens dykes. Note the tabular relict plagioclases replaced by albite, and the calcareous and felsitic groundmass containing chlorite, muscovite, and lozenge-shaped sphene (mostly extinct) alterations products. Field of view 4 mm, XPL.

veins throughout the Ovens anticline (N. Culshaw, pers. comm., 1993) suggests that mineralizing fluids caused this alteration. If the Ovens dykes intruded late in the deformation, fluid-rock interaction possibly occurred soon after emplacement.

2-2.7. Weekend Dyke Lamprophyres Along the Eastern Shore

Field relations

The Weekend dykes constitute a small "swarm" of 10 north-northwesterly oriented, subvertical lamprophyres exposed along the Eastern Shore (Figure 2.18). All dykes have similar appearances and they show intrusive features typical of lamprophyres (Rock, 1990; Tate and Clarke, 1993; Table 2.2). Their consistent orientations and macroscopic features suggest that they represent a related lithologic subset of the LDMI suite and individual dykes fall into two size categories. The narrowest dykes at Borgles Island, Little Harbour coast, and Devils Island have ginger-brown weathering characteristics, they range in width from 0.01-1 m, and they display sharp and discordant contacts approximately perpendicular to regional east-northeast trending folds in the Goldenville Formation (Figure 2.19a). Narrow dykes also have fine-grained porphyritic textures that result from chilling, and they finger out or show intrusive kinks and offsets along strike. At Borgles Island, three narrow dykes occupy late-Acadian, northwesterly-oriented shear fractures (O'Brien, 1983) that presumably represent the magma conduits (Figure 2.19b, c). The Devils Island dyke shows strong propylitic alteration similar to the Ovens dykes.

Wide dykes at Sober Island, Popes Harbour, Pleasant Harbour, Little Harbour road, and East Jeddore range in width from 12-15 m (Figure 2.19d), they have melanocratic appearances and either resist weathering (at Sober Island and Pleasant Harbour), or weather preferentially (at Popes Harbour). All examples show medium-coarse grained, porphyritic textures and have fine-grained chilled margins that form approximately 10% of the total dyke width. Contacts with the Meguma Group appear straight over tens of metres, and contact metamorphism within the

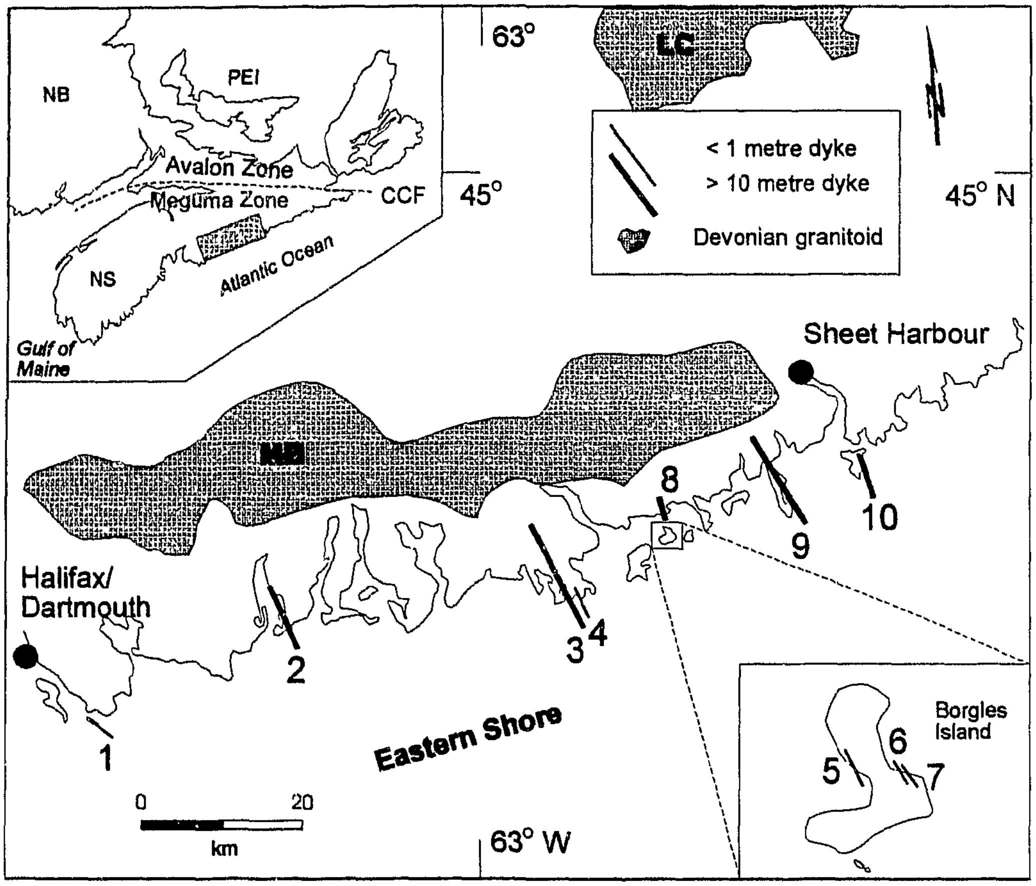

Figure 2.18. Geological map of the Eastern Shore indicating the locations of the currently recognized Weekend dykes. 1 = Devils Island, 2 = East Jeddore, 3 = Little Harbour road, 4 = Little Harbour coast, 5, 6, 7 = Borgles Island dykes, 8 = Pleasant Harbour, 9 = Popes Harbour, 10 = Sober Island. NB = New Brunswick, NS = Nova Scotia, PEI = Prince Edward Island, CCF = Cobequid-Chedabucto Fault, MB = Musquodoboit Batholith, LC = Liscomb Complex.

Table 2.2. Macroscopic characteristics and modal mineralogy of the currently recognized Weekend dykes.

Fig. 2.18 No.	Location	Alternative name	Width (m)	Strike (°)	Dip	Xenoliths	Intrusive offsets	Globular structures	Multiple intrusion	Mode
1	Devils Island	-	≤1	130	90	No	No	No	No	-
2	East Jeddore	-	12.2-13.7	160	90	Rare	No	No	No	$Pl_{46.2}$ $Cpx_{1.3}$ $Kfs_{1.6}$ $Hbl_{45.0}$ $Qtz_{2.1}$ $Cal_{0.8}$ $Ep_{0.6}$ $Opq_{0.1}$ $Chl_{2.8}$
3	Little Harbour road	-	11.9-14.6	155	85NE	No	No	No	No	$Pl_{49.2}$ $Cpx_{4.8}$ $Kfs_{3.5}$ $Hbl_{32.5}$ $Qtz_{3.2}$ $Cal_{0.3}$ $Ep_{3.2}$ $Opq_{3.2}$ $Chl_{0.2}$
4	Little Harbour coast	-	≤1	153	90	No	Yes	No	No	$Cpx_{12.6}$ $Opq_{6.0}$ $Chl_{0.4}$
5, 6, 7	Borgles Island	Charles Island[a]	≤1	161	90	No	Yes	No	No	$Cpx_{17.1}$ $Opq_{>2.5}$ $Chl_{0.6}$
8	Pleasant Harbour	Tuff Island	12.0-13.1	163	80NE	Yes	No	Yes	No	$Pl_{28.0}$ $Cpx_{2.0}$ $Kfs_{2.4}$ $Hbl_{48.6}$ $Qtz_{7.0}$ $Cal_{4.0}$ $Ep_{3.5}$ $Opq_{3.5}$ $Chl_{1.0}$
9	Popes Harbour	Tangier[b]	12.0-15.1	150	86NE	Yes	No	Yes	Yes	$Pl_{38.8}$ $Cpx_{2.3}$ $Kfs_{7.5}$ $Hbl_{31.6}$ $Bt_{11.6}$ $Qtz_{4.8}$ $Cal_{0.5}$ $Ep_{0.3}$ $Opq_{0.5}$ $Chl_{2.2}$
10	Sober Island	-	13.0-14.7	162	89NE	No	No	Yes	Yes	$Pl_{44.0}$ $Cpx_{2.5}$ $Kfs_{9.7}$ $Hbl_{36.3}$ $Qtz_{4.0}$ $Cal_{0.0}$ $Ep_{1.2}$ $Opq_{0.7}$ $Chl_{1.6}$

Modified and updated after Ruffman and Greenough (1990). [a] = Ruffman and Greenough (1990); [b] = Giles and Chatterjee (1987). See Table 2.1 for the point counting strategy and mineral abbreviations. Note that the highly altered Devils Island dyke preserves little primary mineralogy, and groundmass phases within the Little Harbour coast and Borgles Island dykes are too fine grained to determine manually.

Figure 2.19. The intrusive characteristics of the Weekend dyke spessartites. (a) A narrow Weekend dyke exposed on Borgles Island. Note the abrupt intrusive offset and its typical ginger-brown weathering characteristics. View to the southeast, lens cap 7 cm diameter; (b) The fracture occupied by the above Weekend dyke. Narrow dykes commonly finger and pinch out along strike at the current exposure level. View to the southeast, bag approximately 60 cm long; (c) Plan view of the fracture depicted above. The small offset suggests that fracture morphology controlled dyke intrusion and caused intrusive offsets in the small dykes. The perpendicular dextral sigmoids identify the fractures as transtensional brittle-ductile shears recognized by (O'Brien, 1983); (d) The 12 m wide Pleasant Harbour dyke exposed at the southeastern end of Tuff Island (Figure B1.9 in Appendix B-1). This body is typical of wide Weekend dykes. View to the southeast; (e) Autobrecciation of consolidated lamprophyre by late-magmatic fluids at the centre of the Pleasant Harbour dyke. View to the southeast, red package 10 cm long; (f) Panoramic view of the widest Weekend dyke at Popes Harbour. Note the prominent outer chilled margins (behind the figure) and the preferentially weathered central zone that contains high concentrations of exotic lower crustal xenoliths. View to the southeast, boat approximately 4.2 m long; (g) Small, subrounded metawacke and metaarenite xenoliths in the Pleasant Harbour dyke. Note the bleached reaction zones(?) rimming dark xenoliths. Plan view, red package 10 cm long; (h) High concentrations of large crustal xenoliths within the central zone of the Popes Harbour dyke. View to the southeast, hammer shaft 1 m long.

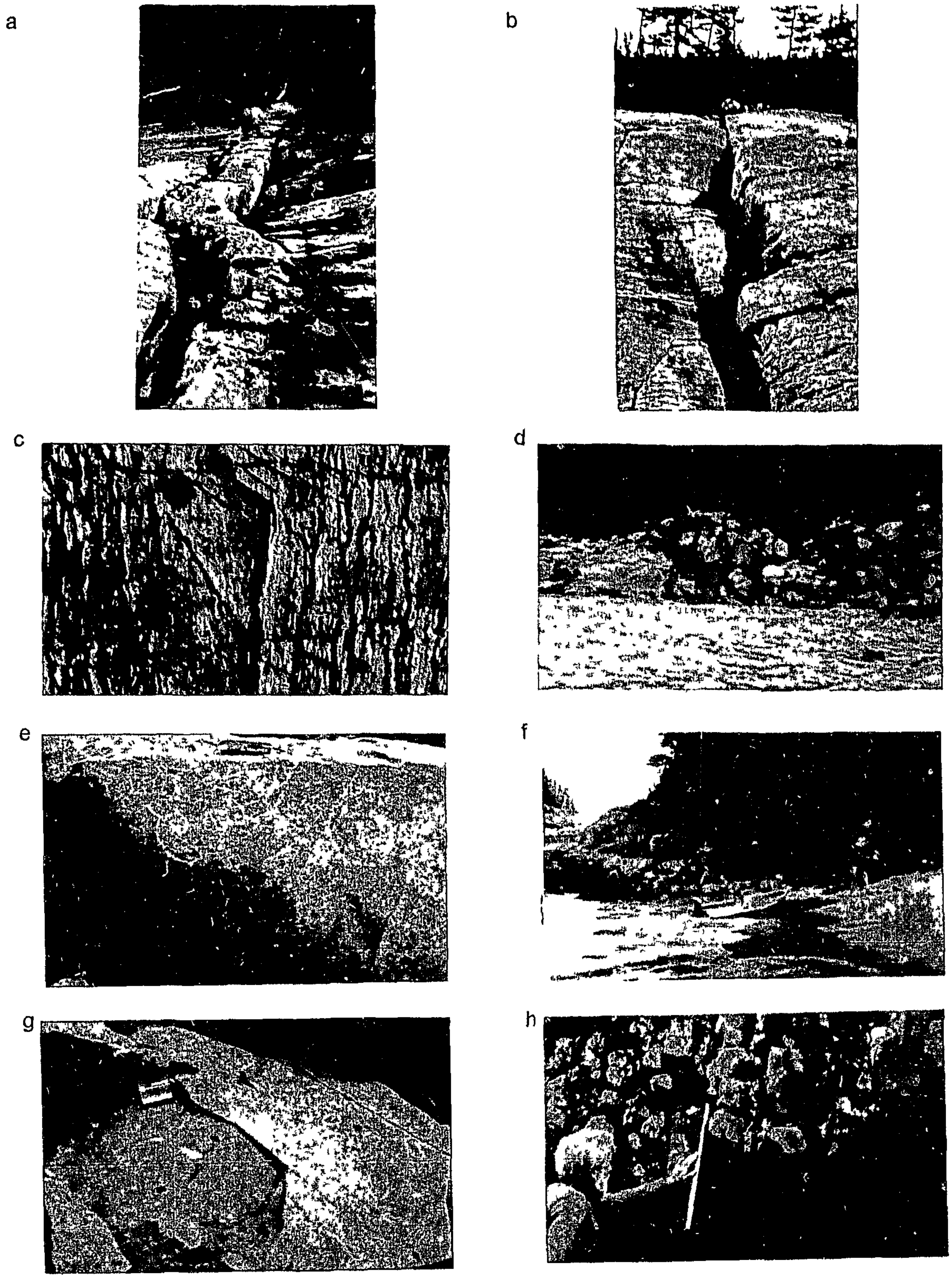

Figure 2.19. The intrusive characteristics of the Weekend dyke spessartites.

country rocks occurs as insignificant bleaching and annealing of tectonic cleavages immediately adjacent to the dyke margins. The Sober Island and Pleasant Harbour dykes occur proximally to *en echelon* 20-70 cm companion dykelets that presumably represent small, upwardly penetrating fingers of dyke material that connect to the main dyke at depth. The Pleasant Harbour and Popes Harbour dykes contain irregular pods and stringers of fractionated, feldspathic lamprophyre, and late-stage mobilization of this material caused autobrecciation at the centre of the Pleasant Harbour dyke (Figure 2.19e). The anomalous Popes Harbour dyke represents a composite body, comprising two outer chill zones approximately 1-2 m wide and separated from a 10-12 m inner zone of xenolithic lamprophyre by a prominent contact (Figure 2.19f). Up to 30% exotic metabasite and metapelitic xenoliths and xenocrysts of lower crustal derivation (Giles and Chatterjee, 1987; Owen et al., 1988) occur in the dykes at Popes Harbour and Pleasant Harbour (Figure 2.19g, h), and the chilled margins contain ovoid, 1 cm diameter quartz-orthoclase-calcite -epidote-pyrite felsic globular structures.

Petrography

Fine-grained, narrow dykes from the coast at Little Harbour and Borgles Island contain elongate, panidiomorphic-hypidiomorphic glomerocrysts of augite or diopside (approximately 20%; $Wo_{22-41}En_{42-75}Fs_{3-29}$), up to 1 mm in length, embedded within an intergranular matrix of plagioclase that poikilitically encloses abundant microscopic magnetite, chrome-spinel, and brown amphibole nuclei (Table 2.2; Figure 2.20a). Calcite and chlorite pseudomorph clinopyroxene phenocrysts within the Devils Island dyke, although the groundmass feldspar and typical lamprophyre textures remain intact and they provide the basis for its inclusion with the Weekend dykes (Perring et al. 1989). In contrast, medium-coarse grained Weekend dykes show crudely aligned, panidiomorphic-hypidiomorphic phenocrysts of normally zoned, elongate brown amphibole (29-51%; magnesio-hornblende, tschermakite, magnesio-hastingsite, and ferroan pargasite) and diopside (0.5-13%; Table 2.2; Figure 2.20b). Rare, ovoid chlorite mats enclosing

a

b

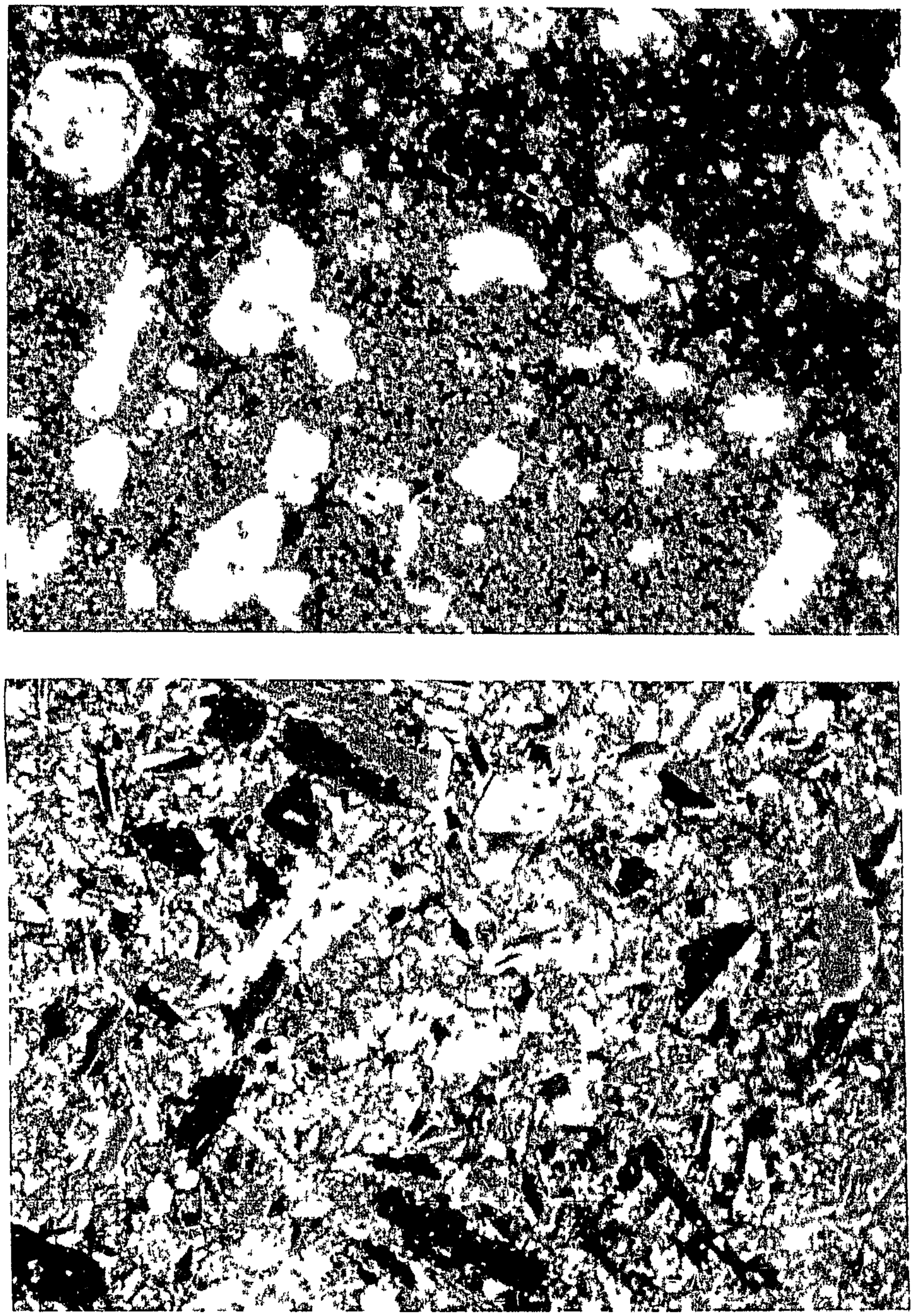

Figure 2.20. Photomicrographs showing the textures of narrow and wide Weekend dykes. (a) Panidiomorphic-hypidiomorphic augite phenocrysts in a chilled matrix consisting of plagioclase, minor amphibole, and magnetite nuclei within the narrow Little Harbour road dyke. Field of view 5.5 mm, PPL; (b) Elongate and seriate amphibole phenocrysts in the typical panidiomorphic coarse-grained texture of the Sober Island dyke. The matrix consists of randomly oriented amphibole (with abundant simple twinning) and minor diopside, plagioclase, quartz, K-feldspar and epidote. Chlorite replaces some acicular amphiboles. Field of view 4 mm, XPL.

chrome-spinel within the Popes Harbour, Sober Island, and Little Harbour road dykes may indicate the previous presence of olivine. Normally zoned plagioclase laths (36-53%; An_{78}-An_{6}) range in size from 0.2 to 1 mm, and they occur only in the groundmass where they nucleated with equant amphibole, clinopyroxene, quartz (0.7-9%) and K-feldspar (2-15%). Biotite (17%; [Mg/(Mg+Fe)] = 0.6) occurs in the central zone of the Popes Harbour dyke, where it represents a phenocryst phase that apparently precipitated partly at the expense of amphibole (9%). Deuteric patches of anhedral calcite, epidote, and chlorite (~5%), coalesce to form pseudomorphs after plagioclase and amphibole phenocrysts at the centres of large Weekend dykes (Kempster, 1988), and the accessory minerals include rutile, perovskite, and sphene.

Preliminary interpretations

Panidiomorphic-hypidiomorphic textures and high modal abundances of deuteric calcite, epidote, and chlorite are diagnostic of lamprophyres (Rock, 1990). The occurrence of augite, diopside, and hornblende as the mafic phenocryst phases, and plagioclase as the dominant groundmass feldspar, confirm the spessartite lamprophyre classification for the Weekend dykes (Streckeisen, 1979). Also, the presence of biotite in the Popes Harbour dyke imparts kersantitic characteristics similar to those of the Forbes Point and Mcleods Cove lamprophyres. Tate and Clarke (1993) recognized the absence of contact metamorphism, the development of felsic globular structures, and the elongate amphibole habits with weak zoning, all of which suggest rapid emplacement and cooling. This rapid undercooling in the narrow dykes probably preserves the early anhydrous crystallizing assemblage. The importance of amphibole over clinopyroxene in all the larger (presumably slower cooled) dykes, suggests that increased volatile exsolution occurred in the lamprophyric magma, probably resulting from decompression during dyke emplacement (Cooper 1979). Silica (atomic) concentrations between 6.9 and 7.2 in amphibole suggest that they crystallized from intratelluric mafic magmas (Pe-Piper 1988) and wide compositional zoning in plagioclases also suggests a predominant mafic magma containing volatiles rather than the purely volatile medium that Rock (1990) considered plausible for lamprophyres. The smallest Weekend dykes intrude Acadian crustal extensional weaknesses ("shear joints"), and the larger dykes and other LDMIs may also mimic this intrusive behaviour.

2-2.8. Gabbro-Diorite at Ten Mile Lake and Bog Island Lake, Liscomb Complex

Field relations

Two black-brown gabbro-diorite plutons crop out in spatial association with high-grade gneisses and peraluminous granitoid plutons in the Liscomb Complex (Figure 2.1). The circa 9 km^2 Ten Mile Lake intrusion discordantly cuts an east-west trending magnetic signature in the Halifax Formation, whereas the smaller (circa 4 km^2) Bog Island Lake body intrudes the Liscomb gneisses (Clarke et al., 1993a). Regional gravity studies identify no positive anomalies associated with either intrusion and suggest that either they form thin sheets or that an extensive volume of granite underlies them (Ryall, 1990). The contacts between the gabbro-diorites and their country rocks do not crop out, but the Ten Mile lake body caused localized anatexis in the adjacent Halifax pelites and a granitoid dyke intrudes it (Clarke et al., 1993a). Both intrusions have coarse grain sizes and inequigranular textures; they also contain miarolitic cavities and patches of late-magmatic felsic fractionates. The Ten Mile Lake intrusion contains abundant enclaves of Liscomb gneiss, gabbro, and exotic lower crustal material (Chatterjee et al., 1989), whereas the Bog Island Lake intrusion contains predominantly feldspar-phyric cumulate enclaves (Clarke et al., 1993a).

Petrography

The Ten Mile Lake body contains porphyritic clusters of amphibole and clinopyroxene set in a plagioclase-rich inequigranular matrix containing biotite, minor chlorite, and accessory spinel, apatite, sphene, and pyrite (Clarke et al., 1993a). Although the Bog Island Lake intrusion contains similar mineral phases, it shows a plagioclase-dominant mode with a cumulate texture, and contains primary magmatic(?) garnet. All minerals show strong normal zoning and both intrusions contain amphiboles with complex microtextural relationships. Amphiboles show extreme compositional variation between primary magmatic kaersutite, cummingtonite, pargasite, and subsolidus magnesio-hornblende and actinolite overgrowths (Chatterjee et al., 1989).

Preliminary interpretations

The Ten Mile Lake and Bog Island Lake gabbro-diorites have the coarse-grained, equigranular textures and the variable accessory mineral assemblages that typify the LDMIs. Amphibole compositional variation in both bodies may be analogous to the complex microtextural assemblages preserved in the Attwoods Brook gabbronorite; perhaps the presence of garnet at Bog Island lake also supports its former presence in the Birchtown diorite. Their hydrous mineral assemblages and miarolitic cavities imply a strongly hydrous parent magma (Clarke et al., 1993a), and amphibole formation at approximately 8 Kbar (circa 25 km depth) (Chatterjee et al., 1989) suggests that volatile saturation occurred early, during the ascent of the parent magmas through the crust.

2-2.9. The Characteristics of Late Devonian Mafic Intrusions

LDMIs in the MZ all crop out as volumetrically minor dykes, plugs, or synplutonic bodies with gabbroic, dioritic, or lamprophyric natures. Compared to the Ordovician and Silurian mafic intrusions, the LDMIs have discordant intrusive relationships with the Meguma Group or their spatial associations with the Late Devonian granitoids confirm the contemporaneity of mafic-felsic magmatism. Currently known bodies generally have ginger-brown weathering characteristics and coarse grain sizes, although they may show dramatic local variations in grain size. They also show no obvious signs of deformation except for slight straining of quartz. Compared to the Jurassic mafic intrusions, LDMIs have abundant magmatic and deuteric amphibole and/or biotite, with or without clinopyroxene and orthopyroxene. The textural and mineralogical similarities of these rocks all indicate their derivation from hydrous magmas and they strongly suggest a genetic relationship between them. The small sizes and preponderance of currently recognized LDMIs to the well exposed coastal regions undoubtedly reflects the poor exposure in the interior of southwestern Nova Scotia (<2%), and it suggests that unexposed mafic bodies may occur inland.

2-3. Geochronology

2-3.1. Previous Geochronology

Previous geochronological studies in the MZ largely concentrated on the South Mountain Batholith and the Meguma Group metagreywackes, but regional dating surveys also generated ages for the LDMIs between 1966 and 1987. Published LDMI geochronology currently relies on Rb-Sr, K-Ar, and $^{40}Ar/^{39}Ar$ isotope systematics (Table 2.3). Ages determined for this study rely on the ^{40}Ar-^{39}Ar (hornblende and phlogopite) and U-Pb (zircon) geochronometers and they take advantage of the increased analytical accuracy achieved in geochronology over the last seven years.

2-3.2. $^{40}Ar/^{39}Ar$ Geochronology

Introduction

Four LDMIs at Attwoods Brook, Birchtown, Mersey Point, and Little Harbour were selected for $^{40}Ar/^{39}Ar$ dating. All analyses rely upon argon systematics within calcic amphiboles (K_2O between 0.01 and 1.14 wt.%), except for a phlogopite analysis from the Mersey Point picrite. Appendix A-3 describes the sample preparation, the mineral separates, and the analytical procedures of the Dalhousie argon laboratory in detail, whereas Figure 2.21 summarizes the argon results as conventional apparent age spectra with the ages determined from weighted

Table 2.3. Compilation of previously determined ages for the Late Devonian mafic intrusions.

Figure 2.1 number	Location	Body	Age (Ma)	Mineral	Isotopic system	Reference
1	Attwoods Brook	-	362±18	Bt	Rb/Sr	1
			344	Bt	$^{40}Ar/^{39}Ar$	2
			372.3±2.7	Hbl	$^{40}Ar/^{39}Ar$	2
			252	Pl	$^{40}Ar/^{39}Ar$	2
2	Birchtown	-	350	Bt	$^{40}Ar/^{39}Ar$	3
			353	Bt	K/Ar	3
			370	Bt	$^{40}Ar/^{39}Ar$	2
			371	Bt	$^{40}Ar/^{39}Ar$	2
3	Forbes Point	-	324	Hbl	$^{40}Ar/^{39}Ar$	4
4	Mcleods Cove	-	324	Hbl	$^{40}Ar/^{39}Ar$	4
5	Mersey Point	-	366±16	-	K-Ar	5
			362±22	Phl	Rb/Sr	1
			367.6±0.8	Phl	$^{40}Ar/^{39}Ar$	6
6	Ovens	-	-	-	-	-
7	Weekend dykes	East Jeddore	370±2	Hbl	$^{40}Ar/^{39}Ar$	7, 8
		Sober Island	368±2	Hbl	$^{40}Ar/^{39}Ar$	7, 8
8	Liscomb complex	Bog Island Lake	377.3±1.3	Bt	$^{40}Ar/^{39}Ar$	9, 10, 11
		Bog Island Lake	377	Bt	$^{40}Ar/^{39}Ar$	10, 11
		Ten Mile Lake	372.8	Bt	$^{40}Ar/^{39}Ar$	9, 10, 11
		Ten Mile Lake	368	Hbl	$^{40}Ar/^{39}Ar$	10, 11
		Ten Mile Lake	370.3	Hbl	$^{40}Ar/^{39}Ar$	10, 11

Mineral abbreviations after Kretz (1983). Note that the Ovens dykes contain no primary igneous geochronometers. 1 = de Albuquerque (1979), 2 = Reynolds et al. (1987), 3 = Reynolds et al. (1983), 4 = Douma (1988), 5 = Wanless et al. (1986), 6 = Elias (1986), 7 = Kempster (1988), 8 = Kempster et al. (1989), 9 = Giles and Chatterjee (1987), 10 = Clarke et al. (1993a), 11 = Kontak and Reynolds (1994).

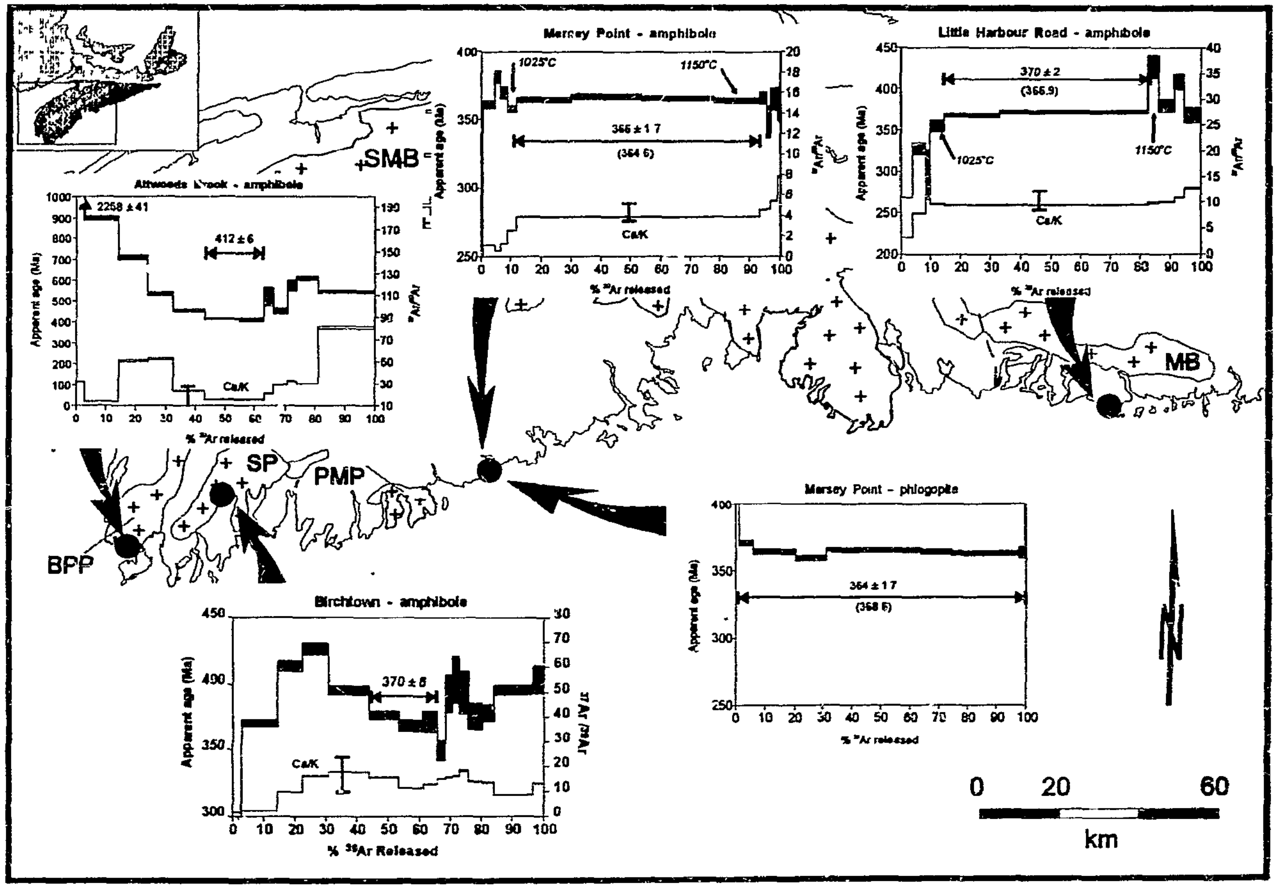

Figure 2.21. The sample locations and ^{40}Ar-^{39}Ar (apparent age vs. cumulative % ^{39}Ar released) spectra for hornblende and phlogopite in Late Devonian mafic intrusions. Uncertainties for individual heating steps are quoted at 1σ. The horizontal arrow shows the plateau used for the age calculation, the age calculated from a weighted average of the plateau steps, and the total gas age (in parentheses, quoted at 0.5%). The hornblende spectra also have the Ca/K release spectra calculated from the observed ^{37}Ar-^{39}Ar ratios with a vertical error bar that indicates the values determined independently by electron microprobe analysis.

averages of contiguous plateau steps.

Attwoods Brook (hornblende)

Stepwise argon release from Attwoods Brook amphibole produced a saddle-shaped spectrum with extreme discordance. The earliest steps define a staircase geometry with ages initially falling from 2258±41 Ma because of excess argon. At 33.4% of the total ^{39}Ar released, the saddle reaches a minimum age of 412±6 Ma over two steps representing 20% of the total gas released. The Ca/K ratio (deduced from observed $^{37}Ar/^{39}Ar$ values during irradiation) broadly mirrors the $^{40}Ar/^{39}Ar$ release spectrum, but it shows variability that implies the presence of high-calcium and low-potassium lamellae within the analyzed grains. Independent petrographic evidence suggests clinopyroxene to be this intergrown phase. Despite the discordance, Ca/K values corresponding to the youngest portion of the saddle correlate with independent amphibole microprobe analyses and its age may correspond to a geologically reasonable maximum age for the Attwoods Brook body.

Birchtown (hornblende)

Bulk amphibole from the Birchtown diorite produced a saddle-shaped spectrum similar to the Attwoods Brook results. Early argon outgassing yields young (<300 Ma) ages, which rise to a maximum of 425 Ma over the first 30% of the total ^{39}Ar released. The ages in subsequent steps fall irregularly to a minimum of 370±6 Ma over two steps containing 14% of the total ^{39}Ar released. The low-potassium content of the amphiboles within this sample (<0.85%) necessitates a large correction for atmospheric argon that reduces the analytical precision. The Ca/K ratio varies gradually throughout the spectrum, and although the values agree with independent microprobe analyses, this variation suggests a complex internal structure within the Birchtown amphiboles that potentially controlled argon release. Low Ca/K ratios over the first two steps (below 1000°C) probably result from contamination by microscopic biotite intergrowths observed in the separate that could not be removed by crushing and hand picking. The high-age artifact at 64% of the ^{39}Ar released possibly results from ^{39}Ar redistribution (recoil) during sample irradiation (McDougall and Harrison, 1988; P. Reynolds pers. comm., 1993).

Mersey Point (hornblende and phlogopite)

Bulk amphibole from the Mersey Point picrite generated a highly concordant plateau spectrum. The initial low-age (217±43 Ma) step corresponds to only 0.5% ^{39}Ar released, but the plateau age consists of four contiguous steps that yield an age of 366±1.7 Ma with 95% confidence. Outgassing below 1025°C at lower Ca/K ratios indicates minor argon contributions from a more potassic phase than amphibole (possibly biotite), but the monotonous Ca/K ratio over the plateau agrees with microprobe analyses of Mersey Point amphiboles. High temperature (>1200°C) discordance over the last four steps occurs at higher Ca/K ratios, but it does not change the age of the sample. A 364.6 Ma total gas age for this sample reflects artificial lowering of the age because of the initial low age step.

Phlogopite produces similar concordant results. The spectrum shows a nearly contiguous plateau over the entire range of temperatures for biotite release (700-1250°C) with only one significant deviation from 95% confidence between 20 and 31% of the total ^{39}Ar released. Despite this inflection (and irrespective of the number of steps included in the age calculation) the plateau age of this sample remains identical to the amphibole age at 364±1.7 Ma, within analytical uncertainty. As with amphibole, the insignificant first step (only 0.5% ^{39}Ar) influences the 368.6 Ma total gas age for this sample. Minor irregularities in the plateau possibly result from minor chloritization observed in thin section, or they may result from isotope fractionation during analysis (Lee, 1993).

Little Harbour (hornblende)

Little Harbour amphibole produced a predominantly concordant release spectrum with marked disturbances before 10%, and after 80%, of the total ^{39}Ar released. The initial discordance corresponds to temperatures below 1025°C, it occurs at lowered Ca/K ratios, and yields a poorly defined age of 298±28 Ma. Considering the narrow width of the Little Harbour dyke, this initial age gradient probably corresponds to slow cooling of the country rocks rather than slow cooling of the intruded dyke. The concordant region of the spectrum consists of only two large steps, but it corresponds to 82% of the total gas released and yields a plateau age of 370±2 Ma. The Ca/K ratio over this region agrees with the observed amphibole compositions within all Weekend dykes. High-temperature and high-age discordance occurs at the same temperatures (>1150°C) as the phenomena observed within the Mersey Point amphibole spectrum and it also corresponds to increasing Ca/K ratios. Perhaps this feature results from structural breakdown of the amphiboles during step heating (Lee et al., 1991; Lee, 1993).

Discussion

Except for the discordant spectra from Attwoods Brook and Birchtown, the results of this study compare favourably with previous $^{40}Ar/^{39}Ar$ age determinations (Table 2.3):

(1) *Birchtown and Attwoods Brook.* The saddle-shaped spectra for both bodies appear similar to the partial Alleghanian thermal resetting artifacts in Meguma Group spectra documented by Muecke et al. (1988). Reynolds et al. (1987) generated two concordant biotite spectra from Birchtown that give 370-371 Ma ages (Table 2.3), and a more concordant amphibole spectrum from the Attwoods Brook gabbronorite (372 Ma) than this study achieved; these new data possibly imply excess argon distributed irregularly throughout the Attwoods Brook and Birchtown bodies, although the synplutonic intrusion of the gabbronorite into the Barrington Passage Pluton (385 Ma; Reynolds et al., 1987) suggests a 385 Ma age. Figure 2.22 shows that the Attwoods Brook sample contains $^{40}Ar/^{36}Ar$ values over twice the atmospheric ratio of 296, and the isochron age of 353±20 Ma is poorly constrained. The Birchtown diorite contains much less excess argon

a

b

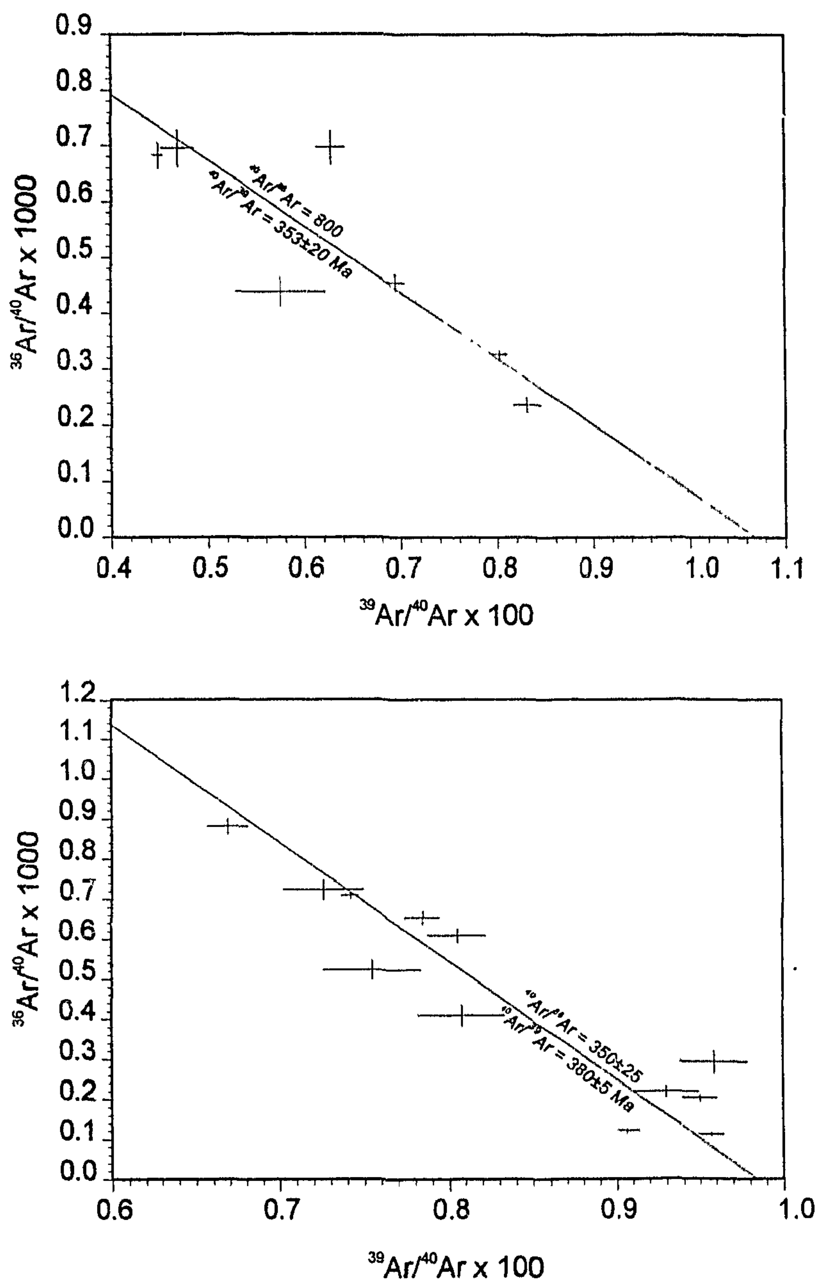

Figure 2.22. ^{36}Ar/^{40}Ar-^{39}Ar/^{40}Ar isochron plots for disturbed hornblendes from the Late Devonian mafic intrusions. (a) The Attwoods Brook gabbronorite; (b) The Birchtown diorite. All of the data come from contiguous heating steps between 1025 and 1300°C that have Ca/K ratios corresponding to independent microprobe analyses for the hornblende grains.

($^{40}Ar/^{36}Ar$ ~350) and its isochron age of 380±5 Ma represents the best estimate of the diorites age, although it predates both the minimum age obtained from the release spectrum and the previously determined plateau ages by at least 5 Ma.

(2) *Mersey Point.* Concordant amphibole and biotite ages appear approximately 2 Ma younger than the 368 Ma phlogopite spectrum of Elias (1986). If geologically significant, this more precise result suggests either that the Mersey Point picrite intruded slightly after 370 Ma, or that its country rocks cooled below the argon blocking temperatures slightly after 370 Ma. The low ages yielded from low temperature steps indicate some discordance that may result from late-stage open system behaviour during either slow Acadian regional cooling or Alleghanian resetting (Reynolds et al., 1987).

(3) *Weekend dykes.* The 370 Ma age for the Little Harbour dyke is identical to the recently determined ages for the Sober Island and East Jeddore dykes (Kempster et al., 1989) and if the analysis represents an intrusion age, then it suggests that the Weekend dykes intruded during one event. Lower ages for the initial steps in the Little Harbour dyke occur at similar temperatures to the low age steps in the Mersey Point spectra, and they may reflect an Alleghanian overprint because Eastern Shore rocks generally record less severe Acadian thermal histories than those intruding southwesterly areas of the MZ (Muecke et al., 1988).

2-3.3. U-Pb Zircon Geochronology

U-Pb (zircon) dating overcomes the excess argon problems encountered in hornblende from the Birchtown diorite. Appendix A-4 summarizes the sample preparation and analytical procedures of the Royal Ontario Museum. Hand picking distinguishes three zircon morphologies in the diorite: fractured equidimensional grains (fraction B8-1), slightly turbid acicular grains (fraction B8-2), and clear acicular grains (fraction B8-3). Figure 2.23 shows the analyzed zircon morphologies, Table 2.4 summarizes the analytical results, and Figure 2.24 is the resulting

a

b

c

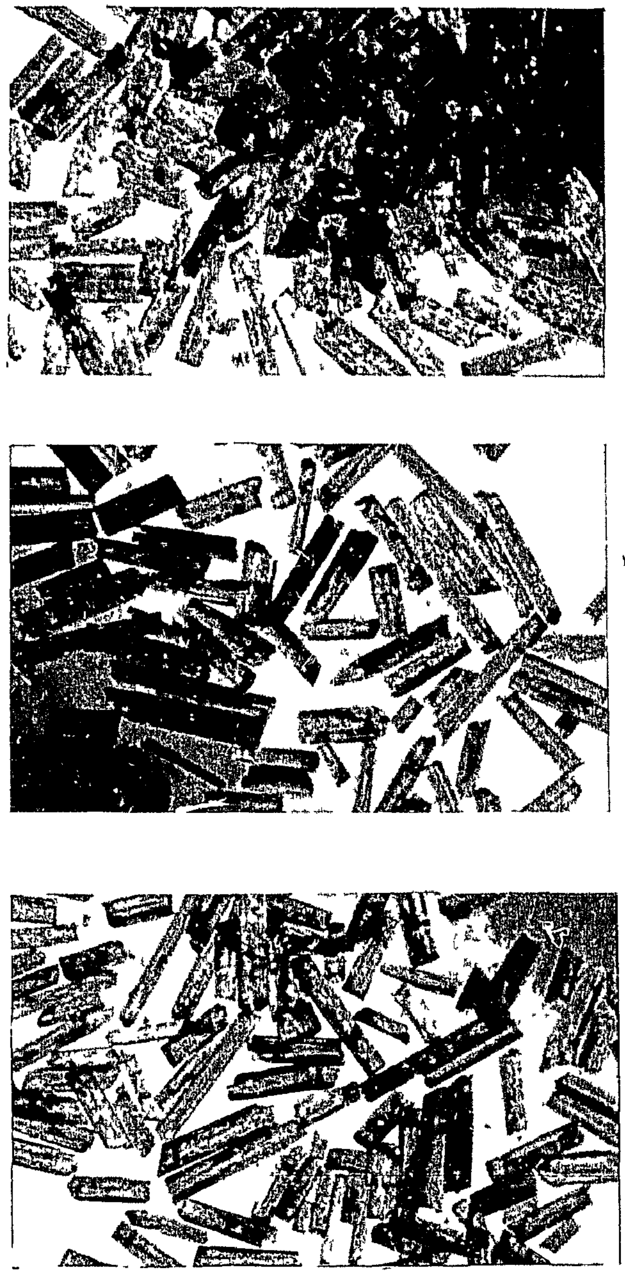

Figure 2.23. Photographs showing the morphological differences between three zircon fractions separated from the Birchtown diorite. (a) Fraction B8-1, dark brown, fractured, and equant zircons. Magnification x25; (b) Fraction B8-2, dark brown, acicular and slightly fractured zircons. Magnification x25; (c) Fraction B8-3, dark brown, acicular, and clear zircons. Magnification x25.

Table 2.4. U-Pb results for zircon fractions separated from the Birchtown diorite

Frac No	Description[a]	Wt (μg)	U (ppm)	Pb_{rad} (ppm)	Pb_{com} (ppm)	$^{206}Pb/^{238}U^b$	$^{207}Pb/^{235}U^b$	$^{207}Pb/^{206}Pb^b$	$^{206}Pb/^{238}U$	$^{207}Pb/^{235}U$	$^{207}Pb/^{206}Pb$	Disc
B8-1	Zrn,0M,E,B,Abr (43)	71	2,346 04	140 43	1 8	0 05904±7	0 44092±65	0 05416±3	369 79	370 9	377 81	2 18
B8-2	Zrn,0M,N,L,Abr (75)	68	1,514.9	91 06	7 65	0 05927±8	0 44203±116	0 05409±12	371.2	371 68	374 7	0 96
B8-3	Zrn,0NM,N,B (25)	48	1,983 8	123 05	0 19	0 05912±9	0 44121±71	0 05413±2	370 24	371 1	376 48	1 7

[a]Mineral analyzed (mineral abbreviations after Kretz, 1983), Magnetic susceptibility (0M = Final Frantz magnetic fraction at 0 degree side tilt, 0NM = Final Frantz non-magnetic fraction at 0 degree side tilt, M1 0A = Initial Frantz 1 0A magnetic fraction (Krogh, 1981a, Morphology (E = equant, N = acicular needle), Colour (B = Brown, L = Light Brown, R = Red, Y = Yellow); Abr = Abrasion (Krogh, 1981b), The number in parentheses denotes the number of grains analyzed [b]Atomic ratios corrected for blank (Pb = 2 pg, U = 0 5 pg), analytical mass fractionation, and initial common Pb calculated using the model of Stacey and Kramers (1975) Pb_{rad} = radiogenic lead, Pb_{com} = common lead

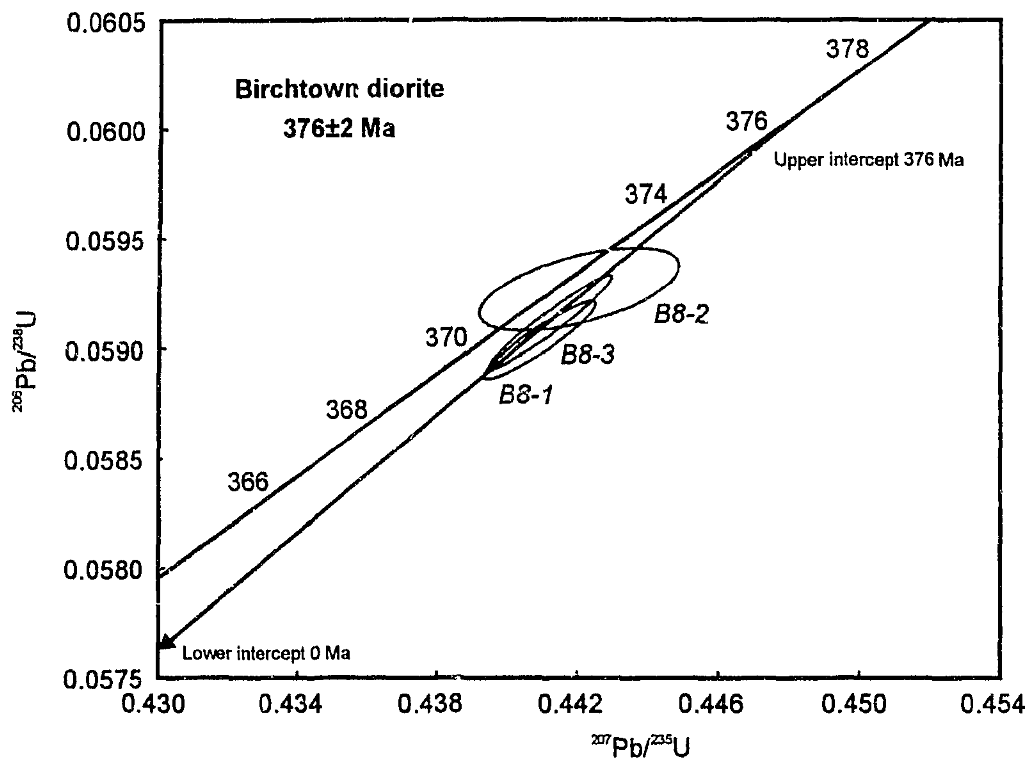

Figure 2.24. U-Pb concordia plot for zircon fractions separated from the Birchtown diorite. Sample numbers in italics, see Table 2.4 for the analytical data.

concordia diagram. The analyzed grains all have dark brown colours, very high U contents (1515-2346 ppm), and predominantly low common Pb (0.19-7.65 ppm). They also have similar ages (370-372) and they underwent a recent lead loss that produced 1.0-2.0% discordance in the analyses. The three fractions, therefore, lie along a single discordia line (with 35% confidence of fit) that intersects concordia at 0 Ma and provides an upper intercept age for the samples of 376±2 Ma. This age represents the best estimate of the intrusion age for the Birchtown diorite, and it agrees with the $^{40}Ar/^{39}Ar$ isochron age for this body.

2-3.4. Geochronological Conclusions

New data for this study provide a range of Late Devonian ages between 366 and 412 Ma for the LDMIs. The analyses agree with, but show less variation than, the previously published $^{40}Ar/^{39}Ar$ analyses, which provide ages between 324 Ma and 377 Ma. If the new data all record the time of intrusion, then they require that LDMI emplacement occurred over a circa 46 Ma interval and they do not suggest a related lithologic suite. However, Douma (1988) interpreted the low age spectra (circa 324 Ma) from the Forbes Point and Mcleods Cove amphiboles as reset Alleghanian ages, and P.H. Reynolds (pers. comm., 1994; Reynolds et al., 1987) suggested that all $^{40}Ar/^{39}Ar$ ages below 370 Ma reflect either partial Alleghanian resetting or slow regional cooling after the Acadian Orogeny. Micas from the LMDIs in southwestern Nova Scotia show ages younger than 370 Ma (Table 2.3), and the circa 376 Ma U-Pb age for the Birchtown diorite does imply that both the amphibole and biotite data for this body (circa 370 Ma) record cooling rather than intrusion. Also, the saddle-shaped Attwoods Brook and Birchtown spectra suggest Alleghanian overprinting in these intrusions (Muecke et al., 1988). Perhaps all of the circa 370 Ma (amphibole and biotite) ages for LDMIs emplaced into southwestern parts of the MZ reflect slow cooling after amphibolite grade metamorphism that occurs abundantly southwest of the South Mountain Batholith, in some cases combined with an Alleghanian overprint (Figure 1.3 in Chapter 1; Elias, 1986; Muecke et al., 1988).

Currently available geochronology suggests two possibilities for the intrusion of the LDMIs: (1) slow Acadian cooling and/or Alleghanian tectonothermal resetting at least partially affect all $^{40}Ar/^{39}Ar$ (hornblende and biotite) data, and so the circa 376 Ma Birchtown U-Pb analysis accurately reflects the intrusion of mafic magmas; or (2) tectonothermal events do not appreciably alter the $^{40}Ar/^{39}Ar$ data. This study favours the first hypothesis for mafic intrusions in southwestern Nova Scotia, and the second hypothesis for the Liscomb Complex gabbro-diorites and the Weekend dykes exposed along the eastern shore; the LDMIs probably intruded the Meguma crust between circa 380 and circa 370 Ma. Given that accepted intrusion ages for the peraluminous granitoids indicate tonalite emplacement at 385-378 Ma and the intrusion of more evolved lithologies in the SMB and Canso plutons at 372±3 Ma (Hill, 1991; Clarke et al., 1993b), the mafic intrusions are approximately contemporaneous with the tonalites and probably also contemporaneous with the younger peraluminous granitoid rocks. No geochronology exists for other granitoid bodies, but the synplutonic intrusion of mafic material into the Shelburne and Port Mouton plutons (considered further in Chapter 3) supports the contemporaneity of mafic and felsic magmas and, therefore, a circa 376 Ma age for the Shelburne Pluton. Geochemical similarities among the LDMIs (considered below) suggest that the LDMIs are genetically related.

2-4. Geochemical Characteristics

2-4.1. Introduction

Previously-published major element oxide, trace and rare-earth element, and Sr, Sm, and Nd isotopic analyses for the LDMIs were compiled and combined with analyses determined specifically for this study. Appendices A-5, A-6, and A-7 describe the sample preparation and analytical procedures, whereas Appendix B-3 contains the geochemical database and indicates the sources of data and the methods of recalculation. Appendix B-4 contains a compilation of analyses of Ordovician, Silurian, and Jurassic mafic intrusions for comparison with the LDMIs.

2-4.2. Major Oxide Characteristics and Variation Among Late Devonian Mafic Intrusions

The LDMIs collectively show a wide range of SiO_2 (45.7-65.7 wt.%), Al_2O_3 (8.9-26.5 wt.%), FeOT (4.2-10.9 wt.%), MgO (2.8-26.5 wt.%), and CaO (1.2-11.2 wt.%) that reflects the lithological variety of currently exposed mafic material. On an AFM diagram (Figure 2.25a), they plot within the calc-alkaline field and define a weak evolutionary trend with moderate enrichment of total iron relative to MgO and alkalies. A K_2O-SiO_2 Harker diagram (Figure 2.25b) shows the calc-alkaline and high-K calc-alkaline nature of most intrusions, but the Forbes Point and Mcleods Cove synplutonic lamprophyres have shoshonitic characteristics. All LDMIs show similar CIPW-normative compositions (Fe_2O_3/FeO recast to 0.23; see Appendix B-3) with normative anorthite generally exceeding normative albite, and hypersthene (10-32%) generally exceeding normative diopside. All bodies contain 2-27% normative quartz, except for the silica-undersaturated Mersey Point picrite that instead contains 25-36% normative olivine. High normative orthoclase (12-17%) within the Forbes Point and Mcleods Cove bodies indicates the potassic nature of these intrusions, whereas up to 7% normative corundum in the Ovens and Devils Island bodies probably reflects the alteration of mafic mineral phases to clays during propylitization. High LOI values (up to 6.6 wt.%) generally reflect the hydrous mineral assemblages of these rocks, although the highest values occur in the altered Devils Island and Ovens dykes.

Figure 2.26 shows a series of variation diagrams plotted against Mg-number ([100(MgO/(MgO+FeOT)]). Regardless of the element used as the ordinate, the Weekend dykes, Birchtown diorite, four Attwoods Brook samples, and a Ten Mile Lake gabbro-diorite sample have similar compositions and they define a relatively coherent group at Mg-numbers between 47 and 64. Three other Attwoods Brook samples plot separately at higher TiO_2 and CaO, and lower FeOT and K_2O, which probably discriminates these plagioclase-cumulate samples. The Mersey Point picrite consistently defines a separate tight cluster at Mg-numbers above 67,

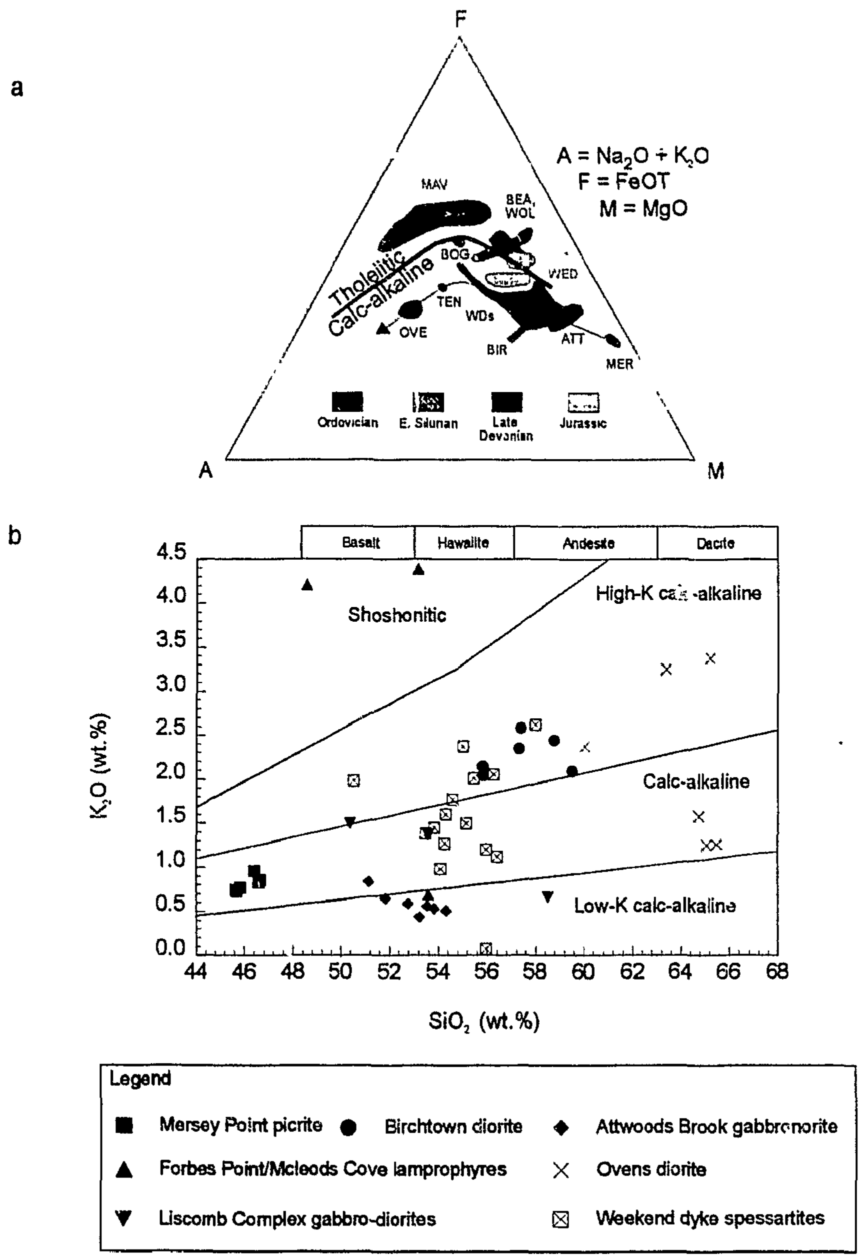

Figure 2.25. Geochemical classification of magma series for the Late Devonian mafic intrusions. (a) The AFM diagram after Irvine and Baragar (1971). MAV = Mavillette intrusion, BEA = Bear River dykes and sills, WOL = Wolfville dykes and sills, SHE = Shelburne dyke, WED = Wedgeport dykes. OVE = Ovens dykes, TEN = Ten Mile Lake gabbro-diorite, BOG = Bog Island Lake gabbro-diorite, WDs = Weekend dykes, BIR = Birchtown diorite, ATT = Attwoods Brook gabbronorite, MER = Mersey Point picrite. See Figure 2.1 for their locations and Appendices B-3 and B-4 for the sources of data; (b) Plot of K_2O-SiO_2 for LDMIs. Comparative volcanic nomenclature after Gill (1981).

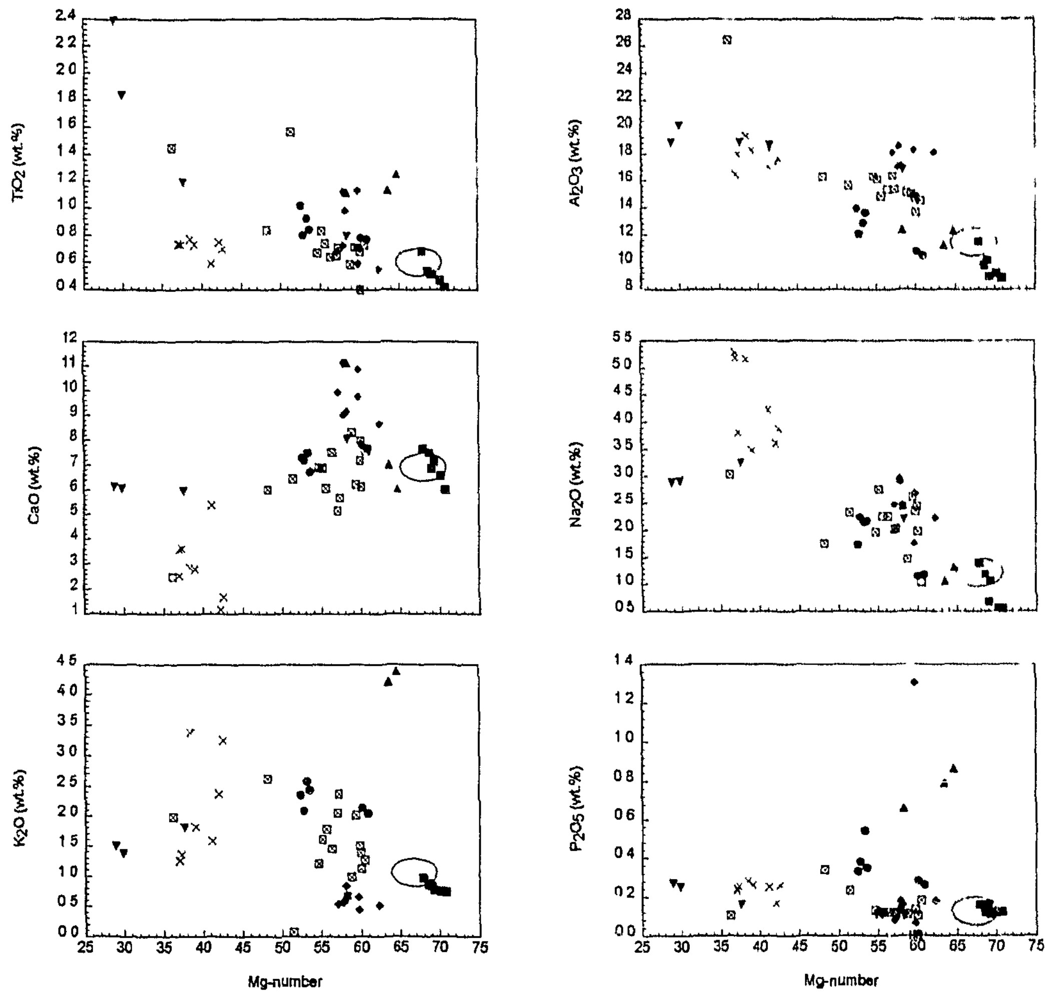

Figure 2.26. Mg-number variation diagrams illustrating major oxide variation among members of the Late Devonian mafic intrusion suite. Only Al_2O_3 shows an evolutionary trend and much scatter exists, especially for the alkalies. The large ellipse marks a hypothetical estimate of their parent magma composition. See the text for an explanation, other symbols as in Figure 2.25.

probably resulting from olivine and hypersthene accumulation. In contrast, the Ovens dykes have the lowest FeOT, MgO, and CaO of all LDMIs, and high Na_2O and K_2O that probably marks the breakdown of pre-existing mafic phases during alteration. Scatter exists for the Devils Island and Liscomb bodies (particularly for the alkalies), although the high TiO_2 and Al_2O_3 characteristics of the Liscomb rocks argue for clinopyroxene, amphibole, and/or plagioclase accumulation, as the field relations suggest.

2-4.3. Trace Element and Rare-earth Element Variation

Trace element abundances also show considerable diversity within the unaltered LDMIs. Chromium and nickel have wide variations from 21-1222 ppm and 10-349 ppm (respectively), and each body has a unique Cr-Ni signature (Figure 2.27). Although most intrusions contain basaltic Ni concentrations, anomalously high Cr in the Mersey Point picrite suggests the accumulation of chrome-spinel as inclusions within olivine and orthopyroxene. Figure 2.28a shows chondrite-normalized spider diagrams for individual LDMIs. All bodies contain high concentrations of large-ion lithophile elements (LILE; e.g. Ba 167-1920 ppm, Sr 176-1235 ppm) relative to high field strength elements (HFSE; e.g. Y 11-37 ppm, Zr 40-248 ppm). Ignoring the LILE-depleted characteristics of the altered Devils Island sample (Figure 2.28a inset), the overall spider diagram patterns appear similar for all bodies. Particularly obvious peaks occur at Rb, K, Sr, and P, with pronounced troughs at Nb ($12\text{-}70_{CN}$) and in many cases also at Ti. The Mersey Point picrite contains the lowest concentrations of most trace elements relative to the other LDMIs, and the Ovens, Forbes Point, and Mcleods Cove intrusions have the highest LILE abundances. The Attwoods Brook gabbronorite shows a similar LILE pattern to the Devils Island dyke, suggesting that mobile element loss explains its anomalous low-K calc-alkaline characteristics on Figure 2.25b. Although the average Weekend dyke pattern appears identical to those of the other LDMIs, individual Weekend dykes (Figure 2.28a inset) span a range of trace element concentrations comparable to the entire mafic intrusion suite.

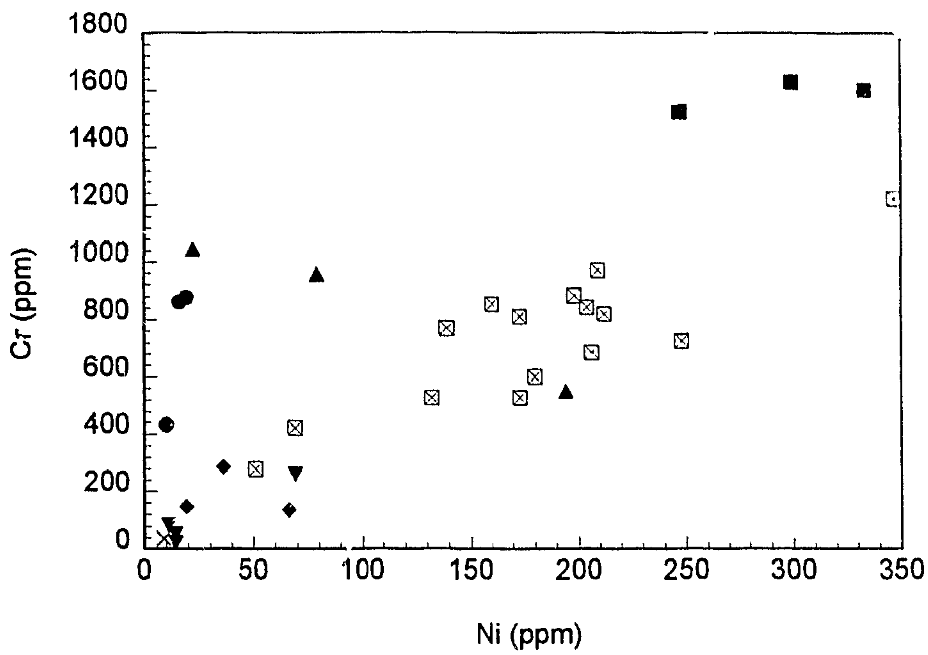

Figure 2.27. Plot of Cr-Ni for the Late Devonian Mafic Intrusions. Note the high Cr content of the Mersey Point picrite that probably results from chrome-spinel retention into accumulating hypersthene and olivine. Symbols as in Figure 2.25.

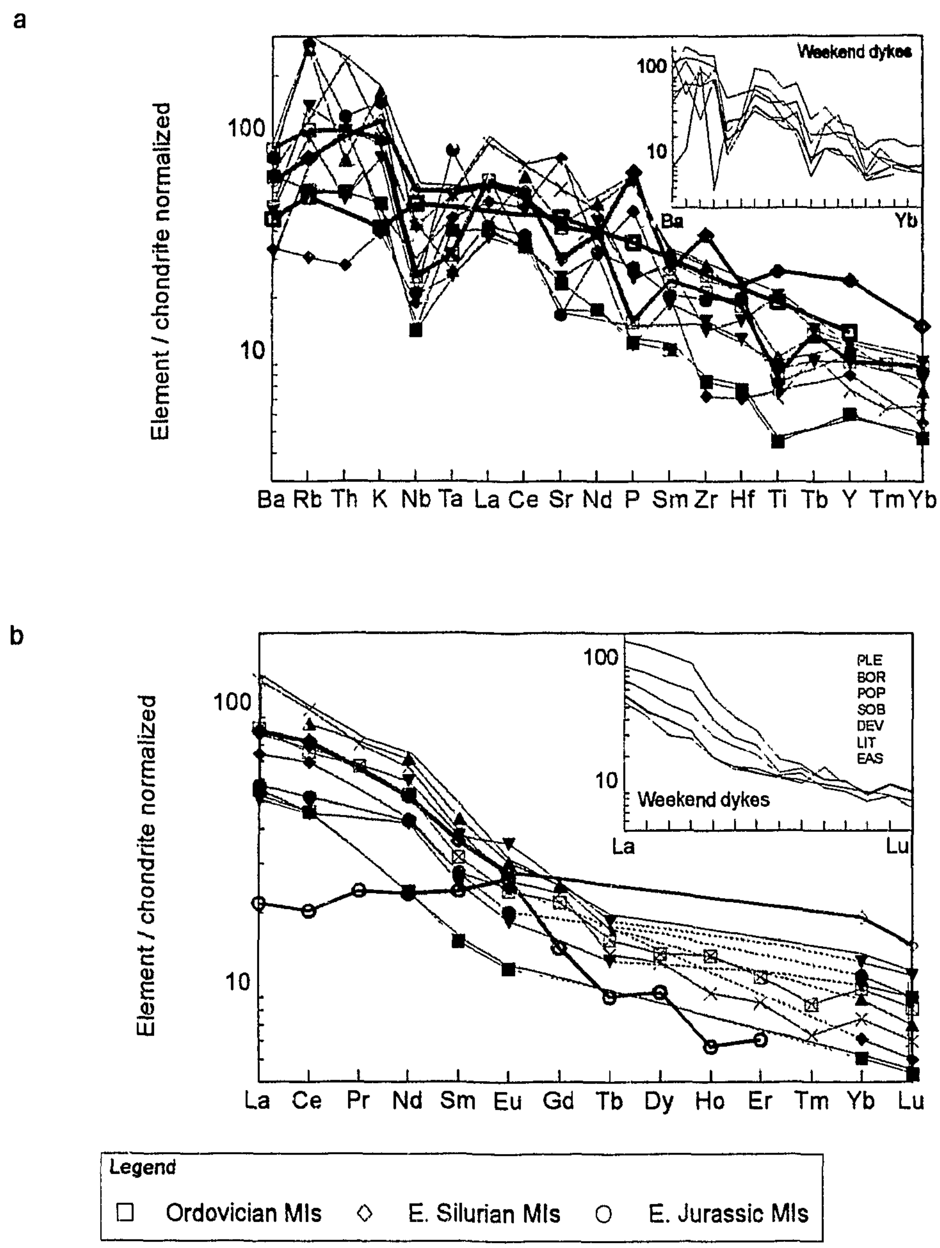

Figure 2.28. Chondrite-normalized spider diagrams. (a) Chondrite normalized trace element diagram. Normalization factors after Thompson et al. (1984); (b) Chondrite-normalized rare-earth diagram. Normalization factors after Nakamura (1974). The grey fields represent the LDMIs and the insets show spiderdiagrams for individual Weekend dykes: PLE = Pleasant Harbour, BOR = Borgles Island, POP = Popes Harbour, SOB = Sober Island, DEV = Devils Island, LIT = Little Harbour, EAS = East Jeddore. Refer to Figure 2.18 for their locations. Symbols as in Figure 2.25. MIs = mafic intrusions.

Variable rare-earth element concentrations also exist in the LDMIs (Σ_7REE 42-148; Figure 2.28b), although all bodies show similar chondrite-normalized spider diagrams. Light rare-earth elements (LREE; e.g. La 7-42 ppm) have higher concentrations than heavy rare-earth elements (HREE; e.g. Yb 0.9-3.5 ppm, Lu 0.1-6.5 ppm), and the overall spider diagram patterns for each body appear broadly concave upwards. The Ovens, Forbes Point, and Mcleods Cove bodies consistently have the highest concentrations of all rare-earths and the high incompatible trace element concentrations in the Ovens rocks perhaps argue for metasomatism not apparent in the Devils Island analysis (Figure 2.28b inset). The Mersey Point picrite contains the lowest rare-earth abundances and is the most primitive composition. Only the Bog Island Lake gabbro-diorite has a small positive Eu anomaly (Eu/Eu* 1.3) that agrees with the petrographic evidence for plagioclase accumulation (Clarke et al., 1993a).

2-4.4. Sr, Sm, and Nd Isotope Systematics

Although the intrusion ages of the LDMIs may span a circa 10 Ma interval, their initial Sr ratios remain insensitive to the age of the rocks within 370 Ma^{+13}_{-17}. LDMIs intruding the Meguma Group show wide variation of initial $^{87}Sr/^{86}Sr$ ratios between 0.7043 and 0.7079, and variable $^{144}Nd/^{143}Nd$ (0.51222-0.512654) and $^{147}Sm/^{144}Nd$ (0.09349-0.13736) isotopic values. εSr also ranges widely between 3.41 and 54.43, although εNd shows less variation between -4.36 and 3.69. All bodies except those from the Liscomb Complex, lie close to the "array" of values compatible with mantle derivation (Figure 2.29). The Liscomb Complex gabbro-diorites have the highest $^{87}Sr/^{86}Sr_i$ value (0.7079) and the lowest εNd value (-4.36). The Forbes Point and Mcleods Cove synplutonic bodies both contain very similar initial $^{87}Sr/^{86}Sr$ ratios (0.70509 and 0.70567, respectively), but the Forbes Point dyke has a low εNd value (-0.96±0.17); this value correlates with unusually high alkalies, LILE, and LREE in the synplutonic intrusions, which result from mafic-granitoid hybridism (Chapter 3). Model ages (T_{CHUR}) for the LDMIs lie at markedly younger

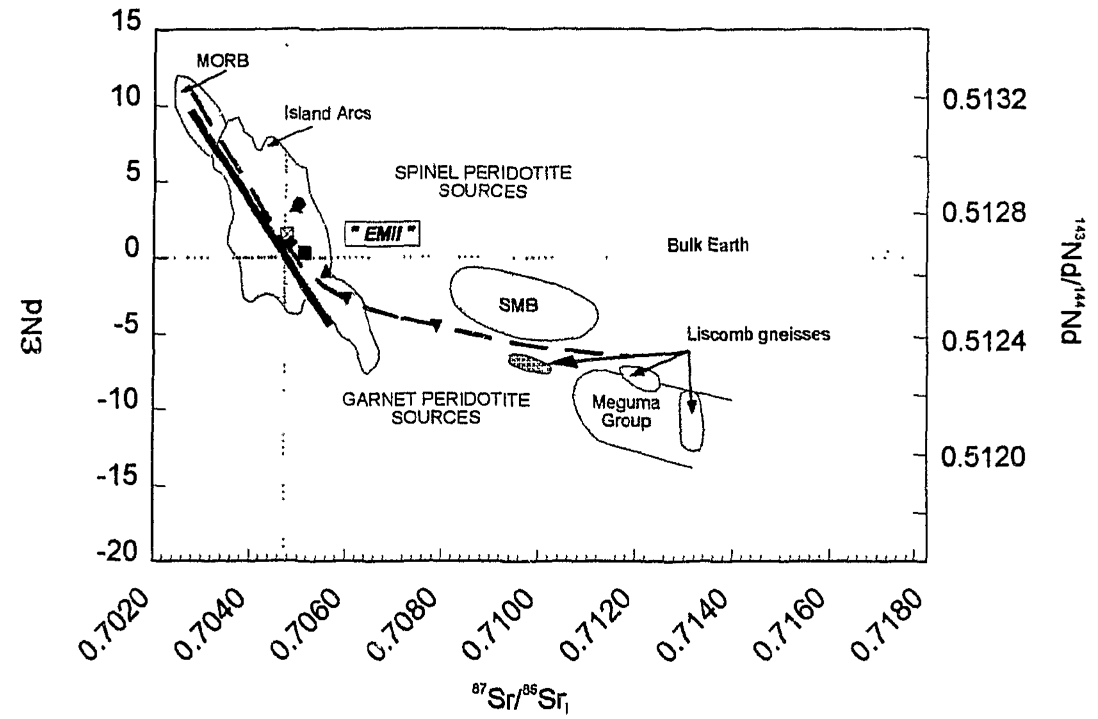

Figure 2.29. Plot of εNd-$^{87}Sr/^{86}Sr_i$ for the Late Devonian mafic intrusions. Most bodies plot close to the modern mantle trend (solid line), in the field for modern island arcs. The Liscomb Complex gabbro-diorites instead plot along a hyperbolic mixing line between the compositions of MORB and those of the Meguma Group metasediments, Liscomb Complex gneisses, or the South Mountain Batholith (SMB). Note that the uncontaminated intrusions plot in the spinel peridotite field. Island arc field after Hawkesworth et al. (1993), "EMII" compositions after Hart (1988). Meguma Group and SMB isotopic compositions taken from Clarke et al. (1988) and Clarke and Halliday (1980) respectively. Other comparative data from DePaolo (1988). All data recalculated to t = 370 Ma, symbols as in Figure 2.25.

ages than the circa 370 Ma intrusion ages of individual bodies (56-357 Ma), whereas depleted mantle (T_{DM}) model ages (658-1370 Ma) predate their intrusion by more than 280 Ma.

2-4.5. Geochemical Comparison of the Late Devonian Mafic Intrusions with Other Mafic Intrusions in the Meguma Zone

Unaltered LDMIs contain variably evolved major oxide compositions, but they generally have high concentrations of alkalies (especially K_2O) and LILE (approximately 100 times chondritic abundances) relative to HFSE (occurring at 10-50 times chondritic values). They also have strong LREE fractionation (La/Lu 29.6-161), variable but high initial Sr isotopic ratios, and variable Sm and Nd isotopic values. The internally consistent trace element spider diagrams of the LDMI suite suggest that these rocks represent a suite of genetically related intrusions. Statistical comparisons with the Ordovician, Silurian, and Jurassic tholeiites cannot be made for many trace elements because of the limited nature of the previously published geochemical data (Appendix B-4). However, although the LDMIs span a similar evolutionary range to other intrusions (SiO_2 46-66 wt.%), the Ordovician, Silurian, and Jurassic tholeiites have higher TiO_2 and FeOT, generally lower MgO, and sodi-potassic characteristics. Where trace element and rare-earth element data exist, the LDMIs consistently have different chondrite-normalized spider diagram patterns (Figure 2.28). Figure 2.30 establishes useful major oxide criteria for LDMI fingerprinting, and the AFM diagram (Figure 2.25a) also effectively separates the tholeiitic characteristics of these rocks from the calc-alkaline LDMIs, although the alkaline Wedgeport lamprophyres do transgress the calc-alkaline field towards the total alkali apex.

2-5. Petrogenesis of the LDMI Suite

The internally consistent mineral assemblages, mineral compositions, and chondrite normalized trace element characteristics of the LDMIs all support the notion of a related suite of

a

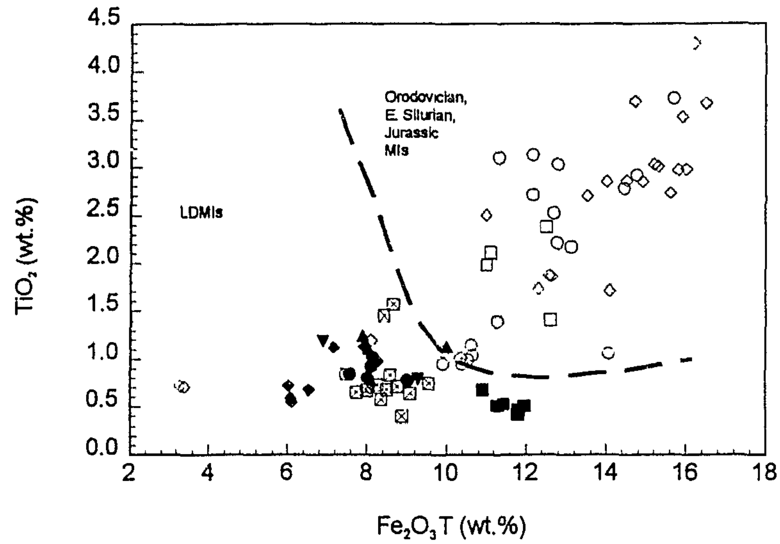

b

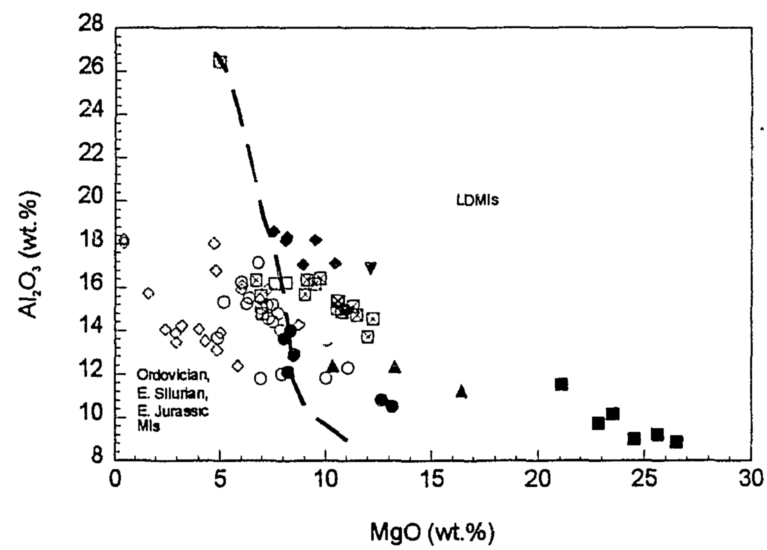

Figure 2.30. Major oxide discrimination of the unaltered Late Devonian mafic intrusions from the Ordovician, Silurian, and Jurassic mafic intrusions in the Meguma Zone. (a) Plot of TiO_2-Fe_2O_3; (b) Plot of Al_2O_3-MgO. The dashed line defines the areas of least overlap between the compositions of the Late Devonian and the other mafic intrusions. Symbols as in Figures 2.25 and 2.28.

Late Devonian calc-alkaline mafic intrusions. Conventional interpretations of Recent and modern calc-alkaline lavas suggest the derivation of most lithologic suites from primitive parent magma compositions by the fractionation of phenocryst assemblages, with or without crustal contamination (e.g. Green and Ringwood, 1968b; Yagi and Takeshita, 1987). This discussion evaluates plausible evolutionary paths and appropriate mantle sources for the LDMIs, recognizing the caution that must be exercised in the interpretation of these coarse-grained rocks as analogues of magma compositions. It ignores the altered Devils Island and Ovens dykes and the synplutonic lamprophyres at Forbes Point and Mcleods Cove (Section 3 of Chapter 3 considers the geochemical consequences of hybridism in detail).

2-5.1. Evolutionary Processes

The lack of strong evolutionary correlations on Figure 2.26 neither supports nor rejects the possibility of a genetic relationship between the LDMIs. Dispersed major oxide variations for the collective suite probably reflects the cumulate characteristics of the Attwoods Brook, Mersey Point, and Bog Island Lake bodies. However, their similar spider diagram patterns on Figure 2.28 suggest that they may be related by phenocryst fractionation or accumulation from similar parent magmas. Figure 2.31 relates the major element chemistry of all LDMIs to the atomic proportions of Mg and Ca in magnesio-hornblende and, therefore, preferentially emphasizes correlations attributable to amphibole fractionation (Russell and Nicholls, 1988). Except for the Mersey Point picrite, LDMI samples collectively define an array paralleling the amphibole fractionation trend (slope = 1.0). The weak correlation coefficient of this regression (r = 0.55) results from scatter that precludes amphibole as the only fractionating phase; both clinopyroxene and plagioclase occur in the LDMIs and could also affect trends on this diagram. The Mersey Point samples instead plot along a steep linear trend (r = 0.97). On a 0.5(Fe+Mg) diagram (Figure 2.31 inset), it has a slope of unity and it supports olivine and/or orthopyroxene as the primary accumulating phases.

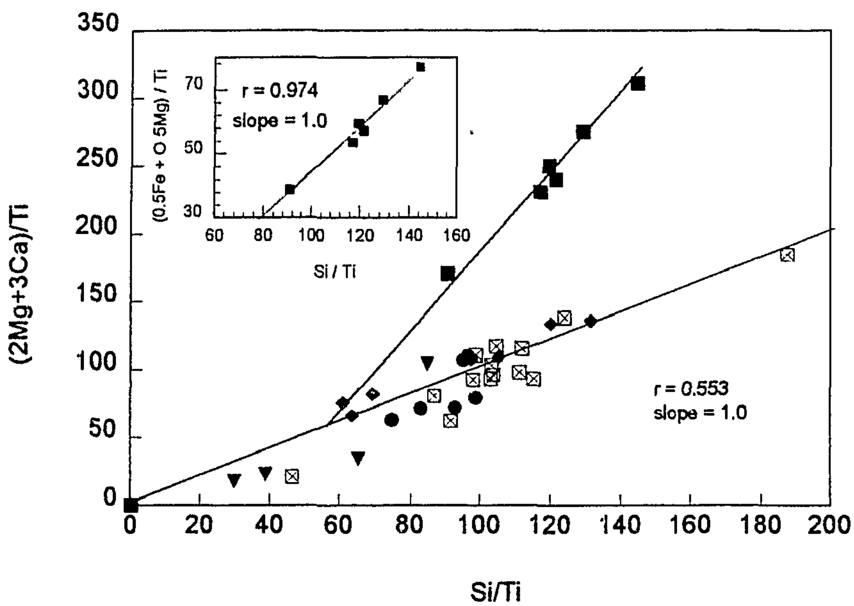

Figure 2.31. Pearce element ratio plot of 2Mg+3Ca/Ti-Si/Ti for the Late Devonian mafic intrusions. It excludes highly fractionated or altered samples. The Pearson correlation coefficients, slopes, and ordinate intercepts were calculated using the Pearce.Plot program of Stanley and Russell (1989). Symbols as in Figure 2.25.

If the chemical intersection between these regressions implies a similar parent for all bodies (as their similar spider diagram morphologies on Figure 2.28 suggest), then the Mersey Point picrite evolved from it by olivine and orthopyroxene accumulation, and the other bodies evolved by the fractionation or accumulation of all their major modal constituents. Petrographic information in the intrusions support this evolutionary sequence, which appears similar to that postulated for other calc-alkaline intrusive suites (e.g. Smith et al., 1983; Yagi and Takeshita, 1987). The Mersey Point picrite consistently plots below all other LDMIs on Figure 2.28 and it represents the most primitive composition. Although the cumulate picrite cannot represent a liquid composition, microprobe analyses of its unzoned cumulus olivines indicate that they formed in equilibrium with primitive magma characterized by a Mg-number of 70±1 (Roeder and Emslie, 1970). This value is similar to the value for the picrite whole-rock, but accounting for the enhanced MgO and FeOT abundances promoted in this lithology by olivine and orthopyroxene accumulation, the parent probably plotted between the Attwoods Brook gabbronorite and the picrite samples (Figure 2.26).

Assuming that all LDMIs crystallized similar phenocryst assemblages, then crystal fractionation would shift their spider diagram patterns to higher values on the ordinate axis without affecting their morphologies (Pearce, 1983). Figure 2.28 shows this general similarity, but non-parallel trends do exist for some elements. They may result from the fractionation of phenocrysts in different proportions in each body, but Green and Ringwood (1968b) also advocated crustal contamination as a major evolutionary process in cogenetic calc-alkaline rocks. Despite the variable occurrence of elevated and scattered Zr/Y, Sr/Y, and La/Nb, Sr/Ba ratios in contaminated magmas (Thompson and Fowler, 1986; Wyman and Kerrich, 1989), and to some extent in the LDMIs, trace element data cannot unequivocally separate the effects of crustal assimilation from those of fractional crystallization without knowledge of the contaminant composition (McBirney et al., 1987). Strontium-neodymium isotope data indicate that most of the LDMIs plot on or close to the modern mantle array and that they may represent mantle compositions (Figure 2.29), but the Liscomb Complex gabbro-diorites have more enriched Sr and more depleted Nd isotopic compositions and they plot on a mixing line between the Meguma Group, SMB, or sub-Meguma basement gneiss compositions. The presence of abundant crustal xenoliths, εNd <0, and initial $^{87}Sr/^{86}Sr$ >0.707 in the Liscomb intrusions, suggests a strong crustal influence in their petrogenesis (Venturelli et al., 1984; Frost and O'Nions, 1985). The occurrence of crustal xenoliths in the Mersey Point picrite and the Popes Harbour dyke suggest that contamination may account for isotopic scatter (Hergt et al., 1989) if it does not reflect the nature of the source (considered below).

In summary, currently exposed LDMIs probably represent a discontinuous series of fractionated products derived from similar parent magma batches by the variable fractionation of all their major modal phases. Only the Liscomb Complex gabbro-diorites contain isotopic evidence for crustal contamination. The cumulate characteristics of some bodies implies that fractionation occurred *in situ*, and unzoned cumulus olivine compositions in the primitive Mersey Point body have Mg-numbers (>70) that may be appropriate for partial melts in equilibrium with the upper mantle (Roeder and Emslie, 1970; Eggler and Burnham, 1973; Grove and Baker, 1984). To explain the modal and chemical characteristics of the LDMIs, the parent magmas must have been a primitive (Mg-number >60), hydrous basalt or peridotite (Cawthorn and O'Hara, 1976; Ulmer, 1988).

2-5.2. Source(s) of the Magmas

The evidence for fractionation does not suggest the use of LDMI compositions as probes of the mantle, but it did not significantly change their spider diagram patterns. Recognizing the limited influence of crustal contamination in most intrusions, their high-LILE and LREE characteristics cannot entirely result from infracrustal processes and must originally emanate from the mantle source. Assuming that the parent plotted between the gabbronorite and the picrite on Figure 2.28, high concentrations of the first transition series metals (e.g. Ti, Sc, V, Co) and both Ti/V and Ti/Sc ratios similar to those of MORB, suggest a depleted source within the upper mantle for this composition (Rock, 1990). A chondrite-normalized Ce/Yb-Ce diagram (Figure 2.32) suggests that somewhat similar modal source compositions existed for all LDMIs and chondrite-normalized Ce and Yb abundances between 7 and 11 largely preclude major garnet in the residuum. The lack of Eu anomalies in most LDMIs also suggests a depleted source without major plagioclase fractionation. As de Albuquerque (1979) suggested, harzburgite-wehrlitic (peridotitic) compositions may be appropriate sources.

However, high incompatible trace element concentrations in even the most primitive LDMIs apparently contradict the supposition of a depleted source. With little evidence for abundant residual garnet, incompatible element enrichments cannot result from preferential HREE and HFSE retention by garnet (Salters and Hart, 1991). Furthermore, MORB-normalized HFSE abundances close to unity (see below) cannot result from small degrees of partial melting, and small-proportion melts may be difficult to mobilize from the source region (Arndt and Christensen, 1992). Abundances of Rb, K, and Th between 10 and 100 times chondrite argue strongly against chondritic source alternatives. Instead, εNd values with more enriched compositions than those of MORB (Figure 2.29) and variable initial $^{87}Sr/^{86}Sr$ ratios up to 0.7055, suggest the possibility of isotopic enrichments in the source (Wyman and Kerrich, 1989). Three explanations exist: (1) the ascent of juvenile asthenospheric plumes into depleted upper mantle sources; (2) the percolation of fluids derived from small degrees of partial melting of chondritic or otherwise enriched mantle sources (e.g. Neal, 1988); or (3) metasomatism of depleted upper mantle sources by "IRS" (incompatible element, radiogenic isotope, and silica enriched) fluids and/or lithospheric partial melts derived from subducted ocean lithosphere (Hawkesworth et al., 1993).

Tate and Clarke (1993) preferred the derivation of the Weekend dykes from sources modified by subducted ocean lithosphere to explain the volatile magmas and their depletion of Nb relative to Ta and Ce. The collective LDMI suite has similar characteristics to the Weekend dykes (Figure 2.28a). Most intrusions show troughs at Nb, and in some cases also coupled with smaller troughs at Ta and Ti constituting the classical negative "TNT" anomaly subduction tracer (Beard and Day, 1988; Figure 2.28; Figure 2.33a). High and variable initial $^{87}Sr/^{86}Sr$ isotope ratios at more limited εNd values in the uncontaminated bodies correlate with quoted values for island arc and continental margin arc basalts (Arndt and Christensen, 1992) and the intrusions plot towards the "EMII" subduction-derived enriched mantle component that Hart (1988) identified in ocean island basalts (Figure 2.29). The LDMIs also have MORB-normalized LILE abundances similar to those of island arc basalts (Pearce, 1983; Figure 2.33b), but they contain more abundant HFSE and they have less pronounced TNT anomalies. Most HFSE occur at within-plate basalt concentrations (Figure 2.33c) and the chaotic peaks and troughs in the MORB-normalized spider diagrams suggest the generation of LDMIs from sources containing erratic fractionation of HFSE (Wyman and Kerrich, 1989; Salters and Hart, 1991). Their geochemical similarities to within-plate basalts suggest that appropriate sources resided in the subcontinental lithospheric mantle (Brown et al., 1984; Hawkesworth et al. 1990).

In summary, LDMIs were probably derived from a depleted mantle source similar to that of MORB, but erratically metasomatized and enriched by an externally-derived fluid or melt phase to explain the high LILE, LREE, and $^{87}Sr/^{86}Sr$ values. The existence of negative Ta-Nb-Ti anomalies (Figure 2.33a) and Sr isotopic similarities with island arc basalts suggest a subduction origin for this enrichment, and the high and erratically fractionated HFSE suggest a subcontinental lithosphere source. Enrichments of HFSE and negative TNT anomalies possibly imply that metasomatism also stabilized amphibole, phlogopite, or a titanian accessory phase in the source to form the TNT anomalies (McCulloch and Gamble, 1991; Hawkesworth et al., 1993). Following Pearce's method for the quantification of source contributions in multi-component rocks, 39-83% of all LILE could be derived from subduction-derived contaminants, 6-25% of LILE and up to 50% of HFSE may originate from the depleted mantle source (Figure 2.33d).

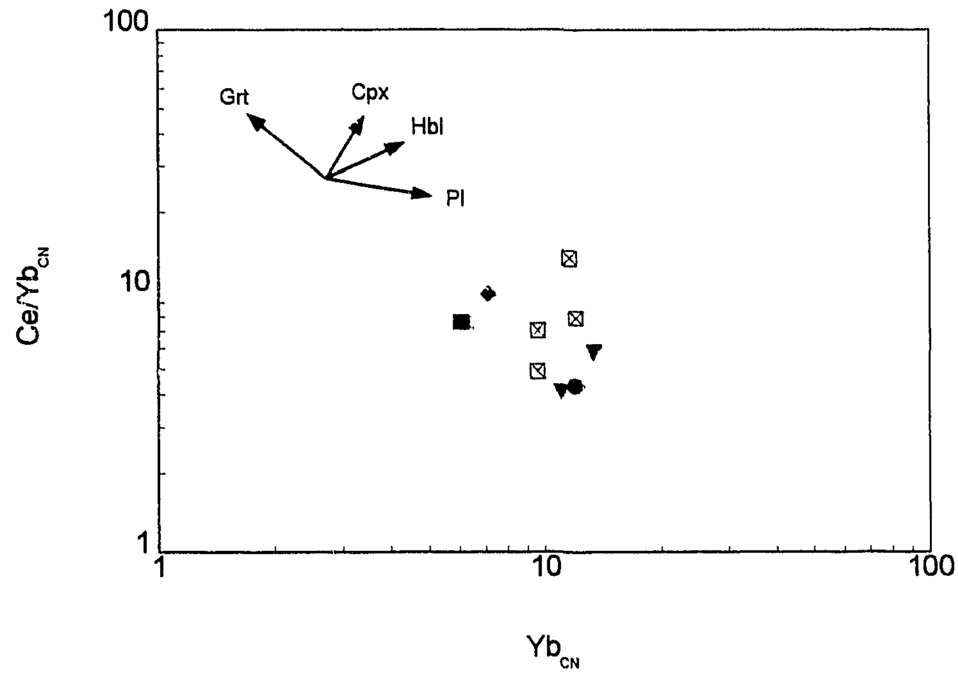

Figure 2.32. Chondrite-normalized Ce/Yb-Yb diagram for the Late Devonian mafic intrusions. All compositions form a cluster at Ce/Yb and Yb ~10 that largely precludes the major presence of garnet in the residuum. The intrusions probably formed as partial melts derived from similar sources. Vectors after Venturelli et al. (1984) and mineral abbreviations after Kretz (1983). Symbols for the LDMIs as in Figure 2.25.

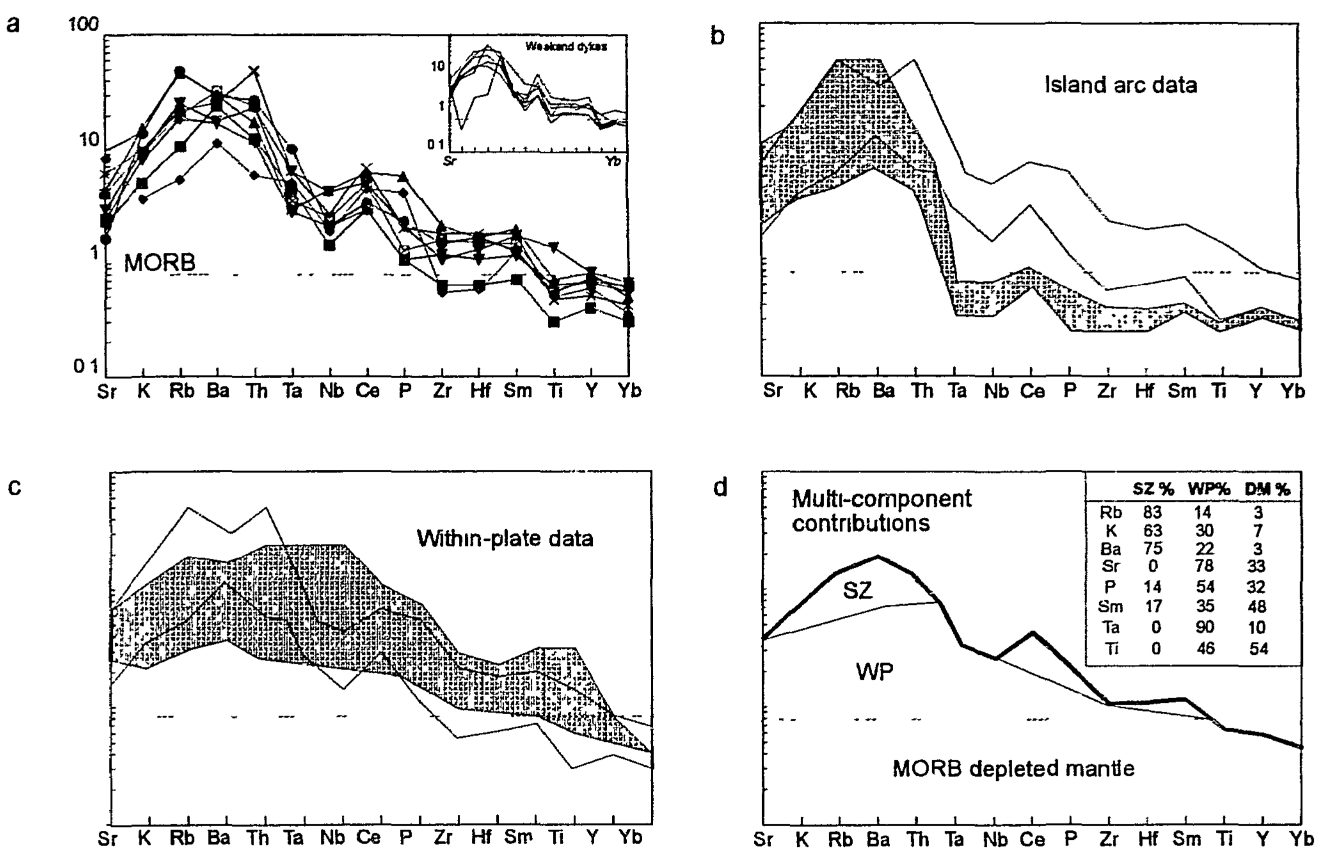

Figure 2.33. Comparative MORB-normalized spider diagrams for the Late Devonian mafic intrusions. (a) The MORB-normalized characteristics of the intrusions; (b) Comparison of the intrusions (unshaded) with the characteristics of modern island arc basalts (shaded in grey); (c) Comparison of the intrusions (unshaded) with the characteristics of within-plate basalts (shaded in grey); (d) Graphical and numerical summary of the multi-component source contributions in the intrusions calculated with the method of Pearce (1983). All comparative data from Pearce (1983). SZ = subduction zone contaminants, WP = Within-plate contributions from the subcontinental lithosphere. MORB = Mid-Ocean Ridge Basalt, DM = depleted mantle. Symbols as in Figure 2.25.

2-5.3. Palaeotectonic Environment and the Timing of Metasomatism

Well-established tectono-magmatic discriminators based on immobile elements derived from the mantle, not a putative metasomatic source, support a subduction-related petrogenesis for the LDMIs (Figure 2.34). The TiO_2-Na_2O-MnO (in clinopyroxene) diagram of Nisbet and Pearce (1977) identifies LDMIs as both volcanic arc and within-plate basalts. A Nb/3-Th-TiO_2 diagram discriminates LDMIs as within-plate basalts, and on a Nbx2-Y-Zr/4 diagram, the LDMI compositions applicable for the diagram plot in the field for both volcanic arc and within-plate basalts. These variable volcanic arc and within-plate characteristics probably reflect the supposed multi-component nature of the LDMI source (containing both subduction-derived and lithospheric mantle components) and they suggest that the intrusions formed in a continental margin arc environment. The Ta/Yb-Th-Yb and Zr/Y-Zr diagrams of Pearce (1983) both directly identify LDMIs as continental margin arc rocks derived from re-enriched depleted mantle sources. Suppression of the variation attributable to fractional crystallization on these diagrams probably suggests that varying amounts of subduction-zone contamination in the source accounts for the scatter.

Contamination of anhydrous upper mantle sources by fluids emanating from subducted oceanic lithosphere probably lowered the mantle solidus and caused partial melting; the model ages for subduction-related rocks reflect either this melting event or they reflect a mixture of ages for the components in the source (Hawkesworth et al., 1993). Given that neither chondritic nor depleted mantle sources alone produced the LDMI compositions, neither T_{CHUR} model ages (younger than the LDMI intrusion ages) nor T_{DM} model ages (anomalous Proterozoic ages) reflect the time of magma generation. In rocks with multi-component source regions (containing both depleted and enriched components) appropriate model ages cannot be calculated without knowledge of the isotopic compositions of the source components. However, re-enrichment of a depleted source should evolve the mantle from the depleted mantle evolution curve towards

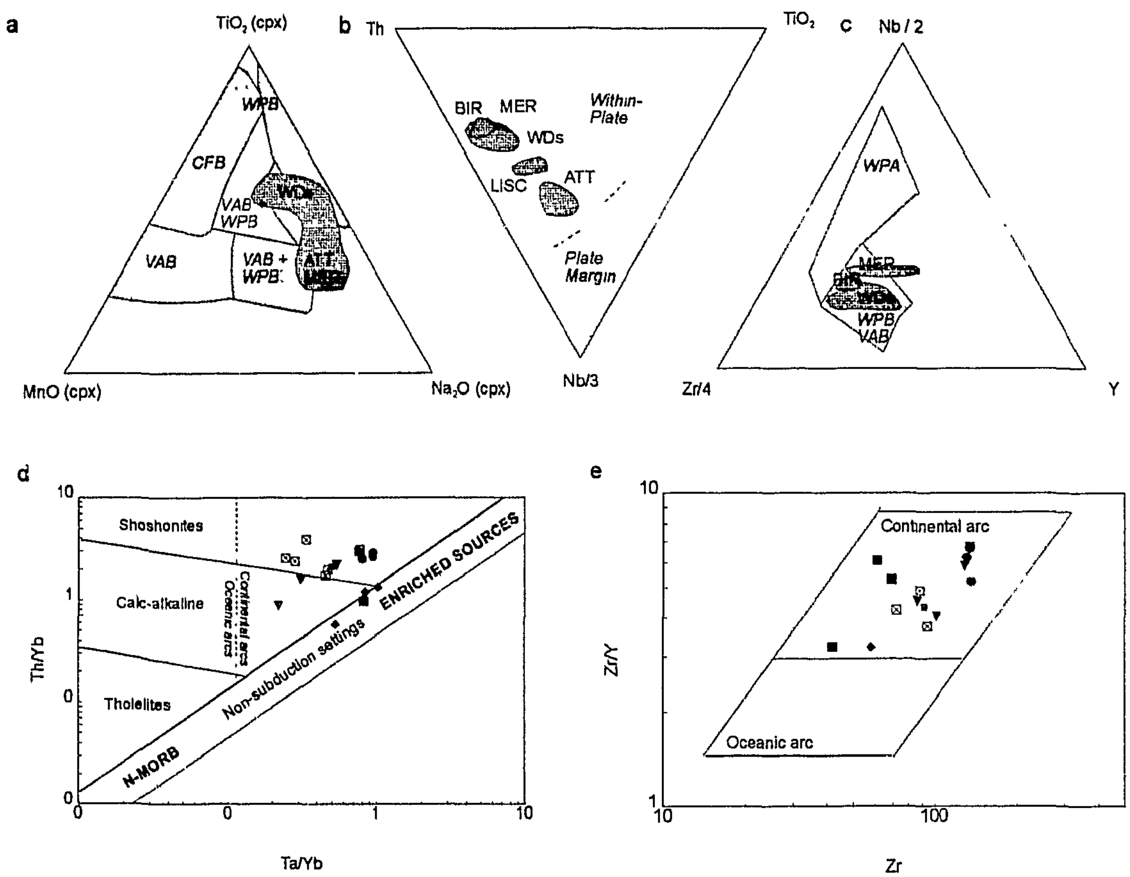

Figure 2.34. Selected immobile element tectonomagmatic discriminators for the Late Devonian mafic intrusions. (a) Plot of MnO-TiO_2-Na_2O in clinopyroxene (Nisbet and Pearce, 1977); (b) Plot of whole-rock TiO_2-Nb/3-Th (Meschede, 1986); (c) Plot of whole-rock Zr/4-Nb/2-Y (Holm, 1985); (d) Plot of whole-rock Th/Yb-Ta/Yb (Pearce, 1983); (e) Plot of whole-rock Zr/Y-Zr (Pearce, 1983). Abbreviations: CFB = continental flood basalts, WPA = within-plate alkaline, WPB = within-plate basalts, VAB = volcanic arc basalts. Symbols and abbreviations as in Figure 2.25.

lower εNd values. The slope of this line reflects the compositions, relative proportions, and degree of equilibrium between the depleted and enriched components (Hawkesworth et al., 1993). Figure 2.35 illustrates this situation and shows two potential source compositions for the LDMIs (notated 1 and 2) and their model age ranges (notated T_{ENRICH}). It illustrates the sensitivity of the calculation on the composition of the enriched mantle and suggests only that prospective regional tectonic models for the LDMIs should recognize the possibility of circa 370-1000 Ma ages in the source.

2-6. Proposed Regional Tectonic Model

Poorly constrained palaeomagnetic interpretations hinder the development of regional plate tectonic models for the Meguma terrane and most other Appalachian zones (Williams and Hatcher 1982). However, recent correlations of Appalachian tectonics suggest that after the Iapetus Ocean opened in the Late Proterozoic, continued rifting of the palaeo-Gondwanan margin generated a series of microcontinental fragments that separated the Theic and Iapetus oceans (Hon and Piqué, 1989; Figure 2.36). Although the events are poorly constrained, microcontinents amalgamated to form the Avalon Zone throughout the Late Silurian and the Early Devonian (Keppie, 1985) and the composite Avalon terrane collided with the North America as Iapetus closed (Piqué and Skehan, 1992; Keppie et al., 1992). Diachronous ocean closure and oblique subduction prevented Avalon accretion until the Middle Devonian (circa 380-390 Ma) in the Canadian Appalachian region (Keppie et al., 1992). Continued closure of the Theic Ocean proceeded throughout the Devonian by northwesterly subduction beneath the accreted Avalon terrane (Piqué and Skehan, 1992) and it culminated with the accretion of the MZ during the Acadian Orogeny (Keppie, 1985; Keppie, 1989).

Historically, the MZ represented the only northern Appalachian terrane with a paucity of evidence for a subduction-related tectonic emplacement. Direct structural evidence and the presence of Avalonian basement below the Meguma Group (Eberz et al., 1991; Clarke et al.,

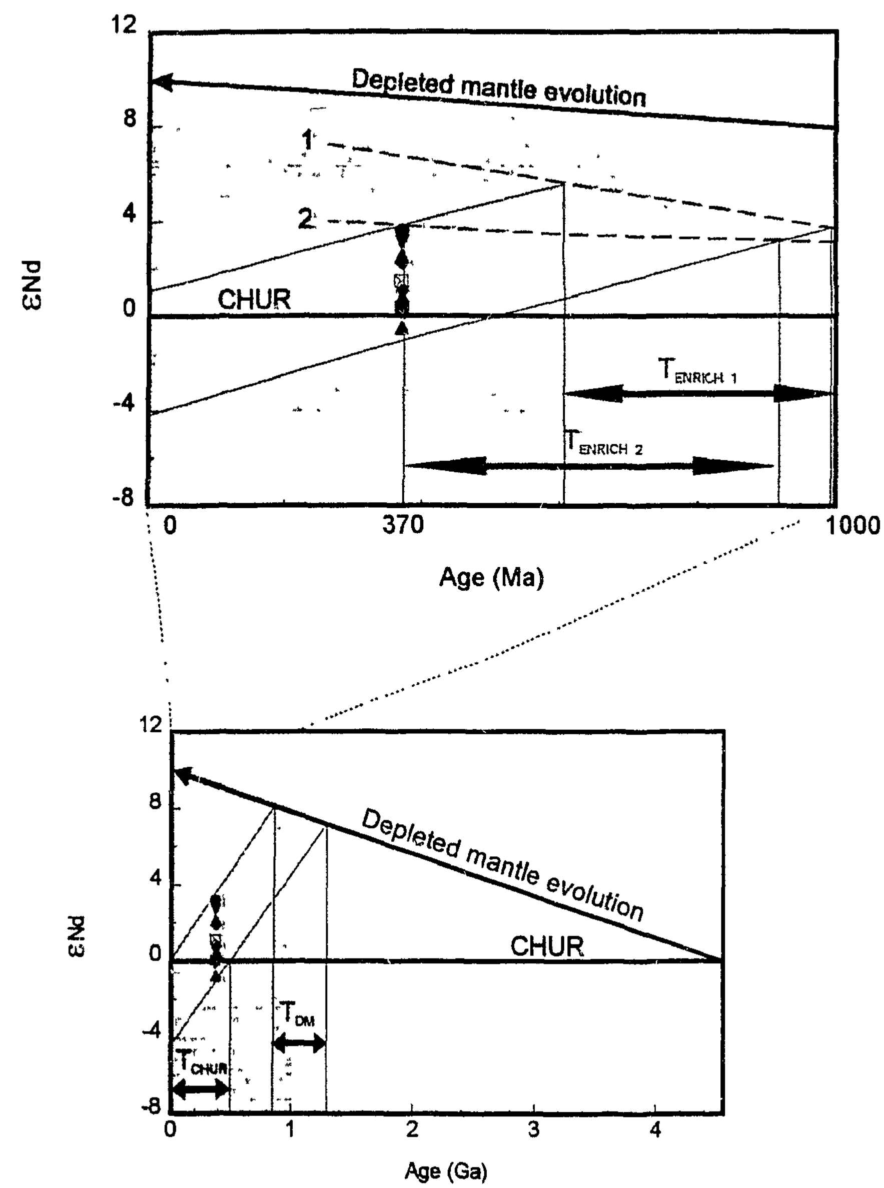

Figure 2.35. εNd evolution diagram for the Late Devonian mafic intrusions illustrating the difficulty of determining source model ages for rocks with multi-component sources. The dashed lines 1 and 2 represent arbitrary evolutionary curves for depleted mantle sources after different degrees of isotopic re-enrichment. See the text for a discussion. All data recalculated to t = 370 Ma. Symbols for the intrusions as in Figure 2.25.

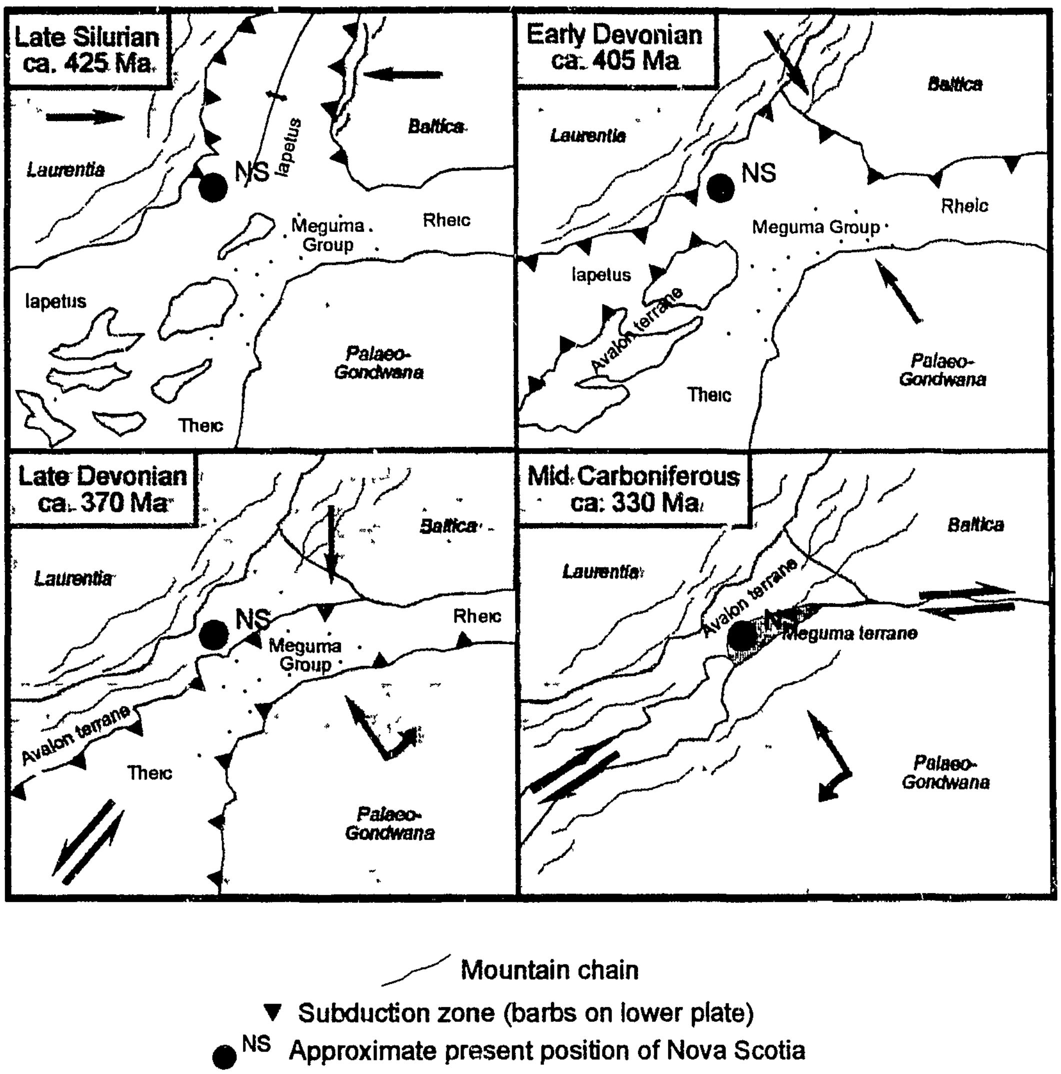

Figure 2.36. Schematic palaeogeographic reconstruction of the northern Appalachians from the Late Silurian to the Carboniferous. The positions of the continents, terranes, and oceans were compiled from Rast and Skehan (1993), Kent and Keppie (1988), and Hatcher (1988) See the text for details.

1993a) necessitate only the northwesterly obduction of Meguma lithologies onto the Avalon terrane along the Cobequid-Chedabucto Fault (Mawer and White, 1987). However, Keen et al. (1991) recently interpreted northerly-dipping mantle reflectors in deep seismic reflection studies across the Gulf of Maine as remnants of subducted ocean lithosphere, and Keppie and Dostal (1991) interpreted the offshore Collector Anomaly as a potential mafic and ultramafic ophiolite preserved along the Cobequid-Chedabucto Fault. The characteristic subduction fingerprint preserved in the LDMIs apparently provides additional evidence for subduction and two competing hypotheses explain their characteristics:

(1) *Subduction associated with Avalon accretion.* Keppie (1977) initially postulated the presence of a pre-Acadian, southeasterly dipping subduction zone beneath the Avalon and Meguma terranes and likened the Canadian Appalachians to the present-day western margin of North America. The accepted Late Palaeozoic tectonic framework for the Canadian Appalachian region suggests that this event correlates with the closure of Iapetus and Figure 2.37a illustrates the tectonic setting. Southeasterly subduction occurs beneath the Avalon terrane until the Middle Devonian and generates metasomatized mantle sources above the Benioff Zone. The Meguma terrane then overrides these sources in the Late Devonian during the closure of the Theic Ocean, and subduction-type magmas invade the Meguma crust late in the Acadian Orogeny. This hypothesis suggests that the LDMIs represent analogues of the Siluro-Devonian lamprophyric and appinitic province of southern Scotland and northern England (MacDonald et al., 1985; Rock et al., 1986; Fowler, 1988). Striking geochemical similarities between the Weekend dykes and the Scottish lamprophyres possibly support it (Tate and Clarke, 1993).

(2) *Subduction associated with Meguma accretion.* Keppie (1985) instead described an obliquely subducting Benioff Zone with northwesterly polarity beneath the Avalon terrane during the closure of the Theic Ocean (Figure 2.37b). Throughout the Late Silurian and Early Devonian, the Meguma Group lies outboard of the North American continental margin, behind the subduction

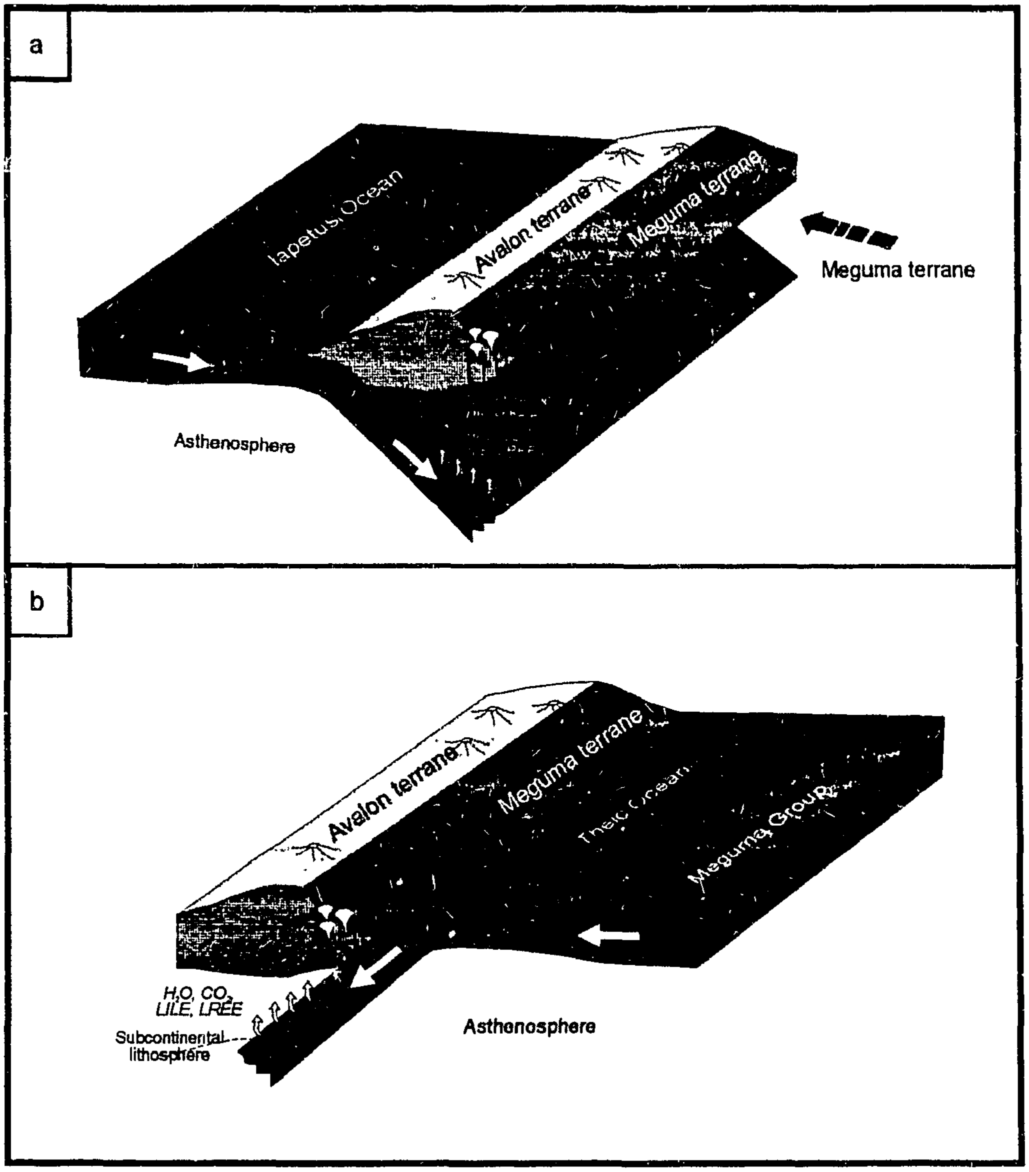

Figure 2.37. Schematic representations of two subduction-related tectonic models for the emplacement of the Meguma terrane and the formation of the Late Devonian mafic intrusions. (a) Late Silurian - Mid Devonian; (b) Mid - Late Devonian. Diagrams modified after Keppie and Dostal (1991). See the text for details.

zone. Continued closure of the Theic Ocean obducts Meguma sediments onto Avalon, and subduction-type mafic magmas intrude late in the Acadian Orogeny. This scenario implies that the LDMIs record subduction directly associated with the emplacement of the Meguma terrane, and suggests that metasomatized mantle sources formed before, during, and/or after terrane emplacement (Harris et al., 1986). The suggestion of Keen et al. (1991) of northwesterly dipping subducted ocean lithosphere beneath the Meguma terrane potentially strengthen this argument.

The wide range of enriched mantle model ages (T_{ENRICH}) for the LDMIs precludes any attempts to evaluate these hypotheses because of the small time gap in the Mid-Late Devonian that separates the closure of the Iapetus and Theic oceans. Young model ages (circa 370 Ma) may reflect mantle metasomatism and partial melting immediately prior to Meguma emplacement, or old model ages (circa 1 Ga) may indicate metasomatic contributions from Proterozoic ocean lithosphere. If subduction occurred immediately prior to the Acadian Orogeny then the second hypothesis provides the simplest explanation for the subduction fingerprint, and it supports the interpretations of Keen et al. (1991) and Keppie and Dostal (1991). However, both Wyman and Kerrich (1989) and Hart (1988) agree that the subcontinental mantle represents an isolated yet long-lived repository for miscellaneous mantle signatures generated during enrichment events. Also, Johnson (1987) documented modern calc-alkaline magmatism without active subduction in western Melanesia that supports this suggestion. It is, therefore, possible that the LDMIs record a much older subduction event; perhaps they record subduction associated with an inboard Appalachian terrane.

Penecontemporaneous mafic lithologies in the Avalon terrane do not have the subduction signature that exists in the LDMIs. Lithologically similar gabbros, diorites, and kersantites intruded along the Cobequid-Chedabucto fault at circa 360 Ma (J. Nearing, pers. comm., 1994), and mafic volcanics with unconstrained Middle Devonian-Carboniferous ages occur in the McAras Brook, Fountain Lake, and Fisset Brook Groups of Cape Breton Island (Dostal et al., 1983). However, petrogenetic studies indicate that these rocks have tholeiitic and alkaline intraplate compositions, and they probably relate to Alleghanian transtensional rifting that occurred after the accretion of the Meguma terrane (Dostal et al., 1983; Figure 2.36). Wones and Sinha (1988) and Wiebe (1993) also documented similar scenarios for Late Devonian mafic intrusions in the Avalon Zone to the southwest. Emplacement of the Weekend dykes occurred along late-Acadian shear fractures, and if the other LDMIs mimic this behaviour, then the formation of Acadian crustal weaknesses provides an explanation for their intrusion into the thickened Meguma crust after terrane accretion (Chapter 1; Section 4). Their distinctive compositions may reflect a localized source region that lies only beneath the MZ.

2-7. Summary and Conclusions

LDMIs in the MZ all crop out as variably coarse-grained gabbros, diorites, and lamprophyres with plug-like or dyke-like morphologies. Currently recognized bodies occur in the Meguma Group metasediments and within the peraluminous granitoid batholiths. Their lack of deformation and discordant field relationships with the Meguma Group distinguish them from the Ordovician and Early Silurian mafic intrusions, whereas their amphibole and biotite-bearing mineral assemblages separate them from the Early Jurassic intrusive magmatism. They have similar hydrous mineral assemblages and similar mineral compositions that suggest a genetically-related suite of intrusions, and U-Pb and $^{40}Ar/^{39}Ar$ geochronology constrains their intrusion to either circa 376 Ma or circa 380-370 Ma, respectively. All of the LDMIs have calc-alkaline or shoshonitic characteristics, and their variable major oxide compositions reflect the lithological diversity of the intrusions in outcrop. The intrusions all contain consistently high LILE and LREE (10-100 times chondrite) relative to HFSE (10-50 times chondrite), and they have variable but high initial Sr isotopic ratios (0.7043 to 0.7079) and variable εNd values (-4.36 to 3.69). However, their similar trace element spider diagram patterns also support the notion of a related suite of Late Devonian mafic bodies.

Geochemical assessment of LDMI petrogenesis suggests that: (1) the LDMIs formed by fractionation or accumulation of all their major mineral phases from similar hydrous mafic magmas. Evolution of the parent melts in the lower crust probably also induced some chemical differences, but only the Liscomb Complex parent melts experienced recognizable contamination by continental crust; (2) the parent magmas emanated from depleted upper mantle peridotite or pyroxenite, but the sources contained enrichments of incompatible trace elements and radiogenic isotopes derived from subducted ocean lithosphere. This enrichment event occurred between 0.37 and 1 Ga; (3) if subduction occurred immediately prior to the Acadian Orogeny, then the source metasomatism occurred during the closure of the Iapetus Ocean in the Early-Mid Devonian or (most likely) during the closure of the Theic Ocean in the Mid-Late Devonian. Acadian transtension during dextral terrane rotation probably reactivated crustal weaknesses and allowed Late Devonian mafic magmas to intrude the thickened Meguma crust.

Chapter 3

INTERACTION BETWEEN MAFIC AND GRANITOID MAGMAS

3-1. Introduction

Late Devonian mafic intrusions (LDMIs) in the Meguma Zone (MZ) have poorly constrained absolute ages, but the range of ages obtained from $^{40}Ar/^{39}Ar$ dating does at least partly overlap with intrusion ages for the peraluminous granitoids. In addition, four of these mafic bodies represent synplutonic intrusions and their spatial relationships with peraluminous granitoid strongly suggest the petrogenetic importance of mantle-derived mafic material. Accordingly, this chapter documents the contacts of the texturally, mineralogically, and geochemically similar synplutonic mafic bodies at Mcleods Cove, Forbes Point, and Birchtown (Figure 2.1 in Chapter 2). It ascertains the nature and extent of interaction between mafic and granitoid melts and proposes a model for hybridism. (Although the Attwoods Brook occurrence may also be synplutonic, the paucity of outcrop prevents assessment of hybridism at this locality.) The results provide the foundation for subsequent studies of enclaves (Chapter 4), and for a reinterpretation of geochemical characteristics in all MZ granitoids (Chapter 5).

3-2. Principles of Mafic-Granitoid Magma Interaction

Four related variables control the products of interaction between mafic and granitoid magmas in the plutonic environment (Frost and Mahood, 1987; Davidson et al., 1990). Their viscosities, liquidus temperatures, melt densities, and volatile contents reflect the nature and composition of the magma, its degree of crystallinity, and the level of evolution from a more primitive parent. Three examples demonstrate variations in the above parameters and describe the operative processes when a crystallizing mafic magma intrudes an evolving granitoid magma chamber:

(1) *Mingling.* Rapid synplutonic intrusion of mafic magma causes chilling and crystallization in the mafic end-member because of its strong thermal contrast with the granitoid (Campbell and Turner, 1985). Chilling forms rounded or ovoid mafic "pillows" at the contacts of synplutonic mafic sheets and dykes (Cook, 1988; Michael, 1991), somewhat analogous to the development of subaqueous pillow lavas. Cooling and contraction of the pillows produces sharp and cuspate contacts that develop crenulations in fractal arrangements on the metric, centimetric, and millimetric scales (Blundy and Sparks, 1992). The size and concavity of the crenulations increases with increasing viscosity and thermal contrasts, and with an increasing proportion of liquid remaining in the interacting magmas (Cook, 1988). If residual mafic magma exists after quenching, then the large viscosity contrast may inhibit chemical interaction (Gamble, 1979; Seaman, 1991), but the mafic pillow structures may be partially disrupted *in situ* to form relict dykes and composite dykes (Noblett and Staub, 1990). Disaggregated pillows may be transported by granitoid convection to form mafic igneous enclaves (Frost and Mahood, 1987; Vernon, 1990; Blundy and Sparks, 1992).

(2) *Commingling.* If the equilibrium temperature of the mingled mafic and granitoid magmas lies above the solidus of the mafic end-member, then the mafic pillows and granitoid magma coexist and may attempt to reach equilibrium by physically transferring phenocrysts and lithic fragments, and/or by chemical diffusion (Wiebe, 1980). Commingled pillows have diffuse contacts that show mineralogical disequilibrium phenomena and record the previous existence of localized geochemical gradients (Dorais et al., 1989). The degree of equilibrium achieved depends on the distribution coefficients for elements transferred under the conditions of interaction, and, therefore, diffusion is selective. Chemical equilibrium rarely occurs at the commingling stage.

(3) *Magma mixing (hybridism).* Under exceptional circumstances, complete homogenization of the mafic and granitoid end-members produces hybrid lithologies with intermediate mineralogical and geochemical characteristics (Zorpi et al., 1989). Convection in the granitoid may shear and

disrupt the mingled or commingled pillows and flux lithic transfers and chemical diffusion between the magmas to form a hybrid (Reid et al., 1983; Oldenburg et al., 1989). If the reaction goes to completion, macroscopically and microscopically homogenous hybrids result (Gamble, 1979), although equilibrium rarely occurs in nature (Oldenburg et al., 1989). Physical blending of the mafic and granitoid magmas occurs only when the magma temperatures are similar or high, and their viscosities are similar or low (Kouchi and Sunagawa, 1985; Sparks and Marshall, 1986). High convective velocities and extended time periods increase the likelihood of mixing (Frost and Mahood, 1987; Campbell and Turner, 1985); ideally, the mafic magma must have an evolved composition, and the granitoid magma must be superheated and convecting chaotically (Eberz and Nicholls, 1988; Wiebe, 1993).

Mingling, commingling, and mixing operate as a continuum in nature and are not clearly separated (Foster and Hyndman, 1990). If multiple synplutonic intrusions occur at the same locality, then the first intrusion chills rapidly and both heats and mingles with the granitoid host. Subsequent mafic injections over short periods of geological time cool more slowly and may further superheat the granitoid host. Assuming that the mafic and granitoid magmas have similar properties and contain few suspended crystals during interaction, then commingled rocks and ultimately homogenized hybrids may form (Grove et al., 1982; Kouchi and Sunagawa, 1985). Figure 3.1 illustrates the plausible evolutionary paths for bimodal magmatic systems and shows the products of interaction, whereas Table 3.1 summarizes previously published macroscopic and microscopic evidence for these processes.

3-3. Mingling, Commingling, and Hybridism within the Meguma Zone

3-3.1. Mingling and Commingling of the Forbes Point Synplutonic Dyke (Port Mouton Pluton)

Section 2.3 in Chapter 2 notes the arcuate nature of this body and suggests its lateral discontinuity on the basis of a ground magnetic survey. Figure 3.2 shows the synplutonic dyke

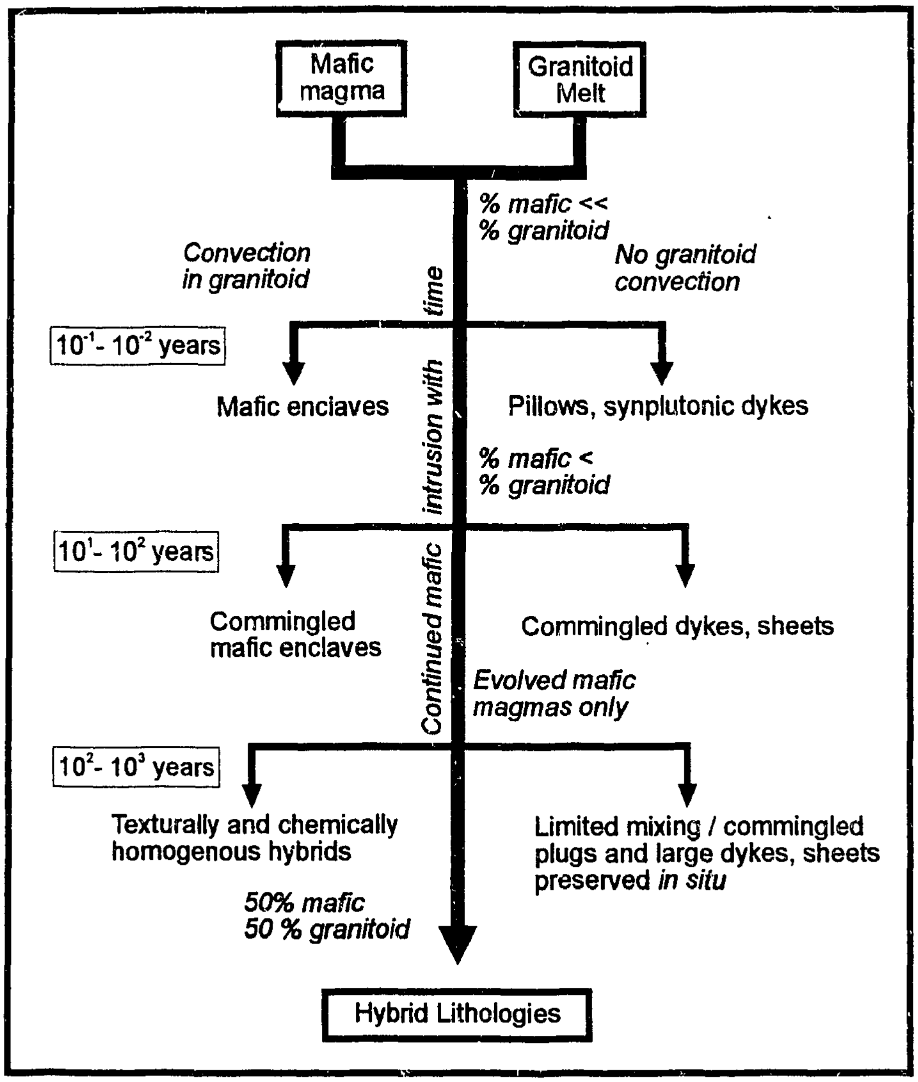

Figure 3.1. Summary of the potential evolutionary paths and products resulting from mafic-granitoid magma interaction in the plutonic environment. Timescales for interaction summarized after Lesher (1990).

Table 3.1. Published macroscopic and microtextural criteria for the recognition of mingled, commingled, and hybrid lithologies.

Evidence	Scale	Example	Reference
sharp, pillowed, or lobate contacts	cm-m	synplutonic dykes	1, 2
gradational, pillowed, or lobate contacts	cm-m	synplutonic dykes	3, 4, 5
liquid immiscibility menisci	mm-cm	mafic igneous enclaves	12, 6, 13
crenulations on pillowed contacts	mm	mafic igneous enclaves	6, 5, 7
acicular and/or spherulitic mineral phases	mm	apatite, plagioclase	8, 9, 10
hopper crystals	mm	plagioclase, amphibole, orthopyroxene	6, 11
dendritic opaque phases	mm	ilmenite and magnetite	6, 9, 11
epitaxial overgrowths and intergrowths	mm	patchily zoned plagioclase	14, 15, 7
corona textures	mm	bronzite rims enclosing plagioclase	16, 11
corona textures	mm	magnetite rims on amphibole	17, 15
ocellar felsic mineral phases	mm	amphibole or biotite rims on quartz	17, 7
synneusis textures	mm	amphibole breakdown to biotite	17, 18
corroded crystals with reaction rims	mm	rapakivi texture	15, 19, 20
oscillatory zoning and abrupt zoning	mm	in all solid solution minerals	14, 6, 17
reversed zoning	mm	albite cores with anorthite rims	14, 7
grain boundary intergrowths	mm	perthite, antiperthite, microcline	15, 11
undeformed, thermally-shattered phenocryst phases	mm	quartz, plagioclase, sphene, apatite	21, 6, 22, 23

1 = Hyndman and Foster (1988), 2 = Furman and Spera (1985), 3 = Wiebe (1980), 4 = Wiebe (1993), 5 = Cook (1988), 6 = Vernon (1990), 7 = Eberz and Nicholls (1988), 8 = Reid et al. (1983), 9 = Gamble (1979), 10 = Seaman (1990), 11 = Castro et al. (1990), 12 = Bacon and Metz (1984), 13 = Kouchi and Sunagawa (1985), 14 = Hibbard (1981), 15 = Zorpi et al. (1989), 16 = Chen et al. (1990), 17 = Blundy and Sparks (1992), 18 = Orsini et al. (1989), 19 = Dorais et al. (1989), 20 = Lindberg and Eklund (1988), 21 = Wall et al. (1987), 22 = Nakada (1991), 23 = Shearer et al. (1988).

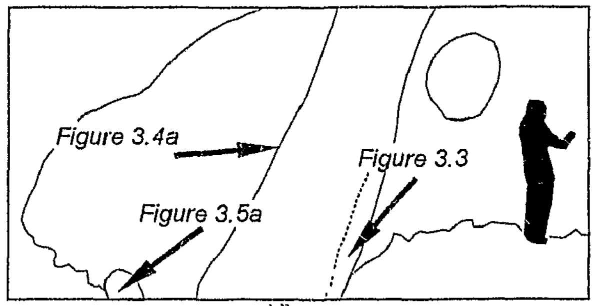

Figure 3.2. Macroscopic characteristics of the Forbes Point synplutonic dyke. Note the arcuate shape of the dyke in its tonalite host and the metric enclave at the centre of the intrusion. The easternmost contact of the dyke lies unexposed in the overburden below the tree. View to the northwest, figure approximately 1.8 m tall. See the text for details, Figure 2.8 in Chapter 2, and Figure B1.4 in Appendix B for the location of this body in the MZ.

and the surrounding tonalite of the Port Mouton Pluton (PMP). Cross-cutting relationships between the dyke and its tonalite host require that spessartite lamprophyre intruded either during or after solidification of the PMP. Detailed analysis of subtle macroscopic, microscopic, and geochemical features at this locality suggest that the dyke intruded, mingled, and commingled with magmatic tonalite.

Contact relationships with the host tonalite

The lamprophyre has an equigranular texture and a medium grain size (≤2 mm) within 20 cm of its westernmost contact with the tonalite. Where no lamprophyre pegmatite stringers obscure the dyke margins, the contact surface is sharp at the top of the outcrop, but becomes a gradational decrease in amphibole and biotite at its base (Figure 3.3). The gradational contact, in conjunction with the arcuate attitude of the dyke, suggests that it intruded partially molten granitoid. The coarse-grained (>1 cm) pegmatitic material preferentially concentrated at the lamprophyre-tonalite contact (not characteristic of any other LDMI) suggests that exceptionally high volatile contents existed in the lamprophyre magma. This feature may reflect prolonged insulation of lamprophyre by magmatic tonalite, and it probably also records magmatic and/or deuteric volatile transfers across the lamprophyre-tonalite interface after dyke emplacement.

Textural variation in the host tonalite

A sharp contact separates two textural varieties of tonalite in the vicinity of the synplutonic dyke (Figure 3.4a). Normal tonalite of Unit 1 contains an equigranular quartzo-feldspathic groundmass (1.5 mm) with panidiomorphic phenocrysts of rounded oligoclase (An_{20}) up to 5 mm long (Douma, 1988), which have patchy and reversed zoning patterns (Figure 3.4b). In contrast, coarse tonalite immediately adjacent to the dyke contains patchily zoned and reversely zoned hypidiomorphic andesine (An_{45}) and rounded quartz grains up to 1 cm in diameter. All felsic minerals appear resorbed and have rims of biotite, chlorite, and

Figure 3.3. The western contact of the Forbes Point dyke at the base of the outcrop. Note the irregular chilled margin and the gradational decrease in amphibole abundance over approximately 20 cm. View to the northwest, hammer handle 1 m long. See Figure 3.2 for the location of this photograph.

a

b

c

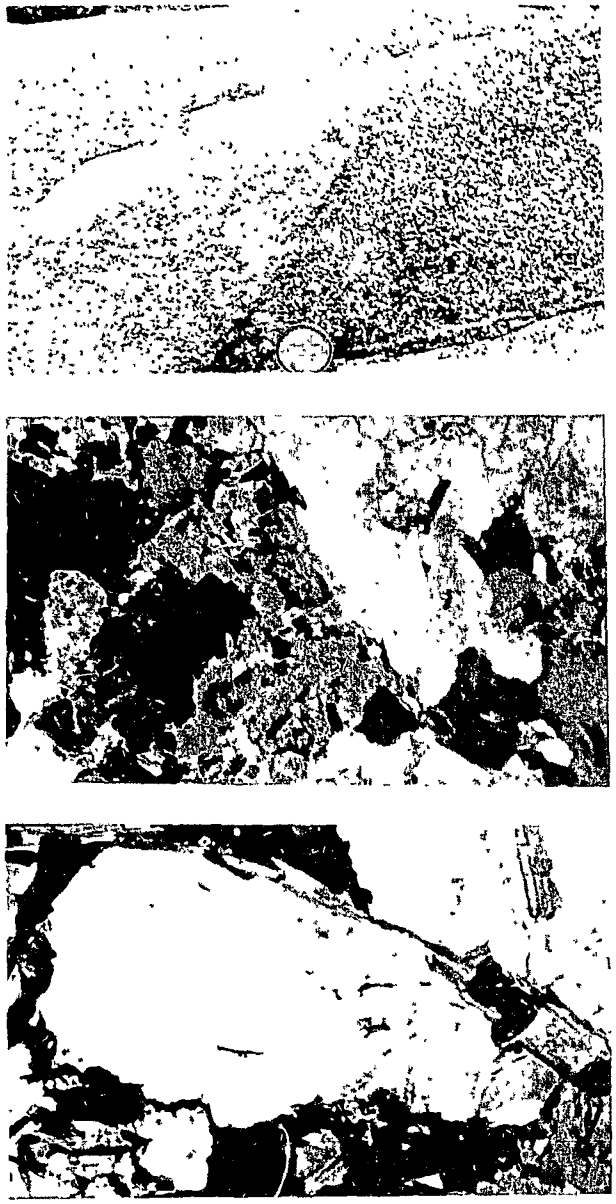

Figure 3.4. Characteristics of the tonalite at Forbes Point. (a) The sharp contact between medium tonalite (left) and coarse tonalite (right) to the west of the synplutonic dyke. View to the northwest, lens cap 7 cm diameter. See Figure 3.2 for the location of this photograph; (b) Photomicrograph of the normal medium-grained tonalite. Note the inequigranular texture typical of granitoid rocks and the lack of ocellar grains. Field of view 12 mm, XPL; (c) Photomicrograph of the coarse-grained tonalite adjacent to the dyke. Note the large quartz ocellus with a biotite mantle, and the magnesio-hornblende crystal to the lower right. Field of view 12 mm, XPL.

minor magnesio-hornblende in an ocellar arrangement (Douma, 1988; Figure 3.4c). Coarsening of the tonalite occurs only adjacent to the synplutonic dyke. The resorption of plagioclase and quartz suggests that it formed during heating (or superheating?) in response to dyke intrusion and the magnesio-hornblende and strongly zoned feldspars suggest that chemical modification by the lamprophyre also occurred. If the coarse tonalite underwent an extended magmatic history because of the lamprophyre dyke, then the sharp contact between the tonalite subunits probably preserves the limit of heating.

Lamprophyre pillow development

Approximately 2 m west of the main dyke exposure (Figure 3.2), a small and irregular patch of pillowed lamprophyre occurs as an inclusion within the fine-grained tonalite host (Figure 3.5a). The equidimensional pillows range in size from 1 cm to 20 cm, and the lamprophyre has a fine grain size and an equigranular texture. The pillow contacts are sharp and an irregular carapace of "aplitic" tonalite surrounds them. Pillowed lamprophyre has an equigranular groundmass consisting of quartz, patchily zoned and hypidiomorphic plagioclase, and biotite, enclosing variolitic and acicular apatite inclusions (Figure 3.5b). Clusters of biotite up to 3 mm in diameter represent either glomerophenocrysts or a magmatic reaction phenomenon; if biotite is more stable during mingling, then perhaps the biotite clusters pseudomorph pre-existing hornblende (justified below). The equigranular groundmass and variolitic apatites in the pillowed material probably record rapid quenching of the lamprophyre against the tonalite (Seaman, 1990), whereas the presence of "aplitic" backveins penetrating lamprophyre pillows demands the fluid and magmatic nature of the host during interaction. Intrusion of lamprophyre into magmatic tonalite probably disrupted the pillows from the main dyke, and the sharp pillow contacts suggest that only minor chemical diffusion accompanied mingling.

a

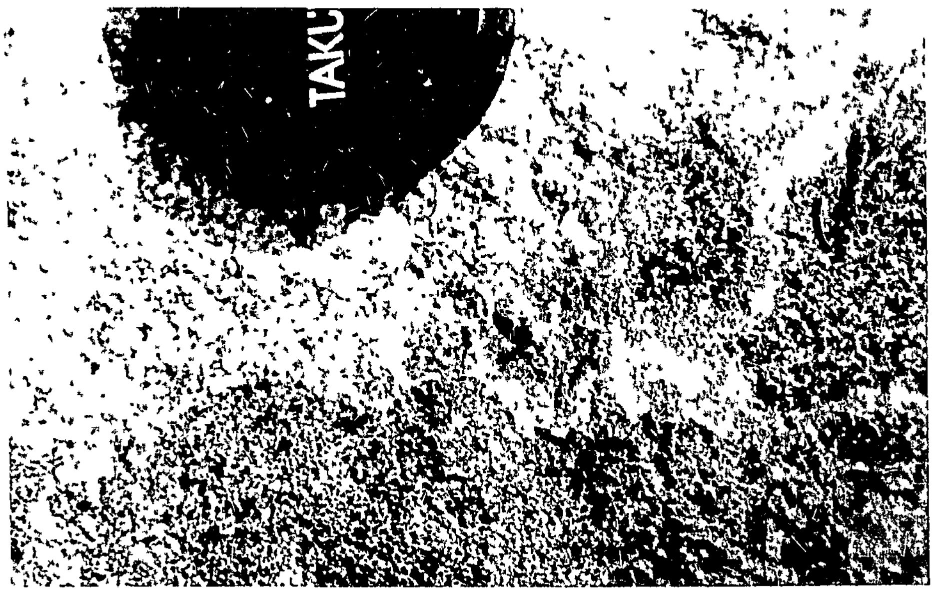

b

Figure 3.5. Characteristics of the pillowed lamprophyre at Forbes Point. (a) 10-20 cm lamprophyre pillows with sharp and cuspate contacts in aplitic tonalite to the west of the lamprophyre dyke. View to the north, lens cap 7 cm diameter. See Figure 3.2 for the location of this photograph; (b) Photomicrograph of the pillowed lamprophyre contact. The pillowed contact is irregular and shows a peripheral chilled margin of aligned biotite crystals. Note the absence of amphibole in the lamprophyre. Field of view 1 cm, PPL.

Petrographic aspects of the igneous enclave

The metric enclave in the main dyke (Figure 3.2) has a sharp contact with the lamprophyre and a leucocratic and equigranular appearance. It consists of fine-grained (<0.5 -1 mm) feldspathic lamprophyre with elongate hornblende phenocrysts (14.1%) in a granoblastic groundmass containing panidiomorphic and hypidiomorphic andesine (37.5%), biotite (34%), and quartz (12.6%) (Figure 3.6). Randomly distributed biotite clusters up to 5 mm occur throughout the enclave, and unusually high concentrations of sphene (1.8%) are distributed in the groundmass. Compared with the main dyke, the enclave has similar concentrations of biotite, less amphibole, and more sphene. The fine quartzo-feldspathic groundmass and macroscopic biotite clusters impart characteristics similar to those of the pillowed lamprophyre and the lamprophyre at Mcleods Cove (considered below). If the biotite clusters pseudomorph amphibole, then the enclave probably also represents mingled or commingled lamprophyre. Its occurrence within the main dyke suggests that mafic-granitoid interaction occurred at depth prior to the intrusion of the dyke, probably during the upward penetration of lamprophyre through magmatic tonalite.

Geochemical characteristics

The composition of the Forbes Point dyke is similar to the other LDMIs, but it shows significant chemical differences. Despite the primitive chemical characteristics of this lithology (MgO 16.41 wt.%, Cr 957 ppm), the lamprophyre contains shoshonitic concentrations of K_2O (4.2 wt.%), and it has P_2O_5 (0.79 wt.%) approximately twice their abundances within non-synplutonic LDMIs (Appendix B-3). Concentrations of Ba (817 ppm), Rb (167 ppm), Sr (420-598 ppm), Y (28 ppm), Zr (135-248 ppm), and LREE (e.g. Ce 61 ppm, Nd 33 ppm) also occur at levels above those of other non-synplutonic mafic intrusions, although the dyke contains similar concentrations of HREE. Slight increasing of the initial $^{87}Sr/^{86}Sr$ ratio (0.70509) towards the value for the tonalite ($^{87}Sr/^{86}Sr_i$ 0.70630), a negative εNd value (-0.96), and the physical evidence for

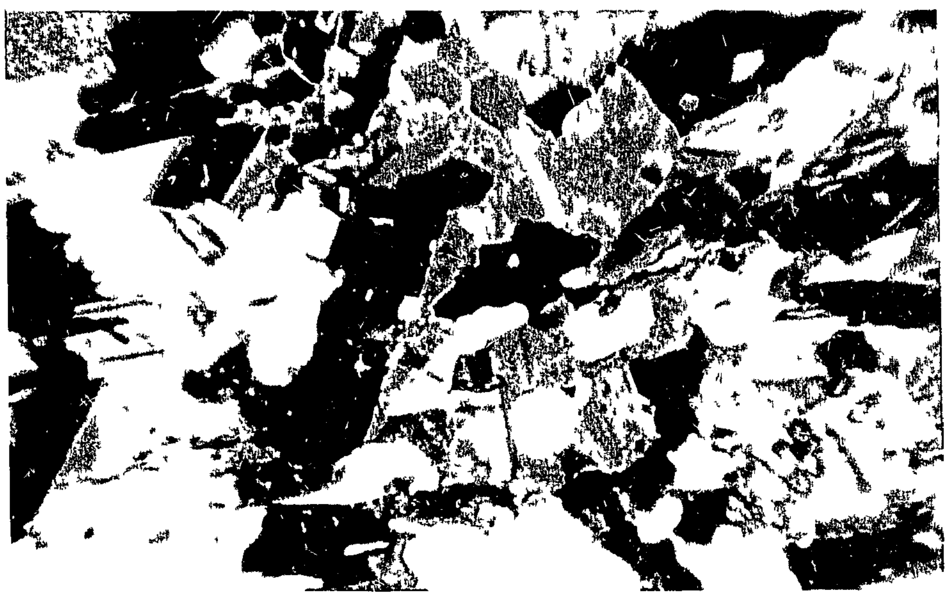

Figure 3.6. Photomicrograph of the inequigranular texture in the enclave at Forbes Point. Note the equigranular patches in the groundmass, the patchily zoned hornblende and plagioclase phenocrysts, and the abundant rounded sphene grains. Field of view 1 cm, XPL.

magma mingling at this locality, strongly suggest a contamination origin for these differences.

3-3.2. The Commingled Contact of the Mcleods Cove Synplutonic Sheet (Port Mouton Pluton)

Four spatially associated lamprophyres crop out at Mcleods Cove (Figure 3.7). Three 10-15 m long lamprophyric rafts and numerous centimetric enclaves occur as disrupted inclusions within coarse tonalite of Unit 1 and medium-grained monzogranite of Unit 8 (Douma, 1988). The largest body is 84 m long and it has a pillowed basal contact with the host tonalite (Figure 3.8). Disruption of the lamprophyre by numerous monzogranitic, leucomonzogranitic, and pegmatitic dykes assigned to Units 7, 8, and 9 by Douma (1988), unequivocally constrains the synplutonic intrusion of this sheet; dyking probably disrupted the smaller lamprophyres from it. Detailed petrographic examination of the pillowed lamprophyre-tonalite contact indicates that lamprophyre and tonalite commingled at Mcleods Cove.

Characteristics of lamprophyre close to the contact

Pillows at the basal contact of the lamprophyre range in size from 5 cm to 1 m and lie within "aplitic" tonalite, similar to the pillows at Forbes Point. Figure 3.9 shows details of a typical lamprophyre pillow at Mcleods Cove and emphasizes its important features. Compared with lamprophyre from the centre of the intrusion (described and photographed in Section 2.4 of Chapter 2), pillowed marginal lamprophyre has a fine (0.1 mm) grain size and an equigranular texture (Figure 3.10) that contains amphibole (23.6%), biotite (28.7%), plagioclase (24.1%), microcline (9.3%), and quartz (11.3%). Close to the contact, biotite clusters develop around internally aggregated amphibole grains (Figure 3.11a) and subrounded quartz ocelli with amphibole rims appear in the groundmass (Figure 3.11b). Biotite occurs as weakly pleochroic crystals ([Mg/(Mg+Fe)] = 0.62-0.69) or as strongly pleochroic grains with zircon inclusions

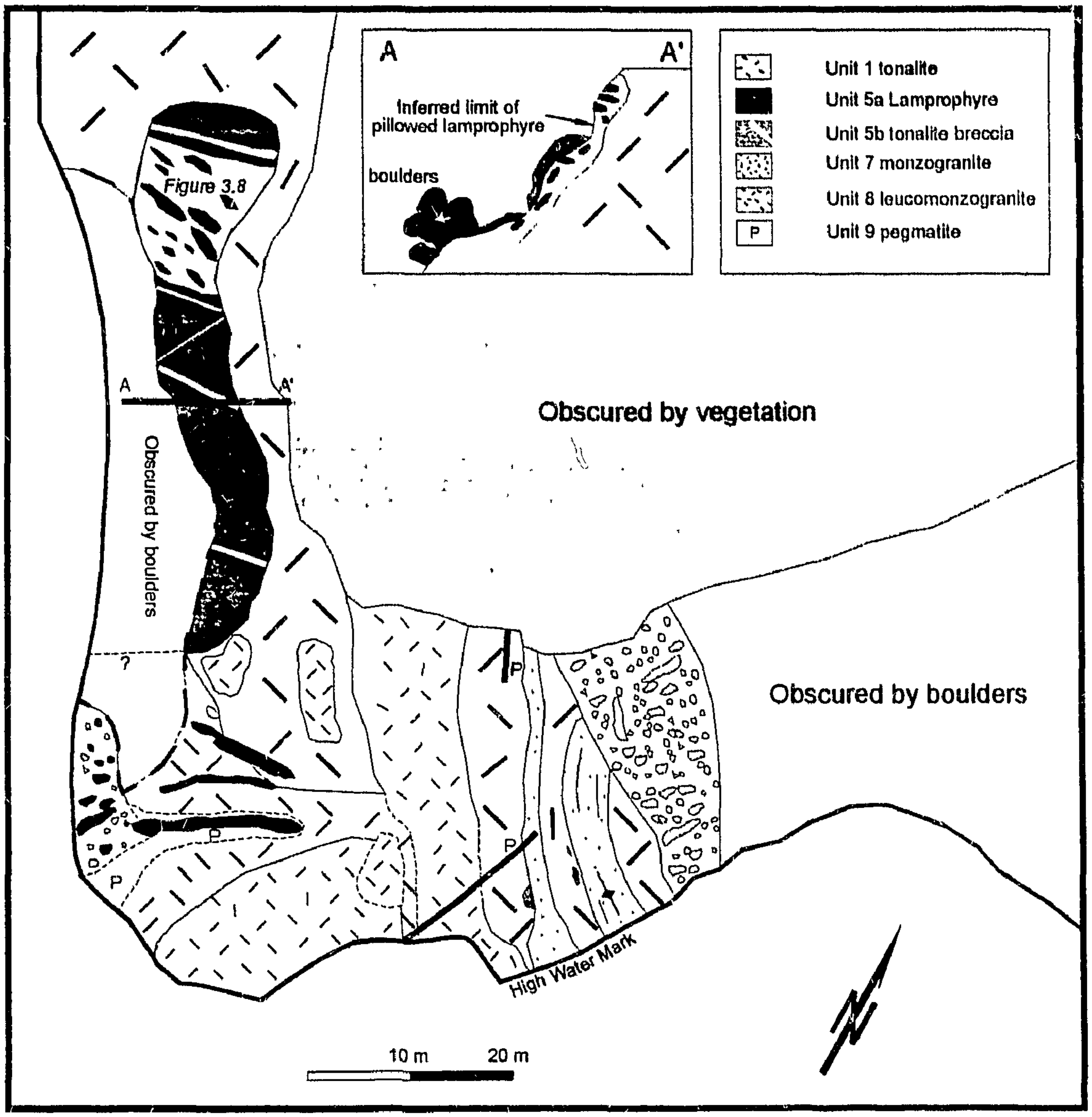

Figure 3.7. Detailed geological map of the Mcleods Cove area. The high water mark is approximate and the lithologic nomenclature is after Douma (1988). See Figure B1.4 in Appendix B for the location of this map in the MZ.

Figure 3.8. Well-developed lamprophyre pillows at the base of the Mcleods Cove synplutonic sheet. Note that the adjacent pillows impinge upon each other, which constrains their formation prior to the crystallization of the aplitic tonalite host. Plan view, notebook 16 cm long. See Figure 3.7 for the location of this photograph, and also Figure 2.11 in Chapter 2.

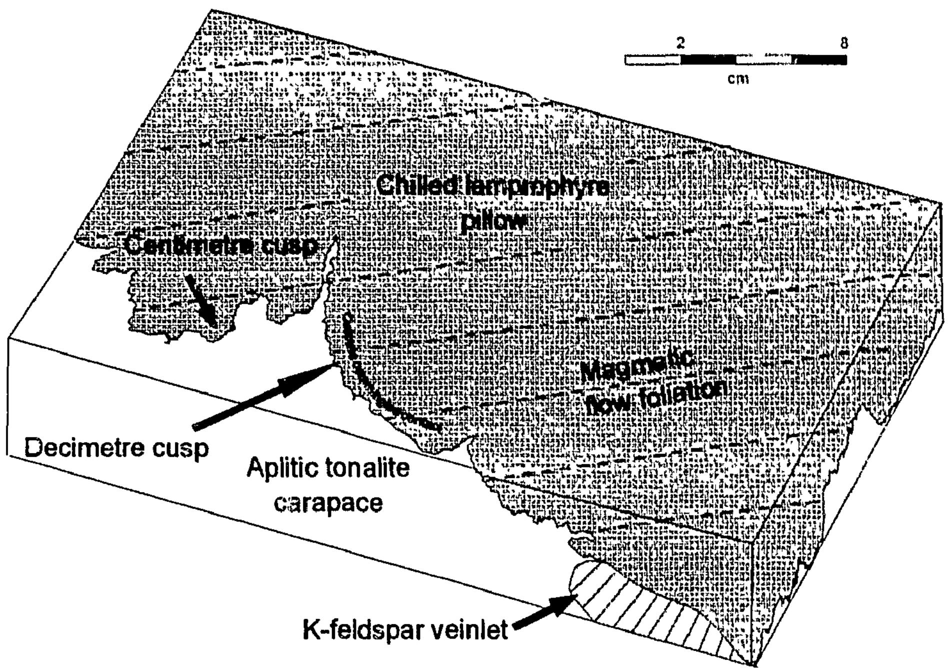

Figure 3.9. Three-dimensional reconstruction of the macroscopic features shown by pillows at Mcleods Cove. Note the discontinuous K-feldspar veinlet.

([Mg/(Mg+Fe)] ≤0.55) (Figure 3.11c), and plagioclase oikocrysts show distinct cores of andesine (An_{36}) with oscillatory or patchily zoned envelopes of oligoclase (An_{21}) (Figure 3.11d). Cracked sphene and acicular apatite crystals reach 2-4% of the mode (Figure 3.11e).

Observations at the contact

A 2 cm wide veinlet discontinuously occupies the pillow contact and contains tabular K-feldspar crystals oriented with their longest crystallographic axes perpendicular to the pillow margins. In the absence of this vein, the contact supports both centimetric and millimetric satellite crenulations (Figure 3.9) and it consists of a grain size contrast between the "aplitic" tonalite and the lamprophyre (Figure 3.12a). The tonalite at the contact contains abundant patchily zoned and reversely zoned plagioclase phenocrysts and equant microcline shows myrmekite at its grain boundaries with quartz. Fractured garnets and muscovite up to 1 mm occur with rounded magnetite blebs, and with both the weakly pleochroic biotite (found in the tonalite) and strongly pleochroic biotite (found in the lamprophyre). Allotriomorphic amphibole, sphene, and millimetric lamprophyre lithoclasts also occur in this contact-proximal region. Apatite locally accounts for at least 5% of the "aplitic" tonalite within approximately 0.8 mm of the contact. They range from stubby and equant hexagonal crystals with 5:1 aspect ratios observed elsewhere in the tonalite host, to highly acicular, cracked, and skeletal examples with up to 50:1 aspect ratios (Figure 3.12b).

Comparisons with Forbes Point

Lamprophyre pillows at Mcleods Cove are more abundant than those at Forbes Point, and they generally have larger sizes that suggest interaction between fluid magmas. Preservation of amphibole-biotite synneusis textures confirms the instability of amphibole during interaction at both localities, and the diffuse pillowed contact suggests that commingling allowed physical transfers and chemical diffusion to occur after mingling. The existence of siliceous ocelli

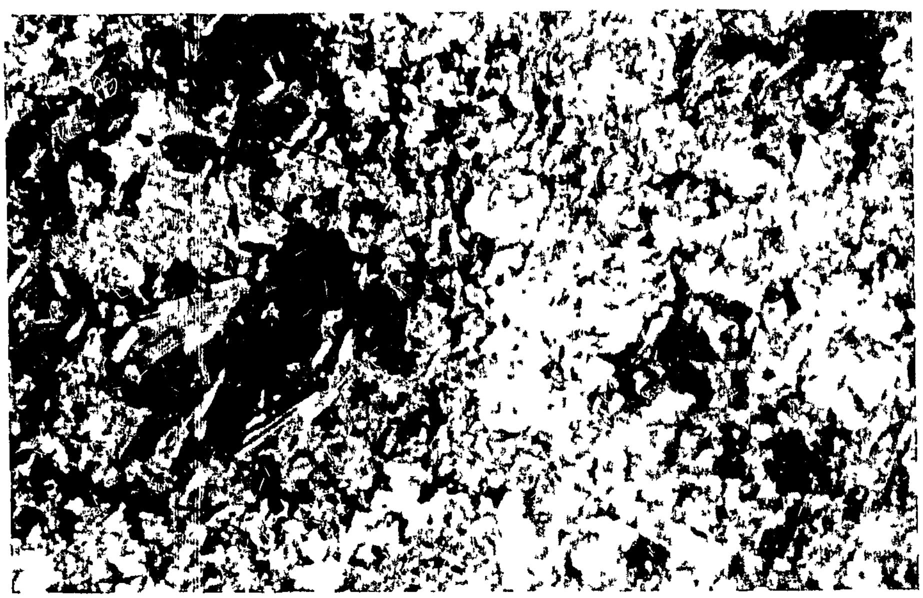

Figure 3.10. Photomicrograph of the pillowed lamprophyre at Mcleods Cove. Note the fine-grained and equigranular groundmass, and the replacement of amphibole by biotite, sphene, quartz, and magnetite. Figure 2.11 in Chapter 2 shows the texture of the lamprophyre away from the contact. Field of view 1 cm, XPL.

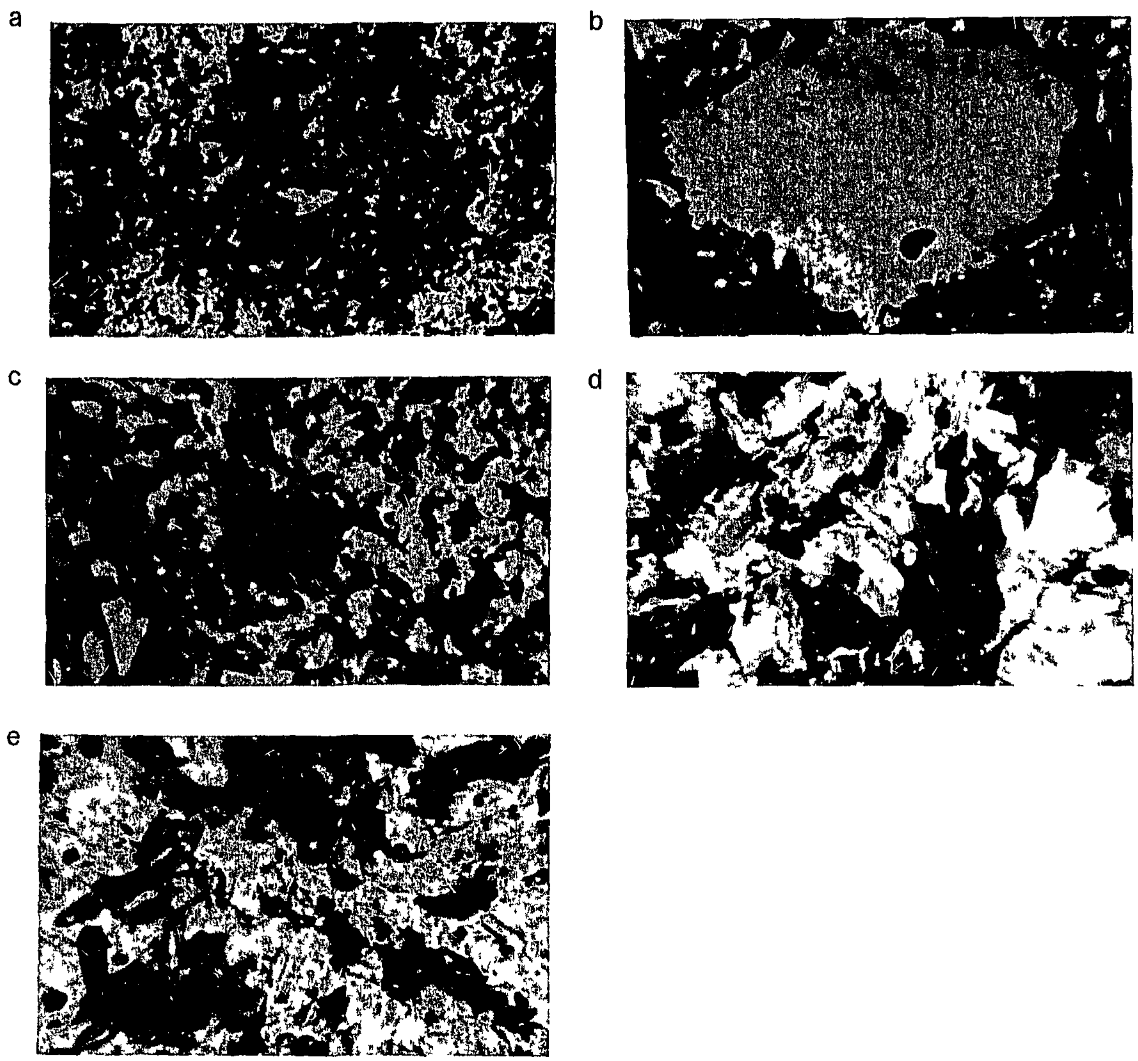

Figure 3.11. Textural disequilibrium features in pillowed lamprophyre at Mcleods Cove. (a) Amphibole-biotite synneusis clusters. Field of view 1cm, XPL; (b) A large quartz ocellus with a discontinuous rim of amphibole. Field of view 3 mm, XPL; (c) Two distinct biotite morphologies. The large, dark grain in the centre has apatite inclusions and pleochroic haloes and has the composition of tonalitic biotite. The smaller, more euhedral biotites crystallized from the lamprophyre magma. Field of view 6 mm, XPL; (d) Patchily zoned oikocrysts of plagioclase associated with resorbed amphiboles. Field of view 3 mm, XPL; (e) Acicular apatite and sphene euhedra at the contact. Field of view 3 mm, PPL.

a

b

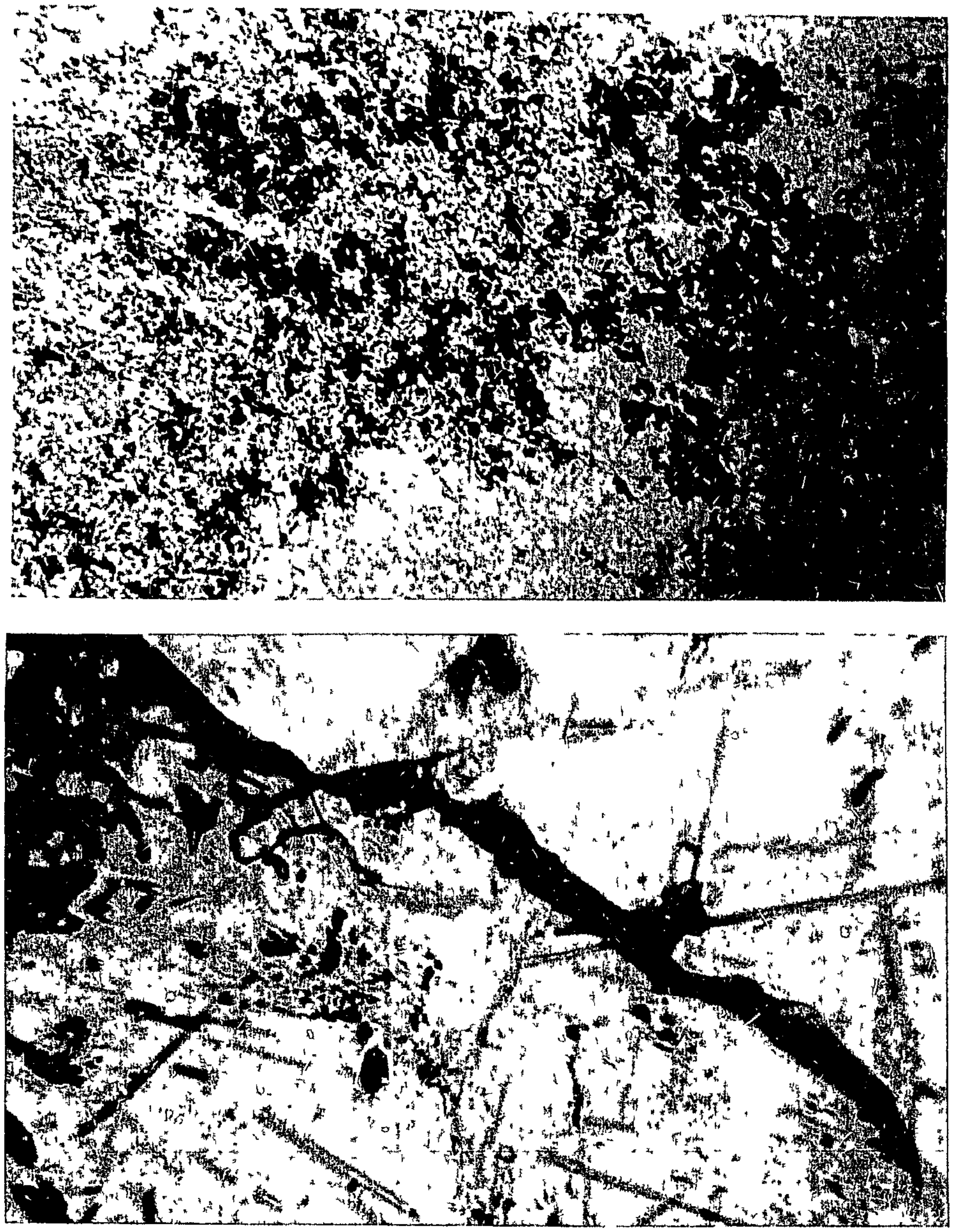

Figure 3.12. Photomicrographs of the pillowed lamprophyre-tonalite contact at Mcleods Cove. (a). The irregular, cuspate morphology of the contact. Note the aplitic texture of the host tonalite. Field of view 2 cm, PPL; (b) Highly acicular apatites with fractures in aplitic tonalite at the contact. Field of view 0.5 mm, PPL.

and evolved tonalitic biotite in the lamprophyre suggests that the tonalite contributed quartz and biotite crystals to the lamprophyre (Vernon, 1990). The primitive lamprophyric biotite, resorbed amphibole, and the lithified fragments of lamprophyre in the "aplitic" carapace indicate that mechanical transfers also occurred from the lamprophyre to the tonalite. Plagioclase zoning in the lamprophyre at the contact also ranges between the compositions of lamprophyric and tonalite plagioclase away from the contact. Nucleation of acicular apatite and sphene close to the contact records rapid undercooling of the lamprophyre in the tonalite, and it probably also records the previous existence of phosphorus and titanium gradients between the two magmas (Reid et al., 1983). The K-feldspar vein at the pillowed contact may record a chemical gradient for potassium.

Figure 3.13 shows that pillowed lamprophyre at Mcleods Cove has a more evolved mode than the putative mingled enclave and pillowed lamprophyre at Forbes Point, and it lies between the compositions of the Forbes Point lamprophyre and the Unit 1 tonalite. Geochemistry corroborates the textural evidence for more advanced interaction at Mcleods Cove. The lamprophyre contains slightly lower MgO (13.27 wt.%) values, and slightly higher Al_2O_3 (12.34 wt.%) values than the Forbes Point body, which probably reflect the more advanced development of groundmass quartzo-feldspathic minerals close to the contacts. The high CIPW-normative K-feldspar value (27%) reflects K_2O concentrations similar to Forbes Point (4.39 wt.%), and P_2O_5 (0.86 wt.%) and Rb (132 ppm) also exist at Forbes Point concentrations. However, Ba (1920 ppm), Sr (2567 ppm), and Zr (421 ppm) occur at levels at least two orders of magnitude above those at Forbes Point, and LREEs are more fractionated (La/Lu = 317) than in all other LDMIs (La/Lu <161). Figure 3.14 shows that Mcleods Cove lamprophyre also has a relatively high initial $^{87}Sr/^{86}Sr$ ratio (0.70567) that is similar to the value for the Forbes Point body. Both lamprophyres have isotopic compositions between the tonalite and the non-synplutonic LDMIs and they plot away from the mantle array.

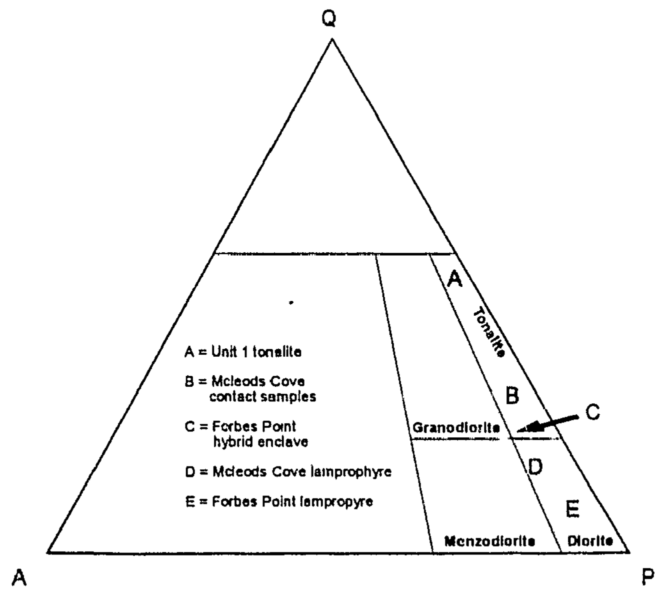

Figure 3.13. Modal Quartz-K-feldspar-Plagioclase (QAP) classification for the Forbes Point and Mcleods Cove samples. Comparative data for the Unit 1 tonalite of the Port Mouton Pluton is from Douma (1988). Q+A+P = 100 after Streckeisen (1976).

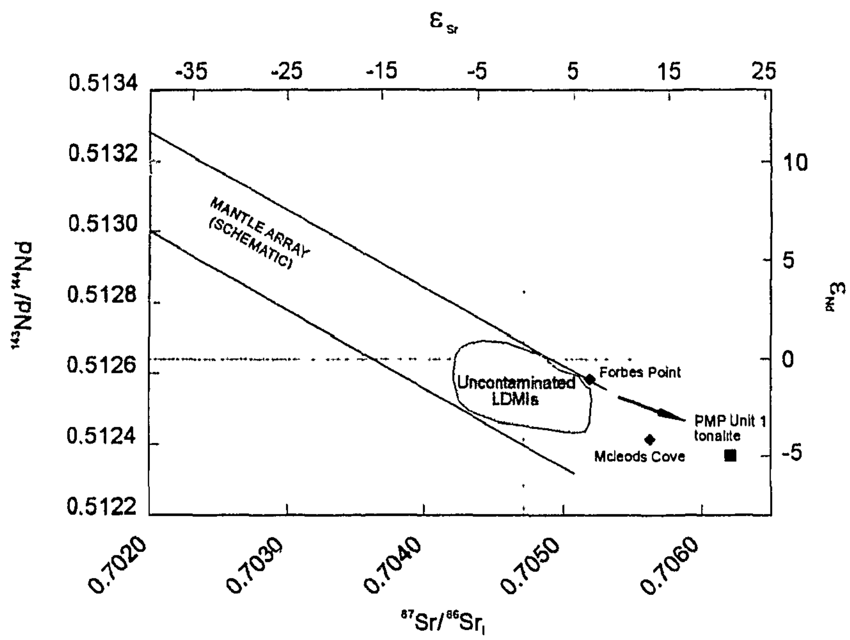

Figure 3.14. Plot of initial $^{87}Sr/^{86}Sr$-$^{143}Nd/^{144}Nd$ for the Forbes Point and Mcleods Cove lamprophyre and the Unit 1 tonalite. The lamprophyres lie between the composition of the tonalite and the other LDMIs. All data recalculated to t = 370 Ma.

3-3.3. Open System Mixing at Birchtown (Shelburne Pluton)

Recent quarrying at Birchtown reveals the nature of the contact between the synplutonic diorite and its granodiorite host. No sharp lithologic discontinuity marks this boundary, which instead consists of a gradational contact zone of tonalite exposed discontinuously over approximately 50 m. Figure 3.15 shows a detailed geological map of the quarry and marks the contact zone transect (CZT). The field relationships suggest that the tonalite represents either a diorite fractionate or a diorite-granodiorite hybrid. Documentation of the modal, mineral chemical, and whole-rock geochemical variations across the gradational CZT suggest that open-system hybridism between granodioritic and dioritic magmas generated the tonalites.

Lithologic variation across the CZT

Sampling with circa 5 m spacing extends from the Birchtown diorite, across the CZT, and into a granodiorite phase of the Shelburne pluton. Table 3.2 contains the petrographic and modal characteristics of each sample and Section 2.2 of Chapter 2 describes the diorite in detail. The Shelburne Pluton (SP) granodiorite has a medium to coarse (1-4 mm) grain size and an equigranular to subporphyritic texture. It consists of hypidiomorphic intergrowths of plagioclase and K-feldspar, biotite, and quartz, and contains accessory muscovite, garnet, apatite, and zircon (Rogers, 1984). Little textural or modal variation occurs within this lithology. The tonalite instead represents a heterogeneous unit that is texturally intermediate between the diorite and the granodiorite (Figure 3.16). It has variably coarse grain sizes (2-7 mm) and contains a hypidiomorphic intergrowth of plagioclase, amphibole, biotite, and quartz. A magmatic flow foliation of inequidimensional biotite and plagioclase occurs intermittently throughout the unit, and coarse leucocratic patches probably represent fractionated tonalitic material (Figure 3.17). All tonalite samples have modal compositions between those of the granodiorite and the diorite, but they show significant skewness towards the diorite (Figure 3.18a); they also overlap with the mingled and commingled facies at Forbes Point and Mcleods Cove. De Albuquerque (1977)

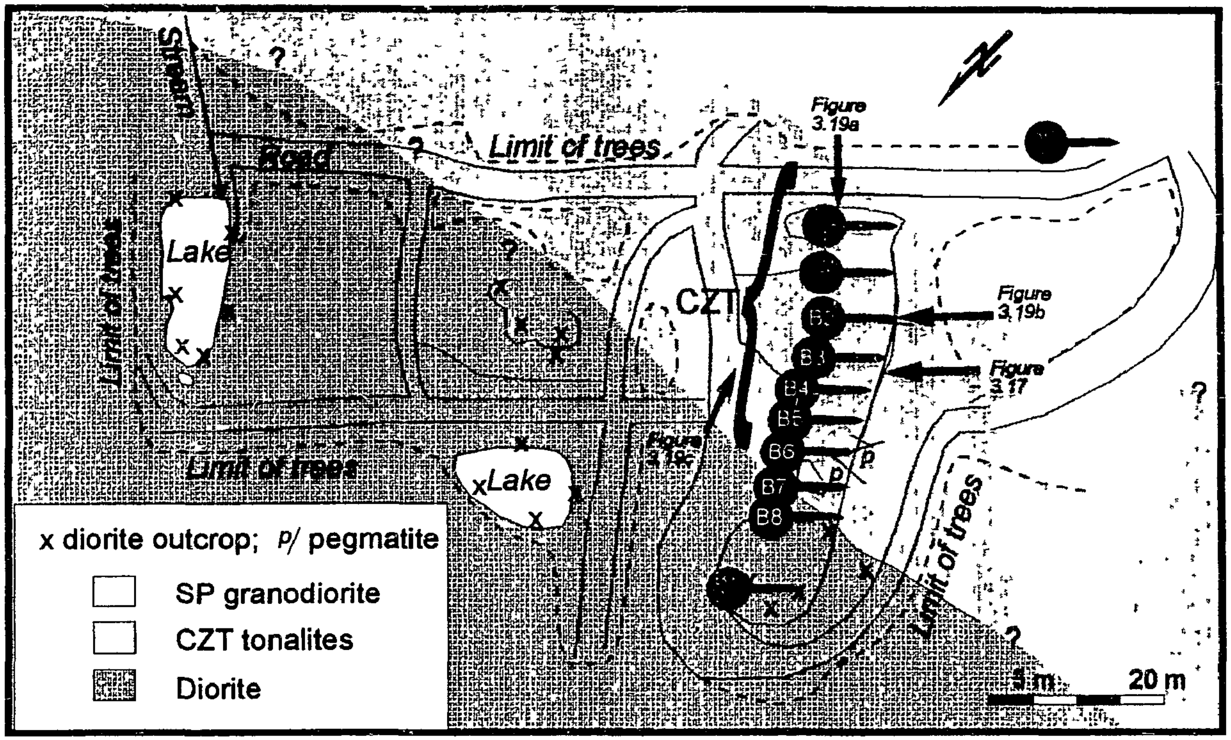

Figure 3.15. Geological sketch map of the Contact Zone Transect in Birchtown Quarry, showing the sample locations. See Figure B1.3 in Appendix B for the location of this map in the Meguma Zone.

Table 3.2. Macroscopic, textural, and modal characteristics of the Contact Zone Transect tonalite samples.

Sample	Lithology	Colour	Grain size	Texture	Mode	QAP	C.I.
SPGD	Granodiorite	Bu	M-C (1-3 mm)	Equ SuP	$Qtz_{32.9}\ Kfs_{2.8}\ Pl_{52\,1}\ Ms._{48}\ Bt_{7\,4}$	$Q_{32.9}A_{2.8}\ P_{52.1}$	7.4
BQ-4	Tonalite	LG	C (0.5-5 mm)	Ine SuP	$Qtz_{15\,35}\ Kfs_{2.7}\ Pl_{72.5}\ Ms_{0\,3}\ Bt_{8\,2}\ Ap_{0\,45}\ Hbl_{0\,5}$	$Q_{15\,35}\ A_{2.7}\ P_{72.5}$	8.7
BM-6	Tonalite	LG	C (0.5-5 mm)	Ine SuP	$Qtz_{12.8}Kfs_{0\,1}Pl_{49.5}\ Ms_{0\,5}Bt_{22.3}Ap_{0\,3}\ Hbi_{14\,5}$	$Q_{12\,8}\ A_{0\,1}\ P_{49\,5}$	36.8
B2	Tonalite	LG	C (0.5-7 mm)	Ine SuP	$Qtz_{12.7}\ Kfs_{1\,6}Pl_{48\,9}\ Bt_{25\,2}Ap_{0.3}\ Hbl_{11.3}$	$Q_{12\,7}\ A_{1\,6}\ P_{48\,9}$	36.5
B3	Tonalite	DG	C (0.3-5 mm)	Ine Por	$Qtz_{27}\ Plg_{40}\ Bt_{27}\ Ap_{2}\ Hbl_{4}$	$Q_{27}\ A_{0}\ P_{40}$	31
B4	Tonalite	DG	C (1-4 mm)	Equ Por	$Qtz_{15}\ Kfs_{1}\ Pl_{44}\ Bt_{14}\ Ap_{1}\ Hbl_{25}$	$Q_{15}\ A_{1}\ P_{44}$	39
B5	Tonalite	DG G	C (1-4 mm)	Equ Por	$Qtz_{11\,9}\ Pl_{31\,2}\ Bt_{25\,4}\ Ap_{0.2}\ Hbl_{31\,3}$	$Q_{11\,9}\ A_{0}\ P_{31\,2}$	56.7
B7	Tonalite	LG	C (0.5-2 mm)	Equ Por	$Qtz_{17\,7}\ Pl_{51\,55}\ Bt_{30\,2}\ Ap_{0.25}Hbl_{0\,3}$	$Q_{17\,7}\ A_{0}\ P_{51.55}$	30.5
B8	Diorite	G	C (0.5-1.5 mm)	Ine Por	$Qtz_{12}\ Pl_{28}\ Ab_{1}\ Bt_{17}\ Hbl_{42}$	$Q_{12}\ A_{1}\ P_{28}$	59
BIR-20	Diorite	G	C (0.5-5 mm)	Ine Por	$Qtz_{13\,41}\ Kfs_{0.29}\ Pl_{21\,4}\ Bt_{23\,9}\ Hbl_{41}$	$Q_{13\,41}\ A_{0.29}\ P_{21\,4}$	64.9

Modal analyses are averages of at least three thin sections (approximately 4500 counts per thin section) using the Dalhousie Link image analysis system and the methodology of Van der Plas and Tobi (1965). Lithological nomenclature (Q+A+P = 100) after Streckeisen (1976) and mineralogical abbreviations after Kretz (1983). C = coarse-grained, M-C = medium-coarse-grained. Bu = buff, LG = light grey, DG = dark grey, G = green, Gr = grey. Equ = equigranular, SuP = subporphyritic, Por = porphyritic, In = inequigranular. C.I. (colour index) is the sum of modal amphibole, biotite, and muscovite. See Figure 3.15 for the sample locations in the CZT.

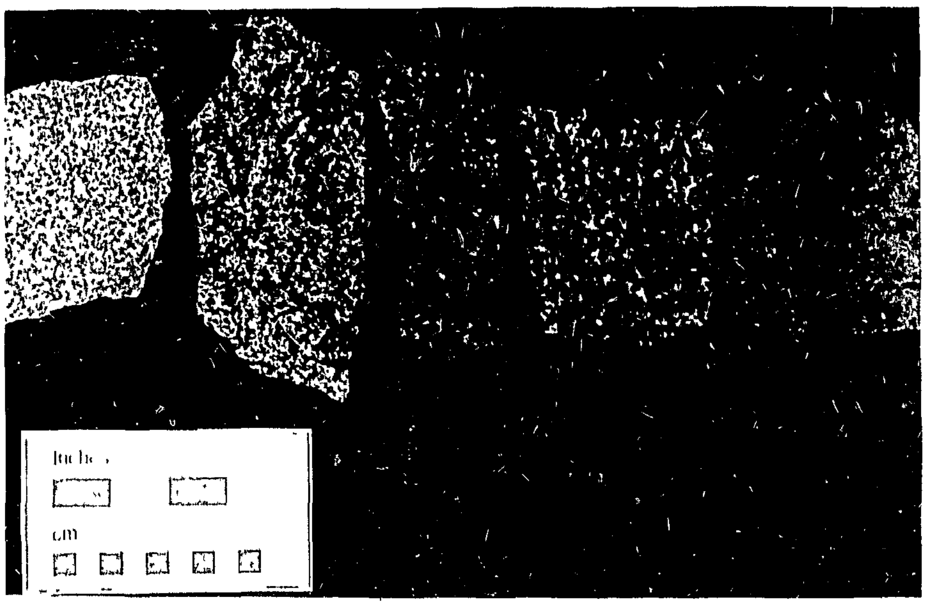

Figure 3.16. Textural variation among the granodiorite, tonalite, and the diorite in the Contact Zone Transect. From left to right: granodiorite (sample SPGD), tonalite (samples B3, B4, and B5), and the diorite (sample B8).

considered the tonalite to be a trondhjemite, but these rocks contain more abundant biotite and amphibole than trondhjemites *sensu stricto*, and they have less quartz and more calcic plagioclase compositions (Barker, 1979; Figure 3.18b). However, they do have equigranular groundmass textures like the granodiorite and coarse-grained phenocrysts like those in the diorite. The tonalite samples are also heterogeneous and contain modal amphibole; all of these observations strongly support a hybrid origin for them.

Local cross-cutting inter-relationsips in the CZT

Four distinct intrusions occur in the CZT and their cross-cutting relationships with the tonalite constrain the intrusive history of these rocks. Numerous garnet-bearing pegmatites and a small diorite tongue intrude the tonalites to the north of the CZT, and a medium-grained granitoid dyke with pillowed contacts intrudes tonalite to the south (Figure 3.19a). Subrounded-rounded enclaves of tonalite up to 20 cm in diameter, occur within a dyke of fractionated tonalite that has similar characteristics to the fractionated tonalite patches in Figure 3.17. The enclaves locally impinge upon each other, and they were apparently incorporated as magmatic inclusions (Figure 3.19b) and the fractionated material in the matrix also occurs as angular enclaves within the tonalites (Figure 3.19c). Truncation of tonalite by (presumed) externally-derived pegmatites and leucogranitic dykes constrains its formation prior to solidification of the Shelburne Pluton, and granitoid-tonalite mingling indicates that the tonalite and the leucogranite existed as melts simultaneously. The diorite intrusion into the tonalite indicates only that these lithologies are penecontemporaneous, whereas the disruption of tonalite by fractionated material (and *vice versa*) suggests that strong convective stirring of the magmas occurred.

Figure 3.17. An irregular patch of coarse-grained fractionate within the Contact Zone Transect tonalite. View to the southeast, lens cap 7 cm diameter. See Figure 3.15 for the location of the photograph.

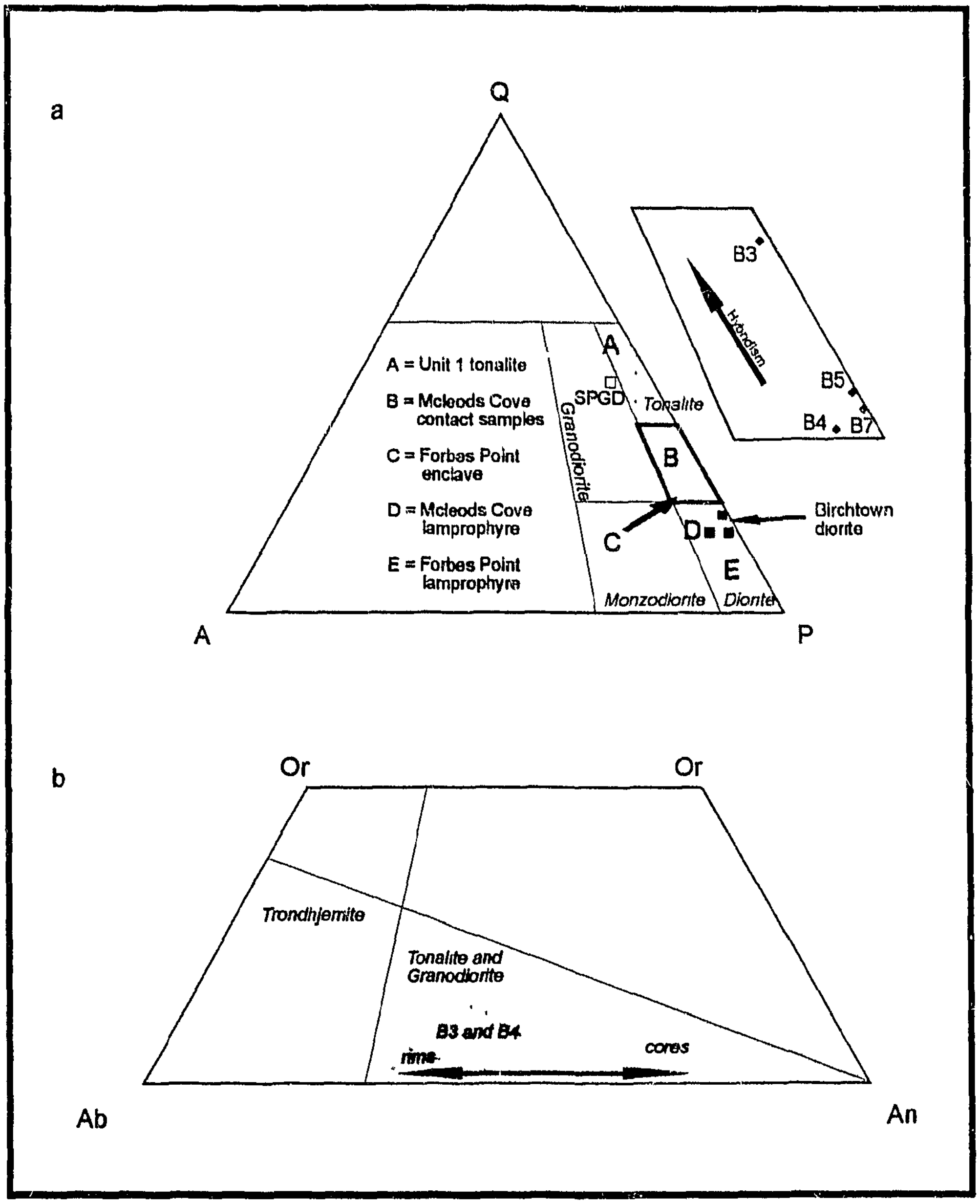

Figure 3.18. Modal and mineral chemical classification of the Contact Zone Transect lithologies and comparison of their characteristics with the Forbes Point and Mcleods Cove lamprophyres. (a) Modal QAP plot. Comparative data for the Unit 1 tonalite of the Port Mouton Pluton is from Douma (1988). The vector shows the effects of hybridism towards sample SPGD; (b) Plot of Ab-Or-An in plagioclase after Barker (1979). The tonalites do not have trondhjemitic characteristics.

a

b

c

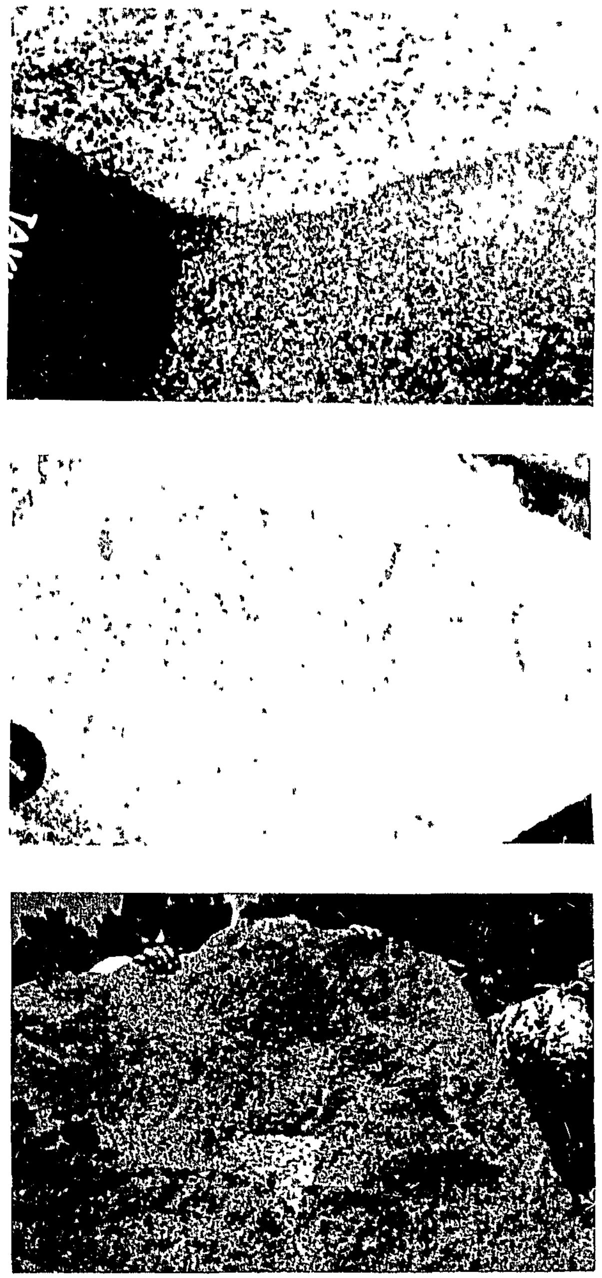

Figure 3.19. Cross-cutting field relationships in the Contact Zone Transect. (a) The crenulate, mingled contact between a granitoid dyke and the tonalite. Note the biotite selvage that forms the sharp contact, and the truncation of a micaceous schlieren by the contact. Small red garnets nucleated in the leucogranite at the contact, presumably because of chemical diffusion. View to the southeast, lens cap 7 cm diameter; (b) Pillowed enclaves of tonalite in a dyke of fractionated tonalite similar to that in Figure 3.17. Plan view, lens cap 7 cm diameter; (c) Angular enclaves of fractionated tonalite in the tonalite. Photograph of a loose boulder, lens cap 7 cm diameter. See Figure 3.15 for the location of the photographs.

U-Pb geochronology across the CZT

Extensive U-Pb dating of zircon, sphene, and monazite in the CZT yields the contemporaneous ages for the diorite and tonalite that their juxtaposed field relationships suggest. Appendix A-4 describes the sample preparation and analytical procedures, Table 3.3 summarizes the sample numbers and the analytical results, and Section 3.3 of Chapter 2 describes the morphology of dioritic zircons. The tonalite contains both fractured and clear acicular zircons similar to those of the diorite, and it has red sphene grains with yellow sphene overgrowths (Figure 3.20). The zircons have very high U contents (1750-2807 ppm) and low common lead contents (generally 0.17-0.55 ppm), but sphene contains less U (298-852 ppm) and it also has more common lead (<2.58 ppm). The granodiorite contains abundant equant zircon, but all the grains have xenocrystic cores and only thin magmatic overgrowths; they largely represent inherited xenocrysts from the Meguma Group or the sub-Meguma basement (T.E. Krogh, pers. comm., 1993) and do not occur in the tonalite. This study concentrates on yellow monazite, which is variably abundant in the granodiorite. Monazite contains higher U than either the zircon or the sphene (5760 ppm), but also contains high common Pb (1.66 ppm).

The most concordant zircon data from the tonalite and the diorite give identical ages of 376±2 Ma with less than 5.46% discordance in the unfractured grains. Both the yellow and the red sphene from the tonalite give circa 376 Ma ages, but they have <1.43% discordance (Figure 3.21). Linear regression of the zircon and sphene data produces a single discordia line that intersects concordia at 0 Ma and provides an upper intercept age of $376^{+2.3}_{-1.7}$ Ma (2σ with 35% confidence of fit). All grains, therefore, suffered the same recent lead loss event, and the age represents the best estimate possible from the zircon and sphene data. Monazite from the granodiorite plots above concordia with -1.47% discordance because of excess ^{206}Pb resulting from Th decay. The data shown on Figure 3.21 are arbitrarily corrected for Th/U = 1 in the granodiorite magma, and give a more concordant ^{207}Pb/^{235}U age of 370.4±2 Ma. Although this

Table 3.3. U-Pb results for zircon, sphene, and monazite fractions separated from the Contact Zone Transect

CZT Unit	Fraction No	Description[a]	Wt (µg)	U (ppm)	Pb_{rad} (ppm)	Pb_{com} (ppm)	$^{206}Pb/^{238}U^{b}$	$^{207}Pb/^{235}U^{b}$	$^{207}Pb/^{206}Pb^{b}$	$^{206}Pb/^{238}U$	$^{207}Pb/^{235}U$	$^{207}Pb/^{206}Pb$	Disc
Diorite	B8-1	Zrn,0M,E,B,Abr (43)	71	2,346 04	140 43	1 8	0 05904±7	0 44092±65	0 05416±3	369 79	370 9	377 81	2 18
Diorite	B8-2	Zrn,0M,N,L,Abr (75)	68	1,514 9	91 06	7 65	0 05927±8	0 44203±116	0 05409±12	371 2	371 68	374 7	0 96
Diorite	B8-3	Zrn,0NM,N,B (25)	48	1,983 8	123 05	0 19	0 05912±9	0 44121±71	0 05413±2	370 24	371 1	376 48	1 7
Tonalite	B3-1	Zrn,0M,E,B,Abr (58)	90	2,806 96	164 25	0 29	0 05888±9	0 43937±70	0 05412±2	368 83	369 81	375 92	1 94
Tonalite	B3-2	Zrn,0M,E,B,Abr (63)	129	2,417 88	134 73	0 55	0 05682±11	0 42407±84	0 05413±3	356 29	358 96	376 26	5 46
Tonalite	B3-3	Spn,M1 0A,E,R (80)	1,128	852 25	49 82	2 58	0 05982±13	0 44715±118	0 05421±7	374 55	375 28	379 82	1 43
Tonalite	B3-4	Spn,M1 0A,E,Y (>100)	1,315	298 19	16 96	2 3	0 05962±10	0 44501±164	0 05414±17	373 29	373 78	376 78	0 95
Tonalite	B3-5	Zrn,0M,N,L,Abr (46)	32	1,749 93	102 64	0 17	0 05950±8	0 44358±63	0 05407±4	372 6	372 77	373 86	0 35
Tonalite	B3-6	Zrn,0M,N,L (47)	144	2,295 99	132 39	0 28	0 05869±8	0 43822±62	0 05415±3	367 68	369	377 27	2 62
Granod	SPGD	Mnz,M0 75A,E,Y (8)	4	5,760 42	1,026 27	1 66	0 05925±9	0 44016±72	0 05388±4	371 09	370 37	365 86	-1 47

[a]Mineral analyzed (mineral abbreviations after Kretz, 1983), Magnetic susceptibility (0M = Final Frantz magnetic fraction at 0 degree side tilt, 0NM = Final Frantz non-magnetic fraction at 0 degree side tilt, M1 0A = Initial Frantz 1 0A magnetic fraction (Krogh, 1981a), Morphology (E = equant, N = acicular needle), Colour (B = Brown, L = Light Brown, R = Red, Y = Yellow), Abr = Abrasion (Krogh, 1981b), number in parentheses denotes the number of grains analyzed [b]Atomic ratios corrected for blank (Pb = 2 pg, U = 0 5 pg), analytical mass fractionation, and initial common Pb calculated using the model of Stacey and Kramers (1975) Pb_{rad} = radiogenic lead, Pb_{com} = common lead

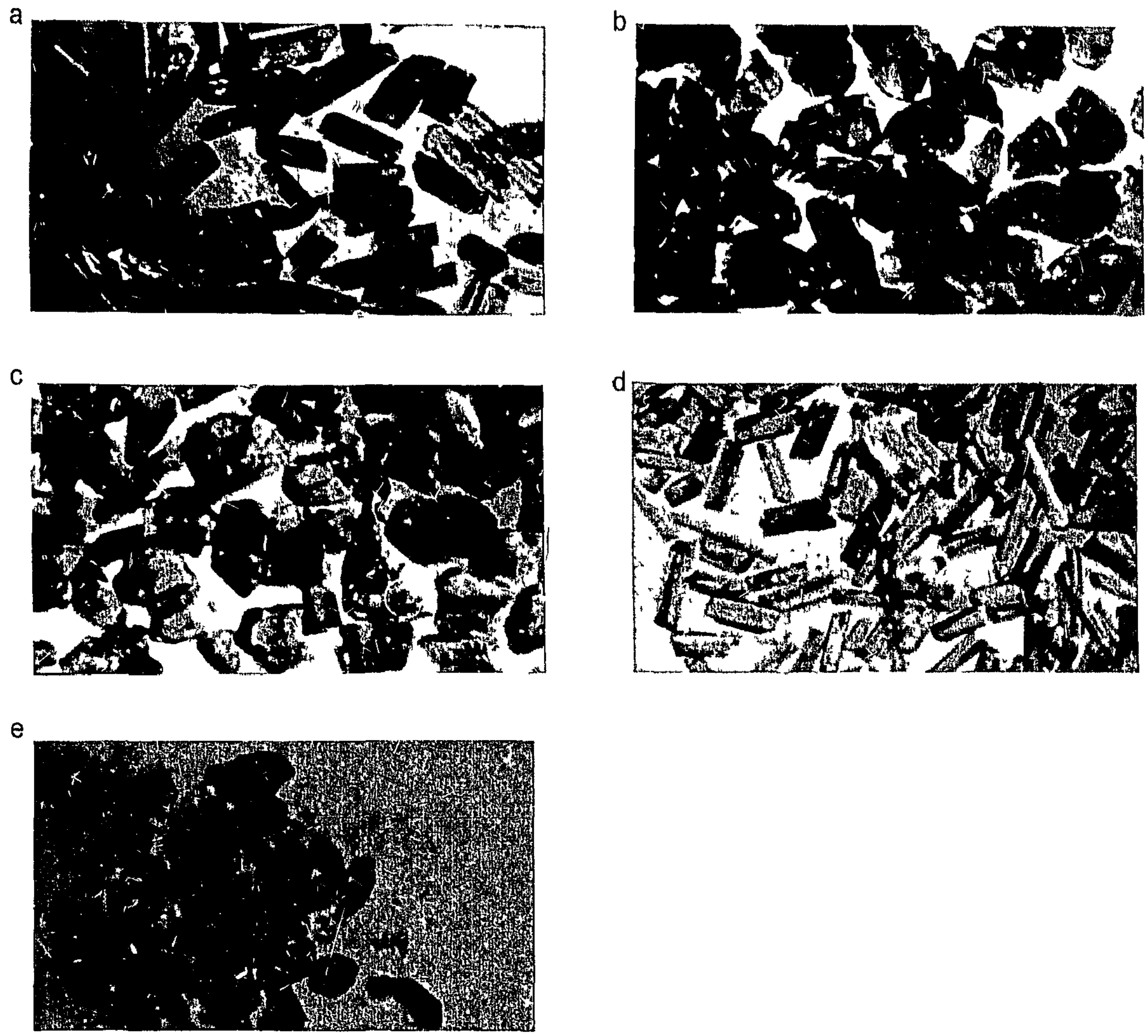

Figure 3.20. Microphotographs of zircon, sphene, and monazite fractions used in the U-Pb isotopic analysis of the tonalite and granodiorite. (a) Fraction B3-1 dark brown, equant zircon. Magnification x25; (b) Fraction B3-3 red sphene cores. Magnification x25; (c) Fraction B3-4 yellow sphene rims. Magnification x25; (d) Fraction B3-6 light brown, acicular zircon. Magnification x25; (e) SPGD yellow monazite. Magnification x50. See Figure 2.23 in Chapter 2 for zircon morphologies extracted from the diorite.

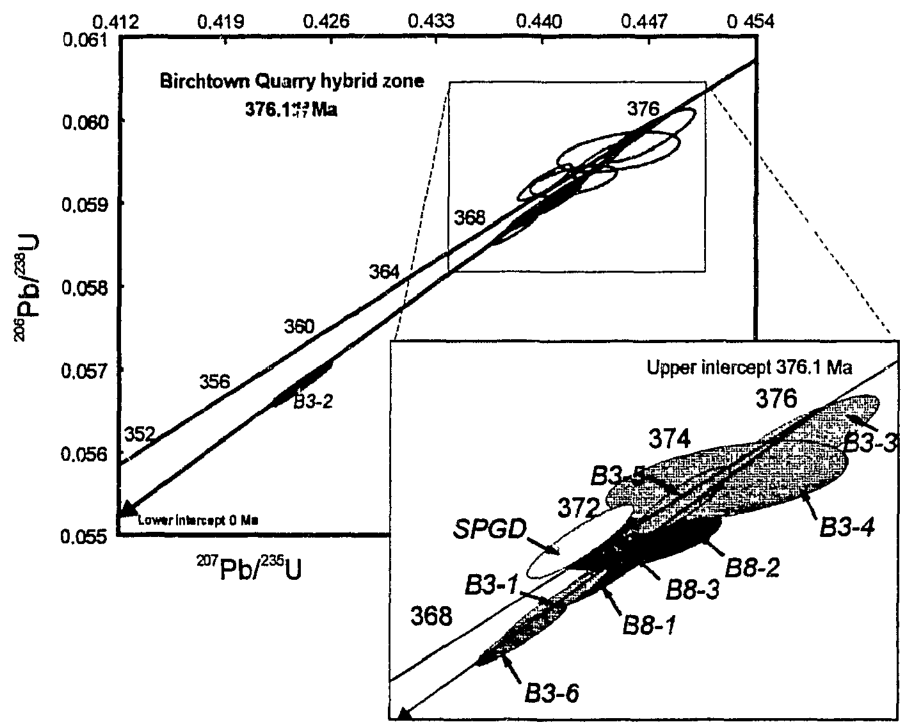

Figure 3.21. U-Pb concordia plot for zircon, sphene, and monazite fractions separated from the Contact Zone Transect lithologies. Sample numbers in italics; see Table 3.3 for the analytical data.

age is the best possible estimate for the intrusion of the granodiorite, it does not represent an intrusion age. Mingling between the granitoid dyke and its tonalite host does not support such a young age for the granodiorite and no U-Pb constraint exists for the mixing hypothesis at Birchtown.

Tonalite hybrid petrography and mineral chemistry

Tonalite shares petrographic characteristics with both the granodiorite and the diorite. Figure 3.22 shows the textures of all three units and Figure 3.23 summarizes their similarities and differences. The tonalite has an equigranular quartzo-feldspathic groundmass identical to that of the granodiorite and it contains similar plagioclase morphologies. Euhedral phenocrysts have unzoned cores with oscillatory zoned rims, whereas hypidiomorphic crystals in the groundmass show strong patchy zoning (Figure 3.24a). Poikilitic microclines occur only rarely, but they consistently have perthitic intergrowths and myrmekitic rims. As at Mcleods Cove, two biotite populations exist (Figure 3.24b). Abundant orange-brown crystals (>1.1 mm) cluster together into diffuse patches reminiscent of the diorite, whereas dark brown grains with kinked cleavage, pleochroic haloes, and equant apatite inclusions occur only rarely as isolated crystals smaller than 1 mm; they resemble biotite crystals from the granodiorite. As in the diorite, tonalite commonly contains abundant chalcopyrite blebs associated with biotite and it also has anhedral magnetite. No tonalite samples contain the primary magmatic muscovite, garnet, or other aluminosilicate phases that occur in the granodiorite.

Amphibole phenocrysts form the dominant ferromagnesian phase in the most mafic tonalite samples. They resemble their counterparts in the diorite and they have well-developed cleavage and simple twinning. However, amphibole becomes less abundant in leucocratic tonalites and individual grains are smaller (0.5 mm), anhedral, they lack twinning or cleavage, and they routinely contain inclusions and overgrowths of biotite and ilmenite (Figure 3.24c). Apatite and sphene show particularly high abundance in the tonalites relative to the either the

a

b

c

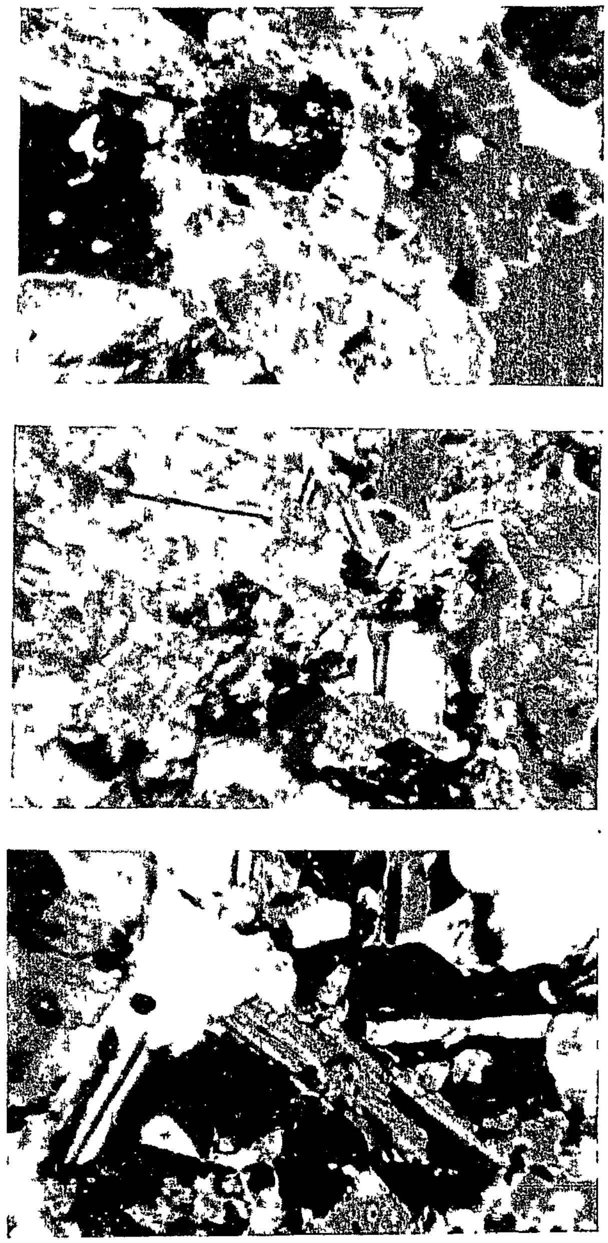

Figure 3.22. Textural characteristics of the Contact Zone Transect lithologies. (a) Photomicrograph of the granodiorite (sample SPGD). Note the hypidiomorphic inequigranular texture. Field of view 6 mm, XPL; (b) Photomicrograph of the diorite (sample B8). Note the panidiomorphic inequigranular texture and abundant intergrowths of amphibole, biotite, and plagioclase. Field of view 6 mm, XPL; (c) Photomicrograph of the tonalite (sample B4). Note that it has the groundmass texture of the granodiorite, and it has the amphibole (centre) and panidiomorphic plagioclase and biotite phenocrysts that occur in the diorite. Field of view 6 mm, XPL.

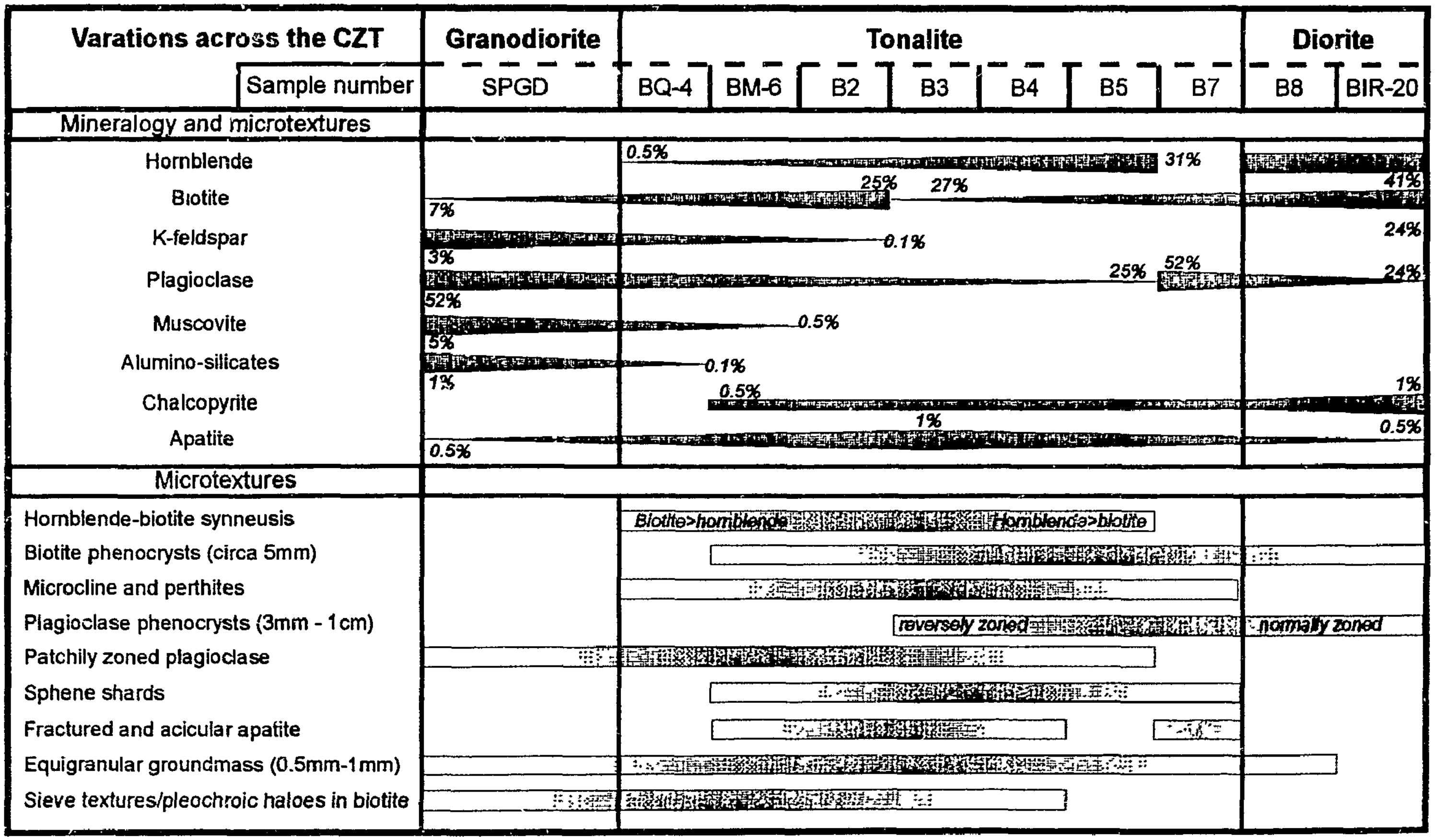

Figure 3.23. Summary of the mineralogical and microtextural variations across the Contact Zone Transect. The horizontal triangles and rectangles indicate the range of pertinent phenomena caused by hybridism in the heterogeneous tonalites. The samples are organized sequentially according to their positions in the transect. See Figure 3.15 for the sample locations.

granodiorite or the diorite. Acicular apatite occurs as inclusions within all other mineral phases or as large crystals in the groundmass. Most examples have very high aspect ratios (<30:1) and they have numerous fractures that dissect individual crystals (Figure 3.24d). Their fractured and quenched morphologies resemble those of apatites at the Mcleods Cove commingled contact; perhaps the Birchtown apatites also formed at a commingled contact. Sphene preferentially occurs with apatite as panidiomorphic fractured grains or as broken shards.

Appendix C-2 contains representative mineral analyses for major modal constituents of the diorite, tonalite, and granodiorite, and Figure 3.25 illustrates the changes in mineral chemistry across the CZT. All minerals in the tonalite show compositional characteristics that vary between their compositions in the diorite and granodiorite end-members. Andesine (An_{32}-An_{47}) represents the dominant plagioclase composition in the tonalites, but crystals of bytownite (An_{74}) and oligoclase (An_{27}) also occur; they compositionally overlap with those of the diorite and granodiorite. Tabular plagioclase crystals generally have reversed zoning with oligoclase cores and andesine and bytownite oscillatory rims, whereas patchily zoned grains show predominantly andesine or bytownite compositions (Figure 3.25a). Tonalitic biotites are unzoned, but they have more evolved compositions than those within the diorite (Figure 3.25b). Most compositions lie between the dioritic and granodioritic compositions at higher Al_2O_3, FeOT, TiO_2, and alkalies, although overlap exists with dioritic biotite compositions. Unzoned amphiboles in the tonalite have lower SiO_2, MgO, and CaO, and they accommodate increased pargasitic and edenitic substitution than those in the diorite (Figure 3.25c). Chemical modification of the amphibole phenocrysts accompanied their breakdown to biotite.

Major oxide, trace element, and isotopic variation within putative hybrids

Appendix C-3 contains ten major oxide, trace element, and isotopic analyses that encompass all lithologic variation within the CZT. Most tonalites have clustered compositions for SiO_2 (58.2-63.0 wt.%) and Al_2O_3 (16.2-17.8 wt.%) that reflects the broadly similar feldspathic

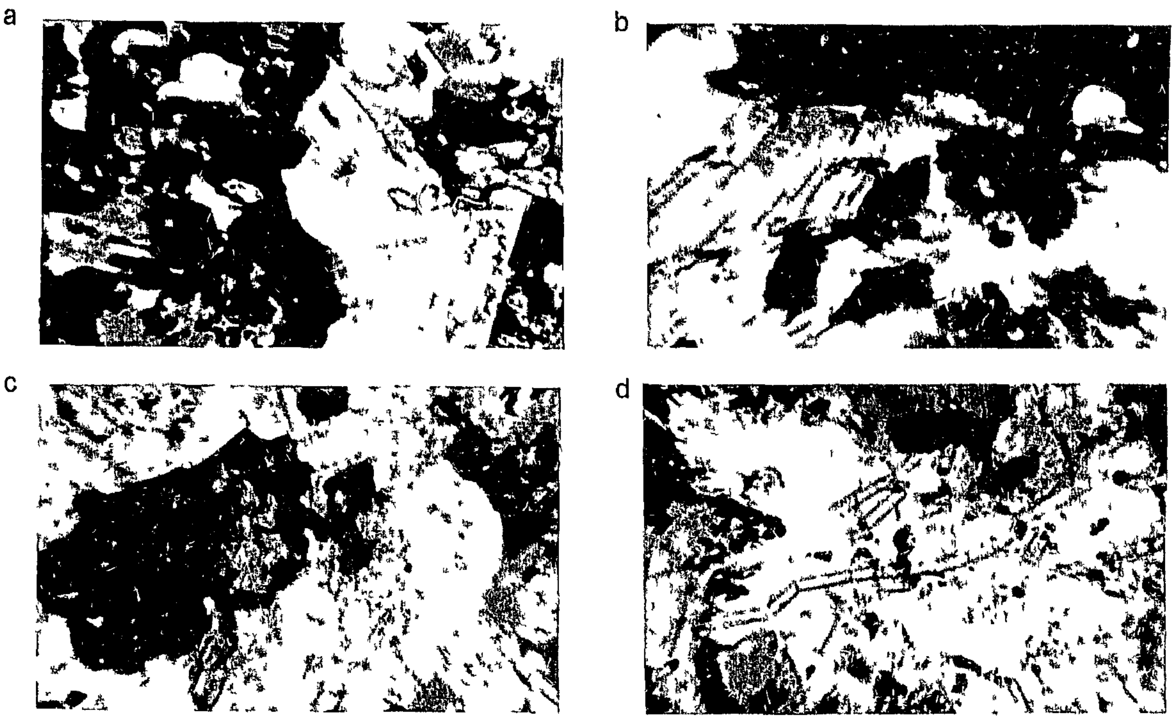

Figure 3.24. Textural disequilibrium features in the Contact Zone Transect tonalite. (a) Photomicrograph of strongly zoned plagioclases. Note that the groundmass grains have patchy zoning and the phenocrysts have reversed oscillatory zoning. Some phenocrysts also have distinct cores. Field of view 6 mm, XPL; (b) Photomicrograph of the two biotite morphologies. The pale grains (bottom left) originated in the diorite, whereas the abundant dark brown grains have pleochroic haloes and probably originated in the granodiorite. Field of view 6 mm, PPL; (c) Photomicrograph of amphibole-biotite synneusis. Note that the biotites do not have zircon inclusions, and that sphene associates with amphibole Field of view 6 mm PPL; (d) Highly acicular and cracked apatite crystals and broken shards of red sphene Field of view 3 mm, PPL.

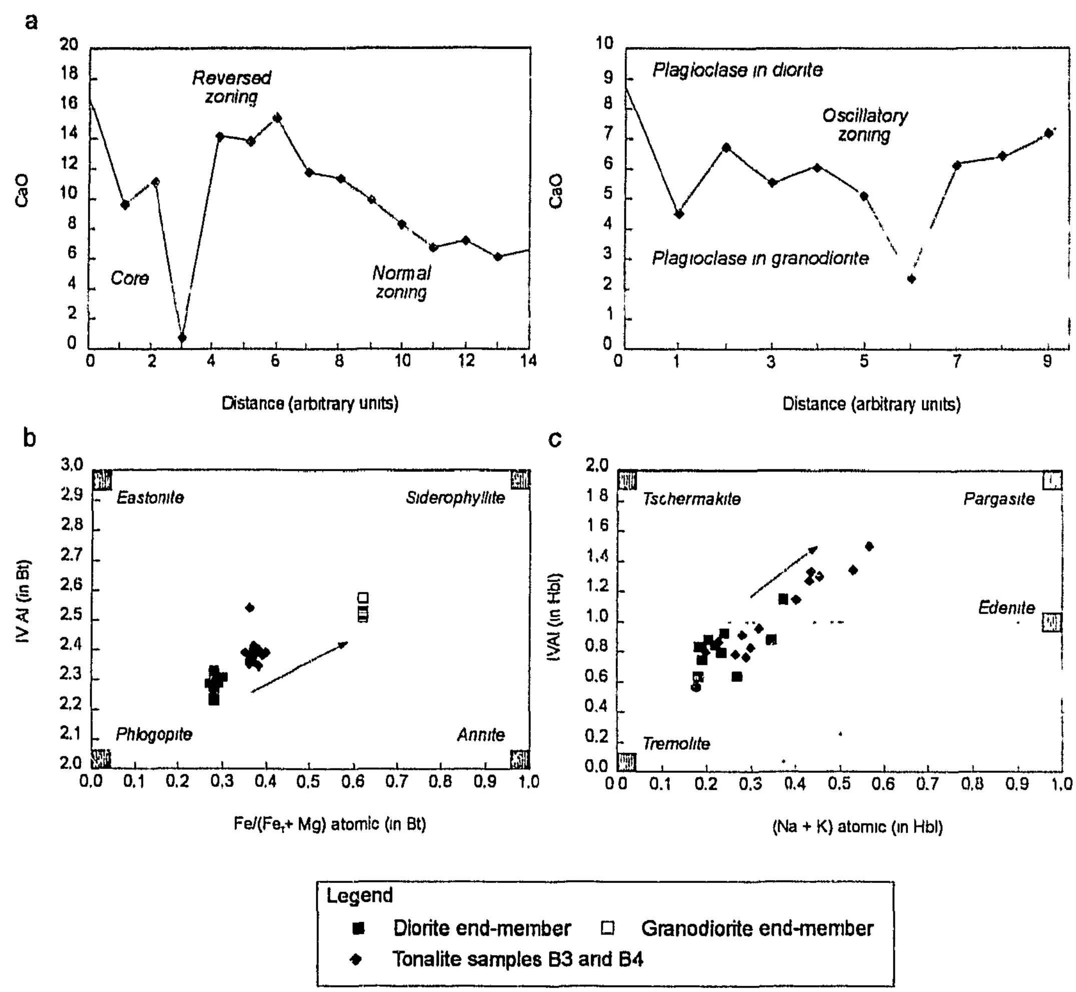

Figure 3.25. Modal mineral zoning patterns and compositional variation across the Contact Zone Transect. (a). Plots of CaO-arbitrary distance across the grain, for a reversely zoned phenocryst in tonalite sample B4 and a patchily zoned groundmass crystal in tonalite sample B3; (b) Plot of IVAl-Fe/(Fe+Mg) atomic for biotite, showing that the tonalite contains biotite compositions similar to those in the granodiorite and diorite, and it also contains biotite grains with intermediate compositions that crystallized from the tonalitic magma. (c) Plot of IVAl-(Na+K) atomic for amphibole, showing the increased pargasitic substitution in tonalitic amphibole xenocrysts; the vectors illustrate the compositional effects of hybridism. Mineral abbreviations after Kretz (1983).

mineral assemblages and modal proportions in these samples (Figure 3.26). The widest chemical variation exists for MgO (0.7-9.4 wt.%), FeOT (1.8-7.6 wt.%), CaO (2.06-6.9 wt.%), P_2O_5 (0.3-0.9 wt.%), and TiO_2 (0.3-0.7 wt.%); the highest values for these oxides correspond to intermediate samples containing abundant amphibole, apatite, and sphene. Tonalites have transitional metaluminous-peraluminous characteristics (A/CNK 0.86-1.27) that reflect the variable presence of amphibole and the absence of aluminosilicate mineral phases. Tonalite compositions lie between those of the diorite and granodiorite for all major element oxides except Al_2O_3 and P_2O_5, and for all minor and trace elements except Cr, Ni, and Sr, although they show significant skewness towards the diorite composition (Figure 3.26).

Of all trace elements Cr (17-341 ppm), Th (0.6-4.9 ppm), Pb (6-29 ppm), V (51-192 ppm), and Y (11-23 ppm) show the widest chemical variation in the tonalites. Low concentrations of Sr and Ba correlate with low K_2O in the granodiorite and argue for post-emplacement loss of mobile elements. Tonalites contain variable abundances of rare-earth elements (REE; La 8.4-13.9 ppm, Sm 2.6-4.3 ppm; Yb 1.0-2.0 ppm, Lu 0.14-0.29, ΣREE 52.2-88.2), but their chondrite-nomalized pattems generally lie between those of the diorite and the granodiorite (Figure 3.27). They also have small negative Eu anomalies (Eu/Eu* = 0.70-0.86), except for sample B7 that has a positive Eu anomaly. Small positive anomalies occur in the middle rare-earths (MREE) at Gd, Dy, and Er (in sample B7) and they may reflect matrix calibration effects during mass spectrometric analysis (S. Jackson, pers. comm., 1993). Strontium and Nd isotope ratios for the tonalite samples B3 and B7 lie close to the diorite values, whereas tonalite sample BQ-4 has a Sr-Nd isotopic composition that resembles the granodiorite (Figure 3.28).

Comparisons with Forbes Point and Mcleods Cove

The Birchtown tonalite contains similar microtextures and modes to the Forbes Point and Mcleods Cove contact lamprophyres, and they support a hybrid petrogenesis for it. Tonalite has identical amphibole-biotite synneusis textures and it has the acicular apatites and cracked

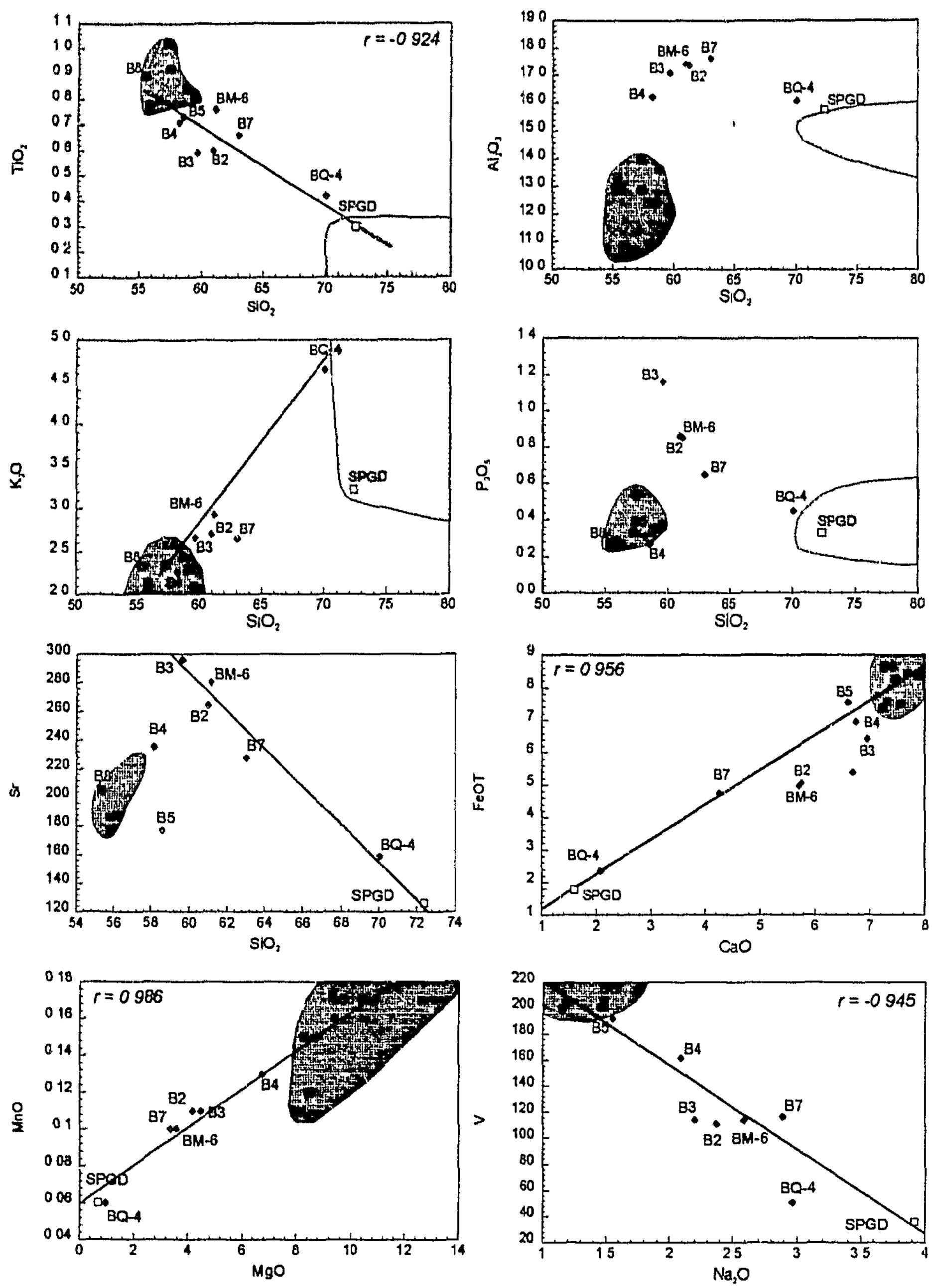

Figure 3.26. Harker plots and other miscellaneous variation diagrams for the Contact Zone Transect tonalites. The solid lines indicate regressions of linear data, and r is the Pearson correlation coefficient. The diorite end-member is outlined in dark grey and the granodiorite endmember is outlined in light grey. Comparative data for the granodiorite is from Rogers (1984). Symbols as in Figure 3.25. See the text for details.

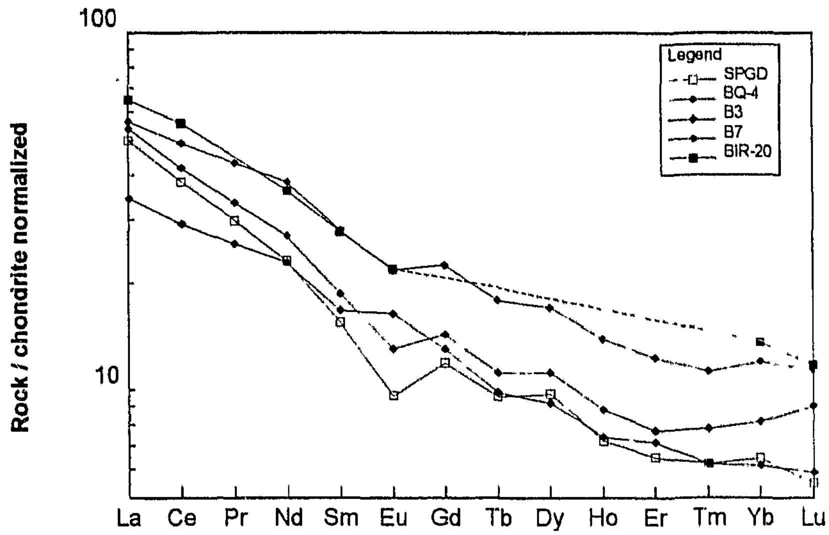

Figure 3.27. Chondrite-normalized REE spider diagram for the Contact Zone Transect lithologies. See the text for details.

sphene crystals. In addition, it is lithologically and texturally intermediate between the putative granodiorite and diorite end-members. The equigranular groundmass of the tonalite appears similar to that in the granodiorite and the coarse-grained phenocrysts of plagioclase and biotite resemble those in the diorite. Biotite grains derived from both the diorite and the granodiorite exist in the tonalite, and the patchily zoned plagioclase crystals span the range of compositions that typify the end-members. Furthermore, the transitional metaluminous-peraluminous characteristics and predominantly mafic trace element and isotopic compositions of the tonalite contrast with the predominantly peraluminous compositions of other MZ granitoids (Richard, 1988), and they lie between the compositions of the diorite and granodiorite for most major oxides and trace elements. Cross-cutting field relationships indicate that the granodiorite and tonalite existed as magmas simultaneously, and microtextures in conjunction with modal mineral assemblages in the tonalite suggest that mixing occurred between the granodiorite and diorite, despite the young $^{207}Pb/^{235}U$ age of the granodiorite.

Current knowledge predicts that for closed system (ideal) mixing topologies, hybrid lithologies lie along linear chords between the end-member compositions in element-element compositional space, and they lie along hyperbolic trends in ratio-ratio plots. Recognizing that the tonalite data set includes only 10 analyses, Figure 3.26 illustrates the somewhat linear correlations for some elements across the CZT, and Figure 3.29 shows the corresponding Pearson correlation matrix for a wider number of elements and oxides. Both the lever rule and the IGPET mixing module suggest that the tonalites could result from mixing up to 83% diorite (sample BIR-20) and at least 17% granodiorite (sample SPGD) with relatively low residuals (Σresiduals^2 = 1.966-2.306) for all elements except Al_2O_3, P_2O_5, Sr, Cr, and Ni. The pronounced curved variation trends for these elements and oxides and the non-hyperbolic Sr-Nd isotope ratio distributions (Figure 3.28) indicate that ideal mixing did not occur.

Ried et al. (1983), Frost and Mahood (1987), Davidson et al. (1990), and Ayuso and Arth (1992) recognized that fractional crystallization commonly accompanies mixing, and, therefore,

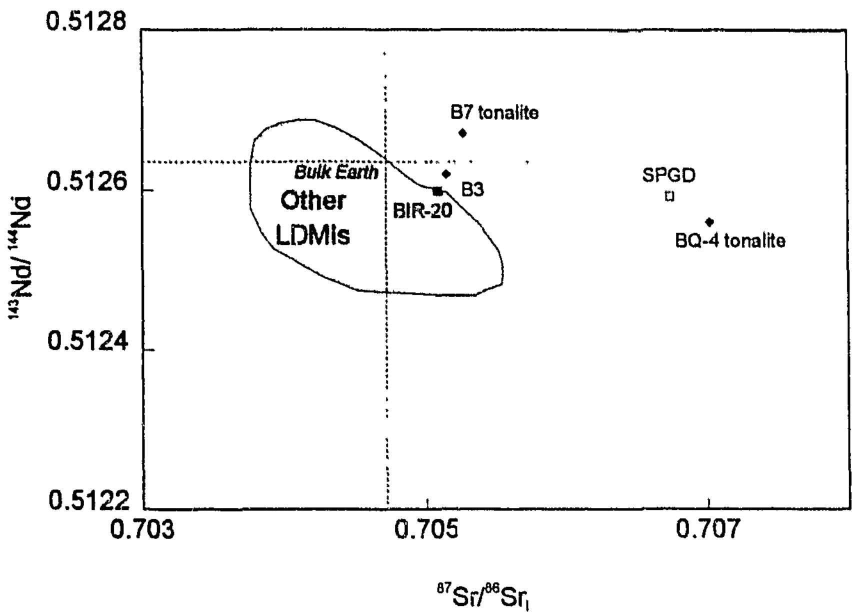

Figure 3.28. Plot of initial $^{87}Sr/^{86}Sr$-$^{143}Nd/^{144}Nd$ for the Contact Zone Transect lithologies and the other Late Devonian mafic intrusions. All data recalculated to t = 370 Ma. Symbols as in Figure 3.25; see the text for details.

	SiO_2	TiO_2	Al_2O_3	FeOT	MnO	MgO	CaO	Na_2O	K_2O	P_2O_5	Ba	Rb	Sr	Y	Pb	Ni	V
SiO_2	1.000																
TiO_2	**-0.924**	1.000															
Al_2O_3	0.131	-0.217	1.000														
FeOT	**-0.967**	**0.926**	-0.370	1.000													
MnO	**-0.937**	**0.891**	-0.444	**0.992**	1.000												
MgO	**-0.889**	**0.852**	-0.560	**0.973**	**0.986**	1.000											
CaO	**-0.985**	**0.896**	-0.164	**0.956**	**0.931**	**0.885**	1.000										
Na_2O	**0.954**	**-0.890**	0.314	**-0.962**	**-0.948**	**-0.925**	**-0.939**	1.000									
K_2O	0.579	-0.492	0.274	-0.633	-0.654	-0.633	-0.640	0.438	1.000								
P_2O_5	-0.216	0.062	0.758	-0.004	-0.074	-0.198	0.219	-0.089	0.074	1.000							
Ba	-0.370	0.377	0.248	0.270	0.219	0.179	0.256	-0.443	0.488	0.354	1.000						
Rb	0.345	-0.230	0.476	-0.420	-0.466	-0.502	-0.469	0.309	0.736	0.227	0.581	1.000					
Sr	-0.746	0.636	0.513	0.560	0.485	0.365	0.739	-0.606	-0.287	0.770	0.449	-0.034	1.000				
Y	**-0.881**	**0.862**	-0.139	**0.834**	0.802	0.758	**0.909**	**-0.866**	-0.409	0.250	0.316	-0.439	0.725	1.000			
Pb	**0.849**	0.749	0.200	**-0.856**	**-0.843**	-0.798	**-0.891**	0.755	**0.868**	-0.175	0.094	0.558	-0.603	-0.685	1.000		
Ni	-0.603	0.697	-0.796	0.761	0.791	**0.845**	0.608	-0.713	-0.433	-0.367	0.114	-0.434	0.038	0.577	-0.546	1.000	
V	**-0.940**	**0.946**	-0.411	**0.988**	**0.985**	**0.968**	**0.923**	**-0.945**	-0.601	-0.092	0.282	-0.389	0.502	0.817	-0.575	**0.936**	1.000

Figure 3.29. Pearson correlation matrix for selected major and trace element data from the diorite, granodiorite, and tonalite. Somewhat linear correlations (>0.83) are emphasized in bold type.

fractionation of amphibole, biotite and/or plagioclase may account for non-ideal mixing behaviour in the CZT samples. Figure 3.30 overlays the calculated liquid lines of descent for diorite fractionation, diorite-granodiorite mixing, and diorite fractional crystallization accompanied by diorite-granodiorite mixing, with the observed major oxide variation. In these models, diorite fractionation alone consistently underfractionates most major oxides relative to the tonalite compositions, whereas fractional crystallization-mixing models produce curved variation trends that mimic the CZT variation for MgO, CaO, and Na_2O. The tonalite compositions lie between the bulk mixing and diorite fractionation trends for other oxides, suggesting that small amounts of fractionation occurred in the tonalite during, or after, mixing. Feldspathic patches of tonalite within the CZT support the fractionation hypothesis and may explain the non-linear variation trends for Al_2O_3 and Sr. Perhaps fractionation of apatite, amphibole, and magnetite also explain the curved variation trends shown by P_2O_5, Cr, and Ni.

However, crystal fractionation cannot separate the small mass differences that exist between Sr and Nd isotopes, and it does not explain their non-hyperbolic variation in the CZT. Lesher (1990) documented a similar decoupling of Sr and Nd isotopes in hybrid rocks and attributed it to the slow diffusivities of Nd isotopes relative to Sr isotopes in granitoid magmas, and to the different structures of juxtaposed mafic and granitoid melts. Davidson et al. (1990) also documented small-scale trace element and isotopic heterogeneities in a hybrid and suggested that they resulted from incomplete mixing between the end-members on a local scale. The Birchtown tonalites show extreme modal and microtextural heterogeneity that could result from different degrees of mixing in addition to, or instead of fractionation. The lack of equilibrium achieved by Sr and Nd isotopes may result from small degrees of mixing or incomplete mixing, and this hypothesis also explains the absence of linear trends for all major oxides and trace elements. The presence or absence of linear compositional features, therefore, probably depends on the behaviour of elements in the granodiorite-diorite mixture, and also on the nature and extent of the mixing process (considered below).

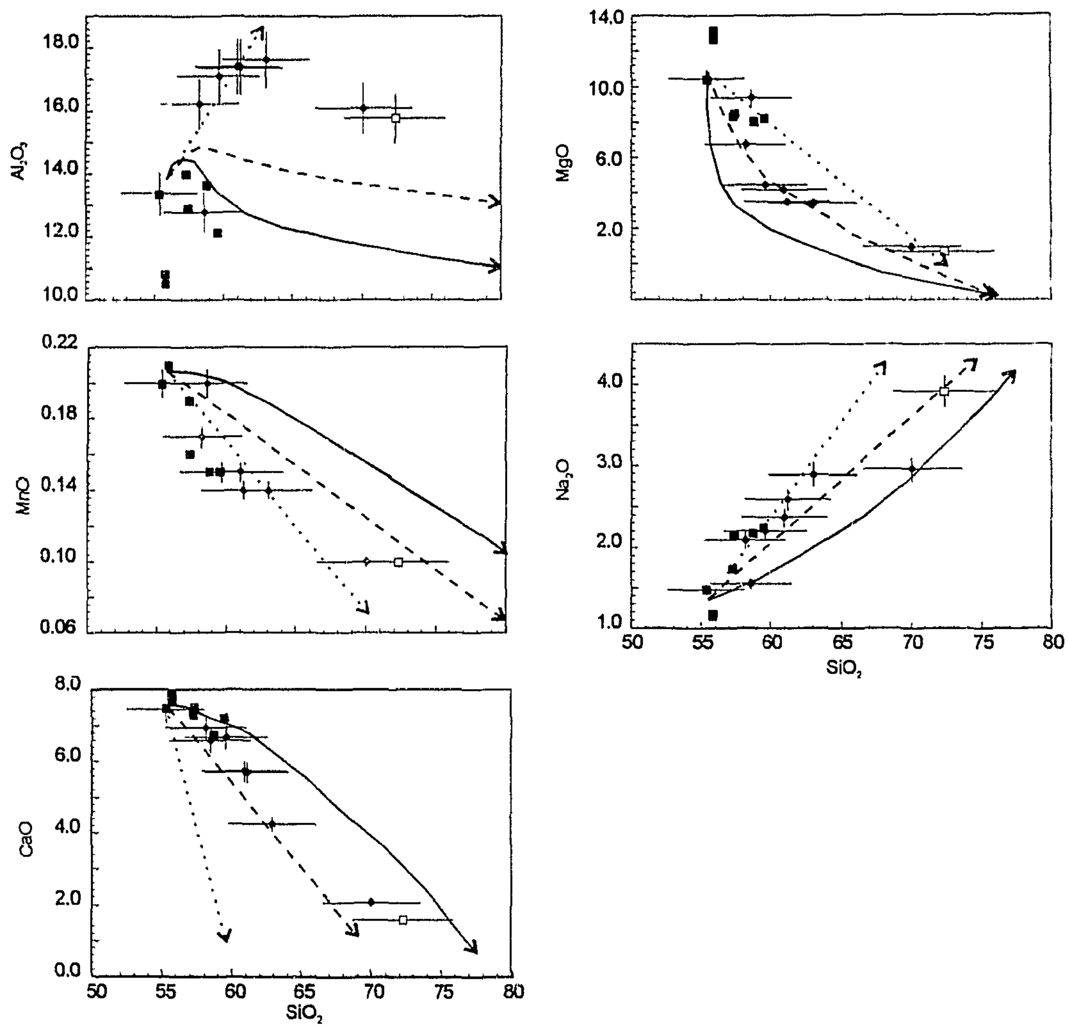

Figure 3.30. Harker variation diagrams for the Contact Zone Transect data compared with the variation trends expected from bulk diorite-granodiorite mixing (straight dotted arrow), 1:1 mixing combined with amphibole, biotite, and plagioclase fractionation (dashed arrow), and fractionation of amphibole, biotite, and plagioclase from the diorite (solid arrow). All models were simulated with the TRACE3 computer program of Nielsen (1988) using samples BIR-20 and SPGD as the diorite and granodiorite end-member compositions (respectively). Error bars for the data points calculated at 2σ. Symbols as in Figure 3.25, see the text for discussion, and see Figure 3.26 for the sample numbers.

3-4. The Nature of Mafic-Granitoid Magmatic Interaction in the Meguma Zone

The products of mafic-granitoid hybridism depend on the nature of the consanguineous magmas, and on the degree and type of interaction between them. In the MZ, lithological similarities between the synplutonic mafic bodies at Forbes Point, Mcleods Cove, and Birchtown, suggest that they record the progressive products of magmatic interaction between peraluminous granitoid and hydrous mafic material. Figure 3.31 summarizes their behaviour with time, and a specific details of the interactive sequence appear below:

(1) *Initial synplutonic intrusion at Forbes Point.* The well-constrained nature of the dyke (albeit with an arcuate attitude) and its sharp-gradational contacts, suggest that lamprophyre intruded magmatic but highly competent tonalite. Experiments predict the critical melt fraction for transitional fluid-solid behaviour at crystal contents of approximately 60-70% in the tonalite (Van der Molen and Paterson, 1979; Hibbard and Watters, 1985). Intrusion of the dyke apparently caused the conduction of heat into the adjacent tonalite, and disruption of the dyke during intrusion formed mingled mafic pillows. The occurrence of hornblende in the tonalite, in conjunction with K_2O, Ba, Rb, Sr, Y, Zr, and LREE, and Sr isotopic enrichments in the lamprophyre, suggests that the juxtaposed magmas commingled slightly before the lamprophyre completely solidified.

(2) *Commingling at Mcleods Cove.* The development of metric pillows with millimetric crenulations at Mcleods Cove requires that both the tonalite and lamprophyre contained fewer crystals, and they probably interacted at higher temperatures than the Forbes Point magmas (Cook, 1988). As the juxtaposed magmas cooled, their miscibilities probably increased and chemical equilibration began across the pillowed zone (Dorais et al., 1989). The magmatic pillows commingled with the tonalite host by diffusion of alkalies, LILE, Zr, LREE,and Sr isotopes, as at Forbes Point. Mechanical transfer of lithic fragments and amphibole and biotite

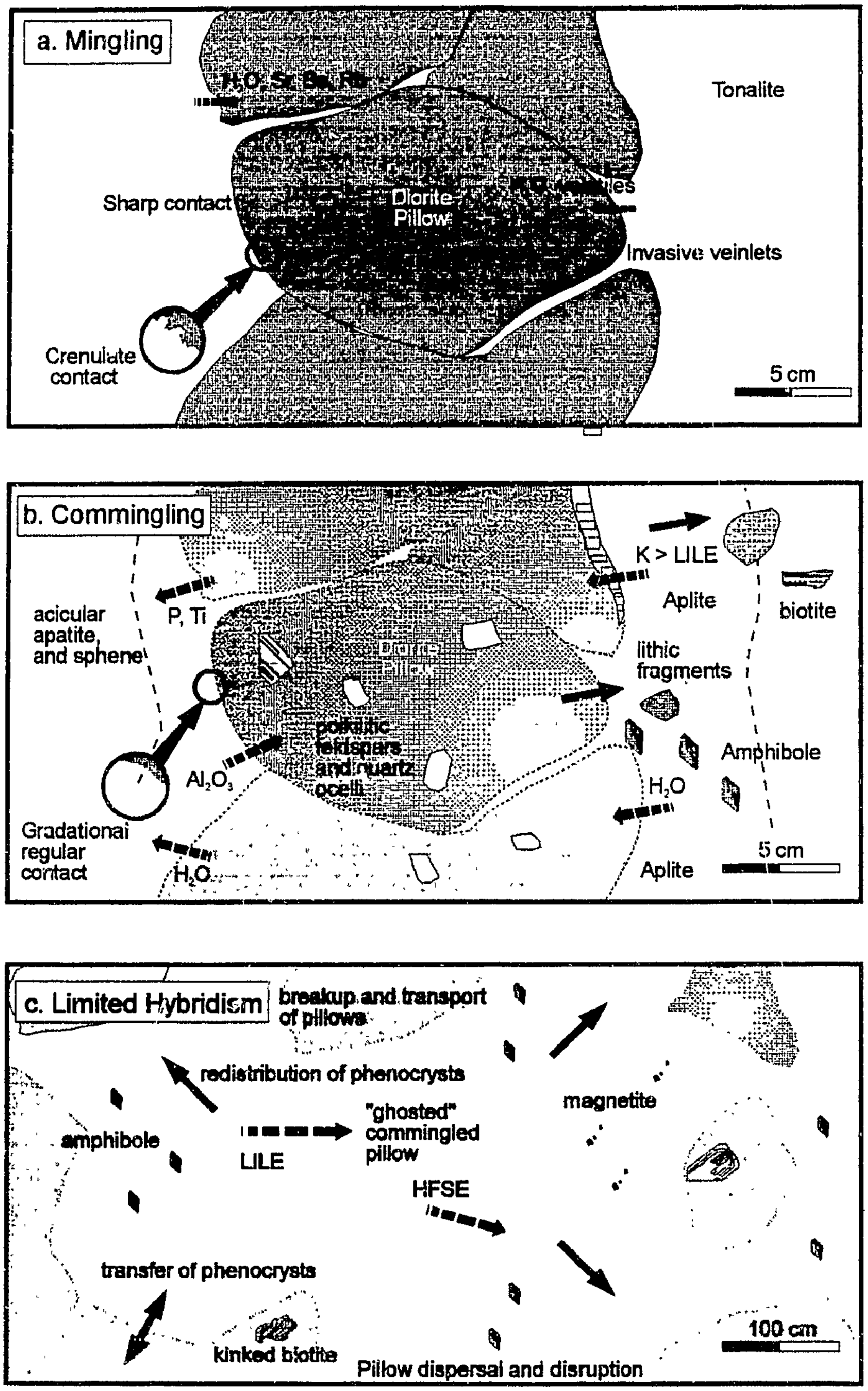

Figure 3.31. Schematic representation of the processes of mafic-granitoid interaction in the Meguma Zone. (a) Initial synplutonic intrusion and pillow formation; (b) Commingling across the pillowed contact; (c) Hybridism by phenocryst transfers. Refer to Figure 3.1 for the time scales involved and see the text for an explanation. Broken arrows represent chemical transfers and solid arrows represent physical transport of phenocryst phases.

phenocrysts accompanied apatite nucleation within 1 m of the lamprophyre-tonalite contact before the lamprophyre solidified, perhaps because of convection in the granitoid in response to heating by the lamprophyric sheet (Gamble, 1979).

(3) *Mixing at Birchtown.* The large volume of the diorite at Birchtown, relative to the Forbes Point and Mcleods Cove intrusions, potentially facilitated slower cooling after synplutonic intrusion, and probably allowed the most advanced magmatic interaction to occur (Oldenburg et al., 1989). Both the diorite and the granodiorite apparently contained abundant crystals during interaction, however, and they probably prevented physical blending of the magmas (Grove et al., 1982). The occurrence of acicular and fractured apatites, similar to those at Mcleods Cove, suggests that the magmas initially established a commingled contact. However, convection in the granitoid probably destroyed the pillows and transported them into the granodiorite as amphibole, biotite, and plagioclase xenocrysts. A tonalite hybrid, therefore, currently occupies the granodiorite-diorite contact, and its compositional characteristics probably result from a combination of variable amounts of mixing coupled with fractionation.

Experiments indicate that alkalies, LILE, and Sr-Nd isotopes equilibrate readily and they contaminate synplutonic mafic bodies soon after emplacement (Shearer et al., 1988; Van der Laan and Wyllie, 1993), whereas network forming elements and Cr, Ni, V, and most HFSE diffuse slowly in bimodal magmatic systems (Johnston and Wyllie, 1988). Observations in the MZ support some of these results. The late-stage pegmatites at Forbes Point probably represented the only residual liquid that existed after crystallization of the dyke, and exchange of volatiles may have helped to exchange Sr, Ba, Rb, alkalies (especially K_2O), and LREE between the tonalite and the lamprophyre (Gamble, 1979). The residual magma at Mcleods Cove was probably also enriched in volatiles, LILE, LREE and P_2O_5 and its putative higher temperature possibly allowed chemical diffusion to operate longer than the interaction at Forbes Point. However, in Birchtown Quarry, wide chemical variation is shown by network modifying elements, LILE, and HFSE, suggesting, perhaps, that these elements have somewhat similar distribution coefficients in mixed systems. High values for TiO_2, MgO, FeOT, CaO, Cr, Th, Pb, V, and Y may result from the transfer and breakdown of amphibole, biotite, and plagioclase as xenocrysts during mixing. Perhaps the breakdown of amphibole phenocrysts in the lamprophyre and diorite at Mcleods Cove and Birchtown (respectively) released them into the granitoid host according to the equation: amphibole + Al + K $\Rightarrow$ biotite + Si (quartz) + Fe + Mg + Ti + Ca (sphene) + Cr + V + Pb + Y. This process also explains the abundance of sphene at all three synplutonic intrusion sites.

If the transfer of chemically variable elements occurred in amphibole and/or biotite phenocrysts, then the variable occurrence and only partial breakdown of ferromagnesian xenocrysts may also explain the lack of equilibrium (linear and hyperbolic trends) in the Birchtown tonalites. However, Mysen (1992) suggested that phosphorus complexes with iron and HFSE. If phosphorus complexed with these elements and carried them as it diffused into the granitoid, then apatite crystallization probably released the complexed elements. Phosphorus also polymerizes silicate melts (Mysen, 1992) and this ability explains the unusual existence of fine grain sizes and equigranular quench textures in the tonalite adjacent to the lamprophyre at Forbes Point and Mcleods Cove. Despite strong heating by the lamprophyre, the aplitic texture of the marginal tonalite probably resulted from rapid crystallization induced by high phosphorus concentrations at the commingled contact. Formation of a solid "aplitic" carapace probably isolated the magmatic lamprophyre from the tonalite and it potentially inhibited further chemical diffusion.

3-5. Conclusions

The synplutonic mafic intrusions at Forbes Point, Mcleods Cove, and Birchtown have similar macroscopic, microtextural, and geochemical characteristics, and they probably document the progressive thermal and chemical effects of hybridism between calc-alkaline mafic magmas and peraluminous granitoid melts. The Forbes Point dyke may record the rapid cooling and intense heating associated with the initial synplutonic intrusion. It has small mafic pillows that show the breakdown of amphibole to biotite under the mingling conditions, but the lack of residual magma after crystallization allowed only the partial equilibration of Sr (and its isotopes), Ba, and Rb. At Mcleods Cove larger pillows potentially formed during the interaction of hotter and more fluid magmas. Rapid crystallization did not solidify the lamprophyre and residual magma exchanged volatiles, alkalies, P_2O_5, TiO_2, LILE (especially Ba, Sr, and Rb), LREE, and Y and Zr by diffusion. The tonalite and lamprophyre also transferred amphibole, biotite, plagioclase, and quartz phenocrysts within 1 m of this contact at a late stage. At Birchtown, slower cooling and the larger volume of dioritic magma probably allowed the most advanced interaction. After commingling occurred, convection probably destroyed the pillowed contact and amphibole, biotite, and plagioclase phenocrysts were transferred up to 30 m into a zone of hybrid lithologies. The hybrids have modal, microtextural, and geochemical characteristics that lie between those of the end-member compositions for MgO, FeOT, CaO, TiO_2, Cr, Th, Pb, V, Y, and REEs. The presence of phenocrysts probably prevented the physical blending of diorite and granodiorite magmas to form a homogeneous intermediate composition characterized by linear trends for all elements.

Chapter 4

ENCLAVES IN FOUR MEGUMA ZONE GRANITOIDS

4-1. Introduction

The term enclave refers to "material totally enclosed within and differing in some way from the otherwise fairly homogenous igneous rock in which it is found" (Didier, 1973; p. 1). An enclave is, therefore, any inclusion within a granitoid rock, regardless of its physical appearance, mode of occurrence, or supposed derivation. Abundant enclaves occur in most granitoids, and the diversity of enclave lithotypes provides a possible means to assess the source of the granitoid magmas and the material with which they interacted after leaving the site of melting (Barbarin and Didier, 1992a). The nature of the enclave assemblage in the Meguma Zone (MZ) granitoids is poorly known. Although previous workers reported abundant enclaves, Jamieson (1974) provided the only detailed study and focused on metasedimentary xenoliths in a local part of the South Mountain Batholith. Given that synplutonic mafic intrusions and hybrid granitoid lithologies occur, the enclave population may also contain mafic and/or hybrid igneous enclaves. This chapter documents in detail the enclave assemblage preserved within four MZ granitoids. It classifies the enclaves discovered and proposes origins for them.

4-2. The Variety of Enclaves in Granitoid Rocks

Didier (1973) standardized the classification of enclaves and recognized six distinct lithotypes in granitoid rocks on the basis of textural and mineralogical criteria. Figure 4.1 shows both their descriptive and genetic nomenclature and Table 4.1 contains criteria for enclave identification. Four arbitrary enclave groupings have important implications for petrogenetic studies and are distinguishable with field-based criteria:

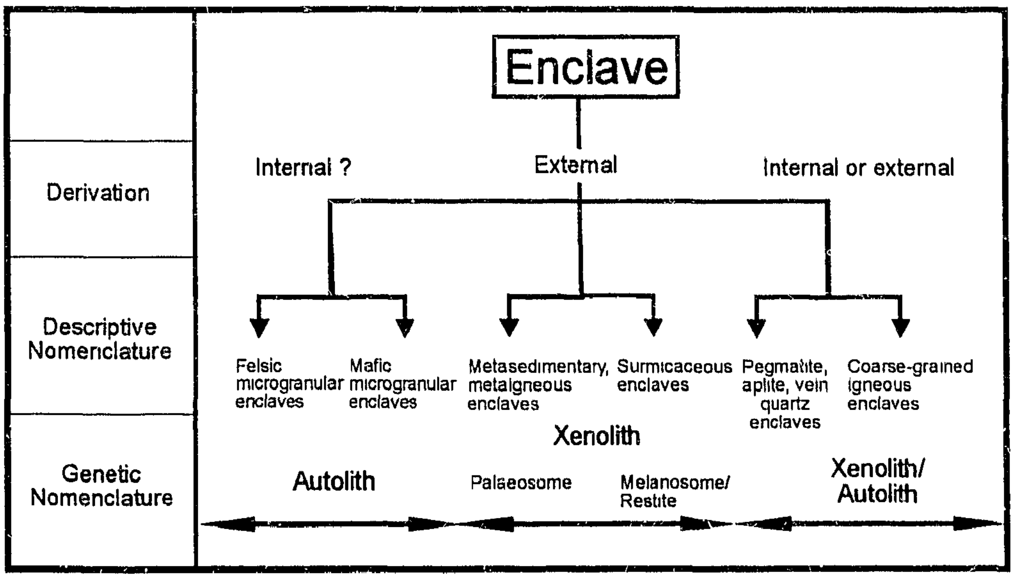

Figure 4.1. Descriptive and genetic classifications for enclaves in granitoid rocks. Nomenclature after Didier (1973) and Didier and Barbarin (1992).

Table 4.1. Criteria for the identification and classification of the six main enclave lithotypes.

Enclave type	Rounding (morphology)	Colour	Grain size	Contact Features	Other characteristics	References
Metasedimentary and metaigneous	angular-rounded or ellipsoidal	melanocratic to leucocratic	fine-coarse	sharp or diffuse	High temperature metamorphic mineralogy with hornfels texture. Appearance and mineralogy vary with protolith composition and degree of assimilation by host. May record relict sedimentary bedding and show strong micaceous foliations	1, 2, 3
Surmicaceous	angular-subangular (lenticular)	melanocratic	fine-coarse	sharp or diffuse	High-grade metamorphic textures and refractory mineralogy e.g. biotite, garnet, corundum, zircon, apatite. Generally foliated with >90% micas and aluminosilicate polymorphs	1, 4
Coarse-grained igneous	subangular-subrounded (ellipsoidal)	melanocratic to leucocratic	coarse	sharp or crenulate	Igneous textures and either mafic or granitoid compositions. Mafic compositions may show textural evidence for hybridism (see Table 3.1)	5, 6, 7
Mafic microgranular	subrounded-rounded (ellipsoidal)	melanocratic	fine	sharp, diffuse, or crenulate	Igneous textures and mafic or felsic mineralogies. May contain amphibole, clinopyroxene, and/or calcic plagioclase. May also show chilled margins, vesicles, and other textural evidence for hybridism	8, 9, 10, 11, 12
Felsic microgranular	subrounded-rounded (ellipsoidal)	leucocratic	fine	sharp or diffuse	Inequigranular textures and granitoid mineralogies dominated by biotite and plagioclase. Generally tonalitic modes	13, 14, 2, 15
Other	variable	variable	variable	sharp	Lithological characteristics of aplites, pegmatites, and vein quartz	1

1 = Didier (1973), 2 = Vernon (1983), 3 = Didier et al. (1982), 4 = Didier (1987), 5 = Fershtater and Borodina (1976), 6 = Bacon (1988), 7 = Larsen and Smith (1990), 8 = Eberz and Nicholls (1988), 9 = Castro et al. (1990), 10 = Chen et al. (1990), 11 = Blundy and Sparks (1992), 12 = Barbarin and Didier (1992b), 13 = Flood and Shaw (in press), 14 = Vernon (1990), 15 = Vernon (1984).

(1) *Metasedimentary and metaigneous enclaves.* Hornfelsed metasedimentary and metaigneous rocks show variable mineral assemblages and textures that reflect both their original protolith and the effects of contact metamorphism resulting from incorporation into the granitoid magma. These enclaves occur in all granitoids, where they may concentrate preferentially at intrusive contacts (Barbarin, 1992). Presumably they represent fragments of country rock.

(2) *Surmicaceous enclaves.* Enclaves consisting almost totally of biotite, muscovite, and aluminosilicate polymorphs occur only in migmatitic and deep-seated peraluminous granitoids (Didier, 1973; Didier et al., 1982). The preservation of microfolds within some enclaves indicates an external derivation and precludes their formation as magmatic biotite cumulates (Didier, 1973). Refractory mineral assemblages and sieve-textured biotites instead suggest a melanosome origin for many surmicaceous enclaves (Didier, 1987).

(3) *Microgranular enclaves.* Fine-grained igneous enclaves occur only in epizonal granitoids (Barbarin and Didier, 1992a; Vernon, 1984). Felsic microgranular enclaves are leucocratic relative to their host and have microgranitic textures and primitive granitoid compositions (Fershtater and Borodina, 1976), whereas mafic microgranular enclaves have higher colour indices than the host and may show granitoid, dioritic, diabasic, or cumulate textures (Orisini et al., 1992; Vernon, 1990; Vernon, 1992); they commonly occur near synplutonic mafic intrusions (Holden et al., 1987; Pitcher, 1992; Barbarin and Didier, 1992b, c). The presence of flow foliations and chilled margins in both mafic and felsic examples indicate the incorporation of magmatic enclaves. Fine-grained enclaves with mafic compositions may also have pillowed morphologies and crenulate contacts that provide well-established evidence for hybridism between the enclave and its host (Didier et al., 1982; Bowden et al., 1984; Larsen and Smith, 1990; Barbarin and Didier, 1992d).

(4) *Coarse-grained igneous enclaves.* Granitoid enclaves occur in multiply-intrusive hypabyssal or mesabyssal granitoids, where they may be comagmatic with their host and represent primitive

lithologies derived from depth, or have external derivation if suitable country rocks exist (Fershtater and Borodina, 1976). The presence of rounded shapes and magmatic flow foliations suggest their incorporation as magmas, whereas sharp contacts and angular morphologies instead suggest solid enclave incorporation. Truly mafic igneous lithologies may show mingling features similar to those of mafic microgranular enclaves, and they only occur abundantly in peralkaline or metaluminous granitoids (e.g. Eberz and Nicholls, 1988; Chen et al., 1992).

4-3. Approach

In this thesis, systematic enclave studies focus on the Barrington Passage Pluton (BPP), Shelburne Pluton (SP), Port Mouton Pluton (PMP), and the South Mountain Batholith (SMB) (Figure 4.2). These intrusions range in composition from tonalite to leucogranite, encompassing the wide range of granitoid lithologies present in the MZ. Also, they contain little obvious deformation, afford good access, and previous field studies established their lithological variation. All granitoid lithologies and known outcrops within the BPP, SP, and PMP were sampled. Within the SMB, sampling relied on the published 1:50,000 scale maps published by the Nova Scotia Department of Natural Resources (MacDonald et al., 1986), which report both the presence and abundance of enclaves within the batholith. At each locality, every enclave with a different appearance was sampled to yield an unbiased data set that delineates the effects of incorporation by the granitoid host. This work resulted in a total of 140 enclave samples (BPP 15%, SP 5%, PMP 26%, and SMB 54%). The number of samples from each intrusion approximately equals the abundance and variety of enclaves and the amount of exposed granitoid. After assigning the samples to descriptive groupings on the basis of their macroscopic characteristics, they were classified within Didier's (1973) scheme; 82 thin sections were made to aid the identification of fine-grained samples. Appendix D-1 summarizes all of the samples collected for this study, and specific details regarding the abundance, distribution, and nature of enclaves in each intrusion appear below.

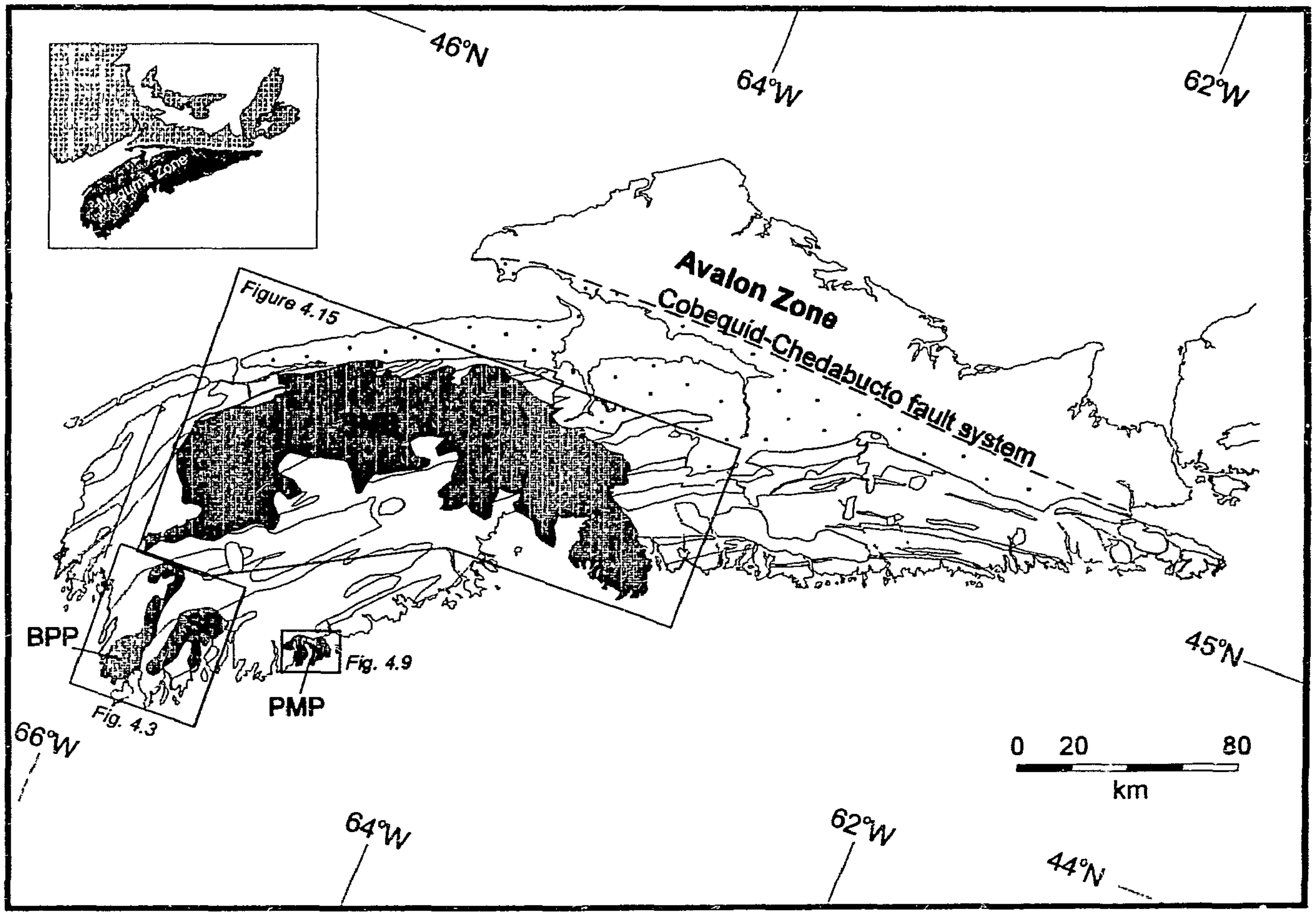

Figure 4.2. Geological map of the Meguma Zone showing the locations of the granitoid bodies included in the enclave study (shaded in grey) and the relative locations of Figures 4.3, 4.9, and 4.15. See Figure 1.3 in Chapter 1 for an explanation of the ornament. BPP = Barrington Passage Pluton, SP = Shelburne Pluton, PMP = Port Mouton Pluton, SMB = South Mountain Batholith.

4-4. Enclaves in Meguma Zone Granitoids

4-4.1. The Barrington Passage Pluton

The BPP forms a lobate intrusion of porphyritic tonalite at the southernmost onshore extent of the MZ (Rogers, 1984; Figure 4.2). Although poor exposure exists inland, good coastal outcrop occurs in the vicinity of Shag Harbour and Highway 103 provides a discontinuous section through the centre of the pluton. Coastal and highway localities, and two small quarries indicated on Figure 4.3 provided the most abundant enclaves, which show patchy distribution and rarely exceed 1% of any outcrop by area. No clear relationship exists between the abundance of enclaves and their proximity to the contacts.

Metasedimentary enclaves (45%)

Concentrated screens of parautochthonous Meguma Group enclaves up to 5 m long, occur at the southernmost contact of the pluton (Rogers, 1984) where they grade outwards into migmatite complexes (Rogers and White, 1984; Figure 4.3). Along the western margin of the pluton near Shag Harbour, metasedimentary enclaves range in length from 20-90 cm and show high aspect ratios (length/width 2.5-4) with lenticular to ellipsoidal morphologies. Most examples appear massive and have 0.05-0.5 cm grain sizes, but the elongate enclaves show indistinct contacts and have foliations parallel to the magmatic flow foliation in the host (Gallant, 1991; Figure 4.4a). The largest metasedimentary enclaves contain alternating horizons of foliated biotite and granoblastic quartz and feldspar, whereas smaller examples have gneissic appearances and coarser grain sizes and show 0.5 cm plagioclase porphyroblasts that resemble phenocrysts in the host. Magnetite, pyrite, anhedral cordierite, and subhedral andalusite may occur with biotite (Figure 4.4b), but garnet porphyroblasts occur only in sample NQ-1. One exotic enclave (SH-2) consists entirely of 1 mm granoblastic scapolite, amphibole, pyrite, and minor quartz (Figure 4.5).

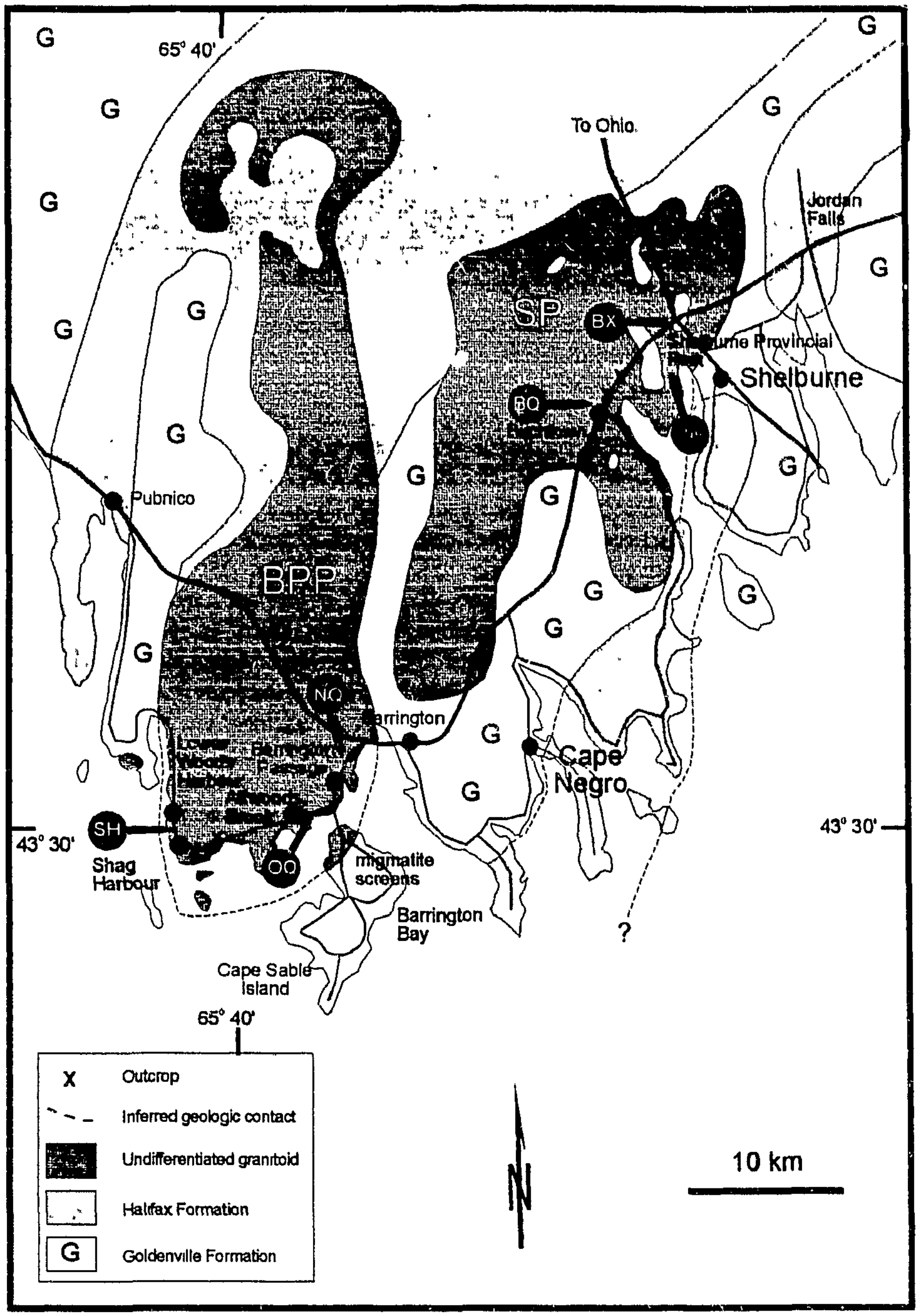

Figure 4.3. Geological sample location map for the Barrington Passage and Shelburne plutons. Modified after Rogers and Barr (1988). See Figure 4.2 for its location and the pluton abbreviations, and Table D1.1 in Appendix D for the location abbreviations.

a

b

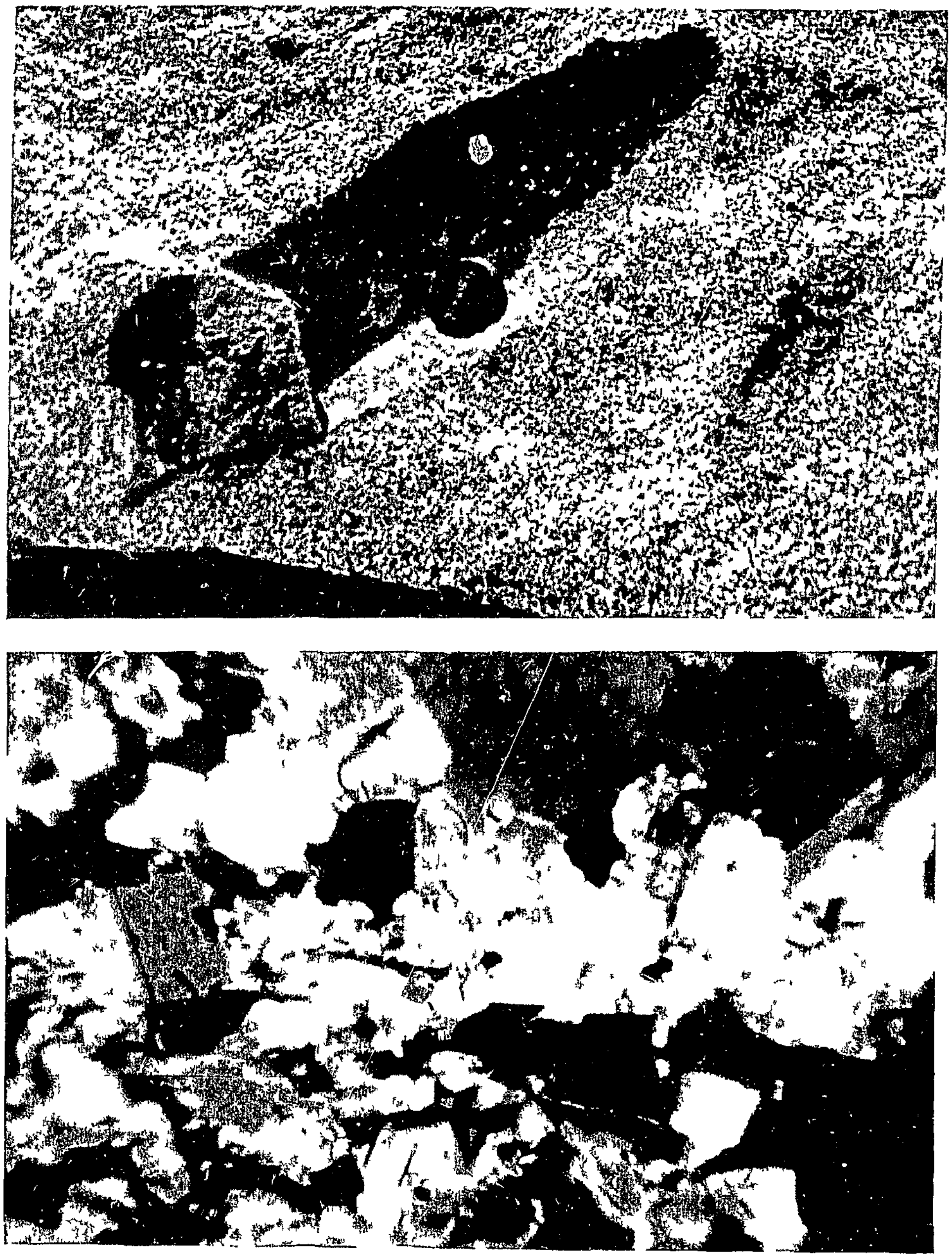

Figure 4.4. A typical metasedimentary enclave in the Barrington Passage Pluton (Sample NQ-2). (a) Note the elongate and lenticular shape and the plagioclase porphyroblasts. Plan view, lens cap 7 cm diameter; (b) Photomicrograph showing the weakly developed hornfels texture with granoblastic quartz, equant biotite, and plagioclase oikocrysts. Field of view 6 mm, XPL.

Surmicaceous Enclaves (55%)

Strongly foliated micaceous enclaves occur away from the contacts with the Meguma Group, where they range in size from 0 07-1 m and reach abundances of approximately 2% in monogenic clusters Most samples have subangular to lenticular morphologies and resemble metasedimentary enclaves, except that they are friable have millimetric thicknesses, and lie secant on the foliation of their host (Figure 4 6a) All samples contain >70% sieve-textured biotite with euhedral apatite and zircon inclusions Sulphides and magnetite also occur with secondary muscovite and chlorite in most enclaves, and samples OQ-4 OQ-5, and NQ-3 contain trace amounts of andalusite and cordierite (Figure 4 6b, Appendix D-1) Centimetric plagioclase oikocrysts with patchy zoning appear similar to phenocrysts in the host, and they suggest that chemical modification occurred after the incorporation of the enclaves (Jamieson, 1974)

4-4 2 The Shelburne Pluton

The SP forms an irregularly shaped granitoid body and a thin zone of Meguma Group metasediments separates it from the BPP to the south (Rogers and White, 1984, Figure 4 2) This pluton consists of equigranular tonalite, granodiorite, and minor monzogranite, although Rogers (1984) distinguishes no formal lithologic map units Highway 103 road cuts and two small quarries provided the samples (Figure 4 3) Enclaves occur most commonly in the monzogranites and granodiorites, but they account for less than 0 2% of the available outcrop Thick vegetation precludes determination of the overall enclave distribution within the pluton

Metasedimentary enclaves (53%)

Angular-subangular enclaves of Meguma Group metawackes range in size from 10-50 cm, and they occur in proximity to Meguma Group roof pendants along Highway 103 (Rogers,

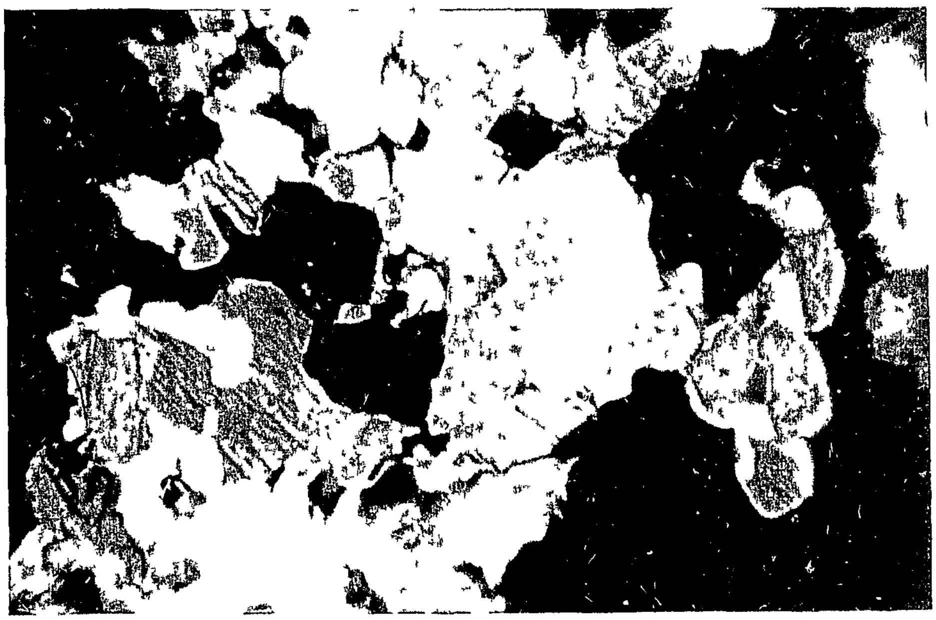

Figure 4.5. Photomicrograph of the granoblastic texture in exotic enclave SH-2 Scapolite and hornblende form the high relief and high birefringence minerals. The extinct areas are holes in the slide Field of view 6 mm XPL

a

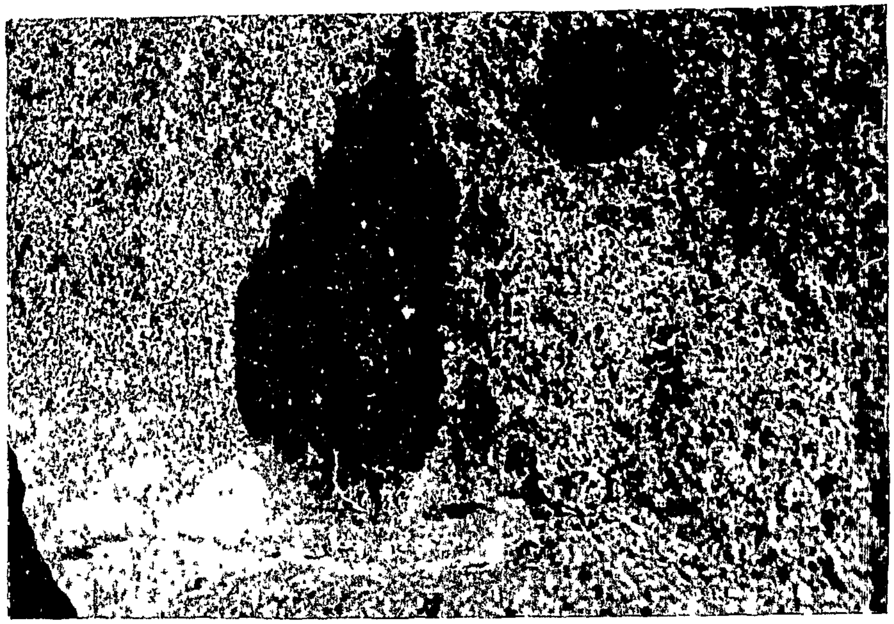

b

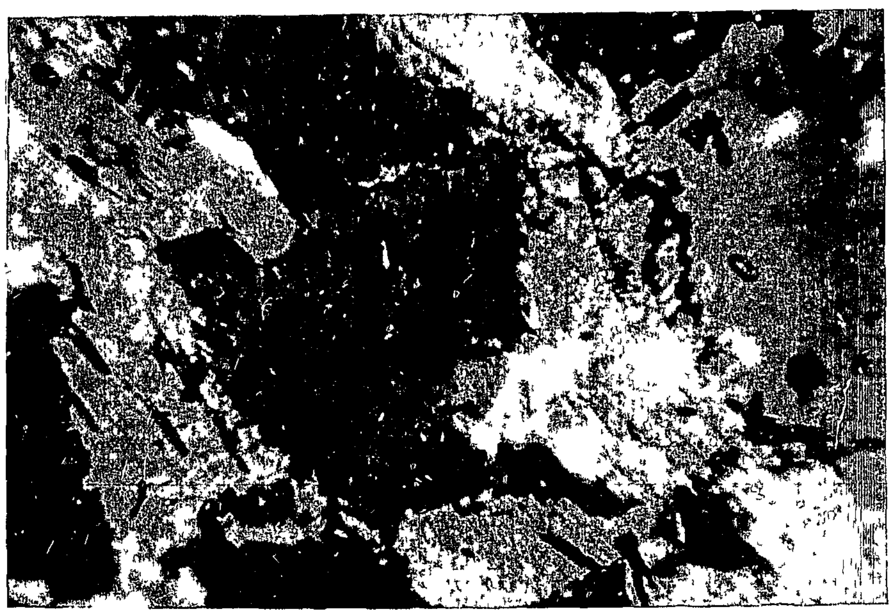

Figure 4.6. A typical surmicaceous enclave in the Barrington Passage Pluton (Sample OQ-4). (a) The enclave has an ellipsoidal shape, millimetric thickness, and consists largely of friable biotite. Plan view, lens cap 7 cm diameter; (b) Photomicrograph showing the abundance of biotite containing apatite and zircon inclusions. Many of the extinct interstitial areas are cordierite and andalusite. Field of view 6 mm, PPL.

1984; Figure 4.7a). All samples have sharp contacts and fine grain sizes and they contain no plagioclase or quartz oikocrysts (Figure 4.7b). Along the coast and within a small quarry at the Shelburne Provincial Park, subangular-subrounded hornfelses occur up to 20 cm in diameter. These enclaves show granoblastic hornfels textures and medium-coarse grain sizes that probably formed during recrystallization and partial assimilation.

Surmicaceous enclaves (47%)

Lenticular micaceous enclaves range in length from 3-5 cm; they occur along Highway 103 and in Birchtown Quarry (Figure 4.8a). These friable samples contain >90% decussate biotite with euhedral zircon and apatite inclusions (Figure 4.8b). They also have indistinct contacts and contain corundum euhedra and albite oikocrysts up to 1 cm. Unlike analagous enclaves in the BPP, all surmicaceous enclaves have centimetric thicknesses and no examples appear texturally intermediate between surmicaceous enclaves and metasediments.

4-4.3 The Port Mouton Pluton

The PMP is a complex, multiply-intrusive elliptical pluton that crops out south of Liverpool (Figure 4.2). This intrusion contains ten cross-cutting lithologic units that range in composition from biotite-muscovite-tonalite to granodiorite and monzogranite, which Douma (1988) assigned to three mafic-felsic intrusive cycles. Enclaves exist in all units, but they occur most abundantly (1-2%) in the Unit 1 tonalite and the Unit 4 granodiorites and monzogranites (Douma, 1988). At the interior of the pluton, enclaves become less abundant and show patchy distribution. Sampling concentrates on the tonalites of Unit 1 along the coast, in Unit 4 monzogranites along Saint Catherines River Road, and along Highway 103 at the interior of the pluton (Figure 4.9).

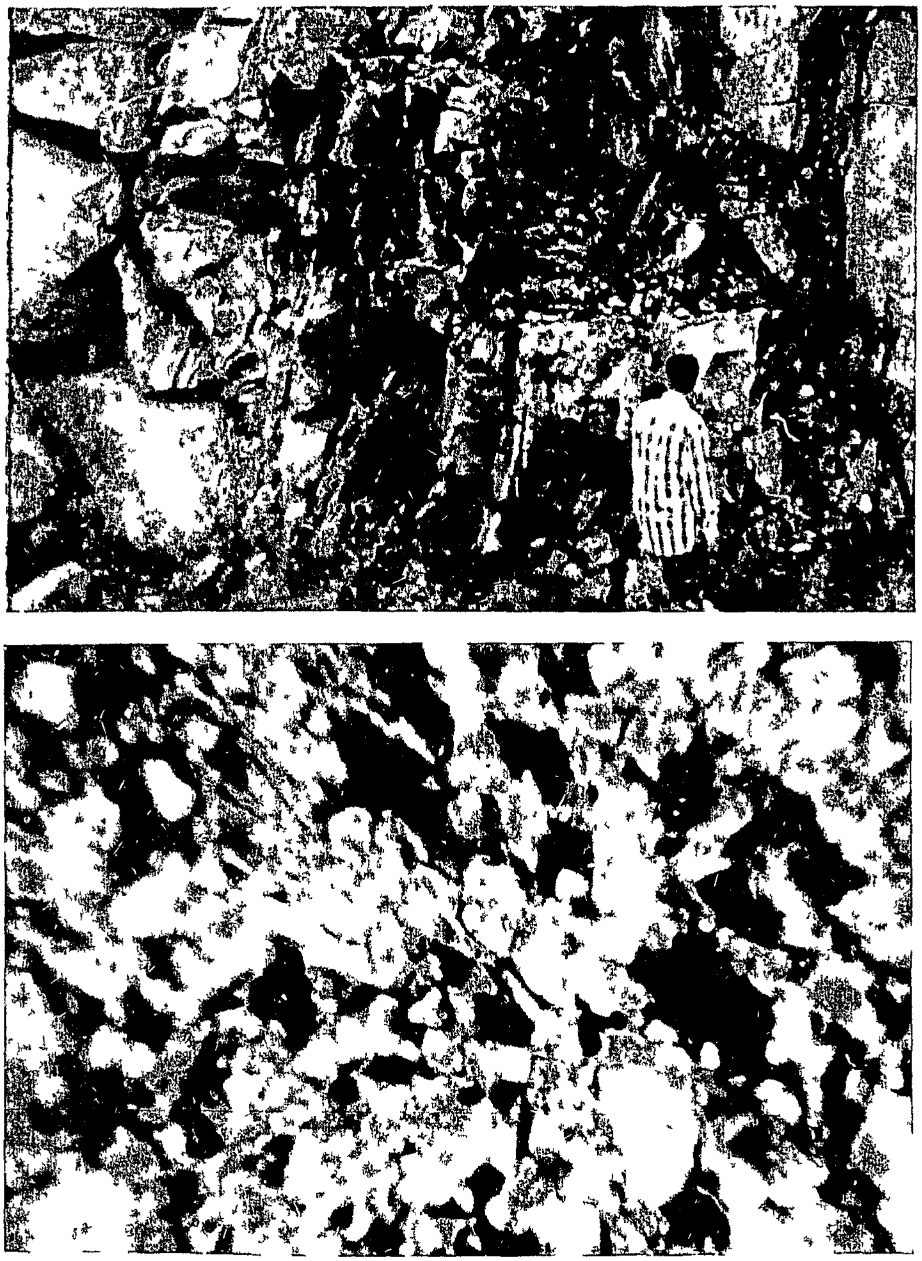

Figure 4.7. Typical metasedimentary enclaves in the Shelburne Pluton (a) Samples taken from near a roof pendant (central area with shattered appearance) at locality BX on Highway 103 Figure approximately 1 5 m tall; (b) Photomicrograph of the fine-grained granoblastic texture in metasedimentary enclaves at locality BX Field of view 6 mm, XPL

a

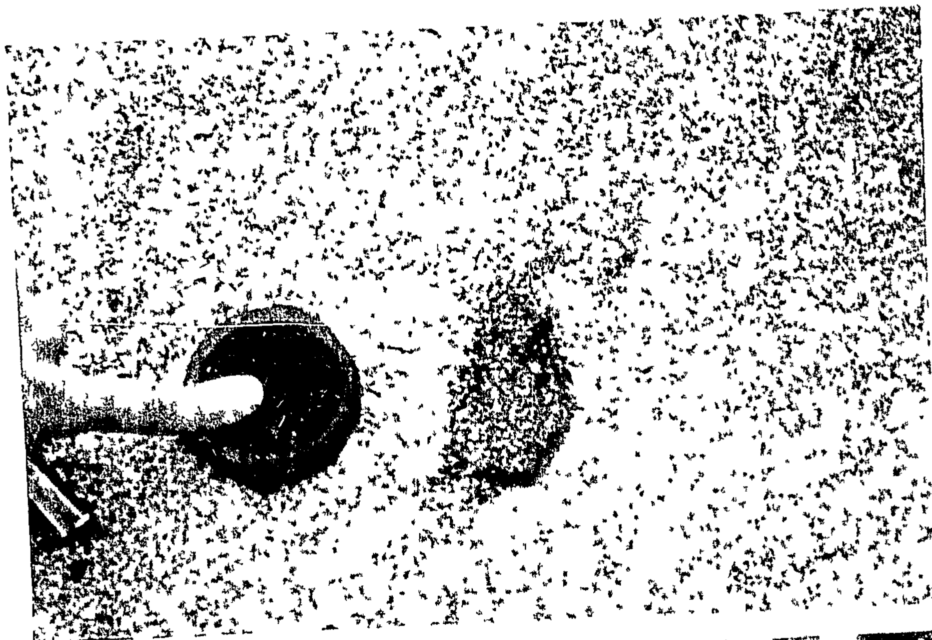

b

Figure 4.8. A typical surmicaceous enclave in the Shelburne Pluton (Sample BX-3). (a) Note the abundance of biotite and its similarity to sample OQ-4 (Figure 4.6). Plan view, lens cap 7 cm diameter; (b) Photomicrograph of randomly oriented biotites with large apatite and zircon inclusions. Note the sieve texture in the large biotite crystal at the far right. Field of view 6 mm, PPL.

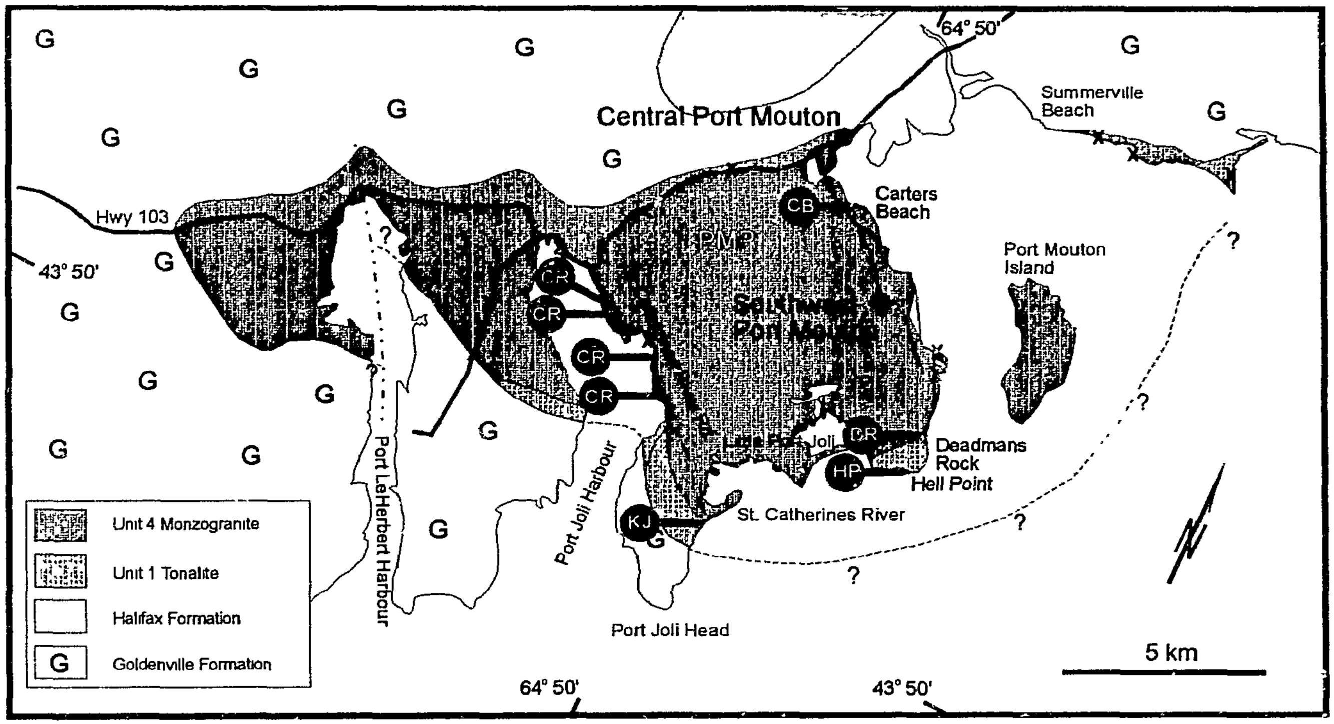

Figure 4.9. Geological sample location map for the Port Mouton Pluton. Modified after Douma (1988). See Figure 4.2 for its location and the pluton abbreviations, Figure 4.3 for other symbols, and Table D1.1 in Appendix D for the location abbreviations. The extreme internal complexity of this pluton on the metric scale prevents any representation of all ten lithologic units in this diagram (see Figure 3.7 in Chapter 3).

Metasedimentary enclaves (46%)

Large rafts of Meguma Group metasedimentary rocks up to 35 m long occur in migmatite complexes at Saint Catherines River beach near locality KJ (Figure 4.10; Douma, 1988). Transported enclaves range in size from 0.3-1 m and have subangular to subrounded shapes; pelites are dark brown, whereas psammites have grey colours and commonly show biotite selvages at their contacts (Figure 4.11a). Within Unit 1, metasedimentary lithologies are similar to Meguma Group enclaves within the screens at the contact; they show foliated biotite horizons alternating with quartzo-feldspathic layers that probably mimic sedimentary bedding (Figure 4.11b). Non-recrystallized examples show mild deformation manifested as strained quartz with undulose extinction, and they have porphyroblasts of garnet, cordierite, and andalusite. At one locality near Mcleods Cove a concentrated tonalite breccia (Unit 5b of Douma, 1988; Figure 3.7 in Chapter 3) contains up to 80% garnet-, andalusite-, and cordierite-bearing hornfelses from 0.02-2 m long. Metasedimentary enclaves in Unit 4 are smaller, coarser grained, and contain millimetric porphyroblasts of garnet, cordierite, and/or corundum.

Surmicaceous enclaves (<2%)

Surmicaceous enclaves occur only at Carters Beach in the Unit 4 monzogranite, where they form 2-30 cm, angular-subangular rafts of foliated biotite and chlorite (Figure 4.12). They constitute less than 0.5% of the exposed granitoid.

Microgranular enclaves (25%)

Microgranular enclaves occur rarely in the Unit 1 tonalite, but they show greater abundances in the Unit 4 granodiorites and monzogranites along Saint Catherines River road. They range in size from 10-35 cm, have subrounded to rounded shapes, and exhibit sharp or gradational contacts with their host (Figure 4.13a). Some examples resemble psammites because they have surficial weathered rinds, but internally, their fine grain sizes

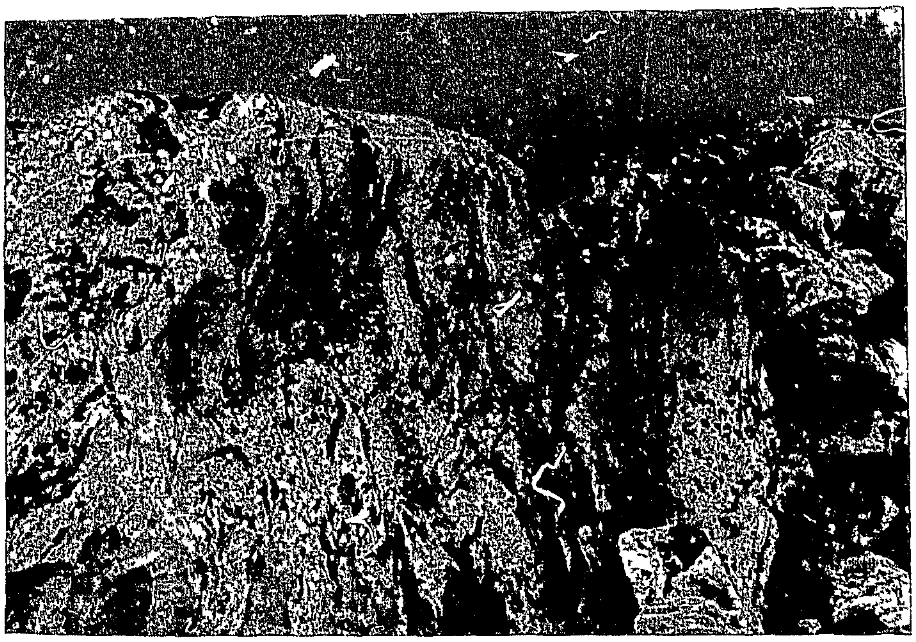

Figure 4.10. Screens of migmatite in the Port Mouton pluton at Saint Catherines River beach. The migmatites contain abundant enclaves of recrystallized pelite (dark grey) and recrystallized psammite (light grey). View to the northeast, cliff face 2 5 m high.

a

b

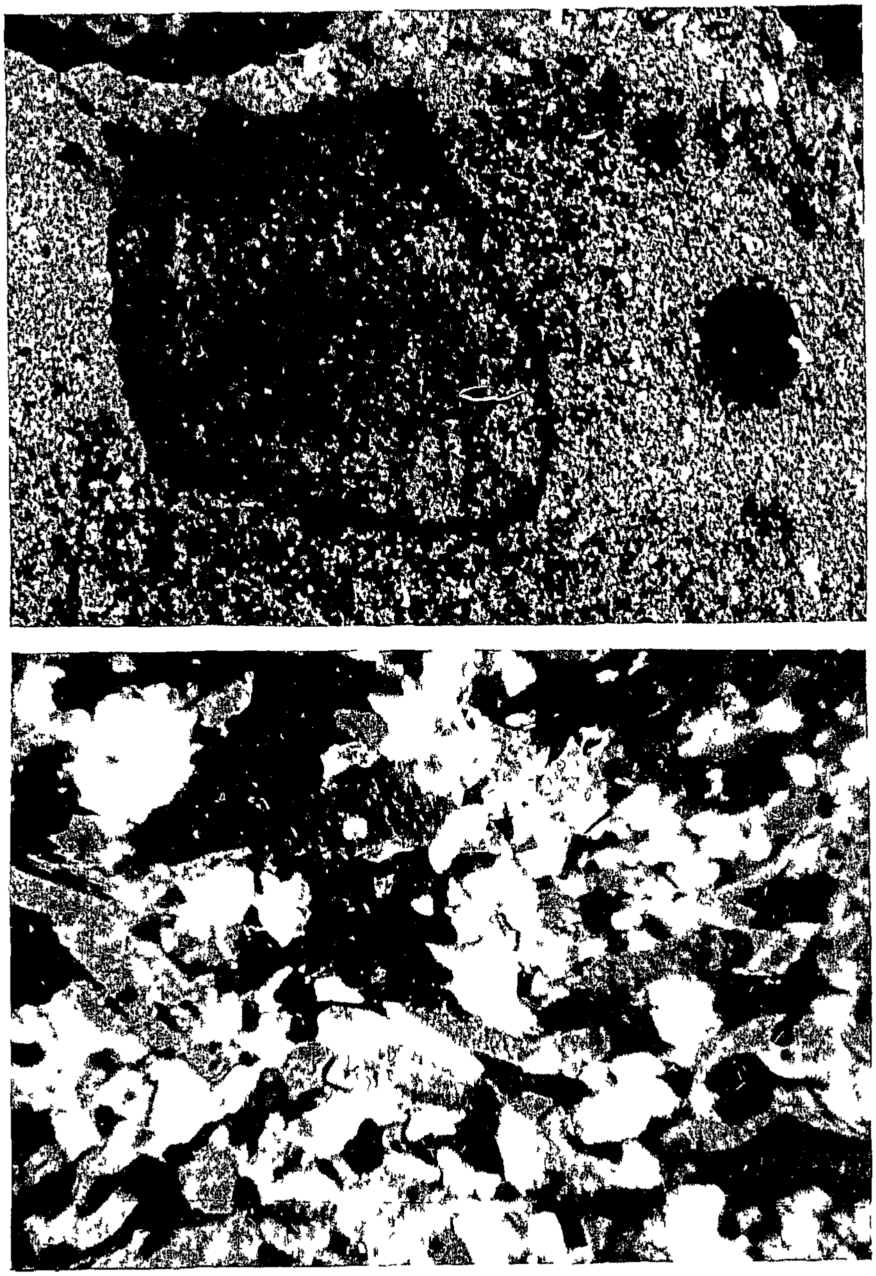

Figure 4.11. Typical metasedimentary enclaves in the Port Mouton Pluton (a) The subrounded shape and marginal biotite rind shown by psammitic sample CR-14 collected along Saint Catherines River Road The coarse grain size results from hornfelsing and chemical assimilation. Plan view, lens cap 7 cm diameter; (b) Photomicrograph of the well-developed granoblastic groundmass in sample HP-1. Fine grain sizes and aligned biotites typify pristine metasedimentary enclaves Field of view 6 mm, XPL

Figure 4.12. A coarse-grained surmicaceous enclave in the Port Mouton Pluton at Carters Beach (sample CB-2). The green colouration of the enclave results from chloritization, and the outcrop discolouration results from weathering. Plan view, lens cap 7 cm diameter.

(circa 0.5 mm) and equigranular but igneous textures impart melanocratic colourations. They all have tonalitic modes and contain biotite (15%), normally zoned plagioclase (53%), rare K-feldspar (<1%), interstitial quartz (27%), and up to 6% muscovite (Figure 4.13b). All mineral phases apparently crystallized concurrently and rapidly to form a pseudo-aplitic texture. Many examples also develop centimetric oikocrysts of albite, K-feldspar, and quartz, similar to those in the metasedimentary enclaves.

Coarse-grained granitoid enclaves (27%).

Abundant coarse-grained granitoid enclaves occur in both Unit 1 and Unit 4, where they form "patch breccias" containing up to 80% inclusions, as at Hell Point and Deadmans Rock (Figure 4.14a). Most examples range in size from 0.1-1 m, and they have white, grey, or buff colours and rounded morphologies, porphyritic, megacrystic, or equigranular textures, and 1-2 mm grain sizes. Granitoid enclaves contain subgrained quartz, with plagioclase, biotite, muscovite, and rare K-feldspar (Figure 4.14b). Their compositions apparently range between tonalite and monzogranite and match all of the ten lithologies exposed in the pluton (Douma, 1988), although no examples were explicitly slabbed and stained.

4-4.4. The South Mountain Batholith

The SMB represents a polyintrusive granitoid complex covering an area of approximately 7500 km^2 southwest of Halifax (Abbott, 1989; Figure 4.2). Regional mapping subdivides the SMB into at least 13 discrete plutons that range in composition from granodiorite to leucogranite (MacDonald et al., 1990; Clarke et al., 1993b; Figure 4.15). The SMB has a discontinuous marginal tonalite-granodiorite carapace at its contact with the Meguma Group, but monzogranite forms the most common internal lithology. Poor exposure and weathered outcrops south of Lequille, restrict most sampling to coastal exposures within the Halifax Pluton, and to major roads throughout the rest of the batholith (Figure 4.15). The most abundant enclaves occur

a

b

Figure 4.13. Typical microgranular enclaves in the Port Mouton Pluton. (a) The well-rounded shape and sharp-indistinct contacts of sample DR-2. Note its fine grain size and homogenous appearance relative to metasedimentary enclaves. Plan view, lens cap 7 cm diameter; (b) The inequigranular igneous texture of sample CR-9. Note the lack of mineral alignments and the occurrence of primary magmatic (?) muscovite similar to that of the host. Field of view 6 mm, XPL.

a

b

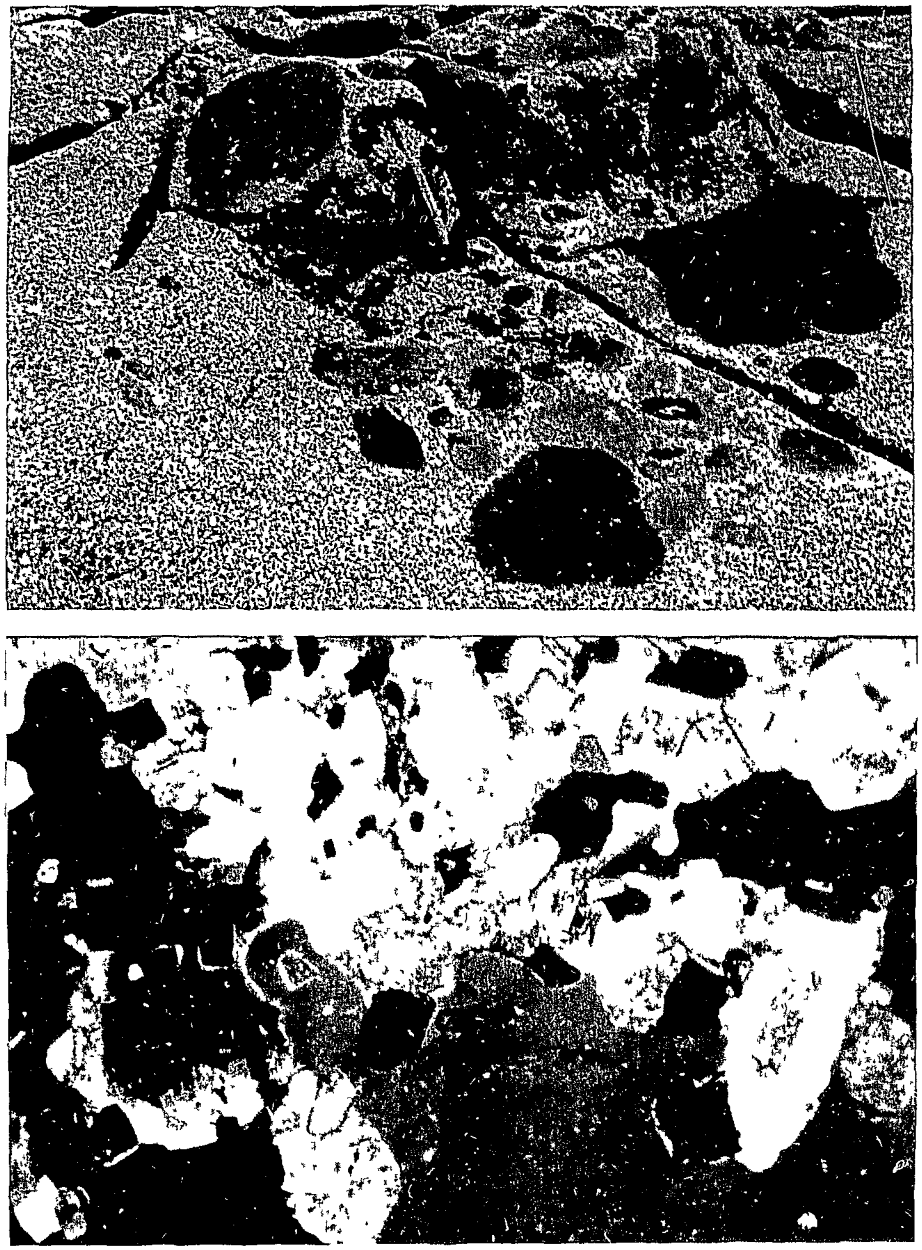

Figure 4.14. Coarse-grained granitoid enclaves in the Port Mouton Pluton. (a) A polygenic cluster of rounded granitoid enclaves and microgranular enclaves at Hell Point. The two dark patches are tidal pools. View to the west, hammer 50 cm long; (b) The inequigranular-subporphyritic texture of sample HP-4. The granitoid enclaves appear similar to in situ granitoid lithologies. Field of view 1 cm, XPL.

a

b

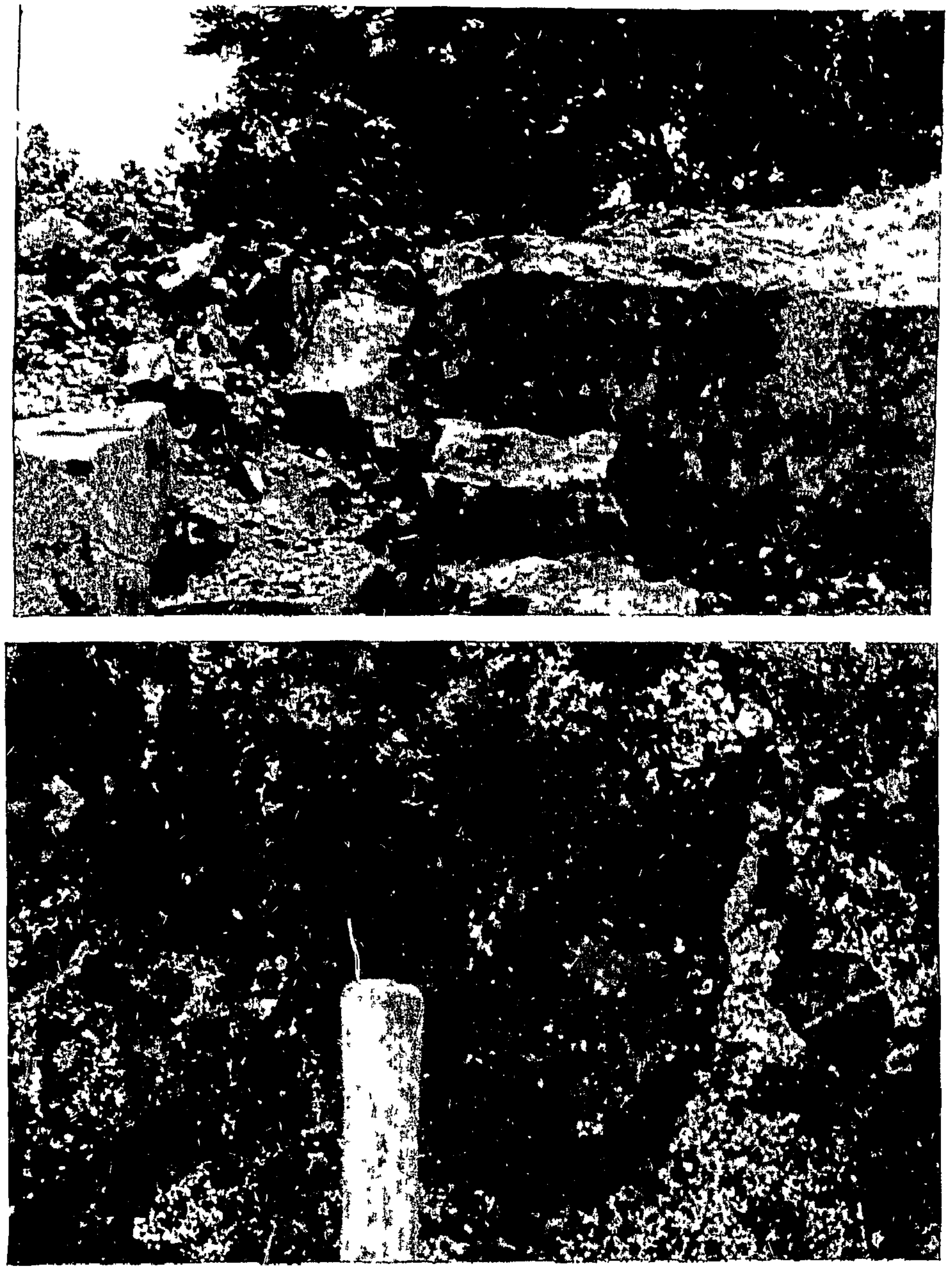

Figure 4.17. Enclaves in a "breccia pipe" at Northwest Arm drive (ND samples). (a) The vertical pipe contains a polygenic assemblage of centimetric metasedimentary and microgranular enclaves. View to the northeast, pipe structure approximately 1.5 m wide; (b) Hornfelsed metasedimentary enclaves in the matrix-supported "breccia pipe". Note the plagioclase, quartz, and garnet porphyroblasts. View to the northeast, observable hammer handle 20 cm long.

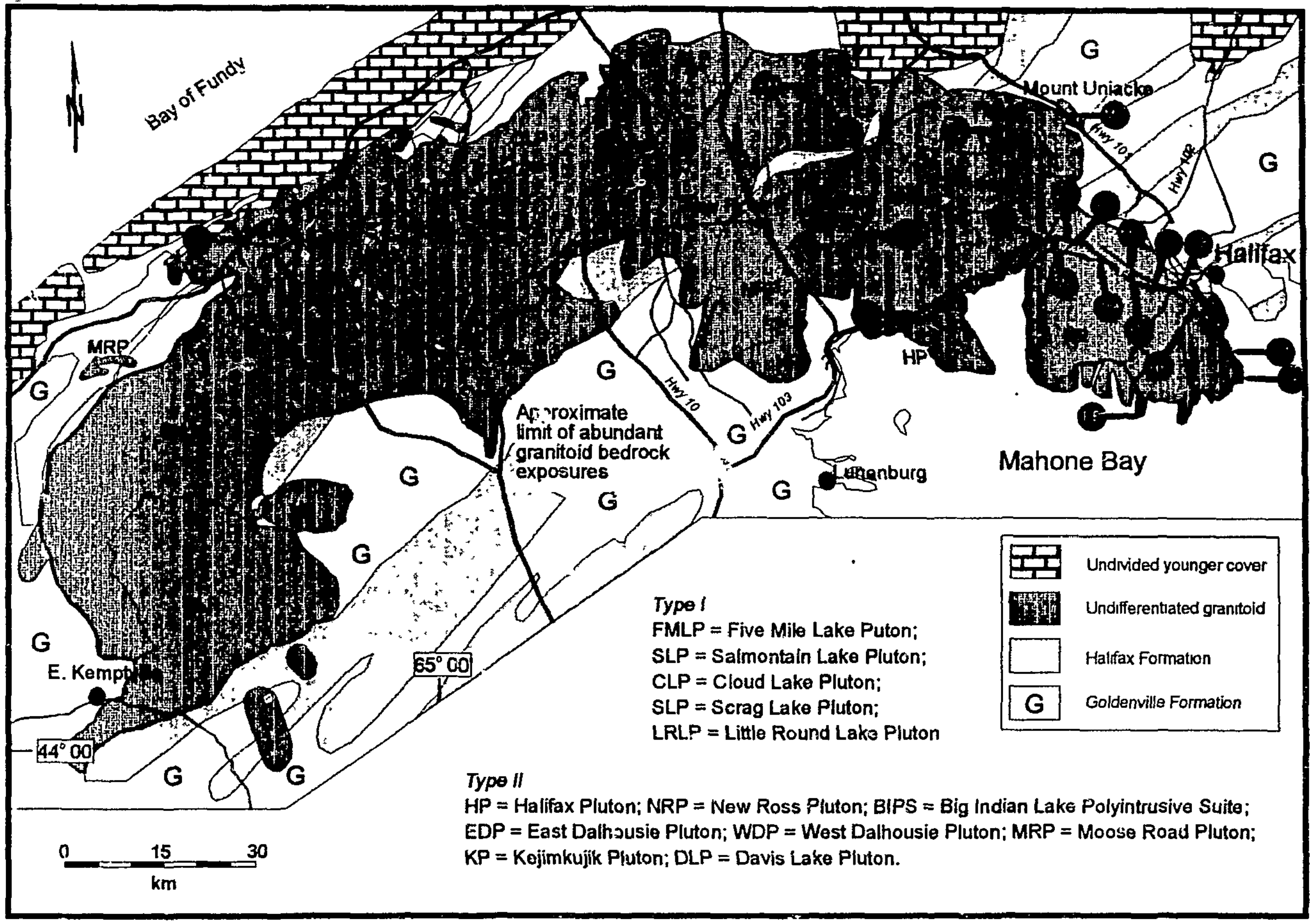

Figure 4.15. Geological sample location map for the South Mountain Batholith. Base map after MacDonald et al. (1992) and the granitoid bedrock limit stylized after Stea et al. (1992). See Figure 4.2 for its location and the batholith abbreviation, and Table D1.1 in Appendix D for the location abbreviations.

in the marginal lithologies, especially at their contacts with the Meguma Group. Internally, the leucomonzogranites and leucogranites contain the fewest, smallest, and most assimilated enclaves, whereas the most abundant pristine (unassimilated) enclaves occur at intrusive contacts between individual plutons. Enclave abundance drops sharply to approximately 2% within 10-20 m of the contact, and enclaves cluster into swarms or intrusive "pipes" that locally reach 80% total included material at the pluton interiors.

Metasedimentary enclaves (57%).

Metasedimentary inclusions occur within most plutons of the SMB, but they show particular abundance and variety in the marginal granodiorite. At Mount Uniacke and Northwest Arm Drive (Figure 4.15) angular-subangular pelites and psammites up to 20 cm, occur at various stages of disaggregation and assimilation; they locally represent approximately 60% of the total outcrop. Psammites are massive and equigranular, whereas pelites contain foliated biotite and abundant opaque minerals. Pristine hornfelses preserve relict sedimentary bedding, which commonly controls the distribution of cordierite, andalusite, and garnet porphyroblasts (Figure 4.16a, b). Their considerable variety probably reflects a range of sources and different residence times in the granodiorite magma. At Portuguese Cove, Prospect Bay, and Chebucto Head, in the Halifax Pluton monzogranites, metasedimentary enclaves constitute 1-5% of the outcrop; they have variable colouration, 0.03-1 m sizes, and subangular to subrounded morphologies. Matrix-supported intrusive breccias at Portuguese Cove and Northwest Arm Drive contain polygenic assemblages of rounded hornfelses with garnet porphyroblasts (Figure 4.17a, b).

Towards the centre of the batholith at Upper Vaughan, Smiths Corner, Dead Brook, and within the Big Indian Lake Polyintrusive Suite, subrounded-rounded enclaves occupy less than 0.1% of the available outcrop where concentrated monogenic swarms occur. Most examples have grey-buff colouration and they show gradational contacts marked by biotite selvages. They commonly also have cordierite, garnet, and/or andalusite porphyroblasts, and pyrite,

a

b

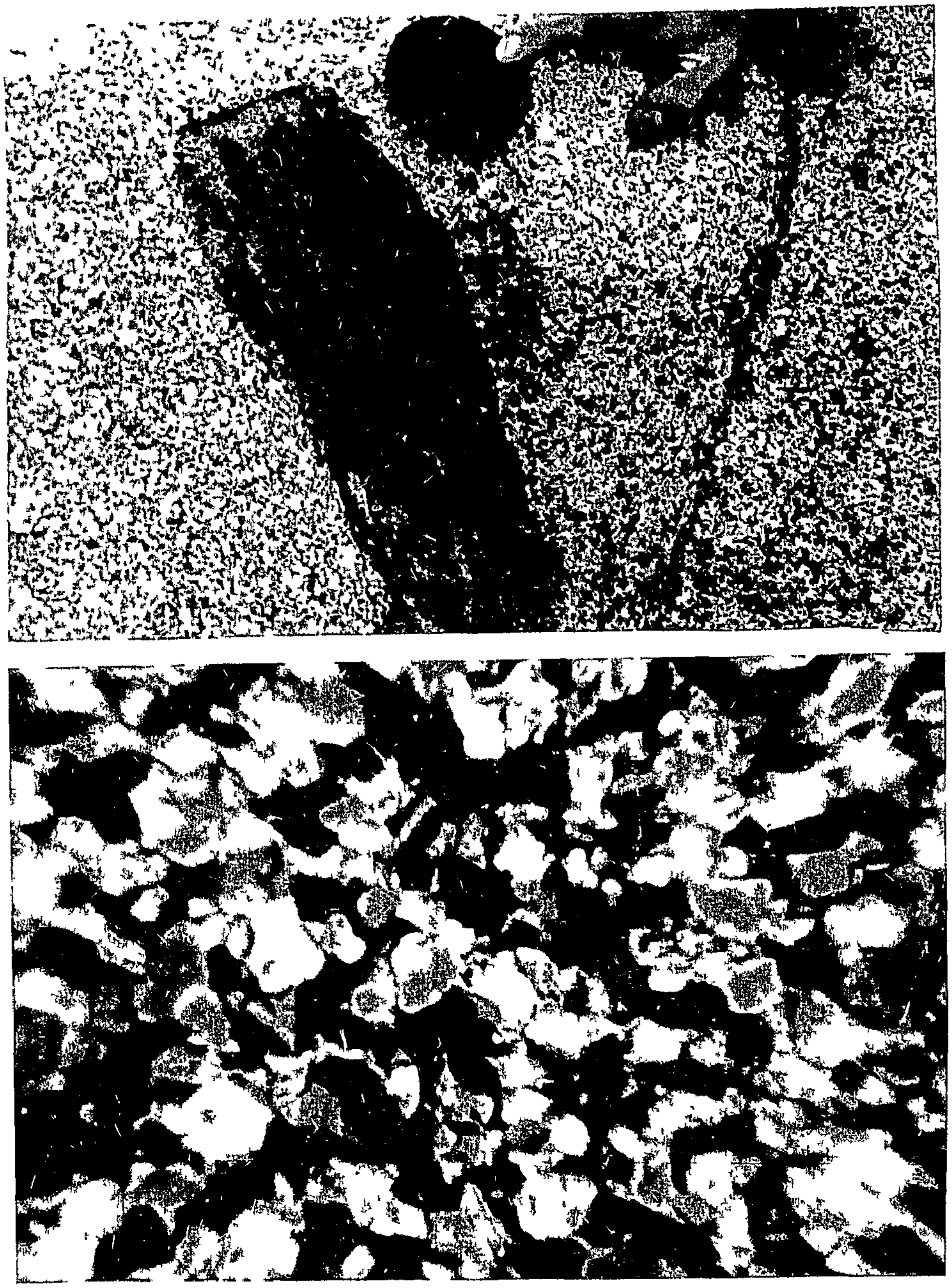

Figure 4.16. Metasedimentary enclaves in the South Mountain Batholith. (a) An elongate, foliated and garnet-bearing enclave at Peggys Cove. View to the west, lens cap 7 cm diameter; (b) Photomicrograph of the granoblastic quartzo-feldspathic matrix with weakly foliated muscovite and biotite in sample MU-4 from Mount Uniacke. Field of view 6 mm, XPL.

chalcopyrite, and magnetite inclusions in biotite. At Lequille and Hemlock Hill (within the volumetrically minor "mafic porphyry" unit) enclaves are angular to subrounded hornfelses that have leucocratic colours and indistinct contacts. Their leucocratic colour at least partly reflects the growth of feldspar and quartz porphyroblasts during assimilation to produce a pseudo-granitic texture that resembles the host.

Surmicaceous enclaves (<1%).

Surmicaceous enclaves occur rarely within the SMB. Minor 2-8 cm lenticular examples contain centimetric feldspar porphyroblasts. They occur in leucomonzogranites throughout the batholith, where they represent the only enclave lithotype. One 3 m example in monzogranite at Portuguese Cove, consists entirely of randomly oriented biotite, and it has K-feldspar megacrysts similar to those present in the host (Figure 4.18). However, its irregular shape and gradational contacts alternatively suggest that it may represent a biotite-cumulate schlieren.

Microgranular enclaves (26%).

Fine-grained igneous enclaves occur commonly throughout the batholith, but they show particular abundance and diversity within the Peggys Cove monzogranite and Halifax Peninsula leucomonzogranite, near the contact of the Halifax pluton. Typical examples range in size from 0.1-1 m at Portuguese Cove and Chebucto Head, where they constitute 10% of the enclave assemblage. Subrounded, well-rounded, or irregular shapes all exist, and they have light grey colours and fine grain sizes (average 0.5 mm). Exceptionally large examples (1-2 m) also enclose angular metasedimentary enclaves (Figure 4.19a). They consist of equigranular biotite (9.4-18.0%), muscovite and/or cordierite (0.4-1.0%), normally zoned or oscillatory zoned plagioclase (26.1-40.4%; An_{50}-An_{10}), K-feldspar (0.04-1.5%), and quartz (32.8-35.5%) (Figure 4.19b). All of the microgranular enclaves have tonalitic compositions, and their textural and

Figure 4.18. A potential surmicaceous enclave at Portuguese Cove (sample PC-5). Its large size and irregular shape suggests that it might also represent a biotite cumulate. View to the northeast, hammer handle 50 cm long.

a

b

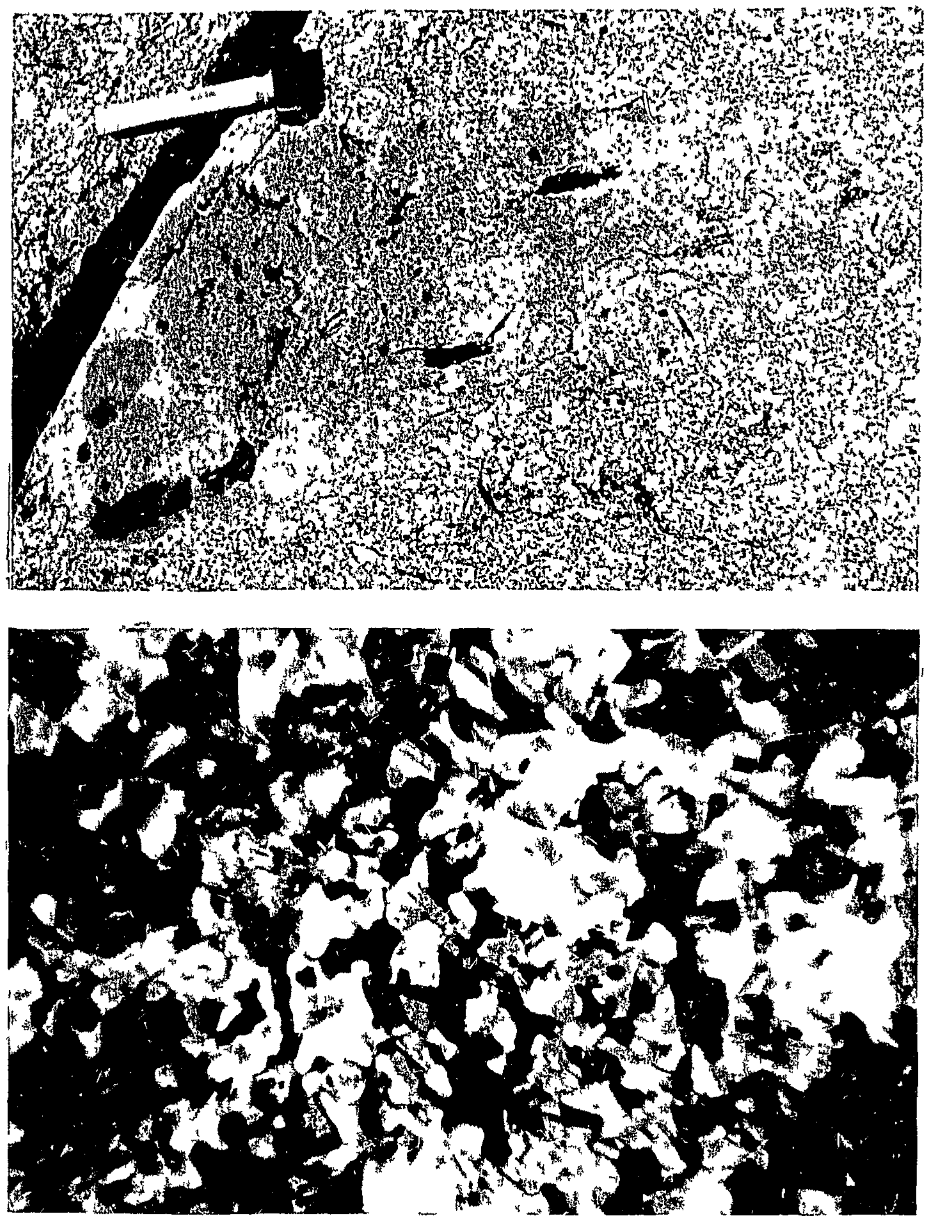

Figure 4.19. Typical microgranular enclaves in the South Mountain Batholith. (a) A composite microgranular enclave at Portuguese Cove. It contains angular, centimetric metasedimentary enclaves (sample PC-3) Plan view, hammer approximately 50 cm long; (b) Photomicrograph of the inequigranular and randomly oriented texture in microgranular sample RM-2. Note the quartz porphyroblast at the top of the slide. Field of view 6 mm, XPL

compositional similarity with analogous enclaves in the PMP suggests that they formed by similar processes.

Unusual dark grey examples occur at Northwest Arm Drive, Portuguese Cove, and along Highway 103 near Timberlea and Nine Mile River, where a concentrated monogenic swarm contains approximately 2% ellipsoidal enclaves (Figure 4.20a). The melanocratic enclaves have similar mineral assemblages and compositions to their leucocratic counterparts, but they show inequigranular or subporphyritic textures with magmatic flow foliations and idiomorphic plagioclase microphenocrysts (Figure 4.20b). The foliation lies parallel to their longest axes and it possibly implies their incorporation in a magmatic state. Oikocrysts that resemble megacrysts in the host, grew after enclave solidification and they locally cross-cut the flow foliations or the enclave-host contacts. Their dark colour apparently results from high concentrations of biotite (the only ferromagnesian mineral) and no enclaves have compositions more primitive than tonalite. Rare examples show concentric zoning and they are surrounded by leucocratic haloes in the host granitoid. These features probably preserve the effects of a chemical disequilibrium reaction between the enclave and its host.

Coarse-grained granitoid enclaves (<16%).

No mineralogical distinction exists between coarse-grained enclaves and the microgranular enclaves in the SMB. Porphyritic or megacrystic granitoids occur as inclusions within the granodiorites and monzogranites, but they do not occur within the leucomonzogranites and leucogranites. Grey, subangular enclaves up to 1 m, subangular shapes occur at Lakeside, Little Indian Lake, Portuguese Cove, Prospect Bay, and Lequille. Small (<10 cm) examples also occur in the "breccia pipes" at Northwest Arm Drive. They all have medium-coarse grain sizes and they consist of biotite, muscovite and/or cordierite, plagioclase, K-feldspar, and quartz (Figure 4.21). Their similar textures and modes to all *in situ* rocks in the SMB except leucomonzogranite and leucogranite support an internal origin for them.

a

b

Figure 4.20. Unusually melanocratic microgranular enclaves at Nine Mile River. (a) The monogenic swarm of dark grey, ellipsoidal, and highly elongate enclaves. View to the southeast, figure approximately 1.5 m tall; (b) Photomicrograph of the inequigranular, medium-grained texture of sample NMR-3. Field of view 6 mm, XPL.

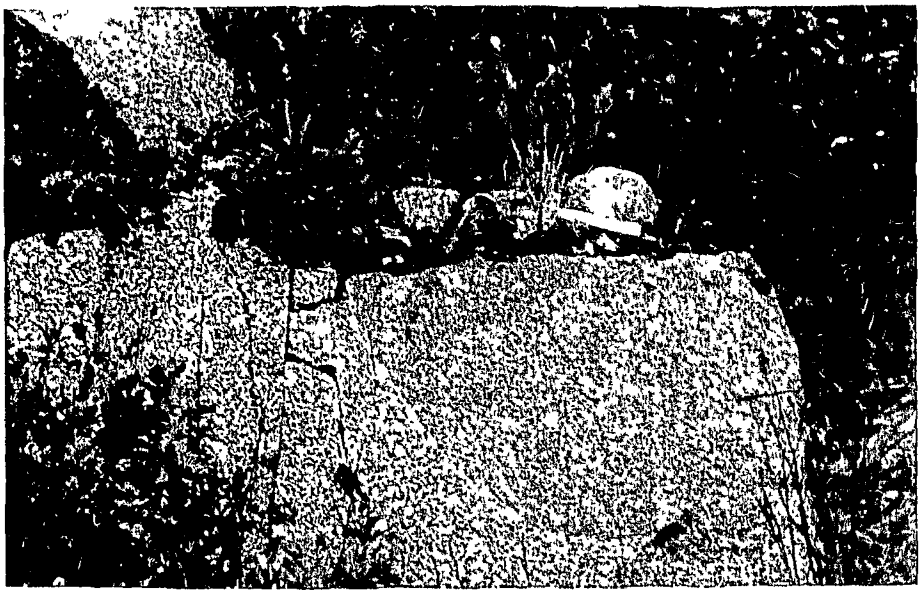

Figure 4.21. A typical coarse-grained granitoid enclave in the South Mountain Batholith at Little Indian Lake. Note its similar colour to the host, the alignment of plagioclase megacrysts in the host around it, and the concentration of megacrysts at the enclave contact. View to the north, hammer approximately 50 cm long.

4-5. Implications of the Enclave Studies for Granitoid Petrogenesis

The BPP, SP, PMP, and SMB contain a typical enclave assemblage for peraluminous granitoids, which consists of metasedimentary, surmicaceous, coarse-grained granitoid, and microgranular enclaves (Barbarin, 1992). No coarse-grained mafic igneous enclaves occur in any lithology. Given that the studied intrusions encompass all of the granitoid lithologies currently exposed in the MZ, they are potentially representative of all MZ granitoids. This discussion considers the origins of the micaceous and igneous enclaves separately.

4-5.1. The Origin of Metasedimentary and Surmicaceous Enclaves

Metasedimentary and surmicaceous material accounts for all of the enclaves within the BPP and SP, and it represents circa 50% of the enclaves in the PMP and SMB. Pristine metasediments at the contacts of all plutons, or close to roof pendants, are lithologically similar to Meguma Group lithologies. In the SMB, they probably represent locally stoped xenoliths, and both S isotopic analyses of the marginal granodiorite and Nd isotopic analyses of micaceous enclaves support this interpretation (Clarke et al., 1988). In all of the studied intrusions, xenoliths show variable lithologies that probably reflect a variety of Meguma Group protoliths; perhaps exotic enclave SH-2 from the BPP represents a hornfelsed calcareous nodule from the Halifax Formation (Graves and Zentilli, 1988). Although the White Rock Formation possibly contributed xenoliths to northerly areas in the SMB, no enclaves have gneissic textures with high-grade metamorphic mineral assemblages that suggest a derivation as palaeosomes derived from the sub-Meguma basement. Towards the centres of the granitoids, metasediments generally have smaller sizes, more rounded shapes, and coarser grain sizes. These features probably form during hornfelsing and disaggregation in the granitoid host after incorporation. Many examples also have centimetric plagioclase and K-feldspar porphyroblasts that result from alkali metasomatism during assimilation (Jamieson, 1974).

Textural and mineralogical similarities between the surmicaceous enclaves and the type examples described by Didier (1973) support a melanosome origin for these structures. The gradation from micaceous xenoliths to surmicaceous enclaves at the interior of the BPP strongly suggests that hot tonalite magmas (e.g. Wyllie, 1977) partially melted the xenoliths to form a biotite- and aluminosilicate-rich residue, and the migmatitic contacts of the pluton lend support to this hypothesis. The rare but mineralogically similar surmicaceous enclaves in the other granitoid bodies probably also formed by partial melting of xenoliths, but they could represent transported enclaves of restite from the granitoid source region. The absence of a lithologic continuum with the xenoliths neither supports nor refutes a restite origin for them. Regardless of the ultimate origin for surmicaceous enclaves, they indicate a strong crustal component in the granitoids that their peraluminous compositions suggest (Didier, 1987).

4-5.2. The Origin of Granitoid and Microgranular Igneous Enclaves

Mineralogical similarities between the coarse-grained granitoid enclaves and *in situ* lithologies in the PMP and SMB strongly suggest that they represent stoped autoliths of early crystallized granitoid material. The multiply-intrusive nature of both bodies, the absence of enclaves more evolved than monzogranite, and the forceful emplacement of magmas in the SMB (Horne et al., 1990) all lend support to this hypothesis. No clear distinction exists between models for the origin of mafic and felsic microgranular enclaves in the literature and three main hypotheses apply to both types:

(1) *Restites or assimilated metasediments.* Chen et al. (1990) considered the lack of suitable country rock and granitoid protoliths in granitoids from the Lachlan Fold Belt of southeastern Australia as an indication of deep, restitic sources for microgranular enclaves. If they form as

restites, then their igneous microtextures result from reaction and assimilation with the host (Chen et al., 1992).

(2) *Quenched hybrids, mingled magmas, or assimilated mafic igneous material.* Chapter 3 documents the effects of magmatic interaction between mafic and granitoid magmas. Emplacement of mafic magma into a crystallizing granitoid magma chamber causes rapid quenching and potentially produces fine-grained mafic igneous enclaves and mafic microgranular enclaves that convection re-distributes (Eberz and Nicholls, 1988; Barbarin, 1992). Castro et al., (1990) and Cantagrel et al. (1984) describe "pillow-like" microdioritic enclaves with chilled and crenulate margins that probably result from commingling. Tonalitic enclaves containing quartz ocelli, rapakivi feldspars, reversely zoned calcic plagioclases, and vesicles may also result from hybridism (Larsen and Smith, 1990; Pin et al., 1990; Bacon, 1988; Dodge and Kistler, 1988).

(3) *Autoliths, chilled margins, or crystal cumulates.* Didier (1973) refined the term autolith to represent early crystallizing primitive lithologies that are comagmatic with their hosts and Vernon (1992) considered their formation as crystal cumulates. To explain their fine grain sizes, Fershtater and Borodina (1976) suggested that initial incursions of granitoid magma at any crustal level may chill rapidly because of strong undercooling, and form an aplitic carapace at the contact. Flood and Shaw (in press) instead suggested that they form by pressure quenching against the roof and wall rocks at the margins of the pluton.

The similar mineralogy and tonalitic modes of the microgranular enclaves in the PMP and SMB support a similar origin for them, and their igneous microtextures argue strongly against a restite or assimilated metasediment paragenesis. Melanosomes and palaeosomes should exhibit variable mineral assemblages similar to those of the hornfelsed xenoliths and surmicaceous enclaves; also, they may show relict metasedimentary or granoblastic textures. Although assimilation induces granoblastic textures in the xenoliths, microgranular enclaves have inequigranular igneous textures and they consistently lack the sieve-textured biotite and opaque mineralogy of surmicaceous enclaves. Instead, the existence of metasedimentary and microgranitoid material within composite microgranular enclaves at Portuguese Cove, necessitates a magmatic origin for them. Biotite and muscovite constitute the only ferromagnesian mineral phases and no enclaves have modes more mafic than tonalite; they are not simply quenched mafic magmas. Furthermore, the enclaves in granitoids of the MZ are unlikely to form as hybrids because they lack typical hybrid microtextures, particularly the amphibole-biotite synneusis, and fractured sphene and apatite identified in hybrid tonalites at Birchtown (Chapter 3, Section 3.3). Although their ellipsoidal or subspherical shapes may appear pillow-like, xenoliths apparently also developed ellipsoidal shapes during assimilation.

Although many of the enclaves have darker colourations than the host, their microgranitoid textures and modes suggest that they represent felsic rather than mafic microgranular types. Also, the peraluminous mineral assemblages of both the enclaves and their granitoid hosts in both the PMP and SMB imply that they crystallized from similar magmas. The lack of cumulate textures suggests that they do not represent conventional crystal accumulations, but their fine grain sizes and acicular apatites do imply rapid rates of crystallization. Perhaps the plagioclase microphenocrysts in some samples formed nuclei for a quench process that occurred close to the pluton margins, as Flood and Shaw (in press) suggested. Despite the record of widespread quenching in enclaves from the PMP and the SMB, no granitoids in the MZ have fine-grained and equigranular carapaces at currently exposed contacts, or at the peripheries of roof pendants. Nevertheless, the primitive tonalitic compositions of the enclaves may suggest that they formed by marginal quenching of early intruded magmas at depth, although the reason for quenching may be related to either temperature or pressure.

4-6. Conclusions

Peraluminous granitoids in the MZ contain metasedimentary, surmicaceous, microgranular, and coarse-grained granitoid enclaves. The metasedimentary material largely originates in the Meguma Group, but the strata overlying the Meguma Group possibly also contributed metasedimentary material. Surmicaceous enclaves probably formed as melanosomes after partial melting of included xenoliths, but they could also be restites from the anatectic source region of the granitoids. Both the coarse-grained granitoid and microgranular granitoid enclaves apparently represent autoliths of early crystallized granitic magma, but the fine-grained textures of the microgranular material requires quenching. The cause of this process is related either to temperature or pressure; perhaps it occurred at depth close to the granitoid contacts. None of the studied intrusions contains enclaves with mafic igneous characteristics or known hybrid microtextures.

Chapter 5

THE GEOCHEMICAL CHARACTERISTICS OF MEGUMA ZONE GRANITOIDS

5-1. Introduction

Chapter 3 documents the nature of interaction between Late Devonian mafic and peraluminous granitoid magmas in the Meguma Zone (MZ), and it demonstrates that mingled, commingled, and mixed lithologies occur locally in the Port Mouton and Shelburne plutons. Richard (1988) compiled a geochemical database for MZ granitoids and recognized fundamental major oxide and trace element differences between these and other southern intrusions, compared to their more northerly counterparts. This chapter presents an updated compilation of more comprehensive major oxide, trace element, and Sr-Nd-O-S isotopic data for MZ granitoid rocks, and uses it to rule out the formation of all these differences by formerly known petrogenetic processes that operated in the granitoid bodies. Instead, recognition of hybridization at the synplutonic intrusion sites aids the assessment of a plausible role for mantle chemical input into some of the small peraluminous granitoid intrusions peripheral to the South Mountain Batholith (SMB).

5-2. Lithological and Geochemical Characteristics of the Meguma Zone Granitoids

Wide lithological variety exists in peraluminous granitoids of the MZ. The SMB forms the largest granitoid body (Figure 5.1) and it consists of four dominant lithologies. Inside a primitive and early-intruded carapace of biotite granodiorite and minor tonalite, two-mica monzogranites and subordinate leucomonzogranites formed before late-stage leucogranites; monzogranite is the most abundant lithology (MacDonald et al., 1989; Clarke et al., 1993b). Because of the large areal extent of the SMB (circa 7500 km^2) compared to the surrounding plutons, monzogranite also represents the most voluminous granitoid composition in the entire MZ (Poulson et al.,

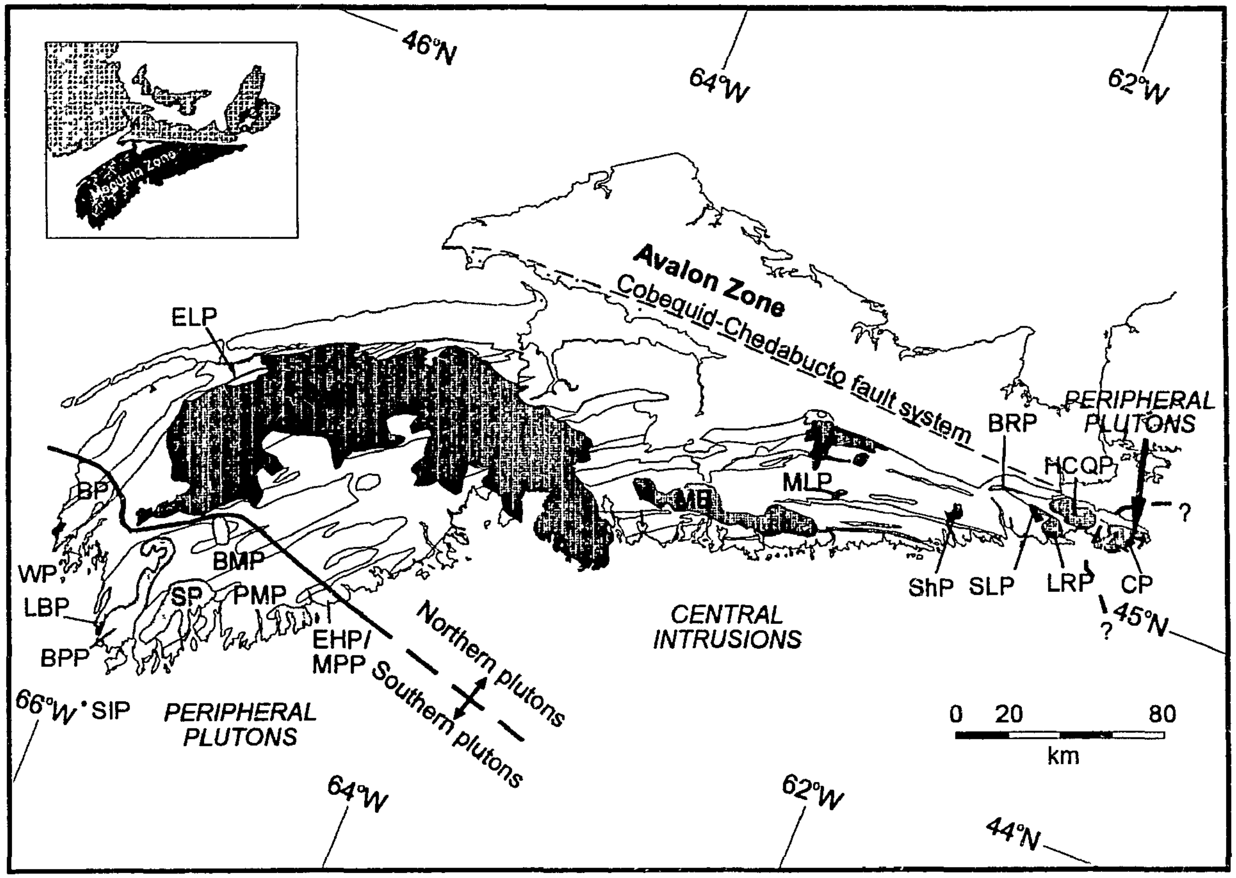

Figure 5.1. Geological map of the Meguma Zone distinguishing the northern plutons (shaded in dark grey) from the southern plutons (shaded in light grey). The geographic boundary between north and south is after Richard (1988). BMP = Bald Mountain Pluton, BP = Brenton Pluton, BPP = Barrington Passage Pluton, BRP = Bull Ridge Pluton, EHP = Eastern Head Pluton, ELP = Ellison Lake Pluton, CP = Canso plutons, HCQP = Halfway Cove-Queensport Pluton, LBP = Lyons Bay Pluton, LC = Liscomb Complex, LRP = Larrys River Pluton, MLP = Mulgrave Lake Pluton, MB = Musquodoboit Batholith, MPP = Moose Point Pluton, PMP = Port Mouton Pluton, ShP = Sherbrooke Pluton, SIP = Seal Island Pluton, SLP = Sangsters Lake Pluton, SP = Shelburne Pluton, SMB = South Mountain Batholith (undivided), WP = Wedgeport Pluton.

1991). Several much smaller granitoid intrusions crop out around the SMB. The Barrington Passage Pluton (BPP) and Lyons Bay Pluton consist of homogeneous hornblende-bearing tonalite, and the Shelburne Pluton (SP) contains mainly tonalite and granodiorite (de Albuquerque, 1977; Rogers, 1984). In contrast, the internally complex Port Mouton Pluton (PMP) encompasses three tonalite-leucomonzogranite cycles (Douma, 1988), and the Liscomb Complex (LC) is an irregular collection of predominantly granodioritic and monzogranitic plutons. The Musquodoboit Batholith consists largely of monzogranite, whereas the Halfway Cove-Queensport Pluton (HCQP) and the Canso plutons (CP) contain monotonous monzogranite and leucomonzogranite. The CP also contain large enclaves and poorly exposed bodies of hornblende-tonalite (Ham, 1988; Hill, 1991).

Previous studies have documented the modal mineralogical and peraluminous chemical compositions (molar A/CNK 1.1-1.3) of MZ granitoid rocks, and have accounted for the existence of lithologic variation from tonalite to leucomonzogranite and leucogranite in each intrusion by fractional crystallization, contamination by Meguma Group lithologies, and interactions with fluids. The most primitive tonalites and granodiorites show strongly correlated variations for most major and trace elements that apparently reflect fractionation and accumulation of plagioclase, biotite, K-feldspar, and quartz, with accessory zircon, monazite, and apatite from the parent melts (McKenzie and Clarke, 1975; MacDonald, 1981; Clarke and Muecke, 1985; Rogers and Barr, 1988; Ham, 1988). In the SMB, the marginal granodiorite also shows Sr, Nd, and S isotopic evidence for contamination by Meguma Group metagreywackes that agrees with its abundant Meguma Group xenoliths (Clarke et al., 1988; Poulson et al., 1991; Chapter 4, Section 4.4). More evolved monzogranites, leucomonzogranites, and leucogranites in all intrusions show scatter for most mobile elements, and (to a lesser extent) rare-earth elements (REEs), that probably results from late-stage fluid interaction effects (Muecke and Clarke, 1981; Douma, 1988; Clarke et al., 1993b).

Magmatic and hydrothermal processes do not, however, explain all of the geochemical variation among the MZ granitoids. For example, marked compositional breaks in the PMP, HCQP, and the CP may distinguish separate magma batches or reflect heterogeneous basement sources (Douma, 1988; Ham, 1988; Hill, 1991). If variable initial $^{87}Sr/^{86}Sr$ ratios and εNd values in the SMB and LC do not entirely result from Meguma Group contamination, then they probably also reflect compositional heterogeneity in the source (Clarke et al., 1988; Clarke et al., 1993b). Intrinsic compositional differences also exist between the southwesterly plutons and more northerly granitoid bodies. Richard (1988) used a multivariate statistical treatment based on discriminant function analysis to manipulate major and trace element data and subdivide the MZ granitoids into chemically different "northern" and "southern" plutons (Figure 5.1). No explanations currently exist for these differences, and so this study uses an updated geochemical database (removed of strongly altered analyses and alleviated of some limitations associated with missing data) to test petrogenetic processes as possible causes of the north-south geochemical divide.

5-3. Geochemical Differences Among Meguma Zone Granitoids

5-3.1. Data Compilation and Manipulation

Analyses compiled for this chapter consist of Richard's (1988) database, augmented with new analyses published over the last six years for SP monzogranite and granodiorite (Appendix C-2), the PMP (D.B. Clarke and S.L. Douma, unpublished), the SMB (Ham et al., 1989; Ham et al., 1990; Clarke et al., 1993b), the LC (Clarke et al., 1993a), and the CP (Hill, 1991). Lithogeochemistry now represents all of the northern and southern granitoids exposed in the MZ with 990 and 163 samples, respectively. Collectively, the northern and southern pluton data contain circa 20% analyses of tonalite and granodiorite, 50% analyses of monzogranite, and 30% analyses of leucomonzogranite; these percentages approximately equal the relative proportions of granitoid lithologies defined petrographically in the Meguma crust. The 1153 analyses in the new geochemical compilation contain major oxide (SiO_2, TiO_2, Al_2O_3, FeOT, MgO, CaO, Na_2O, K_2O, P_2O_5) analyses with up to 26 trace elements (Ba, Rb, Sr, Y, Zr, Nb, Th, Pb, Ga, Zn, Cu, Ni, V, Cr, Hf, Cs, Sc, Ta, Co, Li, Be, B, U, W, Sn, Mo), and up to eight REEs. Appendix E-1 contains the data and their sources, and summarizes the initial selection criteria for analyses of unaltered, barren rocks.

A K-Rb diagram plotted from these data (Figure 5.2) shows that many evolved compositions contain 300-1200 ppm Rb and 4-6 wt.% K_2O; the low K-Rb ratios (<160) for some of these analyses probably record fluid-rock interaction (Reynolds, 1972). Excluding these potentially altered samples removes greisenized rocks from consideration, and it also eliminates the altered Brenton Pluton (Longstaffe et al., 1980) and the "associated" leucogranites produced by fluid-rock interaction in the SMB (Clarke et al., 1993b). Ranges and standard deviations for the remaining 155 southern pluton samples do not differ significantly from those of Richard (1988; Table 5.1), but a greater number of analyses for the northern plutons (by a factor of approximately three) expands the ranges and standard deviations for major oxides, Ba, Rb, Sr, Y, Zr, Nb, Th, Pb, Cr, V, and Ga (Table 5.2). Despite these new data, however, considerable heterogeneity remains in the database for other trace elements, particularly the REEs (Appendix E-1). Use of the available data requires the assumption that interlaboratory analytical differences and contamination during sample preparation are negligible, and Appendix E-2 describes the approach. Data for the CP are excluded until Section 5-4 to simplify the arguments presented below because Richard's (1988) classification did not involve these granitoid bodies.

5-3.2. Geochemical Differences between the Northern and Southern Plutons

Figure 5.3 shows crust-normalized spider diagrams for the northern and southern plutons. All granitoids have predominantly similar spider diagram patterns that show enrichments of Rb, K, Pb, Zn, and Zr approximately twice those of the average crust and prominent troughs between 0.1 and 0.3 times average crust at Ca-Fe, Ni-Mg, and Ti. Major and trace elements

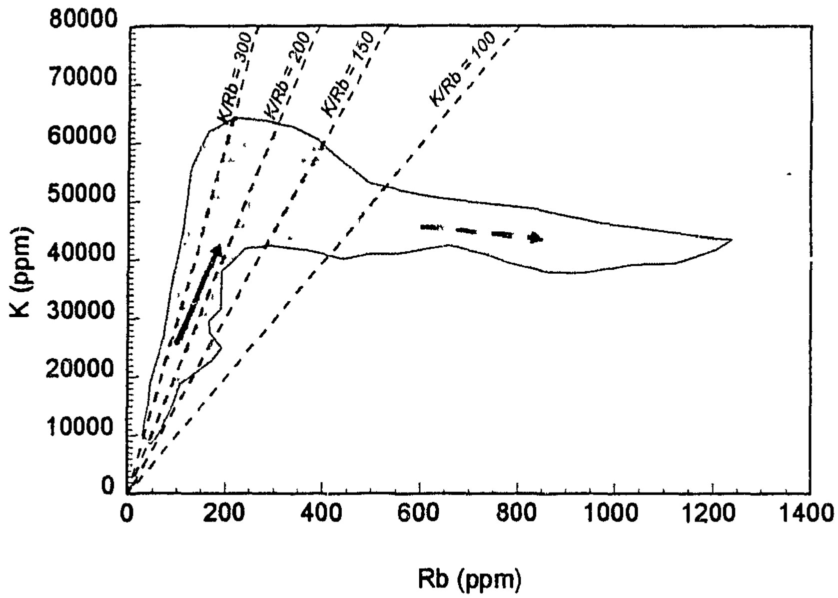

Figure 5.2. Plot of K-Rb for all compiled analyses of Meguma Zone granitoid rocks. The solid arrow represents the effects of magmatic evolution, and the dashed arrow shows the presumed lowering of K/Rb below 160 because of fluid-rock interaction. The northern and southern plutons completely overlap on this diagram.

Table 5.1. Summary of basic statistics describing geochemical analyses for all of the southern plutons depicted on Figure 5.1.

	SiO_2	TiO_2	Al_2O_3	MnO	MgO	CaO	Na_2O	K_2O	P_2O_5	FeOT
Mean	70.83	0.37	15.2	0.06	0.93	1 79	3.73	3.61	0.22	2.23
SD	3.61	0.24	1.32	0.03	0.75	1.19	0.57	1.29	0.1	1.24
n	155	155	155	153	155	155	155	155	155	155
Min	59.75	0.04	12.14	0.01	0.07	0.19	1.52	1 15	0.03	0.42
Max	76.7	1.07	20.18	0.3	3.62	5.19	5.82	6.4	0.82	5.99

	A/CNK	Ba	Rb	Sr	Y	Zr	Nb	Th	Pb	Ga
Mean	1.15	525.75	140.34	189.91	16.56	143.33	11.15	7 02	19 48	18.76
SD	0.1	215.69	59.77	134.2	5.7	63.61	5.15	7 46	6.66	4.03
n	155	138	149	149	100	117	106	123	128	108
Min	0.86	156	36	7	1	34	3	0 4	6	4
Max	1.46	1,200	330	720	35	389	29	44	41	26

	Zn	Ni	V	Cr	Li	Be	U	Sn
Mean	63.07	10.25	39.37	38.68	82.33	4.72	5.06	10.87
SD	79.96	6.65	34.32	27.46	48.77	3.52	13.16	12.15
n	124	105	98	106	88	66	80	80
Min	5	0.5	1	3	19	0.5	0.8	1
Max	770	47	136	111	262	20	120	80

The ordering of elements, and the elements included, allow comparison with the database of Richard (1988). See Figure 5.6b for a summary of the sparse rare-earth data.

Table 5.2. Summary of basic statistics describing geochemical analyses for all of the northern plutons depicted on Figure 5.1.

	SiO_2	TiO_2	Al_2O_3	MnO	MgO	CaO	Na_2O	K_2O	P_2O_5	FeOT
Mean	70.99	0.36	14.76	0.07	1.08	1.07	3.42	4.47	0.22	2.45
SD	2.88	0.21	0.89	0.04	0.54	0.66	0.4	0.65	0.06	1.2
n	678	678	678	678	678	678	678	678	678	609
Min	54.9	0.02	11.39	0.01	0.03	0.05	2.13	1.02	0.02	0.15
Max	78.13	0.96	21.3	0.6	4.84	3.48	5.64	7.84	0.49	5.72
	A/CNK	Ba	Rb	Sr	Y	Zr	Nb	Th	Pb	Ga
Mean	1.12	428.81	213.48	100.95	24.55	123.59	11.31	10.89	25.17	19.36
SD	0.07	203.16	56.13	55.18	9.47	58.57	3.17	4.58	19.24	3.47
n	678	670	672	670	600	654	607	589	494	516
Min	0.94	5	44	2	6	10	3	0.8	2	11
Max	1.65	1,101	380	520	50	294	31	26	267	53
	Zn	Ni	V	Cr	Li	Be	U	Sn		
Mean	58.7	9.52	28.26	35.34	72.95	8.29	5.75	7.79		
SD	48.21	9.01	20.47	58.72	32.47	20.52	21	4.25		
n	648	90	484	80	591	107	617	533		
Min	5	1	1	2	6	2	1	1		
Max	790	66	106	404	323	205	380	31		

The ordering of elements, and the elements included, allow comparison with the database of Richard (1988). See Figure 5.6a for a summary of the sparse rare-earth data.

show variably wide compositional ranges (2-400 times enrichment in the database) and considerable geochemical overlap occurs between these two intrusive groups. Richard (1988) discovered that TiO_2 (48 times enrichment), FeOT (40 times enrichment), CaO (140 times enrichment), K_2O (7 times enrichment), Rb (9 times enrichment), Ba (220 times enrichment), Sr (360 times enrichment), and Pb (130 times enrichment) provide the most complete separation of northern and southern intrusions. New data for the northern plutons in this study indicate that Al_2O_3 (2 times enrichment), Cr (200 times enrichment), V (100 times enrichment), Ga (5 times enrichment), and Y (8 times enrichment) also effectively separate the northern and southern granitoid bodies.

The discriminating major element oxides define irregular fields that approximate magmatic evolutionary trends (Figure 5.4). Some southern pluton compositions have higher TiO_2, Al_2O_3, FeOT, and CaO than northern plutons. Higher FeOT and CaO values in the southern plutons may define separate evolutionary trends, and the BPP defines a separate low-K_2O field that does not overlap with the northern plutons or other southern bodies (de Albuquerque, 1977). Also, southern lithologies in the PMP and (to a lesser extent) in the BPP show high Al_2O_3 coupled with low A/CNK ratios (>0.86), presumably because of high CaO and Na_2O (not shown) concentrations in these analyses. These compositional features (especially for TiO_2, CaO, and FeOT) partly reflect the occurrence of tonalite analyses (n ~50) with SiO_2 <64.0 wt.% in the southern plutons; the northern pluton data instead contain no analogous tonalitic analyses, and have a predominance of data for monzogranites (n = 304) and leucomonzogranites (n = 157). Despite these lithological differences, however, both groups span similar ranges for SiO_2 and neither the major oxide discriminators nor silica clearly distinguish the lithologies defined on the basis of modal mineralogy. North-south geochemical differences (particularly for Al_2O_3 and CaO) persist in lithologies with similar silica values, and so do not entirely represent a simple function of lithologic classification.

In Figure 5.5, the mobile trace element discriminators Ba, Rb, and Sr show considerable

a

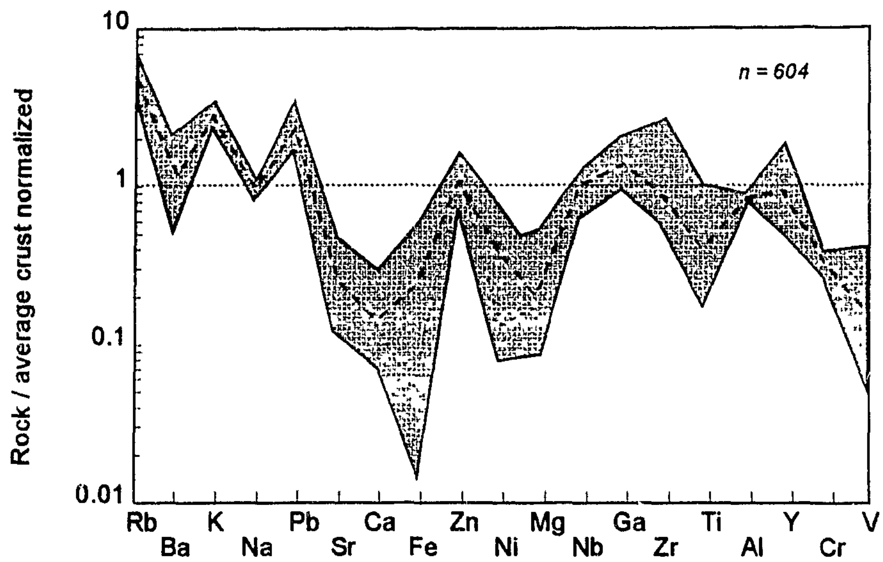

b

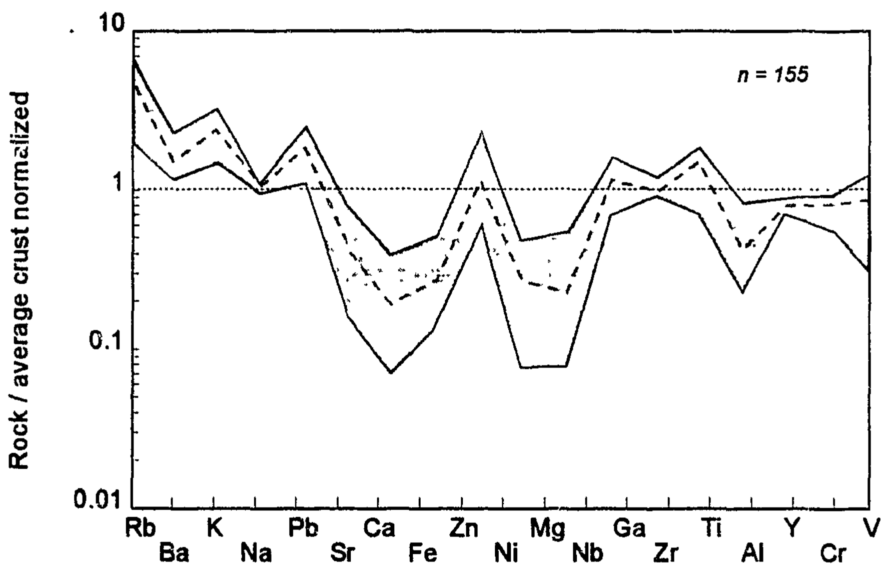

Figure 5.3. Spider diagrams normalized to average continental crust. (a) The field occupied by the northern plutons (BRP, ELP, HCQP, LC, LRP, MB, ShP, SLP, and all constituent plutons of the SMB). The dashed line is the mean northern pluton composition and the dotted line shows the mean SMB composition; (b) The field occupied by the southern plutons (the BMP, BPP, BRP, EHP, LBP, MPP, PMP, SIP, SP, and the WP). The dashed line is the mean southern pluton composition. n = the number of analyses included. Normalization constants after Taylor and McLennan (1985). The colour scheme follows Figure 5.1; see the text for a discussion.

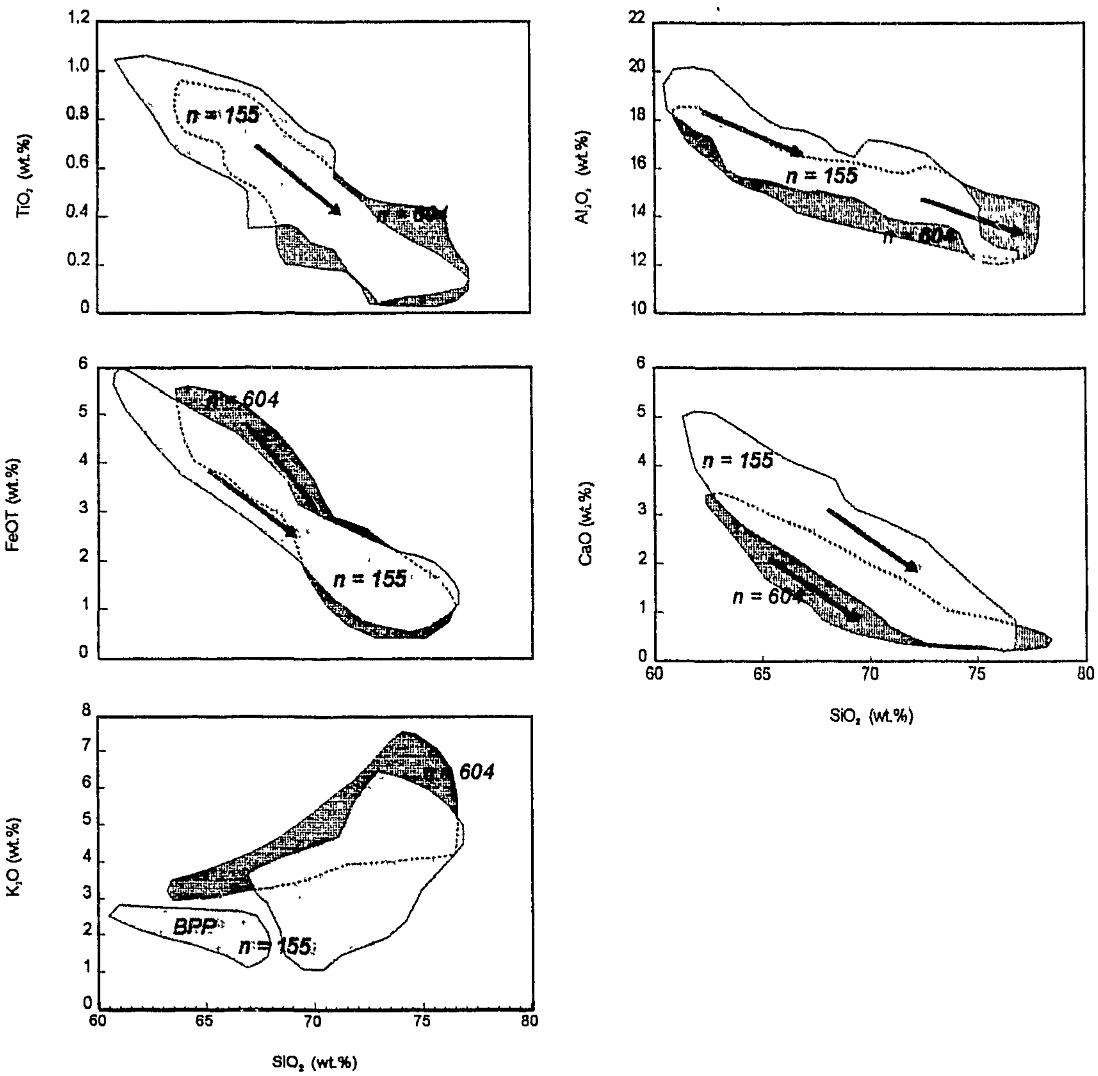

Figure 5.4. Harker variation diagrams for major element oxides discriminating the northern plutons from the southern plutons. The colour scheme follows Figure 5.1 and the solid arrows represent the potential effects of magmatic phenocryst fractionation. Outlying data points (<10 per plot) were excluded from this diagram; n = the number of samples plotted. See Figure 5.1 for the pluton abbreviation and the text for a discussion.

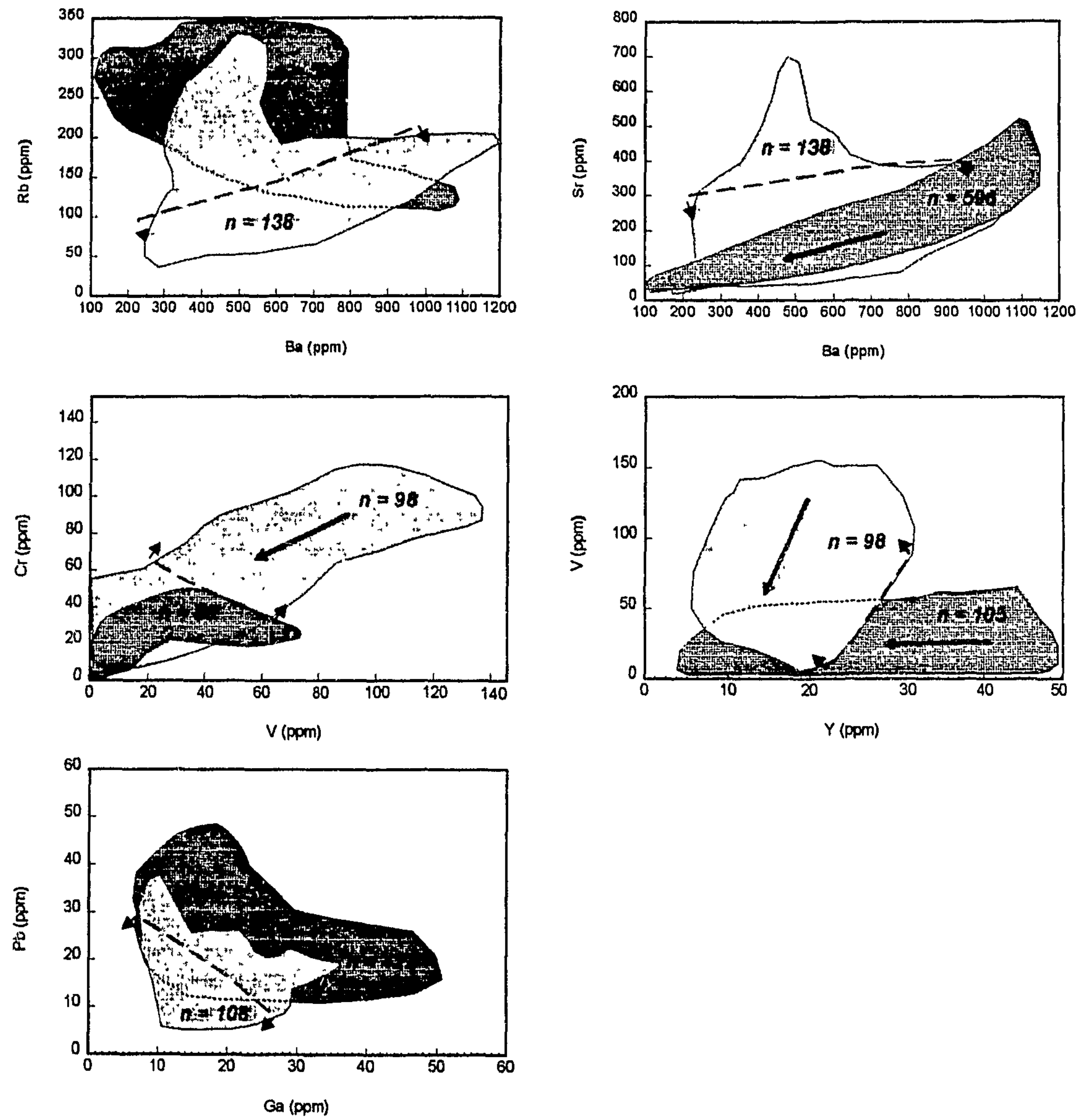

Figure 5.5. Selected trace element variation diagrams for discriminators of the northern and southern plutons. Colour scheme as in Figure 5.1 and arrow ornamentation as in Figure 5.4. The thick, double-headed arrow marks the limit of tonalite analyses in the southern pluton field. Outlying data points (<10 per plot) were excluded from this diagram; n = the number of analyses plotted. See the text for a discussion.

scatter for both the northern and southern plutons. Increasing Rb and linearly decreasing Sr with decreasing Ba characterizes the northern plutons, whereas the southern pluton lithologies collectively have higher Sr concentrations and show no obvious trends for Rb. A plot of less mobile Cr-V shows much wider compositional variation for both elements in the southern plutons; northern plutons instead contain a wide compositional range for Y, and somewhat higher Pb and Ga concentrations. As with the major oxide discriminators, no clear distinction exists between granodiorites, monzogranites, and leucomonzogranites on the basis of these trace elements, although very high Cr and V concentrations do occur only in the southern pluton tonalites. The much smaller amount of data for Ga, Cr, and V may also account for some separation of the northern and southern geochemical fields, although the ratio of analyses for northern and southern plutons is <10:1 for these elements and artificially-induced separation is statistically insignificant (Richard, 1988). A valid statistical treatment cannot, however, be undertaken for the new discriminators because the new southern pluton data do not change the problematic sample to variable ratio limitation that Richard and Clarke (1989) experienced.

Where data exist for at least seven REEs, no significant differences separate the northern and southern plutons (Figure 5.6). Intrusions from both groups have very similar patterns with approximately six times enrichment of light REE relative to heavy REE (La/Lu 335-696). Tonalites and granodiorites have less pronounced negative Eu anomalies (Eu/Eu* 0.39-0.58) than the monzogranite and leucomonzogranite analyses (Eu/Eu* <0.16), and the smaller Eu anomalies in the southern plutons reflect the predominance of tonalite analyses. The small peak at Gd in the southern plutons may be an analytical phenomenon (Figure 5.6b; Chapter 3, Section 3.3), and the data may not accurately reflect all characteristics of the northern and southern plutons. The available radiogenic and stable isotope data for unaltered rocks is also limited, but gives much more obvious north-south separations (Table 5.3). Figure 5.7 shows that a wide variation of Sr, O, and S isotopic values characterizes lithologies in both the northern and southern plutons, but the northern and southern plutons do represent clearly separated

a

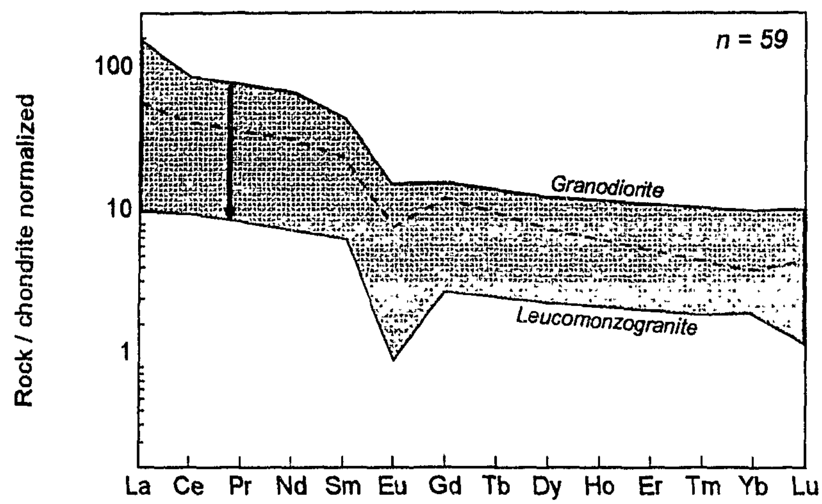

b

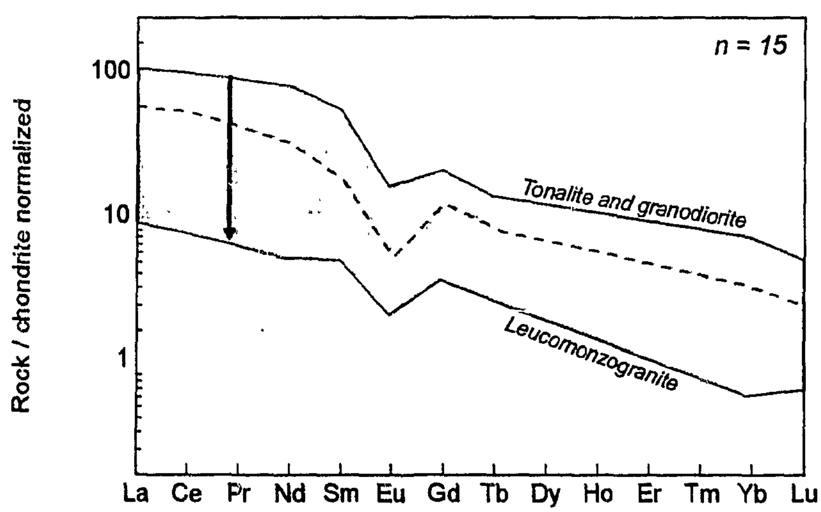

Figure 5.6. Chondrite-normalized rare-earth spider diagrams. (a) The field occupied by normalized rare-earth element abundances for three northern plutons (the HCQP, LC, and SMB); (b) The field occupied by normalized rare-earth element abundances for two southern plutons (the SP and PMP). The dashed lines are the average compositions of the northern and southern plutons, the arrow shows the effects of phenocryst fractionation, and n is the number of analyses plotted. Normalization constants after Nakamura (1974) and the colour scheme follows Figure 5.1. See the text for a discussion.

Table 5.3. Summary of the available radiogenic and stable isotopic data for the northern, southern, and unclassified plutons in the Meguma Zone.

Intrusion	Classification	Lithology	$^{87}Sr/^{86}Sr_i$	εNd	$\delta^{18}O$	$\delta^{34}S$	Reference
BPP	Southern	Ton	-	-	8.3-9	0-5	1, 2
SP	Southern	Ton	0.7052-0.7067	1.75-3.3	8.8-10.1	1-4	1, 2, 3, 4
	Southern	Mzg	0.7100	-	8.4-9.3	1-4	1, 2, 4, 5
PMP	Southern	Ton	0.7036-0.7079	-0.10 to 1.65	-	-	4, 6
	Southern	Grd	0.7046-0.7090	-0.10 to 1.65	8.9	1-4	1, 2, 5, 6
	Southern	Mzg	0.7100	-	9.4-10.4	-	1, 6
SMB	Northern	Grd	0.7076-0.7090	-1.4 to -2.9	9.6-11.4	5.0-10.0	1, 2, 7
	Northern	Mzg	0.7095-0.7102	-2.8 to -5.2	10.9-12	5.0-14.0	1, 2, 7, 8
	Northern	Lmzg	0.7095-0.7108	-	10.15-12.7	5.0-14.0	1, 2, 8, 9
LC	Northern	Grd	0.7100	-2	-	-	10
	Northern	Mzg	0.7100	-4	-	-	10
	Northern	Lmzg	0.7100	-6	-	-	10
CP	Unclassified	Ton	0.7057-0.7069	-	-	-	11, 12
	Unclassified	Grd	0.7100	-	-	-	11, 12
	Unclassified	Mzg	0.7030-0.7093	-	-	-	11, 12

Tonalite data are recalculated to t = 378 Ma and analyses for all other lithologies are recalculated to t = 372 Ma. Ton = tonalite, Grd = granodiorite, Mzg = monzogranite, Lmzg = leucomonzogranite and leucogranite. Data for the SP tonalite represents an average for the Birchtown hybrids. 1 = Longstaffe et al. (1980), 2 = Poulson et al. (1991), 3 = Tate (this study), 4 = Kubilius and Ohmoto (1984), 5 = Rogers and Barr (1988), 6 = D.B. Clarke and S.L. Douma (unpublished data), 7 = Clarke et al. (1988), 8 = Clarke and Halliday (1980), 9 = Clarke et al. (1993b), 10 = Clarke et al. (1993a), 11 = Hill (1988), 12 = Hill (1991). Refer to Figure 5.1 for the intrusion abbreviations and locations.

populations. Partial overlap exists for Sr and O isotopic compositions between these compositional groups, but the BPP, SP, and the PMP generally have lower $\delta^{18}O$ values (8.3-10.4 ‰) than the SMB (9.6-12.7 ‰), and also lower Sr isotopic compositions (0.705-0.710 and 0.708-0.711, respectively). Low $\delta^{34}S$ (0-5 ‰) and high εNd (-0.1 to 1.65) values to the south do not overlap with the SMB values of 5-14 ‰ and -1.4 to -6, respectively.

In summary, the northern and southern plutons do not represent two clearly separated geochemical groups, but southern pluton lithologies (particularly the tonalites) have higher TiO_2, Al_2O_3, FeOT, CaO, Ba, Sr, Cr, and V than their northern plutons, which instead show higher values for K_2O, Rb, Y, Ga, and Pb. Although considerable overlap exists between the two groups for major oxides and trace elements, the available radiogenic and stable isotope data provide much greater separations; southern plutons consistently have much lower $^{87}Sr/^{86}Sr_i$ (<0.710), $\delta^{18}O$ (<10.4), and $\delta^{34}S$ (<5.0), and higher εNd (>-0.1) compared to the northern values of >0.708, >9.6, >5.0, and <-1.4, respectively. The number of trace element analyses in the populations of each group is not a significant cause of separation between the northern and southern plutons, but the dominance of monzogranite data and the lack of tonalite analyses in the northern plutons is an important factor. A valid petrogenetic hypothesis for the cause of these intrinsic geochemical differences must, therefore, explain separate northern and southern evolutionary trends for FeOT and CaO, coupled with the bimodal distribution of K_2O in the southern plutons, and the existence of metaluminous southern tonalites.

5-3.3. Potential Explanations for the North-South Geochemical Differences

The existence of somewhat different geochemical trends and distinct isotopic signatures for the northern and southern plutons suggests that these geochemical groupings represent two subtly different magmatic suites that do not necessarily share the same combination of sources and processes, as Tilling (1973) proposed for the Boulder Batholith. In the MZ, the geochemical

a

b

c

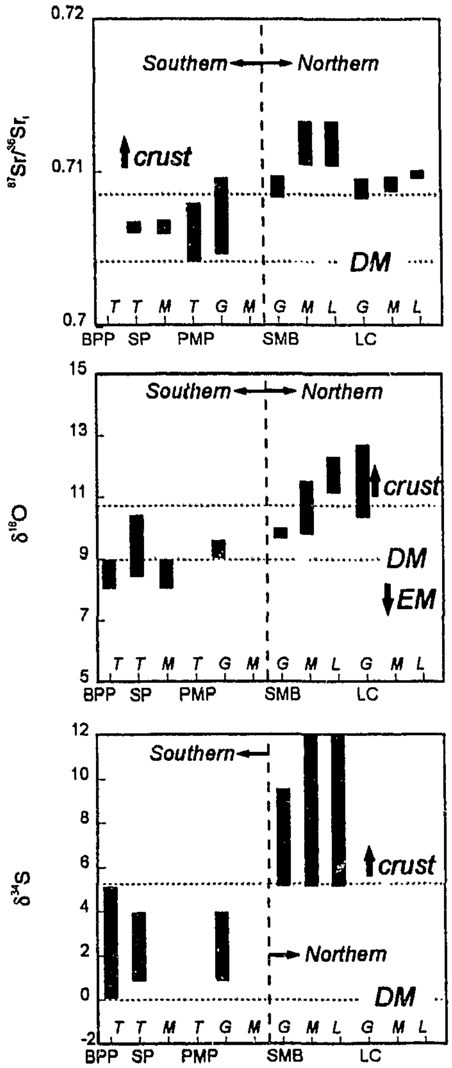

Figure 5.7. Graphical summary of isotopic variation among the northern and southern plutons in the Meguma Zone. (a) Range plot of $^{87}Sr/^{86}Sr_i$ for all analyzed intrusions; (b) Range plot of $\delta^{18}O$ for all analyzed intrusions; (c) Range plot of $\delta^{34}S$ for all analyzed intrusions. The plots use the data in Table 5.3 and the approximate compositions for depleted mantle (DM) and enriched mantle (EM) come from Harmon and Halliday (1980), DePaolo (1981), and Frost and O'Nions (1985). The compositions for supposedly crust-derived granitoids represent averages after Currie and Pajari (1981), DePaolo (1981), O'Neil et al. (1977), and Poulson et al. (1991), and all data sources indicate that isotopic analyses record magma compositions (Longstaffe et al., 1980; Clarke et al., 1988; Poulson et al., 1991). T = tonalite, G = granodiorite, M = monzogranite, L = leucomonzogranite.

characteristics of granitoid rocks result from a combination of identified open system magma-rock and fluid-rock processes superimposed on supposedly closed system compositional effects attributable to fluid-rock and crystal-melt equilibria and the nature of the protolith. These possibilities will be evaluated as explanations for the major oxide, trace element, and Sr-Nd-O-S isotopic differences between the northern and southern plutons, recognizing that they are not mutually exclusive. Evidence for synplutonic mafic intrusions in three southern plutons (Chapter 2, Section 2.2; Chapter 3, Section 3) also requires an evaluation of the compositional effects attributable to mafic-granitoid magma mixing.

Crystal-liquid equilibria

Fractionation and/or accumulation of modal phenocryst phases can account for the existence of major oxide and trace element evolutionary trends. For example, decreasing TiO_2, Al_2O_3, FeOT, and Rb strongly suggest biotite fractionation or accumulation as an important process (Rogers and Barr, 1988; Douma, 1988), and decreasing CaO, Al_2O_3, Ba, and Sr, coupled with increasing Eu anomalies support the removal of plagioclase and/or K-feldspar (Rogers and Barr, 1988; Ham, 1988; Hill, 1991; Figure 5.4; Figure 5.5). Also, lower total REE and higher La/Lu ratios in the most evolved leucomonzogranites (Figure 5.6), implicate the separation of accessory zircon, apatite, and possibly also garnet (Hanson, 1978; Muecke and Clarke, 1981; Ham, 1988). High values for these elements and oxides in the southern plutons (particularly the tonalites) may, therefore, result from the accumulation of biotite, plagioclase, and accessory minerals (Rogers and Barr, 1988). However, metaluminous A/CNK values in many southern pluton tonalites are inconsistent with this process, no samples show the positive Eu anomalies that should occur in plagioclase cumulates, and no explanation exists for separate FeOT and CaO evolutionary trends. The rare presence of hornblende as a minor component in the BPP and PMP (Rogers, 1984; Douma, 1988) probably explains the presence of metaluminous compositions and perhaps also the presence of separate evolutionary trends (discussed further below), but crystal-liquid processes cannot significantly affect the Sr, Nd, O, and S isotopic data.

Hydrothermal alteration

Despite the exclusion of analyses for altered rocks, subsequent K-Rb ratio filtering of the database, and the exclusion of outlying data points on Figures 5.4 and 5.5, scatter observed for the alkalies and mobile trace elements (Rb, Ba, and Sr) may result from subsolidus or magmatic interactions with fluids (Muecke and Clarke, 1981). Leucomonzogranites from the SMB that have A/CNK values <1.0 and show unusually low concentrations of Fe for northern plutons (Figure 5.3a) may be remanent analyses showing the effects of alteration processes. Perhaps the low K_2O samples in the BPP tonalite (Figure 5.4) also reflect alkali loss during alteration. Regardless of these observations, however, the immobile nature of TiO_2, CaO, Cr, V, Y, Ga, and Pb suggest that alteration did not significantly change the values. Also, oxygen isotopic equilibrium for all minerals in the samples of Longstaffe et al. (1980) suggests that interaction with isotopically depleted meteoric fluids did not cause low values for $\delta^{18}O$ in the southern plutons, although it can account for low values (circa 9.6 ‰) in the SMB (Clarke et al., 1993b; Figure 5.7).

Crustal contamination

The abundance of Meguma Group xenoliths in both northern and southern plutons (Chapter 4, Section 4) suggests a plausible role for crustal contamination. Increasing $^{87}Sr/^{86}Sr_i$, decreasing εNd, and increasing $\delta^{34}S$ with evolution in the SMB (Table 5.3; Figure 5.7) may all reflect the incorporation of Meguma Group metasedimentary lithologies (Clarke et al., 1988; Poulson et al., 1991). High Al_2O_3 in some southern pluton samples can also be a product of Meguma Group contamination, but its control on other north-south discriminators depends on the compositions of Meguma Group lithologies incorporated and is unlikely to account for metaluminous compositions or separate evolutionary trends (Poulson et al., 1991). Although the variable isotopic compositions of individual lithologies in the southern plutons may reflect Meguma Group contamination, low values for Sr, Nd, O, and S isotopes cannot entirely result from the incorporation of isotopically enriched Meguma Group lithologies (Longstaffe et al., 1980; Poulson et al., 1991) unless the northern plutons all contain much higher levels of contamination. Northern plutons do not contain more abundant Meguma Group xenoliths (Chapter 4, Section 5), which perhaps argues against this hypothesis. Furthermore, whole-rock sulphur concentrations show wide variation and overlap in both the northern and southern plutons (4-600 ppm; Kubilius and Ohmoto, 1984).

Compositionally distinct protoliths

Orthogneisses and paragneisses representing the sub-Meguma basement occur in the Liscomb Complex and as xenoliths within the Popes Harbour dyke (Eberz et al., 1991; Clarke et al., 1993a). Lithologically variable metabasic and metapelitic lithologies comprise these units, some of which have Sr and Nd isotopic compositions capable of producing SMB magmas (Eberz et al., 1991). Lithological heterogeneity in the exposed basement may account for TiO_2, Zr, Hf, and Y, and Sr and Nd isotopic variations within lithologies and differences between intrusions in the northern plutons (Clarke et al., 1988; MacDonald et al., 1992). Analyzed basement metapelites, however, all have very restricted ranges for Sr and Nd isotopes that have much smaller magnitudes than the north-south isotopic differences. Consequently, a distinct protolith for the southern plutons must contain a significant component of isotopically depleted material with low Rb concentrations (Harmon and Halliday, 1981; Hill, 1991), and it may also be different in age and geological affiliation to the exposed material. However, no high-grade gneissic lithologies interpretable as basement crop out in association with the southern plutons, and so no currently known evidence exists to either support or refute a suggestion of compositionally distinct domains (perhaps corresponding to tectonic terranes) in the sub-Meguma basement (Baird and Meisch, 1984; Todd and Shaw, 1985; Ayuso, 1986; Fleck, 1990).

Restite unmixing

Progressive separation of peraluminous silica-poor enclaves and/or monomineralic inclusions derived from melanosomes in the protolith, may account for compositional diversity in some granitoid suites (White and Chappell, 1977; Zeck, 1992). In the MZ, increasing normative corundum and La/Lu values with increasing silica (Figure 5.6), the absence of linear geochemical trends, and the presence of chemically variable, euhedral aluminosilicate mineral phases, are more consistent with magmatic crystallization, hydrothermal processes, and/or Meguma Group contamination than restite unmixing (Clarke and Muecke, 1985; Chappell et al., 1987). Also, no analyzed peraluminous xenoliths show Sr and Nd isotopic equilibrium with their granitoid hosts, and no known surmicaceous enclaves contain high-pressure metamorphic minerals appropriate for restitic material (Clarke and Muecke, 1985; Wall et al., 1987). High concentrations of surmicaceous enclaves in the BPP tonalite probably reflect *in situ* partial melting of Meguma Group xenoliths (Chapter 4, Section 5.1), and their equally low abundances in all other studied northern and southern intrusion lithologies (regardless of composition) do not suggest unmixing. The restite hypothesis is unlikely to represent an important evolutionary process or a cause of north-south compositional differences in the MZ.

Mafic-granitoid magma mixing

Longstaffe et al. (1980) originally suggested the possibility of a mantle component in the BPP, SP, and PMP on the basis of O isotope data, and the more recently determined Sr-Nd-S isotopic data support this hypothesis. Analyzed lithologies in the PMP consistently have positive εNd values that resemble those of the Birchtown hybrids (Table 5.3), and all of the southern plutons have $^{87}Sr/^{86}Sr_i$, $\delta^{18}O$, and $\delta^{34}S$ compositions corresponding to mantle-crust mixtures on Figure 5.7. Compared to other granitoids that contain putative mantle components (Table 5.4), the southern plutons have compositional ranges that could accommodate mantle input, and they completely overlap with these intrusions for $^{87}Sr/^{86}Sr_i$ and have εNd and $\delta^{18}O$ values approaching

Table 5.4. Comparison of selected granitoid lithologies from the Meguma Zone with the characteristics of published granitoids in bimodal complexes that contain mantle signatures.

Pluton/Batholith	Geographic location	$^{87}Sr/^{86}Sr_i$	εNd	$\delta^{18}O$	Reference
Northern plutons	Meguma Zone	0.7030-0.7108	-1.4 to -6	9.6-12.7	-
Southern plutons	Meguma Zone	0.7040-0.7100	1.8-3.3	8.3-10.4	-
Ploumanac'h	Brittany	0.7100	-	8.8-9.5	1
Lachlan S-types	Australia	0.7069-0.7153	-	-	2
Lachlan I-types	Australia	0.7041-0.7065	-	-	2
Lachlan M-types	Australia	0.7035-0.7039	3.3-6.1	7.9-9.6	3
Caledonian S-type	Scotland	>0.7080	-	-	4
Caledonian I-type	Scotland	0.7040-0.7090	-	-	4
Peninsular Ranges S-types	USA	-	-	11.8-13.8	5
New England S-types	Australia	-	-	>10.4	6
New England I-types	Australia	-	-	7.7-9.9	6
Sierra Nevada granodiorite	USA	0.7041-0.7073	-3.5 to 5.1	7.5-8.2	7
Sierra Nevada monzogranite	USA	0.7074-0.7098	-3.9 to -7.6	8.2-11	7
Peninsular Ranges ton	USA	0.7048-0.7056	-0.8 to 1.9	9.2-9.7	7
Peninsular Ranges Grd	USA	0.7043-0.7074	-4.1 to 5.1	9.8-10.8	7
Peninsular Ranges Mzg	USA	0.7100	1.3	8	7

Ton = tonalite, Grd = granodiorite, Mzg = monzogranite. 1 = Alberede et al. (1980) , 2 = Gray (1984), 3 = Chappell and Stephens (1988), 4 = Frost and O'Nions (1985); 5 = Todd and Shaw (1985), 6 = O'Neil et al. (1977), 7 = DePaolo (1981). Data for the northern and southern plutons is summarized from Table 5.3.

those of the supposedly mantle-derived ("M-type") granitoids (Didier et al., 1982). Of all the north-south geochemical discriminators, higher TiO_2, V, and Cr in the southern plutons match the findings of published investigations for mixed rocks (e.g. Dickin and Exley, 1981; Vogel, 1982; Gray, 1984). Most importantly, however, hornblende-bearing synplutonic mafic intrusions occur preferentially in the southern plutons (Chapter 2, Section 2), and so the presence of amphibole (and metaluminous compositions) may be manifestations of the mixing process. Separate evolutionary trends for FeOT and CaO may also be mixing rather than fractionation features.

5-4. Evaluation of the Mafic-Granitoid Magma Mixing Hypothesis

In combination, all of the previously identified evolutionary processes can explain some north-south geochemical differences for major oxides and trace elements, but only the hypothesis of mafic-granitoid magma mixing in the southern plutons provides a satisfactory explanation for the tonalites, synplutonic mafic intrusions, and the available Sr-Nd-O-S isotopic and A/CNK data. Further study of the major oxide and trace element characteristics of the Birchtown hybrids below, shows that interaction with mafic magmas in the south also explains many of the other north-south discriminators, and allows the delineation of some compositional features and trends attributable to hybridism from the effects of other evolutionary mechanisms. Quantitative comparison of the Birchtown hybrids with the northern and southern plutons requires the use of an internal standard to emphasize geochemical features attributable solely to MZ processes; this study uses an average of all northern pluton analyses (ANP) in the database (except those for the CP) for this purpose. Northern and southern analyses that lie within specific SiO_2 ranges are directly compared, recognizing that the Birchtown hybrids are southern lithologies, and that northern pluton analyses are compared with an average of northern pluton data.

Tonalite at Birchtown represents a transitional metaluminous-peraluminous unit (A/CNK 1.0-1.3) that formed by variable degrees of mixing between a synplutonic diorite and its granodiorite host (Chapter 3, Section 3.3). The hybrid tonalites show the strongest compositional resemblance to the southern lithologies classified as tonalite (SiO_2 55.0-63.9 wt.%) and granodiorite (SiO_2 64.0-69.9 wt.%) in the database; they have very similar A/CNK values (0.9-1.3) and a somewhat similar range of SiO_2 abundances (59.8-69.9 wt.%). Figure 5.8a shows that, compared to the average of northern pluton compositions, the Birchtown hybrids have 4-6 times enrichment of MgO, Ca, V, and Cr, and 2-4 times enrichment of P, Ti, and Sr, and a smaller peak at Fe. In Birchtown Quarry, high Sr may in part be a function of plagioclase accumulation and high P probably results from commingling, but the other compositional features exist in the hybrid because it contains high-titanium calcic amphibole, biotite, and calcic plagioclase xenocrysts derived from the synplutonic diorite during mixing. Southern pluton tonalites show smaller peaks for all of these elements at >2 times enrichment, small peaks for Ca, V, Sr, and (to a lesser extent) Ti and Cr occur in the granodiorites (Figure 5.8b) but not the monzogranites (Figure 5.8c). Northern pluton granodiorites show enriched Ti, Ca, V, and Sr to a much lesser extent and have different patterns that lack a peak at Ce (Figure 5.8d, e).

Except for MgO and Ni, all peaks in southern pluton lithologies correspond to north-south geochemical discriminators. Enrichments for all of the discriminators do not occur in the Birchtown tonalite patterns, but of all the north-south discriminators, only Al_2O_3, K_2O, mobile trace elements, Cr, and Ga do not show linear covariation (see Figure 3.29 in Chapter 3) that results from their involvement in the mixing process at Birchtown. Assuming, therefore, that the northern plutons represent a hybrid-free baseline (as the lack of synplutonic intrusions and the Sr-Nd-O-S isotopic data suggest), these comparisons suggest the presence of major oxide and trace element compositional effects attributable to mafic-felsic magma mixing in the southern pluton tonalites and granodiorites, and probably also to a lesser extent in the monzogranites. Depleted Sr-Nd-O-S isotopic signatures in all of these lithologies preclude the direct evolution of tonalites into granodiorites and monzogranites by plagioclase and biotite fractionation and/or fluid interaction processes alone. Also, fractional crystallization models suggest that tonalites in

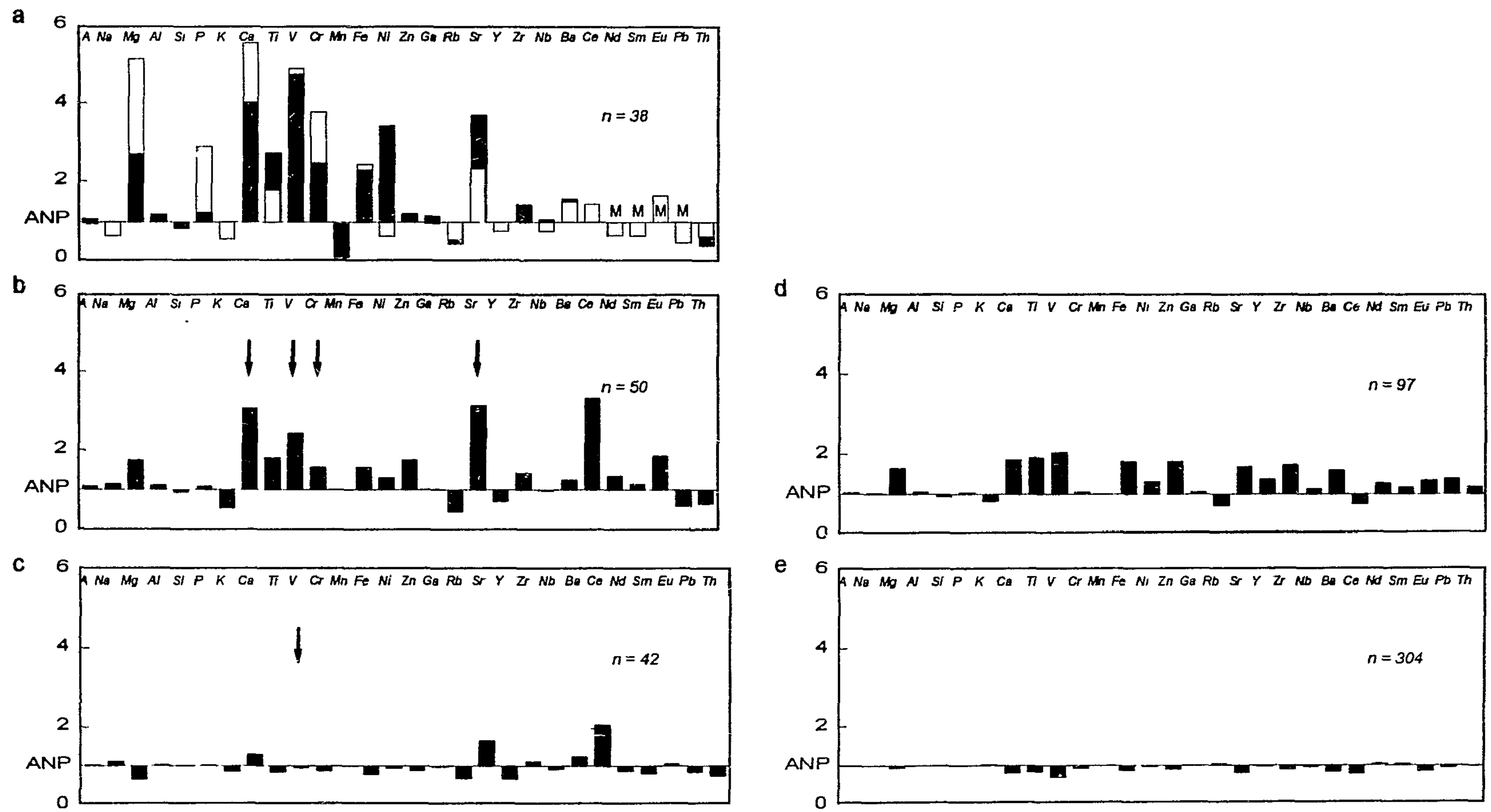

Figure 5.8. Enrichment and depletion of elements in northern and southern pluton lithologies. (a) Average southern tonalite (shown in black) with average Birchtown hybrid tonalite (SiO_2 55.0-63.9 wt.%, shown in white; n = 6); (b) Average southern granodiorite (SiO_2 64.0-69.9 wt.%); (c) Average southern monzogranite (SiO_2 70.0-74.9 wt.%); (d) Average northern granodiorite (SiO_2 64.0-69.9 wt.%; (e) Average northern monzogranite SiO_2 70.0-74.9 wt.%). Elements are arranged in order of increasing atomic number, and the data are normalized to an average of the 604 northern pluton lithologies in the database (ANP). Data presentation follows the style of Hildreth (1981). A = A/CNK, M = missing data, and n = the number of analyses averaged. The vertical arrows mark important elements; see the text for a discussion.

the PMP do not represent suitable parental compositions (Douma, 1988), and hornblende fractionation from metaluminous melts produces peraluminous compositions inefficiently (Zen, 1986). In addition to these processes, therefore, a plausible role exists for variable degrees of mafic-granitoid magma mixing in constituent lithologies of the southern plutons.

Tonalites, granodiorites, and monzogranites from the CP have compositions that resemble the southern plutons, despite their occurrence at the northeastern onshore extent of the MZ and the lack of critical data for Cr and V. Figure 5.9 shows that enrichment factors for Ti, Mg, Ca, and Sr are 1.5-3.8 times ANP in the CP tonalite. Enrichment patterns for the granodiorites and monzogranites that show a Ce peak and resemble those of equivalent lithologies in the southern rather than northern plutons, and $^{87}Sr/^{86}Sr_i$ values for all lithologies (0.703-0.710; Table 5.3) also overlap with the southern plutons. Although no substantative Nd or stable isotope data currently exist, Hill (pers. comm., 1994) describes the existence of small hornblende-tonalite bodies with compositions that closely resemble the Birchtown diorite and the hybrid tonalites. As in the PMP, fractional crystallization models for the REEs suggest that these rocks are not entirely comagmatic with the granodiorites and monzogranites and ages for the tonalites also predate them by 6 Ma (Hill, 1991; Chapter 1, Section 4). To account for the new geographic distribution of compositionally similar groups, this study correlates the CP with the southern plutons and collectively imposes the non-geographic and non-genetic term "peripheral plutons" to describe them. Hereafter, the remaining granitoid bodies in the MZ are termed "central intrusions" including the SMB (Figure 5.1). Further study of the magma mixing hypothesis includes the CP analyses as peripheral plutons below .

The persistence of high Ca, and to a lesser extent Fe, Ti, Cr and V, in primitive peripheral lithologies suggests that either these elements were transferred preferentially during mixing and/or were least affected by other magmatic processes, notably crystal fractionation. The effects of mixing and crystal-liquid fractionation are not clearly separable in binary compositional space (see Figure 3.30 in Chapter 3), but Figure 5.10 shows that the linearly

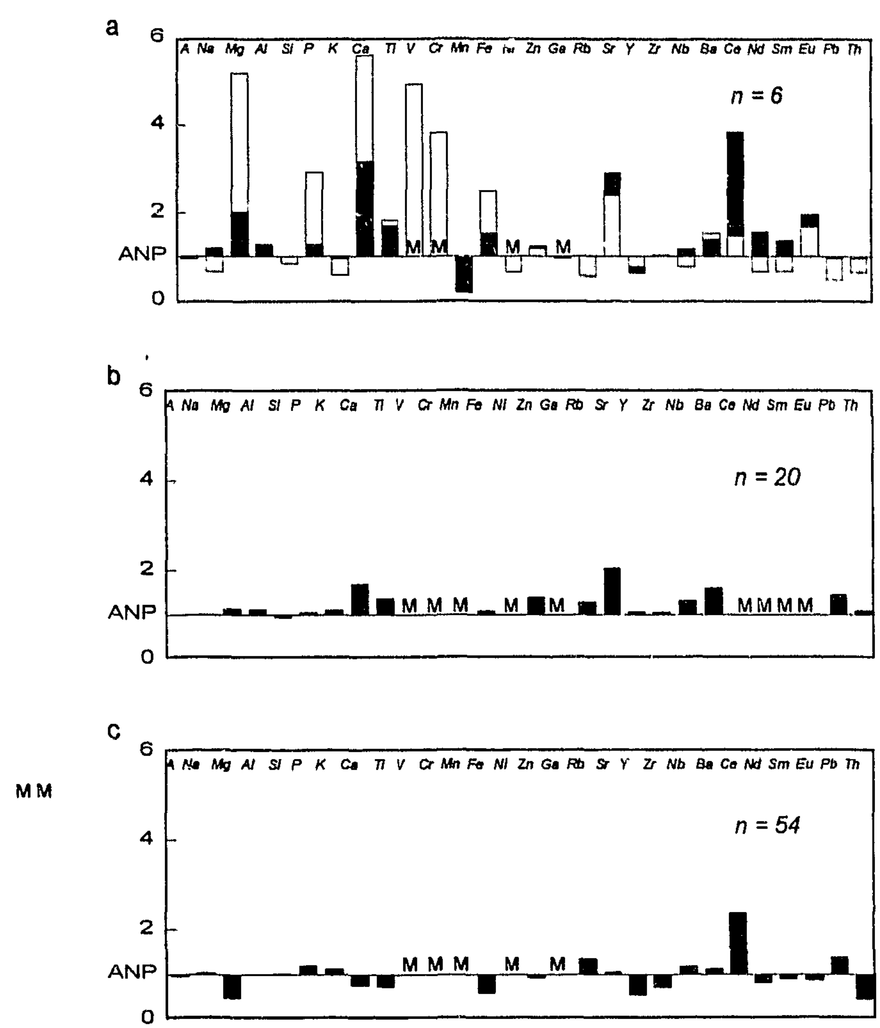

Figure 5.9. Enrichment and depletion of elements in the Canso plutons. (a) Average Birchtown hybrid tonalite (shown in white; n = 6) with average Canso pluton tonalite (SiO_2 55.0-63.9 wt.%, shown in black); (b) Average Canso pluton granodiorite (SiO_2 64.0-69.9 wt.%); (c) Average Canso pluton monzogranite (SiO_2 70.0-74.9 wt.%). Elements are arranged in order of increasing atomic number, and the data are normalized to an average of the 604 northern pluton lithologies in the database (ANP). Data presentation follows the style of Hildreth (1981). A = A/CNK, M = missing data, and n = the number of analyses averaged. See the text for a discussion.

correlated discriminators in Birchtown Quarry (TiO_2, FeOT, CaO, and particularly V) most effectively separate the peripheral and central intrusions into two trends. On all of the plots, peripheral lithologies suggests that either these elements were transferred preferentially during mixing and/or were least affected by other magmatic processes, notably crystal fractionation. The effects of mixing and crystal-liquid fractionation are not clearly separable in binary compositional space (see Figure 3.30 in Chapter 3), but Figure 5.10 shows that the linearly correlated discriminators in Birchtown Quarry (TiO_2, FeOT, CaO, and particularly V) most effectively separate the peripheral and central intrusions into two trends. On all of the plots, partial overlap between the fields indicates that some peripheral pluton analyses resemble the central intrusions compositionally, but the central intrusion field always has a different slope. Furthermore, the hybrid tonalite trend mostly lies parallel to, and partially overlaps with, the peripheral pluton compositions and extends away from the field occupied by the Late Devonian mafic intrusions (LDMIs). Where the hybrid and peripheral pluton trends are not parallel, the peripheral plutons always plot closer to the Birchtown tonalite trend. Given that the Birchtown compositions probably result from variable degrees of mixing with mafic magma, these relationships also strongly suggest that the central pluton trend records the combined effects of magmatic and hydrothermal processes, whereas the peripheral pluton trend (marked by a regression) represents a hybridized mafic-felsic modification of it.

Assuming that hybridism of mafic and felsic magmas represents an important petrologic process in peripheral areas of the MZ, and that simple bulk mixing occurs between two end-members, then isotopic ratios should show hyperbolic variation in a suite of hybrids (DePaolo, 1981; Gray, 1984). On a plot of εNd-$^{87}Sr/^{86}Sr_i$ (Figure 5.11) analyses for the peripheral plutons do plot between the inferred end-member compositions, which correspond to isotopic values for the LDMIs (Appendix B-3) and metapelitic Popes Harbour basement gneisses (Eberz et al., 1991). Although most peripheral plutons lack Nd isotope data (a line represents the range of $^{87}Sr/^{86}Sr_i$ in the CP), a poorly constrained hyperbola would fit through their Sr and Nd isotopic

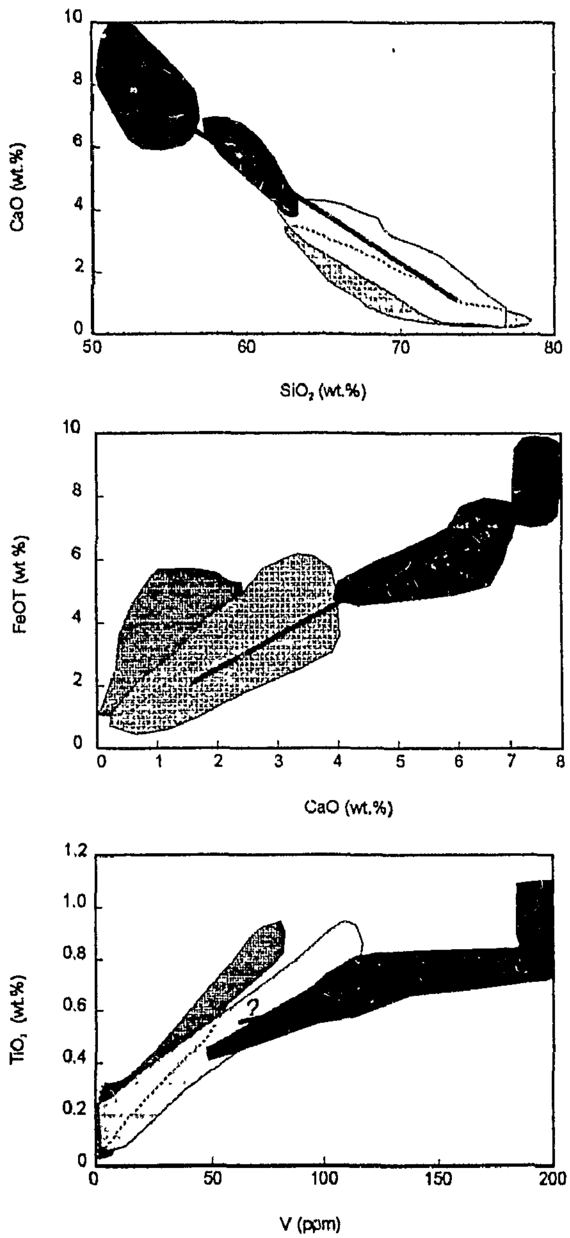

Figure 5.10. Variation diagrams that show intermediate relationships for the Birchtown hybrids (shaded in dark grey) and the peripheral plutons (shaded in light grey). The estimated regressions show possible linear trends using the Late Devonian mafic intrusions (shaded in black) and the central intrusions (shaded in medium grey) as end-members. Data for the mafic intrusions comes from Appendix B-3 and Appendix C-2 contains the hybrid geochemical data. Figure E2.1 in Appendix E shows least squares linear regressions for the plot of FeOT-CaO.

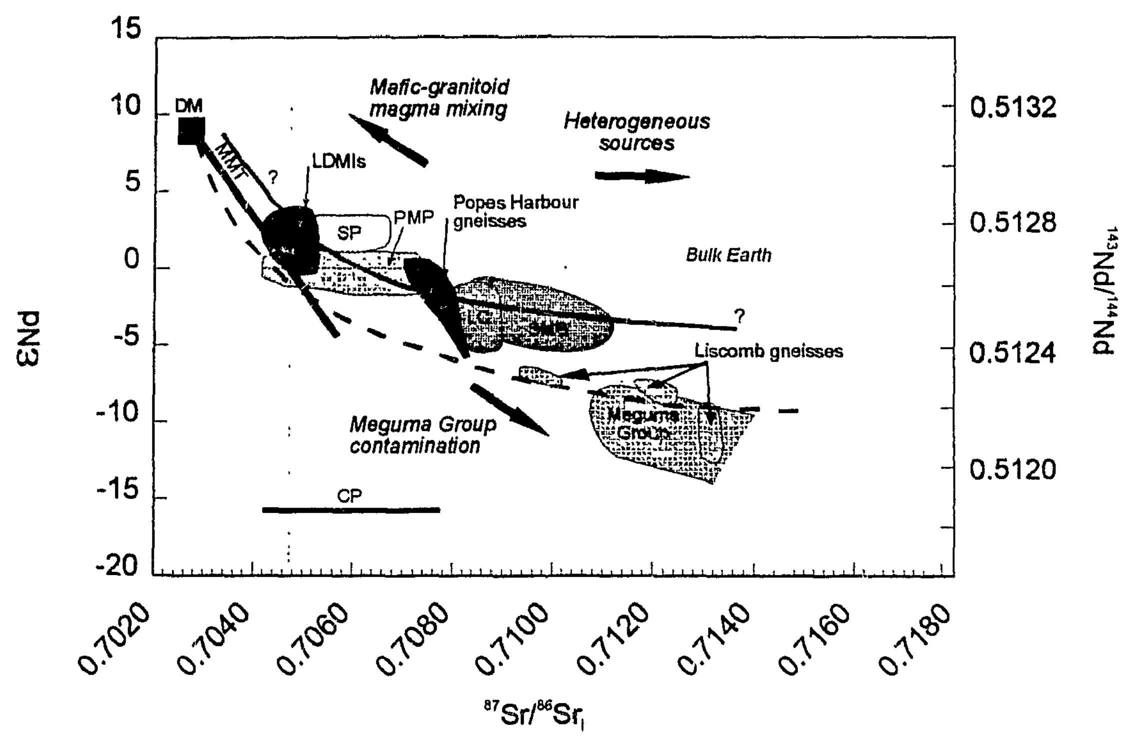

Figure 5.11. Plot of εNd-^{87}Sr/^{86}Sr$_i$ for the Meguma Zone granitoids. Table 5.3 describes the data recalculation. DM = depleted mantle, LDMIs = Late Devonian mafic intrusions. The solid line is a putative mixing hyperbola through the peripheral plutons, using the LDMIs and sub-Meguma basement at Popes Harbour (Eberz et al., 1991) as end-members. The dashed line is the hyperbola between depleted mantle and Meguma Group metagreywackes that Clarke et al. (1988) predicted. MMT = the modern mantle trend. Refer to Figure 5.1 for the intrusion abbreviations and Figure 5.10 for the colour scheme.

compositions; the peripheral LC and SMB instead plot to the right of the sub-Meguma basement field and apparently do not participate in mixing. Wide Sr isotopic variation in both peripheral and central intrusions may in part result from heterogeneous protoliths, although the fields for central intrusions also show some extension towards the Meguma Group metagreywacke compositions. Current data, therefore, allow for compositional variation attributable to heterogeneous sources and Meguma Group contamination in central bodies, coupled with mafic-granitoid magma mixing in the peripheral intrusions.

In summary, the currently available data comply with the results of previous studies, which suggest that peraluminous granitoids in the MZ result from a combination of chemical effects attributable to crystal fractionation, fluid interaction, crustal contamination, and/or heterogeneous crustal sources. The existence of an additional, variably strong component derived by mafic-granitoid magma mixing in the peripheral plutons, also provides an adequate explanation for the presence of many major oxide, trace element, and isotopic peripheral-central differences. Problems with missing data limit the current exploration of this hypothesis, which requires: (1) additional whole-rock major oxide and trace element analyses to increase the number of peripheral pluton samples and variables (particularly for the CP) and eliminate the possibility of geochemical separation resulting from different population sizes; (2) further characterization of the chondrite normalized REE patterns and elemental distributions in both the peripheral and central intrusions, which may identify new discriminators (perhaps Ce); and (3) determination of at least $^{87}Sr/^{86}Sr$, εNd, $\delta^{18}O$, and $\delta^{34}S$ values for different lithologies within all currently exposed peripheral and central intrusions. With these expansions of the database, quantitative appraisal of the mafic-granitoid magma mixing hypothesis could also use mathematical modelling and/or statistical treatments (e.g. Baird and Meisch, 1984; Ayuso and Arth, 1992) to test these graphical results.

5-5. Conclusions

The MZ contains two subtly different magmatic suites that Richard (1988) recognized as "northern" and "southern" plutons, and this study renames "central" and "peripheral" after the inclusion of data for the CP. These geochemical groups are not clearly separated, but peripheral plutons (particularly the tonalites) have higher TiO_2, Al_2O_3, FeOT, CaO, Ba, Sr, Cr, V, and εNd (>-0.1), coupled with lower $^{87}Sr^{86}Sr_i$ (<0.710), $\delta^{18}O$ (<10.4), and $\delta^{34}S$ (<5.0) values than their central counterparts, which instead show higher K_2O, Rb, Y, Ga, and Pb, $^{87}Sr/^{86}Sr_i$ (>0.708), $\delta^{18}O$ (>9.6), and $\delta^{34}S$ (>5.0), in conjunction with lower εNd (<-1.4); these geochemical groups cannot share the same combination of sources and processes. Accumulation of plagioclase, biotite, and accessory minerals can explain high Al_2O_3 and Sr in the peripheral plutons, and scatter for Ba, Rb, and Sr may at least partly result from subsolidus or magmatic interactions with fluids. The presence of synplutonic intrusions in the peripheral plutons suggest that high TiO_2, FeOT, CaO, Cr, and V, and depleted isotopic signatures allow for the possibility of mantle chemical input in addition to the evidence for open system crystal-liquid, Meguma Group contamination, and hydrothermal processes, and closed system effects attributable to heterogeneous protoliths in the central intrusions.

Chapter 6

THEORETICAL HEAT FLOW SIMULATIONS

6-1. Introduction

The Meguma Zone (MZ) contains contemporaneous mafic and granitoid intrusions of Late Devonian age and evidence exists for mechanical and chemical magmatic interaction between them on both the local and regional scales. The "mafic intrusion model" (MIM) advocates mantle-derived mafic magma as an anatectic heat source in such bimodal magmatic suites, and assessment of its thermal capabilities must rely on mathematical modelling. This chapter uses theoretical simulations of heat output associated with turbulently convecting mafic sills to test the thermal effects of mafic magmas in the Late Devonian crust of the MZ. The numerical models predict the minimum volumes of mafic magma emplaced into the sub-Meguma basement that could generate calculated volumes for exposed peraluminous granitoids. If the models adequately describe the behaviour of mafic intrusions, then the results provide some suggestions for the use of mafic magma heat sources during the Acadian Orogeny.

6-2. Approaches to Lithospheric Heat Flow Modelling

Assuming geothermal gradients of approximately 20-30°C km^{-1}, the 'normal thickness' continental crust at plate boundaries lies below its melting temperature at all depths above the Moho (Younker and Vogel, 1976; Sclater et al., 1980; Fowler and Nisbet, 1988). England and Thompson (1984; 1986) simulated the effects of instantaneous crustal-scale thrusting causing homogeneous pure shear thickening on a hypothetical steady-state geothermal gradient. Davy and Gillett (1986) and Zen (1988) used a similar one-dimensional finite difference approach to consider the effects of repetitively emplaced upper crustal thrust sheets (Figure 6.1a). With the

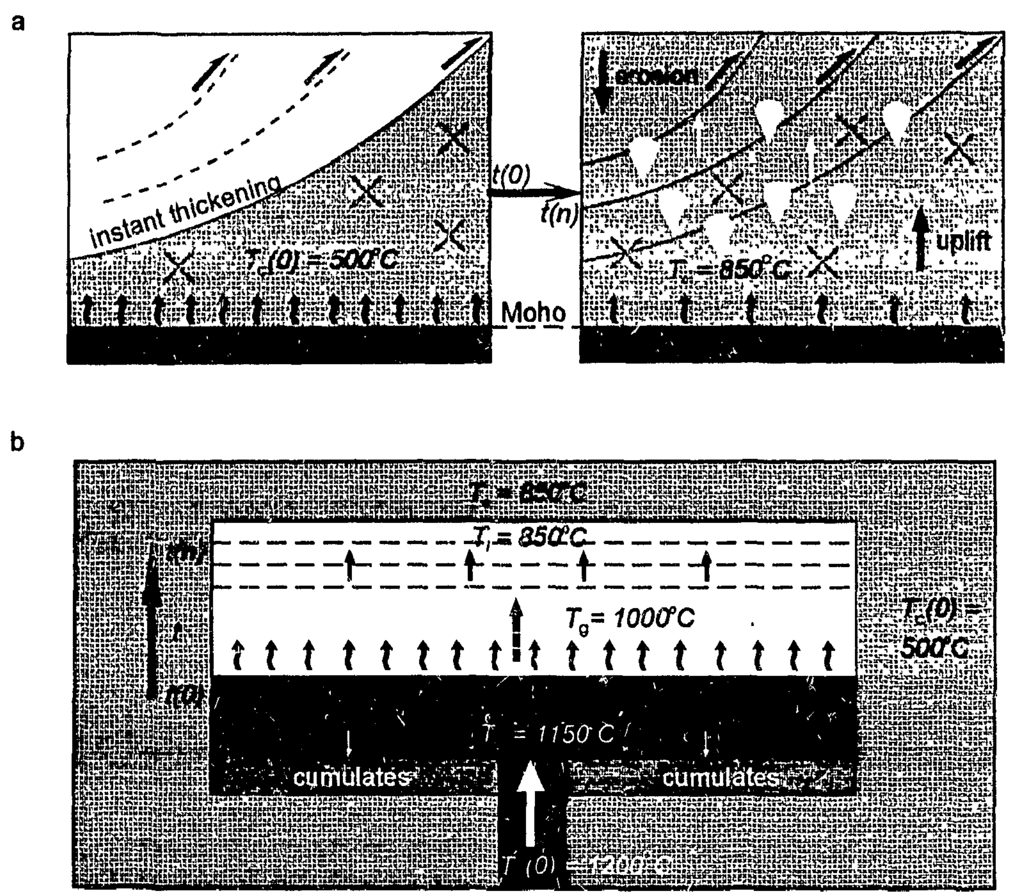

Figure 6.1. Schematic representation of two approaches to lithospheric heat flow modelling, showing the nomenclature adopted in the text. (a) Infracrustal heating by thrusting followed by thermal relaxation and uplift of 'normal thickness' (circa 35 km thick) crust. The main heat sources are the mantle heat flux (small vertical arrows), and radionuclides in the crust (crossed arrows); (b) Intracrustal heating by conduction above a mafic intrusion. T_b = the temperature of basalt, T_g = the temperature of anatectic granitoid, T_c = the temperature of the crust, T_i = the temperature of the crust-basalt interface, t = time from *t(0)* to *t(n)* where $n > 0$. Granitoid melt is shown in white. See Table 6.1 for other abbreviations and the text for a discussion.

scatter for both the northern and southern plutons. Increasing Rb and linearly decreasing Sr with decreasing Ba characterizes the northern plutons, whereas the southern pluton lithologies collectively have higher Sr concentrations and show no obvious trends for Rb. A plot of less mobile Cr-V shows much wider compositional variation for both elements in the southern plutons; northern plutons instead contain a wide compositional range for Y, and somewhat higher Pb and Ga concentrations. As with the major oxide discriminators, no clear distinction exists between granodiorites, monzogranites, and leucomonzogranites on the basis of these trace elements, although very high Cr and V concentrations do occur only in the southern pluton tonalites. The much smaller amount of data for Ga, Cr, and V may also account for some separation of the northern and southern geochemical fields, although the ratio of analyses for northern and southern plutons is <10:1 for these elements and artificially-induced separation is statistically insignificant (Richard, 1988). A valid statistical treatment cannot, however, be undertaken for the new discriminators because the new southern pluton data do not change the problematic sample to variable ratio limitation that Richard and Clarke (1989) experienced.

Where data exist for at least seven REEs, no significant differences separate the northern and southern plutons (Figure 5.6). Intrusions from both groups have very similar patterns with approximately six times enrichment of light REE relative to heavy REE (La/Lu 335-696). Tonalites and granodiorites have less pronounced negative Eu anomalies (Eu/Eu* 0.39-0.58) than the monzogranite and leucomonzogranite analyses (Eu/Eu* <0.16), and the smaller Eu anomalies in the southern plutons reflect the predominance of tonalite analyses. The small peak at Gd in the southern plutons may be an analytical phenomenon (Figure 5.6b; Chapter 3, Section 3.3), and the data may not accurately reflect all characteristics of the northern and southern plutons. The available radiogenic and stable isotope data for unaltered rocks is also limited, but gives much more obvious north-south separations (Table 5.3). Figure 5.7 shows that a wide variation of Sr, O, and S isotopic values characterizes lithologies in both the northern and southern plutons, but the northern and southern plutons do represent clearly separated subcrustal mantle heat flux augmenting heat produced by radionuclides in the crust, lithospheric thickening by thrusting (under a variety of crustal conditions and tectonic configurations) may produce small amounts of granitoid melt in circa 10 Ma. More voluminous melting occurs in circa 40-60 Ma, in response to thermal relaxation and the subsequent elevation of heated crust into shallower crustal regions containing volatiles because of erosion and/or uplift (De Yoreo et al., 1989; Gray and Cull, 1992). Although the lack of empirical data for the thermal behaviour of both the mantle and the crust (especially at depth) limits the usefulness of the models as analogues of natural processes, thrusting, thermal relaxation, and uplift alone generate anatectic melt slowly and inefficiently because of the low thermal conductivities of most crustal rocks (Fowler et al., 1988; Zen, 1992).

Greater crustal thickening lengthens the incubation period for the deep crust, and a longer incubation period between the thickening and uplift stages directly increases the amount of melt generated, but infracrustal processes may not generate sufficient melt in the short time intervals imposed by geological constraints in many ancient orogens. Also, the temperatures attained in the crust may be insufficient for the generation of hot tonalitic melts (Wyllie, 1977; Clemens and Vielzeuf, 1987). In the MZ, anatexis occurred rapidly and proceeded with the formation of tonalites (Chapter 5, Section 4.2). Dating of granitoid rocks indicates that the Barrington Passage Pluton (BPP) and the Canso pluton (CP) tonalites intruded the Meguma crust only 30 Ma after the onset of the Acadian terrane collision (Chapter 1, Section 4). The voluminous South Mountain Batholith (SMB), and presumably the other granitoid bodies that lack dates, intruded 40 Ma after the onset of terrane collision, contemporaneous with tectonic uplift at circa 372 Ma (Clarke et al., 1988). Although crustal thickening and tectonic uplift probably generated granitoid melt, plausible thermal roles exist for Late Devonian mafic intrusion (LDMI) magmas as an assisting thermal influence throughout the sub-Meguma basement, as an important heat source in the protoliths for at least the early-intruded peripheral BPP and CP, and perhaps also as a supplier of heat to some degree in the protoliths for the voluminous SMB.

One-dimensional thermal models of mafic intraplating suggest that mafic dykes and sills may generate voluminous melts at their emplacement level, and sills have the greatest thermal potential (Younker and Vogel, 1976; Bergantz, 1989). Thermal conduction above an intraplated mafic sill rapidly heats the crust to temperatures close to the basalt liquidus and causes partial melting under vapour-absent conditions (Irvine, 1970; Figure 6.1b). Bergantz (1989) predicted the presence of a substantial temperature gradient above the basalt sill and estimated that a 450 m thick intrusion intruded into crust at circa 500°C generates approximately 225 m of granitoid melt in less than 5000 years. The volume of granitoid increases with the thickness of the sill, and with the initial regional temperature of the crust, although crystal accumulations may insulate the crust below the base of the sill and prevent major melting there (Irvine, 1970). The first granitoids produced above the sill may be superheated and represent very high degrees of partial melting of the country rocks (Huppert and Sparks, 1988a), and, therefore, primitive tonalites and granodiorites may form soon after basalt intrusion with appropriate crustal compositions (Younker and Vogel, 1976; Vielzeuf and Holloway, 1988).

Given the probability of convection in mafic magmatic systems (Hanson and Barton, 1989), Huppert and Sparks (1988a, b, c) developed and described in detail a new one-dimensional model for mafic intraplating that integrates the results of quantitative fluid dynamical experiments with theoretical assumptions regarding the behaviour of mafic and granitic liquids. This method balances the thermal budget of a partial melting system by considering the vertical thermal effects of turbulent convection in the crystallizing mafic sills, and convection in the superheated melt layer that they form. To allow for the likelihood of repetitive injections (e.g. Hildreth, 1981), intracrustal heat flow simulations in this study use both static (single intrusion) and dynamic (repeated intrusion) models based on this approach (Younker and Vogel, 1976), using reasonable estimates for the nature and temperatures of the parent magmas to the LDMIs and the sub-Meguma basement during the Acadian Orogeny. Direct application of these intraplating models to a specific geological situation illustrates both the capabilities of, and the potential problems with, the use of mafic magma heat sources.

6-3. The Convective Intracrustal Model

6-3.1. The Static Scenario

Introduction

The convective intracrustal model uses parameterized equations that describe the temperatures of convecting mafic and granitoid magmas, and the thickness of a granitoid melt layer as a function of time, assuming that mafic magma forms a turbulently convecting sill (Huppert and Sparks (1988a, c). These mathematical relationships represent geological modifications of equations governing the thermal behaviour of a rectangular, homogeneous region of fluid constrained by rigid boundary conditions and containing an internal heat source. Jaeger (1957), Turner (1973), and Denton and Woods (1979) explored the conductive heat transfer equations that provide the basis for this work, and Huppert and Sparks (1988c) show the derivation of the ten main equations (described briefly below) for the special cases of turbulent convection in the fluid and fusion of the upper boundary. Hereafter, the subscripts *b*, *g*, *c*, and *i* refer to the basalt, the granitoid, the crust, and the interfaces between them, respectively. Table 6.1 shows the complete nomenclature for these modelling procedures, and Appendix F-1 summarizes variables critical to the modelling results. Equations 1 and 2 describe changes in the temperature of the intruded and anatectic melts with respect to time.

$$\frac{dT_b}{dt} = -(J_b/D)(T_b - T_i)^{4/3}/[1 - L_b c_b^{-1} x_b'(T_b)]. \tag{1}$$

$$\frac{dT_g}{dt} = (J_g/a)\{[T_i - T_g)^{4/3} - (T_g - T_m)^{4/3}] - \frac{da}{dt}[T_g - T_m - L_g c_g^{-1} x_g(T_g)]\}/\ldots$$

$$[1 - L_g c_g^{-1} x_g'(T_g)], \tag{2}$$

where *T* is a magma temperature, *D* is the thickness of the basalt sill, *L* is the latent heat of a

Table 6.1. Summary of initial conditions and results for static models calculated with HTFLOW31.

Model name	D (m)	$T_b(0)$ (°C)	$T_c(0)$ (°C)	T_m (°C)	% H_2O	T_I (°C)	Ra_g	a (m)	anatectic efficiency (%)
S1	10	1,150	500	850	2-6	830	-	-	-
S2	10	1,200	500	850	2-6	854	1.41	4.9	49
S3	10	1,200	600	850	2-6	903	6.96	6	60
S4	10	1,200	700	850	2-6	953	33.62	7.6	76
S5	10	1,200	500	950	0	804	-	-	-
S6	50	1,150	500	850	2-6	830	-	-	-
S7	50	1,200	500	850	2-6	854	176.12	24.8	50
S8	50	1,200	600	850	2-6	903	870.25	30.1	60
S9	50	1,200	700	850	2-6	953	6.21E+03	38.2-53.6	76-107
S10	50	1,200	500	950	0	804	-	-	-
S11	100	1,150	500	850	2-6	830	-	-	-
S12	100	1,200	500	850	2-6	854	2.16E+03	49.6-61.0	50-61
S13	100	1,200	600	850	2-6	903	9.77E+03	60.1-75.6	60-76
S14	100	1,200	700	850	2-6	953	4.47E+04	76.5-98.2	76-98
S15	100	1,200	500	950	0	804	-	-	-
S16	500	1,150	500	850	2-6	830	-	-	-
S17	500	1,200	500	850	2-6	854	1.83E+05	267.2-303.3	53-61
S18	500	1,200	600	850	2-6	903	9.11E+05	325.6-374.6	65-75
S19	500	1,200	700	850	2-6	953	4.51E+06	414.8-484.3	83-97
S20	500	1,200	500	950	0	804	-	-	-
S21	1,000	1,150	500	850	2-6	830	-	-	-
S22	1,000	1,200	500	850	2-6	854	1.44E+06	519.8-570.4	53-57
S23	1,000	1,200	600	850	2-6	903	7.10E+06	625.8-690.6	63-69
S24	1,000	1,200	700	850	2-6	953	3.45E+07	795.0-888.0	80-89
S25	1,000	1,200	500	950	0	804	-	-	-
S26	5,000	1,150	500	850	2-6	830	-	-	-
S27	5,000	1,200	500	850	2-6	854	1.75E+08	2478.2-2577.4	50-52
S28	5,000	1,200	600	850	2-6	903	8.70E+08	3006.8-3129.5	60-63
S29	5,000	1,200	700	850	2-6	953	4.20E+09	3822.3-3975.5	76-80
S30	5,000	1,200	500	950	0	804	-	-	-

D = the thickness of the basalt sill, $T_b(0)$ = the initial temperature of the basalt, $T_c(0)$ = the initial regional temperature of the crust, T_m = the melting temperature of the crust, % H_2O = the volatile content of the crust, T_l = the maximum crustal temperature at the interface above the basalt intrusion, Ra_g = the maximum Rayleigh number of the granitoid melt layer and, *a* = the maximum thickness of the granitoid melt layer, and the anatectic efficiency is the ratio between *D* and *a* expressed as a percentage.

magma, c is a specific heat capacity, x is the magma crystal content, x' is the first derivative of this crystal content, and a represents the thickness of the granitoid melt layer formed. Magma temperatures depend on their rheological characteristics, their thickness, and on the temperature of the interface between the basalt and the crust, which relies on the $^4/_3$ relationship to describe a linearly averaged thermal profile above a turbulent convective boundary layer (Turner, 1973). The temperature of the granitoid also depends on the melting temperature of the crust T_m, and on the temperature of the crust-basalt interface T_i; the heat flux out of the basalt controls this property. Equation 3 gives the parameter J_b

$$J_b = 0.1(\alpha_b g \kappa_b^2 / \nu_b)^{1/3}, \tag{3}$$

which represents the heat flux out of the basalt in the turbulent convection case (Turner, 1973); g is the acceleration due to gravity, κ is a thermal diffusivity, α is a coefficient of thermal expansion, and ν is a kinematic viscosity. The heat flux out of the basalt is assumed to equal the heat flux supplied to the overlying granitoid, and, therefore, $J_b = J_g$.

Equation 4 predicts the thickness of granitoid formed with time above the basalt sill.

$$\frac{da}{dt} = k_g H^{-1}(T_i - T_m)/a, \tag{4}$$

where, k is the thermal conductivity of a magma. Parameter H represents the heat required to raise the crust from any starting temperature $T_c(0)$ to its melting temperature T_m

$$H = \rho_c[c_c(T_m - T_c(0)) + L_c], \tag{5}$$

and ρ represents a density for the crust. The heat required for melting (and so the thickness of granitoid melt generated) depends critically on the interval between the regional crustal temperature and its solidus, and on the composition of the crust and its volatile content. These parameters determine the density, specific heat capacity, and latent heat of fusion of the crust.

The numerical algorithm

The iterative computer program HTFLOW31 (Appendix F-2) encapsulates relationships derived from these equations with respect to the temperature of the basalt. The algorithm emulates the methodology of Huppert and Sparks (1988a, c) in three stages with time (Figure 6.2 and Figure 6.3).

(1) *Emplacement of a convecting basalt sill.* A basalt sill of known thickness and magma temperature instantaneously intrudes lower crustal country rocks of known initial regional temperature T_c at time zero, with the initial conditions a = 0, $T_b(0) = T_b$, and $T_c < T_m$. If the basalt convects turbulently at T_b according to Equation 6 (critical Rayleigh number of basalt $Ra_b > 10^6$), where

$$Ra_b = x_b g(T_i - T_m)D^3/\kappa_b \nu_b, \tag{6a}$$

and the crystal content of basalt x_b represents a simple function of temperature based on experimental results (Huppert and Sparks, 1988a)

$$x_b = 7200T_b^{-1} - 6, \tag{6b}$$

then turbulent convection in the basalt magma heats the country rocks at and above the crust-basalt interface to the temperature T_i

$$T_i = T_m + \rho_b^2 c_b^2 D J_b H^{-1} k_b^{-1}[T_b(0) - T_b + L_b c_b^{-1} x_b(T_b)](T_b - T_i)^{4/3}. \tag{7}$$

If $T_i \geq$ the melting temperature of the crust T_m then the overlying crust melts to form a thickness of superheated granitoid *a*

$$a = H^{-1}\{\rho_b c_b D[T_b(0) - T_b] + \rho_b L_b D x_b(T_b)\}. \tag{8}$$

The thickness of granitoid depends on the difference between the intrusion temperature and the current temperature of the basalt. This relationship approximates time because the basalt

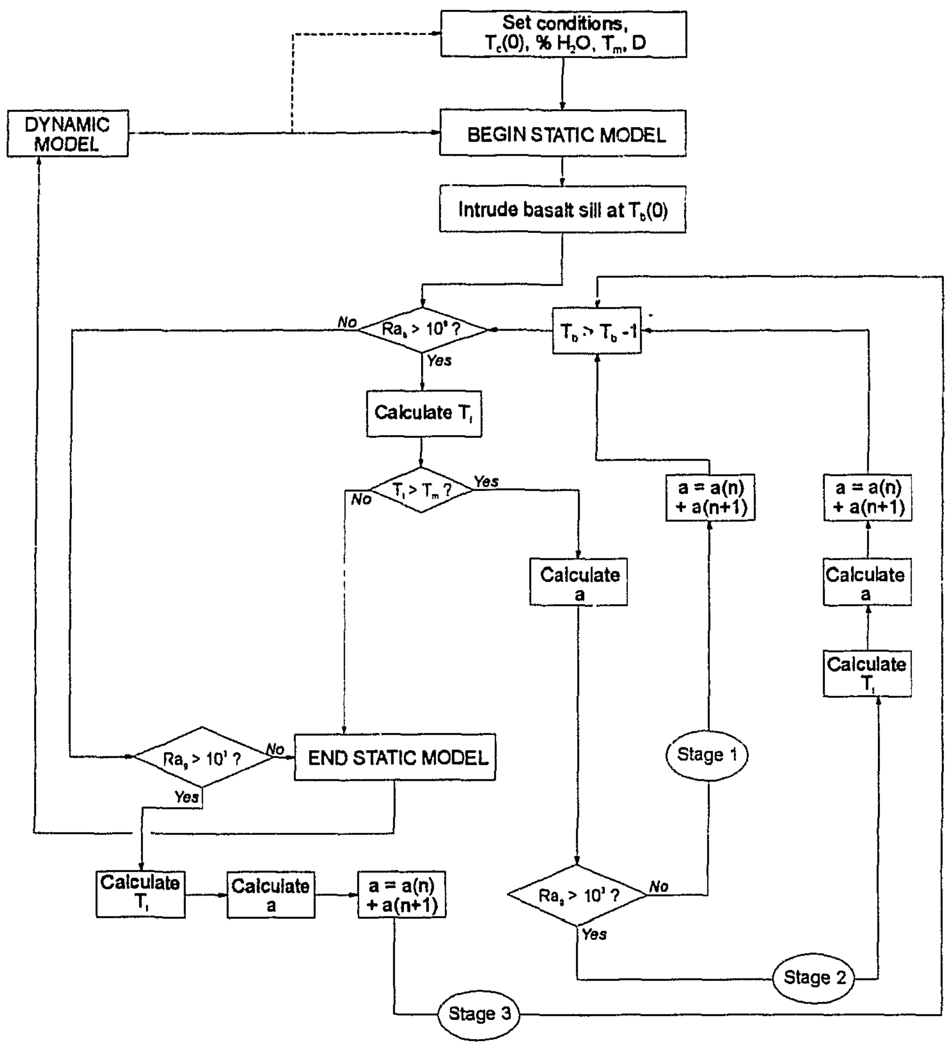

Figure 6.3. Flow chart illustrating the algorithm for HTFLOW31. The program recognizes the three stages of the static model illustrated in Figure 6.2, and it also includes an iterative dynamic scenario. Symbols as in Table 6.1.

cooling rate in the model is uniform; the algorithm decreases the basalt temperature in discrete 1°C increments to ensure stable results (Appendix F-3). As the mafic sill cools, the thickness of granitoid increases from *a(0)* to *a(n)* at time *n*, when it reaches the critical Rayleigh number for the onset of convection (Ra_g >2000), which is calculated by substituting parameters for the granitoid into Equation 6a and using Equation 9 instead of Equation 6b to determine a crystallinity. The crystal content of granitoid melt x_g is a function of temperature and the percentage of volatiles derived from the crust during melting. Melts with 2-6% vapour use a constant of 1000 and dry melts use a constant of 1100 in Equation 9.

$$x_g = 0.65(1000 \rightarrow 1100 - T_g)/150. \quad (9)$$

If the basalt ceases to convect turbulently during this initial stage then no further melting occurs if convection did not initiate in the granitoid, otherwise the model progresses to the second stage.

(2) *Convection in both the basalt and the granitoid.* Assuming that both the basalt sill and the overlying granitoid melt layer convect simultaneously, then the basalt advects heat to the granitoid while the granitoid advects heat to its roof. Equations 7 and 8 also describe the melting process for the granitoid if Equation 10 substitutes for Equation 7 when calculating the crust temperature above the granitoid, assuming that the heat flux out of the basalt equals the heat flux into the overlying granitoid.

$$T_i = (T_b + yT_g)/(1 + y), \quad (10)$$

where

$$y = (p_g c_g J_g / p_b c_b J_b)^{3/4}.$$

If the basalt ceases to convect turbulently during this second stage, then the granitoid continues to convect and generates small amounts of additional crustal melt in Stage 3.

(3) *Convection in the granitoid alone.* The mafic sill ceased turbulent convection at Ra_b <10^6 and a critical melt fraction of 55%, but the granitoid melt layer may continue to convect and generate

new melt according to equations 8, 9, and 10, until Ra_g <2000 and the critical melt fraction equals 70% (Huppert and Sparks, 1988a; Van der Molen and Paterson, 1979). As the granitoid melt layer propagates, the mafic sill undergoes double-diffusive convection before ultimately conducting heat to the granitoid. As a first approximation, the model ignores these processes (Huppert and Sparks, 1988a) and no further crustal melting occurs after the granitoid solidifies.

Modelling results

Table 6.1 summarizes the results of 123 static model runs designed to test the capabilities of the equations. It shows the thickness of granitoid that basaltic sills with different thicknesses emplaced at 1150-1200°C produce in crust at 500-700°C that arbitrarily has a pelitic composition and a solidus at 850°C under vapour-absent conditions with 2% H_2O in hydrous silicates, and under excess vapour (6% H_2O) conditions. The latent heat of fusion of the crust remains constant at 70 cal g^{-1} for all temperatures below the solidus and is lowered to 45 cal g^{-1} at temperatures at or above the solidus. Models run with these conditions (e.g. models S1-S4 for a 10 m sill) allow comparison of the results with those of the conductive infracrustal models, and with the original results of Huppert and Sparks (1988a, c). Excess vapour models do not take into account any decrease in the solidus temperature and so indicate the sensitivity of the calculations to the volatile content of the crust. In contrast, models run with a dry pelitic solidus at 950°C (0% H_2O) simulate the production of high temperature melts (e.g. model S5 for 10 m sills). In all models, constants describing the rheology of the mafic and granitoid magmas follow those of Huppert and Sparks (1988a; Appendix F-4) and the plots use the temperature of the basalt as an approximate indicator of time because cooling of the basalt occurs at a uniform rate with time, and it controls the evolution of the model.

Figures 6.4 and 6.5 summarize the changes in the rheological parameters of the granitic and basaltic magmas that affect the melting process. All basaltic sills thicker than 50 m convect turbulently on intrusion, and their Rayleigh numbers decrease progressively with crystallization

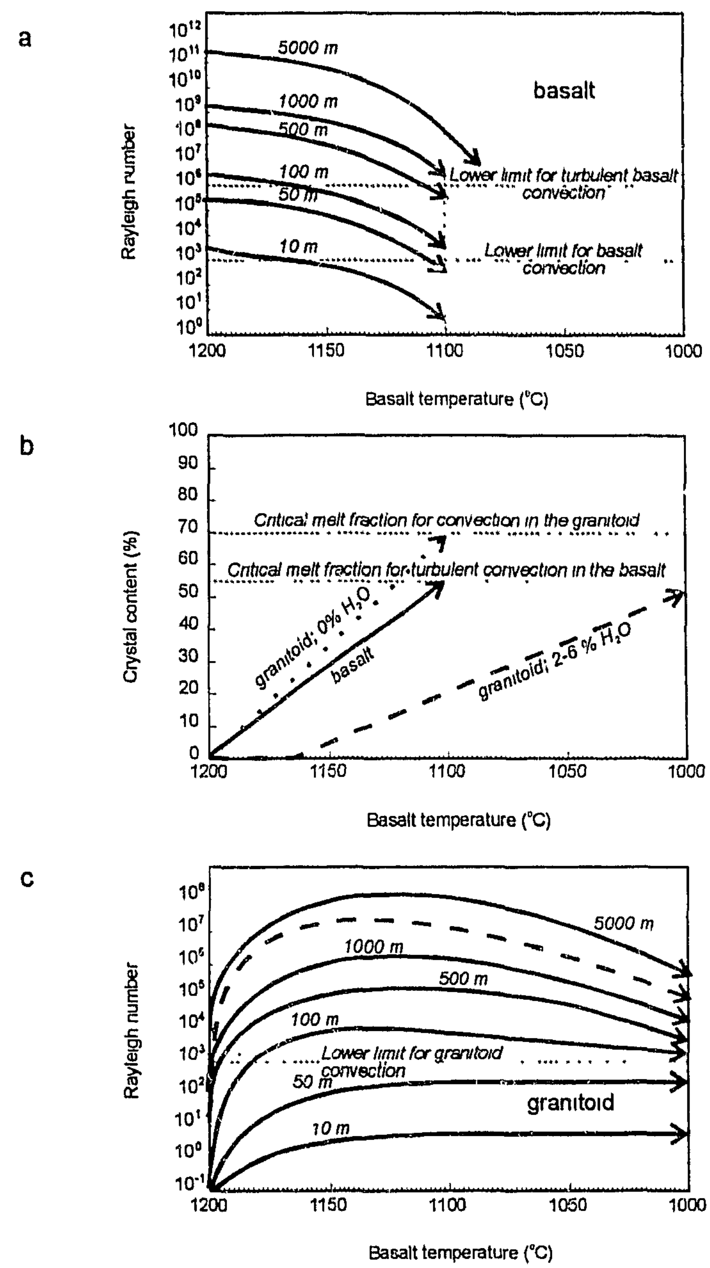

Figure 6.4. Calculated changes in the convective potential of the mafic and granitoid magmas as the basalt cools with time. (a) Plot of Rayleigh number-basalt temperature for different basalt sill thicknesses; (b) Plot of crystal content-basalt temperature for the basalt (solid arrow) and for the granitoid with different volatile contents (dotted and dashed arrows); (c) Plot of Rayleigh number-basalt temperature for granitoid melt layers with 2% volatiles produced above different basalt sill thicknesses. The effect of 6% volatiles is illustrated with a dashed line for granitoid produced by a 1000 m basalt sill.

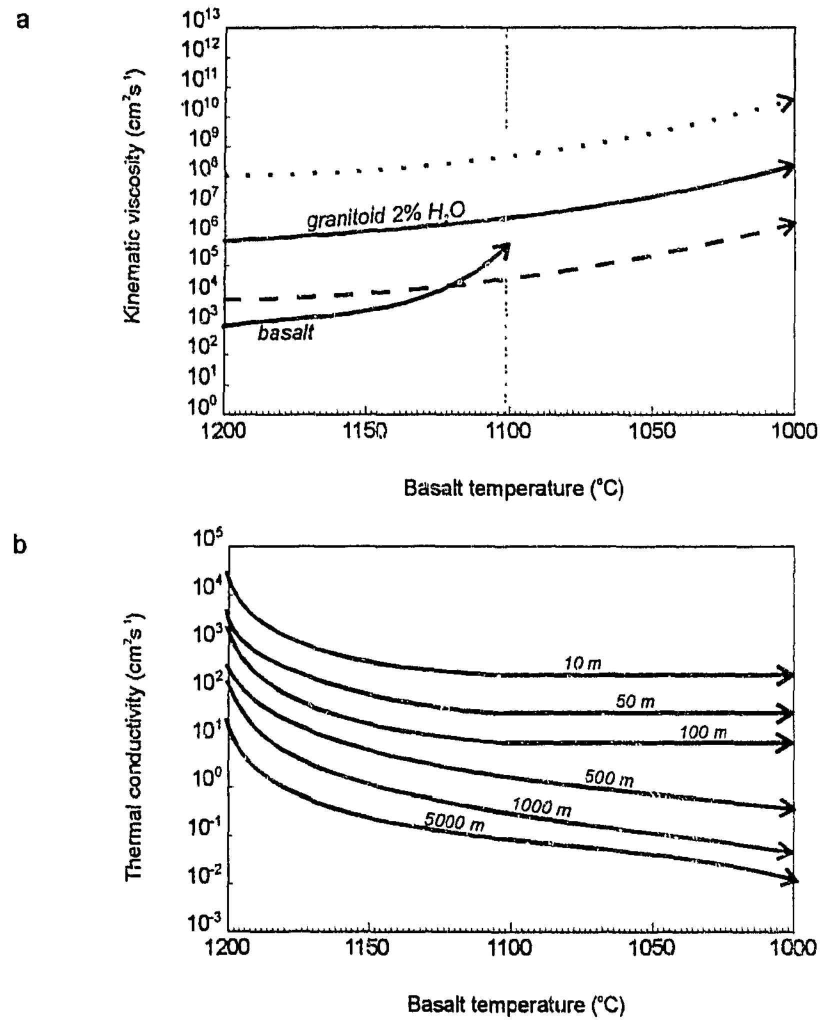

Figure 6.5. Calculated rheological changes for the basalt and granitoid magmas as the basalt cools with time. (a) Plot of kinematic viscosity-basalt temperature; symbols as in Figure 6.4c; (b). Plot of thermal conductivity-basalt temperature for granitoids containing 2% H_2O. See the text for details.

(Figure 6.4a); regardless of the ambient crustal conditions, basalt sills <5000 m thick cease turbulent convection at 1100°C when the magma contains 55% crystals (Figure 6.4b). The initial crustal conditions and the nature of the underlying basalt sill do, however, profoundly affect granitoid crystallization. Crystal contents and Rayleigh numbers for the granitoid initially rise with time as the thickness of the melt layer increases rapidly above the mafic sill (Figure 6.4b, c), and melts produced above sills greater than 50 m thick convect with the basalt but cool much more slowly. Unless the crust is dry, solidification of the granitoid occurs after the basalt no longer convects turbulently because the crystal content of the granitoid eventually affects its Rayleigh number more than any increase in melt layer thickness after the basalt sill ceases to supply heat. Mafic sills smaller than 50 m, or those emplaced with liquidus temperatures below 1200°C, do not produce convecting granitoid and the static model does not provide a valid description of the melting process for these situations.

For basalt sills ≥100m thick, Figure 6.5a shows that crystallization in both the granitoid and the basalt increases their viscosities, although the presence of vapour in the granitoid magma has a more profound effect on the rheology of the melt region than its crystal content. In Figure 6.5b, the thermal conductivity of the granitoid decreases as the basalt sill thickness increases, and this effect progressively reduces the thickness of granitoid melt formed above sills with increasing thickness by a maximum of 27% if the crust contains excess vapour (compare models S9 and S29 in Table 6.1); the geological relevance of this effect is not known. However, granitoid melts containing 2-6% vapour propagate additional melting and the quantity of this melt depends on the crust temperature. Figure 6.6 summarizes the thermal regime near a sill. The crust at the interface immediately attains temperatures well above the solidus and any granitoid formed represents an almost total partial melt and becomes superheated to temperatures between those of the basalt and this hot crust; lower degrees of partial melting occur at the lower temperatures prevalent with increasing distance from the crust-basalt interface. Increasing the starting temperature of the crust increases the attainable temperatures

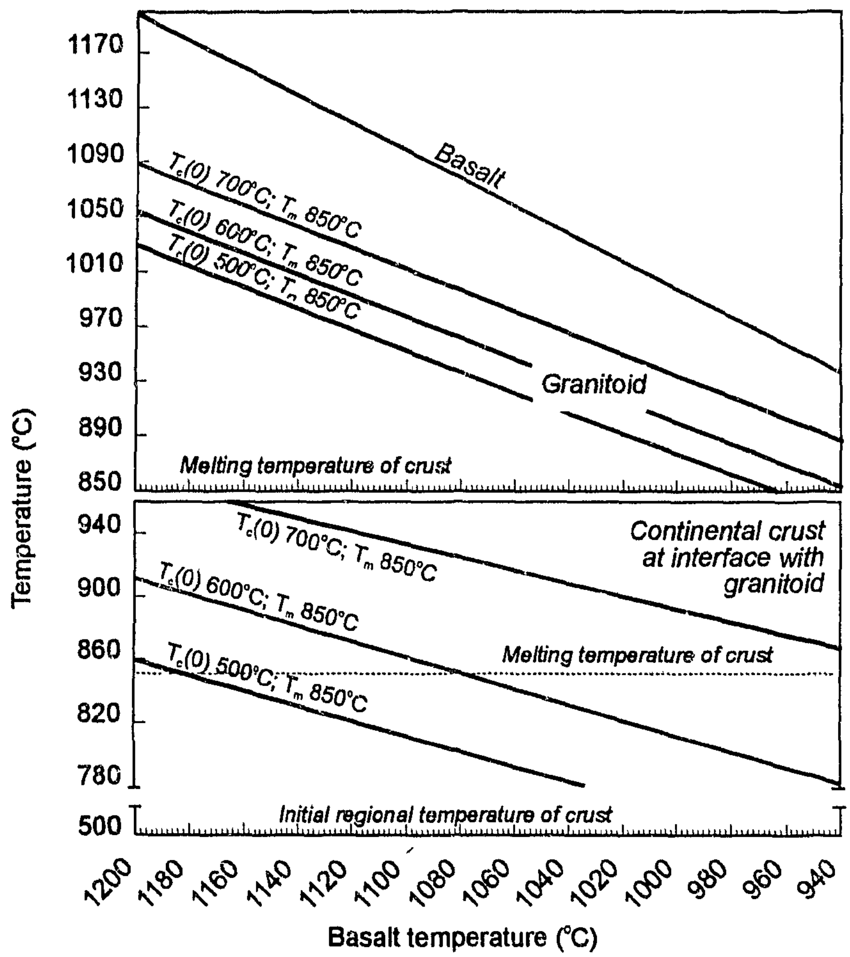

Figure 6.6. Predicted temperatures for the basalt and granitoid magmas and their country rocks as the basalt cools with time after the emplacement of a 500 m basalt sill. Symbols as in Table 6.1.

of the crust and the granitoid over a narrow range of circa 100°C (compare models S2-S4 in Table 6.1). Crust containing volatiles in hydrous silicates cools below its solidus after the sill solidifies (at circa 1100°C) in all models where a sill intrudes hot crust at >500°C. Progressively smaller degrees of partial melting occur as the crust immediately above the basalt cools.

Increasing the crustal temperature, or its volatile content, increases the thickness of melt generated by approximately 50 m for each 100°C temperature increase or 2% increment for the volatile content (Figure 6.7a). The thickness of granitic melt increases linearly until the basalt temperature reaches 1100°C, as both the basalt and the granitoid generate additional melt and the model progresses through the first and second stages. After the basalt ceases turbulent convection, the granitoid generates small amounts of additional melt in the third stage if the crust contains volatiles, and crust with 6% H_2O produces approximately 20% more melt than crust with 2% H_2O. The ratio of the basalt thickness to the total thickness of granitoid produced at the end of the model approximately indicates the anatectic efficiency of the melting process (Bergantz, 1989), and it rises from 0.5:1 (granitoid:mafic) in crust at 500°C to 0.8:1 in hot crust at 700°C; a 500 m mafic sill, therefore, liberates 267-484 m of granitoid melt in an absolute time period of approximately 267 years (Huppert and Sparks 1988b) and the granitoid generates more melt in circa 10^5-10^6 years. Although decreased thermal conductivity values for granitoid melt produced above thick sills slightly reduce the efficiency of melting in models with excess vapour, the absolute thickness of melt increases with the sill thickness (Figure 6.7b). Therefore, 5000 m sills produce 2478-3975 m of granitoid (models S27-S29 in Table 6.1) over their longer cooling history of approximately 1000 years.

In summary, turbulently convecting basalt generates melt layers that account for circa 50% of the sill thickness in vapour-absent crust at 500°C, achieve maximum thicknesses equivalent to circa 80% of the basalt sill in hotter crust vapour-absent crust at 700°C, but may attain thicknesses equal to the sill thickness if the crust contains excess (6%) volatiles. The temperature difference between the liquidus basalt and the ambient conditions in the crust

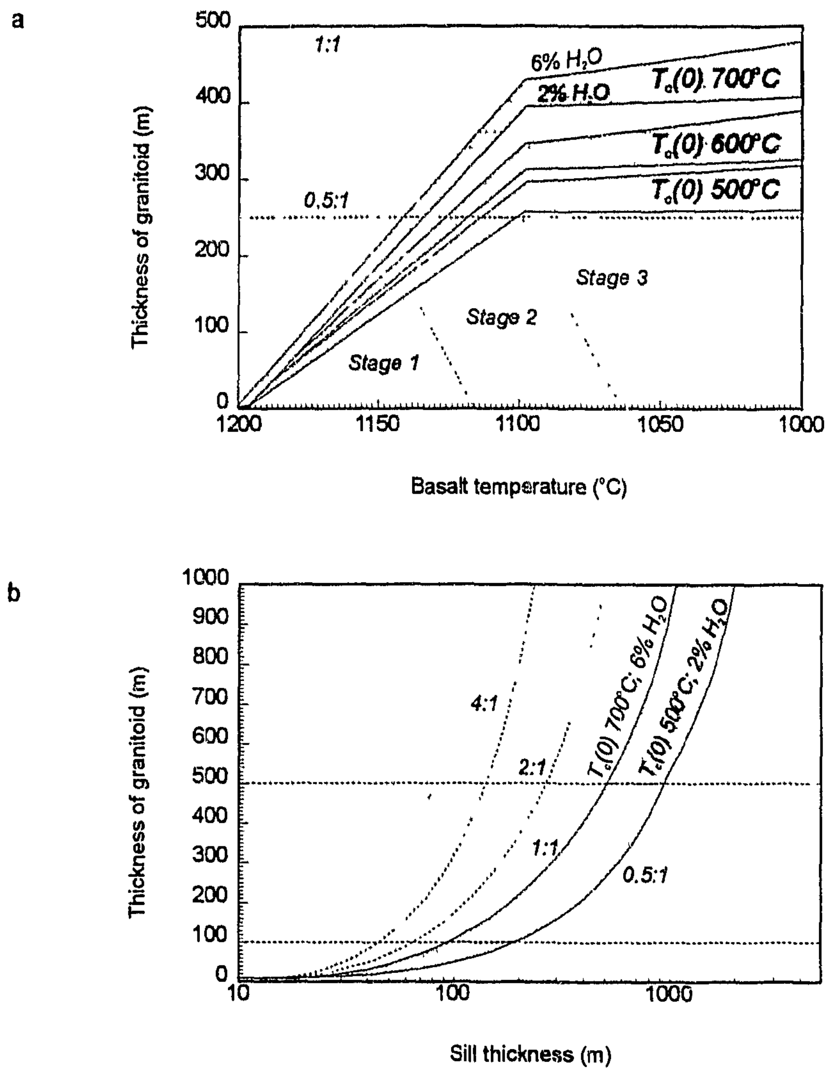

Figure 6.7. Variation of the granitoid melt layer thickness in the static model. (a) Plot of granitoid thickness-basalt temperature for a 500 m basalt sill showing the effects of volatiles in the crust and its ambient temperature; Figure 6.2 describes the stages in the static model; (b) Plot of granitoid thickness-basalt sill thickness under different crustal conditions. The ratio is the anatectic efficiency and the shaded regions mark the modelling results. See the text and Table 6.1 for details.

critically controls the thickness of melt that forms, and no melting occurs if this temperature difference exceeds 350°C and if the crust is dry (e.g. models S10, S15, and S20 in Table 6.1). The volatile content of the crust allows slower cooling and aids convection in the granitoid magma, which promotes further melting by self-propagation. These results agree with the expected control of dissolved volatiles on the crystallization history of natural granitoid magmas (e.g. Scarfe, 1986), and they also match the initial findings of Huppert and Sparks (1988a). The models in Table 6.1 produce granitoid thicknesses within 5% of the published values; these small differences result from assumptions regarding the density of the crust; explicit values do not appear in Huppert and Sparks (1988a).

Assumptions, limitations, and boundary conditions

All static models assume that the crust above the intrusion site has a thickness much greater than that of the mafic sill, that a chilled margin never stabilizes on the upper margin of the sill, that all crystals in the sill remain in suspension, and that the crust above the sill undergoes equilibrium melting at a constant rate. The requirement of turbulent convection in the sill probably justifies these conditions because the basalt might scavenge a chilled margin and suspend early-formed crystals above melt fractions of circa 50% (Huppert and Sparks, 1988c), while ensuring homogeneous temperatures in the basalt to produce a steady heat source. However, the calculations make no provision for potentially significant non-Newtonian behaviour in crystal-rich magmas (Hardee, 1981), and they ignore heat advection by volatiles exsolved from the basalt (Fowler and Nisbet, 1988). The models do account for the changing thermal conductivities and kinematic viscosities of both the mafic and granitoid magmas as functions of crystal content as they cool with time (Huppert and Sparks, 1988a), but they assume constant magma densities (despite crystallization and cooling), and use averaged values for specific heat capacity and the latent heat of crystallization over the temperature ranges considered for magmatic crystallization. Also, external temperature gradients and geological processes do not affect partial melting because the mafic intrusion site is assumed to be a closed thermal system.

Although the crust may be dry, vapour-absent, or contain excess volatiles, individual models assume a homogenous crust composition, with an averaged latent heat of fusion, that melts congruently above a single solidus temperature determined by its composition. Anatexis in nature depends on a combination of the ambient temperatures, pressures, and compositions of the crust (Zen, 1988), and phase changes associated with dehydration prevent steady-state melting (Clemens and Vielzeuf, 1987; Bergantz, 1989), although experiments do suggest that vapour-absent partial melting occurs over a narrow temperature interval at depth (Wyllie, 1977). Finally, this model may underestimate the volume of granitoid melt produced because anatexis occurs only directly above the sill, contrary to the suggestion of Hodge (1974) and Younker and Vogel (1976). Although basal cumulates in the basalt probably inhibit melting below the base of the sill after turbulent convection ceases, lateral melting may occur in nature because of advective heat transfers through the sides of the basalt intrusion (Irvine, 1970). Perhaps the large horizontal extent of a sill relative to its thickness minimizes the effect of this process (Huppert and Sparks, 1988a, b) and ensures that all heat is transferred vertically into overlying crust or granitoid melt as a one-dimensional process.

6-3.2. Dynamic Models

Given the assumptions and limitations of the conductive static model, and recognizing that the calculations simulate only the early magmatic history of basaltic magmas, the convective model for heat transport generates circa 3% more melt than the conductive approaches of Younker and Vogel (1976) and Bergantz (1989) in vapour-absent crust at 500°C because the anatectic granitoid can propagate small amounts of additional melting. However, convection generates this melt in substantially less time (Huppert and Sparks, 1988b, c); 500 m sills cool and crystallize in <300 years, compared to the 2000-4500 year estimates of Hodge (1974) and Bergantz (1989) with similar crustal conditions and physical parameters for the melts.

Static models of basaltic sills intruding hotter crust at 700°C generate up to 30% more granitoid melt, and suggest further study of dynamic intrusion models. Natural situations probably involve repeated injections of basalt into a contiguous region of the crust, and any existing granitoid would trap subsequent basaltic sills in the hot crust that exists after the first basalt intrusion (e.g. Michael, 1991; Chapter 1, Section 2). A model simulating repeated basaltic injections could, therefore, generate substantially more anatectic granitoid than static models under similar regional thermal regimes (Huppert and Sparks, 1988a; R.S.J. Sparks pers. comm., 1992).

The HTFLOW31 algorithm includes a dynamic model component that describes multiple injections of basalt sills of the same thickness by iterating the static model for each intrusion (Figure 6.3). In the static model, the crust heats up from its regional temperature to the solidus before cooling occurs (Figure 6.6; Figure 6.8a). By setting the initial crustal conditions for the second and subsequent sills in the dynamic model to the thermal regime prevailing at the end of the previous static run, a constant cooling interval exists between intrusions. For any regional crustal temperature, the crust cools to 700-780°C before the next intrusive event (Figure 6.8b). Dynamic models run with the initial regional temperature of the crust equal to its melting temperature simulate a situation where the sills intrude simultaneously and no cooling occurs. The first sill heats the crust to the solidus and all subsequent sills maintain the melting temperature (Figure 6.8c), and so the entire fusion process occurs in crust that has a lowered latent heat of fusion of 45 cal g^{-1} to describe its partially molten state. These findings match the suggestions of Huppert and Sparks (1988b) and assume that repeated basaltic intrusions do not involve significantly different fluid dynamics. Table 6.2 summarizes the dynamic models simulating 1-10 basaltic intrusions of equal thickness with this methodology, and Figure 6.9a summarizes the results for 10-5000 m thick basalt sills .

For any initial regional crustal temperature in the range 500-700°C with vapour-absent conditions and a constant cooling interval (e.g. models D1, D2 and D3 for 10 m sills), the first sill heats the crust and melts it with 0.5:1-0.8:1 anatectic efficiency, as in the static model (Figure

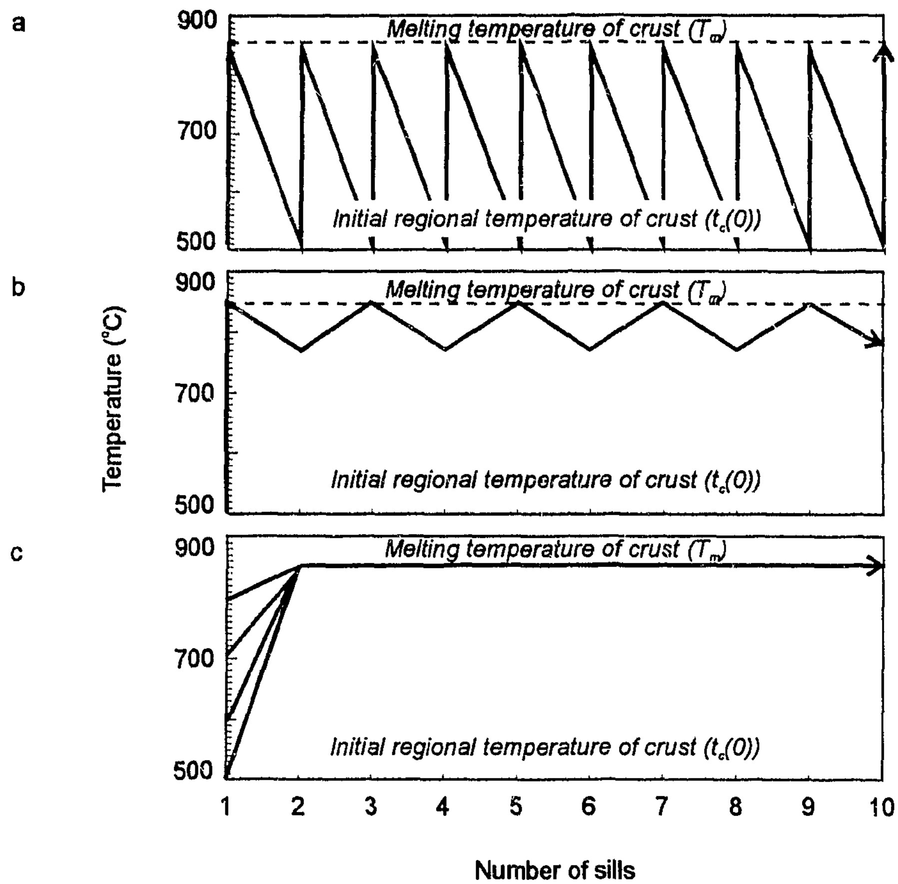

Figure 6.8. Postulated variations in the ambient temperature of crust for different intrusive scenarios. (a) Plot of temperature-number of basalt sills for the static model; (b) Plot of temperature-number of basalt sills for a dynamic model where the crust cools between each incursion of basalt; (c) Plot of temperature-number of basalt sills for a dynamic model where no crustal cooling occurs between basalt incursions. See the text for details.

Table 6.2. Summary of initial conditions and results for dynamic models calculated with HTFLOW31.

Model name	n	D (m)	$T_b(0)$ (°C)	$T_c(0)$ (°C)	T_m (°C)	% H_2O	T_l (°C)	a (m)	anatectic efficiency (%)
D1	1-10	10	1,200	500	850	2	854	4.9-100.3	49-106
D2	1-10	10	1,200	600	850	2	903	6.0-122.1	60-129
D3	1-10	10	1,200	700	850	2	953	7.6-123.7	76-129
D4	1-10	10	1,200	850	850	2	1026	21.5-215.0	215
D5	1-10	50	1,200	500	850	2	854	24.8-503.6	50-106
D6	1-10	50	1,200	600	850	2	903	30.1-609.7	60-129
D7	1-10	50	1,200	700	850	2	953	38.2-617.8	76-129
D8	1-10	50	1,200	850	850	2	1026	181.2-1812.0	362
D9	1-10	100	1,200	500	850	2	854	49.6-1007.2	50-106
D10	1-10	100	1,200	600	850	2	903	60.1-1220.2	60-129
D11	1-10	100	1,200	700	850	2	953	76.5-1656.0	76-176
D12	1-10	100	1,200	850	850	2	1026	339.1-3391.0	339
D13	1-10	500	1,200	500	850	2	854	267.2-5246.9	53-111
D14	1-10	500	1,200	600	850	2	903	325.6-6219.7	65-131
D15	1-10	500	1,200	700	850	2	953	414.8-6802.1	83-142
D16	1-10	500	1,200	850	850	2	1026	1238.3-12383.0	248
D17	1-10	1,000	1,200	500	850	2	854	519.8-9869.9	53-104
D18	1-10	1,000	1,200	600	850	2	903	625.8-11009.1	63-115
D19	1-10	1,000	1,200	700	850	2	953	795.0-12441.9	80-129
D20	1-10	1,000	1,200	850	850	2	1026	2333.1-23331.0	233
D21	1-10	1,000	1,200	500	950	0	1028	0-8058.6	0-90
D22	1-10	1,000	1,150	500	850	2	953	0-86818.4	0-96
D23	1-10	1,000	1,150	700	950	0	1002	0-8568.0	0-95
D24	1-10	5,000	1,200	500	850	2	854	2478.2-42683.0	50-89
D25	1-10	5,000	1,200	600	850	2	903	3006.8-247621.0	60-99
D26	1-10	5,000	1,200	700	850	2	953	3822.3-53829.0	76-111
D27	1-10	5,000	1,200	850	850	2	1026	10738.9-107389.0	215
D28	1-10	5,000	1,200	500	950	0	1,028	0-40294.8	0-90
D29	1-10	5,000	1,150	500	850	2	953	0-42820.2	0-96
D30	1-10	5,000	1,150	700	950	0	1002	0-43162.2	0-95

The initial run conditions and physical parameters for the crust resemble those for the static models to facilitate comparison (Table 6.1). *n* = the number of basaltic sills intruded, *D* is the thickness of each individual sill, *a* is the thickness of granitoid formed after the first and tenth sill intruded, and the anatectic efficiency is shown for the first and tenth sills. See Table 6.1 for the other abbreviations.

6.8a). Subsequent sills then raise the crust from circa 780°C to its melting temperature of 850°C and generate melt with anatectic efficiencies approaching 1.3:1. Ten 100 m sills, therefore, produce up to 100% more melt than a single 1000 m sill given similar initial conditions (compare model D9 with S22 in Table 6.1). Decreasing the initial regional temperature of the crust decreases the amount of melt produced because each sill generates less melt, but melting still occurs under conditions that produce no melt under the static model (compare models D21 and D22 with S21 and S25 in Table 6.1). For the models without cooling (e.g. model D4 for 10 m sills), all sill thicknesses generate approximately four times the thickness of granitoid generated by equivalent static models (Figure 6.9b) under vapour-absent conditions, in part because of the low latent heat of fusion assumed for partially molten crust. Increasing the sill thickness increases the thickness of granitoid proportional to the static model results (Figure 6.9b), and so decreasing it also reduces the amount of melt; anatectic efficiencies range between 2.2:1 and 3.6:1 for the range of sill thicknesses considered. Excess vapour in the protoliths would increase these efficiencies by a maximum of 20%, as in the static model results presented in Table 6.1.

In summary, dynamic models simulating the repeated intrusion of basalt sills with the same thickness have higher anatectic efficiencies than static models run with equivalent initial conditions. Models run with a constant cooling interval generated 200% more melt than equivalent static models with equal thicknesses of basalt intruded. The amount of granitoid generated does depend on the ambient regional temperature of the crust, but repeated intrusion raises the crust temperature and increases the amount of melt with time. Melting occurs when the basalt sills are <100 m thick, intrude with suspended crystals at 1150°C, and where the crust initially resides at >350°C below its solidus. For the models without cooling, each individual sill generates four times more melt than all static models with similar basalt thicknesses, with anatectic efficiencies up to 3.6:1. In all dynamic models, the melting occurs less rapidly; Huppert and Sparks (1988a, c) estimate the life of a dynamic intrusion site at between 10^5-10^7 years to account for the slower cooling of basaltic sills in the hot crust.

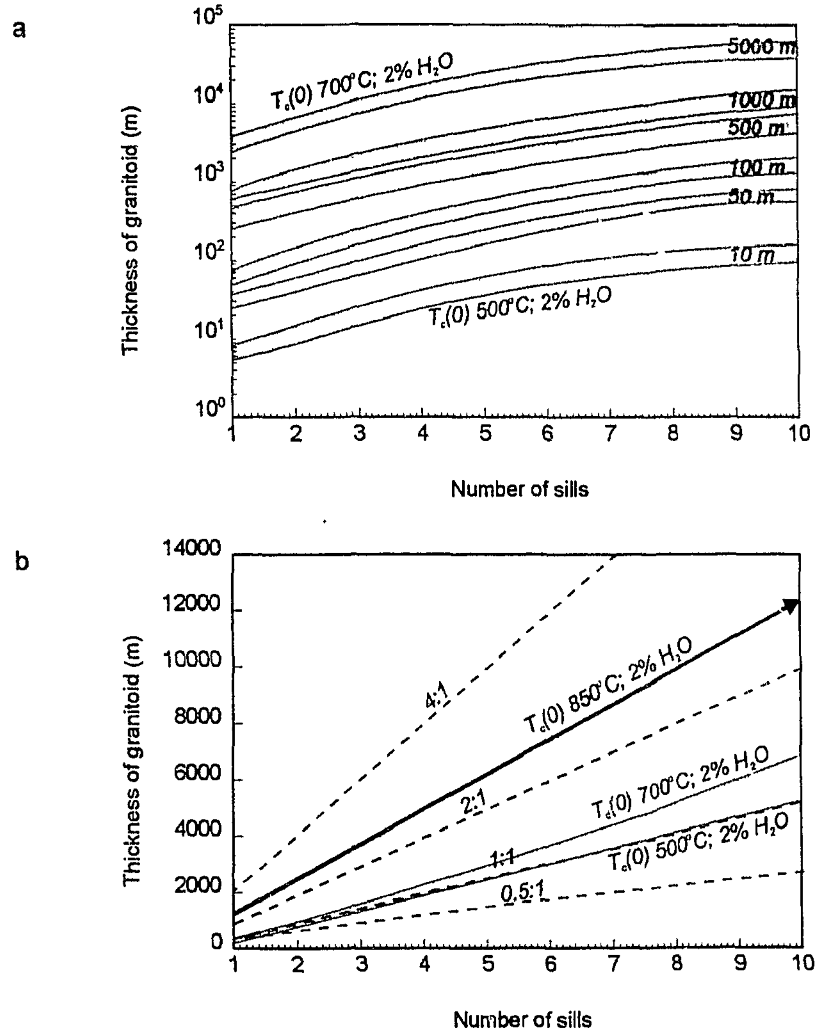

Figure 6.9. Variations of the granitoid melt layer thickness in the dynamic model. (a) Plot of granitoid thickness-number of basalt sills intruded for different basalt sill thicknesses emplaced into crust with different initial temperatures and volatile contents; (b) Plot of granitoid thickness-number of 500 m thick basaltic sills intruded, comparing the effects of crustal cooling between each intrusive event in the static model ($T_c(0)$ 500°C), constant cooling in the dynamic model ($T_c(0)$ 700°C), and no cooling in the dynamic model ($T_c(0)$ 850°C). Figure 6.7 indicates the significance of the ratios.

6-4. Late Devonian Heat Flow Modelling in the Meguma Zone

6-4.1. Parameters and Constraints

General application of the convective dynamic models to the study of mafic intraplating in the MZ recommends some parametal changes to reflect the rheology of the LDMIs and the thermal state of the lower crust during the Acadian Orogeny and also explore the sensitivity of the calculations to changes of the initial conditions. The LDMIs represent a series of variably evolved mafic-intermediate intrusions, which probably formed from hydrous parent magmas with potentially high liquidus temperatures up to 1250°C (Rock, 1990; Chapter 2, Section 5.1). Empirical data generally exist only for dry silicate liquids, but Lange and Carmichael (1987) determined the densities of analogous liquids with volatiles at 2.6-2.7 g cm^{-3}. Density determinations for the range of granitoid compositions in the Meguma crust lie between 2.63 and 2.73 g cm^{-3} (O'Reilly, 1975) and the average of 2.68 g cm^{-3} matches densities for the solid samples of Lange and Carmichael (1987); their melt densities for these samples range from 2.3-2.4 g cm^{-3}. Sass et al. (1984) determined thermal conductivities for granitoid compositions of 2.25 w m^{-1} K^{-1}, which is the value that appears in Appendix F-4. Parameters that lack empirical data remain those that appear in this appendix.

The MZ granitoids probably emanated from paragneisses in crystalline basement below the Meguma Group (Clarke et al., 1988), and gneissic lithologies that may represent this material crop out in the Liscomb Complex and as xenoliths in the Popes Harbour dyke (Clarke et al., 1993a; Owen et al., 1988; Sections 3.3 and 4 of Chapter 5). Sillimanite-grade Liscomb metapelitic rocks record rapidly changing P-T conditions that mostly do not exceed 760°C at pressures of 0.64-0.82 GPa. Popes Harbour metapelites record retrograde conditions of 600°C at 0.6 GPa; the sub-Meguma basement apparently resided at 600-760°C and circa 0.6-0.8 GPa (with 10-15% uncertainties) during the Acadian Orogeny. Densities for the gneisses are assumed to be greater than the lowest value that O'Reilly (1975) determined for the Halifax Formation (2.76 g cm^{-3}), probably within the range 2.80-2.89 with circa 2% volatiles present only in hydrous silicates (Clemens and Vielzeuf, 1987). Fusion temperatures for crustal lithologies decrease with increasing pressure, and under vapour-absent conditions at 0.8 GPa, kyanite-sillimanite metapelitic gneisses melt at 780-850°C, dependent upon modal mineralogy (Thompson and Tracy, 1979; Clemens and Wall, 1981; Vielzeuf and Holloway, 1988).

6-4.2. Mafic Heat Sources for the Meguma Zone Granitoids

Table 6.3 contains the results of dynamic models that have a constant cooling interval between LDMI sills at 1250°C emplaced into sub-Meguma basement with initial regional temperatures of 600-700°C (e.g. models MZ1 and MZ2 for 10 m sills), and have no cooling interval between sills emplaced into partially molten basement at 850°C (e.g. model MZ3 for 10 m sills). All of the model runs use values of ρ_b = 2.65 g cm^{-3}, ρ_g = 2.35 g cm^{-3}, and ρ_c = 2.89 g cm^{-3}. Increasing the density of the crust and granitoid melts by 0.29 and 0.05 g cm^{-3}, respectively, and decreasing the density of the mafic magmas by 0.05 g cm^{-3}, cumulatively increases the anatectic efficiency of the melting process by 3-4% in all models because the decreased kinematic viscosity and increased thermal conductivity of the basalt promote convective heating in the denser crust (compare models D2 and MZ2 for 10 m sills). Furthermore, the slightly higher liquidus temperatures for the basalt extend its cooling history and allow the attainment of higher interface temperatures up to 1042°C in sub-Meguma basement with a solidus at 850°C. If the basement solidus instead occurred at 780°C, then the decreased interval between the crusts regional and melting temperatures would increase the anatectic efficiency by 7% and change the composition of the granitoid melts produced.

Assuming that the basement thermometry reflects peak Acadian metamorphic conditions and that the lithologies analyzed represent the nature of the lower crust throughout southwestern Nova Scotia, LDMI magmas could melt the sub-Meguma basement metapelitic gneisses with anatectic efficiencies of 1:1 to 1.8:1 (average 1.3:1) in the models with cooling, and with anatectic efficiencies of 2.3:1 to 3.7:1 (average 3:1) under vapour-absent conditions in the

Table 6.3. Summary of initial conditions and results for Meguma Zone models calculated with HTFLOW31.

Model name	n	D (m)	$T_b(0)$ (°C)	$T_c(0)$ (°C)	T_m (°C)	% H_2O	T_l (°C)	a (m)	anatectic efficiency (%)
MZ1	1-10	10	1,250	600	850	2	913	6.3-123.3	63-130
MZ2	1-10	10	1,250	700	850	2	964	8.0-129.5	80-135
MZ3	1-10	10	1,250	850	850	2	1042	22.5-225.0	225
MZ4	1-10	50	1,250	600	850	2	913	31.4-614.6	63-130
MZ5	1-10	50	1,250	700	850	2	964	40.0-646.6	80-135
MZ6	1-10	50	1,250	850	850	2	1042	183.8-1838.0	368
MZ7	1-10	100	1,250	600	850	2	913	63.9-1231.2	63-130
MZ8	1-10	100	1,250	700	850	2	964	79.9-1677.4	80-178
MZ9	1-10	100	1,250	850	850	2	1042	343.0-3430.0	343
MZ10	1-10	500	1,250	600	850	2	913	382.8-6345.3	77-133
MZ11	1-10	500	1,250	700	850	2	964	489.9-7194.0	98-149
MZ12	1-10	500	1,250	850	850	2	1042	1279.4-12794.0	256
MZ13	1-10	1,000	1,250	600	850	2	913	711.1-11293.3	71-118
MZ14	1-10	1,000	1,250	700	850	2	964	902.5-12749.2	90-132
MZ15	1-10	1,000	1,250	850	850	2	1042	2404.0-24040.0	240
MZ16	1-10	1,000	1,250	700	950	0	964	0-9621	0-107
MZ17	1-10	5,000	1,250	600	850	2	913	3242.7-49111.2	65-102
MZ18	1-10	5,000	1,250	700	850	2	964	4126.3-55843.0	83-115
MZ19	1-10	5,000	1,250	850	850	2	1042	11228.9-112289.0	225
MZ20	1-10	5,000	1,250	700	950	0	964	0-50806.8	0-113

The initial run conditions and physical parameters for the crust resemble those for the static models to facilitate comparison (Table 6.1). *n* = the number of basaltic sills intruded, *D* is the thickness of each individual sill, *a* is the thickness of granitoid formed after the first and tenth sill intruded, and the anatectic efficiency is shown for the first and tenth sills. See Table 6.1 for the other abbreviations.

dynamic model without cooling. High liquidus temperatures and low melt densities implemented for the LDMIs represent maxima designed to indicate the greatest possible thermal effects of intruded sills, and, therefore, the amount of crystallized mafic magma present at depth beneath the MZ must be 30-77% of any volume calculated for exposed granitoids if intraplating is an important anatectic process. Appendix F-5 contains details of the volume estimates for onshore granitoids, which suggest a minimum value of order 10^5 km^3 $\pm$30% for the SMB, 2×10^4 km^3 for all of the peripheral and central plutons (see Figure 5.1 in Chapter 5), and approximately 3×10^3 km^3 for the BPP. Despite the slightly increased anatectic efficiencies of dynamic convective models applied to the MZ, these results do not differ significantly from those of Hodge (1974), Younker and Vogel (1976), and Bergantz (1989), which require the presence of large volumes of basalt in the lower crust if intraplating generated granitoid melt on the regonial scale.

On the basis of the assumptions and results of the dynamic models, two main end-member scenarios illustrate the potential effects of intruded mafic magmas, which may be complementary in nature: (1) mafic sills intruded pervasively in low concentrations throughout the sub-Meguma basement would effectively heat the crust to temperatures >900°C and generate relatively small amounts of granitoid melt, as in the dynamic models with cooling; and (2) repeated intrusion of mafic sills into contiguous regions of the crust could generate the much larger quantities of melt necessary to form the discrete granitoid intrusions typical of the MZ; dynamic models without cooling mimic this situation. Using the dynamic model results, the sub-Meguma basement lithologies must contain at least 3×10^4 km^3 of basalt to account for the SMB, circa 6×10^3 km^3 to form the collective volume of the peripheral and central plutons, and circa 9×10^2 km^3 to account for the BPP or other isolated granitoid plutons. Simple regional gravity calculations (shown below) estimate the anomalies produced by intrusion sites capable of producing the BPP and SMB (Figure 6.10a) and attempt to provide constraints for the large volumes of basaltic magma required.

Given 35 km thick crust (Marillier et al., 1989), the sub-Meguma basement (ρ = 2.8-2.9 g

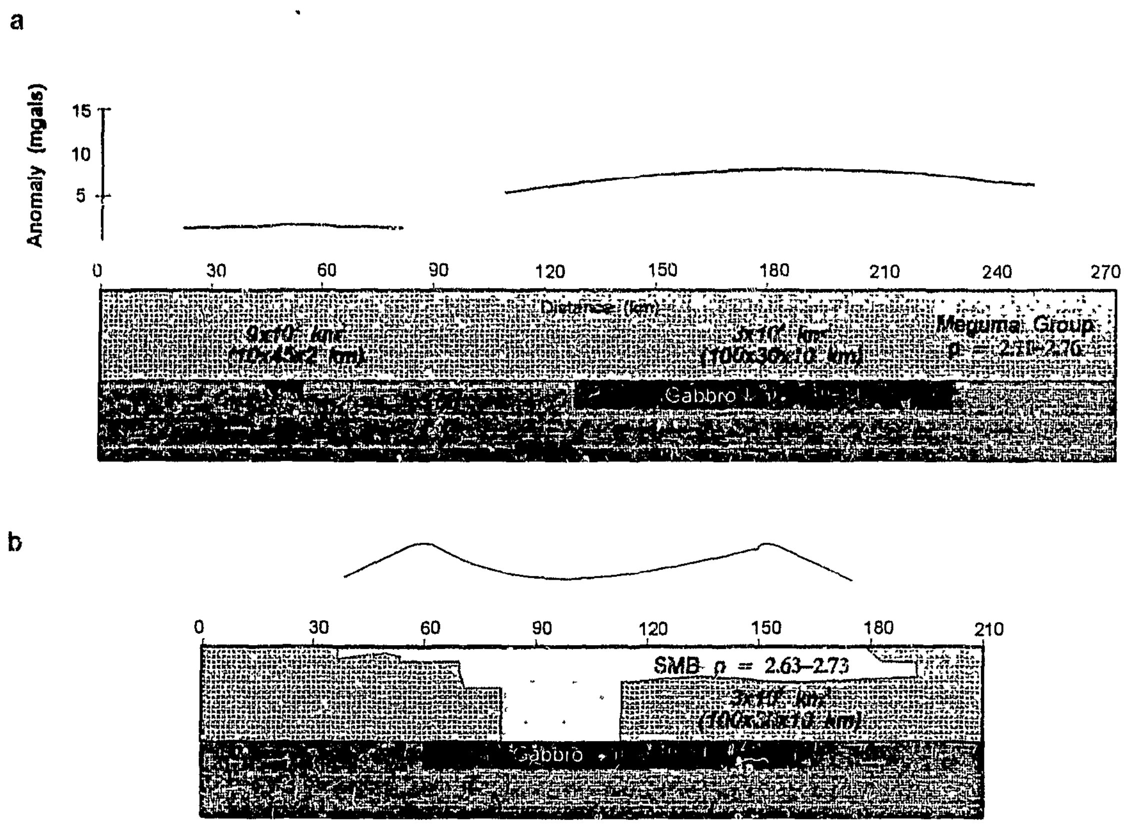

Figure 6.10. Regional gravity models for basalt intrusion sites capable of generating the Barrington Passage Pluton and the South Mountain Batholith (SMB). (a) Predicted anomalies for mafic intrusion sites emplaced below Meguma Group lithologies; (b) Predicted anomaly for a mafic intrusion site emplaced below the SMB. Gravity anomalies were calculated using the MAGRAV 2.5-dimensional computer program (Broom, 1986) assuming that mafic intrusion sites have strike lengths of 30-45 km in the third dimension and hypothetically intrude the uppermost levels of the sub-Meguma basement to maximize the anomalies produced. Vertical exaggeration 150%; densities for the Meguma Group and the SMB are from O'Reilly (1975).

cm^{-3}; mean = 2.85 g cm^{-3}) occupies its lowermost 15 km (Owen et al., 1988; Keen et al., 1991), the Meguma Group (ρ = 2.71-2.76 g cm^{-3}; mean = 2.73 g cm^{-3}) overlies it, and most of the SMB (ρ = 2.63-2.73 g cm^{-3}; mean = 2.68 g cm^{-3}) extends to a maximum depth of 18 km (Douma, 1978). Basaltic sills (ρ =3.0-3.1 g cm^{-3}) occupying 10^2-10^4 km^3, account for regions 10-100 km long and produce broad gravitational perturbations of between 2 and 10 mgals over areas of approximately 60 to >150 km at the surface. To satisfy the MIM, the anomaly produced by a 10^4 km^3 intrusion site emplaced below the SMB is shown in Figure 6.10b to be indistinguishable from the large (circa 60 mgal) negative anomaly associated with the batholith (see also Figure F3.1 in Appendix F), except, perhaps, for the marginal positive anomalies caused by the broader gravitational effects of the more deeply intruded mafic intrusions. Such features do not occur in the MZ and so all mafic sills intruding below granitoid bodies would be gravitationally undetectable in the sub-Meguma basement. Individual sills smaller than 5 km thick and distributed throughout the MZ crust would also not contribute appreciably to the regional gravity field, especially if they intruded at greater depths below the Meguma Group-basement boundary.

Regional gravity data, therefore, cannot constrain these results, but reasonable application of the intrusive scenarios to the MZ recommends that pervasively intruded sills would efficiently heat the overlying sub-Meguma basement and aid the formation of anatectic melts produced by thermal relaxation approximately 30 Ma after the superposition of Meguma Group lithologies. Unexplained southerly-dipping high-amplitude reflectors identified in the lower crust of the Meguma and Avalon Zones (Keen et al., 1991) may be sill-like mafic intrusions that provide independent support for this hypothesis. No seismic profiles across the MZ intersect granitoid intrusions and so seismic data cannot recommend or rule out the use of focused intrusion sites capable of generating observed plutons or batholiths. Instead, at least three factors must be recognized.

(1) *Volume considerations.* The large volume of intraplated mafic material required to produce the SMB may be difficult to accommodate in the crust without commensurate tectonic

compensation by uplift. Epizonal crustal levels now exposed in the MZ suggest that erosion and/or uplift removed 10-14 km of the upper crust. Although the component attributable to uplift alone is unknown and 14 km represents a maximum, this value must encompass the response of the crust to both tectonic and magmatic processes (Gupta and Sutcliffe, 1990). The existence of mafic sills occupying 10^4 km^3 in a region 10 km thick below the SMB (Figure 6.10) is unlikely unless ascending granitoid melts at least partly create room. Mafic sills occupying 900 km^3 in a region 2 km thick below the BPP do not create such major problems with the accommodation of mafic magmas.

(2) *Melt extraction efficiencies.* The models require that all anatectic melt leaves the source and rises to the 10-14 km crustal depths now exposed in the MZ (Douma, 1988; Ham, 1988). Clemens and Vielzeuf (1987) allow nearly 100% extraction for melts with 2% volatiles at superheated temperatures >950°C, but more conservative estimates of melt extraction efficiencies by Bergantz (1989) suggest that only 40-60% of any melt generated leaves its source at pressures >0.5 GPa, especially without high concentrations of volatiles. Circa 50% melt extraction clearly doubles the quantity of mafic magma required and exacerbates potential problems with the accommodation of this material in the crust, especially for the generation of the SMB.

(3) *Magma emplacement style.* Current models assume that all LDMI magma forms sills that melt the crust. Although the supposed layered nature of the lower crust favours the formation of sill-like intrusions (Huppert and Sparks, 1988a), natural situations should involve significant quantities of magma emplaced as dykes that supply the sills and may heat the crust, but do not trigger voluminous melting (Huppert and Sparks, 1988a). Furthemore, the models assume that all LDMI magma intrudes the crust. Underplated mafic magmas could heat the lowermost crust and generate granitoid melt without creating room problems (Hogan and Sinha, 1989; Pin et al., 1990; Gray and Cull, 1992).

Most of these factors significantly reduce the efficiency of melting by mafic intraplating and are difficult to quantify with geological constraints. However, increasing the volatile content of the crust to the unlikely value of 6% would not increase anatectic efficiency by the required 200% to compensate for problems with melt extraction (Table 6.1), and lowering of the latent heat of fusion of the sub-Meguma basement below 45 cal g^{-1} may not realistically mimic natural situations; the calculations are not particularly sensitive to changes of the other parameters that rely on empirical measurements. Consequently, any use of repetitively emplaced mafic magmas in focused intrusion sites must minimize the potential effects of these factors and this study favours the use of mafic magma heat to produce peripheral and, perhaps also, central plutons, particularly the early-intruded CP and BPP. The results do not currently suggest a major role for intruded mafic material in protoliths for the extensive SMB, although widely distributed sills could be a partial thermal influence and/or smaller focused intrusion sites could form some of its 13 constituent plutons. Underplated mafic magmas may also have a plausible thermal role in the petrogenesis of this large granitoid intrusion. Section 3 in Chapter 7 considers these ideas further, in conjunction with the nature and distribution of observed spatial mafic-granitoid field relationships.

6-5. Conclusions

Widely distributed LDMI magmas emplaced as sills with liquidus temperatures at 1250°C into metapelitic sub-Meguma basement gneisses at 600-850°C under vapour-absent conditions would cause rapid heating on a regional scale, but would only generate small amounts of granitoid melt equivalent to circa 130% of the mafic magmas volume. Repeatedly intruded LDMI magmas forming focused intrusion sites would require the presence of basaltic sills that account for 30% of any volume calculated for exposed granitoid intrusions; the BPP would require approximately 900 km^3 of basalt and the SMB would require circa 10^4 km^3 of basalt. Regional gravity data permit such high volumes of mantle-derived material if they occur below the granitoid bodies, as the MIM predicts. Assuming that the models accurately describe partial melting in response to intraplating, potential problems with the accommodation of voluminous mafic magmas, granitoid melt extraction efficiencies, and mafic magma emplacement style, recommend the use of important mafic magma heat in the sources of small granitoid plutons rather than the voluminous SMB.

Chapter 7

THE APPLICATION OF A "MAFIC INTRUSION MODEL" TO GRANITOID PETROGENESIS IN THE MEGUMA ZONE

7-1. Introduction

The "mafic intrusion model" (MIM) proposes that in granitoid terrains containing temporally and spatially related mafic and granitoid intrusions, the mafic end-members represent a potential source of chemical components and, therefore, heat during the formation of crustal melts. In this thesis, evaluation of the MIM in the Meguma Zone (MZ) required a thorough investigation of all the currently recognized physical, geochronological, and geochemical evidence for contemporaneous mafic-felsic magmatism; one-dimensional thermal models of mafic intraplating into the sub-Meguma basement also applied some constraints. This chapter evaluates the nature and distribution of exposed mafic-granitoid field relationships and establishes the evidence for a chemical and thermal genetic relationship between the Late Devonian mafic intrusions (LDMIs) and the peraluminous granitoids. The results are applied to models of granitoid petrogenesis in the MZ, with suggestions for other potential sources of heat and a summary of the assumptions and limitations inherent to the MIM.

7-2. Evaluation of the Late Devonian Mafic-Granitoid Relationships

The MZ contains all of the required evidence to support a genetic relationship between the LDMIs and the peraluminous granitoids except enclaves. $^{40}Ar/^{39}Ar$ age ranges and a U-Pb date for the LDMIs overlap with U-Pb intrusion ages for the South Mountain Batholith and the Canso plutons (the only granitoid bodies with reliable intrusion ages), suggesting that mantle-derived mafic magmas coexisted in the crust with peraluminous granitoid melts (Chapter 2, Section 3.4). Although the interpretation of argon geochronological data for the LDMIs is problematic given the evidence for slow regional cooling after Acadian metamorphism and/or partial Alleghanian tectonothermal resetting, the occurrence of synplutonic mafic bodies in the Barrington Passage, Shelburne, and Port Mouton plutons provides physical evidence that supports this temporal relationship. Mingling, commingling, and mixing also occurred locally at the synplutonic intrusion sites (Chapter 3, Section 4), and the peripheral plutons probably represent homogenized hybrids on the pluton scale (Chapter 5, Section 4). The LDMIs do, therefore, represent plausible sources of chemical components in some granitoids, and the magnitude and distribution of mafic-felsic magmatic interaction has important implications for the use of LDMI magmas as heat sources.

Table 7.1 shows that synplutonic dykes and mafic igneous enclaves form the most abundant evidence for mantle involvement in well-documented peraluminous granitoids, and none of these intrusions shows all of the evidence for the MIM. Peraluminous granitoids generally contain less evidence for mafic-felsic interaction than alkaline or metaluminous granitoids, probably reflecting the much smaller chemical influence of the mantle on these bodies (Bussy, 1992; Pin et al., 1990). However, where synplutonic dykes and enclaves do crop out, they occur in large numbers that suggest a significant intrusive process (Foster and Hyndman, 1988; Larsen and Smith, 1990). The MZ granitoids show a wider variety of physical and chemical evidence than many peraluminous intrusions, but the localities with mafic bodies are sparse. Although the mafic end-members of bimodal suites may be substantially less abundant than contemporaneous granitoid lithologies (Wiebe, 1980), the LDMIs have only a 1000:1 volumetric ratio with the granitoids in the MZ (Clarke et al., 1993a), and only four small synplutonic intrusions occur. Three main factors (considered below) can adversely affect the abundance and nature of evidence required to support mafic-granitoid genetic relationships:

(1) *Amount of exposure.* Poor exposure (<2%) exists throughout the interior of southwestern Nova Scotia (Chapter 2, Section 2.9). Given that currently recognized LDMIs have small areal extents (mostly <100 m^2), their restriction to well-exposed coastal localities or inland quarries

Table 7.1. Comparison of criteria required for the "Mafic Intrusion Model" between the Meguma Zone and other Phanerozoic bimodal magmatic centres containing peraluminous granitoids.

Intrusive suite	Location	Age	Maf	Syn	Hyb	Enc	Che
Wilson Ridge Pluton	USA	Tertiary	Y	N	N	Y	N
Adamello Massif	Italy	Tertiary	N	Y	Y	Y	Y
Monte Caponne	Italy	Tertiary	N	N	N	Y	N
Idaho-Bitteroot Batholith	USA	Cretaceous	N	Y	N	Y	N
Smartville Complex	USA	Jurassic	Y	Y	N	Y	N
Velay granite	France	Carboniferous	N	N	N	Y	N
Meguma Zone	Canada	Late Devonian	Y	Y	Y	N	Y
Older granites	Scotland	Late Silurian	Y	N	N	Y	Y
Pleasant Bay Intrusion	USA	Late Silurian	Y	Y	Y	N	Y

These observations assume that exposure and the level of erosion do not significantly affect the evidence described. Maf = contemporaneous satellite mafic intrusions; Syn = synplutonic mafic intrusions with or without pillowed contacts; Hyb = localized hybrid granitoid lithologies, commingled pillows, or composite dykes, Enc = mafic igneous or hybrid granitoid enclaves, Che = regional low Sr, Nd, or O isotope ratios. See Table 1-1 in Chapter 1 for the sources of this summarized information.

may be a function of the lack of outcrop. With this premise, low abundances of LDMIs do not necessarily argue against the MIM as a viable petrogenetic process.

(2) *Level of crustal exhumation.* Hyndman and Foster (1988) suggested that the granitoid bodies trap most mafic incursions at the lower levels of granitoid intrusions, and Wiebe (1993) documented this tendency in the Coastal Maine Magmatic Province, which may be the type area for studying mafic-granitoid genetic relationships (Hogan and Sinha, 1989). Supposed roof pendants do occur in the Barrington Passage Pluton (BPP) and Shelburne Pluton (SP), and in the South Mountain Batholith (SMB) and Halfway Cove-Queensport Pluton (Rogers, 1984; Horne et al., 1988; Ham, 1988; Chapter 4, Sections 4.1 and 4.2). Furthermore, MacDonald (1981) interpreted the abundance of granitoid dykes, magmatic foliations, and Meguma Group xenoliths in the Musquodoboit Batholith (MB) as indicators of shallow exhumation. If the apparent rarity of LDMIs in the MZ reflects shallow exhumation of the uppermost levels in granitoid intrusions, their small sizes may reflect the inability of voluminous mafic magmas to ascend through partially molten lower crust and reach the epizone.

(3) *Timing of mafic magma emplacement.* Mafic intrusions in bimodal complexes commonly bracket the granitoids in both space and time (Rock, 1990) and so ages for some mafic intrusions may be slightly older or younger than spatially contemporaneous granitoids. Synplutonic mafic intrusions into convecting granitoid bodies should be disrupted and disaggregated to form mafic igneous enclaves (Blundy and Sparks, 1992). Their preservation as coherent intrusions in the MZ implies that magma emplacement occurred after the cessation of strong convection in the granitoid surrounding the synplutonic intrusion site (Furman and Spera, 1985; Eberz and Nicholls, 1988; Foster and Hyndman, 1988). The Forbes Point synplutonic dyke apparently intruded partially solidified tonalite in the Port Mouton Pluton (Chapter 3, Section 4), and disruption of the Mcleods Cove sheet by the subsequent intrusion of granitoid and pegmatite dykes occurred over only 15 m at the current exposure level (Figure 3.7 in Chapter 3). This late

emplacement, therefore, possibly explains the absence of mafic igneous or hybridized enclaves at epizonal exhumation depths.

The absolute effects of poor exposure, shallow exhumation, and the timing of interaction are difficult to establish unequivocally. This study recognizes the potential relevance of such factors and suggests only that currently exposed temporal and spatial relationships between mafic and granitoid intrusions suggest a genetic role the LDMI magmas as suppliers of heat if much more voluminous mafic magmas also intruded the sub-Meguma basement at depth. The occurrence of high TiO_2, FeOT, CaO, Cr, and V in conjunction with $^{87}Sr/^{86}Sr_i$ values of 0.704-0.710, $\delta^{18}O$ <10.4, εNd >-0.1 and $\delta^{34}S$ <5.0 (Chapter 5, Section 4) in the peripheral plutons (see Figure 5.1 in Chapter 5), suggest that mafic-granitoid interaction occurred at depth in the sub-Meguma basement source or during the ascent of granitoid melts. The four small synplutonic mafic bodies exposed in these plutons are unlikely to entirely account for their geochemical characteristics; hybridism at Birchtown occurs only within circa 30 m of the synplutonic diorite intrusion (Figure 3.15 in Chapter 3). Peripheral plutons exposed at the extreme northeastern and southwestern onshore areas of the MZ, therefore, also contain the strongest indications of thermal influence by intruded mafic magmas.

One-dimensional heat flow models suggest that circa 10^3 km^3 of LDMI magmas emplaced as sills could form sufficient granitoid to account for the small peripheral granitoid plutons (Chapter 6, Section 4.2), and these mafic intrusion sites would not be detected if they were emplaced below the granitoid bodies. Elias (1986) and Longstaffe et al. (1980) suggested that amphibolite metamorphic grades in these areas reflect exposures of deeper crustal levels (see Figure 1.3 in Chapter 1), which could explain the preferential abundance of synplutonic mafic intrusions. Given that low topographic relief occurs throughout the MZ, however, this hypothesis requires that tectonic tilting or faulting uplifted southwestern and northeastern portions of the Meguma crust. No currently identified fault system separates the central intrusions and peripheral plutons, and the facies-series metamorphic grades (see Figure 1.3 in

Chapter 1) exposed in northeasterly areas of the MZ reflect locally elevated temperatures with no evidence for higher pressures (Raeside et al., 1988). The amphibolite metamorphic culminations that mostly correspond to these areas may instead represent the product of heating by either mafic magmas or ascending hot granitoid melts generated above mafic sills (Hanson and Barton, 1989; Chapter 6, Section 4.2).

In addition to peripheral regions, however, satellite mafic bodies do occur in the Liscomb Complex and the Weekend dykes may be spatially restricted to the peripheries of the MB (see Figure 2.18 in Chapter 2). Although intraplated LDMI magmas could not independently generate the voluminous SMB (Chapter 6, Section 4.3), some support does exist for mafic heat influence throughout the sub-Meguma basement, and the small central plutons may at least partly represent the products of heating above mafic sills. The lack of hybrid geochemical signatures and synplutonic mafic bodies in these intrusions does not entirely argue against this hypothesis because the Sr-Nd isotopic effects of Meguma Group contamination do counteract those of mafic-granitoid magma mixing (see Figure 5.11 in Chapter 5; Clarke et al., 1988) and the potential for isotopic heterogeneity in the sub-Meguma basement could also mask hybridized granitoid compositions (Chapter 5, Section 3.3; Ayuso, 1986; Todd and Shaw, 1985). If mixed lithologies do not occur at depth in these bodies, then perhaps mafic sills dispersed throughout the sub-Meguma basement heated sources for the central intrusions without forming abundant granitoid melts (Chapter 6, Section 4.3) or underplated LDMI magmas melted the lower crust without forming hybrids or affecting metamorphic conditions at shallower crustal levels (De Yoreo et al., 1989; Hogan and Sinha, 1989; Pin et al., 1990).

7-3. Application of the "Mafic Intrusion Model" to the Meguma Zone

This study advocates that the observed mafic-granitoid genetic relationships in the peripheral plutons reflect the chemical and strongest thermal contributions from LDMI magmas in peripheral onshore areas of the MZ, and that intraplating may be a necessary thermal supplement for the generation of central intrusions, especially considering the large size of the SMB. These inferences warrant a modified petrogenetic model for the generation of granitoids in the MZ, which recognizes the petrogenetic history of the LDMIs, the granitoids, and the established tectonic history of the MZ. In this model, the Theic Ocean separated the MZ and Avalon terrane (Piqué and Skehan, 1992), and subduction metasomatized and partially melted the subcontinental mantle below the MZ (Chapter 2, Section 6). At circa 410 Ma, obduction of the Meguma Group onto Avalonian basement occurred along the Cobequid-Chedabucto Fault (Dallmeyer and Keppie, 1986; Keppie and Dallmeyer, 1987; Eberz et al., 1991). Moderate Acadian crustal thickening by folding and thrusting (N. Culshaw, pers. comm., 1993) accompanied greenschist metamorphism in the Meguma Group (Raeside et al., 1988), and presumably generated higher temperatures in the sub-Meguma basement until at least 380 Ma.

Dispersed mafic magmas emplaced as sills beneath southwesterly and northeasterly onshore regions probably augmented thermal relaxation heat and focused intrusion sites probably formed hybridized partial melts parental to the BPP and Canso pluton (CP) tonalites between 385 and 378 Ma, only circa 30 Ma after the onset of Acadian crustal thickening (Figure 7.1a). Between 375 and 370 Ma, Alleghanian strike-slip reactivation of the Cobequid-Chedabucto fault formed extensional fractures during dextral terrane rotation (O'Brien, 1983) and uplift of the thickened Meguma crust (Figure 7.1b). Further incursions of mafic magma presumably intruded these crustal weaknesses and evolved in a series of crustal magma chambers throughout the crust of southwestern Nova Scotia (Chapter 2, Section 2.7 and Section 5.1). In peripheral regions of the terrane, mafic magmas continually formed hybridized melts for the SP at circa 376 Ma, the Port Mouton Pluton, and the CP until 372 Ma; rapid emplacement of the voluminous SMB at circa 372 Ma, and the intrusion of other small central intrusions at this time may reflect a combination of crustal melting by uplift of the hot sub-Meguma basement aided by heat emanating from widely distributed intruded sills and/or underplated LDMI magmas. Continued uplift into the Carboniferous then exposed the shallowest vestiges of bimodal intrusive

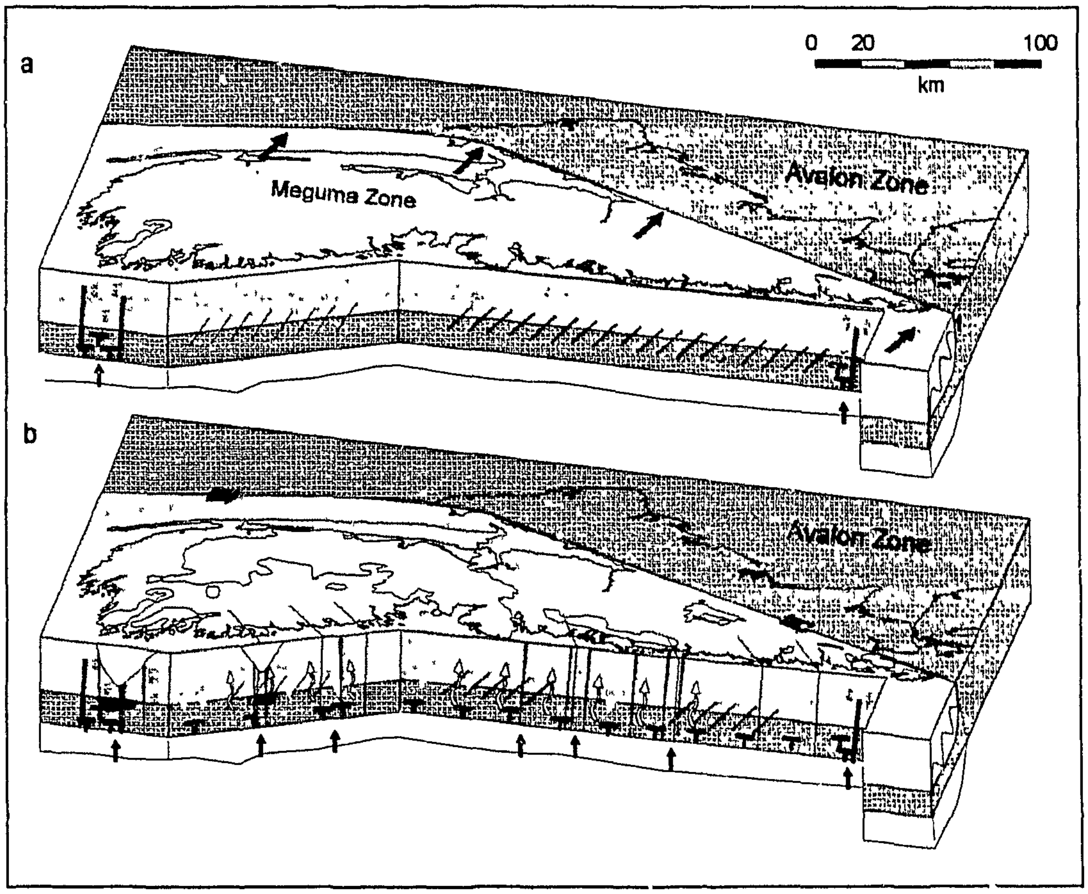

Figure 7.1. Orthographic three-dimensional projection summarizing the application of a "mafic intrusion model" to the Meguma Zone. (a) The state of the Meguma crust between approximately 410 and 385 Ma; (b) Events in the Meguma crust between approximately 385 Ma and 370 Ma. Diagonal rulings indicate thermal relaxation heating, white arrows show the ascent of granitoid melts, and black arrows mark the intrusion of mafic magmas. Thin vertical lines mark faults and thicker vertical lines mark faults containing dykes. The Meguma Group is shown in light grey, the sub-Meguma basement is shown in dark grey, and white represents granitoid melt. The unshaded region below the crust represents the source for LDMI magmas. See the text for a discussion. Horizontal and vertical scales, and the location of the Cobequid-Chedabucto Fault at the Meguma-basement boundary, are approximate only; no vertical exaggeration.

magmatism to erosion by approximately 365 Ma (Mawer and Williams, 1986; Muecke et al., 1988).

7-4. Other Sources of Localized Heat

Future interpretations of granitoid petrogenesis in the MZ must test this model by constraining the Acadian thrusting history, determining the degree and timing of crustal thickening associated with folding and thrusting in the Meguma Group, and calculating the volumes of granitoid that orogenic crustal thickening generates from the sub-Meguma basement in <40 Ma. A valid description of crustal melting for the MZ granitoids must include thermal input from the LDMIs in at least the peripheral plutons, but mafic magma heat influence in the central intrusions would also help to compensate for any discrepancies in the volumes of infracrustal granitoid melt generated. In many orogens, granitoid melts may be the products of various tectonic processes in combination with mafic magmatism, as Gray and Cull (1992) proposed for the Lachlan Fold Belt of southeastern Australia. With this premise, the following factors also require consideration:

(1) although granitoids in the MZ do not show spatial relationships with the exposed trace of the Cobequid-Chedabucto Fault (Hill, 1991), the lateral ramp morphology assumed for this structure (Clarke et al., 1993a) suggests that it underlies all granitoid bodies at the interface between the Meguma Group basement (Figure 7.1) and may be a source of frictional heat (Molnar et al., 1983; Gray and Cull, 1992);

(2) fluid influx and ultrametamorphism hypotheses are difficult to evaluate for granitoids that do not intrude their source rocks at the current level of exposure, but the MZ granitoids do not show spatial relationships to specific structural horizons in the Meguma Group and no exposed evidence exists to support the thermal focusing hypothesis;

(3) average concentrations of heat-producing elements in the granitoids (K_2O 4.43 wt.%, U 4.0 ppm, Th 12.9 ppm; n = 833), and in the sub-Meguma basement (K_2O 2.65 wt.%, U 4.2 ppm Th 9.2 ppm; n = 16), which were calculated using the data in Appendix E-1 and Eberz et al. (1991), do not reflect anomalously radioactive crust (Zen, 1992); and

(4) the potential thermal effects of a subduction-related tectonic regime prior to and during the obduction of the Meguma Group onto the Avalon terrane (Chapter 2, Section 6) include delamination of the subcontinental lithosphere (Pin et al., 1990), roll-back of subducted ocean lithosphere (Sandiford et al., 1992), and/or other resultant thermal anomalies in the mantle (Pitcher, 1979). Such factors may be responsible for controlling lithospheric heat flow, the styles and timing of tectonic processes, and the liberation of mafic magmas (e.g. Gray and Cull, 1992; C. Beaumont, pers. comm., 1994); perhaps they contributed to the generation of both mafic and granitoid magmas in the MZ.

7-5. Assumptions and Limitations of the "Mafic Intrusion Model"

The MIM recognizes upper crustal evidence for mechanical and/or chemical interaction between contemporaneous mafic and granitoid intrusions, and assumes that the intruded mafic magmas represent at least a partial thermal influence at depth in the protoliths for these granitoids. In the MZ, satellite and synplutonic mafic intrusions (supported to some extent by geochronology) demonstrate the contemporaneity of mafic and granitoid intrusive magmatism. Given that poor exposure and epizonal exhumation probably affect the abundance of mafic intrusions, only the existence of putative hybrid granitoid compositions in the peripheral plutons demand widespread mafic-granitoid magmatic hybridization at depth in the crust of the Meguma Zone. If this interaction occurred in the sub-Meguma basement source, then the mafic end-members represent a permissible thermal influence during the generation of peripheral pluton partial melts. It is, however, possible that mafic magmas coincidentally encountered pre-existing granitoid magmas (perhaps during their ascent through the crust) and do not represent a significant source of anatectic heat. Only the amphibolite-grade metamorphic culminations in peripheral areas of the MZ can independently support the production of superheated partial melts above mafic sills (Chapter 7, Section 2).

In addition to problems with exposure and exhumation, at least three limiting factors influence interpretations of mafic-granitoid temporal and spatial relationships as indicators of thermal processes: (1) thermal transfer above mafic sills could conceivably occur without exchange of mass or chemical components. For example in the MZ, the central intrusions may contain no synplutonic mafic intrusions, mafic igneous enclaves, or hybridized granitoid lithologies because hot partial melts ascended rapidly from mafic intrusions in their protoliths; (2) the distribution of mafic intrusions in the upper crust may reflect tectonic controls on magma ascent rather than the distribution of intrusive processes operating at depth. Currently exposed LDMI magmas did not directly participate in anatexis unless they emanated at some stage from sills emplaced into the sub-Meguma basement, and the availability of late-Acadian crustal weaknesses potentially controlled the occurrence of currently exposed bodies; and (3) field-based temporal and spatial relationships primarily bias mafic intraplating relative to underplating. Central intrusions may represent the products of widespread crustal melting above underplated mafic magmas where few opportunities for hybridization exist, whereas hybridized peripheral intrusions may result from localized partial melting above intruded mafic bodies.

Future applications of the MIM to bimodal intrusive suites emplaced into crust exposed at exhumation depths approaching those of granitoid melt generation may overcome some of these limitations and constrain the importance of mafic magma heat sources more precisely than this study. Quantitative modelling of mafic underplating, in conjunction with infracrustal sources of heat, is essential to reliably suggest the importance of both underplated and intraplated mafic magma as either a localized thermal influence in regions with otherwise heated crust, or as an independent cause of widespread partial melting.

Chapter 8

CONCLUSIONS AND RECOMMENDATIONS

8-1. Conclusions

(1) The Meguma Zone contains 14 volumetrically minor mafic intrusions that intruded as dykes, sheets, and plugs with Late Devonian ages (circa 380-370 Ma $^{40}Ar/^{39}Ar$; 376 Ma U-Pb). Mafic magmas probably intruded contemporaneously with the peraluminous granitoids (385-372 Ma).

(2) Late Devonian mafic magmas probably evolved from similar parental compositions by the fractionation and/or accumulation of ferromagnesian modal phases, with some evidence for Meguma Group contamination in the Liscomb Complex gabbro-diorites. Their calc-alkaline compositions potentially indicate subduction prior to terrane collision of the Acadian Orogeny.

(3) Four of the Late Devonian mafic intrusions are synplutonic into the Barrington Passage, Shelburne, and Port Mouton plutons. These mafic bodies confirm the spatial and temporal intimacy of mafic and peraluminous granitoids in the crust of the Meguma Zone.

(4) The three well-exposed synplutonic intrusion sites in the Port Mouton and Shelburne plutons probably record the progressive thermal and chemical effects of localized interaction between mafic magmas and granitoid melts by early exchange of volatiles, alkalies, and mobile trace elements (Rb, Ba, Sr), diffusion of Ti, P, and LILE, and by the transfer of at least Ca, Ti, Fe, and V in ferromagnesian and calcic plagioclase phenocrysts.

(5) The Barrington Passage and Shelburne plutons contain abundant Meguma Group xenoliths and surmicaceous melanosomes that probably formed by partial melting of the xenoliths. The Port Mouton Pluton and South Mountain Batholith also contain coarse-grained granitoid autoliths and quenched microgranitoid enclaves. None of the studied intrusions contains mafic igneous

enclaves with microtextures or modal mineralogies resembling the Late Devonian mafic intrusions or the known hybrids.

(6) Subtly different geochemical characteristics subdivide peraluminous granitoid intrusions into peripheral pluton and central intrusion suites. Peripheral plutons at the northeastern and southwestern onshore extents of the Meguma Zone contain high values for Ti, Ca, Fe, Cr, V, and εNd coupled with low values for $^{87}Sr/^{86}Sr_i$, $\delta^{18}O$, and $\delta^{34}S$, which probably reflect mantle chemical input not evident in central intrusions.

(7) One-dimensional heat transfer resulting from repeated intrusion of hydrous mafic magmas into the sub-Meguma basement suggest that dispersed Late Devonian mafic intrusions could heat the lower crust throughout southwestern Nova Scotia and aid the generation of melts by tectonic thickening of the Meguma Group. Focused intrusion sites containing high concentrations of mafic sills could plausibly generate discrete peripheral and central plutons, although they could not plausibly generate the voluminous South Mountain Batholith indepe ,dently.

(8) The proposed "mafic intrusion model" requires that mafic magmas emplaced into the sub-Meguma basement contributed heat and chemical components during the formation of the peripheral plutons between 385-372 Ma. Mafic magmas potentially also heated the crust below centrally located onshore areas of southwestern Nova Scotia at circa 376-372 Ma, perhaps in conjunction with thermal relaxation heat and local thermal effects attributable to a variety of other tectonic processes.

8-2. Recommendations for Further Work

Further studies of mafic-granitoid genetic relationships in the entire Meguma Zone require new outcrops for the recognition of additional mafic intrusions and hybrid lithologies based on the results of this study. However, the present work uncovered six specific problems relating to Late Devonian mafic and granitoid magma petrogenesis. The following recommendations (in no particular order of importance) lay beyond the scope of this regional petrogenetic study.

(1) *Identification and petrogenesis of new Late Devonian mafic intrusions.* Currently exposed post-Acadian mafic intrusions crop out only in the Meguma Zone, but no logical restriction precludes their existence in the adjacent Avalon terrane of Cape Breton Island, Nova Scotia, and New Brunswick. The discovery and study of small mafic intrusions, with 385-370 Ma ages, hydrous modal mineral assemblages, and calc-alkaline-shoshonitic geochemical characteristics, may expand the current knowledge of their petrogenesis and provide evidence supporting pre-Acadian subduction over a larger geographic area.

(2) *U-Pb dating of granitoid bodies and the Late Devonian mafic intrusions.* Slow regional cooling after the Acadian Orogeny and/or Alleghanian tectonothermal resetting require that future dating studies of the mafic intrusions rely on U-Pb isotopic systematics in zircon. High-precision analyses for the Attwoods Brook gabbronorite, the Mersey Point picrite, Liscomb Complex gabbro-diorites, and at least one Weekend dyke will constrain the emplacement of these rocks to either one intrusive event (circa 376 Ma) or a series of events between 385 and 370 Ma. Also, U-Pb dating of zircon and/or monazite from at least the Barrington Passage and Port Mouton plutons, the Musquodoboit Batholith, and the Liscomb Complex, will provide intrusion ages for all of the largest granitoid bodies in the Meguma Zone. Future studies of mafic-granitoid genetic relationships require these crucial data to precisely constrain the contemporaneity of mafic and felsic magmatism.

(3) *Processes of deuteric alteration in the Late Devonian mafic intrusions.* The hydrous nature of the parent mafic magmas produced deuteric alteration assemblages characterized by clinopyroxene-amphibole textural relationships, and amphiboles with complex internal structures, variable compositions and potentially different parageneses. The Attwoods Brook gabbronorite,

Birchtown diorite, Liscomb Complex gabbro-diorites, and the Weekend dykes typify this behaviour and represent candidates for detailed documentation of late-magmatic and hydrothermal processes.

(4) *Geochemical investigation of microgranitoid enclaves.* A comprehensive geochemical comparison of the microtonalite enclaves with both the peraluminous and metaluminous (hybridized) granitoid lithologies in the Meguma Zone will help to constrain them as quenched autoliths of primitive, but otherwise typical granitoid material, or (less likely) as hybridized granitoid lithologies. Such a study could profitably use the enclaves sampled for this study.

(5) *Geochemical study of the peripheral plutons.* Recent geochemical studies in the Meguma Zone concentrate on the voluminous South Mountain Batholith and other central plutons. Expansion of the major oxide, trace element, rare-earth element, and Sr-Nd-O-S isotopic database for the peripheral plutons would remove problems with missing data and increase the number of samples and variables necessary for a multiple discriminant function analysis including V, Cr, Y, and Ga. Also, mathematical modelling and/or statistical manipulation of these more comprehensive data may allow quantitative estimates for the degree of mantle input into the peripheral plutons.

(6) *Infracrustal heat flow models.* Quantification of a plausible thermal role for mafic intrusions emplaced into the sub-Meguma basement requires knowledge of the absolute need for an external heat source in the Meguma Zone during the Acadian Orogeny. Currently available one- and two-dimensional infracrustal models of crustal thickening by upper crustal thrusting will suggest the volumes of granitoid that thermal blanketing, erosion, and/or tectonic uplift can generate in the 30-40 Ma period that separates the onset of terrane accretion from granitoid intrusion, as more detailed interpretations of Meguma tectonics emerge.

Appendix A

ANALYTICAL AND QUANTITATIVE PROCEDURES

A-1. Microprobe Operating Conditions

Single mineral analyses were obtained from polished thin sections using the Dalhousie Link eXL system and JEOL 733 electron microprobe operating under EDS at 15 kV accelerating voltage, 15 nA probe current, 137 ev detector resolution, 12 μm beam diameter, and a counting time of 40 s (approximately 7600 counts per second). Calibration used geological standards, and data were reduced using the Oxford Link ZAF matrix correction program. Data recalculation and classification for pyroxenes (recalculated to 6 oxygens), olivine (recalculated to 4 oxygens), plagioclases (recalculated to 32 oxygens), and biotites (recalculated to 24 oxygens and 4 OH-groups) used the MINPET data processing program of Richard (unpublished). Amphibole recalculation and classification used the AMPHIBOL program of Richard and Clarke (1990) and assumed that average total cations equalled 13 (excluding Ca, Na, and K). Replicate spot analyses indicate that values for SiO_2, TiO_2, Al_2O_3, FeO, MgO, CaO, and alkalies are better than 2% and values for MnO are better than 5%.

A-2. Ground Magnetic Survey Methodology

Semi-quantitative ground magnetic surveys occurred at Attwoods Brook, Birchtown, Forbes Point, and Mersey Point to identify buried geological contacts between the Late Devonian mafic intrusions (LDMIs) and their country rocks, and to constrain their shapes and lateral extents for the production of detailed geological location maps (Appendix B-1). All surveys used the Dalhousie Scintrex MP2 proton precession magnetometer and the maps in Appendix B-1 show the survey lines where appropriate. At each locality, compass bearings aided the location of parallel survey lines across the mafic intrusions. Repeated measurements at a designated base station near the outcrops allowed for instrumental drift compensation.

A-3. $^{40}Ar/^{39}Ar$ Sample Preparation and Analytical Procedures

The author prepared and analyzed bulk mineral separates of amphibole and phlogopite at the Dalhousie argon laboratory. The Attwoods Brook (amphibole) sample comes from a coarse-grained gabbroic pegmatite vein, whereas the Birchtown (amphibole), Mersey Point (amphibole and phologopite), and Little Harbour (amphibole) samples came from representative material described in Sections 2.1, 2.2, 2.5, and 2.7 of Chapter 2, respectively. All samples were disaggregated as described in Appendix A-5 and crushed to <0.1 mm grain sizes in a tungsten carbide shatter box. After several washes in deionized water and alcohol to remove dust, mineral separation used a Frantz™ isodynamic separator operating at 15° side tilt and 25° forward slope to concentrate amphibole and biotite in the 0.4 and 0.5A magnetic fractions, respectively. The Mersey Point amphibole sample underwent a bromoform (ρ = 2.85) heavy liquid separation to eliminate olivine, and all samples passed over an improvized shaking table to remove adhering biotite grains (the Mersey Point phlogopite sample was collected at this time). The mineral concentrates were then washed for approximately 20 minutes in an ultrasonic bath, hand picked to select the best grains in fractions with >99.5% purity, and accurately weighed on a Mettler™ single pan electronic balance (model H1OW).

Hand picked fractions (approximately 12-16 mg) were loaded into aluminium irradiation canisters interspersed with standard flux monitors (approximately 8-10 flux monitors per canister) and irradiated in the McMaster University reactor. The standards comprise both the NS 231 Dalhousie standard biotite (368 Ma; Reynolds et al., 1973) and the accepted standard MMHb-1 hornblende (519 Ma; Alexander et al., 1978). After irradiation, analysis occurred with a VG 3600 mass spectrometer connected to a double-vacuum tantalum resistance furnace and equipped with an 11 sample cassette holder. Amphibole samples underwent heating from 750-1300°C in

27-75°C steps and the phlogopite sample underwent heating from 650-1250°C in 50-100°C increments; all heating steps lasted for approximately 20 minutes. Corrections for interfering Ca and K isotopes vary between 0.5-2.1% and atmospheric argon corrections are all less than 10% over the designated age plateaus. All ages were calculated with J interpolated from the flux monitors at 0.002317.

A-4. U-Pb Sample Preparation and Analytical Procedures

Preparation of U-Pb (zircon, sphene, and monazite) samples followed the meticulous cleaning procedures established and practiced by the staff of the Jack Satterley Geochronology Laboratory at the Royal Ontario Museum. Only filtered reagents and ultrasonically cleaned glassware and utensils contacted the samples during the liberation of accessory minerals. Bulk hand samples of the Birchtown granodiorite (sample SPGD, 12.7 kg) diorite (sample B8, 14.5 kg), and hybrid (sample B3, 18.1 kg), were disaggregated in a jaw crusher and subsequently pulverized to a <400μ powder in a Bico™ disk mill. The heavy mineral fraction was separated on a Wilfley™ table, reducing the volume of each sample by approximately 90% (Heaman and Parrish, 1991). The heavy fractions were washed in alcohol, dried in air, and sieved at 70 mesh. Freefall magnetic separation of the fine material then occurred across the pole pieces of a modified Frantz™ isodynamic separator at 1.7A with 90° side tilt and 5° forward slope, to remove strongly magnetic particles (generally magnetite, sulphides, and weathered or multiple grains in these samples).

Quartz and feldspar were floated from samples SPGD and B3 using bromoform (ρ = 2.85) heavy liquid separation, and the heavy separate was washed in alcohol and then dried in air. A Frantz isodynamic separator subdivided all three samples into magnetic fractions at 0.1A, 0.3A, 0.5A, 0.8A, 1.0A (monazite in sample SPGD), and 1.7A (sphene in sample B3, zircon in samples B8 and B3) with 10° side tilt. After this "initial Frantz" stage, samples SPGD and B3 underwent a methylene iodide separation (ρ = 3.29) to isolate zircons from apatite in the 1.7A initial Frantz non-magnetic fraction. For sample B8, the methylene iodide separation occurred between the 0.8A and 1.0A initial Frantz stages to remove quartz, feldspar, and apatite, and reduce sample size to compensate for the lack of a prior bromoform treatment. For all samples, a "final Frantz" step for the 1.7A non-magnetic initial Frantz fraction, occurred at 1.7A with progressively smaller side tilts (5°, 3°,1°, and 0°) and 10° forward slope. The most concordant zircons generally occur in the smallest side tilt (non-magnetic) fractions (Krogh, 1981a).

The 1.0A magnetic (monazite) and 1.7A magnetic (sphene) initial Frantz fractions, and the 0° magnetic and non-magnetic final Frantz (zircon) fractions were hand picked in alcohol under a binocular microscope at 25-50 times magnification, to produce monomineralic separates with 100% purity. Both black and white backgrounds facilitated the rejection of grains with observable cores, inclusions, fractures, and turbidity (Heaman and Parrish, 1991). All equant zircon fractions were abraded in a compressed air chamber with ~5 mg of a purified pyrite polishing agent for approximately 5 hours at 4 p.s.i. (Krogh, 1981b); any remaining pyrite was subsequently floated from the samples by a warm 2N nitric acid wash. Sphene and monazite populations were not abraded. The selected final populations were then rinsed in both warm 4N nitric acid, distilled water, and distilled acetone in an ultrasonic bath for 1 minute, dried in air, and weighed accurately on an electronic Cann (Model 400) balance in disposable aluminium boats (Heaman and Machado, 1992). The U content of the grains was estimated from the sample weight and guided by the colour of the grains and their hardness during abrasion.

Zircon and monazite samples were placed into sealed teflon bombs containing 50% HF and 8N HNO_3 (30:1), with an appropriately measured dope of a mixed $^{205}Pb/^{235}U$ isotope dilution spike (~7pg/ml) (Krogh and Davis, 1975), and refluxed in an oven at 220°C for at least 5 days in a clean laboratory. Sphene dissolution occurred in 10 ml Savillex capsules at 100°C on a hotplate for 5 days. Prior to the introduction of samples, all bombs and capsules were cycled at least 4 times with an alternating mixture of lead-free 50% HF and 8N HNO3 (30:1), or 6.2N HCl. After dissolution, the monazite and zircon samples were evaporated to dryness in the bombs to remove silica, and loaded onto miniaturized anion exchange columns (10 mm diameter) with 0.05 ml anion exchange resin equilibrated with 3.1N HCl (Krogh, 1973). Sequential elution of the columns with 3.1N HCl (to remove Zr, Hf, and LREE), 6.2N HNO_3 (to remove Pb), and double-distilled water (to remove U) allowed for simultaneous collection of purified Pb and U in one aliquot. Sphene samples instead experienced 1N HBr and 6.2N HCl elution in larger columns (Heaman and Machado, 1992). Total analytical blanks for Pb and U in all columns were 2 and 0.5 pg, respectively for HCl chemistry and 5 and 1 pg for HBr chemistry.

After evaporation of the U and Pb mixture to dryness, the sample aliquot was combined with a phosphoric acid binding agent and a silica gel ionization enhancer (Cameron et al., 1969), loaded onto outgassed rhenium single filaments, and analyzed in a VG 354 solid source thermal ionization mass spectrometer operating in single collector mode. All U and Pb isotope ratio measurements occurred at temperatures between 1520-1680°C with the Faraday cup, except for measurements of small ^{205}Pb/ ^{204}Pb values with the Daly photomultiplier detector. Analytical uncertainties (1σ) are 0.2% for U/Pb ratios and less than 0.1% for ^{207}Pb/^{206}Pb ratios and all data were corrected for mass fractionation, spike, and procedural blank. Initial common Pb at t = 370 Ma was calculated from the model of Stacey and Kramers (1975) and decay constants were derived from Steiger and Jäger (1977). Data analysis utilized in-house software developed by the laboratory for age recalculation, concordia plotting, regression, and error analysis (Davis, 1982; Heaman, unpublished).

A-5. Geochemical Sample Preparation

4-5 kg specimens from Attwoods Brook, Birchtown, Forbes Point, Mcleods Cove, Mersey Point, the Ovens, and the Weekend dykes were lapped with a diamond saw to remove weathered surfaces at Dalhousie University. The sawn surfaces were then polished with tungsten carbide powder on a glass plate to remove Fe and Cr contamination from the saw blade. The remainder was broken into circa 5 cm pieces with a hammer and a Meker Cutrock™, and then disaggregated into 5 mm chips with a Bico™ pulveriser in a clean crushing room. At this stage, fragments from the Pleasant Harbour dyke were picked to remove obvious xenolithic and xenocrystic material. All samples were then crushed in a Siebtechnik tungsten carbide ring mill to grain sizes below 200 mesh after pre-contaminating the mill with a random aliquot of the sample to minimize W, Nb, and Ta contamination. After homogenization of the powder by inversion, approximately 300 g aliquots were contained in inert plastic containers for storage prior to analysis.

A-6. Major Oxide, Trace Element, and Rare-earth Element Analytical Procedures

Powdered samples for all LDMIs (prepared following the procedure outlined in Appendix A-5) were analyzed for major and minor element oxides (SiO_2, TiO_2, Al_2O_3, MgO, Fe_2O_3T, CaO, Na_2O, K_2O, and P_2O_5) and trace elements (Ba, Rb, Sr, Y, Zr, Nb, Pb, Ga, Zn, Cu, Ni, V, Cr) by Sally Stanford at Saint Mary's University. Oxide determinations were made from circa 5 g fused glass disks, and trace elements were determined from pressed powder pellets. All analyses used a Philips PW 1400 sequential X-ray fluorescence spectrometer equipped with a Rhenium anode tube. Prior to fusion, loss on ignition (LOI) was determined by heating 1 g of each sample at 1050°C in an electric furnace for 90 minutes. Instrumental calibration relies upon 30 international standards (Govindaraju, 1989) in conjunction with in-house standards of the Saint Mary's geochemical centre. Duplicate analyses of the standards indicate that analytical precision is better than 5% for major and minor elements and between 5% and 10% for minor and trace elements.

Seven rare-earth elements (La, Ce, Nd, Sm, Eu, Yb, and Lu), with Hf, Ta, Th, U, Sc, and Co, were resolved for the Attwoods Brook gabbronorite, Birchtown diorite, Mersey Point picrite, and Popes Harbour and Little Harbour spessartites by instrumental neutron activation analysis (INAA) at Saint Mary's University. 0.5 g powdered samples were simultaneously irradiated with at least two geological standards approaching the composition of the unknowns, and determined with a high resolution Aptec coaxial germanium detector according to the method described in Gordon et al. (1968). Y, Nb, Hf, Ta, Th, and all 14 rare-earths for the Birchtown diorite, Forbes Point kersantite, and the Ovens, Devils Island, and Pleasant Harbour dykes were determined by Beverly Chapman using ICP-MS analysis at Memorial University of Newfoundland, following a sodium peroxide sintering procedure to ensure the complete dissolution of resistant accessory phases (Longerich et al., 1990). 0.2 g aliquots of all samples were sintered with sodium peroxide. After dissolution of the sinter cake, REEs were separated in a hybroxide-bearing precipitate. Analysis by ICP-MS used a pure quartz reagent blank and internal standards to correct for matrix effects and instrumental drift. Although insignificant blank concentrations were not subtracted from the samples, corrections were applied for Ba, Eu, and Gd interference during LREE determinations. Certified geological reference standards MRG-1 (gabbro), DNC-1 (diabase), W-2 (diabase), USGS BIR-1 (basalt) (Govindaraju, 1989; Jenner et al., 1990) were also analyzed with the samples. Replicate rare-earth determinations at Saint Mary's University indicate that determinations of La, Ce, Eu, Tb, Yb, Lu, Th, Sc, and Co are better than 5% and analyses for Nd, Sm, Hf, Ta, and U are better than 10%. ICP-MS determinations at Memorial University are better than 5% for all elements with detection limits at less than 10% of their chondritic abundances (0.008 ppm at 3σ background).

A-7. Sr, Sm, and Nd Isotope Analytical Procedures

Powdered isotopic samples for all unaltered LDMIs were prepared at Dalhousie University according to the procedures outlined in Appendix A-5. Patricia Horan analyzed all the samples at Memorial University of Newfoundland, except for the Liscomb Complex samples LC5, LC6, LC7, and LC8, which were taken from Clarke et al. (1993a). Approximately 0.1 g aliquots from each powdered sample (weighed accurately to 5 decimal places) were refluxed in a teflon bomb with a 1:1 mixture of 8 N nitric and hydrofluoric acid for up to one week. The refluxed solution was then desiccated, and the sample cake was repeatedly dissolved in 6 N HCl and evaporated to dryness before splitting into separate fractions for the determination of Sr, Nd, and Sm isotopic composition and isotopic ratio (IR) fractions. The IR fraction was doped with a $^{150}Nd/^{147}Sm$ spike proportional to the Nd content of the sample (determined by ICP-MS at Memorial University according to the procedures outlined in Appendix A-6), and both fractions were evaporated to dryness and filtered. Bulk Rb, Sr, Nd, and Sm separation for both fractions occurred in teflon chromatography columns filled with quartz wool, washed with 1.5 N nitric acid to neutralize remanent organic material, and dissolved in 0.15 N HCl before loading onto the outgassed rhenium double filament of a Finnigan MAT 262V thermal-induction mass spectrometer. Isotopic abundances were determined with the Faraday detector cup using static simultaneous multicollector and multicollector peak jumping routines, which contain statistical corrections for instrumental drift and isotopic mass fractionation during analysis. Isotopic measurements were made by reference to the NBS 987, LaJolla, and AMES standards for Sr, Nd, and Sm, respectively. Analytical uncertainties (1σ) for $^{87}Sr/^{86}Sr$, $^{143}Nd/^{144}Nd$, and $^{147}Sm/^{144}Nd$ measurements appear with the data in Table B3.1 and Table C2.1 of Appendices B-3 and C-2, respectively.

Appendix B

GEOGRAPHIC LOCATIONS, MICROPROBE DATA, AND GEOCHEMICAL DATA FOR CHAPTER 2

B-1. Location Maps

Before this study, adequate location maps existed only for the Ovens dykes (Hall, 1979) and the Ten Mile Lake and Bog Island Lake intrusions of the Liscomb Complex (Clarke et al., 1993a). For the benefit of subsequent workers, new location maps were compiled from detailed compass surveys superimposed on published 1:50,000 and 1:25,000 scale topographic maps and/or 1:10,000 scale air photographs and orthophotographs available in 1991. Figure B1.1 shows the explanation and map conventions and Figures B1.2 to B1.11 contain the location maps for the Attwoods Brook gabbronorite, the Birchtown diorite and CZT, the Forbes Point and Mcleods Cove lamprophyres, the Mersey Point picrite, and the Weekend dyke spessartites. To help locate these important but volumetrically minor intrusions, each figure includes the coastline of Nova Scotia, an excerpt from Donohoe and Grantham (1989) to show the major access roads and settlements, and one or more detailed maps in the vicinity of the mafic intrusion at circa 1:10,000 scale or less. The maps were continuously updated to August 1992 and show the locations for geochemical samples analyzed by the author.

Appendix B-3 contains geochemical data for these samples; refer to Douma (1988) for the locations of samples collected from the Forbes Point and Mcleods Cove lamprophyres, Hall (1979) for the locations of some samples collected from the Ovens dykes (prefixed AO), Clarke et al., (1993a) for the locations of samples collected from the Liscomb Complex gabbro-diorites, Kempster (1988) for the locations of samples collected from the East Jeddore and Sober Island Weekend dykes, and de Albuquerque (1979) for the locations of some samples collected from the Attwoods Brook gabbronorite, Birchtown diorite, and Mersey Point picrite (prefixed DEA).

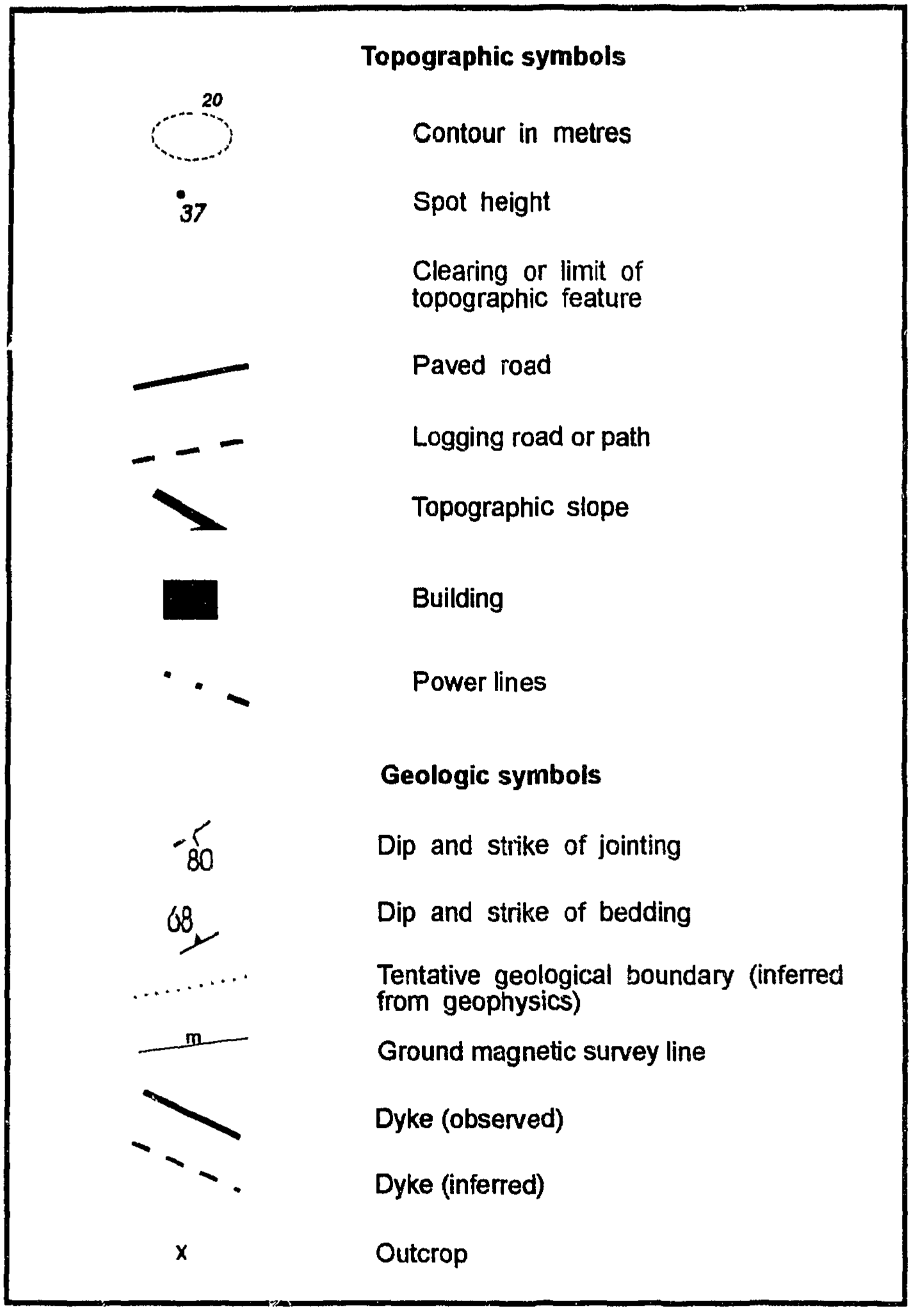

Figure B1.1. Legend for the Late Devonian mafic intrusion location maps.

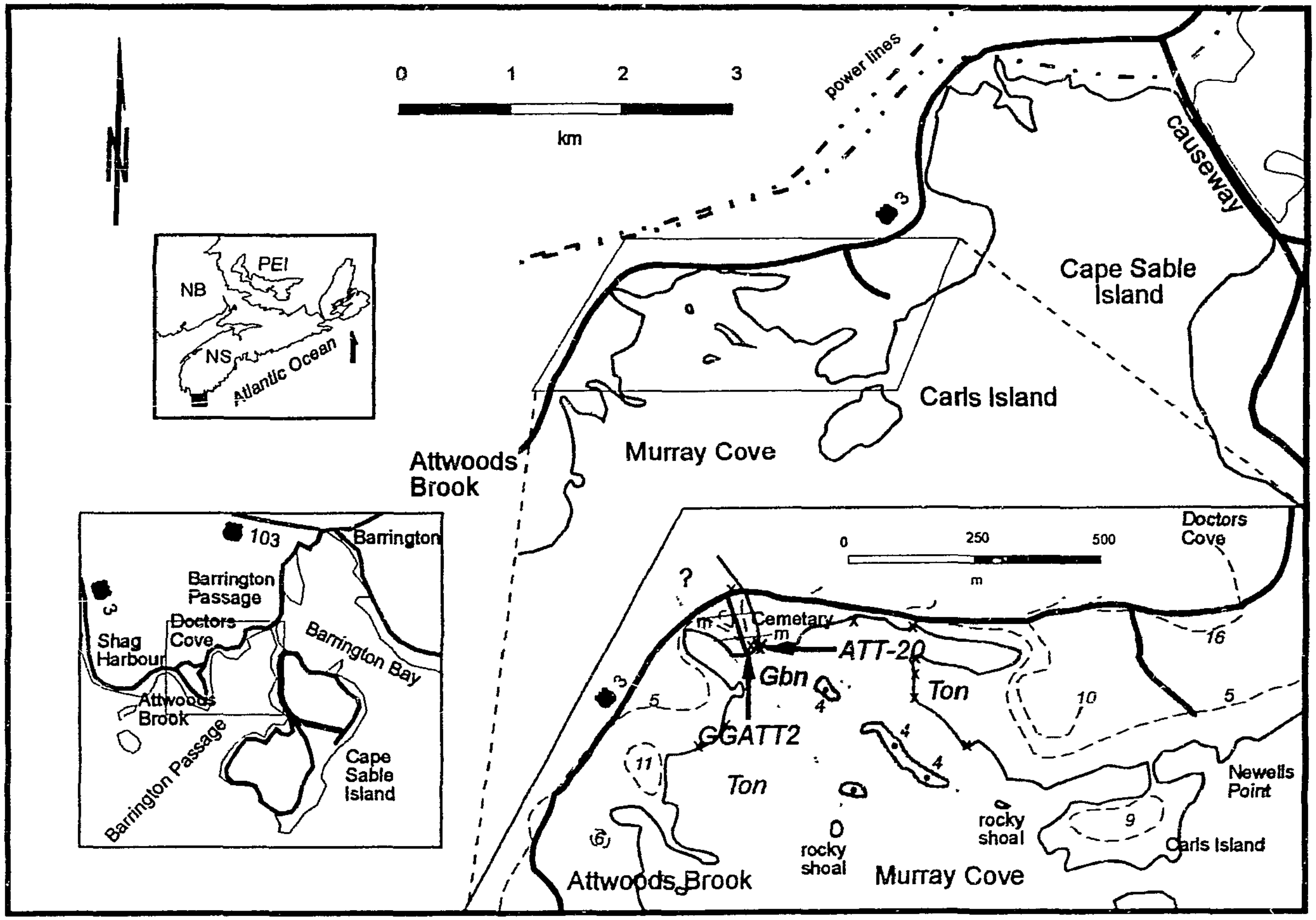

Figure B1.2. Location of the Attwoods Brook gabbronorite. Ton = Tonalite, Gbn = gabbronorite. See Figure B1.1 for the explanation.

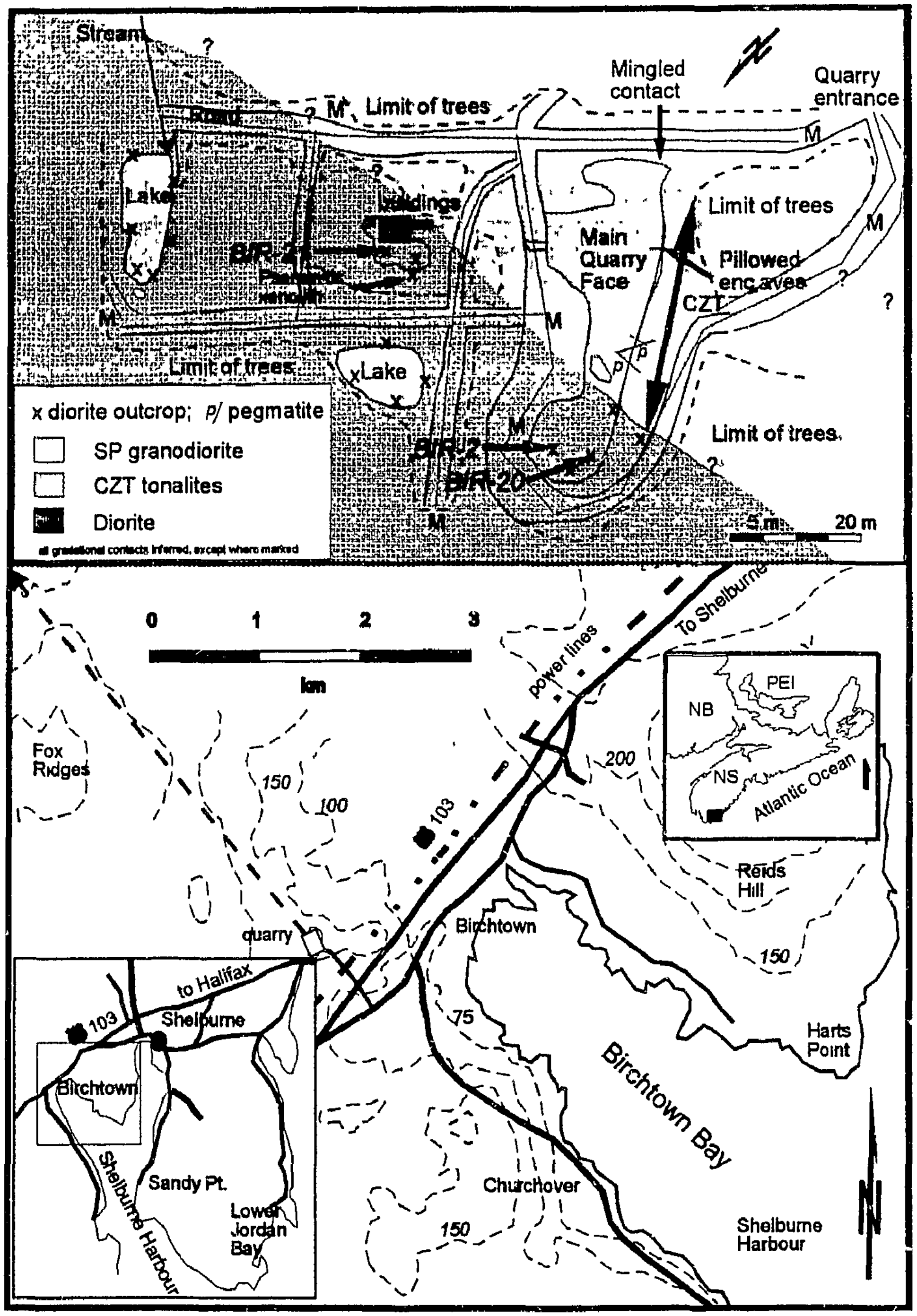

Figure B1.3. Location of the Birchtown diorite and its hybrid contact with the Shelburne Pluton. CZT = Contact Zone Transect. See Figure B1.1 for the explanation.

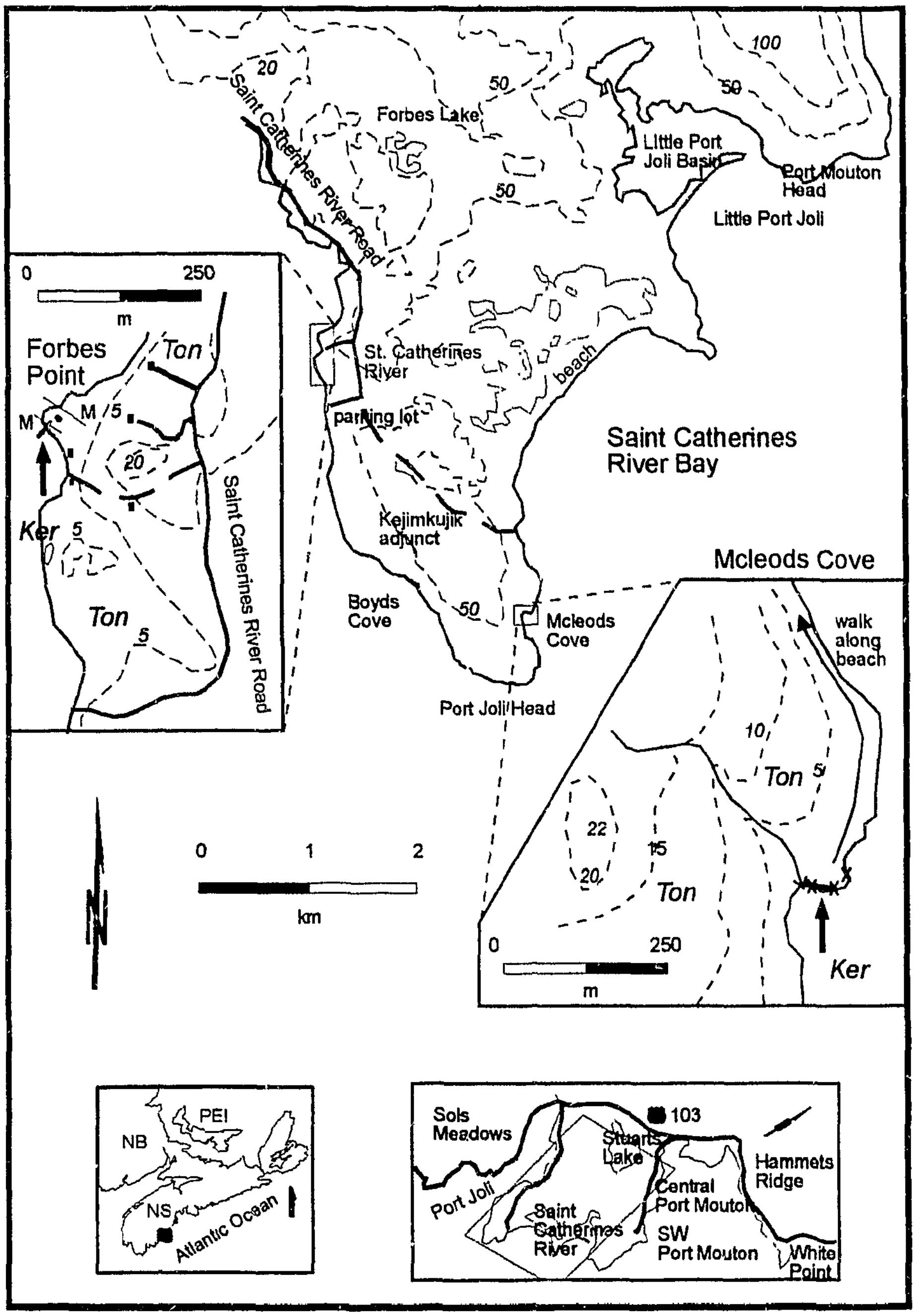

Figure B1.4. Location of the Forbes Point and Mcleods Cove kersantites in the Port Mouton Pluton. Ton = tonalite, Ker = Kersantite. See Figure B1.1 for the explanation.

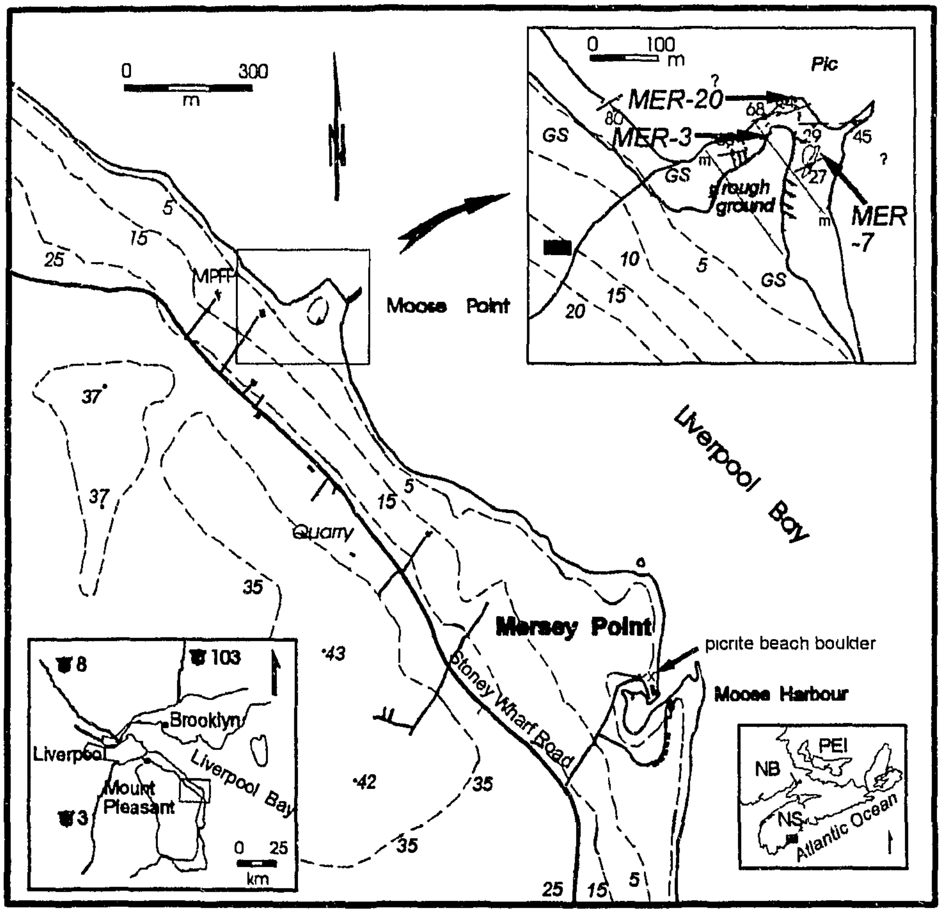

Figure B1.5. Location of the Mersey Point picrite. GS = Goldenville Formation sandstone, Pic = picrite. MPFP = Mersey Point Fish Products. The circular dashed pattern represents an aeromagnetic survey over the picrite (Geological Survey of Canada, 1986), see Figure B1.1 for the explanation.

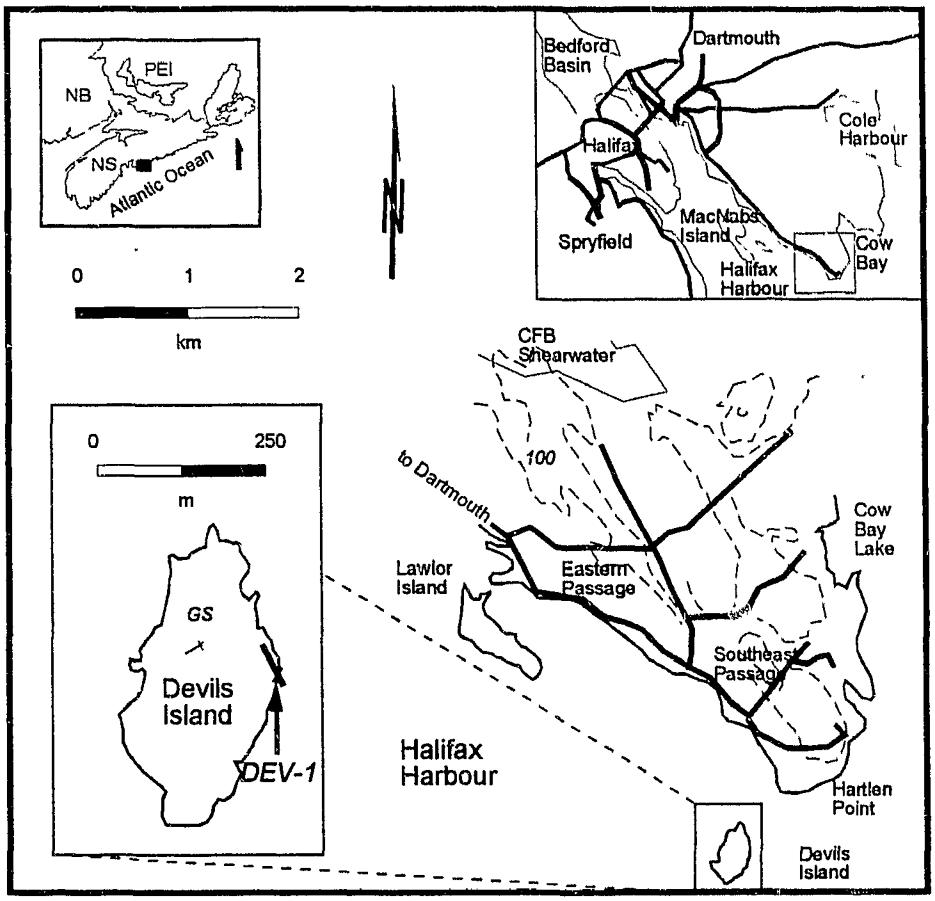

Figure B1.6. Location map for the Devils Island dyke. GS = Goldenville Formation sandstone. See Figure B1.1 for the explanation.

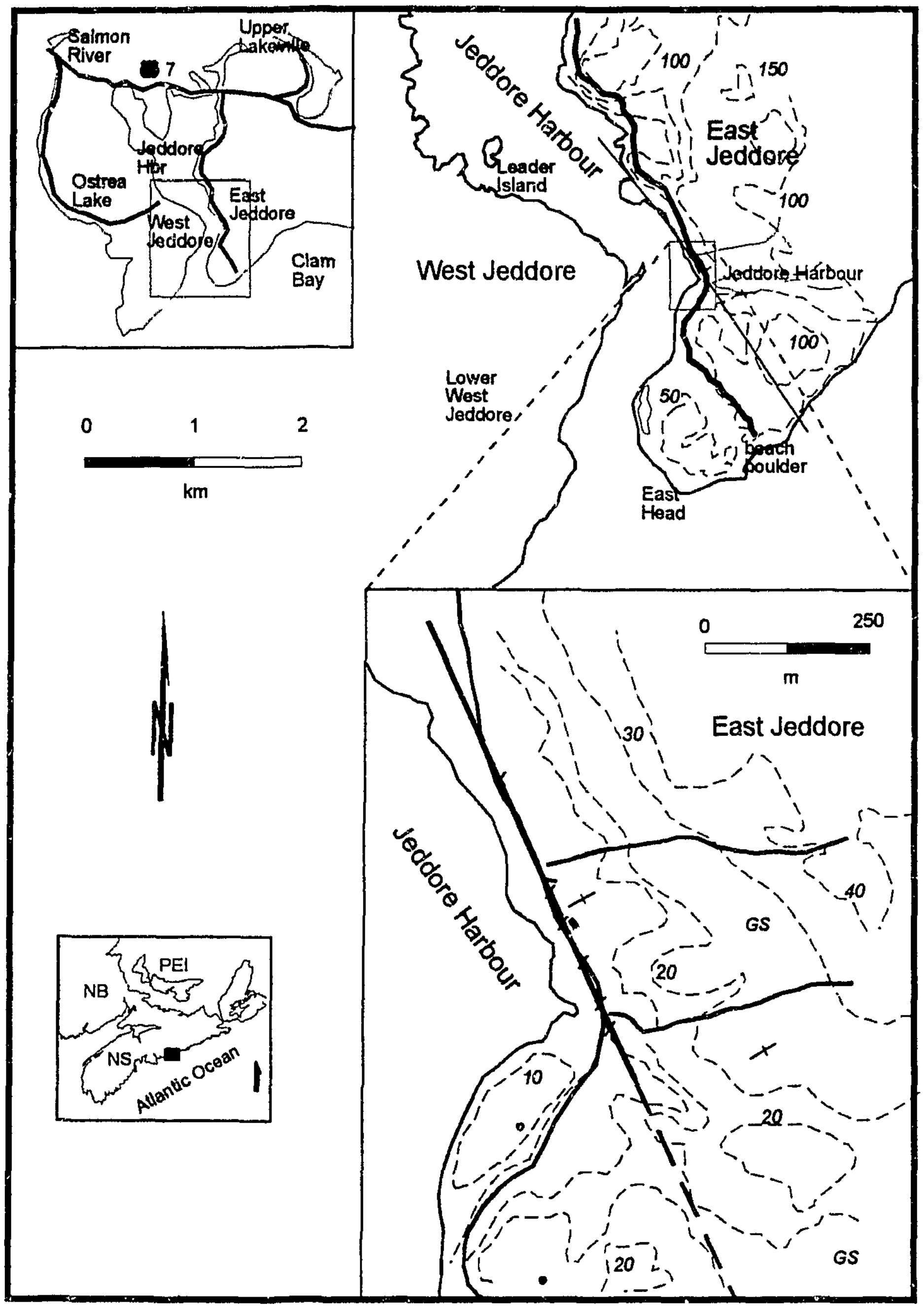

Figure B1.7. Location map for the East Jeddore dyke. GS = Goldenville Formation sandstone. See Figure B1.1 for the explanation.

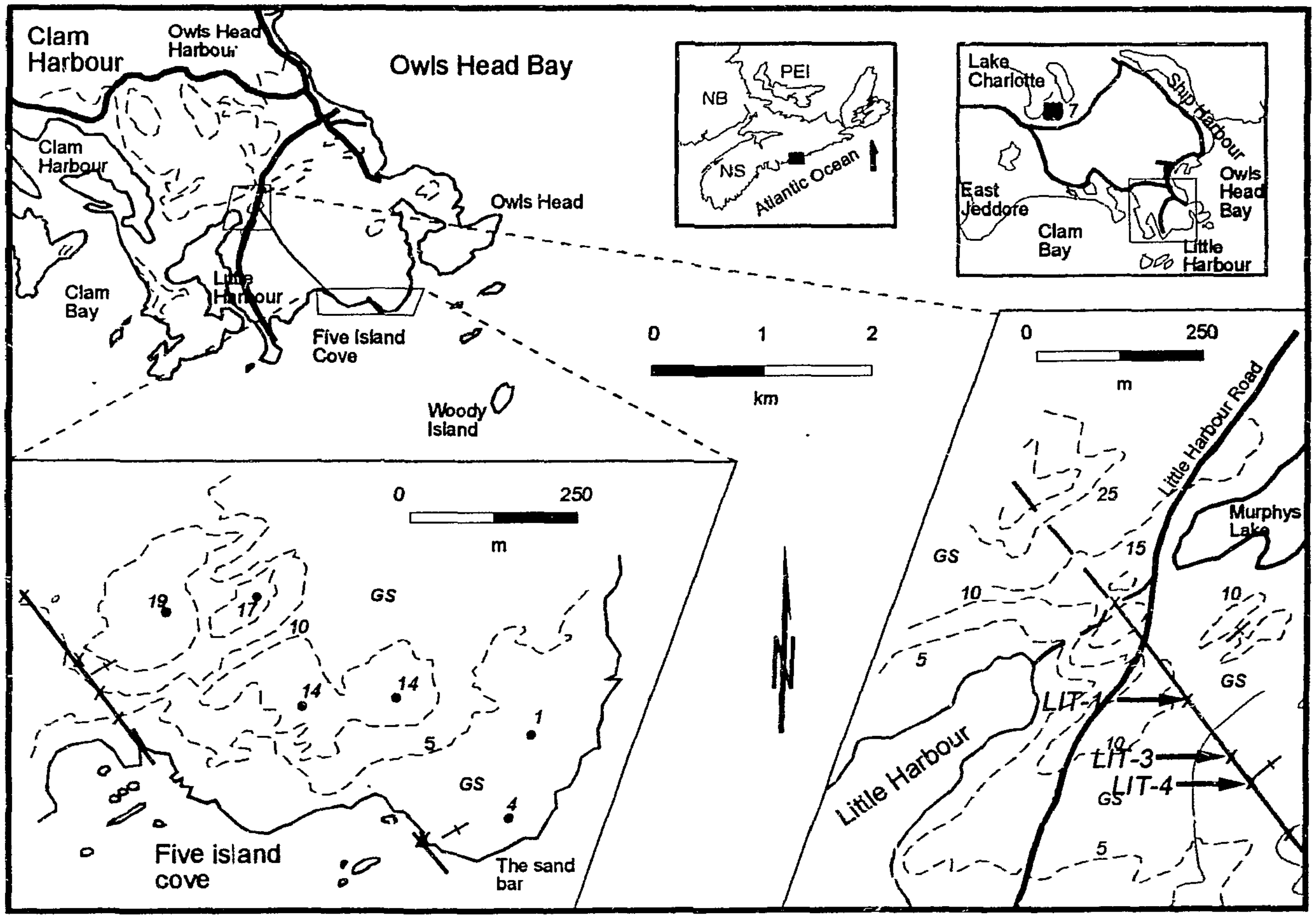

Figure B1.8. *Location map for the Little Harbour (road and coast) dykes.* GS = Goldenville Formation sandstone. See Figure B1.1 for the explanation.

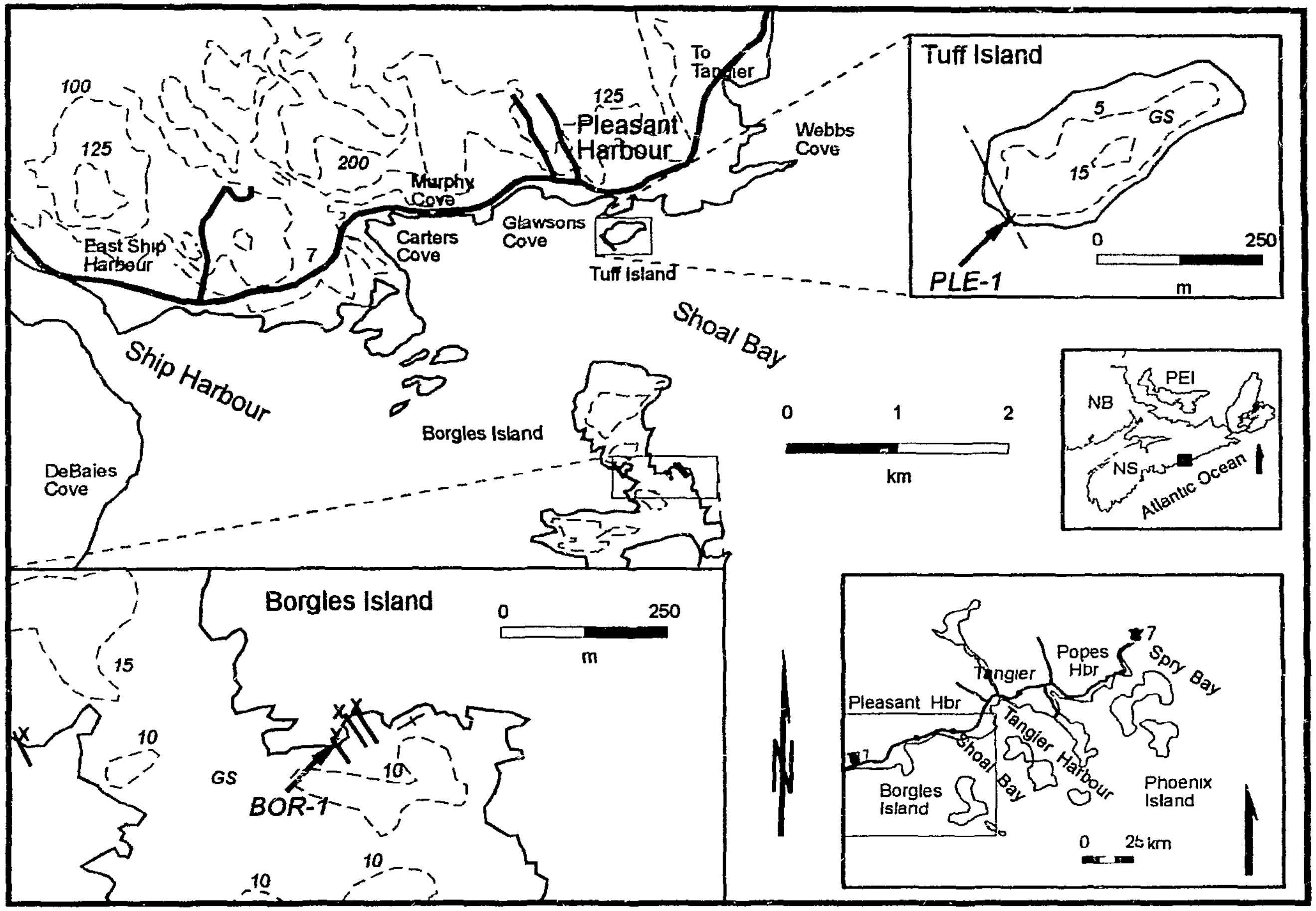

Figure B1.9. Location map for the Pleasant Harbour and Borgles Island dykes. GS = Goldenville Formation sandstone. See Figure B1.1 for the explanation.

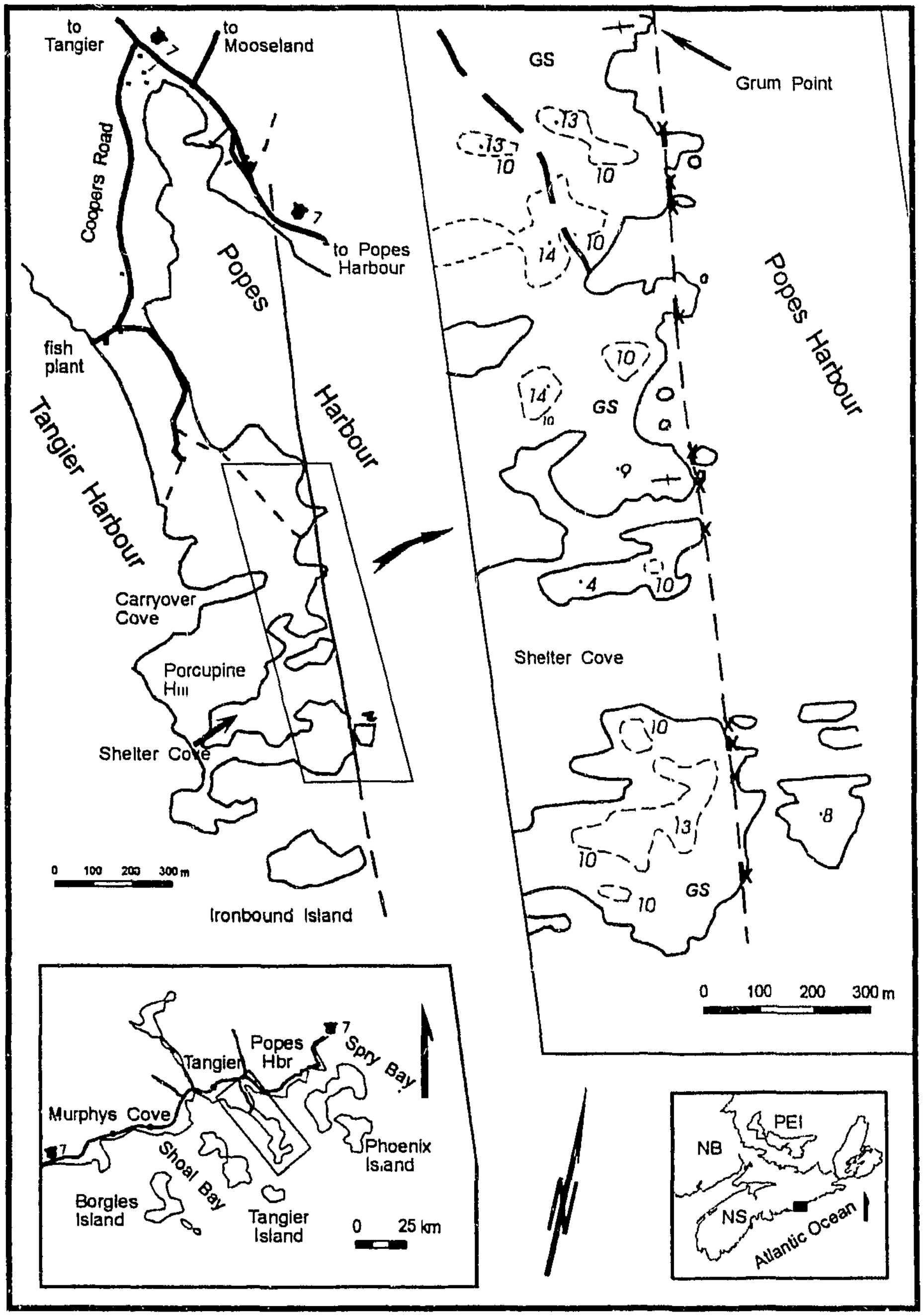

Figure B1.10. Location map for the Popes Harbour dyke. GS = Goldenville Formation sandstone. See Figure B1.1 for the explanation.

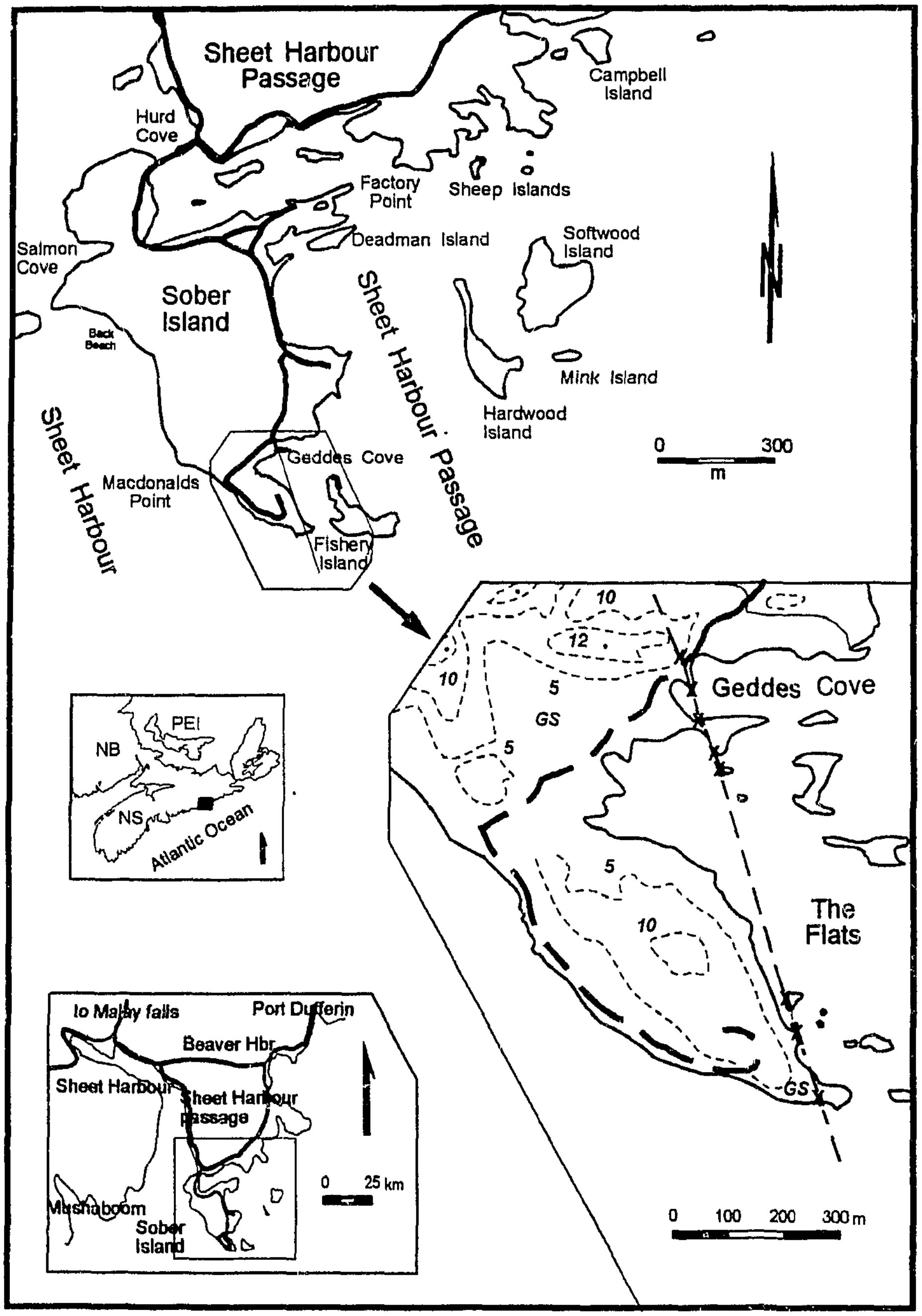

Figure B1.11. Location map for the Sober Island dyke. GS = Goldenville Formation sandstone. See Figure B1.1 for the explanation.

B-2. Microprobe Data for the Late Devonian Mafic Intrusions

Representative microprobe data for olivines, pyroxenes, amphiboles, biotite and phlogopite, and feldspars generated by this study appear in Tables B2.1 to B2.5, respectively. Appendix A-1 contains the analytical and data recalculation procedures. Abbreviations: ATT = Attwoods Brook gabbronorite, BIR = Birchtown diorite FOR = Forbes Point kersantite, MCL = Mcleods Cove kersantite, MER = Mersey Point picrite, DEV = Devils Island "diorite", EAS = East Jeddore spessartite, LIT = Little Harbour spessartites, PLE = Pleasant Harbour spessartite, BOR = Borgles Island spessartites, POP = Popes Harbour spessartite, SOB = Sober Island spessartite; C = core, M = middle, R = rim. Mineralogical abbreviations after Kretz (1983). Amphibole nomenclature: Act = actinolite, Act Hbl = actinolitic hornblende, Ed = edenite, Ed Hbl = edentic hornblende, F Parg Hbl = ferroan pargasitic hornblende, M Hbl = Magnesio-hornblende, M Hs = Magnesio-hastingsite, M Hs Hbl = Magnesio-hastingsitic hornblende, Prg = pargasite, Prg Hbl = pargasitic hornblende, Tr = tremolitic hornblende.

Table B2.1. Microprobe analyses for olivine from the Mersey Point picrite.

Intrusion	MER	MER	MER	MER
Mineral	Ol	Ol	Ol	Ol
Location	C	R	C	C
SiO_2	39.14	38.87	39.13	38.93
TiO_2	0.00	0.03	0.00	0.01
Al_2O_3	0.00	0.00	0.00	0.00
FeO	18.48	19.05	17.53	17.72
MnO	0.36	0.29	0.23	0.28
MgO	41.85	41.57	42.62	42.28
CaO	0.06	0.02	0.09	0.05
Na_2O	0.33	0.42	0.30	0.19
K_2O	0.05	0.00	0.00	0.00
P_2O_5	0.00	0.00	0.00	0.00
Total	100.27	100.26	99.89	99.46
% Fo	80.14	79.54	81.25	80.96
% Fa	19.86	20.46	18.75	19.04

Table B2.2. Microprobe analyses of clino- and orthopyroxene from the Attwoods Brook gabbronorite, Mersey Point picrite, and the Weekend dykes.

Intrusion	ATT	ATT	EAS	LIT	LIT	MER	MER	POP	POP
Mineral	Cpx	Cpx	Cpx	Cpx	Cpx	Cpx	Cpx	Cpx	Cpx
Location	-	-	C	C	R	C	R	C	C
SiO_2	53.04	50.38	48.60	51.02	50.16	51.31	52.11	52.02	46.17
TiO_2	0.18	1.05	0.73	0.73	0.77	0.48	0.31	0.53	1.29
Al_2O_3	1.65	7.01	6.91	4.05	4.60	4.46	3.28	3.21	8.42
FeO	5.88	8.68	14.39	6.70	6.21	4.90	5.58	6.14	11.37
MnO	0.00	0.09	0.37	0.17	0.31	0.10	0.08	0.11	0.25
MgO	15.01	17.60	15.27	16.93	16.09	16.39	16.76	17.81	16.33
CaO	23.25	12.08	10.69	20.38	21.00	22.00	22.18	20.61	11.19
Na_2O	0.46	0.95	1.46	0.34	0.38	0.58	0.53	0.42	1.80
K_2O	0.00	0.41	0.25	0.01	0.00	0.00	0.00	0.00	0.48
P_2O_5	0.00	0.00	0.00	0.09	0.21	0.00	0.00	0.03	0.00
Total	99.47	98.23	98.67	100.42	99.73	100.21	100.83	100.88	97.30
Wo	47.53	22.96	18.49	39.56	41.30	43.78	43.90	39.92	17.09
En	44.32	60.27	59.03	54.07	52.55	53.09	52.80	55.52	74.78
Fs	8.15	16.78	22.48	6.37	6.15	3.13	3.30	4.56	8.14

Intrusion	POP	POP	POP	POP	POP	POP	ATT	MER	MER
Mineral	Cpx	Cpx	Cpx	Cpx	Cpx	Cpx	Opx	Opx	Opx
Location	-	-	-	-	R	R	-	C	R
SiO_2	51.11	52.84	52.68	50.64	52.51	49.68	54.63	56.15	55.51
TiO_2	0.47	0.41	0.27	1.14	0.44	0.86	0.00	0.19	0.09
Al_2O_3	5.33	3.50	2.02	5.13	2.93	7.26	0.54	1.81	1.51
FeO	9.18	8.96	16.50	10.74	5.31	12.14	18.86	11.09	11.94
MnO	0.22	0.24	0.64	0.33	0.02	0.33	0.00	0.21	0.33
MgO	18.65	19.96	13.45	18.13	17.87	17.07	24.77	31.05	30.36
CaO	12.06	10.77	11.92	11.31	20.89	11.40	0.36	1.23	1.17
Na_2O	1.06	0.59	0.34	1.24	0.35	1.56	0.12	0.24	0.31
K_2O	0.25	0.13	0.06	0.25	0.00	0.39	0.00	0.00	0.02
P_2O_5	0.00	0.00	0.00	0.00	0.00	0.07	0.00	0.00	0.00
Total	98.33	97.40	97.88	98.91	100.32	100.76	99.29	101.97	101.24
Wo	22.93	22.06	28.75	21.51	40.74	18.37	-	-	-
En	63.35	61.92	41.53	62.45	54.21	57.90	69.10	85.61	81.53
Fs	13.72	16.02	29.71	16.04	5.06	23.74	30.90	14.39	14.11

Table B2.3. Microprobe analyses of amphiboles from all Late Devonian mafic intrusions.

Intrusion	ATT	ATT	ATT	ATT	ATT	ATT	ATT	ATT	ATT	ATT
Mineral	Am	Am	Am	Am	Am	Am	Am	Am	Am	Am
Location	C	R	R	C	R	C	C	C	R	C
SiO_2	43.91	45.20	43.49	47.73	45.00	43.65	52.89	55.94	57.37	50.46
TiO_2	1.98	2.23	2.06	1.44	1.86	2.46	0.07	0.13	0.07	0.88
Al_2O_3	11.70	10.77	10.88	9.10	9.48	11.27	4.59	2.32	0.96	6.80
FeO	14.10	11.94	11.75	11.15	11.67	12.78	11.26	11.17	7.89	10.83
MnO	0.04	0.03	0.10	0.14	0.21	0.24	0.32	0.38	0.11	0.12
MgO	12.72	13.95	13.65	14.75	14.17	12.82	16.79	19.76	20.00	16.25
CaO	12.38	12.14	12.59	12.60	12.15	12.30	12.34	9.47	13.27	12.61
Na_2O	1.16	0.94	1.07	0.75	1.30	1.20	0.83	0.42	0.27	0.65
K_2O	1.14	1.08	1.13	0.82	0.94	1.20	0.07	0.01	0.01	0.48
P_2O_5	0.00	0.00	0.00	0.00	0.00	0.00	0.00	0.00	0.00	0.00
Total	99.13	98.28	96.72	98.48	96.78	97.92	99.16	99.60	99.95	99.08
Classification	Ts Hbl	M Hbl	M Hs	M Hbl	M Hbl	Ts Hbl	Act Hbl	Tr Hbl	Act Hbl	M Hbl

Intrusion	BIR	BIR	BIR	BIR	BIR	BIR	BIR	BIR	BIR	BIR
Mineral	Am	Am	Am	Am	Am	Am	Am	Am	Am	Am
Location	C	R	C	R	C	R	C	C	R	-
SiO_2	52.24	52.40	53.52	54.00	54.69	55.69	56.59	49.32	49.85	48.61
TiO_2	0.22	0.31	0.47	0.41	0.30	0.15	0.14	0.55	0.69	0.62
Al_2O_3	5.50	6.38	5.05	5.05	4.24	3.03	2.17	7.42	6.67	7.42
FeO	9.34	9.04	8.78	8.18	8.17	7.68	7.58	12.10	12.31	12.08
MnO	0.35	0.39	0.32	0.33	0.35	0.34	0.21	0.47	0.38	0.35
MgO	17.54	17.57	18.18	17.81	18.51	19.38	19.95	14.96	15.12	14.91
CaO	12.42	12.37	12.71	12.44	12.82	12.76	12.96	12.90	12.85	12.61
Na_2O	0.91	0.92	0.88	0.72	0.74	0.49	0.43	1.08	0.78	0.95
K_2O	0.29	0.19	0.17	0.12	0.07	0.04	0.03	0.46	0.59	0.51
P_2O_5	0.00	0.00	0.00	0.00	0.00	0.00	0.00	0.00	0.00	0.00
Total	98.81	99.57	100.08	99.06	99.89	99.56	100.06	99.26	99.23	98.04
Classification	Act Hbl	M Hbl	Act Hbl	Act Hbl	Act	Act	Act	Act	Act	Act

Table B2.3. (Continued) Microprobe analyses of amphiboles from all Late Devonian mafic intrusions.

Intrusion	BIR	EAS	EAS	EAS	EAS	EAS	EAS	EAS	EAS	EAS
Mineral	Am	Am	Am	Am	Am	Am	Am	Am	Am	Am
Location	-	C	C	C	C	C	C	R	R	R
SiO_2	47.23	42.90	44.40	43.87	44.01	42.80	43.79	42.97	45.75	44.90
TiO_2	0.84	2.85	1.73	2.04	1.77	2.55	2.91	2.81	1.05	1.79
Al_2O_3	8.20	11.21	10.20	10.49	10.35	11.55	10.47	10.98	9.40	10.44
FeO	13.17	12.20	12.85	12.66	13.26	11.69	11.12	11.95	13.13	13.46
MnO	0.27	0.23	0.25	0.27	0.34	0.00	0.00	0.00	0.24	0.26
MgO	13.84	14.94	14.49	14.79	14.60	15.10	15.77	14.49	15.23	14.63
CaO	12.40	11.40	11.18	11.03	10.71	11.14	11.00	11.34	11.18	11.06
Na_2O	1.20	2.29	2.03	2.16	1.85	2.21	1.99	2.23	1.87	1.93
K_2O	0.95	0.54	0.46	0.43	0.41	0.46	0.54	0.51	0.38	0.42
P_2O_5	0.00	0.00	0.00	0.00	0.00	0.00	0.00	0.00	0.00	0.00
Total	98.10	98.56	97.59	97.74	97.30	97.50	97.59	97.28	98.23	98.89
Classification	Act	M Hs	Ed Hbl	Prg Hbl	M Hbl	Prg	Prg Hbl	F Prg Hbl	Ed Hbl	F Prg Hbl

Intrusion	EAS	EAS	EAS	EAS	FOR	FOR	FOR	FOR	LIT	MCL
Mineral	Am	Am	Am	Am	Am	Am	Am	Am	Am	Am
Location	R	R	R	R	C	R	-	-	R	C
SiO_2	43.25	46.55	42.58	43.81	49.32	49.85	47.23	48.61	49.13	51.79
TiO_2	2.61	0.96	2.73	2.41	0.55	0.69	0.84	0.62	1.25	0.27
Al_2O_3	11.11	8.71	11.57	10.76	7.42	6.67	8.20	7.42	5.90	4.54
FeO	11.52	13.06	11.62	12.38	12.10	12.31	13.17	12.08	12.72	11.19
MnO	0.27	0.51	0.00	0.00	0.47	0.38	0.27	0.35	0.45	0.37
MgO	15.03	14.66	14.72	14.92	14.96	15.12	13.84	14.91	15.23	16.45
CaO	11.48	11.00	11.38	11.22	12.90	12.85	12.40	12.61	11.14	12.68
Na_2O	2.09	1.55	2.18	2.07	1.08	0.78	1.20	0.95	1.11	0.60
K_2O	0.46	0.35	0.47	0.44	0.46	0.59	0.95	0.51	0.22	0.33
P_2O_5	0.00	0.00	0.00	0.00	0.00	0.00	0.00	0.00	0.18	0.00
Total	97.82	97.35	97.25	98.01	99.26	99.24	98.10	98.06	97.33	98.22
Classification	M Hs Hbl	Ed	Prg Hbl	Prg Hbl	Act Hbl	Act Hbl	M Hs Hbl	Act Hbl	M Hbl	Act Hbl

Table B2.3. (Continued) Microprobe analyses of amphiboles from all Late Devonian mafic intrusions

Intrusion	MCL	MCL	MCL	MER	MER	MER	MER	MER	MER	POP
Mineral	Am	Am	Am	Am	Am	Am	Am	Am	Am	Am
Location	C	R	R	C	C	C	R	R	R	C
SiO_2	51.92	52.44	53.65	45.02	44.28	49.06	44.53	52.30	56.04	43.97
TiO_2	0.39	0.44	0.14	0.19	0.36	0.70	0.33	0.33	0.15	2.45
Al_2O_3	5.56	4.86	3.39	12.28	12.45	8.86	12.83	3.19	2.28	11.07
FeO	11.09	10.57	9.57	8.41	8.38	10.34	8.12	5.25	7.70	11.61
MnO	0.40	0.31	0.39	0.10	0.14	0.28	0.03	0.24	0.27	0.08
MgO	16.23	16.30	17.32	17.74	17.44	15.59	17.04	16.47	19.44	15.57
CaO	12.95	13.01	12.56	12.00	12.06	12.25	12.16	22.33	13.17	11.12
Na_2O	0.78	0.79	0.83	2.49	2.53	1.29	2.42	0.58	0.55	2.22
K_2O	0.37	0.40	0.27	0.92	0.98	0.42	0.92	0.05	0.06	0.70
P_2O_5	0.00	0.00	0.00	0.00	0.00	0.00	0.00	0.00	0.00	0.18
Total	99.69	99.12	98.12	99.15	98.62	98.79	98.38	100.74	99.66	98.97
Classification	Act Hbl	Act Hbl	Act Hbl	M Hs Hbl	M Hs	M Hbl	M Hs Hbl	Act	Act	Prg Hbl

Intrusion	POP	POP	POP	POP	POP	POP	POP	POP	SOB	SOB
Mineral	Am	Am	Am	Am	Am	Am	Am	Am	Am	Am
Location	C	C	C	C	R	R	R	R	C	C
SiO_2	43.29	43.49	43.12	42.47	43.16	44.23	43.16	43.16	44.43	42.43
TiO_2	2.68	2.45	3.00	2.98	2.84	2.36	2.84	2.84	1.35	3.03
Al_2O_3	10.41	11.13	10.92	11.46	11.53	9.76	11.53	11.53	10.57	11.57
FeO	11.54	11.65	11.88	11.60	11.70	11.51	11.70	11.70	13.34	11.10
MnO	0.23	0.30	0.32	0.32	0.02	0.18	0.02	0.02	0.18	0.20
MgO	15.39	15.44	15.37	15.28	15.41	14.94	15.41	15.41	14.81	15.09
CaO	11.08	11.45	11.05	11.39	11.47	11.46	11.47	11.47	11.06	11.39
Na_2O	2.28	2.41	2.42	2.33	2.32	2.03	2.32	2.32	2.09	2.21
K_2O	0.59	0.71	0.66	0.65	0.68	0.64	0.68	0.68	0.55	0.64
P_2O_5	0.00	0.00	0.22	0.00	0.14	0.08	0.14	0.14	0.00	0.00
Total	97.49	99.03	98.96	98.48	99.27	97.19	99.27	99.27	98.38	97.66
Classification	Prg Hbl	Prg Hbl	Prg Hbl	Prg	Prg Hbl	Ed Hbl	Prg Hbl	Prg Hbl	M Hs Hbl	Prg

Table B2.3. (Concluded) Microprobe analyses of amphiboles from all Late Devonian mafic intrusions

Intrusion	SOB	SOB	SOB	SOB	SOB
Mineral	Am	Am	Am	Am	Am
Location	C	C	R	R	R
SiO_2	43.11	42.51	43.54	46.43	48.42
TiO_2	2.63	2.65	1.69	1.36	0.79
Al_2O_3	11.30	11.49	10.95	8.67	7.68
FeO	11.09	10.83	12.31	11.28	11.86
MnO	0.20	0.23	0.07	0.18	0.28
MgO	15.55	15.06	14.77	15.73	16.75
CaO	11.26	11.52	11.12	11.88	10.87
Na_2O	2.23	2.11	1.95	1.37	1.36
K_2O	0.54	0.64	0.62	0.49	0.32
P_2O_5	0.00	0.00	0.00	0.00	0.25
Total	97.91	97.04	97.02	97.39	98.58
Classification	Prg Hbl	Prg Hbl	F Prg Hbl	M Hbl	M Hbl

Table B2.4. Microprobe analyses of micas from all Late Devonian mafic intrusions.

Intrusion	ATT	ATT	ATT	BIR	BIR	BIR	BIR	BIR	BIR	BIR
Mineral	Bt	Bt	Bt	Bt	Bt	Bt	Bt	Bt	Bt	Bt
Location	R	-	-	C	C	R	R	R	C	C
SiO_2	38.16	38.20	37.86	37.98	37.74	39.11	39.07	39.40	38.74	39.28
TiO_2	1.79	2.28	1.95	2.73	3.08	1.45	2.42	1.72	2.76	2.17
Al_2O_3	16.23	15.25	15.53	15.38	15.70	16.83	15.88	16.15	15.79	16.41
FeO	15.73	13.85	14.42	16.74	16.08	13.30	12.72	12.49	12.49	12.23
MnO	0.10	0.01	0.00	0.55	0.55	0.17	0.08	0.07	0.10	0.11
MgO	15.19	16.01	16.31	12.34	12.36	14.73	16.67	16.70	16.78	16.97
CaO	0.12	0.00	0.06	0.05	0.02	0.04	0.11	0.10	0.13	0.02
Na_2O	0.31	0.41	0.70	0.15	0.07	0.16	0.37	0.31	0.43	0.38
K_2O	8.19	8.53	8.23	8.95	9.43	9.22	7.92	7.76	7.91	7.82
P_2O_5	0.00	0.00	0.00	0.00	0.00	0.00	0.00	0.00	0.00	0.00
Total	95.82	94.53	95.06	94.87	95.03	95.01	95.24	94.70	95.13	95.39
Mg/(Mg+Fe)	0.63	0.67	0.67	0.57	0.58	0.66	0.70	0.70	0.71	0.71

Intrusion	BIR	BIR	BIR	BIR	BIR	BIR	BIR	BIR	BIR	BIR
Mineral	Bt	Bt	Bt	Bt	Bt	Bt	Bt	Bt	Bt	Bt
Location	R	R	C	C	C	R	R	C	C	R
SiO_2	39.52	38.98	39.37	38.32	39.60	39.35	39.30	37.97	38.68	38.13
TiO_2	2.54	2.04	2.30	2.23	1.97	1.59	2.10	1.80	1.93	1.86
Al_2O_3	15.96	15.66	15.62	15.80	15.95	15.76	15.81	16.39	16.69	16.57
FeO	11.56	11.57	11.91	12.31	11.77	12.57	11.69	13.88	14.49	14.53
MnO	0.12	0.14	0.13	0.08	0.13	0.08	0.16	0.18	0.16	0.19
MgO	16.98	17.08	17.10	17.29	17.43	17.48	17.51	14.55	14.49	14.64
CaO	0.09	0.06	0.01	0.13	0.10	0.17	0.02	0.04	0.04	0.06
Na_2O	0.31	0.41	0.39	0.24	0.35	0.35	0.34	0.34	0.21	0.38
K_2O	8.24	7.63	7.92	7.91	8.47	7.67	8.15	7.87	6.42	8.55
P_2O_5	0.00	0.00	0.00	0.00	0.00	0.00	0.00	0.00	0.00	0.00
Total	95.32	93.57	94.75	94.31	95.77	95.02	95.08	93.02	93.10	94.91
Mg/(Mg+Fe)	0.72	0.72	0.72	0.71	0.73	0.71	0.73	0.65	0.64	0.64

Table B2.4. (Concluded) Microprobe analyses of micas from all Late Devonian mafic intrusions.

Intrusion	FOR	FOR	FOR	MCL	MCL	MCL	MCL	MCL	MCL	MCL
Mineral	Bt	Bt	Bt	Bt	Bt	Bt	Bt	Bt	Bt	Bt
Location	C	C	R	C	C	C	C	R	R	R
SiO_2	37.67	38.68	38.13	38.06	37.59	39.43	38.63	39.05	37.65	38.95
TiO_2	1.80	1.93	1.86	1.44	1.33	1.49	1.67	1.34	1.47	1.86
Al_2O_3	16.39	16.69	16.57	17.09	17.76	17.29	16.67	17.20	17.19	16.80
FeO	13.88	14.49	14.53	15.13	13.70	13.32	13.25	13.24	14.39	14.04
MnO	0.18	0.16	0.19	0.13	0.16	0.16	0.19	0.10	0.11	0.16
MgO	14.55	14.49	14.64	12.36	13.52	14.34	14.71	14.91	12.17	13.79
CaO	0.04	0.04	0.06	0.00	0.07	0.04	0.13	0.05	0.09	0.02
Na_2O	0.34	0.21	0.38	0.34	0.25	0.19	0.24	0.22	0.28	0.19
K_2O	7.87	6.42	8.59	8.99	8.76	8.99	9.26	9.64	9.73	8.58
P_2O_5	0.00	0.00	0.00	0.00	0.00	0.00	0.00	0.00	0.00	0.00
Total	92.72	93.11	94.95	93.54	93.14	95.25	94.75	95.75	93.08	94.39
Mg/(Mg+Fe)	0.65	0.64	0.64	0.59	0.64	0.66	0.66	0.67	0.60	0.64

Intrusion	MCL	MER	MER	MER	MER	POP
Mineral	Bt	Phl	Phl	Phl	Phl	Phl
Location	R	C	C	C	R	-
SiO_2	40.83	38.57	38.35	37.96	38.72	36.91
TiO_2	0.58	2.56	2.47	2.33	2.20	3.62
Al_2O_3	18.26	15.97	16.49	16.68	16.44	14.14
FeO	13.35	7.48	7.94	6.97	6.79	17.89
MnO	0.23	0.05	0.10	0.10	0.08	0.43
MgO	12.92	21.20	20.91	20.64	22.38	13.37
CaO	0.25	0.04	0.00	0.07	0.00	0.00
Na_2O	1.19	1.19	0.94	0.81	1.28	0.31
K_2O	8.42	7.95	7.93	7.47	8.02	8.91
P_2O_5	0.00	0.00	0.00	0.00	0.00	0.00
Total	96.03	95.01	95.13	93.03	95.91	95.58
Mg/(Mg+Fe)	0.63	0.83	0.82	0.84	0.85	0.57

Table B2.5. Microprobe analyses of plagioclase from all Late Devonian mafic intrusions.

Intrusion	ATT	ATT	ATT	ATT	BIR	BIR	BIR	BIR	BIR	EAS
Mineral	Pl	Pl	Pl	Pl	Pl	Pl	Pl	Pl	Pl	Pl
Location	-	M	C	R	C	R	R	C	R	C
SiO_2	52.43	57.20	54.36	55.51	57.24	58.47	58.34	58.90	58.76	48.28
TiO_2	0.00	0.00	0.02	0.00	0.21	0.21	0.21	0.05	0.17	0.09
Al_2O_3	29.91	26.81	29.11	29.01	26.76	25.68	26.77	26.87	26.56	31.94
FeO	0.00	0.23	0.02	0.19	0.06	0.15	0.06	0.07	0.15	0.38
MnO	0.00	0.00	0.00	0.00	0.20	0.17	0.19	0.06	0.00	0.00
MgO	0.13	0.00	0.04	0.00	0.09	0.09	0.09	0.00	0.10	0.25
CaO	12.66	8.98	11.48	10.98	9.21	8.37	9.20	8.57	8.40	15.54
Na_2O	4.52	6.45	5.40	5.61	6.99	7.37	6.96	6.67	6.86	2.48
K_2O	0.99	0.16	0.00	0.00	0.07	0.11	0.07	0.08	0.11	0.05
P_2O_5	0.00	0.00	0.00	0.00	0.00	0.00	0.00	0.00	0.00	0.00
Total	100.64	99.83	100.43	101.30	100.83	100.62	101.89	101.28	101.09	99.01
Ab	36.85	55.52	45.80	47.71	56.82	60.00	56.73	57.96	58.23	21.58
An	57.84	43.57	54.20	52.29	42.81	39.41	42.89	41.58	41.16	78.13
Or	5.31	0.91	0.00	0.00	0.37	0.59	0.38	0.46	0.61	0.29

Intrusion	EAS	EAS	EAS	EAS	EAS	EAS	EAS	FOR	FOR	MCL
Mineral	Pl	Pl	Pl	Pl	Pl	Pl	Pl	Pl	Pl	Pl
Location	C	C	R	R	R	R	R	C	R	C
SiO_2	65.53	52.93	57.49	64.84	57.59	61.37	54.95	58.90	58.76	65.60
TiO_2	0.00	0.00	0.07	0.05	0.00	0.01	0.00	0.05	0.17	0.08
Al_2O_3	22.24	29.37	26.27	22.64	26.51	23.95	28.27	26.87	26.56	22.91
FeO	0.36	0.22	0.08	0.27	0.21	0.07	0.24	0.07	0.15	0.00
MnO	0.00	0.00	0.00	0.00	0.00	0.07	0.13	0.06	0.00	0.00
MgO	0.06	0.07	0.00	0.06	0.09	0.00	0.02	0.00	0.10	0.10
CaO	2.95	12.22	8.58	3.69	8.49	5.55	10.43	8.57	8.40	3.80
Na_2O	8.85	4.47	6.02	8.07	6.14	7.34	5.28	6.67	6.86	8.21
K_2O	0.94	0.17	0.29	0.68	0.23	0.35	0.19	0.08	0.11	0.04
P_2O_5	0.00	0.00	0.02	0.00	0.03	0.00	0.00	0.00	0.00	0.00
Total	100.93	99.45	98.82	100.30	99.29	98.71	99.51	101.27	101.11	100.74
Ab	78.32	38.91	54.66	75.14	55.10	68.78	46.78	57.75	58.23	78.61
An	16.21	60.12	43.61	20.69	43.54	29.06	52.11	41.79	41.16	21.14
Or	5.47	0.97	1.73	4.17	1.36	2.16	1.11	0.46	0.61	0.25

Table B2.5. (Continued) Microprobe analyses of plagioclase from all Late Devonian mafic intrusions.

Intrusion	MCL	MCL	MCL	MCL	MCL	MCL	MCL	MER	MER	MER
Mineral	Pl	Pl	Pl	Pl	Pl	Pl	Pl	Pl	Pl	Pl
Location	C	C	C	R	R	R	R	C	C	R
SiO_2	64.77	60.03	70.32	65.28	59.77	62.76	60 58	54.10	47.55	54.37
TiO_2	0.00	0.02	0.00	0.00	0.00	0.04	0.00	0.00	0.05	0.06
Al_2O_3	22.59	25.94	20.11	22.46	24.92	23.34	25.11	29.15	33.47	28.67
FeO	0.07	0.17	0.00	0.03	0.01	0.06	0.00	0.18	0.33	0.36
MnO	0.00	0.00	0.05	0.00	0.00	0.00	0.01	0.06	0.00	0.03
MgO	0.01	0.09	0.00	0.00	0.12	0.06	0.06	0.01	0.10	0.01
CaO	3.75	7.27	0.32	3.36	6.35	4.70	6.62	11.59	17.02	11.40
Na_2O	8.23	7.40	8.55	8.05	6.87	8.73	7.43	5.36	2.28	5.35
K_2O	0.04	0.14	0.29	0.04	0.06	0.12	0.19	0.09	0.07	0.07
P_2O_5	0.00	0.00	0.00	0.00	0.00	0.00	0.00	0.00	0.00	0.00
Total	99.46	101.06	99.64	99.22	98.10	99.81	100.00	100.54	100.87	100.31
Ab	79.39	63.46	95.88	80.94	65.33	75.95	65.99	45.01	19.05	45.02
An	20.36	35.75	1.98	18.80	34.29	23.36	32.90	54.49	80.57	54.59
Or	0.25	0.79	2.14	0.26	0.38	0.69	1.11	0.50	0.38	0.39

Intrusion	OVE	OVE	SOB	SOB	SOB	SOB	MCL	MCL	MCL	MCL
Mineral	Pl	Pl	Pl	Pl	Pl	Pl	Kfs	Kfs	Kfs	Kfs
Location	C	R	C	R	R	R	C	C	C	R
SiO_2	67.80	67.70	59.57	51.19	57.37	62.48	66.02	65.96	62.96	67.43
TiO_2	0.00	0.00	0.00	0.04	0.02	0.02	0.00	0.00	0.00	0.04
Al_2O_3	20.69	21.09	25.41	30.77	26.60	22.82	18.78	18.43	17.66	19.34
FeO	0.04	0.00	0.19	0.48	0.11	0.06	0.00	0.05	0.17	0.00
MnO	0.01	0.00	0.00	0.00	0.00	0.00	0.00	0.01	0.05	0.00
MgO	0.17	0.03	0.10	0.05	0.08	0.00	0.05	0.00	0.00	0.00
CaO	1.18	1.50	6.98	13.31	8.40	4.56	0.07	0.03	0.00	0.11
Na_2O	10.54	9.51	6.98	3.82	6.26	8.05	0.62	0.47	0.40	2.87
K_2O	0.06	0.01	0.33	0.11	0.30	0.65	14.98	15.05	15.49	10.97
P_2O_5	0.00	0.00	0.08	0.14	0.03	0.00	0.00	0.00	0.00	0.00
Total	100.49	99.84	99.64	99.91	99.17	98.64	100.52	100.00	96.73	100.76
Ab	92.62	91.72	62.24	33.19	55.81	72.97	5.85	4.53	3.75	28.24
An	7.03	8.22	35.82	66.18	42.43	23.15	0.73	0.00	0.69	0.75
Or	0.35	0.06	1.94	0.63	1.76	3.88	93.43	95.47	95.56	71.01

Table B2.5. (Concluded) Microprobe analyses of plagioclase from all Late Devonian mafic intrusions.

Intrusion	POP	POP
Mineral	Kfs	Kfs
Location	R	R
SiO_2	64.30	66.09
TiO_2	0.25	0.26
Al_2O_3	18.01	18.59
FeO	0.45	0.21
MnO	0.22	0.19
MgO	0.41	0.08
CaO	0.00	0.01
Na_2O	0.32	0.39
K_2O	15.20	15.86
P_2O_5	0.00	0.00
Total	99.16	101.68
Ab	2.93	3.52
An	5.56	2.34
Or	91.51	94.14

B-3. Geochemical Data for the Late Devonian Mafic Intrusions

Whole-rock geochemical analyses generated for the Late Devonian mafic intrusions (LDMIs) by this and other studies appear in Table B3.1; Appendices A-5 to A-7 contain the sample preparation and analytical procedures for analyses determined by this thesis. To encompass the variable reporting of recalculated and unrecalculated analyses by previous workers in the current LDMI database, all data were recast to 100% volatile-free with total iron as FeO for comparative purposes. The inclusion of loss on ignition (LOI) values allow subsequent workers to retrieve unrecalculated analyses. All CIPW norms were calculated after the volatile-free recalculation using the CIPWNORM program for Microsoft® Windows 3.1™ (Tate, unpublished) assuming $Fe_2O_3/FeO = 0.23$ (the average of wet chemical analyses for ferric and ferrous iron in the Attwoods Brook, Birchtown, and Mersey Point bodies by de Albuquerque (1979)); Mg-numbers were also calculated from 100(MgO/(MgO+FeOT)) after the volatile-free recalculation. Σ_7REE = the sum of La, Ce, Nd, Sm, Eu, Yb, and Lu; ΣREE = the sum of all 14 REE. εNd, εSr, T_{CHUR}, and T_{DM} were calculated from the whole-rock $^{143}Nd/^{144}Nd$, $^{147}Sm/^{144}Nd$, and $^{87}Sr/^{86}Sr$ ratios following the methods of DePaolo (1988) and Michard et al. (1985) and the initial $^{87}Sr/^{86}Sr$ ratios were recalculated assuming t = 370 Ma ages for all LDMIs. Values for $^{87}Rb/^{86}Sr$ were calculated from the whole-rock Rb and Sr abundances. Abbreviations as in Appendix B-2. Normative mineral abbreviations after Kretz (1983). Sources of data: 1 = Tate (this study), 2 = de Albuquerque (1979), 3 = Clarke et al. (1993a), 4 = Kempster (1988), 5 = Douma (1988), 6 = Hall (1979), 7 = Eberz et al. (1991). The maps in Appendix B-1 show locations for samples collected by this study.

Table B3.1. Whole-rock geochemistry for the Late Devonian mafic intrusions.

Sample	ATT-20	DEA-ATT1	DEA-ATT2	DEA-ATT3	DEA-ATT4	GGATT2
Intrusion	ATT	ATT	ATT	ATT	ATT	ATT
Source	1	2	2	2	2	1
Major oxides						
SiO_2	54.30	52.76	53.22	51.14	53.53	51.81
TiO_2	0.55	0.72	0.59	0.98	1.12	1.13
Al_2O_3	18.18	18.59	18.33	17.12	17.07	14.97
Fe_2O_3T	6.10	6.02	6.07	8.26	7.16	7.92
FeOT	5.74	5.49	5.50	7.53	6.52	7.46
MnO	0.12	0.08	0.13	0.13	0.12	0.14
MgO	9.49	7.53	8.15	10.44	8.91	11.01
CaO	8.69	11.15	10.88	9.17	9.05	9.78
Na_2O	2.23	2.91	2.69	2.48	2.97	1.76
K_2O	0.51	0.59	0.44	0.84	0.56	0.65
P_2O_5	0.18	0.18	0.06	0.16	0.14	1.30
Total	100.00	100.00	100.00	100.00	100.00	100.00
LOI	2.50	0.73	0.81	1.29	1.26	2.00
Mg-number	62.31	57.83	59.71	58.10	57.74	59.61
CIPW norms						
Qtz	6.78	3.10	3.10	0.00	3.53	6.13
Crn	0.00	0.00	0.00	0.00	0.00	0.00
Kfs	3.10	3.69	2.68	5.13	3.38	3.96
Ab	19.27	26.04	23.26	21.62	25.75	15.32
An	38.94	37.89	37.39	34.06	32.40	31.94
Di	3.18	13.05	13.71	9.25	10.05	7.35
Hy	25.62	13.89	17.02	24.68	20.53	27.90
Ol	0.00	0.00	0.00	0.82	0.00	0.00
Mag	1.61	0.00	1.54	2.12	1.83	2.10
Ilm	1.08	0.18	1.16	1.92	2.19	2.21
Ap	0.40	0.42	0.14	0.36	0.32	2.92
Trace elements						
Ba	202.00	188.00	167.00	222.00	-	288.00
Rb	10.00	19.00	16.00	29.00	-	10.00
Sr	1235.00	597.00	592.00	472.00	-	1233.00
Y	15.00	18.00	11.00	18.00	-	21.00
Zr	40.00	106.00	102.00	127.00	-	51.00
Nb	5.00	9.50	9.00	11.00	-	10.00
Th	1.20	-	-	-	-	1.47
Pb	10.00	-	-	-	-	10.00
Ga	12.00	-	-	-	-	13.00
Zn	65.00	-	-	-	-	78.00
Cu	25.00	-	-	-	-	34.00
Ni	36.00	-	-	-	-	66.00
V	120.00	-	-	-	-	136.00
Cr	285.00	-	-	-	-	136.00
Hf	1.17	-	-	-	-	1.53
Cs	-	-	-	-	-	-

Sample	ATT-20	DEA-ATT1	DEA-ATT2	DEA-ATT3	DEA-ATT4	GGATT2
Sc	26.72	-	-	-	-	26.06
Ta	0.92	-	-	-	-	1.03
Co	59.21	-	-	-	-	56.10
Li	-	-	-	-	-	-
U	0.61	-	-	-	-	0.66
Rare-earth elements						
La	15.70	11.00	8.00	14.50	-	28.48
Ce	36.82	25.50	21.00	34.50	-	73.16
Pr	-	-	-	-	-	-
Nd	17.09	15.50	8.70	18.00	-	35.87
Sm	3.43	3.30	1.70	3.40	-	6.57
Eu	1.34	1.10	0.63	1.15	-	2.04
Gd	-	-	-	-	-	-
Tb	-	-	-	-	-	-
Dy	-	-	-	-	-	-
Ho	-	-	-	-	-	-
Er	-	-	-	-	-	-
Tm	-	-	-	-	-	-
Yb	0.90	1.60	1.20	2.20	-	1.23
Lu	0.14	0.17	0.27	0.00	-	0.18
Σ_7REE	75.42	58.17	41.50	73.75	-	147.53
ΣREE	-	-	-	-	-	-
Isotope ratios						
$^{87}Rb/^{86}Sr$	0.0228900	-	-	-	-	-
$^{87}Sr/^{86}Sr$	0.70496±3	-	-	-	-	-
$^{87}Sr/^{86}Sr_i$	0.7048400	-	-	-	-	-
$^{147}Sm/^{144}Nd$	0.10924±6	-	-	-	-	-
$^{143}Nd/^{144}Nd$	0.51248±15	-	-	-	-	-
εNd	1.05±0.29	-	-	-	-	-
εSr	11.05	-	-	-	-	-
T_{CHUR}	276±26	-	-	-	-	-
T_{DM}	857±19	-	-	-	-	-

Table B3.1. (Continued) Whole-rock geochemistry for the Late Devonian mafic intrusions.

Sample	GGN7	BIR-2	BIR-20	BIR-21	DEA-BIR1	DEA-BIR2
Intrusion	ATT	BIR	BIR	BIR	BIR	BIR
Source	1	1	1	1	2	2
Major oxides						
SiO_2	53.82	55.79	57.28	55.81	58.74	57.36
TiO_2	0.68	0.78	1.02	0.77	0.84	0.92
Al_2O_3	18.16	10.81	13.98	10.52	13.63	12.89
Fe_2O_3T	6.53	9.01	8.13	9.03	7.58	8.10
FeOT	6.08	8.41	7.54	8.45	6.96	7.45
MnO	0.12	0.17	0.15	0.17	0.11	0.12
MgO	8.08	12.64	8.32	13.12	8.03	8.48
CaO	9.96	7.84	7.30	7.68	6.73	7.51
Na_2O	2.48	1.15	1.73	1.18	2.17	2.14
K_2O	0.53	2.14	2.35	2.04	2.44	2.58
P_2O_5	0.08	0.28	0.33	0.26	0.35	0.54
Total	100.00	100.00	100.00	100.00	100.00	100.00
LOI	1.20	1.60	1.00	1.80	1.48	1.57
Mg-number	57.06	60.05	52.46	60.83	53.57	53.23
CIPW norms						
Qtz	5.65	8.49	12.29	8.24	14.69	12.08
Crn	0.00	0.00	0.00	0.00	0.00	0.00
Kfs	3.20	13.07	14.33	12.46	15.51	16.49
Ab	21.50	10.07	15.09	10.36	19.71	19.54
An	37.72	18.60	24.10	17.95	21.71	19.35
Di	9.76	15.58	8.70	15.53	7.05	11.02
Hy	18.94	29.62	20.59	30.93	18.31	17.81
Ol	0.00	0.00	0.00	0.00	0.00	0.00
Mag	1.70	2.38	2.13	2.39	0.00	0.00
Ilm	1.33	1.53	2.00	1.51	0.25	0.28
Ap	0.19	0.63	0.74	0.59	0.82	1.27
Trace elements						
Ba	198.00	584.00	628.00	555.00	565.00	796.00
Rb	12.00	95.00	104.00	92.00	89.00	107.00
Sr	554.00	187.00	228.00	176.00	202.00	270.00
Y	18.00	20.00	26.00	21.00	20.00	24.00
Zr	58.00	134.00	136.00	131.00	131.00	173.00
Nb	5.00	7.00	9.00	6.00	7.80	13.00
Th	0.86	4.80	5.98	5.64	-	-
Pb	10.00	10.00	10.00	10.00	-	-
Ga	14.00	13.00	12.00	10.00	-	-
Zn	58.00	78.00	65.00	67.00	-	-
Cu	12.00	13.00	8.00	9.00	-	-
Ni	19.00	19.00	10.00	16.00	-	-
V	147.00	200.00	213.00	204.00	-	-
Cr	147.00	877.00	433.00	861.00	-	-
Hf	1.53	3.90	4.16	3.94	-	-
Cs	-	-	-	-	-	-

Sample	GGN7	BIR-2	BIR-20	BIR-21	DEA-BIR1	DEA-BIR2
Sc	33.66	42.75	35.99	44.57	-	-
Ta	0.79	1.52	2.14	1.84	-	-
Co	55.81	92.94	102.40	85.74	-	-
Li	-	-	-	-	-	-
U	0.55	0.60	1.46	1.00	-	-
Rare-earth elements						
La	9.40	11.81	15.88	13.60	19.00	25.00
Ce	23.43	31.07	35.75	32.68	42.00	53.50
Pr	-	-	-	-	-	-
Nd	8.82	31.07	17.14	12.01	23.50	28.50
Sm	2.55	4.26	4.29	3.99	5.10	4.90
Eu	1.05	1.21	1.27	1.15	1.10	1.10
Gd	-	-	-	-	-	-
Tb	-	-	-	-	-	-
Dy	-	-	-	-	-	-
Ho	-	-	-	-	-	-
Er	-	-	-	-	-	-
Tm	-	-	-	-	-	-
Yb	1.49	1.91	2.26	1.94	2.40	2.50
Lu	0.21	0.30	0.30	0.29	0.15	0.35
Σ_7REE	46.95	81.63	76.89	65.66	93.25	115.85
ΣREE	-	-	-	-	-	-
Isotope ratios						
$^{87}Rb/^{86}Sr$	0.0612400	-	1.2896800	-	-	-
$^{87}Sr/^{86}Sr$	0.70463±5	-	0.71189±5	-	-	-
$^{87}Sr/^{86}Sr_i$	0.7043000	-	0.7050900	-	-	-
$^{147}Sm/^{144}Nd$	0.12531±1	-	0.10256±8	-	-	-
$^{143}Nd/^{144}Nd$	0.512594±13	-	0.512599±7	-	-	-
εNd	2.51±0.26	-	3.69±0.13	-	-	-
εSr	3.41	-	14.63	-	-	-
T_{CHUR}	94±27	-	63±11	-	-	-
T_{DM}	820±20	-	658±9	-	-	-

Table B3.1. (Continued) Whole-rock geochemistry for the Late Devonian mafic intrusions.

Sample	DEA-BIR3	BOR-1	DEV-1	L7	L8	JD-3	JD-4
Intrusion	BIR	BOR	DEV	BOG	BOG	EAS	EAS
Source	2	1	1	3	3	4	4
Major oxides							
SiO_2	59.48	54.26	55.95	53.52	53.54	54.56	55.44
TiO_2	0.80	0.73	1.57	1.84	2.39	0.74	0.71
Al_2O_3	12.11	14.55	15.68	20.13	18.90	14.90	15.02
Fe_2O_3T	8.02	8.25	8.67	10.29	10.87	9.56	8.02
FeOT	7.37	7.99	8.53	9.47	9.96	8.60	7.23
MnO	0.11	0.15	0.16	0.39	0.35	0.23	0.18
MgO	8.22	12.25	9.02	4.03	4.04	10.76	10.56
CaO	7.21	7.57	6.45	6.09	6.16	6.07	6.24
Na_2O	2.24	1.04	2.32	2.92	2.89	2.25	2.61
K_2O	2.09	1.27	0.07	1.37	1.50	1.77	2.01
P_2O_5	0.38	0.18	0.23	0.25	0.27	0.12	0.00
Total	100.00	100.00	100.00	100.00	100.00	100.00	100.00
LOI	1.73	5.20	6.60	1.92	1.61	-	-
Mg-number	52.73	60.52	51.40	29.85	28.86	55.58	59.36
CIPW norms							
Qtz	16.59	11.37	16.96	12.35	12.24	5.48	3.94
Crn	0.00	0.00	0.64	3.92	2.46	0.00	0.00
Kfs	13.46	8.17	0.45	8.41	9.20	10.95	12.36
Ab	20.61	9.56	21.44	25.55	25.39	19.89	22.93
An	18.27	33.97	33.37	28.45	28.76	26.45	24.15
Di	14.00	2.72	0.00	0.00	0.00	3.35	6.28
Hy	16.11	31.91	24.66	13.98	13.31	30.13	27.28
Ol	0.00	0.00	0.00	0.00	0.00	0.00	0.00
Mag	0.00	0.00	0.00	2.69	2.83	1.99	1.66
Ilm	0.00	0.35	0.37	3.63	4.72	1.47	1.40
Ap	0.90	0.43	0.55	0.56	0.62	0.27	0.00
Trace elements							
Ba	586.00	1212.11	62.32	336.00	375.00	661.00	835.00
Rb	81.88	22.00	5.00	49.00	53.00	57.00	59.00
Sr	260.00	546.00	609.00	352.00	354.00	335.00	414.00
Y	21.00	19.87	16.64	25.00	25.00	18.00	17.00
Zr	154.00	134.60	156.23	94.00	101.00	93.00	102.00
Nb	8.70	6.60	10.61	14.30	15.00	7.00	7.00
Th	-	5.23	5.76	4.60	4.90	3.00	4.00
Pb	-	10.00	10.00	11.00	12.00	13.00	11.00
Ga	-	15.00	16.00	26.30	25.80	17.00	19.00
Zn	-	76.00	82.00	-	-	120.00	77.00
Cu	-	17.00	14.00	-	-	13.00	28.00
Ni	-	160.00	173.00	14.00	14.00	173.00	198.00
V	-	193.00	170.00	204.00	262.00	225.00	197.00
Cr	-	854.00	529.00	54.00	22.00	811.00	884.00
Hf	-	3.51	4.15	3.00	3.30	-	-
Cs	-	-	-	-	-	-	-

Sample	DEA-BIR3	BOR-1	DEV-1	L7	L8	JD-3	JD-4
Sc	-	-	-	30.60	30.60	-	-
Ta	-	0.50	0.65	1.10	1.20	-	-
Co	-	-	-	28.00	29.40	-	-
Li	-	-	-	40.20	37.60	-	-
U	-	-	-	1.80	1.36	-	-
Rare-earth elements							
La	21.50	26.15	20.53	19.90	22.06	13.00	14.00
Ce	48.00	60.91	43.29	45.67	54.18	27.00	29.00
Pr	-	7.95	5.25	-	-	3.00	3.00
Nd	25.50	32.10	20.73	25.14	30.65	13.00	14.00
Sm	4.60	5.97	4.42	4.93	6.39	3.00	3.00
Eu	1.00	1.72	1.46	2.26	1.99	1.00	1.00
Gd	-	4.97	4.20	-	-	4.00	3.00
Tb	-	0.60	0.57	0.70	0.80	0.00	0.00
Dy	-	3.97	3.63	-	-	3.00	3.00
Ho	-	0.78	0.67	-	-	1.00	1.00
Er	-	2.14	1.77	-	-	2.00	2.00
Tm	-	0.30	0.26	-	-	0.00	0.00
Yb	1.80	2.05	1.63	2.32	2.23	-	-
Lu	0.25	0.31	0.26	0.37	0.35	-	-
Σ_7REE	102.65	-	-	100.59	117.85	-	-
ΣREE	-	149.92	108.67	-	-	-	-
Isotope ratios							
$^{87}Rb/^{86}Sr$	-	-	-	0.39358	0.42331	-	-
$^{87}Sr/^{86}Sr$	-	-	-	0.70997	0.70833	-	-
$^{87}Sr/^{86}Sr_i$	-	-	-	0.7079	0.706	-	-
$^{147}Sm/^{144}Nd$	-	-	-	0.1175	0.13736	-	-
$^{143}Nd/^{144}Nd$	-	-	-	0.512223	0.512352	-	-
εNd	-	-	-	-4.36	-2.78	-	-
εSr	-	-	-	54.43	27.49	-	-
T_{CHUR}	-	-	-	800	736	-	-
T_{DM}	-	-	-	1298	1370	-	-

Table B3.1. (Continued) Whole-rock geochemistry for the Late Devonian mafic intrusions.

Sample	JD-5	JD-6	JD-7	NPM612	NPM615	LIT-1	LIT-3
Intrusion	EAS	EAS	EAS	FOR	FOR	LIT	LIT
Source	4	4	4	5	5	1	1
Major oxides							
SiO_2	55.14	55.00	53.47	48.53	53.58	54.08	56.25
TiO_2	0.71	0.71	0.68	1.13	1.11	0.58	0.65
Al_2O_3	14.85	15.37	14.71	11.24	12.37	15.13	16.42
Fe_2O_3T	8.03	8.78	8.51	10.01	8.03	8.37	7.75
FeOT	7.23	7.90	7.67	9.45	7.44	7.91	7.34
MnO	0.15	0.23	0.15	0.16	0.22	0.16	0.24
MgO	10.75	10.59	11.49	16.41	10.35	11.28	9.74
CaO	7.20	5.69	8.00	7.02	11.13	8.31	5.16
Na_2O	2.35	2.03	2.44	1.06	2.45	1.47	2.02
K_2O	1.50	2.37	1.38	4.21	0.69	0.98	2.05
P_2O_5	0.13	0.11	0.00	0.79	0.66	0.11	0.12
Total	100.00	100.00	100.00	100.00	100.00	100.00	100.00
LOI	-	-	-	2.50	1.50	3.30	4.30
Mg-number	59.79	57.27	59.97	63.46	58.18	58.78	57.03
CIPW norms							
Qtz	5.60	5.56	1.52	0.00	4.45	7.63	9.85
Crn	0.00	0.00	0.00	0.00	0.00	0.00	1.78
Kfs	9.21	14.61	8.50	25.87	4.21	5.97	12.52
Ab	20.61	17.88	21.49	9.31	21.35	12.84	17.61
An	26.49	26.86	26.09	13.96	21.32	32.79	25.62
Di	7.63	1.43	11.96	13.29	24.51	7.18	0.00
Hy	27.08	30.16	27.32	6.84	18.32	29.97	28.99
Ol	0.00	0.00	0.00	23.91	0.00	0.00	0.00
Mag	1.66	1.82	1.77	2.69	2.10	2.23	2.07
Ilm	1.40	1.41	1.35	2.24	2.18	1.13	1.28
Ap	0.29	0.25	0.00	1.79	1.48	0.24	0.26
Trace elements							
Ba	369.00	798.00	323.00	816.66	394.00	279.00	527.00
Rb	42.00	81.00	35.00	167.00	19.00	22.00	42.00
Sr	361.00	295.00	379.00	420.00	598.00	260.00	294.00
Y	18.00	18.00	18.00	21.00	28.00	17.00	18.00
Zr	97.00	88.00	88.00	135.00	248.00	72.00	88.00
Nb	6.00	6.00	6.00	12.00	18.00	5.00	5.00
Th	3.00	3.00	3.00	4.00	3.00	3.78	2.55
Pb	8.00	43.00	11.00	7.00	2.00	10.00	16.00
Ga	14.00	14.00	15.00	16.00	15.00	12.00	11.00
Zn	70.00	113.00	75.00	89.00	110.00	68.00	96.00
Cu	48.00	14.00	21.00	38.00	16.00	28.00	31.00
Ni	204.00	139.00	209.00	79.00	22.00	212.00	180.00
V	166.00	233.00	186.00	181.00	240.00	203.00	178.00
Cr	843.00	769.00	971.00	957.00	1046.00	820.00	601.00
Hf	-	-	-	3.95	-	2.44	2.06
Cs	-	-	-	-	-	-	-

Sample	JD-5	JD-6	JD-7	NPM612	NPM615	LIT-1	LIT-3
Sc	-	-	-	-	-	24.07	28.46
Ta	-	-	-	0.53	-	0.45	0.67
Co	-	-	-	-	-	43.94	70.39
Li	-	-	-	-	-	-	-
U	-	-	-	0.00	-	1.00	0.60
Rare-earth elements							
La	13.00	12.00	14.00	-	-	12.00	16.71
Ce	27.00	24.00	28.00	60.79	-	25.92	32.05
Pr	3.00	3.00	3.00	-	-	-	-
Nd	13.00	12.00	14.00	33.52	-	11.81	16.82
Sm	3.00	3.00	3.00	6.52	-	2.71	3.02
Eu	1.00	1.00	1.00	1.82	-	0.86	0.98
Gd	3.00	3.00	3.00	5.01	-	-	-
Tb	0.00	0.00	0.00	0.70	-	-	-
Dy	3.00	3.00	3.00	-	-	-	-
Ho	1.00	1.00	1.00	-	-	-	-
Er	2.00	2.00	2.00	-	-	-	-
Tm	0.00	0.00	0.00	-	-	-	-
Yb	-	-	-	1.68	-	1.59	1.47
Lu	-	-	-	0.24	-	0.22	0.22
Σ_7REE	-	-	-	71.75	-	55.11	71.27
ΣREE	-	-	-	-	-	-	-
Isotope ratios							
$^{87}Rb/^{86}Sr$	-	-	-	1.12421	-	-	0.40391
$^{87}Sr/^{86}Sr$	-	-	-	0.70989±2	-	-	0.7071±2
$^{87}Sr/^{86}Sr_i$	-	-	-	0.70509	-	-	0.70487
$^{147}Sm/^{144}Nd$	-	-	-	0.1244±7	-	-	0.12397±1
$^{143}Nd/^{144}Nd$	-	-	-	.512414±7	-	-	512536±13
εNd	-	-	-	-0.96±0.17	-	-	1.44±0.26
εSr	-	-	-	-1.33	-	-	11.46
T_{CHUR}	-	-	-	474±15	-	-	215±28
T_{DM}	-	-	-	1093±11	-	-	899±20

Table B3.1.(Continued) Whole-rock geochemistry for the Late Devonian mafic intrusions.

Sample	LIT-4	NPM485	DEA-MER1	DEA-MER2	DEA-MER3	MER-20	MER-3
Intrusion	LIT	MCL	MER	MER	MER	MER	MER
Source	1	5	2	2	2	1	1
Major oxides							
SiO_2	55.97	53.13	46.64	46.41	45.84	45.65	46.58
TiO_2	0.67	1.25	0.53	0.68	0.51	0.47	0.51
Al_2O_3	16.36	12.34	9.75	11.52	8.99	9.21	10.17
Fe_2O_3T	8.00	7.89	11.44	10.91	11.95	11.81	11.29
FeOT	7.57	7.26	10.44	9.98	10.88	10.89	10.56
MnO	0.14	0.12	0.17	0.17	0.18	0.18	0.19
MgO	9.12	13.27	22.82	21.08	24.50	25.59	23.48
CaO	6.90	6.05	7.49	7.65	7.15	6.58	6.86
Na_2O	1.96	1.32	1.19	1.39	1.07	0.57	0.68
K_2O	1.20	4.39	0.86	0.96	0.77	0.74	0.83
P_2O_5	0.13	0.86	0.12	0.16	0.11	0.12	0.16
Total	100.00	100.00	100.00	100.00	100.00	100.00	100.00
LOI	3.10	1.29	1.43	1.32	1.22	0.50	1.40
Mg-number	54.64	64.64	68.61	67.87	69.25	70.15	68.98
CIPW norms							
Qtz	10.80	0.00	0.00	0.00	0.00	0.00	0.00
Crn	0.00	0.00	0.00	0.00	0.00	0.00	0.00
Kfs	7.31	26.72	5.32	6.31	4.76	4.56	5.13
Ab	17.04	11.48	10.47	13.06	9.48	5.07	5.96
An	33.27	15.19	19.51	24.82	18.20	21.26	23.19
Di	0.93	7.83	14.48	11.15	14.23	9.43	8.87
Hy	26.91	30.11	15.04	17.53	13.45	22.81	26.43
Ol	0.00	2.14	30.87	24.98	35.50	32.53	26.03
Mag	2.13	2.04	2.98	0.00	3.11	3.11	3.01
Ilm	1.32	2.44	1.05	0.40	1.01	0.94	1.01
Ap	0.28	1.93	0.28	0.39	0.25	0.28	0.36
Trace elements							
Ba	464.00	1920.00	462.00	494.00	411.00	492.00	529.00
Rb	24.00	132.00	29.00	30.50	25.00	20.00	24.00
Sr	343.00	2567.00	287.00	324.00	273.00	276.00	291.00
Y	21.00	18.84	13.50	11.00	11.00	10.00	13.00
Zr	91.00	420.56	92.00	105.00	8.00	61.00	69.00
Nb	5.00	36.34	7.80	0.80	8.00	5.00	5.00
Th	3.84	-	-	-	-	3.10	3.54
Pb	10.00	-	-	-	-	10.00	14.00
Ga	16.00	19.00	-	-	-	7.00	10.00
Zn	78.00	105.00	-	-	-	74.00	77.00
Cu	27.00	41.00	-	-	-	30.00	28.00
Ni	206.00	194.00	-	-	-	247.00	299.00
V	178.00	144.00	-	-	-	139.00	151.00
Cr	686.00	551.00	-	-	-	1525.00	1630.00
Hf	2.57	8.87	-	-	-	1.64	1.71
Cs	-	-	-	-	-	-	-

Sample	LIT-4	NPM485	DEA-MER1	DEA-MER2	DEA-MER3	MER-20	MER-3
Sc	25.16	-	-	-	-	24.78	25.72
Ta	0.91	-	-	-	-	0.78	0.88
Co	71.53	-	-	-	-	118.80	111.50
Li	-	-	-	-	-	-	-
U	1.66	-	-	-	-	-	0.54
Rare-earth elements							
La	17.05	79.12	16.00	18.00	13.50	13.19	15.01
Ce	32.69	167.60	33.50	43.00	30.00	29.73	32.97
Pr	-	19.29	-	-	-	-	-
Nd	16.48	73.15	13.80	22.50	11.30	10.87	12.00
Sm	3.23	11.55	2.30	3.60	1.85	2.34	2.60
Eu	1.02	3.15	0.70	1.00	0.60	0.73	0.82
Gd	-	7.52	-	-	-	-	-
Tb	-	0.80	-	-	-	-	-
Dy	-	4.33	-	-	-	-	-
Ho	-	0.75	-	-	-	-	-
Er	-	1.92	-	-	-	-	-
Tm	-	0.25	-	-	-	-	-
Yb	1.83	1.59	1.20	1.40	1.10	1.03	1.14
Lu	0.26	0.24	0.00	0.27	0.00	0.17	0.17
Σ_7REE	72.56	72.56	67.50	89.77	58.35	58.06	64.71
ΣREE	-	-	-	-	-	-	-
Isotope ratios							
$^{87}Rb/^{86}Sr$	-	0.14539	-	-	-	-	0.23318
$^{87}Sr/^{86}Sr$	-	0.70446±1	-	-	-	-	0.70637±3
$^{87}Sr/^{86}Sr_i$	-	0.70567	-	-	-	-	0.70514
$^{147}Sm/^{144}Nd$	-	0.09349±1	-	-	-	-	0.11434±2
$^{143}Nd/^{144}Nd$	-	.512566±5	-	-	-	-	512449±26
εNd	-	3.47±0.1	-	-	-	-	0.2±0.51
εSr	-	-5.32	-	-	-	-	15.30
T_{CHUR}	-	107±8	-	-	-	-	351±48
T_{DM}	-	651±6	-	-	-	-	942±37

Table B3.1. (Continued) Whole-rock geochemistry for the Late Devonian mafic intrusions.

Sample	MER-7	AO80087	AO80088	AO80090	AO80092	AO80094	AO80150T
Intrusion	MER	OVE	OVE	OVE	OVE	OVE	OVE
Source	1	6	6	6	6	6	6
Major oxides							
SiO_2	45.67	65.71	64.65	65.07	65.49	63.35	60.01
TiO_2	0.42	0.74	0.73	0.70	0.75	0.59	0.77
Al_2O_3	8.86	16.48	16.53	17.71	17.30	17.11	19.39
Fe_2O_3T	11.79	5.10	5.10	4.50	5.50	4.60	4.80
FeOT	10.94	4.85	4.86	4.24	5.25	4.37	4.96
MnO	0.20	0.06	0.06	0.07	0.07	0.07	0.09
MgO	26.48	2.85	2.86	3.14	3.82	3.06	3.10
CaO	6.03	2.54	3.60	1.68	1.17	5.38	2.87
Na_2O	0.55	5.28	5.19	3.88	3.61	4.22	5.16
K_2O	0.73	1.25	1.26	3.25	2.37	1.58	3.38
P_2O_5	0.12	0.24	0.23	0.26	0.17	0.25	0.28
Total	100.00	100.00	100.00	100.00	100.00	100.00	100.00
LOI	0.70	4.20	3.00	4.25	5.50	6.00	4.00
Mg-number	70.76	37.01	37.05	42.55	42.12	41.18	38.46
CIPW norms							
Qtz	0.00	20.81	17.81	22.22	27.33	17.27	6.31
Crn	0.00	2.45	0.63	5.47	7.22	0.00	2.71
Kfs	4.53	7.52	7.61	19.54	14.30	9.53	20.42
Ab	4.83	45.52	44.76	33.33	31.15	36.33	44.51
An	20.41	11.22	16.69	6.73	4.82	23.40	12.69
Di	7.89	0.00	0.00	0.00	0.00	1.68	0.00
Hy	24.44	9.13	9.18	9.56	11.87	8.82	9.83
Ol	33.64	0.00	0.00	0.00	0.00	0.00	0.00
Mag	3.13	1.35	1.36	1.18	1.47	1.22	1.38
Ilm	0.84	1.43	1.42	1.36	1.46	1.14	1.49
Ap	0.28	0.54	0.52	0.58	0.37	0.56	0.61
Trace elements							
Ba	440.00	-	-	-	-	-	-
Rb	20.00	-	-	-	-	-	-
Sr	257.00	-	-	-	-	-	-
Y	13.00	23.00	18.00	25.00	18.00	16.00	13.00
Zr	42.00	83.00	78.00	75.00	74.00	92.00	74.00
Nb	5.00	-	-	-	-	-	-
Th	0.89	-	-	-	-	-	-
Pb	10.00	-	-	-	-	-	-
Ga	10.00	-	-	-	-	-	-
Zn	77.00	-	-	-	-	-	-
Cu	23.00	-	-	-	-	-	-
Ni	333.00	-	-	-	-	-	-
V	131.00	-	-	-	-	-	-
Cr	1602.00	22.00	22.00	18.00	21.00	21.00	24.00
Hf	1.27	-	-	-	-	-	-
Cs	-	-	-	-	-	-	-

Sample	MER-7	AO80087	AO80088	AO80090	AO80092	AO80094	AO80150T
Sc	23.75	-	-	-	-	-	-
Ta	0.74	-	-	-	-	-	-
Co	117.30	-	-	-	-	-	-
Li	-	-	-	-	-	-	-
U	0.65	-	-	-	-	-	-
Rare-earth elements							
La	11.38	-	-	-	-	-	-
Ce	25.95	-	-	-	-	-	-
Pr	-	-	-	-	-	-	-
Nd	10.68	-	-	-	-	-	-
Sm	2.18	-	-	-	-	-	-
Eu	0.72	-	-	-	-	-	-
Gd	-	-	-	-	-	-	-
Tb	-	-	-	-	-	-	-
Dy	-	-	-	-	-	-	-
Ho	-	-	-	-	-	-	-
Er	-	-	-	-	-	-	-
Tm	-	-	-	-	-	-	-
Yb	0.91	-	-	-	-	-	-
Lu	0.14	-	-	-	-	-	-
Σ_7REE	51.96	-	-	-	-	-	-
ΣREE	-	-	-	-	-	-	-
Isotope ratios							
$^{87}Rb/^{86}Sr$	-	-	-	-	-	-	-
$^{87}Sr/^{86}Sr$	-	-	-	-	-	-	-
$^{87}Sr/^{86}Sr_i$	-	-	-	-	-	-	-
$^{147}Sm/^{144}Nd$	-	-	-	-	-	-	-
$^{143}Nd/^{144}Nd$	-	-	-	-	-	-	-
εNd	-	-	-	-	-	-	-
εSr	-	-	-	-	-	-	-
T_{CHUR}	-	-	-	-	-	-	-
T_{DM}	-	-	-	-	-	-	-

Table B3.1. (Continued) Whole-rock geochemistry for the Late Devonian mafic intrusions.

Sample	OVE-1	OVE-2	AVGE(16)	PLE-1	SID-1	SID-2	SID-3
Intrusion	OVE	OVE	POP	PLE	SOB	SOB	SOB
Source	1	1	7	1	4	4	4
Major oxides							
SiO_2	64.72	65.20	50.52	57.98	54.27	56.40	53.80
TiO_2	0.73	0.73	1.45	0.84	0.83	0.40	0.64
Al_2O_3	18.00	18.31	26.45	16.35	16.17	13.70	15.35
Fe_2O_3T	4.97	4.76	8.42	7.49	8.60	8.89	9.09
FeOT	4.67	4.46	8.73	7.21	7.74	8.00	8.18
MnO	0.08	0.07	0.18	0.14	0.14	0.15	0.15
MgO	2.78	2.86	4.96	6.71	9.50	12.01	10.54
CaO	3.62	2.81	2.50	6.04	6.88	6.15	7.53
Na_2O	3.80	3.48	3.04	1.76	2.76	1.97	2.25
K_2O	1.35	1.81	1.98	2.62	1.60	1.12	1.45
P_2O_5	0.25	0.26	0.10	0.34	0.11	0.10	0.12
Total	100.00	100.00	100.00	100.00	100.00	100.00	100.00
LOI	2.50	2.20	2.24	4.50	-	-	-
Mg-number	37.32	39.07	36.21	48.20	55.10	60.02	56.30
CIPW norms							
Qtz	22.85	25.26	10.55	16.90	3.77	9.57	4.27
Crn	4.29	6.13	0.00	0.46	0.00	0.00	0.00
Kfs	7.99	10.71	8.75	16.70	9.85	6.91	8.95
Ab	32.12	29.41	25.63	16.03	24.29	17.36	19.84
An	16.34	12.26	27.88	29.93	28.07	26.27	28.65
Di	0.00	0.00	2.20	0.00	5.30	3.84	7.50
Hy	14.46	14.25	18.85	18.08	25.03	33.18	27.33
Ol	0.00	0.00	0.00	0.00	0.00	0.00	0.00
Mag	0.00	0.00	3.77	0.00	1.78	1.85	1.89
Ilm	1.39	1.39	1.98	0.32	1.64	0.79	1.27
Ap	0.55	0.57	0.37	0.80	0.25	0.23	0.27
Trace elements							
Ba	485.97	538.21	1053.00	862.58	337.00	320.00	392.00
Rb	39.00	50.00	60.00	78.00	45.00	20.00	29.00
Sr	801.00	659.00	372.00	855.00	464.00	295.00	399.00
Y	16.14	14.55	37.00	20.04	18.00	13.00	12.00
Zr	173.70	152.91	242.00	205.43	97.00	95.00	99.00
Nb	9.79	8.98	20.00	8.13	4.00	4.00	5.00
Th	10.56	9.01	6.71	7.79	4.00	0.00	0.00
Pb	12.00	10.00	16.00	10.00	5.00	0.00	0.00
Ga	20.00	19.00	22.00	18.00	14.00	15.00	17.00
Zn	57.00	60.00	173.00	56.00	56.00	66.00	75.00
Cu	5.00	5.00	22.00	16.00	29.00	40.00	79.00
Ni	9.00	9.00	51.00	69.00	132.00	349.00	248.00
V	93.00	99.00	285.00	152.00	204.00	158.00	168.00
Cr	33.00	39.00	278.00	423.00	526.00	1222.00	726.00
Hf	4.72	3.99	3.05	5.31	-	-	-
Cs	-	-	5.77	-	-	-	-

Sample	OVE-1	OVE-2	AVGE(16)	PLE-1	SID-1	SID-2	SID-3
Sc	-	-	-	-	-	-	-
Ta	1.38	0.94	-	0.67	-	-	-
Co	-	-	-	-	-	-	-
Li	-	-	-	-	-	-	-
U	-	-	-	-	-	-	-
Rare-earth elements							
La	34.45	30.90	23.62	42.00	15.00	-	-
Ce	70.09	66.89	48.56	99.83	29.00	-	-
Pr	8.54	7.55	6.03	13.30	4.00	-	-
Nd	33.43	29.28	23.83	52.96	15.00	-	-
Sm	6.23	5.56	5.52	8.99	3.00	-	-
Eu	1.64	1.51	1.40	2.49	1.00	-	-
Gd	5.08	4.34	5.43	6.46	3.00	-	-
Tb	0.59	0.55	0.95	0.76	0.00	-	-
Dy	3.41	3.25	5.74	4.32	3.00	-	-
Ho	0.65	0.58	1.13	0.78	1.00	-	-
Er	1.69	1.57	3.51	2.15	2.00	-	-
Tm	0.22	0.21	0.52	0.29	0.00	-	-
Yb	1.51	1.35	3.48	1.98	-	-	-
Lu	0.23	0.19	0.54	0.30	-	-	-
Σ_7REE	147.58	135.68	106.95	208.55	-	-	-
ΣREE	167.76	153.72	130.26	236.61	-	-	-
Isotope ratios							
$^{87}Rb/^{86}Sr$	-	-	-	-	-	-	-
$^{87}Sr/^{86}Sr$	-	-	-	-	-	-	-
$^{87}Sr/^{86}Sr_i$	-	-	-	-	-	-	-
$^{147}Sm/^{144}Nd$	-	-	-	-	-	-	-
$^{143}Nd/^{144}Nd$	-	-	-	-	-	-	-
εNd	-	-	-	-	-	-	-
εSr	-	-	-	-	-	-	-
T_{CHUR}	-	-	-	-	-	-	-
T_{DM}	-	-	-	-	-	-	-

Table B3.1. (Concluded) Whole-rock geochemistry for the Late Devonian mafic intrusions.

Sample	L5	L6
Intrusion	TEN	TEN
Source	3	3
Major oxides		
SiO_2	50.36	58.50
TiO_2	0.79	1.19
Al_2O_3	16.87	18.91
Fe_2O_3T	9.28	6.89
FeOT	8.67	6.31
MnO	0.15	0.12
MgO	12.12	3.80
CaO	8.06	5.97
Na_2O	2.21	3.24
K_2O	0.66	1.80
P_2O_5	0.10	0.16
Total	100.00	100.00
LOI	2.23	1.28
Mg-number	58.30	37.59
CIPW norms		
Qtz	0.00	14.52
Crn	0.00	1.49
Kfs	4.06	10.92
Ab	19.30	28.03
An	35.19	28.43
Di	2.69	0.00
Hy	32.38	11.85
Ol	1.40	0.00
Mag	2.45	1.77
Ilm	1.55	2.32
Ap	0.23	0.36
Trace elements		
Ba	167.00	516.00
Rb	18.00	57.00
Sr	273.00	312.00
Y	19.00	22.00
Zr	86.00	129.00
Nb	5.30	9.20
Th	1.60	3.10
Pb	6.00	23.00
Ga	17.30	23.10
Zn	-	-
Cu	-	-
Ni	69.00	11.00
V	146.00	126.00
Cr	260.00	84.00
Hf	2.00	3.20
Cs	-	-

Sample	L5	L6
Sc	22.80	25.20
Ta	0.40	0.60
Co	45.00	18.80
Li	27.50	47.50
U	0.47	1.56
Rare-earth elements		
La	7.01	17.50
Ce	16.65	41.55
Pr	-	-
Nd	11.81	27.65
Sm	2.90	4.74
Eu	0.92	1.31
Gd	-	-
Tb	0.48	0.60
Dy	-	-
Ho	-	-
Er	-	-
Tm	-	-
Yb	1.82	1.94
Lu	0.29	0.30
Σ_7REE	41.40	94.99
ΣREE	-	-
Isotope ratios		
$^{87}Rb/^{86}Sr$	0.18642	0.51654
$^{87}Sr/^{86}Sr$	0.70547	0.70707
$^{87}Sr/^{86}Sr_i$	0.70439	0.70435
$^{147}Sm/^{144}Nd$	0.1526	0.13479
$^{143}Nd/^{144}Nd$	0.512654	0.512512
εNd	2.39	0.46
εSr	4.60	4.04
T_{CHUR}	56	311
T_{DM}	1010	1052

B-4. Geochemical Data for the Ordovician, Silurian, and Jurassic Mafic Intrusions

Table B4.1 contains a comprehensive database of whole-rock geochemical analyses from the Ordovician(?), Early Silurian, and Early Jurassic mafic intrusions in the Meguma Zone for comparison with those of the LDMIs. Appendix B-3 describes the recalculation procedures and conventions, and see Table B3.1 for the abbreviations. Other abbreviations: AUX = Nictaux Falls dykes, BEA = Bear River dykes and sills, TOR = Torbrook dykes and sills, WOL = Wolfville area dykes and sills, NIC = Nickersons Point gabbro, SHE = Shelburne dyke, MAR = Marshdale intrusive, WED = Wedgeport lamrprophyre dykes, LOW = Lower Palmer Lake diabase. Normative mineral abbreviations after Kretz (1983); Ord = Ordovician(?), Sil = Early Silurian, Jur = Early Jurassic. Sources of Data: 1 = Tate (this study), 2 = Barr et al. (1983), 3 = Kempster (1988), 4 = Calder and Barr (1982), 5 = Papezic and Barr (1981), 6 = Cullen (1983).

Table B4.1. Whole-rock geochemistry for the Ordovician(?), Early Silurian, and Early Jurassic mafic intrusions.

Sample	AUX-3	BEA-I	BEA-II	LOW-1	LOW-3	LOW-4	MD-3
Intrusion	AUX	BEA	BEA	LOW	LOW	LOW	MAR
Age	Sil	Ord	Ord	Sil	Sil	Sil	Jur
Source	1	2	2	1	1	1	3
Major elements							
SiO_2	57.06	50.93	49.90	50.46	51.90	50.93	49.36
TiO_2	1.20	1.98	2.11	1.71	1.86	1.87	2.21
Al_2O_3	18.00	16.24	16.18	14.26	14.77	15.44	17.16
Fe_2O_3T	8.11	11.00	11.10	14.08	12.64	12.58	12.77
FeOT	7.83	10.86	10.56	13.06	11.74	11.67	11.49
MnO	0.17	0.18	0.18	0.20	0.19	0.19	0.16
MgO	4.69	8.12	7.61	8.72	6.84	6.89	6.79
CaO	7.32	7.79	8.77	9.21	9.95	10.16	8.99
Na_2O	2.53	2.96	3.59	1.93	2.30	2.35	3.49
K_2O	1.04	0.55	0.74	0.26	0.23	0.29	0.22
P_2O_5	0.16	0.38	0.35	0.20	0.22	0.22	0.14
Total	100.00	100.00	100.00	100.00	100.00	100.00	100.00
LOI	5.60	7.60	4.80	0.40	0.50	0.70	-
Mg-number	37.44	50.92	49.29	52.69	46.64	46.79	46.44
CIPW norms							
Qtz	15.34	3.81	0.00	7.15	9.16	7.00	1.09
Crn	0.00	0.00	0.00	0.00	0.00	0.00	0.00
Kfs	6.35	3.39	4.57	1.61	1.41	1.79	1.38
Ab	22.07	26.18	31.71	17.18	20.41	20.83	31.34
An	35.76	30.69	26.91	31.08	30.70	32.19	32.37
Di	0.54	5.63	12.79	12.57	15.62	15.31	11.08
Hy	14.99	22.35	13.00	22.74	15.10	15.30	15.23
Ol	0.00	0.00	2.98	0.00	0.00	0.00	0.00
Mag	2.21	3.10	3.01	3.77	3.37	3.35	2.70
Ilm	2.36	3.92	4.19	3.43	3.70	3.72	4.46
Ap	0.36	0.88	0.79	0.45	0.50	0.50	0.32
Trace elements							
Ba	208.00	341.00	566.00	108.00	128.00	218.00	87.00
Rb	39.00	24.00	24.00	5.00	5.00	9.00	3.00
Sr	351.00	472.00	553.00	258.00	312.00	365.00	557.00
Y	37.00	33.00	30.00	27.00	31.00	26.00	11.00
Zr	164.00	182.00	169.00	115.00	131.00	130.00	53.00
Nb	7.00	20.00	18.00	10.00	10.00	12.00	4.00
Th	4.48	-	-	1.82	1.61	1.19	0.00
Pb	15.00	-	-	10.00	10.00	10.00	5.00
Ga	15.00	-	-	21.00	19.00	18.00	20.00
Zn	128.00	-	-	126.00	110.00	106.00	133.00
Cu	5.00	-	-	30.00	28.00	63.00	65.00

Sample	AUX-3	BEA-I	BEA-II	LOW-1	LOW-3	LOW-4	MD-3
Ni	5.00	-	-	147.00	47.00	97.00	165.00
V	213.00	-	-	226.00	270.00	243.00	168.00
Cr	80.00	-	-	514.00	254.00	492.00	159.00
Hf	4.59	-	-	3.48	3.50	2.95	-
Cs	-	-	-	-	-	-	-
Sc	26.63	-	-	27.04	30.77	26.19	-
Ta	1.20	-	-	1.78	1.29	1.13	-
Co	48.39	-	-	79.21	74.35	88.98	-
Li	-	-	-	-	-	-	-
U	1.66	-	-	0.57	0.82	0.67	-
Rare-earth elements							
La	21.42	-	-	11.79	13.32	13.91	4.00
Ce	52.84	-	-	30.07	35.08	34.13	10.00
Pr	-	-	-	-	-	-	2.00
Nd	24.51	-	-	15.89	17.65	17.98	8.00
Sm	5.41	-	-	4.29	4.71	4.65	3.00
Eu	1.69	-	-	1.48	1.63	1.59	1.00
Gd	-	-	-	-	-	-	2.00
Tb	-	-	-	-	-	-	0.00
Dy	-	-	-	-	-	-	2.00
Ho	-	-	-	-	-	-	0.00
Er	-	-	-	-	-	-	1.00
Tm	-	-	-	-	-	-	0.00
Yb	3.28	-	-	1.96	2.04	1.86	-
Lu	0.46	-	-	0.26	0.31	0.26	-
Σ_7REE	109.61	-	-	65.74	74.74	74.38	-
ΣREE	-	-	-	-	-	-	-

Table B4.1. (Continued) Whole-rock geochemistry for the Ordovician(?), Early Silurian, and Early Jurassic mafic intrusions.

Sample	MD-4	MD-5	MD-6	MD-7	MAV1	MAV10	MAV11
Intrusion	MAR	MAR	MAR	MAR	MAV	MAV	MAV
Age	Jur	Jur	Jur	Jur	Sil	Sil	Sil
Source	3	3	3	3	4	4	4
Major elements							
SiO_2	49.03	50.69	48.86	49.81	46.83	48.47	47.04
TiO_2	2.78	3.72	2.92	2.17	3.67	3.53	2.85
Al_2O_3	15.18	13.65	15.03	17.14	13.88	13.10	16.80
Fe_2O_3T	14.44	15.69	14.75	13.10	16.50	15.90	14.90
FeOT	12.99	14.12	13.27	11.79	15.15	14.42	13.65
MnO	0.17	0.20	0.17	0.15	0.26	0.23	0.19
MgO	7.48	4.87	6.96	6.82	5.00	4.84	4.79
CaO	8.61	7.88	8.97	7.95	9.79	8.77	9.27
Na_2O	3.33	4.21	3.41	3.63	3.47	4.64	3.67
K_2O	0.27	0.37	0.26	0.43	1.22	1.31	1.12
P_2O_5	0.16	0.29	0.16	0.11	0.73	0.71	0.62
Total	100.00	100.00	100.00	100.00	100.00	100.00	100.00
LOI	-	-	-	-	1.30	1.00	1.70
Mg-number	48.86	38.34	47.06	46.55	38.97	38.19	37.94
CIPW norms							
Qtz	2.10	5.67	2.10	1.15	0.00	0.00	0.00
Crn	0.00	0.00	0.00	0.00	0.00	0.00	0.00
Kfs	1.71	2.36	1.65	2.71	7.71	8.22	7.01
Ab	30.15	38.35	30.92	32.65	31.19	37.77	32.76
An	27.47	18.57	26.72	31.04	19.84	11.72	27.54
Di	13.52	16.91	15.67	8.04	21.37	23.56	13.45
Hy	15.92	6.43	13.44	16.98	4.64	0.00	2.26
Ol	0.00	0.00	0.00	0.00	1.62	3.67	5.80
Mag	3.08	3.37	3.15	2.78	4.41	4.18	3.95
Ilm	5.66	7.62	5.95	4.39	7.43	7.11	5.73
Ap	0.37	0.68	0.37	0.26	1.71	1.63	1.43
Trace elements							
Ba	66.00	152.00	94.00	61.00	-	505.00	342.00
Rb	8.00	4.00	6.00	10.00	31.00	23.00	17.00
Sr	443.00	458.00	479.00	469.00	-	-	-
Y	10.00	24.00	14.00	8.00	43.00	50.00	30.00
Zr	62.00	99.00	62.00	51.00	200.00	220.00	115.00
Nb	6.00	8.00	5.00	4.00	18.00	20.00	15.00
Th	0.00	1.00	0.00	0.00	-	-	-
Pb	5.00	6.00	4.00	3.00	-	-	-
Ga	22.00	28.00	26.00	23.00	-	-	-
Zn	102.00	102.00	111.00	58.00	-	-	-
Cu	71.00	100.00	98.00	44.00	-	-	-

Sample	MD-4	MD-5	MD-6	MD-7	MAV1	MAV10	MAV11
Ni	188.00	29.00	169.00	179.00	39.00	52.00	58.00
V	231.00	264.00	243.00	192.00	-	-	-
Cr	150.00	22.00	112.00	157.00	30.00	13.00	32.00
Hf	-	-	-	-	-	-	-
Cs	-	-	-	-	-	-	-
Sc	-	-	-	-	-	-	-
Ta	-	-	-	-	-	-	-
Co	-	-	-	-	-	-	-
Li	-	-	-	-	-	-	-
U	-	-	-	-	-	-	-
Rare-earth elements							
La	4.00	9.00	5.00	4.00	-	-	-
Ce	11.00	23.00	12.00	9.00	-	-	-
Pr	2.00	4.00	2.00	2.00	-	-	-
Nd	10.00	19.00	10.00	8.00	-	-	-
Sm	3.00	6.00	3.00	3.00	-	-	-
Eu	1.00	3.00	2.00	1.00	-	-	-
Gd	3.00	5.00	3.00	2.00	-	-	-
Tb	0.00	1.00	1.00	0.00	-	-	-
Dy	2.00	4.00	3.00	2.00	-	-	-
Ho	0.00	1.00	1.00	0.00	-	-	-
Er	1.00	2.00	1.00	1.00	-	-	-
Tm	0.00	0.00	0.00	0.00	-	-	-
Yb	-	-	-	-	-	-	-
Lu	-	-	-	-	-	-	-
Σ_7REE	-	-	-	-	-	-	-
ΣREE	-	-	-	-	-	-	-

Table B4.1. (Continued) Whole-rock geochemistry for the Ordovician(?), Early Silurian, and Early Jurassic mafic intrusic

Sample	MAV12	MAV14	MAV15	MAV17	MAV19	MAV2	MAV3
Intrusion	MAV	MAV	MAV	MAV	MAV	MAV	MAV
Age	Sil	Sil	Sil	Sil	Sil	Sil	Sil
Source	4	4	4	4	4	4	4
Major elements							
SiO_2	48.73	52.96	46.11	47.84	48.18	51.59	51.55
TiO_2	3.69	2.85	2.98	2.86	2.97	3.03	2.73
Al_2O_3	14.05	14.06	15.92	16.77	13.50	13.89	13.47
Fe_2O_3T	14.70	14.00	16.00	14.50	15.80	15.20	15.60
FeOT	13.57	13.32	14.79	13.34	14.54	14.28	14.21
MnO	0.26	0.26	0.22	0.19	0.26	0.26	0.27
MgO	4.00	2.43	5.96	4.80	4.30	2.92	2.94
CaO	9.03	6.55	9.24	8.89	9.00	5.85	7.39
Na_2O	4.41	4.65	3.08	3.37	3.68	5.43	4.25
K_2O	1.44	1.80	1.13	1.33	1.84	1.36	2.23
P_2O_5	0.82	1.11	0 58	0.59	1.74	1.39	0.95
Total	100.00	100.00	100.00	100.00	100.00	100.00	100.00
LOI	1.30	5.40	2.10	2.30	1.30	2.30	1.10
Mg-number	33.82	23.69	43.21	38.03	35.43	27.19	27.28
CIPW *norms*							
Qtz	0.00	5.92	0.00	0.00	0.97	2.38	3.04
Crn	0.00	0.00	0.00	0.00	0.00	0.00	0.00
Kfs	8.98	11.22	7.10	8.30	11.56	8.51	13.97
Ab	38.74	41.51	27.67	30.11	33.03	48.66	38.10
An	15.09	12.83	27.87	28.13	15.75	10.06	11.71
Di	21.19	11.30	13.49	11.51	15.79	9.02	16.77
Hy	0.00	4.94	7.33	10.47	8.43	7.73	4.46
Ol	2.30	0.00	4.84	0.44	0.00	0.00	0.00
Mag	3.92	3.84	4.30	3.85	4.22	4.14	4.12
Ilm	7.42	5.73	6.01	5.74	5.98	6.10	5.51
Ap	1.89	2.56	1.33	1.37	4.03	3.21	2.20
Trace elements							
Ba	410.00	605.00	315.00	384.00	502.00		
Rb	23.00	29.00	27.00	30.00	36.00	35.00	42.00
Sr	-	-	-	-	-	-	-
Y	41.00	66.00	31.00	32.00	34.00	64.00	62.00
Zr	220.00	406.00	120.00	130.00	230.00	340.00	310.00
Nb	21.00	28.00	16.00	16.00	22.00	29.00	28.00
Th	-	-	-	-	-	-	-
Pb	-	-	-	-	-	-	-
Ga	-	-	-	-	-	-	-
Zn	-	-	-	-	-	-	-
Cu	-	-	-	-	-	-	-

Sample	MAV12	MAV14	MAV15	MAV17	MAV19	MAV2	MAV3
Ni	50.00	11.00	95.00	111.00	34.00	58.00	32.00
V	-	-	-	-	-	-	-
Cr	18.00	17.00	52.00	28.00	26.00	16.00	32.00
Hf	-	-	-	-	-	-	-
Cs	-	-	-	-	-	-	-
Sc	-	-	-	-	-	-	-
Ta	-	-	-	-	-	-	-
Co	-	-	-	-	-	-	-
Li	-	-	-	-	-	-	-
U	-	-	-	-	-	-	-
Rare-earth elements							
La	-	-	-	-	-	-	-
Ce	-	-	-	-	-	-	-
Pr	-	-	-	-	-	-	-
Nd	-	-	-	-	-	-	-
Sm	-	-	-	-	-	-	-
Eu	-	-	-	-	-	-	-
Gd	-	-	-	-	-	-	-
Tb	-	-	-	-	-	-	-
Dy	-	-	-	-	-	-	-
Ho	-	-	-	-	-	-	-
Er	-	-	-	-	-	-	-
Tm	-	-	-	-	-	-	-
Yb	-	-	-	-	-	-	-
Lu	-	-	-	-	-	-	-
Σ_7REE	-	-	-	-	-	-	-
ΣREE	-	-	-	-	-	-	-

Table B4.1. (Continued) Whole-rock geochemistry for the Ordovician(?), Early Silurian, and Early Jurassic mafic intrusi

Sample	MAV4	MAV5	MAV6	MAV7	MAV8	MAV9	NIC-II
Intrusion	MAV	MAV	MAV	MAV	MAV	MAV	NIC
Age	Sil	Sil	Sil	Sil	Sil	Sil	Sil
Source	4	4	4	4	4	4	2
Major elements							
SiO_2	55.07	51.17	46.31	46.53	64.30	64.08	50.40
TiO_2	2.50	2.70	3.01	4.30	0.71	0.72	1.73
Al_2O_3	15.72	14.22	16.09	12.37	18.04	18.19	15.92
Fe_2O_3T	11.00	13.50	15.30	16.20	3.40	3.30	12.30
FeOT	9.91	12.16	14.29	14.91	3.12	3.07	11.29
MnO	0.22	0.25	0.22	0.24	0.06	0.06	0.22
MgO	1.60	3.20	6.02	5.83	0.41	0.41	7.24
CaO	6.11	8.61	8.72	9.92	0.92	1.03	9.28
Na_2O	5.71	4.81	3.63	3.89	7.95	7.86	2.86
K_2O	2.20	1.70	1.04	1.23	4.38	4.44	0.82
P_2O_5	0.95	1.16	0.65	0.80	0.12	0.12	0.23
Total	100.00	100.00	100.00	100.00	100.00	100.00	100.00
LOI	1.40	1.30	2.20	1.40	1.00	0.80	1.30
Mg-number	16.99	29.04	43.48	42.68	4.95	5.02	48.05
CIPW norms							
Qtz	2.64	0.20	0.00	0.00	0.00	0.00	2.24
Crn	0.00	0.00	0.00	0.00	0.00	0.00	0.00
Kfs	13.56	10.58	6.51	7.72	26.24	26.61	5.05
Ab	50.21	42.69	32.56	31.97	67.13	65.96	25.28
An	11.18	12.79	25.97	13.47	0.57	1.23	29.48
Di	11.30	19.46	12.28	26.33	2.65	2.58	13.65
Hy	1.03	2.57	1.90	0.00	0.00	0.00	17.05
Ol	0.00	0.00	8.97	3.96	0.41	0.41	0.00
Mag	2.82	3.49	4.14	4.33	0.86	0.85	3.23
Ilm	4.95	5.40	6.07	8.67	1.37	1.39	3.45
Ap	2.16	2.66	1.51	1.85	0.27	0.27	0.54
Trace elements							
Ba	-	423.00	445.00	380.00	1292.00	137.50	242.00
Rb	33.00	32.00	23.00	21.00	36.00	31.00	34.00
Sr	-	-	-	-	-	-	474.00
Y	57.00	55.00	32.00	42.00	61.00	75.00	27.00
Zr	380.00	245.00	135.00	200.00	430.00	590.00	138.00
Nb	29.00	25.00	17.00	17.00	28.00	26.00	15.00
Th	-	-	-	-	-	-	-
Pb	-	-	-	-	-	-	-
Ga	-	-	-	-	-	-	-
Zn	-	-	-	-	-	-	-
Cu	-	-	-	-	-	-	-

Sample	MAV4	MAV5	MAV6	MAV7	MAV8	MAV9	NIC-II
Ni	24.00	39.00	76.00	26.00	0.00	0.00	-
V	-	-	-	-	-	-	-
Cr	15.00	22.00	58.00	27.00	19.00	41.00	-
Hf	-	-	-	-	-	-	-
Cs	-	-	-	-	-	-	-
Sc	-	-	-	-	-	-	-
Ta	-	-	-	-	-	-	-
Co	-	-	-	-	-	-	-
Li	-	-	-	-	-	-	-
U	-	-	-	-	-	-	-
Rare-earth elements							
La	-	-	-	-	-	-	16.00
Ce	-	-	-	-	-	-	27.00
Pr	-	-	-	-	-	-	-
Nd	-	-	-	-	-	-	-
Sm	-	-	-	-	-	-	-
Eu	-	-	-	-	-	-	-
Gd	-	-	-	-	-	-	-
Tb	-	-	-	-	-	-	-
Dy	-	-	-	-	-	-	-
Ho	-	-	-	-	-	-	-
Er	-	-	-	-	-	-	-
Tm	-	-	-	-	-	-	-
Yb	-	-	-	-	-	-	-
Lu	-	-	-	-	-	-	-
Σ_7REE	-	-	-	-	-	-	-
ΣREE	-	-	-	-	-	-	-

Table B4.1. (Continued) Whole-rock geochemistry for the Ordovician(?), Early Silurian, and Early Jurassic mafic intrusi

Sample	112	116	120	G-1	P-3	R-7	S-1
Intrusion	SHE	SHE	SHE	SHE	SHE	SHE	SHE
Age	Jur	Jur	Jur	Jur	Jur	Jur	Jur
Source	5	5	5	5	5	5	5
Major elements							
SiO_2	53.44	54.16	54.24	53.51	53.56	53.50	52.61
TiO_2	0.95	1.39	1.15	0.95	1.08	1.04	1.06
Al_2O_3	15.17	15.34	15.51	14.80	16.24	14.41	15.24
Fe_2O_3T	10.39	11.28	10.62	9.92	9.92	10.65	14.05
FeOT	9.51	10.45	9.82	9.04	9.18	9.94	13.81
MnO	0.17	0.18	0.17	0.17	0.16	0.18	0.18
MgO	7.24	5.15	6.33	7.76	5.98	7.52	6.23
CaO	10.56	9.61	9.59	11.07	10.43	10.29	8.06
Na_2O	2.17	2.39	2.39	2.02	2.34	2.22	2.18
K_2O	0.66	1.04	0.64	0.56	0.90	0.76	0.43
P_2O_5	0.13	0.29	0.15	0.12	0.11	0.16	0.19
Total	100.00	100.00	100.00	100.00	100.00	100.00	100.00
LOI	1.41	1.85	2.51	1.45	1.47	1.97	4.20
Mg-number	48.03	39.67	44.70	49.79	43.31	48.98	44.33
CIPW norms							
Qtz	11.04	14.11	13.25	10.99	10.86	10.97	16.26
Crn	0.00	0.00	0.00	0.00	0.00	0.00	0.00
Kfs	4.32	6.87	4.20	3.64	5.86	5.00	2.95
Ab	20.28	22.56	22.40	18.78	21.79	20.85	21.38
An	32.80	31.29	32.90	32.59	34.27	30.08	35.38
Di	16.31	11.86	11.75	18.44	14.28	16.93	4.78
Hy	12.47	8.88	12.11	12.81	9.86	13.05	15.86
Ol	0.00	0.00	0.00	0.00	0.00	0.00	0.00
Mag	0.00	0.00	0.00	0.00	0.00	0.00	0.00
Ilm	0.40	0.43	0.40	0.40	0.38	0.43	0.45
Ap	0.31	0.71	0.36	0.29	0.26	0.39	0.48
Trace elements							
Ba	194.00	269.00	158.00	207.00	242.00	175.00	134.00
Rb	25.00	36.00	28.00	22.00	36.00	30.00	17.00
Sr	197.00	223.00	211.00	199.00	231.00	198.00	177.00
Y	23.00	30.00	26.00	22.00	23.00	25.00	26.00
Zr	97.00	132.00	112.00	91.00	100.00	102.00	106.00
Nb	10.00	13.00	11.00	11.00	10.00	9.00	11.00
Th	5.00	4.00	5.00	4.00	6.00	4.00	6.00
Pb	7.00	9.00	13.00	7.00	10.00	8.00	11.00
Ga	20.00	21.00	22.00	20.00	23.00	22.00	22.00
Zn	80.00	86.00	94.00	67.00	71.00	75.00	95.00
Cu	105.00	136.00	112.00	103.00	107.00	131.00	100.00

Sample	112	116	120	G-1	P-3	R-7	S-1
Ni	83.00	54.00	73.00	88.00	62.00	87.00	74.00
V	256.00	227.00	274.00	218.00	247.00	259.00	252.00
Cr	227.00	105.00	125.00	273.00	143.00	234.00	193.00
Hf	-	-	-	-	-	-	-
Cs	-	-	-	-	-	-	-
Sc	-	-	-	-	-	-	-
Ta	-	-	-	-	-	-	-
Co	-	-	-	-	-	-	-
Li	-	-	-	-	-	-	-
U	-	-	-	-	-	-	-
Rare-earth elements							
La	22.00	22.00	26.00	27.00	26.00	20.00	24.00
Ce	28.00	36.00	29.00	30.00	31.00	26.00	25.00
Pr	-	-	-	-	-	-	-
Nd	-	-	-	-	-	-	-
Sm	-	-	-	-	-	-	-
Eu	-	-	-	-	-	-	-
Gd	-	-	-	-	-	-	-
Tb	-	-	-	-	-	-	-
Dy	-	-	-	-	-	-	-
Ho	-	-	-	-	-	-	-
Er	-	-	-	-	-	-	-
Tm	-	-	-	-	-	-	-
Yb	-	-	-	-	-	-	-
Lu	-	-	-	-	-	-	-
Σ_7REE	-	-	-	-	-	-	-
ΣREE	-	-	-	-	-	-	-

Table B4.1. (Concluded) Whole-rock geochemistry for the Ordovician(?), Early Silurian, and Early Jurassic mafic intrusi

Sample	S-3	SH-1	77-26-6	78-17-7	78-19-8	78-27-10	78-27-9
Intrusion	SHE	SHE	WED	WED	WED	WED	WED
Age	Jur	Jur	Jur	Jur	Jur	Jur	Jur
Source	5	5	6	6	6	6	6
Major elements							
SiO_2	53.66	53.89	52.54	50.24	48.17	47.41	48.92
TiO_2	0.99	1.01	3.03	3.10	3.13	2.71	2.52
Al_2O_3	14.01	14.55	11.79	12.02	11.82	13.57	12.30
Fe_2O_3T	10.53	10.35	12.78	11.32	12.16	12.15	12.69
FeOT	9.76	9.55	11.59	10.29	11.21	11.51	11.98
MnO	0.18	0.17	0.15	0.18	0.20	0.19	0.19
MgO	7.89	7.30	6.95	7.95	10.02	10.05	11.06
CaO	10.66	10.41	8.33	10.89	10.79	8.98	8.98
Na_2O	2.10	2.13	1.79	2.13	0.63	2.91	2.30
K_2O	0.63	0.83	3.82	3.20	4.04	2.67	1.75
P_2O_5	0.12	0.15	0.00	0.00	0.00	0.00	0.00
Total	100.00	100.00	100.00	100.00	100.00	100.00	100.00
LOI	1.85	-	-	-	-	-	-
Mg-number	50.19	48.26	47.04	50.39	56.14	56.22	58.55
CIPW norms							
Qtz	11.34	11.60	5.26	0.00	0.00	0.00	0.00
Crn	0.00	0.00	0.00	0.00	0.00	0.00	0.00
Kfs	4.13	5.43	24.02	19.98	25.33	16.81	11.04
Ab	19.68	19.91	16.12	19.00	5.60	17.38	20.69
An	29.83	30.58	13.61	14.52	18.55	17.05	19.21
Di	19.13	17.32	23.71	33.11	29.83	23.71	22.16
Hy	13.02	12.16	8.44	2.14	7.74	0.00	13.48
Ol	0.00	0.00	0.00	2.64	4.02	12.15	5.51
Mag	0.00	0.00	2.73	2.40	2.63	2.71	2.83
Ilm	0.43	0.40	6.13	6.22	6.30	5.46	5.10
Ap	0.29	0.36	0.00	0.00	0.00	0.00	0.00
Trace elements							
Ba	205.00	205.00	-	-	-	-	-
Rb	22.00	33.00	-	-	-	-	-
Sr	183.00	208.00	-	-	-	-	-
Y	23.00	23.00	-	-	-	-	-
Zr	95.00	100.00	-	-	-	-	-
Nb	-	9.00	-	-	-	-	-
Th	4.00	6.00	-	-	-	-	-
Pb	5.00	7.00	-	-	-	-	-
Ga	20.00	19.00	-	-	-	-	-
Zn	74.00	76.00	-	-	-	-	-
Cu	99.00	110.00	-	-	-	-	-

Sample	S-3	SH-1	77-26-6	78-17-7	78-19-8	78-27-10	78-27-9
Ni	9.00	87.00	-	-	-	-	-
V	252.00	247.00	-	-	-	-	-
Cr	286.00	251.00	-	-	-	-	-
Hf	-	-	-	-	-	-	-
Cs	90.00	-	-	-	-	-	-
Sc	-	-	-	-	-	-	-
Ta	-	-	-	-	-	-	-
Co	-	-	-	-	-	-	-
Li	-	-	-	-	-	-	-
U	-	-	-	-	-	-	-
Rare-earth elements							
La	23.00	20.00	-	-	-	-	-
Ce	25.00	29.00	-	-	-	-	-
Pr	-	-	-	-	-	-	-
Nd	-	-	-	-	-	-	-
Sm	-	-	-	-	-	-	-
Eu	-	-	-	-	-	-	-
Gd	-	-	-	-	-	-	-
Tb	-	-	-	-	-	-	-
Dy	-	-	-	-	-	-	-
Ho	-	-	-	-	-	-	-
Er	-	-	-	-	-	-	-
Tm	-	-	-	-	-	-	-
Yb	-	-	-	-	-	-	-
Lu	-	-	-	-	-	-	-
Σ_7REE	-	-	-	-	-	-	-
ΣREE	-	-	-	-	-	-	-

Table B4.1. (Concluded) Whole-rock geochemistry for the Ordovician(?), Early Silurian, and Early Jurassic mafic intrusions.

Sample	WOL-I	WOL-II
Intrusion	WOL	WOL
Age	Ord	Ord
Source	2	2
Major elements		
SiO_2	51.93	51.03
TiO_2	2.38	1.41
Al_2O_3	14.79	15.60
Fe_2O_3T	12.50	12.60
FeOT	12.14	12.28
MnO	0.18	0.17
MgO	7.02	6.93
CaO	7.34	9.43
Na_2O	2.81	2.71
K_2O	0.86	0.22
P_2O_5	0.54	0.22
Total	100.00	100.00
LOI	6.30	5.60
Mg-number	47.27	46.97
CIPW norms		
Qtz	7.93	5.68
Crn	0.00	0.00
Kfs	5.37	1.35
Ab	24.93	24.07
An	26.45	31.26
Di	6.46	13.14
Hy	19.32	17.64
Ol	0.00	0.00
Mag	3.49	3.53
Ilm	4.74	2.81
Ap	1.24	0.50
Trace elements		
Ba	153.00	188.00
Rb	21.00	11.00
Sr	673.00	468.00
Y	29.00	20.00
Zr	226.00	116.00
Nb	26.00	10.00
Th	-	-
Pb	-	-
Ga	-	-
Zn	-	-
Cu	-	-

Sample	WOL-I	WOL-II
Ni	-	-
V	-	-
Cr	-	-
Hf	-	-
Cs	-	-
Sc	-	-
Ta	-	-
Co	-	-
Li	-	-
U	-	-
Rare-earth elements		
La	-	-
Ce	-	-
Pr	-	-
Nd	-	-
Sm	-	-
Eu	-	-
Gd	-	-
Tb	-	-
Dy	-	-
Ho	-	-
Er	-	-
Tm	-	-
Yb	-	-
Lu	-	-
Σ_7REE	-	-
ΣREE	-	-

Appendix C

MICROPROBE AND GEOCHEMICAL DATA FOR CHAPTER 3

C-1. Microprobe Data for Contact Zone Transect Lithologies

Representative microprobe analyses for amphiboles, biotite, and plagioclase from the granodiorite, tonalite, and diorite in Birchtown Quarry appear in Tables C1.1 to C1.3, respectively. Appendix A-1 contains the analytical and data recalculation procedures. Mineralogical abbreviations after Kretz (1983) and other abbreviations appear in Appendix B-2. Lithologic abbreviations: Dio = diorite, Grd = granodiorite, Ton = tonalite. Figure 3.15 in Chapter 3 shows the sample locations.

Table C1.1. Microprobe analyses of amphibole from the Birchtown diorite and tonalite.

Sample	B8	B8	B8	B8	B8	B8	B8	B8	B8
Lithology	Dio	Dio	Dio	Dio	Dio	Dio	Dio	Dio	Dio
Mineral	Am	Am	Am	Am	Am	Am	Am	Am	Am
SiO_2	50.91	50.59	50.53	50.23	52.31	52.33	51.62	50.32	48.21
TiO_2	0.62	0.66	0.66	0.72	0.35	0.28	0.20	0.36	0.72
Al_2O_3	6.84	6.78	6.54	6.73	4.95	4.86	5.64	6.88	9.23
FeO	10.49	10.26	10.34	10.61	9.53	8.54	8.84	9.40	10.64
MnO	0.33	0.34	0.36	0.30	0.33	0.26	0.24	0.20	0.28
MgO	15.99	16.08	16.08	16.05	17.25	17.97	17.77	16.86	15.26
CaO	12.79	12.84	12.71	12.67	12.86	13.21	12.53	13.04	12.76
Na_2O	0.80	0.84	0.75	0.82	0.78	0.82	0.86	1.06	1.27
K_2O	0.19	0.23	0.27	0.30	0.16	0.29	0.38	0.42	0.43
P_2O_5	0.00	0.00	0.04	0.00	0.00	0.00	0.02	0.00	0.00
Total	98.95	98.62	98.29	98.44	98.52	98.55	98.11	98.53	98.81
Class.	M Hbl	M Hbl	M Hbl	M Hbl	Act Hbl	Act Hbl	Act Hbl	M Hbl	M Hbl

Sample	B8	B4	B4	B4	B4	B4	B4	B4	B3
Lithology	Dio	Ton	Ton	Ton	Ton	Ton	Ton	Ton	Ton
Mineral	Am	Am	Am	Am	Am	Am	Am	Am	Am
SiO_2	51.04	50.38	50.96	50.60	51.07	49.74	49.49	50.86	45.70
TiO_2	0.65	0.58	0.38	0.48	0.29	0.55	0.52	0.46	0.75
Al_2O_3	6.64	6.53	5.88	6.18	5.63	6.23	7.23	5.66	9.62
FeO	8.74	11.74	11.49	11.54	11.41	11.89	12.11	11.10	14.33
MnO	0.28	0.33	0.40	0.39	0.37	0.36	0.34	0.27	0.40
MgO	16.87	15.57	15.98	15.75	16.23	15.75	15.10	16.09	12.88
CaO	12.90	12.70	12.78	12.99	12.95	12.96	13.03	13.00	12.78
Na_2O	0.91	0.73	0.67	0.85	0.82	0.72	0.79	0.80	0.96
K_2O	0.17	0.54	0.43	0.50	0.43	0.55	0.61	0.47	0.89
P_2O_5	0.03	0.06	0.04	0.11	0.11	0.00	0.10	0.03	0.08
Total	98.24	99.16	99.01	99.39	99.31	98.74	99.31	98.73	98.40
Class.	M Hbl	M Hbl	M Hbl	M Hbl	M Hbl	M Hbl	M Hbl	M Hbl	M Hbl

Table C1.1. (Concluded) Microprobe analyses of amphibole from the Birchtown diorite and tonalite.

Sample	B3	B3	B3	B3	B3
Lithology	Ton	Ton	Ton	Ton	Ton
Mineral	Am	Am	Am	Am	Am
SiO_2	47.02	45.48	46.57	49.62	52.81
TiO_2	0.62	0.74	0.59	0.58	0.27
Al_2O_3	8.29	9.69	9.40	6.92	4.12
FeO	13.82	14.52	14.24	12.53	10.85
MnO	0.53	0.45	0.52	0.39	0.29
MgO	13.35	12.31	13.10	14.85	16.88
CaO	12.57	12.53	12.61	12.82	13.15
Na_2O	1.07	0.97	1.14	0.70	0.60
K_2O	0.72	1.06	0.86	0.47	0.16
P_2O_5	0.00	0.04	0.22	0.16	0.00
Total	97.98	97.76	99.25	99.04	99.13
Class.	M Hbl	M Hbl	M Hbl	M Hbl	Act Hbl

Table C1.2. Microprobe analyses of biotite the Birchtown diorite, tonalite, and granodiorite.

Sample	B8	B8	B8	B8	B8	B8	B8	B8	B8
Lithology	Dio	Dio	Dio	Dio	Dio	Dio	Dio	Dio	Dio
Mineral	Bt	Bt	Bt	Bt	Bt	Bt	Bt	Bt	Bt
SiO_2	39.47	38.73	37.96	37.90	38.03	39.02	39.51	39.35	38.86
TiO_2	2.58	2.52	2.63	2.65	2.45	2.68	2.49	2.37	2.47
Al_2O_3	15.45	14.96	14.76	14.60	14.82	15.47	15.67	15.44	15.07
FeO	11.96	11.75	12.07	11.88	11.73	11.69	11.67	11.90	11.69
MnO	0.08	0.17	0.08	0.20	0.03	0.09	0.17	0.12	0.15
MgO	17.03	16.92	16.19	16.40	16.70	17.09	17.08	17.13	16.86
CaO	0.01	0.01	0.03	0.07	0.00	0.00	0.08	0.08	0.00
Na_2O	0.26	0.45	0.40	0.30	0.49	0.34	0.37	0.38	0.38
K_2O	8.31	8.37	8.67	8.68	8.54	8.40	8.24	8.70	8.86
Total	95.16	93.88	92.77	92.70	92.79	94.78	95.28	95.45	94.34
Mg/(Mg+Fe)	0.72	0.72	0.71	0.71	0.72	0.72	0.72	0.72	0.72

Sample	B8	B8	B8	B8	B8	B8	B8	B8	B4
Lithology	Dio	Dio	Dio	Dio	Dio	Dio	Dio	Dio	Ton
Mineral	Bt	Bt	Bt	Bt	Bt	Bt	Bt	Bt	Bt
SiO_2	38.76	38.94	38.47	37.66	37.20	37.46	37.69	37.56	37.45
TiO_2	2.45	2.60	2.47	2.50	2.51	2.61	2.38	2.44	2.69
Al_2O_3	15.12	15.08	14.73	15.07	14.73	14.90	15.02	14.63	16.01
FeO	11.32	11.62	11.56	11.41	11.13	11.34	11.23	12.10	14.66
MnO	0.14	0.13	0.12	0.11	0.14	0.21	0.14	0.09	0.22
MgO	17.14	17.01	16.70	16.19	16.29	16.45	16.50	16.17	13.73
CaO	0.01	0.04	0.08	0.02	0.06	0.00	0.00	0.07	0.03
Na_2O	0.48	0.32	0.35	0.40	0.57	0.39	0.47	0.41	0.33
K_2O	8.89	8.62	8.59	8.90	8.75	8.72	8.78	9.00	9.46
Total	94.32	94.35	93.06	92.25	91.38	92.09	92.21	92.47	94.57
Mg/ (Mg+Fe)	0.72	0.73	0.72	0.72	0.72	0.72	0.72	0.72	0.70

Table C1.2. (Continued) Microprobe analyses of biotite the Birchtown diorite, tonalite, and granodiorite.

Sample	B4	B4	B4	B4	B4	B4	B3	B3	B3
Lithology	Ton	Ton	Ton	Ton	Ton	Ton	Ton	Ton	Ton
Mineral	Bt	Bt	Bt	Bt	Bt	Bt	Bt	Bt	Bt
SiO_2	37.24	37.27	37.36	37.29	37.36	37.20	37.78	37.30	37.94
TiO_2	2.74	2.67	2.74	3.03	2.84	2.28	1.88	1.97	2.07
Al_2O_3	16.06	16.05	15.74	16.02	15.94	15.74	16.35	16.54	16.83
FeO	14.63	14.71	14.58	14.32	14.77	14.55	14.53	13.86	14.12
MnO	0.20	0.29	0.23	0.24	0.28	0.16	0.35	0.27	0.20
MgO	13.87	13.86	13.85	13.71	13.77	14.12	14.37	14.31	14.17
CaO	0.06	0.00	0.17	0.03	0.00	0.06	0.12	0.22	0.01
Na_2O	0.40	0.25	0.37	0.21	0.20	0.22	0.17	0.27	0.33
K_2O	9.48	9.45	9.84	9.75	9.83	8.99	8.75	9.00	9.24
Total	94.68	94.52	94.88	94.60	94.98	93.32	94.30	93.73	94.91
Mg/(Mg+Fe)	0.63	0.63	0.63	0.63	0.63	0.62	0.63	0.64	0.65

Sample	B3	B3	B3	B3	B3	B3	B3	B3	SPGD
Lithology	Ton	Ton	Ton	Ton	Ton	Ton	Ton	Ton	Grd
Mineral	Bt	Bt	Bt	Bt	Bt	Bt	Bt	Bt	Bt
SiO_2	37.24	37.53	37.44	37.08	37.50	37.44	35.68	37.20	34.42
TiO_2	2.42	1.75	1.90	2.41	2.37	2.41	1.16	2.43	2.45
Al_2O_3	16.66	16.81	16.14	15.82	15.77	16.18	16.31	16.68	18.37
FeO	14.72	14.73	16.09	14.63	15.07	15.11	15.24	14.33	20.56
MnO	0.24	0.22	0.29	0.27	0.12	0.30	0.33	0.17	0.55
MgO	13.18	13.26	13.65	13.81	14.18	13.93	15.19	12.79	7.11
CaO	0.04	0.07	0.04	0.00	0.03	0.03	0.38	0.00	0.03
Na_2O	0.33	0.19	0.26	0.20	0.26	0.30	0.62	0.39	0.30
K_2O	8.90	9.44	9.53	9.24	9.53	9.31	8.10	9.71	9.26
Total	93.75	93.99	95.33	93.45	94.85	95.00	93.01	93.70	93.06
Mg/ (Mg+Fe)	0.64	0.61	0.62	0.60	0.63	0.63	0.62	0.64	0.61

Table C1.2. (Concluded) Microprobe analyses of biotite the Birchtown diorite, tonalite, and granodiorite.

Sample	SPGD	SPGD	SPGD	SPGD	SPGD	SPGD
Lithology	Grd	Grd	Grd	Grd	Grd	Grd
Mineral	Bt	Bt	Bt	Bt	Bt	Bt
SiO_2	35.27	35.12	34.98	35.24	35.35	35.10
TiO_2	2.40	2.33	2.30	2.39	2.53	1.80
Al_2O_3	18.45	18.63	18.44	18.72	18.90	19.20
FeO	20.58	20.50	20.73	20.42	20.43	20.25
MnO	0.71	0.38	0.47	0.39	0.51	0.43
MgO	6.99	7.16	6.98	7.12	7.06	7.06
CaO	0.00	0.00	0.00	0.05	0.01	0.00
Na_2O	0.17	0.20	0.21	0.33	0.39	0.37
K_2O	9.56	9.68	9.31	9.42	9.46	9.30
Total	94.14	93.99	93.42	94.09	94.64	93.51
Mg/ (Mg+Fe)	0.38	0.38	0.38	0.38	0.38	0.38

Table C1.3. Microprobe analyses of plagioclase from the Birchtown diorite, tonalite, and granodiorite.

Sample	B8	B8	B8	B8	B8	B4	B4	B4	B4
Lithology	Dio	Dio	Dio	Dio	Dio	Ton	Ton	Ton	Ton
Mineral	Pl	Pl	Pl	Pl	Pl	Pl	Pl	Pl	Pl
SiO_2	60.19	59.82	52.20	60.36	57.13	53.89	51.70	49.63	54.53
TiO_2	0.10	0.01	0.04	0.00	0.03	0.00	0.02	0.03	0.03
Al_2O_3	25.52	26.02	30.75	25.22	27.84	27.52	30.70	31.77	29.32
FeO	0.07	0.22	0.00	0.15	0.00	0.01	0.00	0.09	0.02
MnO	0.00	0.00	0.00	0.00	0.04	0.05	0.02	0.09	0.09
MgO	0.00	0.04	0.02	0.00	0.07	0.38	0.09	0.04	0.10
CaO	7.57	8.04	13.99	7.40	10.36	9.68	13.94	15.59	11.88
Na_2O	7.48	7.03	3.93	7.33	5.77	2.10	3.89	3.09	5.16
K_2O	0.04	0.01	0.00	0.00	0.00	5.36	0.02	0.00	0.05
P_2O_5	0.07	0.00	0.00	0.01	0.00	0.12	0.08	0.00	0.11
Total	101.02	101.18	100.93	100.47	101.23	99.11	100.46	100.32	101.30
Ab	63.61	60.55	33.61	63.83	49.91	18.63	33.29	26.22	43.52
An	36.17	39.39	66.39	36.17	50.09	50.08	66.59	73.78	56.20
Or	0.22	0.06	0.00	0.00	0.00	31.29	0.11	0.00	0.28

Sample	B4	B4	B4	B4	B4	B4	B4	B4	B3
Lithology	Ton	Ton	Ton	Ton	Ton	Ton	Ton	Ton	Ton
Mineral	Pl	Pl	Pl	Pl	Pl	Pl	Pl	Pl	Pl
SiO_2	54.65	57.03	58.77	60.45	59.86	60.86	56.48	58.70	60.60
TiO_2	-0.04	0.01	0.00	0.00	0.08	0.00	0.00	0.09	0.04
Al_2O_3	28.48	27.12	25.93	24.75	25.62	24.60	26.56	26.55	23.97
FeO	0.02	0.06	0.09	0.14	0.10	0.06	0.02	0.07	0.27
MnO	0.01	0.00	0.00	0.00	0.05	0.00	0.00	0.12	0.00
MgO	0.00	0.00	0.02	0.02	0.07	0.00	0.06	0.00	0.22
CaO	11.43	9.77	8.32	6.86	7.38	6.61	9.46	8.65	6.17
Na_2O	5.38	6.28	7.26	7.75	7.46	7.82	6.39	6.92	6.28
K_2O	0.07	0.12	0.12	0.07	0.02	0.08	0.04	0.09	2.01
P_2O_5	0.05	0.19	0.06	0.00	0.08	0.02	0.01	0.08	0.03
Total	100.06	100.59	100.57	100.04	100.72	100.05	99.03	101.27	99.59
Ab	45.78	53.28	60.55	66.45	63.87	67.70	54.62	58.52	55.51
An	58.83	46.06	38.80	33.15	36.02	31.85	45.15	40.98	32.80
Or	0.39	0.67	0.66	0.39	0.11	0.46	0.22	0.50	11.69

Table C1.3. (Continued) Microprobe analyses of plagioclase from the Birchtown diorite, tonalite, and granodiorite.

Sample	B3	B3	B3	B3	B3	B3	B3	B3	B3
Lithology	Ton	Ton	Ton	Ton	Ton	Ton	Ton	Ton	Ton
Mineral	Pl	Pl	Pl	Pl	Pl	Pl	Pl	Pl	Pl
SiO_2	56.77	56.64	56.29	58.65	59.43	59.46	58.80	56.76	57.65
TiO_2	0.02	0.06	0.00	0.02	0.08	-0.10	0.02	0.03	0.00
Al_2O_3	26.68	27.13	27.37	25.93	25.41	25.48	26.32	27.18	27.01
FeO	0.10	0.00	0.03	0.00	0.03	0.05	0.04	0.00	0.12
MnO	0.00	0.00	0.00	0.00	0.00	0.00	0.00	0.08	0.06
MgO	0.03	0.02	0.00	0.00	0.00	0.00	0.07	0.06	0.04
CaO	9.57	10.05	10.24	8.55	7.64	7.61	8.46	8.51	9.29
Na_2O	6.47	6.26	6.14	7.01	7.32	7.49	7.12	5.98	6.32
K_2O	0.04	0.08	0.04	0.06	0.06	0.04	0.03	0.80	0.05
P_2O_5	0.00	0.16	0.02	0.03	0.04	0.00	0.00	0.01	0.01
Total	99.65	100.39	100.13	100.26	100.01	100.04	100.87	99.40	100.50
Ab	54.56	52.58	51.87	59.50	62.96	63.78	59.86	53.08	54.63
An	45.22	46.98	47.91	40.17	36.70	36.00	39.97	42.25	45.09
Or	0.22	0.44	0.22	0.34	0.34	0.22	0.17	4.67	0.28

Sample	B3	B3	B3	B3	B3	B3	B3	B3	SPGD
Lithology	Ton	Ton	Ton	Ton	Ton	Ton	Ton	Ton	Grd
Mineral	Pl	Pl	Pl	Pl	Pl	Pl	Pl	Pl	Pl
SiO_2	58.46	56.98	61.31	52.41	57.64	56.76	54.02	48.29	65.87
TiO_2	0.04	-0.02	0.00	0.00	0.10	0.00	0.00	0.03	0.04
Al_2O_3	25.92	26.81	23.89	29.36	23.31	27.12	28.50	32.83	21.90
FeO	0.00	0.06	0.00	0.37	1.84	0.10	0.01	0.08	0.00
MnO	0.00	0.00	0.12	0.03	0.01	0.00	0.00	0.00	0.00
MgO	0.00	0.02	0.07	0.00	1.92	0.04	0.03	0.09	0.03
CaO	8.37	9.55	5.66	12.94	5.21	9.71	11.61	16.76	3.02
Na_2O	7.04	6.23	8.43	4.46	6.78	6.13	5.09	2.27	8.78
K_2O	0.09	0.11	0.04	0.16	1.51	0.05	0.12	0.06	0.12
P_2O_5	0.07	0.00	0.13	0.04	0.01	0.00	0.05	0.05	0.09
Total	99.99	99.74	99.66	99.77	98.33	99.91	99.43	100.48	99.84
Ab	59.96	53.61	72.44	37.56	52.31	52.83	43.83	19.42	83.09
An	39.53	45.77	27.34	61.56	40.02	46.88	55.49	80.24	16.16
Or	0.50	0.62	0.23	0.89	7.67	0.28	0.68	0.34	0.75

Table C1.3. (Concluded) Microprobe analyses of plagioclase from the Birchtown diorite, tonalite, and granodiorite.

Sample	SPGD	SPGD	SPGD	SPGD	SPGD	SPGD	SPGD	SPGD	SPGD
Lithology	Grd	Grd	Grd	Grd	Grd	Grd	Grd	Grd	Grd
Mineral	Pl	Pl	Pl	Pl	Pl	Pl	Pl	Pl	Pl
SiO_2	65.99	66.77	66.63	67.75	65.59	65.64	66.24	65.24	65.91
TiO_2	-0.06	0.07	0.05	0.00	0.00	0.02	0.00	0.00	0.03
Al_2O_3	21.64	21.63	21.14	20.26	21.58	21.69	21.52	21.40	22.06
FeO	0.00	0.02	0.01	0.07	0.06	0.00	0.00	0.11	0.03
MnO	0.00	0.00	0.01	0.00	0.00	0.01	0.00	0.07	0.03
MgO	0.04	0.06	0.01	0.00	0.00	0.01	0.09	0.08	0.14
CaO	2.67	2.40	2.14	1.24	2.56	2.53	2.29	2.46	3.27
Na_2O	9.38	9.82	10.05	10.41	9.92	10.11	9.98	9.80	7.53
K_2O	0.12	0.02	0.09	0.01	0.05	0.06	0.04	0.06	0.03
P_2O_5	0.17	0.20	0.18	0.01	0.23	0.28	0.19	0.38	0.16
Total	99.96	100.99	100.32	99.74	99.98	100.34	100.36	99.61	99.19
Ab	85.54	87.35	88.75	93.51	87.07	87.43	88.00	86.67	79.35
An	13.74	12.53	10.72	6.43	12.64	12.23	11.77	12.99	20.44
Or	0.72	0.12	0.52	0.06	0.29	0.34	0.23	0.35	0.21

C-2. Major Oxide, CIPW Normative Mineralogy, Trace and Rare-earth Element, and Sr-Nd Isotope Analyses for Contact Zone Transect Lithologies

Whole-rock geochemical analyses for the diorite, tonalite, and granodiorite in Birchtown Quarry appear in Table C2.1; Appendices A-5 to A-7 contain the sample preparation and analytical procedures. All analyses were recast to 100% volatile-free with total iron as FeO, but the inclusion of LOI values allow subsequent workers to retrieve unrecalculated analyses. Mg-numbers were calculated from [100(MgO/(MgO+FeOT))] after the volatile-free calculation, whereas A/CNK values were calculated from the molecular proportions of Al_2O_3, CaO, Na_2O, and K_2O in recast analyses. CIPW norms for all samples were calculated assuming Fe_2O_3/FeO = 0.27, which de Albuquerque (1979) determined for the diorite by wet chemistry. D.I. = differentiation index (the sum of normative quartz, orthoclase, and albite). Lithological abbreviations: Dio = diorite, Grd = granodiorite, Mzg = monzogranite, Ton = tonalite. Appendix B-3 contains all of the other recalculation procedures. Normative mineral abbreviations after Kretz (1983).

Table C2.1. *Whole-rock geochemistry for Contact Zone Transect lithologies.*

Sample	SP	SPGD	BQ-4	BM-6	B2	B3	B4
Lithology	Mzg	Grd	Ton	Ton	Ton	Ton	Ton
Major oxides							
SiO_2	75.24	72.34	70.03	61.16	60.94	59.63	58.18
TiO_2	0.19	0.30	0.42	0.76	0.60	0.59	0.71
Al_2O_3	14.48	15.77	16.08	17.38	17.42	17.11	16.23
Fe_2O_3T	1.53	1.93	2.49	5.27	5.41	5.77	6.73
FeOT	1.39	1.79	2.35	5.00	5.08	5.40	6.40
MnO	0.05	0.06	0.06	0.10	0.11	0.11	0.13
MgO	0.40	0.68	0.95	3.51	4.18	4.47	6.75
CaO	1.29	1.58	2.06	5.70	5.73	6.68	6.94
Na_2O	4.12	3.92	2.96	2.59	2.37	2.20	2.09
K_2O	2.63	3.23	4.64	2.93	2.70	2.66	2.26
P_2O_5	0.20	0.33	0.45	0.85	0.86	1.16	0.31
Total	100.00	100.00	100.00	100.00	100.00	100.00	100.00
LOI	0.30	0.50	0.80	0.90	0.60	0.90	0.80
Mg-number	22.35	27.53	28.79	41.25	45.14	45.29	51.33
A/CNK	1.24	1.24	1.13	1.09	1.14	1.05	1.02
CIPW norms							
Qtz	38.99	34.35	31.23	20.86	21.82	19.99	15.15
Crn	3.02	3.80	3.58	1.67	2.33	1.28	0.00
Kfs	15.78	19.45	28.11	18.25	16.83	16.63	14.28
Ab	35.32	33.73	25.62	23.05	21.10	19.65	18.87
An	5.17	5.80	7.47	23.96	24.06	27.06	30.11
Di	0.00	0.00	0.00	0.00	0.00	0.00	1.90
Hy	1.01	1.73	2.43	9.24	11.01	11.81	17.15
Ol	0.00	0.00	0.00	0.00	0.00	0.00	0.00
Mag	0.00	0.00	0.00	0.00	0.00	0.00	0.00
Ilm	0.11	0.13	0.13	0.23	0.25	0.25	0.30
Ap	0.44	0.73	1.01	1.95	1.98	2.68	0.72
D.I.	95.26	93.33	92.43	86.12	83.81	83.33	78.41
Trace elements							
Ba	271.00	574.00	884.00	646.00	623.00	704.00	577.00
Rb	106.00	114.00	154.00	125.00	114.00	108.00	99.00
Sr	86.00	126.00	159.00	281.00	264.00	296.00	235.00
Y	8.00	11.46	13.79	23.00	21.00	21.20	21.00
Zr	81.00	93.73	116.38	115.00	104.00	141.56	122.00
Nb	7.00	10.22	10.49	9.00	9.00	9.90	8.00
Th	10.00	5.39	4.89	10.00	10.00	3.55	10.00
Pb	19.00	26.00	29.00	14.00	15.00	10.00	11.00
Ga	18.00	18.00	21.00	20.00	19.00	18.00	19.00
Zn	45.00	50.00	50.00	64.00	64.00	74.00	64.00
Cu	5.00	5.00	5.00	6.00	5.00	6.00	5.00
Ni	5.00	5.00	5.00	5.00	5.00	6.00	5.00
V	12.00	36.00	51.00	114.00	111.00	114.00	162.00
Cr	12.00	11.00	17.00	45.00	65.00	50.00	171.00
Hf	-	2.05	2.78	-	-	3.64	-
Ta	-	2.70	2.60	-	-	1.36	-

Sample	SP	BQ-GD	BQ-4	BM-6	B2	B3	B4
Rare-earth elements							
La	-	12.25	13.21	-	-	13.86	-
Ce	-	24.46	26.73	-	-	31.44	-
Pr	-	2.88	3.22	-	-	4.18	-
Nd	-	10.92	12.85	-	-	18.15	-
Sm	-	2.39	2.87	-	-	4.33	-
Eu	-	0.56	0.76	-	-	1.26	-
Gd	-	2.44	2.94	-	-	4.59	-
Tb	-	0.36	0.42	-	-	0.67	-
Dy	-	2.48	2.85	-	-	4.33	-
Ho	-	0.41	0.50	-	-	0.79	-
Er	-	1.08	1.28	-	-	2.05	-
Tm	-	0.16	0.20	-	-	0.29	-
Yb	-	1.07	1.35	-	-	1.99	-
Lu	-	0.14	0.23	-	-	0.29	-
Σ_7REE	-	51.79	58.00	-	-	71.32	-
ΣREE	-	61.60	69.41	-	-	88.22	-
Isotope ratios							
$^{87}Rb/^{86}Sr$	-	2.73845	2.55809	-	-	1.03161	-
$^{87}Sr/^{86}Sr$	-	0.72144±1	0.72021±5	-	-	0.71050±1	-
$^{87}Sr/^{86}Sr_i$	-	0.70702	0.70674	-	-	0.70515	-
$^{147}Sm/^{144}Nd$	-	0.13636±2	0.1406±3	-	-	0.14668±3	-
$^{143}Nd/^{144}Nd$	-	512560±15	0.512592±18	-	-	0.51262±4	-
εNd	-	1.33±0.29	1.75±0.35	-	-	2.01±0.76	-
εSr	-	41.93	37.94	-	-	15.47	-

Table C2.1. (Concluded) Whole-rock geochemistry for Contact Zone Transect lithologies.

Sample	B5	B7	B8	BIR-20
Lithology	Ton	Ton	Dio	Dio
Major oxides				
SiO_2	58.55	63.00	55.32	57.28
TiO_2	0.73	0.66	0.89	1.02
Al_2O_3	12.78	17.63	13.37	13.98
Fe_2O_3T	8.07	5.19	8.63	8.13
FeOT	7.57	4.77	8.26	7.54
MnO	0.16	0.10	0.16	0.15
MgO	9.39	3.42	10.47	8.32
CaO	6.59	4.24	7.46	7.30
Na_2O	1.55	2.89	1.48	1.73
K_2O	2.42	2.65	2.32	2.35
P_2O_5	0.27	0.65	0.27	0.33
Total	100.00	100.00	100.00	100.00
LOI	1.30	1.20	1.50	1.00
Mg-number	55.37	41.76	55.90	52.46
A/CNK	0.86	1.27	0.85	-
CIPW norms				
Qtz	16.27	24.87	10.56	12.29
Crn	0.00	4.02	0.00	0.00
Kfs	15.48	16.46	14.97	14.33
Ab	14.17	25.65	13.65	15.09
An	22.42	17.65	25.03	24.10
Di	6.99	0.00	8.36	8.70
Hy	22.16	8.98	24.49	20.59
Ol	0.00	0.00	0.00	0.00
Mag	0.00	0.00	0.00	2.13
Ilm	0.37	0.22	0.37	2.00
Ap	0.64	1.49	0.64	0.74
D.I.	68.34	84.63	64.21	-
Trace elements				
Ba	636.00	714.00	689.00	628.00
Rb	109.00	149.00	103.00	104.00
Sr	177.00	228.00	205.00	228.00
Y	20.00	11.29	23.00	26.00
Zr	116.00	149.61	141.00	136.00
Nb	6.00	10.64	8.00	9.00
Th	10.00	0.60	10.00	5.98
Pb	10.00	14.00	10.00	10.00
Ga	16.00	21.00	16.00	12.00
Zn	73.00	72.00	67.00	65.00
Cu	9.00	11.00	10.00	8.00
Ni	9.00	5.00	10.00	10.00
V	192.00	117.00	206.00	213.00
Cr	341.00	47.00	644.00	433.00
Hf	-	3.09	-	4.16
Ta	-	2.54	-	2.14

Sample	B5	B7	B8	BIR-20
Rare-earth elements				
La	-	8.41	-	15.88
Ce	-	18.63	-	35.75
Pr	-	2.48	-	-
Nd	-	10.81	-	17.14
Sm	-	2.58	-	4.29
Eu	-	0.95	-	1.27
Gd	-	2.67	-	-
Tb	-	0.37	-	-
Dy	-	2.34	-	-
Ho	-	0.42	-	-
Er	-	1.19	-	-
Tm	-	0.16	-	-
Yb	-	1.02	-	2.26
Lu	-	0.15	-	0.30
Σ_7REE	-	42.55	-	76.89
ΣREE	-	52.18	-	-
Isotope ratios				
$^{87}Rb/^{86}Sr$	-	1.84771	-	1.2896800
$^{87}Sr/^{86}Sr$	-	0.71500±1	-	0.71189±5
$^{87}Sr/^{86}Sr_i$	-	0.70527	-	0.7050900
$^{147}Sm/^{144}Nd$	-	0.14037±3	-	0.10256±8
$^{143}Nd/^{144}Nd$	-	0.512671±63	-	0.512599±7
εNd	-	3.3±1.2	-	3.69±0.13
εSr	-	17.08	-	14.63

Appendix D

THE ENCLAVE LITHOTYPE DATABASE FOR CHAPTER 4

D-1. Physical and Modal Characteristics of Enclaves in the Meguma Zone Granitoids

Table D1.1 contains a summary of the physical appearances, mineralogical characteristics, and descriptive classifications for the enclaves collected in Meguma Zone granitoids. Modal analyses for some microgranular enclaves represent approximately 4500 counts per slide using the Dalhousie Link image analysis system and the methodology of Van der Plas and Tobi (1965). Modal data for all other enclave types represent approximate estimations made under a petrographic microscope. Enclave shape classification (angularity, roundness, and sphericity) follows the class system that Powers (1953) developed for clastic sedimentary grains, and the aspect ratio was calculated from length/width, where the length is the longest axis of the enclave. Modal mineral abbreviations after Kretz (1983); Opq = the sum of Spl, Py, and Rt.

Nomenclature abbreviations: MSed = Metasedimentary enclave, Surm = Surmicaceous enclave, ME = microgranitoid enclave, Sch = Schlieren. Shape abbreviations: Ang = angular, Sba = subangular, Sbr = subrounded, Rnd = rounded, Wrd = well rounded. Contact abbreviations: Ind = indistinct/variable, Sh = sharp, Var = both sharp and indistinct in different locations on the same enclave. Textural abbreviations: Equ = equigranular, Ine = inequigranular, Fol = foliated (magmatic or metamorphic foliation parallel to the enclaves longest axis). Colour abbreviations: B = black, P = pink, Bu = buff, G = grey (DG = dark grey, LG = light grey), W = white, Br = brown (DB = dark brown, LB = light brown, GB = ginger-brown), Gn = green (OG = olive green). Lithologic abbreviations: Ton = Tonalite, Grd = Granodiorite, Mzg = Monzogranite, Lmzg = Leucomonzogranite, Porp = Mafic porphyry. Figures 4.3, 4.9, and 4.15 in Chapter 4 show the sample locations.

Table D1.1. Macroscopic mineralogical and modal characteristics of enclaves in Meguma Zone granitoids

Nomenclature					Shape			Size			Macroscopic features				Mode	Class
Batholith	Pluton	Sample No (n)	Location	Host Lithology	Angularity	Sphericity	Roundness	Length (cm)	Width (cm)	Aspect ratio	Colour	Contact	Texture	Grain size (mm)		
South Mountain	Big Indian Polyintrusive	BI-2	Big Indian Lake	Mzg	Ang	0 5	0 1	7	2	3 5	B	Sha	Equ	0 2-0 75	Bt_{92} Qtz Ap Opq	Surm
South Mountain	Big Indian Polyintrusive	BI-1	Big Indian Lake	Mzg	Sba	0 5	0 3	17	9	1 89	P B	Sha	Equ	1	Bt_{45} Pl_{45} Qtz	ME
South Mountain	Halifax	BV-1	Beechville	Lmzg	Sba	0 3	0 3	17	7	2.43	DG	Ind	Equ	0 5	Bt Chl Pl Kfs Qtz Opq	ME
South Mountain	Halifax	BV-2	Beechville	Lmzg	Sba	0 5	0 3	17	8	2 13	DG	Ind	Equ	0 5	Bt Ms	MSed
South Mountain	Halifax	CH-1	Chebucto Head	Mzg	Wrd	0 9	0 9	17	12	1 42	G	Sha	Equ	1	Bt Qtz	MSed
South Mountain	Halifax	CH-2	Chebucto Head	Mzg	Sba	0 5	0 5	7	5 5	1 27	G	Sha	Equ	0 1-0 2	Bt Ms Chl Pl Kfs Qtz Ap	ME
South Mountain	Halifax	HF-1	Harrietsfield	Mzg	Rnd	0 5	0 7	8	6	1 33	G	Var	Equ	0 5	Bt_{45} Pl Qtz Opq	MSed
South Mountain	Halifax	HF-3	Harrietsfield	Mzg	Sba	0 5	0 3	6	1	6	DG	Sha	Equ	0 18	Bt Pl Kfs Qtz Ap Opq	ME
South Mountain	Halifax	HH (5)	Hemlock Hill	Porp	Sbr-Rnd	-	-	5-20	5-20	-	G, B	Ind	Ine	1-2	-	MSed
South Mountain	Halifax	IV-1	Indian Village	Lmzg	Sba	0 7	0 3	3 5	2 5	1 4	DG	Ind	Ine	0 5-1 0	Bt_{53} Chl Qtz_{45}	MSed
South Mountain	Halifax	IV-2	Indian Village	Lmzg	Sbr	0 7	0 7	16	8 5	1 88	LG	Sha	Equ	0 8	Bt Qtz	Surm
South Mountain	Halifax	LL-1	Long Lake	Mzg	Rnd	0 9	0 9	5	5	1	LG	Sha	Equ	0 5	Bt_{35} Qtz_{65}	MSed
South Mountain	Halifax	LL-2	Long Lake	Mzg	Sbr	0 7	0 5	7 5	6	1 25	G	Ind	Ine	0 75	Bt Pl Kfs Qtz Ap	MSed
South Mountain	Halifax	LL-3	Long Lake	Mzg	Ang	0 3	0 1	40	16	2.5	B	Sha	Ine fol	0 5	Bt_{70} Qtz_{30}	MSed
South Mountain	Halifax	LL-4	Long Lake	Mzg	Sbr	0 7	0 5	10	7	1 43	LG	Sha	Equ	0 5	Bt Ms Pl Kfs Qtz Ap Opq	ME
South Mountain	Halifax	LL-5	Long Lake	Mzg	Sbr	0 9	0 7	10	7	1 43	LG	Sha	Ine	2-20	-	CGG
South Mountain	Halifax	LS-1	Lakeside	Lmzg	Rnd	0 7	0 7	17	12 5	1 36	G	Ind	Ine	0 5-1.2	Bt_{50} Pl Kfs Qtz_{40}	MSed
South Mountain	Halifax	LS-2	Lakeside	Lmzg	Sba	0 9	0 3	6 5	6 5	1	W	Sha	Equ	1	Bt Crd Ms Pl Kfs Qtz	ME
South Mountain	Halifax	LS-3	Lakeside	Lmzg	Sbr	-	-	-	-	-	B	Ind	Equ	1	Bt Ms Pl Qtz	MSed
South Mountain	Halifax	LS 4	Lakeside	Lmzg	Sbr	0 6	0 5	10	5	2	DG	Sha	Ine	3-6	-	CGG
South Mountain	Halifax	LS-5	Lakeside	Lmzg	Sbr	0 6	0 5	15	12	1 25	DG	Sha	Ine	3-6	-	CGG
South Mountain	Halifax	LS-6	Lakeside	Lmzg	Sbr	0 7	0 5	8 5	8	1 06	G B	Sha	Ine	0 5-1 0	Bt_{30} Ms Pl Kfs Qtz_{70} Ap	ME
South Mountain	Halifax	LS-7	Lakeside	Lmzg	Sbr	0 9	0 5	10	10	1	GB	Sha	Ine	0 5-1 0	Bt Ms Qtz Opq	MSed
South Mountain	Halifax	LS-8	Lakeside	Lmzg	Rnd	0 9	0 9	50	50	1	DG	Sha	Equ	0 75	Bt_{35} Qtz_{65}	MSed
South Mountain	Halifax	ND-1	Northwest Arm Drive	Grd	Sbr	0 5	0 7	9	5 5	1 64	G	Sha	Equ	1	Bt_{30} Ms Pl_{30} Qtz_{30}	ME
South Mountain	Halifax	ND 3	Northwest Arm Drive	Grd	Sba	0 7	0 3	6	5	1 2	DG	Var	Equ	1	Bt_{50} Qtz_{50}	MSed
South Mountain	Halifax	ND 4	Northwest Arm Drive	Grd	Rnd	-	-	-	-	-	G	Ind	Equ	0 75 - 1 0	Bt Pl Qtz Opq	MSed
South Mountain	Halifax	NMR-1	Nine Mile River	Lmzg	Rnd	0 5	0 9	21	7	3	LG	Sha	Equ	0 1-1	Bt_{35} Ms Pl Kfs Qtz_{65} Ap Opq	ME
South Mountain	Halifax	NMR-3	Nine Mile River	Lmzg	Rnd	0 5	0 9	99	60	1 65	LG	Ind	Equ	0 5-0 75	Bt Ms Pl Kfs Qtz Ap Opq	MSed
South Mountain	Halifax	PB-1	Prospect Bay	Mzg	Sbr	0 9	0 7	10 5	7	1 5	DG	Sha	Equ	0 1-1	Bt Ms Pl Kfs Qtz Opq	MSed
South Mountain	Halifax	PB 2	Prospect Bay	Mzg	Sba	0 9	0 5	21	18	1 17	G	Sha	Equ	0 5	Bt_{30} Grt Chl Qtz_{70}	MSed
South Mountain	Halifax	PB 3	Prospect Bay	Mzg	Ang	0 9	0 1	11	8	1 38	B	Sha	Equ	2	Bt_{30} Pl_{35} Kfs Qtz_{35} Ap	ME
South Mountain	Halifax	PB 4	Prospect Bay	Mzg	Sbr	0 9	0 5	62	62	1	LG	Var	Ine	0 75-1 0	Bt_{30} Qtz_{70}	MSed
South Mountain	Halifax	PB 5	Prospect Bay	Mzg	Sbr	0 5	0 7	36	14	2.57	G	Sha	Eau	0 5	Bt Qtz	MSed
South Mountain	Halifax	PB 6	Prospect Bay	Mzg	Rnd	0 7	0 9	99	70	1 41	G	Sha	Equ	0 75	Bt Pl Qtz	MSed

Table D1.1. (Continued) Macroscopic, mineralogical, and modal characteristics of enclaves in Meguma Zone granitoids

Nomenclature				Host	Shape			Size			Macroscopic features				Mode	Class
Batholith	Pluton	Sample No	Location	Lithology	Angularity	Sphericity	Roundness	Length (cm)	Width (cm)	Aspect ratio	Colour	Contact	Texture	Grain size (mm)		
South Mountain	Halifax	PB-7	Prospect Bay	Mzg	Sba	0 7	0 3	8	7	1 14	B	Sha	Equ	1	Bt_{40} Pl_{50} Qtz_{10}	ME
South Mountain	*Halifax*	*PB-8*	*Prospect Bay*	*Mzg*	*Sbr-Rnd*	*0 5*	*0 5*	*28*	*30*	*0 93*	*G*	*Sha*	*Ine*	*2-20*	-	*CGG*
South Mountain	Halifax	PB-9	Prospect Bay	Mzg	Wrd	0 9	0 9	9	8	1 13	G	Var	Equ	0 25-1 0	Bt_{20} Ms Pl_{60} Kfs Qtz_{20} Ap	ME
South Mountain	Halifax	PB-10	Prospect Bay	Mzg	Sbr	0 7	0 5	40	50	0 80	LG	Sha	Ine	2-20	-	CGG
South Mountain	Halifax	PC-1	Portuguese Cove	Lmzg	Wrd	0 5	0 9	28	10	2.8	G	Sha	Equ	0 1-1	Bt Crd Ms Pl Qtz Ap	ME
South Mountain	Halifax	PC-2	Portuguese	Lmzg	Wrd	0 5	0 9	17 5	10 5	1 67	B	Sha	Equ	0 5-0 8	Bt Qtz	MSed
South Mountain	Halifax	PC 3	Portuguese	Lmzg	Wrd	0 5	0 9	84	30	2 8	LG	Sha	Equ	1 0-1 2	Bt_{25} Pl_{30} Qtz_{45}	ME
South Mountain	Halifax	PC-5	Portuguese	Lmzg	Ang	-	-	3	0 5	6	B	Ind	Ine fol	3	Bt_{65} Pl_{35}	Sch
South Mountain	Salmontail Lake	SL (10)	Salmontail Lake	Lmzg	Ang	-	-	5-20	5-20	-	P, Br	Sha	Equ	0 5-1 0	-	MSed
South Mountain	New Ross	SC-1	Smiths Corner	Lmzg	-	-	-	-	-	-	G	Sha	Equ	0 5-1 0	-	MSed
South Mountain	New Ross	SC-2	Smiths Corner	Lmzg	-	-	-	-	-	-	LG	Sha	Equ	0 5-1 0	-	MSed
South Mountain	Halifax	TIM-1	Timberlea	Lmzg	Sbr	0 9	0 5	5	5	1	B	Ind	Equ	0 1	Bt Pl Kfs Qtz Ap	ME
South Mountain	Halifax	TIM-2	Timberlea	Lmzg	Sba	0 3	0 1	4	1	4	DG	Ind	Ine	0 25-0 5	Bt Ms Qtz Opq	MSed
South Mountain	*Halifax*	*QU-1*	*Queensland*	*Lmzg*	*Ang*	*0 9*	*0 3*	*35*	*32*	*1 09*	*G*	*Sha*	*Equ*	*1*	*Bt Pl Qtz*	MSed
South Mountain	New Ross	DB-1	Dead Brook	Lmzg	Sbr	0 5	0 5	36	24	1 5	B	Var	Ine	0 1	Bt Crd Ms Pl Qtz	MSed
South Mountain	New Ross	NV-1	New Ross	Lmzg	Ang	0 5	0 1	6	3	2	GB	Var	Ine fol	1	Bt Pl Qtz Opq	Surm
South Mountain	New Ross	UV-1	Upper Vaughan	Lmzg	Sba	0 7	0 5	6	5	1 2	G	Var	Ine	2	-	MSed
South Mountain	New Ross	UV-2	Upper Vaughan	Mzg	Ang	0 3	0 3	42	28	1 5	P	Sha	Equ	0 1-0 6	Bt Ms Pl Qtz	MSed
South Mountain	Salmontail Lake	RM-1	Round Mountain	Mzg	Ang	0 7	0 3	7	6	1 17	B	Sha	Equ	0 25-0 5	Bt Qtz	MSed
South Mountain	Salmontail Lake	RM-2	Round Mountain	Mzg	Sba	0 5	0 3	7	3	2.33	DG	Var	Equ	0 1	Bt Pl Kfs Ap Opq	ME
South Mountain	Salmontail Lake	RM-4	Round Mountain	Mzg	Sba	0 5	0 5	7	4 5	1 56	B	Sha	Ine	0 75	Bt Pl Qtz	ME
South Mountain	Salmontail Lake	RM-5	Round Mountain	Mzg	Wrd	0 5	0 9	14	7	2	LG	Sha	Equ	0 5-1	Bt Pl Kfs Qtz	MSed
South Mountain	West Dalhousie	LQ-1	Lequille	Porp	Sbr	0 7	0 7	4	4	1	B	Ind	Equ	0 5	Bt Qtz	MSed
South Mountain	West Dalhousie	LQ-2	Lequille	Porp	Rnd	0 5	0 7	10	6	1 67	B	Sha	Equ	0 3	*Bt Grt Ms Pl Kfs* Qtz Opq	ME
South Mountain	West Dalhousie	LQ-3	Lequille	Porp	Ang	0 3	0 1	8	5	1 6	G	Sha	Equ	1	Bt Ms Pl Qtz	MSed
South Mountain	West Dalhousie	LQ-4	Lequille	Porp	Rnd	0 5	0 7	16	5	3 2	DG	Sha	Equ	0 5-1 0	Bt Grt Ms Qtz	Msed
South Mountain	West Dalhousie	LQ-5	Lequille	Porp	Sbr	0 7	0 5	15	10	1 5	G	Sha	Equ	1 5-2 0	Bt Pl Qtz	MSed
South Mountain	West Dalhousie	LQ-6	Lequille	Porp	Sbr	0 5	0 5	7	3	2.33	G	Sha	Equ	1	Bt Ms Pl Qtz Opq	MSed
South Mountain	*West Dalhousie*	*LQ-10*	*Lequille*	*Porp*	*Sbr*	0 6	0 5	16	5	3 2	DG	Sha	Ine	5	-	CGG
South Mountain	West Dalhousie	LQ-11	Lequille	Porp	Sbr	0 7	0 5	3	2 3	1 3	DB	Ind	Ine fol	1 5	Bt_{90} Pl_{5} Qtz_{5}	Surm
South Mountain	Halifax	LIL	Little Indian Lake	Lmzg	Sbr	0 9	0 7	200	200	1	G	Ind	Equ	1	Bt Pl Qtz	ME
South Mountain	Halifax	ML-1	Mill Lake	Lmzg	Sbr	0 9	0 7	8	8	1	DB	Ind	Ine	0 5-1 5	Bt Ms Chl Opq	Surm
South Mountain	Marginal granodiorite	MU-1	Mount Uniacke	Grd	Sba	0 5	0 3	6	4 5	1 33	DG	Sha	Equ	0 1	Bt Ms Pl Kfs Qtz Opq	MSed
South Mountain	Marginal granodiorite	MU-2	Mount Uniacke	Grd	Sba	0 5	0 3	7	4 5	1 56	G	Var	Equ	0 5-1 0	*Bt_{70} Pl Qtz_{30} Opq*	*MSed*
South Mountain	Marginal granodiorite	MU-3	Mount Uniacke	Grd	Sba	0 5	0 3	11	5	2.2	DG	Ind	Equ	0 25-0 5	Bt_{50} Pl Kfs Qtz Ap	ME
South Mountain	Marginal granodiorite	MU-4	Mount Uniacke	Grd	Sba	-	-	-	-	-	DG	Sha	Ine	0 1-1 0	$Bt_{[illegible]}$ Pl Qtz_{50} Opq	MSed
South Mountain	Marginal granodiorite	MU-5	*Mount Uniacke*	*Grd*	*Ang*	*0 5*	*0 1*	*9*	*4*	*2.25*	*DG*	*Ind*	*Equ*	*0 5*	*Bt_{50} Opq*	MSed
-	Barrington Passage	NQ-1	New Quarry	Ton	Sba	0 5	0 3	99	20	4 95	G	Ind	Equ	0 5-1	Bt Pl Qtz Opq	MSed
-	Barrington Passage	NQ-2	New Quarry	Ton	Ang	0 3	0 1	70	21	3 33	DG	Ind	Equ	0 5-2	$Bt_{[illegible]}$ $Pl_{[illegible]}$ $Qtz_{[illegible]}$ Ap Opq Grt_{1}	MSed

Table D1.1. (Continued) Macroscopic, mineralogical, and modal characteristics of enclaves in Meguma Zone granitoids

Nomenclature				Host	Shape			Size			Macroscopic features				Mode	Class
Batholith	Pluton	Sample No	Location	Lithology	Angularity	Sphericity	Roundness	Length (cm)	Width (cm)	Aspect ratio	Colour	Contact	Texture	Grain size (mm)		
-	Barrington Passage	NQ-3	New Quarry	Ton	Wrd	0 5	0 9	42	21	2	LB	Sha	Ine	1-1 5	Bt_{20} And Crd Pl_{54} Qtz_{25} Ap	Surm
-	Barrington Passage	NQ-4	New Quarry	Ton	Srd	0 3	0 7	65	17	3 82	DG	Sha	Ine	0 15-0 3	Bt_{45} Ms_{1} Pl_{45} Qtz_{5} Ap Opq	Surm
-	Barrington Passage	NQ-6	New Quarry	Ton	Rnd	0 5	0 7	14	7	2	DG	Var	Ine	3	Bt_{50} Pl_{25} Qtz_{25}	Surm
-	Barrington Passage	NQ-8	New Quarry	Ton	Sbr	0 5	0 5	35	14	2 5	DB	Ind	Equ	1	Bt_{65} Pl_{25} Qtz_{10} Ap Opq	MSed
-	Barrington Passage	OQ-1	Old Quarry	Ton	Ang	0 5	0 3	14	7	2	DB	Sha	Ine fol	1	Bt_{90} Pl_{5} Qtz_{5} Ap Opq	Surm
-	Barrington Passage	OQ-2	Old Quarry	Ton	Rnd	0 5	0 7	13	7	1 86	B	Sha	Equ	0 5-0 75	Bt_{65} Ms Qtz	MSed
-	Barrington Passage	OQ-3	Old Quarry	Ton	Sba	0 3	0 3	42	14	3	Br	Ind	-	3	-	Surm
-	Barrington Passage	OQ-4	Old Quarry	Ton	Sbr	0 3	0 5	25	7 5	3 33	DB	Ind	Ine	2.5	Bt_{60} And_{1} Crd_{1} Pl_{35} Kfs_{2} Ap Opq	Surm
-	Barrington Passage	OQ-5	Old Quarry	Ton	Ang	0 3	0 1	21	3 5	6	G	Sha	Equ	1-1 75	Bt_{45} Crd_{1} Pl_{8} Qtz_{45} Ap And	Surm
-	Barrington Passage	OQ-6	Old Quarry	Ton	Ang	0 3	0 3	16	5	3 2	B	Ind	Ine fol	3	Bt_{100}	Surm
-	Barrington Passage	OQ-7	Old Quarry	Ton	Ang	0 3	0 1	26	7	3 71	DB	Var	Ine	2	Bt_{90} Pl_{3} Qtz_{5} Ap	Sch
-	Barrington Passage	OQ-9	Old Quarry	Ton	Sbr	0 3	0 5	84	28	3	Br	Sha	Ine	0 5-5	Bt_{30} And_{1} Crd_{1} Pl_{60} Kfs Qtz_{13} Ap	Surm
-	Barrington Passage	OQ-10	Old Quarry	Ton	Sbr	0 5	0 7	20	10	2	G	Sha	Ine	1	Bt_{85} Pl Qtz	Surm
-	Barrington Passage	OQ-11	Old Quarry	Ton	Sbr	0 3	0 7	32	10 5	3 05	B	Ind	Ine fol	1-2 5	Bt_{100}	Surm
-	Barrington Passage	SH-2	Shag Harbour	Ton	Ang	0 3	0 1	70	19	3 68	DG	Ind	Ine	0 25-5	Bt_{40} Pl_{45} Qtz_{15} Ap Opq	MSed
-	Barrington Passage	SH-4	Shag Harbour	Ton	Sba	0 5	0 3	28	12	2 33	OG	Ind	Equ	0 3-1 0	Am Bt_{2} Chl Pl Qtz_{3} Opq	MSed
-	Barrington Passage	SH 5	Shag Harbour	Ton	Sbr	-	-	-	-	-	G	-		1-2 5	Bt_{50} Qtz_{50}	MSed
-	Port Mouton	CB-1	Carters Beach	Mzg	Sba	0 1	0 3	14	5	2 8	Br, G	Sha	Ine	-	-	Surm
-	Port Mouton	CB-2	Carters Beach	Mzg	Sbr	0 8	0 3	7	7	1	Br, G	Sha	Ine	-	-	Surm
-	Port Mouton	CR-1	St. Caths River Rd	Mzg	Sba	0 7	0 3	14	11	1 27	DG	Ind	Ine	1	Bt_{45} Ms Pl Qtz	MSed
-	Port Mouton	CR-2	St. Caths River Rd	Mzg	Rnd	0 7	0 7	10	7	1 43	GB	Var	Ine	2	Bt Ms Pl_{5} Qtz_{50}	MSed
-	Port Mouton	CR-3	St. Caths River Rd	Mzg	Wrd	0 7	0 7	17 5	14	1 25	DG	Ind	Ine	1	Bt Ms Pl Qtz Opq	MSed
-	Port Mouton	CR-4	St. Caths River Rd	Mzg	Rnd	0 5	0 7	28	8	3 5	DB	Sha	Equ	0 5	Bt Pl Qtz Opq	MSed
-	Port Mouton	CR-5	St. Caths River Rd	Mzg	Rnd	0 7	0 7	28	12	2 33	DB	Sha	Equ	0 5	Bt Plg Qtz Opq	MSed
-	Port Mouton	CR-6	St. Caths River Rd	Mzg	Rnd	0 9	0 7	17	17	1	G	Sha	Ine fol	0 8-1 2	Bt_{3}[illegible] Ms_{1} Pl_{34} Qtz_{3} Ap	ME

Table D1.1. *(Concluded) Macroscopic mineralogical, and modal characteristics of enclaves in Meguma Zone granitoids*

Nomenclature				Shape				Size			Macroscopic features				Mode	Class
Batholith	Pluton	Sample No	Location	Host Lithology	Angularity	Sphericity	Roundness	Length (cm)	Width (cm)	Aspect ratio	Colour	Contact	Texture	Grain size (mm)		
-	Port Mouton	CR-7	St. Caths River Rd	Mzg	Rnd	0 7	0 5	16	18	0 89	G	Sha	Ine fol	0 8-1 2	Bt Ms Pl Qtz Ap	ME
-	Port Mouton	CR-8	St. Caths River Rd	Mzg	Wrd	0 5	0 7	28	10 5	2.67	DG	Sha	Equ	0 45	Bt Ms Pl Kfs Qtz Ap	ME
-	Port Mouton	CR-9	St. Caths River Rd	Mzg	Wrd	0 3	0 3	28	10 5	2 67	DG	Sha	Equ	0 45	Bt Ms Pl Qtz Ap	ME
-	Port Mouton	CR-10	St. Caths River Rd	Mzg	Wrd	0 5	0 9	31	24	1 29	LG	Var	Ine	2	Bt_{30}	MSed
-	Port Mouton	CR-11	St. Caths River Rd	Mzg	Sbr	0 5	0 7	31	16	1 94	DG	Sha	Equ	0 15-0 5	Bt Ms Pl Kfs Qtz Ap	ME
-	Port Mouton	CR-12	St. Caths River Rd	Mzg	Rnd	0 9	0 7	18	18	1	G	Sha	Equ	0 6-1 2	Bt_{25} Ms_{3} Pl_{40} $Qtz_{>1}$ Ap	ME
-	Port Mouton	CR-13	St. Caths River Rd	Mzg	Sbr	0 9	0 5	5	5	1	DB	Ind	Ine fol	-	Bt_{80}	MSed
-	Port Mouton	CR-1..	St. Caths River Rd	Mzg	Sbr	0 7	0 5	35	23	1 52	DG	Sha	Ine	3	-	MSed
-	Port Mouton	DR-1	Dead Mans	Ton	Sba	0 9	0 3	5	5	1	DG	Ind	Equ	1 5	Bt Ms Pl Qtz Ap	ME
-	Port Mouton	DR-2	Dead Mans	Ton	Wrd	0 7	0 9	30	20	1 5	DG	Sha	Equ	3	-	ME
-	Port Mouton	DR-3	Dead Mans	Ton	Sbr	0 7	0 7	20	14	1 43	DG	Sha	Equ	0 75-1 5	-	ME
-	Port Mouton	HP-1	Hell Point	Ton	Sba	0 5	0 5	31	14	2.21	G	Sha	Equ	1-2.5	Bt Ms Pl Qtz	MSed
-	Port Mouton	HP-2	Hell Point	Ton	Sba	0 5	0 5	25	18	1 39	Bu	Sha	Equ	1-2 5	Bt Ms Pl Qtz	MSed
-	Port Mouton	HP-3	Hell Point	Ton	Wrd	0 7	0 9	28	16	1 75	LG	Sha	Equ	0 6-1 8	Bt Ms Pl Qtz	ME
-	Port Mouton	HP 4	Hell Point	Ton	Sbr	0 9	0 5	15	15	1	DG	Sha	Equ	0 5-0 75	Bt_{40} Sil And Crd Qtz	CGG
-	Port Mouton	HP-5	Hell Point	Ton	Sba	0 5	0 3	21	7	3	W	Sha	Equ	2	Bt And Crd Ms Chl Pl Kfs Qtz Ap	MSed
-	Port Mouton	KJ (5)	Kejimkujik Adjunct	Ton	Sba	-	-	3 5-41	2 5-22	1 86	DB G	Sha-Ind	-	0 3-3	-	MSed
-	Shelburne	BX-1	nr Birchtown quarry	Mzg	Sbr	0 7	0 7	7	3	2 33	G Br	Ind	Ine fol	1	Bt_{100}	Surm
	Shelburne	BX 2	nr Birchtown quarry	Mzg	Ang	0 1	0 3	[illegible]	1	8	DB	Ind	Equ	1-1 5	Bt And Crd Ms Pl Qtz	Surm
-	Shelburne	BX-3	nr Birchtown quarry	Mzg	Sba	0 7	0 3	7	5	1 4	G Br	Sha	Ine fol	1-1 5	Bt And Crd Ms Pl Qtz Ap	Surm
-	Shelburne	BQ-1	Birchtown	Grd	Sba	0 1	0 1	5	3	1 67	B, DB	Sha	Equ	0 7	-	Surm
-	Shelburne	BQ-2	Birchtown	Grd	Sba	0 1	0 1	3	3	1 00	B DB	Sha	Equ	0 6	-	Surm
-	Shelburne	SPP-1	Shelburne Provincial Park	Mzg	Sbr	-	-	15	11	1 36	LG	Ind	Ine	0 1-0 3	-	MSed
-	Shelburne	SPP-2	Shelburne Provincial Park	Mzg	Sbr	0 3	0 3-0 4	20	21	0 95	LG	Ind	Ine	0 15-0 3	-	MSed

Appendix E

THE GRANITOID GEOCHEMICAL DATABASE FOR CHAPTER 5

E-1. Compiled Granitoid Geochemical Data

Table E1.1 contains a compilation of Meguma Zone granitoid lithogeochemistry. It consists of the unpublished database compiled by Richard (1988), supplemented with analyses derived from publications between 1988 and 1994 (Chapter 5, Section 3.1). Only fresh and unmineralized granitoid data were included in the data set; greisens, pegmatites, and aplites were specifically ignored. Sources of information were scanned with a Hewlett Packard™ page scanner at Dalhousie University. The resulting bitmaps were then converted to ASCII text with OmniPage™ optical character recognition software. Hard copy major oxide, trace element, and rare-earth element data from each source were summed and the totals were compared to the computer-generated totals for each analysis. This procedure eliminated recognition errors, and subsequent random manual checking of the digital data helped to produce a reliable compilation with an estimated accuracy of less than one error per page.

The database contains 1153 analyses and Figure E1.1 shows the names and locations of the analyzed intrusions (sorted alphabetically by pluton name) and indicates the number of analyses for them in the database. All sample numbers are those of the original authors, except where duplication occurred. Refer to the original sources for the sample locations and details of the analytical procedures. To accommodate the variable reporting of incomplete (total iron and loss on ignition) data with analyses containing values for FeO and Fe_2O_3, CO_2, F, Cl, H_2O+, and H_2O-, all analysis totals were calculated with all iron as FeOT and loss on ignition (or the sum of available data for CO_2, F, Cl, H_2O+, and H_2O-). A/CNK values were calculated from the molecular proportions of Al_2O_3, CaO, Na_2O, and K_2O. Lithologic abbreviations: Ton = Tonalite, Grd = Granodiorite, Mzg = Monzogranite, Lmzg = Leucomonzogranite, Lg = Leucogranite, MPOR = "mafic porphyry".

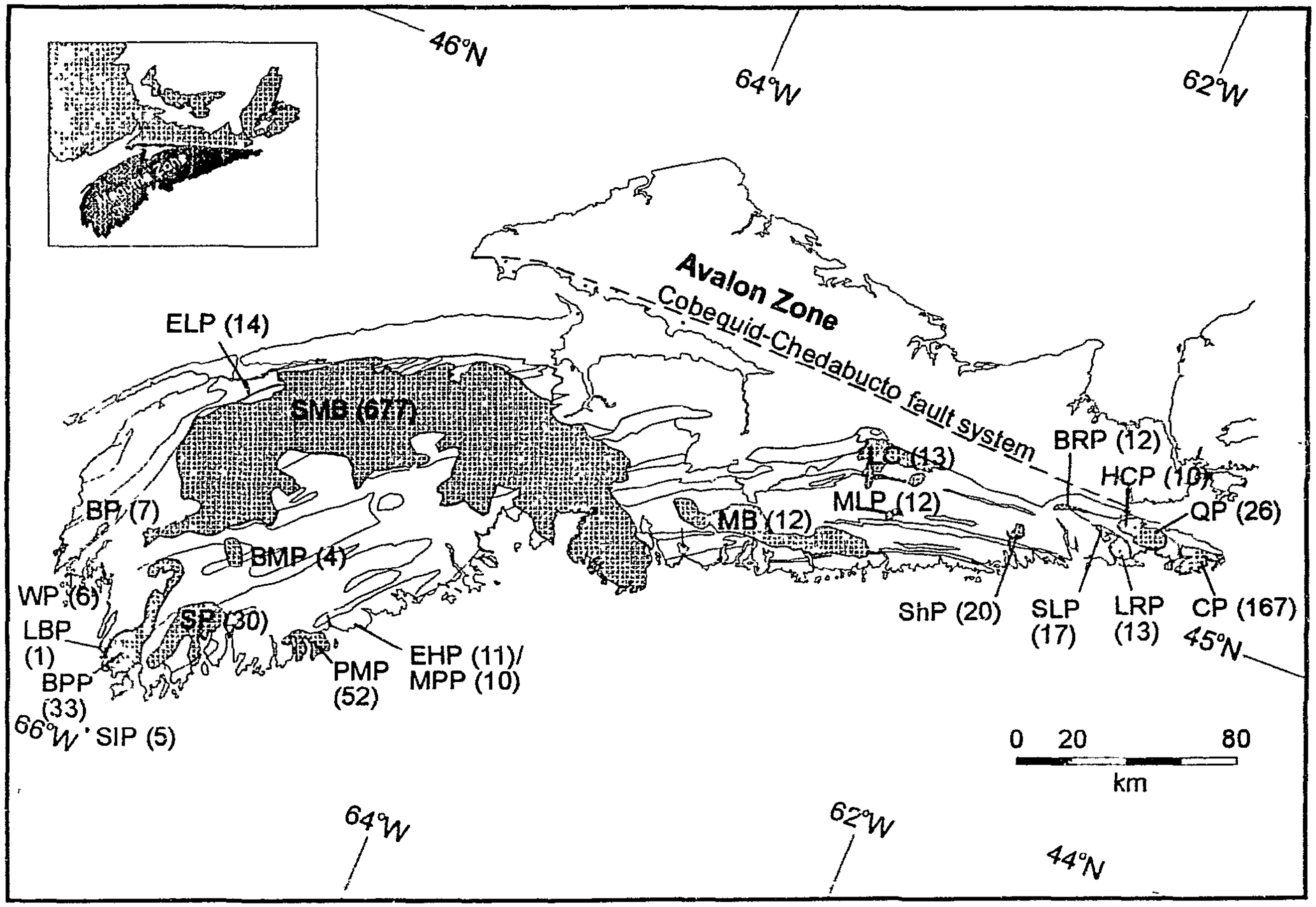

Figure E1.1. Locations of the plutons and batholiths intruded in the granitoid geochemical database (shaded in grey). The number in parentheses indicates the number of analyses for each intrusion. See Figure 4.15 in Chapter 4 for the locations of major plutons that comprise the batholith.

Batholith abbreviations: MB = Musquodoboit Batholith, SMB = South Mountain Batholith. Pluton abbreviations: BBP = Burnt Blanket Pluton (SMB), BuBP = Button Brook Pluton (SMB), BIP = Big Indian Polyintrusive Suite (SMB), BLP = Burnt Lake Pluton = Boot Lake Pluton (SMB), BMP = Bald Mountain Pluton, BP = Brenton Pluton, BPP = Barrington Passage Pluton, BRP = Bull Ridge Pluton, CLP = Cloud Lake Pluton (SMB), DLP = Davis Lake Pluton (South Mountain Batholith), DoLP = Dog Lake Pluton (SMB), EDP = East Dalhousie Pluton (SMB), EHP = Eastern Head Pluton, EKP = East Kemptville Pluton (SMB), ELP = Ellison Lake Pluton, GLP = Gasperaux Lake Pluton (SMB), GRP = Gold River Pluton (SMB), HCP = Halfway Cove Pluton, HP = Halifax Pluton (SMB), HFP = Harrietsfield Pluton (SMB), JSP = Joe Simon Pluton (SMB), KP = Kejimkujik Pluton (SMB), KLP = Kerr Lake Pluton (SMB), LBP = Lyons Bay Pluton, LC = Liscomb Complex, LP = Lequille Pluton (SMB), LGP = Lake George Pluton (SMB), LLP = Lewis Lake Pluton (SMB), LRP = Larrys River Pluton, LRoP = Little Round Lake Pluton (SMB), MLP = Mulgrave Lake Pluton, MuLP = Murphy Lake Pluton (SMB), MHP = Mickey Hill Pluton (SMB), MRP = Morse Road Pluton (SMB), MPP = Moose Point Pluton, NCP = New Cornwall Pluton (SMB), NRP = New Ross Pluton, PCP = Peggys Cove Pluton (SMB), (SMB), PLP = Panuke Lake Pluton (SMB), PMP = Port Mouton Pluton, QP = Queensport Pluton, RLP = Roseway Lake Pluton (SMB), ShP = Sherbrook Pluton, SwP = Sherwood Pluton (SMB), SIP = Seal Island Pluton, SLP = Sangster Lake Pluton, SaLP = Sandy Lake Pluton (SMB), ScLP = Scrag Lake Pluton (SMB), SoLP = Solomon Lake Pluton (SMB), SpLP = Spectacle Lake Pluton (SMB), StLP = Salmontail Lake Pluton (SMB), SP = Shelburne Pluton, TP = Tantallon Pluton (SMB), WP = Wedgeport Pluton, WBP = Walsh Brook Pluton (SMB), WDP = West Dalhousie Pluton (SMB), WLP = Whale Lake Pluton (SMB), WaP = Walden Pluton (SMB).

Sources of data: 1 = de Albuquerque (1979), 2 = McKenzie (1974), 3 = McKenzie and Clarke (1975), 4 = Bernadette, 1982 (uncited reference in Richard (1988)), 5 = Rogers (1984), 6 = Smith (1979), 7 = Charest (1976), 8 = Dwyer (1975), 9 = Weagle (1983), 10 = Richardson (in prep.) (uncited reference in Richard (1988)), 11 = Farley (1979), 12 = Wolfson (1983), 13 =

Alizay (1981) (uncited reference in Richard (1988)), 14 = Ham (1988), 15 = Cameron (1985), 16 = O'Reilly (1988), 17 = MacDonald (1981), 18 = MacDonald and Clarke (1985), 19 = O'Reilly (1976), 20 = Allan (1983) (uncited reference in Richard (1988)), 21 = de Albuquerque (1977), 22 = Douma (1988), 23 = Smith (1977) (uncited reference in Richard (1988)), 24 = Smith et al. (1987) (uncited reference in Richard (1988)), 25 = Hill (1991), 26 = Clarke et al. (1993b), 27 = Ham et al. (1989), 28 = Ham et al. (1990).

Table E1.1. Compilation of Meguma Zone granitoid lithogeochemistry

Sample	NBM106	NBM148	NBM193	NBMA52	NOE42	NOE045	NOE046	NOE047	NOE050	NOE059	NOE061	NAL1	NAL2
Batholith	-	-	-	-	-	-	-	-	-	-	-	-	-
Pluton	BMP	BMP	BMP	BMP	BP	BP	BP	BP	BP	BP	BP	BPP	BPP
Lithology	Mzg	Mzg	Mzg	Mzg	Mzg	Mzg	Mzg	Mzg	Mzg	Mzg	Mzg	Ton	Ton
Source	5	5	5	5	16	16	16	16	19	19	19	1	1
Major oxides													
SiO_2	73.34	74.11	73.23	71.60	75.72	76.00	76.42	75.56	71.68	74.76	75.72	66.39	64.13
TiO_2	0.17	0.17	0.22	0.20	0.12	0.12	0.11	0.16	0.30	0.20	0.21	0.72	0.74
Al_2O_3	14.84	14.21	14.64	15.30	12.51	12.37	12.23	12.14	13.68	12.71	12.55	16.48	17.75
Fe_2O_3	-	-	-	-	0.32	0.38	0.11	0.26	1.51	0.33	0.73	0.70	0.75
FeO	-	-	-	-	1.45	1.28	1.32	1.35	2.15	1.85	1.56	3.12	3.12
MnO	0.03	0.04	0.04	0.02	0.03	0.04	0.03	0.04	0.08	0.06	0.06	0.06	0.06
MgO	0.18	0.22	0.29	0.67	0.10	0.07	0.07	0.13	0.27	0.17	0.13	1.56	1.96
CaO	0.63	0.65	0.67	0.68	0.40	0.33	0.19	0.62	1.05	0.57	0.84	3.66	4.07
Na_2O	3.60	3.50	3.33	3.94	2.69	2.97	3.16	3.20	2.53	2.88	1.52	3.64	3.94
K_2O	4.49	4.50	4.49	4.53	5.59	5.58	5.35	5.21	5.41	5.44	5.44	2.18	2.19
P_2O_5	0.33	0.33	0.32	0.30	0.20	0.10	0.03	0.04	0.21	0.15	0.17	0.18	0.25
H_2O+	-	-	-	-	0.35	0.34	0.23	0.14	0.52	0.61	0.53	1.18	0.78
H_2O-	-	-	-	-	0.06	0.02	0.03	0.06	0.08	0.03	0.13	0.11	0.08
CO_2	-	-	-	-	-	-	-	-	-	-	-	-	-
Cl	-	-	-	-	-	-	-	-	-	-	-	-	-
F	0.03	0.04	0.04	0.04	-	-	-	-	-	-	-	-	-
LOI	0.99	0.84	0.86	1.00	0.41	0.36	0.26	0.20	0.60	0.64	0.66	1.29	0.86
TOTAL	99.76	99.86	99.50	99.48	99.49	99.54	99.25	98.36	99.28	99.70	99.22	99.86	99.69
Fe_2O_3T	1.30	1.45	1.59	1.40	1.93	1.80	1.58	1.76	3.90	2.38	2.16	4.16	4.21
FeOT	1.16	1.29	1.41	1.24	1.72	1.60	1.40	1.56	3.47	2.12	1.92	3.70	3.74
A/CNK	1.15	1.11	1.16	1.13	0.96	0.93	0.94	0.90	1.02	0.95	1.06	1.22	1.23
Trace els													
Ba	453	352	620	410	-	-	-	-	-	-	-	415	445
Rb	219	196	190	174	217	234	243	195	209	173	180	80	85
Sr	59	70	60	60	40	15	7	46	129	56	86	304	346
Y	11	15	-	10	-	-	-	-	-	-	-	-	-
Zr	74	74	-	62	79	90	93	145	293	180	191	-	-
Nb	9	11	-	8	23	26	27	26	29	28	26	-	-
Th	6.3	6.3	-	7.7	-	-	-	-	-	-	-	-	-
Pb	23	30	-	24	-	-	-	-	-	-	-	-	-
Ga	19	17	-	18	-	-	-	-	-	-	-	-	-
Zn	48	39	-	44	-	-	-	-	-	-	-	-	-
Cu	-	-	-	-	-	-	-	-	-	-	-	-	-
Ni	3	1	-	3	-	-	-	-	-	-	-	-	-
V	8	5	-	2	-	-	-	-	-	-	-	-	-
Cr	47	39	-	37	-	-	-	-	-	-	-	-	-
Hf	-	-	-	-	-	-	-	-	-	-	-	-	-
Cs	-	-	-	-	-	-	-	-	-	-	-	-	-
Sc	-	-	-	-	-	-	-	-	-	-	-	-	-
Ta	-	-	-	-	-	-	-	-	-	-	-	-	-
Co	-	-	-	-	-	-	-	-	-	-	-	-	-
Li	154	134	170	158	-	-	-	-	-	-	-	-	-
Be	5.2	5.2	-	7.4	-	-	-	-	-	-	-	-	-
B	-	-	-	-	-	-	-	-	-	-	-	-	-
U	6.1	5.9	-	5.7	-	-	-	-	-	-	-	-	-
W	-	-	-	-	-	-	-	-	-	-	-	-	-
Sn	8	14	-	5	-	-	-	-	-	-	-	-	-
Mo	-	-	-	-	-	-	-	-	-	-	-	-	-
Rare-earths													
La	-	-	-	-	-	-	-	-	-	-	-	-	-
Ce	-	-	-	-	-	-	-	-	-	-	-	-	-
Pr	-	-	-	-	-	-	-	-	-	-	-	-	-
Nd	-	-	-	-	-	-	-	-	-	-	-	-	-
Sm	-	-	-	-	-	-	-	-	-	-	-	-	-
Eu	-	-	-	-	-	-	-	-	-	-	-	-	-
Gd	-	-	-	-	-	-	-	-	-	-	-	-	-
Tb	-	-	-	-	-	-	-	-	-	-	-	-	-
Dy	-	-	-	-	-	-	-	-	-	-	-	-	-
Ho	-	-	-	-	-	-	-	-	-	-	-	-	-
Er	-	-	-	-	-	-	-	-	-	-	-	-	-
Tm	-	-	-	-	-	-	-	-	-	-	-	-	-
Yb	-	-	-	-	-	-	-	-	-	-	-	-	-
Lu	-	-	-	-	-	-	-	-	-	-	-	-	-

Table E1 1 (Continued) Compilation of Meguma Zone granitoid lithogeochemistry

Sample	NAL3	NBP233	NBP243	NBP265	NBP302	NBP344	NBP345	NBP348	NBP361	NBP364	NBP386	NBP387	NBP391
Batholith	-	-	-	-	-	-	-	-	-	-	-	-	-
Pluton	BPP	BPP	BPP	BPP	BPP	BPP	BPP	BPP	BPP	BPP	BPP	BPP	BPP
Lithology	Ton	Ton	Ton	Ton	Ton	Ton	Ton	Ton	Ton	Ton	Ton	Ton	Ton
Source	1	6	6	6	6	6	6	6	6	6	6	6	6
Major oxides													
SiO_2	63 93	69 82	61 95	67 27	65 94	64 28	67 60	63 32	66 01	68 73	67 83	60 91	70 03
TiO_2	0 79	0 68	0 94	0 73	0 76	0 74	0 66	0 48	0 86	0 78	0 64	1 07	0 29
Al_2O_3	17 78	15 02	17 83	15 45	16 20	16 92	15 91	18 93	15 57	15 08	15 55	18 08	16 68
Fe_2O_3	0 59	-	-	-	-	-	-	-	-	-	-	-	-
FeO	3 33	-	-	-	-	-	-	-	-	-	-	-	-
MnO	0 07	0 05	0 12	0 07	0 11	0 06	0 08	0 07	0 10	0 06	0 11	0 11	0 04
MgO	2 11	0 97	2.18	2 10	2.08	2.39	2 12	1 70	2 30	1 61	2.10	2 43	0 81
CaO	3 93	2.63	4 03	3 08	3 59	3 30	3 42	4 13	3 28	2 36	3 05	3 57	2 98
Na_2O	3 74	3 64	3 43	3 81	3 98	3 64	4 09	4 81	2.76	3 11	3 05	3 36	5 44
K_2O	2 33	1 45	2 58	1 96	2 03	2 20	1 98	2 57	2 48	2.13	1 81	2 74	1 15
P_2O_5	0 24	0 13	0 16	0 16	0 26	0 23	0 38	0 82	0 15	0 05	0 16	0 23	0 06
H_2O+	1 15	-	-	-	-	-	-	-	-	-	-	-	-
H_2O-	0,10	-	-	-	-	-	-	-	-	-	-	-	-
CO_2	-	-	-	-	-	-	-	-	-	-	-	-	-
Cl	-	-	-	-	-	-	-	-	-	-	-	-	-
F	-	0 05	0 01	0 04	0 04	0 07	0 09	-	0 05	0 05	0 05	0 06	0 08
LOI	1 25	0 55	0 01	1 61	0 61	0 98	0 69	0 57	0 81	0 90	0 71	0 88	0 49
TOTAL	99 98	98 04	98 52	99 88	99 53	99 15	100 93	100 66	99 17	98 77	99 12	99 37	99 41
Fe_2O_3T	4 29	3 40	5 95	4 10	4 47	4 96	4 50	3 67	5 46	4 46	4 62	6 74	1 62
FeOT	3 81	3 10	5 29	3 64	3 97	4 41	4 00	3 26	4 85	3 96	4 11	5 99	1 44
A/CNK	1 25	1 37	1 25	1 23	1 19	1 30	1 18	1 16	1 28	1 39	1 38	1 31	1 24
Trace els													
Ba	442	1108	1022	355	401	563	-	701	438	718	560	918	156
Rb	86	70	93	79	74	124	-	86	181	81	61	105	36
Sr	352	359	396	341	278	80	-	341	63	311	339	361	720
Y	-	25	23	10	16	15	-	33	12	10	18	26	7
Zr	-	281	246	191	174	51	-	148	88	191	198	245	125
Nb	-	10	12	11	13	8	-	14	8	11	10	12	3
Th	-	2.1	2 8	2 5	3	2	3 2	1 9	2 4	1 6	0 4	4 4	2 7
Pb	-	14	13	15	12	29	-	17	24	18	18	22	11
Ga	-	18	22	20	19	15	-	20	21	18	18	23	21
Zn	-	48	74	71	69	37	-	550	77	57	57	81	44
Cu	-	-	-	-	-	-	-	-	-	-	-	-	-
Ni	-	4	16	12	12	3	-	11	5	8	11	22	7
V	-	52	135	93	83	1	-	54	9	74	83	136	33
Cr	-	38	86	95	80	27	-	44	37	79	66	92	40
Hf	-	-	-	-	-	-	-	-	-	-	-	-	-
Cs	-	-	-	-	-	-	-	-	-	-	-	-	-
Sc	-	-	-	-	-	-	-	-	-	-	-	-	-
Ta	-	-	-	-	-	-	-	-	-	-	-	-	-
Co	-	-	-	-	-	-	-	-	-	-	-	-	-
Li	-	46	48	55	49	61	50	48	78	41	37	52	42
Be	-	2 8	1	2 7	2 3	0 5	3 1	-	1 1	0 9	2 6	3 4	2 5
B	-	-	-	-	-	-	-	-	-	-	-	-	-
U	-	2 8	0 9	1 1	1 9	1 6	1 2	2	1 1	1 7	120	2	2
W	-	-	-	-	-	-	-	-	-	-	-	-	-
Sn	-	7	14	50	7	5	-	2	13	11	11	14	5
Mo	-	-	-	-	-	-	-	-	-	-	-	-	-
Rare-earths													
La	-	-	-	-	-	-	-	-	-	-	-	-	-
Ce	-	-	-		-	-	-	-	-	-	-	-	-
Pr	-	-	-	-	-	-	-	-	-	-	-	-	-
Nd	-	-	-	-	-	-	-	-	-	-	-	-	-
Sm	-	-	-	-	-	-	-	-	-	-	-	-	-
Eu	-	-	-	-	-	-	-	-	-	-	-	-	-
Gd	-	-	-	-	-	-	-	-	-	-	-	-	-
Tb	-	-	-	-	-	-	-	-	-	-	-	-	-
Dy	-	-	-	-	-	-	-	-	-	-	-	-	-
Ho	-	-	-	-	-	-	-	-	-	-	-	-	-
Er	-	-	-	-	-	-	-	-	-	-	-	-	-
Tm	-	-	-	-	-	-	-	-	-	-	-	-	-
Yb	-	-	-	-	-	-	-	-	-	-	-	-	-
Lu	-	-	-	-	-	-	-	-	-	-	-	-	-

Table E1 1 (Continued) Compilation of Meguma Zone granitoid lithogeochemistry

Sample	N3P403	NBP405	N8P415	NBP418	NBP531	NBP560	NBP562	NBP594	NBP608	NEP610	NBP633	NBP642	NBP652
Batholith	-	-	-	-	-	-	-	-	-	-	-	-	-
Pluton	BPP	BPP	BPP	BPP	BPP	BPP	BPP	BPP	BPP	BPP	BPP	BPP	BPP
Lithology	Ton	Ton	Ton	Gra	Ton	Ton	Ton	Ton	Ton	Ton	Ton	Ton	Ton
Source	6	6	6	6	6	6	6	6	6	6	6	6	6
Major oxides													
SiO_2	66 59	65 75	68 95	72 39	63 37	64 42	65 13	66 20	65 86	67 08	70 77	67 10	69 74
TiO_2	0 67	0 81	0 51	0 42	0 95	0 85	0 90	0 71	0 68	0 64	0 69	0 67	0 57
Al_2O_3	15 83	15 58	15 02	14 14	16 52	16 33	15 73	16 30	15 98	15 80	14 19	16 16	14 91
Fe_2O_3	-	-	-	-	-	-	-	-	-	-	-	-	-
FeO	-	-	-	-	-	-	-	-	-	-	-	-	-
MnO	0 08	0 08	0 08	0 07	0 12	0 10	0 14	0 08	0 09	0 09	0 07	0 09	0 09
MgO	2 20	2.20	1 66	1 16	2 08	2 31	2 39	2 41	2.29	2 06	1 64	2 63	1 00
CaO	2 98	2.98	3 03	[illegible]	2 90	3 47	3 27	3 34	3 22	3 23	1 36	3 18	1 96
Na_2O	3 63	3 63	4 07	3 56	3 55	3 24	3 19	3 75	3 94	4 07	2 75	3 66	3 34
K_2O	2 67	2 67	1 66	1 94	2.76	2.70	2 30	2 32	2 06	1 89	2 57	2 49	3 55
P_2O_5	0 25	0 26	0 17	0 11	0 47	0 17	0 20	0 24	0 23	0 20	0 12	0 32	0 33
H_2O+	-	-	-	-	-	-	-	-	-	-	-		-
H_2O-	-	-	-	-	-	-	-	-	-	-	-	-	-
CO_2	-	-	-	-	-	-	-	-	-	-	-	-	-
Cl	-	-	-	-	-	-	-	-	-	-	-	-	-
F	0 04	0 04	0 05	0 03	0 05	0 06	0 04	0 04	0 04	0 04	0 03	0 04	0 08
LOI	0 69	0 99	0 84	0 87	1 07	0 83	0 88	0 61	0 63	0 53	1 05	0 66	0 98
TOTAL	99 60	99 27	99 23	99 30	99 16	99 15	99 12	100 11	99 02	99 42	99 30	101 08	99 70
Fe_2O_3T	4 51	4 86	3 64	2 54	6 04	5 32	5 61	4 67	4 55	4 31	4 00	4 76	3 64
FeOT	4 01	4 32	3 24	2.26	5 37	4 73	4 99	4 15	4 04	3 83	4 09	4 23	3 24
A/CNK	1 19	1 17	1 21	1 26	1 25	1 21	1 26	1 22	1 22	1 21	1 46	1 21	1 16
Trace els													
Ba	270	545	255	345	690	843	735	423	233	225	650	532	156
Rh	92	105	79	74	110	95	85	111	101	91	85	105	36
Sr	250	260	282	228	306	390	339	274	239	231	226	278	720
Y	15	17	9	7	35	17	16	22	22	19	25	31	7
Zr	166	165	164	107	234	215	189	169	157	156	217	178	125
Nb	13	17	15	9	16	10	13	12	15	14	14	13	3
Th	4 6	4 3	1 6	4 7	5 3	1 9	4 3	3 5	1 7	3 6	3 4	3 5	2 7
Pb	18	15	12	17	23	17	11	13	12	17	15	13	11
Ga	19	20	19	15	21	19	18	23	20	22	18	25	21
Zn	75	80	48	52	84	65	76	78	78	68	65	77	44
Cu	-	-	-	-	-	-	-	-	-	-	-	-	-
Ni	10	16	18	10	23	21	17	15	21	15	23	17	7
V	90	102	65	48	103	114	111	84	74	65	73	86	33
Cr	75	97	84	85	73	81	81	74	73	69	84	76	40
Hf	-	-	-	-	-	-	-	-	-	-	-	-	-
Cs	-	-	-	-	-	-	-	-	-	-	-	-	-
Sc	-	-	-	-	-	-	-	-	-	-	-	-	-
Ta	-	-	-	-	-	-	-	-	-	-	-	-	-
Co	-	-	-	-	-	-	-	-	-	-	-	-	-
Li	58	60	40	52	57	34	152	59	59	63	117	54	42
Be	2 6	3 6	3 6	2 6	3 2	2 3	2 2	-	3 3	2 8	2 9	3 4	2 5
B	-	-	-	-	-	-	-	-	-	-	-	-	-
U	3	1	0 8	2	1 9	1 2	1 4	2 8	2 4	2 2	1 7	2	2
W	-	-	-	-	-	-	-	-	-	-	-	-	-
Sn	3	4	1	12	10	80	-	3	8	7	8	-	5
Mo	-	-	-	-	-	-	-	-	-	-	-	-	-
Rare-earths													
La	-	-	-	-	-	-	-	-	-	-	-	-	-
Ce	-	-	-	-	-	-	-	-	-	-	-	-	-
Pr	-	-	-	-	-	-	-	-	-	-	-	-	-
Nd	-	-	-	-	-	-	-	-	-	-	-	-	-
Sm	-	-	-	-	-	-	-	-	-	-	-	-	-
Eu	-	-	-	-	-	-	-	-	-	-	-	-	-
Gd	-	-	-	-	-	-	-	-	-	-	-	-	-
Tb	-	-	-	-	-	-	-	-	-	-	-	-	-
Dy	-	-	-	-	-	-	-	-	-	-	-	-	-
Ho	-	-	-	-	-	-	-	-	-	-	-	-	-
Er	-	-	-	-	-	-	-	-	-	-	-	-	-
Tm	-	-	-	-	-	-	-	-	-	-	-	-	-
Yb	-	-	-	-	-	-	-	-	-	-	-	-	-
Lu	-	-	-	-	-	-	-	-	-	-	-	-	-

Table E1 1 (Continued) Compilation of Meguma Zone granitoid lithogeochemistry

Sample	NBP665	NBPA07	NBPA08	NBPA13	NBPA15	NBPA21	NBC001	NBC002	NBC003	NBC004	NBC005	NBC006	NBC007
Batholith	-	-	-	-	-	-	-	-	-	-	-	-	-
Pluton	BPP	BPP	BPP	BPP	BPP	BPP	BRP	BRP	BRP	BRP	BRP	BRP	BRP
Lithology	Ton	Ton	Ton	Ton	Ton	Ton	Mzg	Mzg	Mzg	Mzg	Mzg	Mzg	Mzg
Source	6	6	6	6	6	6	4	4	4	4	4	4	4
Major oxides													
SiO_2	67 08	66 40	70 13	66 80	66 10	67 50	73 20	73 20	72 50	74 40	73 20	72 60	73 50
TiO_2	0 57	0 64	0 49	0 56	0 66	0 71	0 13	0 22	0 22	0 22	0 15	0 14	0 13
Al_2O_3	14 91	15 80	14 94	15 90	16 10	15 50	15 00	15 10	15 90	14 40	14 00	15 50	15 20
Fe_2O_3	-	-	-	-	-	-	0 19	0 16	0 32	0 11	0 05	0 09	0 19
FeO	-	-	-	-	-	-	0 77	0 90	0 82	1 02	0 90	0 90	0 72
MnO	0 08	0 05	0 07	0 07	0 09	0 07	0 02	0 03	0 03	0 02	0 03	0 02	0 03
MgO	1 00	1 96	1 47	1.77	2 07	1 49	0 30	0 36	0 39	0 40	0 35	0 38	0 27
CaO	1 96	3 29	2.45	2.81	3 42	2.41	0 39	0 50	0 44	0 46	0 47	0 49	0 56
Na_2O	3 34	4 05	3 90	4 06	4 04	3 83	3 90	3 46	3 58	3 20	3 82	3 88	3 96
K_2O	3 55	2 02	2 32	2.70	2 29	2.32	4 83	4 93	5 20	5 36	5 26	5 98	4 52
P_2O_5	0 33	0 21	0 17	0 21	0 22	0 16	0 40	0 44	0 39	[illegible]	0 31	0 34	0 32
H_2O+	-	-	-	-	-	-	-	-	-	-	-	-	-
H_2O-	-	-	-	-	-	-	-	-	-	-	-	-	-
CO_2	-	-	-	-	-	-	-	-	-	-	-	-	-
Cl	-	-	-	-	-	-	-	-	-	-	-	-	-
F	-	0 05	-	0 05	0 04	0 05	0 03	0 04	0 04	0 02	0 02	0 03	0 03
LOI	0 98	0 31	0 83	0 85	1 00	0 85	0 90	1 00	1 00	1 00	0 70	0 60	0 70
TOTAL	97 02	98 77	99 45	99 53	99 87	99 47	99 99	100 27	100 74	100 80	99 72	100 90	100 07
Fe_2O_3T	3 64	4 55	3 02	4 28	4 37	5 21	1 04	1 16	1 23	1 24	1 05	1 09	0 99
FeOT	3 24	4 04	2.68	3 80	3 88	4 63	0 92	1 03	1 09	1 10	0 93	0 97	0 88
A/CNK	1 16	1 19	1 20	1 16	1 16	1 26	1 11	1 14	1 15	1 07	1 02	1 00	1 13
Trace els													
Ba	-	380	-	380	320	540	300	340	350	395	425	520	285
Rb	-	60	-	110	80	90	255	180	280	240	230	200	195
Sr	-	320	-	290	350	400	54	60	55	115	160	170	135
Y	-	-	-	-	-	-	-	-	-	-	-	-	-
Zr	-	-	-	-	200	360	-	-	-	-	-	-	-
Nb	-	-	-	-	-	-	-	-	-	-	-	-	-
Th	-	-	-	-	6	12	4	4	3	8	5	9	2
Pb	-	-	-	-	6	8	20	14	15	22	17	41	27
Ga	-	-	-	-	-	-	-	-	-	-	-	-	-
Zn	-	-	-	-	770	81	58	63	55	53	57	21	27
Cu	-	-	-	-	-	-	9	11	9	8	10	10	10
Ni	-	-	-	-	22	21	-	-	-	-	-	-	-
V	-	-	-	-	-	-	-	-	-	-	-	-	-
Cr	-	-	-	-	-	-	-	-	-	-	-	-	-
Hf	-	-	-	-	-	-	-	-	-	-	-	-	-
Cs	-	-	-	-	-	-	-	-	-	-	-	-	-
Sc	-	-	-	-	-	-	-	-	-	-	-	-	-
Ta	-	-	-	-	-	-	-	-	-	-	-	-	-
Co	-	-	-	-	-	-	-	-	-	-	-	-	-
Li	-	54	-	71	59	53	197	230	203	100	90	60	120
Be	-	-	-	-	-	-	10	6 8	7 5	4 4	6 4	3 7	6 3
B	-	-	-	-	-	-	11	14	6	5	4	4	50
U	-	-	-	-	2.2	2 7	3 8	3 6	3 9	4	3 2	3 5	3 5
W	-	-	-	-	-	-	-	-	-	-	-	-	-
Sn	-	-	-	-	3	3	9 4	8 7	8 9	6 2	6	4 7	7 1
Mo	-	-	-	-	-	-	1	1 3	0 8	0 8	0 8	0 6	0 7
Rare-earths													
La	-	-	-	-	-	-	-	-	-	-	-	-	-
Ce	-	-	-	-	-	-	-	-	-	-	-	-	-
Pr	-	-	-	-	-	-	-	-	-	-	-	-	-
Nd	-	-	-	-	-	-	-	-	-	-	-	-	-
Sm	-	-	-	-	-	-	-	-	-	-	-	-	-
Eu	-	-	-	-	-	-	-	-	-	-	-	-	-
Gd	-	-	-	-	-	-	-	-	-	-	-	-	-
Tb	-	-	-	-	-	-	-	-	-	-	-	-	-
Dy	-	-	-	-	-	-	-	-	-	-	-	-	-
Ho	-	-	-	-	-	-	-	-	-	-	-	-	-
Er	-	-	-	-	-	-	-	-	-	-	-	-	-
Tm	-	-	-	-	-	-	-	-	-	-	-	-	-
Yb	-	-	-	-	-	-	-	-	-	-	-	-	-
Lu	-	-	-	-	-	-	-	-	-	-	-	-	-

Table E1.1 (Continued) Compilation of Meguma Zone granitoid lithogeochemistry

Sample	NBC008	NBC009	NBC010	NBC011	NBC012	NEK1	NEKI0	NEK2	NEK46	NEK47	NEK53	NEK56	NEK57
Batholith	-	-	-	-	-	SMB	SMB	SMB	SMB	SMB	SMB	SMB	SMB
Pluton	BRP	BRP	BRP	BRP	BRP	DLP	DLP	DLP	DLP	DLP	DLP	DLP	DLP
Lithology	Mzg	Mzg	Mzg	Mzg	Mzg	Mzg	Mzg	Mzg	Mzg	Mzg	Mzg	Mzg	Mzg
Source	4	4	4	4	4	10	10	10	10	10	10	10	10
Major oxides													
SiO_2	73 50	72 40	73 40	72 20	72 80	76 50	76 60	77 10	75 70	75 90	7} 40	76 21	76 49
TiO_2	0 15	0 17	0 23	0 22	0 18	0 15	0 15	0 14	0 20	0 11	0 20	0 11	0 12
Al_2O_3	15 00	15 30	15 00	16 30	15 10	12.40	12 00	12.40	12 50	12 60	12 70	12 89	12 73
Fe_2O_3	0 15	0 34	0 30	0 04	0 15	0 45	0 42	0 25	0 50	0 38	0 26	-	-
FeO	0 73	0 56	0 90	0 90	0 86	1 10	1 30	1 20	1 40	1 00	1 70	-	-
MnO	0 03	0 02	0 02	0 03	0 01	0 04	0 04	0 04	0 04	0 04	0 04	0 04	0 03
MgO	0 29	0 25	0 50	0 39	0 33	0 24	0 40	0 20	0 29	0 15	0 24	0 27	0 36
CaO	0 58	0 39	0 58	0 46	0 60	0 50	0 70	0 63	0 62	0 49	0 74	0 38	0 32
Na_2O	3 78	3 71	3 62	4 06	4 01	3 40	3 30	4 10	3 29	3 49	3 41	2 98	3 03
K_2O	4 72	4 76	5 21	5 14	4 86	4 89	4 38	3 31	4 54	4 49	4 71	5 13	4 87
P_2O_5	0 31	0 24	0 32	0 31	0 28	0 06	0 09	0 07	0 10	0 07	0 09	0 10	0 06
H_2O+	-	-	-	-	-	-	-	-	-	-	-	-	-
H_2O-	-	-	-	-	-	-	-	-	-	-	-	-	-
CO_2	-	-	-	-	-	-	-	-	-	-	-	-	-
Cl	-	-	-	-	-	-	-	-	-	-	-	-	-
F	0 03	0 03	0 04	0 04	0 03	0 20	0 13	0 05	0 14	0 23	0 24	0 21	0 06
LOI	0 70	0 90	0 80	0 90	0 80	0 77	0 54	0 85	0 54	0 54	0 39	0 21	0 06
TOTAL	99 91	98 99	100 84	100 93	99 95	100 43	99 85	100 24	99 64	99 20	98 83	99 73	99 64
Fe_2O_3T	0 96	0 96	1 30	1 04	1 10	1 67	1 86	1 58	2 05	1 49	2 15	1 59	1 77
FeOT	0 85	0 85	1,16	0 92	0 98	1 48	1 65	1 40	1 82	1 32	1 91	1 41	1 57
A/CNK	1 11	1 16	1 07	1 13	1 07	0 95	0 96	1 05	0 99	1 00	0 96	1 01	1 03
Trace els													
Ba	380	350	350	500	650	201	157	-	220	170	230	96	128
Rb	190	360	255	295	170	527	397	180	415	530	455	544	495
Sr	135	49	54	61	80	31	24	107	50	18	38	19	41
Y	-	-	-	-	-	44	48	41	40	10	50	45	37
Zr	-	-	-	-	-	89	99	80	110	70	120	79	83
Nb	-	-	-	-	-	15	20	20	20	10	10	0	12
Th	2	2	7	4	7	13	15	18	30	24	34	-	-
Pb	29	21	16	29	22	17	24	22	21	6	13	-	-
Ga	-	-	-	-	-	-	-	-	-	-	-	-	-
Zn	41	49	59	62	40	33	34	36	27	17	26	22	38
Cu	9	9	8	11	11	11	2	6	4	7	5	-	-
Ni	-	-	-	-	-	7	5	6	-	-	-	94	95
V	-	-	-	-	-	8	9	7	-	-	-	4	-
Cr	-	-	-	-	-	27	25	19	220	140	40	37	37
Hf	-	-	-	-	-	3 1	3 2	-	-	-	-	-	-
Cs	-	-	-	-	-	14	11	5	13	16	14	-	-
Sc	-	-	-	-	-	4	4	-	-	-	-	-	-
Ta	-	-	-	-	-	1	0 7	-	-	-	-	-	-
Co	-	-	-	-	-	-	-	-	-	-	-	-	-
Li	214	135	144	130	51	98	79	40	113	138	131	-	-
Be	5 1	4 6	5 6	14	8 5	10	11	37	-	-	-	-	-
B	6	6	3	4	6	25	25	25	-	10 3	-	-	-
U	2.5	7 2	4 6	3 4	3 6	20	26	17	11	15	13	-	-
W	-	-	-	-	-	19	12	10	10	10	10	-	-
Sn	7 1	7	59	7 4	5 2	15	7	13	12	21	8	6	16
Mo	0 7	0 9	0 6	0 7	1	2	4	3	1	1	1	-	-
Rare-earths													
La	-	-	-	-	-	-	-	-	-	-	-	-	-
Ce	-	-	-	-	-	-	-	-	-	-	-	-	-
Pr	-	-	-	-	-	-	-	-	-	-	-	-	-
Nd	-	-	-	-	-	-	-	-	-	-	-	-	-
Sm	-	-	-	-	-	-	-	-	-	-	-	-	-
Eu	-	-	-	-	-	-	-	-	-	-	-	-	-
Gd	-	-	-	-	-	-	-	-	-	-	-	-	-
Tb	-	-	-	-	-	-	-	-	-	-	-	-	-
Dy	-	-	-	-	-	-	-	-	-	-	-	-	-
Ho	-	-	-	-	-	-	-	-	-	-	-	-	-
Er	-	-	-	-	-	-	-	-	-	-	-	-	-
Tm	-	-	-	-	-	-	-	-	-	-	-	-	-
Yb	-	-	-	-	-	-	-	-	-	-	-	-	-
Lu	-	-	-	-	-	-	-	-	-	-	-	-	-

Table E1 1 (Continued) Compilation of Meguma Zone granitoid lithogeochemistry

Sample	NEK9	NEH20	NPL014	NPL015	NPL016	NPL017	NPL018	NPL019	NPL020	NPL021	NPL022	NPL023	NPL024
Batholith	SMB	-	-	-	-	-	-	-	-	-	-	-	-
Pluton	DLP	EHP	ELP	ELP	ELP	ELP	ELP	ELP	ELP	ELP	ELP	ELP	ELP
Lithology	Mzg	Mzg	Grd	Grd	Grd	Grd	Grd	Grd	Grd	Grd	Grd	Grd	Grd
Source	10	9	20	20	20	20	20	20	20	20	20	20	20
Major oxides													
SiO_2	75 70	71 70	68 00	66 00	68 00	67 50	67 00	67 50	67 00	67 00	68 00	67.50	67 70
TiO_2	0 29	0 15	0 60	0 60	0 61	0 60	0 60	0 60	0 60	0 61	0 61	0 60	0 61
Al_2O_3	12 50	14 80	14 98	14 93	14 92	14 97	15 00	14 89	15 01	14 92	14 90	14 95	14 93
Fe_2O_3	0 65	-	-	-	-	-	-	-	-	-	-	-	-
FeO	1 40	-	-	-	-	-	-	-	-	-	-	-	-
MnO	0 03	0 06	0 10	0 10	0 09	0 10	0 09	0 07	0 09	0 11	0 09	0 09	0 10
MgO	0 30	0 70	1 35	1 33	1 30	1 42	1 28	1 18	1 32	1 40	1 31	1 26	1 34
CaO	0 46	1 10	1 67	1 83	2 05	1 67	1 98	1 33	2 05	2 12	2 23	2 10	2 19
Na_2O	3 20	3 90	2.86	2 88	2 88	2.98	2 86	2 74	2 80	2 90	2 76	2 86	2 90
K_2O	4 87	4 40	4 38	4 56	4 11	3 89	4 23	4 30	4 28	3 92	4 08	4 29	4 15
P_2O_5	0 08	0 16	0 19	0 10	0 19	0 20	0 20	0 19	0 19	0 19	0 19	0 19	0 19
H_2O+	-	0 74	-	-	-	-	-	-	-	-	-	-	-
H_2O-	-	-	-	-	-	-	-	-		-	-	-	-
CO_2	-	-	-	-	-	-	-	-	-	-	-	-	-
Cl	0 01	-	-	-	-	-	-	-	-	-	-	-	-
F	0 08	0 04	0 04	0 05	0 06	0 06	0 05	0 05	0 05	0 06	0 06	0 06	0 06
LOI	0 77	0 78	2 05	2 80	0 75	1 69	1 10	1 50	1 35	1 31	0 48	1 01	0 91
TOTAL	100 16	99 17	100 38	99 33	99 13	99 22	98 54	98 48	98 89	98 66	98 85	99 05	99 21
Fe_2O_3T	2 20	1 60	4 72	4 72	4 76	4 73	4 72	4 70	4 72	4 70	4 72	4 73	4 71
FeOT	1 96	1 42	4 20	4 20	4 23	4 20	4 20	4 18	4 20	4 18	4 20	4 20	4 19
A/CNK	0 98	1 07	1 14	1 09	1 13	1 19	1 13	1 20	1 12	1 14	1 12	1 10	1 10
Trace els													
Ba	313	610	850	750	660	760	720	926	746	620	830	740	800
Rb	360	134	154	167	152	139	172	174	187	171	144	176	162
Sr	48	180	240	190	180	245	170	165	190	160	190	200	170
Y	49	-	-	-	-	-	-	-	-	-	-	-	-
Zr	165	-	-	-	-	-	-	-	-	-	-	-	-
Nb	20	-		-	-	-	-	-	-	-	-	-	-
Th	16	4	16	14	17	17	14	14	13	18	14	15	15
Pb	24	29	10	4	10	12	14	[illegible]	16	33	30	33	14
Ga	-	-	-	-	-	-	-	-	-	-	-	-	-
Zn	34	32	59	75	76	36	66	44	59	83	59	69	80
Cu	4	11	13	11	12	10	12	15	13	16	104	13	14
Ni	7	-	-	-	-	-	-	-	-	-	-	-	-
V	19	-	-	-	-	-	-	-	-	-	-	-	-
Cr	20	-	-	-	-	-	-	-	-	-	-	-	-
Hf	4 2	-	-	-	-	-	-	-	-	-	-	-	-
Cs	10	-	-	-	-	-	-	-	-	-	-	-	-
Sc	5	-	-	-	-	-	-	-	-	-	-	-	-
Ta	0 7	-	-	-	-	-	-	-	-	-	-	-	-
Co	-	-	-	-	-	-	-	-	-	-	-	-	-
Li	58	95	77	62	82	86	71	78	89	83	90	87	92
Be	-	4 3	-	-	-	-	-	-	-	-	-	-	-
B	25	4	37	20	51	42	39	58	61	37	48	31	13
U	4	6 4	3 4	2.9	3 3	2.9	3 4	6 9	360	380	3 8	3 9	3 2
W	7	-	-	-	-	-	-	-	-	-	-	-	-
Sn	11	5	5 1	5 2	4 8	4	4 2	4 8	5	5	4 5	4 7	4
Mo	3	0 9	2	1 3	2	2.5	2.1	2 2	2 2	1 5	2 8	1 5	2
Rare-earths													
La	-	-	-	-	-	-	-	-	-	-	-	-	-
Ce	-	-	-	-	-	-	-	-	-	-	-	-	-
Pr	-	-	-	-	-	-	-	-	-	-	-	-	-
Nd	-	-	-	-	-	-	-	-	-	-	-	-	-
Sm	-	-	-	-	-	-	-	-	-	-	-	-	-
Eu	-	-	-	-	-	-	-	-	-	-	-	-	-
Gd	-	-	-	-	-	-	-	-	-	-	-	-	-
Tb	-	-	-	-	-	-	-	-	-	-	-	-	-
Dy	-	-	-	-	-	-	-	-	-	-	-	-	-
Ho	-	-	-	-	-	-	-	-	-	-	-	-	-
Er	-	-	-	-	-	-	-	-	-	-	-	-	-
Tm	-	-	-	-	-	-	-	-	-	-	-	-	-
Yb	-	-	-	-	-	-	-	-	-	-	-	-	-
Lu	-	-	-	-	-	-	-	-	-	-	-	-	-

Table E1 1 (Continued) Compilation of Meguma Zone granitoid lithogeochemistry

Sample	NPL025	NPL025	NPL028	NLHH01	NLHH02	NLHH03	NLHH04	NLHH05	NLHH06	NLHH07	NLHHL18	NLHHL34	NLHHL37
Batholith	-	-	-	-	-	-	-	-	-	-	-	-	-
Pluton	ELP	ELP	ELP	HCP	HCP	HCP	HCP	HCP	HCP	HCP	HCP	HCP	HCP
Lithology	Grd	Grd	Grd	Mzg	Mzg	Mzg	Mzg	Mzg	Mzg	Mzg	Mzg	Mzg	Mzg
Source	20	20	20	14	14	14	14	14	14	14	14	14	14
Major oxides													
SiO_2	68 00	68 50	68 10	72 17	71 40	72 65	72 18	71 56	72.55	71 20	72.37	71 88	74 14
TiO_2	0 61	0 61	0 61	0 30	0 21	0 25	0 28	0 25	0 23	0 18	0 17	0 16	0 02
Al_2O_3	14 92	14 93	14 97	14 75	14 46	14 72	15 42	15 30	14 78	14 99	14 86	14 66	15 32
Fe_2O_3	-	-	-	0 21	0 12	0 02	0 30	0 12	-	-	0 09	-	-
FeO	-	-	-	1 64	1 12	1 38	1 27	1 24	-	-	1 03	-	-
MnO	0 09	0 09	0 09	0 08	0 04	0 03	0 06	0 06	0 04	0 06	0 04	0 03	0 16
MgO	1 28	1 34	1 32	0 50	0 36	0 41	0 45	0 40	0 47	0 34	0 31	0 31	0 07
CaO	1 92	2 07	2.26	0 50	0 54	0 55	0 48	0 52	0 54	0 48	0 52	0 50	0 39
Na_2O	2 92	2 89	2 92	3 18	3 41	3 33	3 39	3 50	3 23	3 61	2 73	3 58	3 35
K_2O	4 13	4 06	4 25	4 63	4 77	5 20	4 94	4 92	5 24	4 75	5 02	4 73	5 26
P_2O_5	0 19	0 18	0 19	0 37	0 31	0 32	0 30	0 35	0 33	0 34	0 31	[illegible]	0 22
H_2O+	-	-	-	1 08	1 00	0 85	0 89	0 88	0 59	0 79	0 90	1 0	0 79
H_2O-	-	-	-	0 48	0 49	0 36	0 42	0 32	0 42	0 33	0 44	0 35	0 35
CO_2	-	-	-	-	-	-	-	-	-	-	-	-	-
Cl	-	-	-	-	-	-	-	-	-	-	-	-	-
F	0 05	0 06	0 06	0 07	0 05	0 05	0 05	0 06	0 05	0 05	0 06	0 05	-
LOI	0 05	1 12	0 85	1 63	1 54	1 26	1 36	1 26	1 06	1 17	1 40	1 47	1 14
TOTAL	98 31	99 98	99 75	99 91	98 25	100 10	100 36	99 45	99 99	98 28	98 82	98 76	100 80
Fe_2O_3T	4 72	4 71	4 71	2 03	1 36	1 55	1 71	1 50	1 71	1 31	1 23	1 24	0 82
FeOT	4 20	4 19	4 19	1 80	1 21	1 38	1 52	1 33	1 52	1 16	1 09	1 10	0 73
A/CNK	1 13	1 13	1 08	1 19	1 11	1 09	1 17	1 15	1 10	1 14	1 20	1 12	1 14
Trace els													
Ba	950	830	680	215	274	364	322	310	378	276	248	240	64
Rb	147	167	163	285	240	217	246	247	225	263	255	226	267
Sr	170	170	240	58	70	90	81	79	80	62	65	66	34
Y	-	-	-	14	11	11	11	11	10	11	9	9	8
Zr	-	-	-	81	74	90	84	81	92	63	62	63	29
Nb	-	-	-	15	10	9	11	11	11	12	10	11	8
Th	17	16	14	10	11	12	11	9	9	8	8	10	2
Pb	18	16	18	22	27	28	28	25	29	27	23	65	32
Ga	-	-	-	24	20	21	23	24	24	22	19	21	21
Zn	77	67	75	90	60	64	53	55	66	49	44	195	13
Cu	19	12	12	-	-	-	-	-	-	-	-	-	-
Ni	-	-	-	10	4	4	4	3	10	10	6	4	6
V	-	-	-	19	3	12	-	13	13	12	5	5	-
Cr	-	-	-	23	12	10	19	15	19	9	13	10	7
Hf	-	-	-	-	-	-	-	-	-	-	-	-	-
Cs	-	-	-	-	-	-	-	-	-	-	-	-	-
Sc	-	-	-	-	-	-	-	-	-	-		-	-
Ta	-	-	-	-	-	-	-	-	-	-	-	-	-
Co	-	-	-	-	-	-	-	-	-	-	-	-	-
Li	76	80	74	164	108	76	95	108	-	-	107	36	-
Be	-	-	-	7	6 5	4 5	4 5	6 5	3 5	4	70	6 5	-
B	27	37	15	15	15	25	10	20	20	20	15	20	-
U	3 3	4 6	3 3	11 5	7 4	6 2	7 2	5 5	-	-	7 7	24 6	-
W	-	-	-	2	5	1	6	4	-	-	1	5	-
Sn	4 8	4 7	4 3	13	10	1	5	9	9	12	8	8	-
Mo	1 7	2	1 4	1	1	1	1	1	2	2	1	1	-
Rare-earths													
La	-	-	-	-	-	-	-	-	-	-	-	-	-
Ce	-	-	-	-	-	-	-	-	-	-	-	-	-
Pr	-	-	-	-	-	-	-	-	-	-	-	-	-
Nd	-	-	-	-	-	-	-	-	-	-	-	-	-
Sm	-	-	-	-	-	-	-	-	-	-	-	-	-
Eu	-	-	-	-	-	-	-	-	-	-	-	-	-
Gd	-	-	-	-	-	-	-	-	-	-	-	-	-
Tb	-	-	-	-	-	-	-	-	-	-	-	-	-
Dy	-	-	-	-	-	-	-	-	-	-	-	-	-
Ho	-	-	-	-	-	-	-	-	-	-	-	-	-
Er	-	-	-	-	-	-	-	-	-	-	-	-	-
Tm	-	-	-	-	-	-	-	-	-	-	-	-	-
Yb	-	-	-	-	-	-	-	-	-	-	-	-	-
Lu	-	-	-	-	-	-	-	-	-	-	-	-	-

Table E1.1 (Continued) Compilation of Meguma Zone granitoid lithogeochemistry

Sample	NTS803	NTS804	NTS805	NTS806	NTS812	NTS813	NTS814	NTS815	NTS816	NTS817	NTS818	NTS819	NTS820
Batholith	SMB	SMB	SMB	SMB	SMB	SMB	SMB	SMB	SMB	SMB	SMB	SMB	SMB
Pluton	HP	HP	HP	HP	HP	HP	HP	HP	HP	HP	HP	HP	HP
Lithology	Lg	Lg	Lg	Lg	Mzg	Mzg	Mzg	Mzg	Mzg	Mzg	Mzg	Mzg	Mzg
Source	24	24	24	24	24	24	24	24	24	24	24	24	24
Major oxides													
SiO_2	75.80	76.43	75.81	78.13	74.14	75.33	73.13	74.03	72.31	72.64	73.49	74.92	71.74
TiO_2	0.16	0.17	0.17	0.18	0.31	0.20	0.34	0.24	0.32	0.30	0.32	0.26	0.34
Al_2O_3	12.71	12.83	12.86	11.39	13.44	13.37	13.41	13.32	13.72	13.69	13.46	12.96	13.65
Fe_2O_3	-	-	-	-	-	-	-	-	-	-	-	-	-
FeO	-	-	-	-	-	-	-	-	-	-	-	-	-
MnO	0.04	0.03	0.05	0.06	0.05	0.05	0.04	0.04	0.05	0.04	0.05	0.05	0.04
MgO	0.16	0.18	0.35	0.29	0.44	0.25	0.48	0.11	0.42	0.31	0.54	0.36	0.45
CaO	0.39	0.39	0.56	0.46	0.74	0.55	0.87	0.63	0.96	0.85	0.85	0.82	0.85
Na_2O	3.09	3.36	3.39	2.21	3.53	3.69	3.29	3.67	3.68	3.36	3.44	3.37	3.49
K_2O	4.59	4.33	4.61	4.10	4.48	4.28	4.33	4.47	4.48	4.10	3.99	4.08	4.58
P_2O_5	0.17	0.18	0.18	0.17	0.25	0.23	0.23	0.21	0.22	0.26	0.26	0.23	0.23
H_2O+	-	-	-	-	-	-	-	-	-	-	-	-	-
H_2O-	-	-	-	-	-	-	-	-	-	-	-	-	-
CO_2	-	-	-	-	-	-	-	-	-	-	-	-	-
Cl	-	-	-	-	-	-	-	-	-	-	-	-	-
F	-	-	-	-	-	-	-	-	-	-	-	-	-
LOI	0.81	0.95	0.78	0.64	0.50	0.89	0.81	1.02	0.77	1.12	1.08	0.93	0.89
TOTAL	99.17	99.95	100.38	99.13	100.00	100.40	99.08	99.30	98.96	98.69	99.61	99.67	98.43
Fe_2O_3T	1.41	1.24	1.82	1.69	2.38	1.76	2.44	1.75	2.28	2.27	2.40	1.88	2.44
FeOT	1.25	1.10	1.62	1.50	2.12	1.56	2.17	1.56	2.03	2.02	2.13	1.67	2.17
A/CNK	1.05	1.07	1.01	1.12	1.04	1.06	1.07	1.02	1.02	1.11	1.10	1.06	1.03
Trace els													
Ba	74	67	78	58	184	35	63	240	276	201	204	206	279
Rb	232	228	262	234	267	300	250	258	249	241	235	224	240
Sr	18	16	25	21	56	20	27	62	69	59	60	57	76
Y	23	18	13	19	17	12	13	17	17	16	17	14	17
Zr	71	72	63	64	112	63	77	130	124	106	120	93	127
Nb	-	-	-	-	-	-	12	15	14	13	15	11	13
Th	-	-	-	-	-	-	-	-	-	-	-	-	-
Pb	-	-	-	-	-	-	-	-	-	-	-	-	-
Ga	-	-	-	-	-	-	-	-	-	-	-	-	-
Zn	-	-	21	12	26	13	6	35	35	37	34	22	27
Cu	4	2	-	4	4	1	-	4	-	1	2	3	34
Ni	2	2	2	3	3	-	1	4	1	1	3	3	2
V	11	11	10	11	21	12	16	26	27	23	24	20	27
Cr	-	-	-	-	-	-	-	-	-	-	-	-	-
Hf	-	-	-	-	-	-	-	-	-	-	-	-	-
Cs	-	-	-	-	-	-	-	-	-	-	-	-	-
Sc	-	-	-	-	-		-	-		-		-	-
Ta	-	-	-	-	-	-	-	-	-	-	-	-	-
Co	2	-	1	1	2	1	3	1	4	3	4	2	5
Li	-	-	-	-	-	-	-	-	-	-	-	-	-
Be	-	-	-	-	-	-	-	-	-	-	-	-	-
B	-	-	-	-	-	-	-	-	-	-	-	-	-
U	-	-	-	-	-	-	-	-	-	-	-	-	-
W	-	-	-	-	-	-	-	-	-	-	-	-	-
Sn	1	2	3	5	-	4	2	3	-	3	3	2	3
Mo	-	-	-	-	-	-	-	-	-	-	-	-	-
Rare-earths													
La	-	-	-	-	-	-	-	-	-	-	-	-	-
Ce	-	-	-	-	-	-	-	-	-	-	-	-	-
Pr	-	-	-	-	-	-	-	-	-	-	-	-	-
Nd	-	-	-	-	-	-	-	-	-	-	-	-	-
Sm	-	-	-	-	-	-	-	-	-	-	-	-	-
Eu	-	-	-	-	-	-	-	-	-	-	-	-	-
Gd	-	-	-	-	-	-	-	-	-	-	-	-	-
Tb	-	-	-	-	-	-	-	-	-	-	-	-	-
Dy	-	-	-	-	-	-	-	-	-	-	-	-	-
Ho	-	-	-	-	-	-	-	-	-	-	-	-	-
Er	-	-	-	-	-	-	-	-	-	-	-	-	-
Tm	-	-	-	-	-	-	-	-	-	-	-	-	-
Yb	-	-	-	-	-	-	-	-	-	-	-	-	-
Lu	-	-	-	-	-	-	-	-	-	-	-	-	-

Table E1.1 (Continued) Compilation of Meguma Zone granitoid lithogeochemistry

Sample	NTS821	NTS822	NTS823	NTS824	NTS825	NTS826	NTS827	NTS828	NTS829	NTS830	NTS831	NTS832	NTS833
Batholith	SMB	SMB	SMB	SMB	SMB	SMB	SMB	SMB	SMB	SMB	SMB	SMB	SMB
Pluton	HP	HP	HP	HP	HP	HP	HP	HP	HP	HP	HP	HP	HP
Lithology	Mzg	Mzg	Mzg	Mzg	Mzg	Mzg	Mzg	Mzg	Mzg	Lg	Lg	Lg	Lg
Source	24	24	24	24	24	24	24	24	24	24	24	24	24
Major oxides													
SiO_2	71.96	72.41	71.97	75.28	72.68	75.28	75.47	73.64	75.02	74.71	75.05	74.54	75.54
TiO_2	0.31	0.18	0.18	0.15	0.18	0.16	0.14	0.16	0.13	0.11	0.11	0.11	0.12
Al_2O_3	13.39	14.12	14.10	13.74	14.58	13.16	13.44	13.39	13.76	13.90	13.78	13.56	13.70
Fe_2O_3	-	-	-	-	-	-	-	-	-	-	-	-	-
FeO	-	-	-	-	-	-	-	-	-	-	-	-	-
MnO	0.05	0.04	0.04	0.04	0.03	0.05	0.04	0.06	0.05	0.04	0.04	0.05	0.05
MgO	0.34	0.70	0.24	0.04	0.05	0.07	0.15	0.09	0.08	0.05	0.18	0.25	0.06
CaO	0.70	0.65	0.62	0.47	0.65	0.48	0.56	0.61	0.55	0.44	0.43	0.44	0.42
Na_2O	3.52	3.49	3.54	3.44	3.99	3.54	3.41	3.59	3.42	3.68	3.72	3.40	3.45
K_2O	4.46	4.43	4.48	4.07	4.66	4.25	4.40	4.26	4.43	4.08	4.12	4.13	4.17
P_2O_5	0.22	0.32	0.30	0.26	0.33	0.20	0.20	0.27	0.20	0.24	0.24	0.23	0.21
H_2O+	-	-	-	-	-	-	-	-	-	-	-	-	-
H_2O-	-	-	-	-	-	-	-	-	-	-	-	-	-
CO_2	-	-	-	-	-	-	-	-	-	-	-	-	-
Cl	-	-	-	-	-	-	-	-	-	-	-	-	-
F	-	-	-	-	-	-	-	-	-	-	-	-	-
LOI	1.04	1.13	1.08	1.06	1.08	0.82	0.88	0.90	0.87	1.05	0.99	1.01	1.01
TOTAL	98.07	98.78	97.92	99.90	99.57	99.62	99.96	98.61	99.78	99.58	100.10	98.83	99.89
Fe_2O_3T	2.34	1.47	1.54	1.52	1.51	1.81	1.43	1.84	1.43	1.44	1.62	1.25	1.31
FeOT	2.08	1.31	1.37	1.35	1.34	1.61	1.27	1.64	1.27	1.28	1.44	1.11	1.16
A/CNK	1.04	1.11	1.10	1.16	1.06	1.07	1.08	1.07	1.10	1.14	1.12	1.15	1.15
Trace els													
Ba	244	269	270	43	286	52	82	72	53	5	6	3	8
Rb	253	218	214	464	215	384	328	353	342	431	413	424	417
Sr	66	52	55	24	57	23	26	34	39	7	7	7	8
Y	17	12	8	3	9	13	13	7	10	7	7	7	7
Zr	115	56	59	43	59	52	48	53	46	41	38	37	36
Nb	13	10	11	15	12	13	9	10	9	12	13	10	11
Th	-	-	-	-	-	-	-	-	-	-	-	-	-
Pb	-	-	-	-	-	-	-	-	-	-	-	-	-
Ga	-	-	-	-	-	-	-	-	-	-	-	-	-
Zn	36	5	17	7	9	23	8	25	10	-	-	11	12
Cu	23	13	5	8	5	2	3	7	-	1	3	9	1
Ni	2	2	3	3	2	1	1	1	-	-	-	3	-
V	24	11	13	9	13	10	9	11	9	7	9	6	6
Cr	-	-	-	-	-	-	-	-	-	-	-	-	-
Hf	-	-	-	-	-	-	-	-	-	-	-	-	-
Cs	-	-	-	-	-	-	-	-	-	-	-	-	-
Sc	-	-	-	-	-	-	-	-	-	-	-	-	-
Ta	-	-	-	-	-	-	-	-	-	-	-	-	-
Co	3	1	2	1	1	2	1	2	2	-	-	2	-
Li	-	-	-	-	-	-	-	-	-	-	-	-	-
Be	-	-	-	-	-	-	-	-	-	-	-	-	-
B	-	-	-	-	-	-	-	-	-	-	-	-	-
U	-	-	-	-	-	-	-	-	-	-	-	-	-
W	-	-	-	-	-	-	-	-	-	-	-	-	-
Sn	4	6	6	-	6	7	9	5	8	14	12	12	12
Mo	-	-	-	-	-	-	-	-	-	-	-	-	-
Rare-earths													
La	-	-	-	-	-	-	-	-	-	-	-	-	-
Ce	-	-	-	-	-	-	-	-	-	-	-	-	-
Pr	-	-	-	-	-	-	-	-	-	-	-	-	-
Nd	-	-	-	-	-	-	-	-	-	-	-	-	-
Sm	-	-	-	-	-	-	-	-	-	-	-	-	-
Eu	-	-	-	-	-	-	-	-	-	-	-	-	-
Gd	-	-	-	-	-	-	-	-	-	-	-	-	-
Tb	-	-	-	-	-	-	-	-	-	-	-	-	-
Dy	-	-	-	-	-	-	-	-	-	-	-	-	-
Ho	-	-	-	-	-	-	-	-	-	-	-	-	-
Er	-	-	-	-	-	-	-	-	-	-	-	-	-
Tm	-	-	-	-	-	-	-	-	-	-	-	-	-
Yb	-	-	-	-	-	-	-	-	-	-	-	-	-
Lu	-	-	-	-	-	-	-	-	-	-	-	-	-

Table E1 1 (Continued) Compilation of Meguma Zone granitoid lithogeochemistry

Sample	NTS834	NTS835	NTS836	NTS837	NTS838	NTS839	NTS840	NLBA05	NLI264	NLI265	NLI266	NLI267	NLI300
Batholith	SMB	SMB	SMB	SMB	SMB	SMB	SMB	-	-	-	-	-	-
Pluton	HP	HP	HP	HP	HP	HP	HP	LBP	LC	LC	LC	LC	LC
Lithology	Lg	Lg	Mzg	Mzg	Lg	Lg	Mzg	Tcn	Grd	Mzg	Mzg	Mzg	Grd
Source	24	24	24	24	24	24	24	5	15	15	15	15	15
Major oxides													
SiO_2	74 81	75 58	74 90	76 60	75 67	75 43	74 69	59 75	66 18	77 72	72.38	72 98	63 93
TiO_2	0 11	0 10	0 17	0 12	0 11	0 13	0 23	0 99	0 82	0 08	0 17	0 17	0 82
Al_2O_3	13 58	14 02	13 09	13 70	13 31	12.95	13 57	17 50	16 30	14 56	15 75	15 71	17 70
Fe_2O_3	-	-	-	-	-	-	-	-	-	-	-	-	-
FeO	-	-	-	-	-	-	-	-	-	-	-	-	-
MnO	0 04	0 03	0 06	0 04	0 05	0 04	0 05	0 07	0 12	0 02	0 02	0 02	0 13
MgO	0 02	0 03	0 14	0 06	0 13	0 08	0 33	3 62	1 55	0 21	0 36	0 34	1 68
CaO	0 40	0 42	0 78	0 39	0 40	0 40	0 58	4 91	2 04	0 31	0 43	0 42	2 31
Na_2O	3 58	3 60	3 14	3 48	3 62	3 53	3 54	3 53	3 51	3 67	3 64	4 14	3 78
K_2O	4 32	3 79	4 22	4 32	4 53	4 76	4 35	2 45	3 71	3 57	5 63	4 48	3 55
P_2O_5	0 22	0 20	0 20	0 22	0 18	0 14	0 24	0 35	0 32	0 34	0 37	0 34	0 29
H_2O+	-	-	-	-	-	-	-	-	-	-	-	-	-
H_2O-	-	-	-	-	-	-	-	-	-	-	-	-	-
CO_2	-	-	-	-	-	-	-	-	-	-	-	-	-
Cl	-	-	-	-	-	-	-	-	-	-	-	-	-
F	-	-	-	-	-	-	-	-	-	-	-	-	-
LOI	1 10	1 20	1 08	1 13	0 91	0 83	1 11	0 54	0 69	0 77	0 77	0 85	0 92
TOTAL	99 36	99 89	99 36	101 46	99 99	99 53	100 41	99 11	99 54	101 90	100 48	100 48	99 87
Fe_2O_3T	1 33	1 03	1 78	1,57	1 21	1 40	1 94	6 07	4 84	0 73	1 08	1 16	5 35
FeOT	1 18	0 92	1 58	1 40	1 08	1 24	1 72	5 40	4 30	0 65	0 96	1 03	4 76
A/CNK	1 10	1 21	1 08	1 12	1 05	1 00	1 08	1 13	1 21	1 30	1 09	1 17	1 27
Trace els													
Ba	6	-	58	34	2	10	116	400	963	82	346	468	869
Rb	417	405	320	324	311	279	327	90	147	160	223	215	149
Sr	7	5	23	12	8	15	38	380	217	24	58	73	248
Y	7	3	14	14	10	14	15	-	30	7	8	8	29
Zr	32	29	59	48	33	36	80	110	232	17	68	60	259
Nb	11	8	12	12	9	9	13	-	14	11	8	9	16
Th	-	-	-	-	-	-	-	5	11	-	7	6	8
Pb	-	-	-	-	-	-	-	6	37	19	24	31	25
Ga	-	-	-	-	-	-	-	-	20	22	21	19	22
Zn	-	-	28	-	-	16	13	65	107	27	50	46	106
Cu	13	12	3	6	2	33	2	-	2	-	-	-	6
Ni	2	-	-	3	-	-	2	47	10	4	4	5	8
V	9	6	12	7	6	7	19	-	51	1	5	-	73
Cr	-	-	-		-	-	-	-	22	4	13	2	26
Hf	-	-	-	-	-	-	-	-	-	-	-	-	-
Cs	-	-	-	-	-	-	-	-	-	-	-	-	-
Sc	-	-	-	-	-	-	-	-	-	-	-	-	-
Ta	-	-	-	-	-	-	-	-	-	-	-	-	-
Co	3	-	3	2	2	-	2	-	-	-	-	-	-
Li	-	-	-	-	-	-	-	40	-	-	-	-	-
Be	-	-	-	-	-	-	-	-	-	-	-	-	-
B	-	-	-	-	-	-	-	-	-	-	-	-	-
U	-	-	-	-	-	-	-	1 9	-	-	-	-	-
W	-	-	-	-	-	-	-	-	-	-	-	-	-
Sn	10	9	9	7	9	7	7	-	-	-	-	-	-
Mo	-	-	-	-	-	-	-	-	-	-	-	-	-
Rare-earths													
La	-	-	-	-	-	-	-	-	-	-	-	-	-
Ce	-	-	-	-	-	-	-	-	-	-	-	-	-
Pr	-	-	-	-	-	-	-	-	-	-	-	-	-
Nd	-	-	-	-	-	-	-	-	-	-	-	-	-
Sm	-	-	-	-	-	-	-	-	-	-	-	-	-
Eu	-	-	-	-	-	-	-	-	-	-	-	-	-
Gd	-	-	-	-	-	-	-	-	-	-	-	-	-
Tb	-	-	-	-	-	-	-	-	-	-	-	-	-
Dy	-	-	-	-	-	-	-	-	-	-	-	-	-
Ho	-	-	-	-	-	-	-	-	-	-	-	-	-
Er	-	-	-	-	-	-	-	-	-	-	-	-	-
Tm	-	-	-	-	-	-	-	-	-	-	-	-	-
Yb	-	-	-	-	-	-	-	-	-	-	-	-	-
Lu	-	-	-	-	-	-	-	-	-	-	-	-	-

Table E1 1 (Continued) Compilation of Meguma Zone granitoid lithogeochemistry

Sample	NLI305	NLI306	NLI307	NLI308	NLR002	NLR003	NLR004	NLR005	NLR006	NLR007	NLR008	NLR009	NLR010
Batholith	-	-	-	-	-	-	-	-	-	-	-	-	-
Pluton	LC	LC	LC	LC	LRP	LRP	LRP	LRP	LRP	LRP	LRP	LRP	LRP
Lithology	Grd	Grd	Mzg	Mzg	Mzg	Mzg	Mzg	Mzg	Mzg	Mzg	Mzg	Mzg	Mzg
Source	15	15	15	15	16	16	16	16	16	16	16	16	16
Major oxides													
SiO_2	64 56	64 28	73 23	71 93	75 87	72 79	73 69	72 91	72 71	73 67	72 84	72 78	71 86
TiO_2	0 82	0 49	0 18	0 19	0 33	0 17	0 24	0 21	0 23	0 17	0 24	0 40	0 40
Al_2O_3	17 47	15 31	15 71	15 51	13 49	14 88	14 70	15 30	14 98	14 52	14 70	14 85	15 17
Fe_2O_3	-	-	-	-	0 04	-	0 04	-	0 01	-	-	0 56	0 12
FeO	-	-	-	-	1 82	-	1 52	-	1 49	-	-	1 70	2 03
MnO	0 11	0 06	0 03	0 02	0 05	0 04	0 05	0 07	0 05	0 05	0 04	0 05	0 05
MgO	1 72	1 15	0 41	0 33	0 64	0 39	0 53	0 55	0 58	0 51	0 47	0 76	0 73
CaO	2 18	1 46	0 45	0 38	0 69	0 58	0 69	0 78	0 85	0 65	0 74	1 08	1 03
Na_2O	3 89	4 07	4 00	3 89	3 21	3 45	3 44	3 56	3 56	3 45	3 61	3 47	3 49
K_2O	3 28	3 91	4 77	4 82	3 26	5 21	4 68	5 04	4 82	4 44	4 38	3 85	4 43
P_2O_5	0 31	0 26	0 34	0 36	0 25	0 30	0 25	0 26	0 25	0 27	0 30	0 26	0 25
H_2O+	-	-	-	-	0 66	0 58	0 80	0 85	0 82	0 70	0 66	1 02	0 81
H_2O-	-	-	-	-	0 12	0 14	0 14	0 12	0 14	0 11	0 08	0 07	0 15
CO_2	-	-	-	-	0 16	0 07	0 19	0 16	0 15	0 16	0 19	0 05	0 13
Cl	-	-	-	-	-	-	-	-	-	-	-	-	-
F	-	-	-	-	0 05	0 04	0 04	0 04	0 04	0 09	0 05	0 06	0 05
LOI	1 23	0 85	0 85	0 85	0 99	0 83	1 17	1 17	1 15	1 06	0 98	1 20	1 14
TOTAL	100 36	94 58	101 03	99 27	100 61	99 46	100 98	101 25	100 66	100 24	99 86	100 87	100 66
Fe_2O_3T	5 39	3 08	1 19	1 11	2 06	1 48	1 73	1 58	1 66	1 63	1 76	2 45	2 37
FeOT	4 79	2.74	1 06	0 99	1 83	1 32	1 54	1 40	1 48	1 45	1 56	2 18	2 11
A/CNK	1 29	1 11	1 15	1 15	1 28	1 08	1 12	1 10	1 09	1 15	1 14	1 20	1 15
Trace els													
Ba	819	563	406	331	219	354	347	433	429	178	174	327	401
Rb	139	191	206	231	213	225	213	210	200	231	237	210	223
Sr	228	148	65	50	79	82	101	117	121	63	61	106	108
Y	21	17	9	6	-	-	-	-	-	-	-	-	-
Zr	263	155	71	71	100	81	79	80	85	71	71	122	115
Nb	15	11	9	8	-	-	-	-	-	-	-	-	-
Th	13	11	6	7	12	8	8	8	9	7	7	14	16
Pb	18	27	31	22	24	29	26	35	29	24	25	27	24
Ga	23	21	17	23	-	-	-	-	-	-	-	-	-
Zn	79	77	52	35	55	56	50	77	74	56	53	73	63
Cu	4	-	-	-	-	-	-	-	-	-	-	-	-
Ni	8	8	5	6	-	-	-	-	-	-	-	-	-
V	69	33	9	2	-	-	-	-	-	-	-	-	-
Cr	25	27	8	6	-	-	-	-	-	-	-	-	-
Hf	-	-	-	-	-	-	-	-	-	-	-	-	-
Cs	-	-	-	-	-	-	-	-	-	-	-	-	-
Sc	-	-	-	-	-	-	-		-	-	-	-	-
Ta	-	-	-	-	-	-	-		-	-	-	-	-
Co	-	-	-	-	-	-	-	-	-	-	-	-	-
Li	-	-	-	-	161	116	152	129	141	159	174	130	125
Be	-	-	-	-	6	5 5	5 5	5 5	4 5	5	6	205	3
B	-	-	-	-	25	20	25	30	25	25	25	25	20
U	-	-	-	-	6 6	4	5 5	3 4	6 8	4 4	5 1	8 5	8 3
W	-	-	-	-	7	3	2	3	2	2	3	1	1
Sn	-	-	-	-	8	2	3	5	4	6	10	5	5
Mo	-	-	-	-	2	1	2	1	1	1	1	1	1
Rare-earths													
La	-	-	-	-	-	-		-	-	-	-	-	-
Ce	-	-	-	-	-	-	-	-	-	-	-	-	-
Pr	-	-	-	-	-	-	-	-	-	-	-	-	-
Nd	-	-	-	-	-	-	-	-	-	-	-	-	-
Sm	-	-	-	-	-	-	-	-	-	-	-	-	-
Eu	-	-	-	-	-	-		-	-	-	-	-	-
Gd	-	-	-	-	-	-	-	-	-	-	-	-	-
Tb	-	-	-	-	-	-		-	-	-	-	-	-
Dy	-	-	-	-	-	-	-	-	-	-	-	-	-
Ho	-	-	-	-	-	-	-	-	-	-	-	-	-
Er	-	-	-	-	-	-	-	-	-	-	-	-	-
Tm	-	-	-	-	-	-	-	-	-	-	-	-	-
Yb	-	-	-	-	-	-		-	-	-	-	-	-
Lu	-	-	-	-	-	-		-	-	-	-	-	-

Table E1 1 (Continued) Compilation of Meguma Zone granitoid lithogeochemistry

Sample	NLR011	NLR012	NLR013	NLR014	NMD10	NMD103	NMD109	NMD22	NMD44	NMD96	NMD97	NDW21	NDW25
Batholith	-	-	-	-	MB	MB	MB	MB	MB	MB	MB	-	-
Pluton	LRP	LRP	LRP	LRP	-	-	-	-	-	-	-	MLP	MLP
Lithology	Mzg	Mzg	Mzg	Mzg	Mzg	Mzg	Mzg	Mzg	Mzg	Mzg	Mzg	Mzg	Mzg
Source	16	16	16	16	17, 18	17, 18	17, 18	17, 18	17, 18	17, 18	17, 18	8	8
Major oxides													
SiO_2	70 53	70 40	74 10	74 27	71 75	71 44	74 23	70 77	72.57	72 26	71 43	74 04	75 27
TiO_2	0 34	0 34	0 22	0 09	0 32	0 38	0 13	0 28	0 27	0 22	0 36	0 21	0 07
Al_2O_3	15 89	15 63	14 40	14 71	14 61	14 76	14 44	14 62	14 34	14 77	14 52	14 52	14 42
Fe_2O_3	0 05	0 36	0 04	-	-	-	-	-	-	-	-	0 14	0 03
FeO	1 68	1 56	1 37	-	-	-	-	-	-	-	-	1 16	0 47
MnO	0 04	0 04	0 04	0 06	0 09	0 07	0 05	0 05	0 04	0 05	0 08	0 04	0 02
MgO	0 60	0 65	0 46	0 14	0 73	0 15	0 35	0 61	0 54	0 52	0 78	0 45	0 13
CaO	0 95	1 01	0 68	0 39	0 83	1 22	0 66	0 86	0 88	0 62	0 92	0 60	0 44
Na_2O	3 52	3 58	3 57	4 37	3 60	3 45	3 74	3 51	3 54	3 75	3 64	3 53	3 91
K_2O	5 44	5 09	4 45	3 67	4 80	4 58	4 92	4 65	4 32	4 62	4 31	4 53	3 89
P_2O_5	0 26	0 27	0 29	0 38	0 20	0 07	0 30	0 30	0 27	0 30	0 30	0 33	0 40
H_2O+	0 73	0 57	0 42	0 36	1 17	0 68	0 84	1 52	1 13	0 91	0 92	0 66	1 49
H_2O-	0 12	0 13	0 07	0 18	0 15	0 11	0 14	0 09	0 07	0 07	0 17	-	-
CO_2	0 16	0 10	0 26	0 13	-	-	-	-	-	-	-	-	-
Cl	-	-	-	-	-	-	-	-	-	-	-	-	-
F	0 04	0 05	0 08	0 07	-	-	-	-	-	-	-	-	-
LOI	1 05	0 85	0 83	0 76	1 32	0 79	0 98	1 61	1 20	0 98	1 09	0 66	1 49
TOTAL	100 32	99 72	100 43	99 52	100 20	98 95	100 79	99 05	99 64	99 47	99 52	100 18	100 53
Fe_2O_3T	1 91	2 09	1 56	0 77	2 19	2 30	1 11	2 01	1 88	1 55	2 35	1 43	0 55
FeOT	1 70	1 86	1 39	0 68	1 95	2 04	0 99	1 79	1 67	1 38	2 09	1 27	0 49
A/CNK	1 08	1 09	1 12	1 19	1 07	1 08	1 04	1 09	1 11	1 11	1 11	1 13	1 18
Trace els													
Ba	591	540	169	12	384	59	161	365	275	252	278	-	-
Rb	229	229	232	333	280	300	300	310	250	300	320	-	-
Sr	123	124	59	13	160	120	60	80	70	60	130	-	-
Y	-	-	-	-	-	-	-	-	-	-	-	-	-
Zr	97	108	70	29	120	130	50	90	80	70	100	-	-
Nb	-	-	-	-	-	-	-	-	-	-	-	-	-
Th	12	12	7	2	9 5	1 3	2 5	7 3	8 1	5	7 1		-
Pb	30	27	23	18	-	-	-	-	-	-	-	-	-
Ga	-	-	-	-	-	-	-	-	-	-	-	-	-
Zn	58	65	49	28	42.2	52 8	[illegible]7 4	70 6	49 5	55 8	72 1	-	-
Cu	-	-	-	-	4 2	7	4 3	50 4	5 6	8 5	16 6	-	-
Ni	-	-	-	-	-	-	-	-	-	-	-	-	-
V	-	-	-	-	-	-	-	-	-	-	-	-	-
Cr	-	-	-	-	-	-	-	-	-	-	-	-	-
Hf	-	-	-	-	3 8	1 4	1 8	2 7	3	2.1	3 1	-	-
Cs	-	-	-	-	13 2	35 3	22 1	37 5	19	20 2	34 3	-	-
Sc	-	-	-	-	5 4	4 6	3 1	4 7	4 2	4 1	5 7	-	-
Ta		-	-	-	5 1	7 5	6 3	6 2	5	3 8	4 9	-	-
Co	-	-	-	-	-	-	-	-	-	-	-	-	-
Li	113	122	173	104	141 2	17[illegible] 1	149 7	257 9	159 5	191 7	197 6	-	-
Be	4 5	2.5	3 5	10 5	-	-	-	-	-	-	-	-	-
B	25	25	25	20	-	-	-	-	-	-	-	-	-
U	8 1	6 8	4 5	14	1 9	12 8	6 1	9 7	3 1	2 7	4	-	-
W	4	1	2	3	-	-	-	-	-	-	-	-	-
Sn	1	3	11	19	-	-	-	-	-	-	-	-	-
Mo	1	1	1	1	-	-	-	-	-	-	-	-	-
Rare-earths													
La		-	-	-	-	-	-	-	-	-	-	-	-
Ce	-	-	-	-	-	-	-		-	-	-	-	-
Pr	-	-	-	-	-	-	-	-	-	-	-	-	-
Nd	-	-	-	-	-	-	-	-	-	-	-	-	-
Sm	-	-	-	-	-	-	-	-	-	-	-	-	-
Eu	-	-	-	-	-	-	-	-	-	-	-	-	-
Gd	-	-	-	-	-	-	-		-	-	-	-	-
Tb	-	-	-	-	-	-	-	-	-	-	-	-	-
Dy	-	-	-	-	-	-	-	-	-	-	-	-	-
Ho	-	-	-	-	-	-	-		-	-	-	-	-
Er	-	-	-	-	-	-	-	-	-	-	-	-	-
Tm	-	-	-	-	-	-	-	-	-	-	-	-	-
Yb		-	-	-	-	-	-	-	-	-	-	-	-
Lu	-	-	-	-	-	-	-		-	-	-	-	-

Table E1 1 (Continued) Compilation of Meguma Zone granitoid lithogeochemistry

Sample	NDW27	NDW4	NMO11	NMO15	NMO16	NMO17	NMO18	NMO6A	NMO6B	NMO6M	NMO7	NMO9	NCH15
Batholith	-	-	-	-	-	-	-	-	-	-	-	-	SMB
Pluton	MLP	MLP	MPP	MPP	MPP	MPP	MPP	MPP	MPP	MPP	MPP	MPP	NRP
Lithology	Mzg	Mzg	Mzg	Grd	Grd	Grd	Lmzg	Grd	Grd	Mzg	Grd	Mzg	Lmzg
Source	8	8	9	9	9	9	9	9	9	9	9	9	7
Major oxides													
SiO_2	73 33	73 51	72 50	64 10	69 20	67 90	73 20	-	70 20	74 50	70 70	73 10	-
TiO_2	0 21	0 20	0 16	0 73	0 47	0 37	0 16	-	0 40	0 16	0 51	0 23	-
Al_2O_3	14 73	14 56	14 50	15 40	14 80	15 10	14 50	-	14 70	14 10	14 90	14 70	-
Fe_2O_3	0 11	0 25	-	-	-	-	-	-	-	-	-	-	-
FeO	1 18	1 0[illegible]	-	-	-	-	-	-	-	-	-	-	-
MnO	0 04	0 04	0 04	0 07	0 06	0 06	-	-	0 05	0 03	0 05	0 05	-
MgO	0 43	0 42	0 30	3 00	1 30	2 00	0 30	-	1 00	0 20	1 50	0 40	-
CaO	0 58	0 52	0 39	3 30	2 40	2 50	0 41	-	1 30	0 40	2 00	0 51	-
Na_2O	3 63	3 64	3 70	3 20	3 40	3 20	2 60	-	3 60	3 60	4 20	3 50	-
K_2O	4 61	4 45	5 10	3 80	4 20	4 40	6 40	-	4 40	5 10	3 00	5 20	-
P_2O_5	0 35	0 38	0 39	0 32	0 37	0 36	0 29	-	0 45	0 31	0 36	0 38	-
H_2O+	0 63	0 72	-	-	-	-	-	-	-	-	-	-	
H_2O-	-	-	-	-	-	-	-	-	-	-		-	-
CO_2	-	-	-	-	-	-	-	-	-	-	-	-	-
Cl	-	-	-	-	-	-	-	-	-	-	-	-	-
F	-	-	0 03	0 05	0 05	0 05	0 03	-	-	-	-	-	-
LOI	0 63	0 72	0 99	0 79	0 60	0 70	0 91	-	1 00	0 67	0 66	1 10	-
TOTAL	99 80	99 70	98 96	98 71	99 20	99 35	#VALUE!	-	99 14	99 87	100 19	100 33	-
Fe_2O_3T	1 42	1 42	1 00	4 50	2 70	3 10	1 00	-	2 30	0 90	2 60	1 30	-
FeOT	1 26	1 26	0 89	4 00	2 40	2 76	0 89	-	2 04	0 80	2 31	1 16	-
A/CNK	1 12	1 14	1 06	1 03	1 01	1 02	1 02	-	1 07	1 04	1 12	1 07	-
Trace els													
Ba	-	-	590	980	1000	1200	900	820	790	630	-	650	12
Rb	-	-	120	174	159	166	192	148	150	127	-	157	590
Sr	-	-	100	300	210	250	110	190	190	108	-	130	6
Y	-	-	-	-	-	-	-	-	-	-	-	-	-
Zr	-	-	-	-	-	-	-	-	-	-	-	-	33
Nb	-	-	-	-	-	-	-	-	-	-	-	-	15
Th	-	-	3	9	9	7	3	10	7	2	-	3	-
Pb	-	-	24	11	21	21	29	28	22	22	-	24	-
Ga	-	-	7	7	7	7	11	-	-	-	-	-	-
Zn	-	-	-	-	-	-	-	45	47	9	-	34	-
Cu	-	-	-	-	-	-	-	8	5	7	-	6	6
Ni	-	-	-	-	-	-	-	-	-	-	-	-	-
V	-	-	-	-	-	-	-	-	-	-	-	-	-
Cr	-	-	-	-	-	-	-	-	-	-	-	-	-
Hf	-	-	-	-	-	-	-	-	-	-	-	-	-
Cs	-	-	-	-	-	-	-	-	-	-	-	-	-
Sc	-	-	-	-	-	-	-	-	-	-	-	-	-
Ta	-	-	-	-	-	-	-	-	-	-	-	-	-
Co	-	-	-	-	-	-	-	-	-	-	-	-	-
Li	-	-	38	100	129	148	55	79	78	19	-	48	3700
Be	-	-	8	5	4 3	6 5	16	8 5	14	8	-	20	-
B	-	-	12	5	4	3	7	10	8	7	-	8	-
U	-	-	4 5	6	2 6	3 4	6 3	3 4	3 6	3 5	-	3 2	-
W	-	-	-	-	-	-	-	-	-	-	-	-	-
Sn	-	-	7 4	6 3	7 8	7 1	10	7 3	7 8	5 6	-	7 7	45
Mo	-	-	0 9	0 9	2.2	0 8	1 2	1 1	1 3	1 7	-	0 8	1
Rare-earths													
La	-	-	-	-	-	-	-	-	-		-	-	-
Ce	-	-	-	-	-	-	-	-	-	-	-	-	-
Pr	-	-	-	-	-	-	-	-	-	-	-	-	-
Nd	-	-	-	-	-	-	-	-	-	-	-	-	-
Sm	-	-		-	-	-	-	-	-		-	-	-
Eu	-	-	-	-	-	-	-	-	-	-	-	-	-
Gd	-	-	-	-	-	-	-	-	-		-	-	-
Tb	-	-	-	-	-	-	-	-	-		-	-	-
Dy	-	-	-	-	-	-	-	-	-	-	-	-	-
Ho	-	-	-	-	-	-	-	-	-	-	-	-	-
Er	-	-	-	-	-	-	-	-	-	-	-	-	-
Tm	-	-	-	-	-	-	-	-	-	-	-	-	-
Yb	-	-	-	-	-	-	-	-	-	-	-		-
Lu	-	-	-	-	-	-	-	-	-	-	-	-	-

Table E1 1 (Continued) Compilation of Meguma Zone granitoid lithogeochemistry

Sample	NCH16	NCH165	NCH16A	NCH17	NCH18	NCHI8A	NCH19	NCH19A	NCH20	NCH3A	NCH4	NCH7A	NGH8
Batholith	SMB	SMB	SMB	SMB	SMB	SMB	SMB	SMB	SMB	SMB	SMB	SMB	SMB
Pluton	NRP	NRP	NRP	NRP	NRP	NRP	NRP	NRP	NRP	NRP	NRP	NRP	NRP
Lithology	Mzg	Mzg	Lmzg	Lmzg	Lmzg	Mzg	Mzg	Lmzg	Mzg	Mzg	Mzg	Mzg	Mzg
Source	7	7	7	7	7	7	7	7	7	7	7	7	7
Major oxidet													
SiO_2	-	-	-	-	-	-	75 18	-	74 21	75 93	74 43	74 92	73 14
TiO_2	-	-	-	-	-	-	0 21	-	0 12	0 09	0 16	0 08	0 03
Al_2O_3	-	-	-	-	-	-	12.70	-	13 93	13 81	13 69	14 07	14 84
Fe_2O_3	-	-	-	-	-	-	0 11	-	0 11	0 11	0 11	0 11	0 22
FeO	-	-	-	-	-	-	1 53	-	1 14	0 96	1 45	1 04	0 63
MnO	-	-	-	-	-	-	0 03	-	0 02	0 02	0 02	0 03	0 04
MgO	-	-	-	-	-	-	0 31	-	0 21	0 11	0 23	0 12	0 06
CaO	-	-	-	-	-	-	0 55	-	0 40	0 38	0 58	0 41	0 63
Na_2O	-	-	-	-	-	-	3 31	-	3 58	4 15	3 62	3 88	4 71
K_2O	-	-	-	-	-	-	3 95	-	5 18	4 76	5 08	4 57	4 24
P_2O_5	-	-	-	-	-	-	0 14	-	0 15	0 20	0 17	0 24	0 39
H_20+	-	-	-	-	-	-	0 89	-	0 72	0 72	0 94	1 07	0 72
H_2O-	-	-	-	-	-	-	-	-	-	-	-	-	-
CO_2	-	-	-	-	-	-	-	-	-	-	-	-	-
Cl	-	-	-	-	-	-	-	-	-	-	-	-	-
F	-	-	-	-	-	-	-	-	-	-	-	-	-
LOI	-	-	-	-	-	-	0 89	-	0 72	0 72	0 94	1 07	0 72
TOTAL	-	-	-	-	-	-	98 88	-	99 75	101 22	100 45	100 51	99 62
Fe_2O_3T	-	-	-	-	-	-	1 81	-	1 38	1 18	1 72	1 26	0 92
FeOT	-	-	-	-	-	-	1 61	-	1 23	1 05	1 53	1 12	0 82
A/CNK	-	-	-	-	-	-	1 10	-	1 02	1 00	0 99	1 07	1 05
Trace els													
Ba	115	257	26	68	-	236	180	17	145	85	180	20	-
Rb	484	407	511	720	847	293	278	931	356	680	173	879	-
Sr	10	37	7	17	22	47	34	8	24	10	28	10	-
Y	-	-	-	-	-	-	-	-	-	-	-	-	-
Zr	95	105	56	61	43	120	94	43	70	60	94	50	-
Nb	14	13	12	16	16	14	10	17	11	14	12	14	-
Th	-	-	-	-	-	-	-	-	-	-	-	-	-
Pb	-	-	-	-	-	-	-	-	-	-	-	-	
Ga	-	-	-	-	-	-	-	-	-		-	-	-
Zn	-	-	-	-	-	-	-	-	-			-	
Cu	6	5	43	8	12	10	7	15	10	4	6	4	-
Ni	-	-	-	-	-	-	-	-	-	-	-	-	-
V	-	-	-	-	-	-	-	-	-	-	-	-	-
Cr	-	-	-	-	-	-	-	-	-	-	-	-	-
Hf	-	-	-	-	-	-	-	-	-	-	-	-	-
Cs	-	-	-	-	-	-	-	-	-	-	-	-	-
Sc	-	-	-	-	-	-	-	-	-	-	-	-	-
Ta	-	-	-	-	-	-	-	-	-	-	-	-	-
Co	-	-	-	-	-	-	-	-	-	-	-	-	-
Li	658	207	450	6680	535	279	221	439	131	438	323	708	-
Be	-	-	-	-	-	-	-	-	-	-	-	-	-
B	-	-	-	-	-	-	-	-	-	-	-	-	-
U	-	-	-	-	-	-	-	-	-	-	-	-	-
W	-	-	-	1	-	1	-	1	-	-	1	-	-
Sn	34	31	43	40	52	6	35	43	6	35	31	48	-
Mo	3	2	2	2	2	2	3	2	1	2	2	2	-
Rare-earths													
La	-	-	-	-	-	-	-	-	-	-	-	-	-
Ce	-	-	-	-	-	-	-	-	-	-	-	-	-
Pr	-	-	-	-	-	-	-	-	-	-	-	-	-
Nd	-	-	-	-	-	-	-	-	-	-	-	-	-
Sm	-	-	-	-	-	-	-	-	-	-	-	-	-
Eu	-	-	-	-	-	-	-	-	-	-	-	-	-
Gd	-	-	-	-	-	-	-	-	-	-	-	-	-
Tb		-	-	-	-	-	-	-	-	-	-	-	-
Dy	-	-	-	-	-	-	-	-	-	-	-	-	-
Ho	-	-	-	-	-	-	-	-	-	-	-	-	-
Er	-	-	-	-	-	-	-	-	-	-	-	-	-
Tm	-	-	-	-	-	-	-	-	-	-	-	-	-
Yb	-	-	-	-	-	-	-	-	-	-	-	-	-
Lu	-	-	-	-	-						-		-

Table E1 1 (Continued) Compilation of Meguma Zone granitoid lithogeochemistry

Sample	NCH9	NCH97	NCH9A	NAL6	NAL7	NAL8	NAL9	NPM10	NPM11	NPM17	NPM2	NPM32	NPM361
Batholith	SMB	SMB	SMB	-	-	-	-	-	-	-	-	-	-
Pluton	NRP	NRP	NRP	PMP	PMP	PMP	PMP	PMP	PMP	PMP	PMP	PMP	PMP
Lithology	Mzg	Mzg	Mzg	Grd	Grd	Mzg	Mzg	Mzg	Ton	Grd	Ton	Mzg	Lmzg
Source	7	7	7	1	1	1	1	22	22	22	22	22	22
Major oxides													
SiO_2	75 00	75 37	-	72 10	73 25	70 02	70 86	73 99	67 23	70 09	70 78	73 30	75 07
TiO_2	0 02	0 07	-	0 23	0 22	0 41	0 41	0 14	0 55	0 42	0 41	0 14	0 10
Al_2O_3	14 31	14 32	-	16 15	15 62	16 44	16 55	14 76	16 87	15 53	15 40	15 01	14 13
Fe_2O_3	0 22	0 22	-	0 31	0 24	0 19	0 33	-	-	-	-	-	-
FeO	0 59	0 68	-	1 37	1 13	1 80	1 63	-	-	-	-	-	-
MnO	0 02	0 05	-	0 03	0 03	0 04	0 04	0 02	0 06	0 05	0 06	0 05	0 02
MgO	0 05	0 03	-	0 33	0 42	0 71	0 62	0 28	1 40	0 84	1 19	0 30	0 13
CaO	0 47	0 34	-	1 36	1 33	1 68	1 74	1 70	3 23	2 17	2 09	0 82	1 12
Na_2O	4 98	4 24	-	3 82	3 79	3 66	3 73	3 12	3 62	4 18	3 92	3 87	4 10
K_2O	3 63	3 48	-	3 54	3 52	4 17	3 80	4 48	2 41	3 19	2 14	4 37	3 77
P_2O_5	0 30	0 16	-	0 06	0 07	0 13	0 11	0 06	0 17	0 30	0 22	0 31	0 16
H_2O+	0 73	1 03	-	0 83	0 73	0 67	0 57	-	-	-	-	-	-
H_2O-	-	-	-	0 08	0 04	0 05	0 10	-	-	-	-	-	-
CO_2	-	-	-	-	-	-	-	-	-	-	-	-	-
Cl	-	-	-	-	-	-	-	-	-	-	-	-	-
F	-		-	-	-	-	-	-	-	-	-	-	-
LOI	0 73	1 03	-	0 91	0 77	0 72	0 67	0 38	0 58	0 41	0 88	0 65	0 44
TOTAL	100 28	99 95	-	100 16	100 34	99 93	100 43	99 84	99 55	99 66	99 90	99 90	99 73
Fe_2O_3T	0 87	0 97	-	1 83	1 49	2 19	2 14	1 02	3 86	2 79	3 16	1 21	0 78
FeOT	0 77	0 86	-	1 63	1 32	1 95	1 90	0 91	3 43	2 48	2 81	1 08	0 69
A/CNK	1 08	1 21	-	1 27	1 24	1 18	1 22	1 08	1 28	1 13	1 32	1 12	1 07
Trace els													
Ba	11	-	398	478	365	836	573	972	718	645	397	374	316
Rb	840	-	444	158	171	158	154	77	82	124	74	181	125
Sr	-	-	-	99	87	198	154	229	370	184	200	64	86
Y	-	-	-	-	-	-	-	10	10	20	14	14	15
Zr	37	-	84	-	-	-	-	53	150	179	127	69	70
Nb	22	-	11	-	-	-	-	6	11	13	10	12	7
Th	-	-	-	-	-	-	-	1	-	9	9	6	3
Pb	-	-	-	-	-	-	-	29	18	26	22	26	25
Ga	-	-	-	-	-	-	-	14	18	19	18	20	15
Zn	-	-	-	-	-	-	-	16	59	57	47	43	26
Cu	15	-	6	-	-	-	-	-	16	-	-	-	-
Ni	-	-	-	-	-	-	-	3	7	10	9	4	10
V	-	-	-	-	-	-	-	16	68	38	52	4	4
Cr	-	-	-	-	-	-	-	12	18	20	47	9	9
Hf	-	-	-	-	-	-	-	-	-	-	-	-	-
Cs	-	-	-	-	-	-	-	-	-	-	-	-	-
Sc	-	-	-	-	-	-	-	-	-	-	-	-	-
Ta	-	-	-	-	-		-	-	-	-	-	-	-
Co	-	-	-	-	-		-	-	-	-	-	-	-
Li	279	-	283	-	-	-	-	-	-	-	-	-	-
Be	-	-	-	-	-	-	-	-	-	-	-	-	-
B	-	-	-	-	-	-	-	-	-	-	-	-	-
U	-	-	-	-	-	-	-	-	-	-	-	-	-
W	-	-	-	-	-	-	-	-	-	-	-	-	-
Sn	34	-	26	-	-	-	-	-	-	-	-	-	-
Mo	1	-	2	-	-	-	-	-	-	-	-	-	-
Rare-earths													
La	-	-	-	-	-	-	-	-	-	-	-	-	-
Ce	-	-	-	-	-	-	-	-	-	-	-	-	-
Pr	-	-	-	-	-	-	-	-	-	-	-	-	-
Nd	-	-	-	-	-	-	-	-	-	-	-	-	-
Sm	-	-	-	-	-	-	-	-	-	-	-	-	-
Eu	-	-	-	-	-	-	-	-	-	-	-	-	-
Gd	-	-	-	-	-	-	-	-	-	-	-	-	-
Tb	-	-	-	-	-	-	-	-	-	-	-	-	-
Dy	-	-	-	-	-	-	-	-	-	-	-	-	-
Ho	-	-	-	-	-	-	-	-	-	-	-	-	-
Er	-	-	-	-	-	-	-	-	-	-	-	-	-
Tm	-	-	-	-	-	-	-	-	-	-	-	-	-
Yb		-	-	-	-	-		-	-	-	-		-
Lu	-	-	-	-	-	-	-	-	-	-		-	-

Table E1 1 (Continued) Compilation of Meguma Zone granitoid lithogeochemistry

Sample	NPM368B	NPM371	NPM440	NPM441	NPM458	NPM464	NPM469	NPM472	NPM477	NPM484	NPM487	NPM491	NPM511
Batholith	-	-	-	-	-	-	-	-	-	-	-	-	-
Pluton	PMP	PMP	PMP	PMP	PMP	PMP	PMP	PMP	PMP	PMP	PMP	PMP	PMP
Lithology	Grd	Mzg	Grd	Mzg	Grd	Mzg	Grd	Mzg	Mzg	Grd	Ton	Ton	Mzg
Source	22	22	22	22	22	22	22	22	22	22	22	22	22
Major oxides													
SiO_2	72 96	75 72	68 15	73 72	72 26	69 03	70 16	73 35	72 61	73 83	70 33	73 94	73 48
TiO_2	0 24	0 26	0 52	0 14	0 31	0 48	0 48	0 13	0 32	0 13	0 37	0 02	0 17
Al_2O_3	14 64	12.51	15 25	14 64	14 90	15 58	15 60	15 17	14 58	14 18	15 92	15 33	14 84
Fe_2O_3	-	-	-	-	-	-	-	-	-	-	-	-	-
FeO	-	-	-	-	-	-	-	-	-	-	-	-	-
MnO	0 05	0 04	0 07	0 04	0 05	0 06	0 04	0 05	0 04	0 10	0 05	0 12	0 04
MgO	0 47	0 39	1 40	0 26	0 84	1 22	1 22	0 66	0 49	0 66	1 03	0 41	0 32
CaO	1 81	1 01	3 67	0 83	1 88	2 21	1 38	0 77	0 85	1 62	2 74	0 33	1 28
Na_2O	4 35	2 72	3 68	3 92	4 54	4 51	3 65	4 28	2 96	3 77	4 05	5 58	3 99
K_2O	2 82	4 62	2.97	4 28	2 29	2 80	3 92	4 03	5 18	2 11	1 94	2 45	3 74
P_2O_5	0 22	0 21	0 20	0 31	0 17	0 31	0 21	0 29	0 27	0 06	0 17	0 33	0 21
H_2O+	-	-	-	-	-	-	-	-	-	-	-	-	-
H_2O-	-	-	-	-	-	-	-	-	-	-	-	-	-
CO_2	-	-	-	-	-	-	-	-	-	-	-	-	
Cl	-	-	-	-	-	-	-	-	-	-	-	-	-
F	-	-	-	-	-	-	-	-	-	-	-	-	-
LOI	0 42	0 55	0 52	0 63	0 20	0 40	0 70	0 30	0 73	0 50	0 61	0 70	0 55
TOTAL	99 83	99 52	99 72	99 85	99 33	99 29	99 70	100 02	99 66	99 63	99 96	99 78	99 94
Fe_2O_3T	2 08	1 68	3 70	1 21	2.13	3 03	2 63	1 11	1 83	3 00	3 09	0 64	1 49
FeOT	1 85	1 49	3 29	1 08	1 89	2.69	2 34	0 99	1 63	2 67	2 75	0 57	1 32
A/CNK	1 13	1 01	1 03	1 10	1 19	1 14	1 19	1 14	1 09	1 32	1 28	1 27	1 13
Trace els													
Ba	316	409	494	386	364	730	823	427	696	446	440	4	261
Rb	126	170	134	189	96	137	152	179	152	65	60	165	152
Sr	108	66	207	67	139	219	161	64	113	304	312	3	70
Y	20	20	17	14	22	22	14	17	16	17	20	8	16
Zr	137	99	169	73	186	202	200	66	160	108	121	32	92
Nb	10	10	11	11	10	12	7	10	9	10	9	14	10
Th	5	13	13	2	9	7	38	7	27	24	6	4	5
Pb	16	25	12	24	16	15	22	20	27	19	24	15	21
Ga	19	19	22	21	18	20	22	17	19	16	18	20	22
Zn	60	56	74	49	49	63	81	44	50	40	43	43	53
Cu	-	3	6	1	2	6	6	-	3	3	2	-	-
Ni	16	17	16	13	9	12	9	16	14	6	10	8	12
V	16	11	55	7	18	32	34	6	13	-	31	1	8
Cr	12	10	42	9	14	14	24	11	8	10	15	5	7
Hf	-	-	-	-	-	-	-	-	-	-	-	-	-
Cs	-	-	-	-	-	-	-	-	-	-	-	-	-
Sc	-	-	-	-	-	-	-	-	-	-	-	-	-
Ta	-	-	-	-	-	-	-	-	-	-	-	-	-
Co	-	-	-	-	-	-	-	-	-	-	-	-	-
Li	-	-	-	-	-	-	-	-	-	-	-	-	-
Be	-	-	-	-	-	-	-	-	-	-	-	-	-
B	-	-	-	-	-	-	-	-	-	-	-	-	-
U	-	-	-	-	-	-	-	-	-	-	-	-	-
W	-	-	-	-	-	-	-	-	-	-	-	-	-
Sn	-	-	-	-	-	-	-	-	-	-	-	-	-
Mo	-	-	-	-	-	-	-	-	-	-	-	-	-
Rare-earths													
La	-	-	-	-	-	-	-	-	-	-	-	-	-
Ce	-	-	-	-	56 8	-	-	-	72 29	-	-	-	-
Pr	-	-	-	-	-	-	-	-	-	-	-	-	-
Nd	-	-	-	-	29 23	-	-	-	44 93	-			
Sm	-	-	-	-	6 39	-	-	-	10 18	-	-	-	-
Eu	-	-	-	-	0 83	-	-	-	0 59	-	-	-	-
Gd	-	-	-	-	5 25	-	-	-	-	-	-	-	-
Tb	-	-			0 67			-	0 48	-	-	-	-
Dy	-	-	-	-	-	-	-	-	-	-	-	-	-
Ho	-	-	-	-	-	-	-	-	-	-	-	-	-
Er	-	-	-	-	-	-	-	-	-	-	-	-	-
Tm	-	-	-	-	-	-	-	-	-	-	-	-	-
Yb	-	-	-	-	2 03	-	-	-	1 11	-		-	-
Lu	-	-	-	-	0 27	-		-	0 12	-		-	-

Table E1 1 (Continued) Compilation of Meguma Zone granitoid lithogeochemistry

Sample	NPM533	NPM535	NPM536	NPM537	NPM538	NPM539	NPM542	NPM543	NPM544	NPM545	NPM546	NPM548	NPM549
Batholith	-	-	-	-	-	-	-	-	-	-	-	-	-
Pluton	PMP	PMP	PMP	PMP	PMP	PMP	PMP	PMP	PMP	PMP	PMP	PMP	PMP
Lithology	Ton	Grd	Grd	Lmzg	Mzg	Grd	Lmzg	Grd	Ton	Grd	Ton	Mzg	Grd
Source	22	22	22	22	22	22	22	22	22	22	22	22	22
Major oxides													
SiO_2	63 65	71 33	71 77	74 56	74 50	71 32	74 26	64 24	67 53	69 28	63 53	72 73	67 10
TiO_2	0 68	0 32	0 25	0 09	0 09	0 36	0 11	0 76	0 51	0 43	0 36	0 21	0 65
Al_2O_3	17 67	15 27	15 20	14 22	14 69	15 57	14 65	17 78	16 22	15 75	20 13	15 10	16 42
Fe_2O_3	-	-	-	-	-	-	-	-	-	-	-	-	-
FeO	-	-	-	-	-	-	-	-	-	-	-	-	-
MnO	0 09	0 05	0 06	0 02	0 02	0 06	0 02	0 05	0 08	0 05	0 05	0 04	0 0[illegible]
MgO	2 02	1 04	0 86	0 16	0 34	0 89	0 51	1 91	1 62	1 00	1 25	0 75	1 7[illegible]
CaO	4 02	1 61	1 59	1 25	0 92	2 14	0 92	3 27	2 77	2 47	4 13	0 87	2 4[illegible]
Na_2O	3 97	4 08	4 66	3 84	3 35	4 35	4 49	4 42	4 10	4 18	5 82	3 99	3 94
K_2O	2 12	3 45	3 13	4 44	4 75	2.87	3 62	2 47	2.12	2 31	1 54	4 22	3 42
P_2O_5	0 19	0 21	0 24	0 11	0 14	0 19	0 13	0 24	0 19	0 32	0 14	0 23	0 21
H_2O+	-	-	-	-	-	-	-	-	-	-	-	-	-
H_2O-	-	-	-	-	-	-	-	-	-	-	-	-	-
CO_2	-	-	-	-	-	-	-	-	-	-	-	-	-
Cl	-	-	-	-	-	-	-	-	-	-	-	-	-
F	-	-	-	-	-	-	-	-	-	-	-	-	-
LOI	0 30	0 40	0 40	0 27	0 56	0 37	0 30	0 50	0 70	0 40	0 60	0 30	0 30
TOTAL	98 83	99 71	99 91	99 64	100 08	100 26	99 66	98 92	98 90	98 99	99 62	99 68	99 19
Fe_2O_3T	4 64	2 19	1 97	0 77	0 81	2 41	0 73	3 69	3 44	3 15	2 33	1 39	3 [illegible]
FeOT	4 12	1 95	1 75	0 68	0 72	2.14	0 65	3 28	3 06	2.80	2 07	1 24	2.94
A/CNK	1 23	1 15	1 12	1 01	1 10	1 15	1 11	1 23	1 27	1 23	1 25	1 13	1 16
Trace els													
Ba	601	383	316	460	244	399	451	683	484	318	175	334	929
Rb	71	139	137	143	133	128	132	112	128	112	75	186	139
Sr	474	124	102	111	63	151	84	278	337	130	389	70	223
Y	17	15	17	15	11	16	10	17	20	24	11	15	15
Zr	182	115	117	76	39	128	47	220	141	229	123	88	206
Nb	12	9	11	5	8	9	6	7	10	12	8	9	8
Th	-	12	7	9	2	11	3	28	13	10	10	12	32
Pb	8	17	19	22	24	22	18	11	17	13	14	22	15
Ga	22	22	19	16	21	22	18	26	23	19	22	21	23
Zn	61	57	60	23	23	57	29	88	65	83	50	51	91
Cu	7	6	-	-	-	-	-	4	4	3	7	-	10
Ni	10	9	9	8	9	13	6	10	14	11	6	10	10
V	77	27	15	3	1	30	3	71	58	37	36	14	53
Cr	21	21	13	3	6	25	8	47	24	13	32	16	32
Hf	-	-	-	-	-	-	-	-	-	-	-	-	-
Cs	-	-	-	-	-	-	-	-	-	-	-	-	-
Sc	-	-	-	-	-	-	-	-	-	-	-	-	-
Ta	-	-	-	-	-	-	-	-	-	-	-	-	-
Co	-	-	-	-	-	-	-	-	-	-	-	-	-
Li	-	-	-	-	-	-	-	-	-	-	-	-	-
Be	-	-	-	-	-	-	-	-	-	-	-	-	-
B	-	-	-	-	-	-	-	-	-	-	-	-	-
U	-	-	-	-	-	-	-	-	-	-	-	-	-
W	-	-	-	-	-	-	-	-	-	-	-	-	-
Sn	-	-	-	-	-	-	-	-	-	-	-	-	-
Mo	-	-	-	-	-	-	-	-	-	-	-	-	-
Rare-earths													
La	-	-	-	-	-	-	-	-	-	-	-	-	-
Ce	38 51	-	-	-	-	43 41	17 54	-	-	-	-	-	-
Pr	-	-	-	-	-	-	-	-	-	-	-	-	-
Nd	18 98	-	-	-	-	22 96	8 17	-	-	-	-	-	-
Sm	3 88	-	-	-	-	4 63	2 03	-	-	-	-	-	-
Eu	1 21	-	-	-	-	0 75	0 48	-	-	-	-	-	-
Gd	4 57	-	-	-	-	3 81	-	-	-	-	-	-	-
Tb	0 41	-	-	-	-	0 47	0 19	-	-	-	-	-	-
Dy	-	-	-	-	-	-	-	-	-	-	-	-	-
Ho	-	-	-	-	-	-	-	-	-	-	-	-	-
Er	-	-	-			-	-	-	-	-	-	-	-
Tm	-	-	-	-	-	-	-	-	-	-	-	-	-
Yb	1 38	-	-	-	-	1 7	0 69	-	-	-	-	-	-
Lu	0 2	-	-	-	-	0 23	0 1	-	-	-	-	-	-

Table E1 1 (Continued) Compilation of Meguma Zone granitoid lithogeochemistry

Sample	NPM551	NPM556	NPM558	NPM560	NPM563	NPM565	NPM566	NPM578	NPM579	NPM580	NPM581	NPM582	NPM583
Batholith	-	-	-	-	-	-	-	-	-	-	-	-	-
Pluton	PMP	PMP	PMP	PMP	PMP	PMP	PMP	PMP	PMP	PMP	PMP	PMP	PMP
Lithology	Mzg	Mzg	Grd	Ton	Grd	Grd	Mzg	Mzg	Grd	Lmzg	Grd	Ton	Ton
Source	22	22	22	22	22	22	22	22	22	22	22	22	22
Major oxides													
SiO_2	68 49	70 33	68 27	70 27	71 12	70 01	72 72	70 93	72 64	72 79	71 45	66 24	72 85
TiO_2	0,42	0 46	0 60	0 35	0 32	0 35	0 22	0 29	0 26	0 14	0 32	0 63	0 35
Al_2O_3	15 98	15 25	16 24	15 76	15 18	15 62	14 64	15 31	14 61	14 89	15 61	17 00	15 02
Fe_2O_3	-	-	-	-	-	-	-	-	-	-	-	-	-
FeO	-	-	-	-	-	-	-	-	-	-	-	-	-
MnO	0 06	0 04	0 04	0 07	0 04	0 05	0 03	0 04	0 03	0 03	0 05	0 07	0 04
MgO	1 43	1 02	1 33	0 77	0 71	1,18	0 34	0 97	0 34	0 30	0 95	1 56	0 72
CaO	2,35	1,74	2.27	2 81	1,92	2 05	0 86	1 88	0 86	0 85	1,76	3 94	2 35
Na_2O	3 97	3 56	3 76	4 44	4 07	4 41	2 85	4 21	2 85	2 56	4 63	3 94	3 58
K_2O	3 69	4 24	3 66	2 25	3 49	2 90	5 86	3 17	5 86	6 30	3 09	1 55	2 19
P_2O_5	0 16	0 22	0 21	0 22	0 23	0 14	0 18	0 20	0 18	0 32	0 27	0 30	0 15
H_20+	-	-	-	-	-	-	-	-	-	-	-	-	-
H_2O-	-	-	-	-	-	-	-	-	-	-	-	-	-
CO_2	-	-	-	-	-	-	-	-	-	-	-	-	-
Cl	-	-	-	-	-	-	-	-	-	-	-	-	-
F	-	-	-	-	-	-	-	-	-	-	-	-	-
LOI	0 30	0 46	0 72	0 42	0 50	0 40	0 47	0 40	0 47	0 61	0 50	0 50	0 64
TOTAL	99 38	99 64	100 01	99 62	99 58	99 36	99 48	99 32	99 41	99 64	100 67	99 07	100 01
Fe_2O_3T	2 85	2 61	3 27	2 54	2 25	2 53	1 47	2 16	1 47	0 96	2 29	3 76	2 38
FeOT	2 53	2.32	2 91	2 26	2.00	2.25	1 31	1 92	1 31	0 85	2 04	3 34	2 12
A/CNK	1 10	1 09	1 15	1 16	1 10	1 16	1 02	1 14	1 02	1 02	1 14	1 28	1 29
Trace els													
Ba	812	781	901	283	546	400	963	497	598	774	461	314	657
Rb	121	166	137	98	123	112	157	130	150	234	156	59	69
Sr	330	163	226	184	157	225	118	137	152	102	116	213	197
Y	18	16	17	15	17	17	16	19	13	19	-	27	22
Zr	123	151	217	210	146	102	112	140	137	60	151	389	209
Nb	10	7	8	10	10	13	10	9	9	8	10	11	8
Th	3	26	44	-	8	5	14	3	14	1	13	4	12
Pb	13	22	21	17	23	15	29	17	26	21	18	13	18
Ga	19	26	25	22	20	21	22	20	20	20	21	18	19
Zn	47	83	90	60	59	57	44	56	54	33	61	66	53
Cu	5	4	8	4	1	2	-	-	1	3	-	19	1
Ni	11	16	14	9	11	9	13	12	13	18	13	8	4
V	52	38	45	27	21	37	5	24	19	6	24	50	24
Cr	19	20	33	12	21	18	7	14	16	8	20	16	14
Hf	-	-	-	-	-	-	-	-	-	-	-	-	-
Cs	-	-	-	-	-	-	-	-	-	-	-	-	-
Sc	-	-	-	-	-	-	-	-	-	-	-	-	-
Ta	-	-	-	-	-	-	-	-	-	-	-	-	-
Co	-	-	-	-	-	-	-	-	-	-	-	-	-
Li	-	-	-	-	-	-	-	-	-	-	-	-	-
Be	-	-	-	-	-	-	-	-	-	-	-	-	-
B	-	-	-	-	-	-	-	-	-	-	-	-	-
U	-	-	-	-	-	-	-	-	-	-	-	-	-
W	-	-	-	-	-	-	-	-	-	-	-	-	-
Sn	-	-	-	-	-	-	-	-	-	-	-	-	-
Mo	-	-	-	-	-	-	-	-	-	-	-	-	-
Rare-earths													
La	-	-	-	-	-	-	-	-	-	-	-	-	-
Ce	-	-	13 46	13 04	-	-	48 7	-	-	-	-	49 3	56 93
Pr	-	-	-	-	-	-	-	-	-	-	-	-	-
Nd	-	-	65 54	7,11	-	-	25 55	-	-	-	-	27 09	25 59
Sm	-	-	13 5	1 81	-	-	6	-	-	-	-	5 96	5 36
Eu	-	-	1 17	0 75	-	-	0 64	-	-	-	-	1 3	1 17
Gd	-	-	15 7	2 35	-	-	3 31	-	-	-	-	4 94	-
Tb	-	-	1 51	0 34	-	-	0 54	-	-	-	-	0 81	0 53
Dy	-	-	-	-	-	-	-	-	-	-	-	-	-
Ho	-	-	-	-	-	-	-	-	-	-	-	-	-
Er	-	-	-	-	-	-	-	-	-	-	-	-	-
Tm	-	-	-	-	-	-	-	-	-	-	-	-	-
Yb	-	-	1 15	1 49	-	-	0 6	-	-	-	-	3 07	2 04
Lu	-	-	0 15	0 21	-	-	0 07	-	-	-	-	0 43	0 29

Table E1 1 (Continued) Compilation of Meguma Zone granitoid lithogeochemistry

Sample	NPM584	NPM593	NPM8B	NLHQ00	NLHQ01	NLHQ02	NLHQ03	NLHQ04	NLHQ05	NLHQ06	NLHQ07	NLHQ08	NLHQO9
Batholith	-	-	-	-	-	-	-	-	-	-	-	-	-
Pluton	PMP	PMP	PMP	QP	QP	QP	QP	QP	QP	QP	QP	QP	QP
Lithology	Ton	Grd	Ton	Mzq	Mzg	Mzg	Mzg	Mzg	Mzg	Mzg	Mzg	Mzg	Mzg
Source	22	22	22	14	14	14	14	14	14	14	14	14	14
Major oxides													
SiO_2	68 14	70 20	73 09	71 05	69 07	69 28	70 10	70 55	71 11	72 25	69 64	69 63	72 65
TiO_2	0 50	0 47	0 04	0 19	0 39	0 43	0 20	0 26	0 26	0 26	0 33	0 39	0 24
Al_2O_3	10 25	15 69	15 50	15 21	15 57	15 46	14 85	14 76	14 84	15 12	15 88	15 21	14 99
Fe_2O_3	-	-	-	-	0 07	0 55	0 03	-	0 14	0 36	-	-	0 03
FeO	-	-	-	-	2.02	1 84	1 12	-	1 28	1 27	-	-	1 36
MnO	0 07	0 05	0 22	0 10	0 10	0 11	0 04	0 04	0 04	0 07	0 09	0 10	0 05
MgO	1 46	1 22	0 08	0 48	0 58	0 88	0 39	0 52	0 49	0 57	0 74	0 90	0 52
CaO	3 12	1 30	0 37	0 93	1 45	1 74	0 53	0 61	0 61	1 03	1 79	1 75	0 55
Na_2O	4 02	3 94	3 10	3 44	3 43	3 52	3 54	3 62	3 60	3 51	3 65	3 48	3 65
K_2O	1 73	3 32	5 69	4 68	4 14	3 67	5 06	4 85	4 77	4 44	4 20	3 86	4 83
P_2O_5	0 13	0 20	0 15	0 22	0 16	0 14	0 22	0 23	0 23	0 18	0 12	0 13	0 25
H_2O+	-	-	-	0 70	1 00	1 10	0 82	0 69	0 78	0 85	0 80	0 83	0 94
H_2O-	-	-	-	0 18	0 27	0 23	0 19	0 37	0 22	0 21	0 25	0 20	0 14
CO_2	-	-	-	-	-	-	-	-	-	-	-	-	-
Cl	-	-	-	-	-	-	-	-	-	-	-	-	-
F	-	-	-	-	0 06	0 07	0 06	0 08	0 07	0 07	0 05	0 05	0 08
LOI	0 50	0 70	0 74	0 88	1 33	1 40	1 07	1 14	1 07	1 13	1 10	1 08	1 16
TOTAL	99 35	99 39	99 93	98 81	98 27	98 93	97 13	98 11	98 41	100 13	99 46	98 86	100 26
Fe_2O_3T	3 86	2 59	1 07	1 83	2 31	2 59	1 27	1 72	1 56	1 77	2 16	2 62	1 54
FeOT	3 43	2.30	0 95	1 63	2.05	2 30	1 13	1 53	1 39	1 57	1 92	2 33	1 37
A/CNK	1 29	1 26	1 13	1 13	1 17	1 19	1 09	1 09	1 11	1 14	1 12	1 14	1 12
Trace els													
Ba	475	768	181	310	419	435	318	386	379	342	527	473	392
Rb	62	115	178	227	187	178	245	268	267	209	175	176	268
Sr	385	194	30	94	6	168	79	82	77	113	184	167	75
Y	11	13	11	13	17	18	10	9	8	14	14	16	10
Zr	156	190	37	69	101	109	80	95	95	79	90	98	90
Nb	9	9	10	10	11	9	8	9	8	11	9	10	9
Th	10	35	2	6	13	14	12	19	19	10	12	12	16
Pb	16	26	36	34	31	26	26	26	25	30	32	30	24
Ga	18	20	19	22	19	19	22	21	23	20	17	20	21
Zn	54	58	18	54	58	55	61	68	67	54	46	54	58
Cu	8	-	-	-	-	-	-	-	-	-	-	-	-
Ni	2	7	5	8	6	6	6	7	3	8	5	7	6
V	37	36	-	11	-	-	-	-	-	13	-	-	-
Cr	14	19	9	15	23	29	8	14	12	14	21	20	13
Hf	-	-	-	-	-	-	-	-	-	-	-	-	-
Cs	-	-	-	-	-	-	-	-	-	-	-	-	-
Sc	-	-	-	-	-	-	-	-	-	-	-	-	-
Ta	-	-	-	-	-	-	-	-	-	-	-	-	-
Co	-	-	-	-	-	-	-	-	-	-	-	-	-
Li	-	-	-	-	93	-	68	96	93	114	79	80	102
Be	-	-	-	-	6	3 5	5	6 5	5 5	7 5	5	5 5	5 5
B	-	-	-	-	20	15	15	-	-	15	10	20	20
U	-	-	-	-	4	-	5 7	2 8	3 6	5 8	6	5 6	2 9
W	-	-	-	-	6	-	10	8	3	3	1	3	5
Sn	-	-	-	-	3	6	9	7	13	9	5	1	9
Mo	-	-	-	-	1	2	1	1	1	1	1	1	1
Rare-earths													
La	-	-	-	-	-	-	-	-	-	34 7	-	-	-
Ce	67 96	-	6 03	-	36 12	-	-	-	-	-	-	-	-
Pr	-	-	-	-	-	-	-	-	-	-	-	-	-
Nd	29 41	-	2.88	-	19 8	-	-	-	-	19 04	-	-	-
Sm	5 19	-	0 87	-	4 67	-	-	-	-	5 1	-	-	-
Eu	1 34	-	0 13	-	0 42	-	-	-	-	0 55	-	-	-
Gd	-	-	-	-	-	-	-	-	-	-	-	-	-
Tb	0 32	-	0 18	-	0 65	-	-	-	-	0 5	-	-	-
Dy	-	-	-	-	-	-	-	-	-	-	-	-	-
Ho	-	-	-	-	-	-	-	-	-	-	-	-	-
Er	-	-	-	-	-	-	-	-	-	-	-	-	-
Tm	-	-	-	-	-		-	-	-	-	-	-	-
Yb	0 87	-	1 22	-	0 69	-	-	-	-	0 51	-	-	-
Lu	0 1	-	0 18	-	0 08	-	-	-	-	0 04	-	-	-

Table E1 1 (Continued) Compilation of Meguma Zone granitoid lithogeochemistry

Sample	NLHQ13	NLHQ14	NLHQ15	NLHQ16	NLHQ17	NLHQ18	NLHQ19	NLHQ20	NLHQ21	NLHQ22	NLHQL14	NLHQL32
Batholith	-	-	-	-	-	-	-	-	-	-	-	-
Pluton	QP	QP	QP	QP	QP	QP	QP	QP	QP	QP	QP	QP
Lithology	Mzg	Mzg	Mzg	Mzg	Mzg	Mzg	Mzg	Mzg	Mzg	Mzg	Mzg	Mzg
Source	14	14	14	14	14	14	14	14	14	14	14	14
Major oxides												
SiO_2	70 90	70 93	71 29	70 91	73 67	70 51	72 61	71 63	71 78	70 51	70 40	71 84
TiO_2	0 27	0 31	0 24	0 28	0 24	0 25	0 26	0 24	0 26	0 38	0 31	0 33
Al_2O_3	14 61	15 36	14 74	14 52	14 90	15 00	14 73	15 05	14 90	15 12	14 90	15 01
Fe_2O_3	0 05	0 28	0 01	0 03	0 18	0 08	0 01	-	0 12	0 40	0 02	0 10
FeO	1 44	1 52	1 38	1 46	1 25	1 34	1 43	-	1 38	2.15	1 55	1 62
MnO	0 06	0 06	0 05	0 06	0 04	0 05	0 04	0 05	0 05	0 12	0 05	0 05
MgO	0 59	0 69	0 50	0 57	0 49	0 49	0 52	0 51	0 54	0 98	0 55	0 69
CaO	0 81	0 86	0 57	0 (	0 62	0 74	0 80	0 61	0 77	1 53	0 77	0 85
Na_2O	3 61	3 55	3 58	3 55	3 64	3 66	3 50	3 62	3 56	3 28	3 54	3 50
K_2O	4 66	4 80	4 62	4 43	4 68	4 70	4 87	4 68	4 78	3 96	4 45	4 51
P_2O_5	0 20	0 26	0 24	0 20	0 24	0 24	0 23	0 23	0 24	0 15	0 20	0 20
H_20+	0 65	0 65	0 78	0 68	0 94	1 02	0 76	0 77	0 89	1 03	1 16	0 71
H_2O-	0 29	0 31	0 35	0 26	0 25	0 28	0 25	0 11	0 21	0 17	0 20	0 37
CO_2	-	-	-	-	-	-	-	-	-	-	-	-
Cl	-	-	-	-	-	-	-	-	-	-	-	-
F	0 10	0 10	-	0 09	0 08	0 10	0 07	0 09	0 08	0 08	0 08	0 11
LOI	1 04	1 06	1 13	1 03	1 27	1 40	1 08	0 97	1 18	1 28	1 44	1 19
TOTAL	98 22	99 63	98 33	97 63	101 19	98 44	100 06	99 05	99 53	99 79	98 16	99 86
Fe_2O_3T	1 65	1 97	1 54	1 65	1 57	1 57	1 60	1 64	1 65	2 79	1 74	1 90
FeOT	1 47	1 75	1 37	1 47	1 40	1 40	1 42	1 46	1 47	2 48	1 55	1 69
A/CNK	1 09	1 12	1 13	1 14	1 12	1 11	1 08	1 14	1 10	1 17	1 15	1 14
Trace els												
Ba	504	567	415	443	370	382	441	408	420	355	464	506
Rb	259	267	282	245	268	275	256	269	266	188	265	262
Sr	93	94	79	79	74	76	85	79	80	137	87	93
Y	11	12	11	13	9	11	9	10	10	21	11	11
Zr	105	124	96	112	97	101	106	95	106	102	113	119
Nb	9	9	10	10	10	10	9	8	10	11	9	10
Th	21	25	20	22	17	18	18	18	19	7	26	25
Pb	25	26	36	25	23	25	27	23	27	21	27	25
Ga	23	24	27	25	26	25	25	27	25	23	21	22
Zn	72	82	64	75	62	62	68	72	69	63	57	62
Cu	-	-	-	-	-	-	-	-	-	-	-	-
Ni	11	12	12	8	11	11	10	9	7	11	9	8
V	19	21	14	15	14	13	20	12	14	28	-	-
Cr	16	19	8	14	19	14	17	11	11	26	19	19
Hf	-	-	-	-	-	-	-	-	-	-	-	-
Cs	-	-	-	-	-	-	-	-	-	-	-	-
Sc	-	-	-	-	-	-	-	-	-	-	-	-
Ta	-	-	-	-		-	-	-	-	-	-	-
Co	-	-	-	-		-	-	-	-	-	-	-
Li	-	-	-	-	-	-	-	-	-	-	-	91
Be	2 5	6	-	2	4	4	3 5	4	3	2 5	5 5	5
B	10	15	-	15	150	10	15	20	15	20	20	15
U	3 1	3 7	-	2 8	3 5	5 9	6 5	3 4	3 3	5 5	6 6	2 9
W	-	-	-	-	-	-	-	-	-		-	4
Sn	8	9	-	6	12	12	11	8	11	10	4	1
Mo	2	2	-	2	2	?	2	2	2	3	1	1
Rare-earths												
La	-	-	-	-	-	-	-	-	-	-	-	-
Ce	-	65 27	-	-	48 99	-	-	-	-	-	-	-
Pr	-	-	-	-	-	-	-	-	-	-	-	-
Nd	-	34 06	-	-	27 77	-	-	-	-	-	-	-
Sm	-	7 71	-	-	6 38	-	-	-	-	-	-	-
Eu	-	0 6	-	-	0 54	-	-	-	-	-	-	-
Gd	-	-	-	-	-	-	-	-	-	-	-	-
Tb	-	0 56	-	-	0 51	-	-	-	-	-	-	-
Dy	-	-	-	-	-	-	-	-	-	-	-	-
Ho	-	-	-	-	-	-	-	-	-	-	-	-
Er	-	-	-		-	-	-	-	-	-	-	-
Tm	-	-	-	-	-	-	-	-	-	-	-	-
Yb	-	0 77	-	-	0 71	-	-	-	-	-	-	-
Lu	-	0 03	-	-	0 07	-	-	-	-	-	-	-

Table E1.1 (Continued) Compilation of Meguma Zone granitoid lithogeochemistry

Sample	NLHQL38	NKA003	NKA014	NKA015	NKA019	NKA022	NKA028	NKA029	NKA049	NKA049A	NKA052	NKA062
Batholith	-	-	-	-	-	-	-	-	-	-	-	-
Pluton	QP	ShP	ShP	ShP	ShP	ShP	ShP	ShP	ShP	ShP	ShP	ShP
Lithology	Mzg	Mzg	Mzg	Mzg	Mzg	Mzg	Mzg	Mzg	Mzg	Mzg	Mzg	Mzg
Source	14	13	13	13	13	13	13	13	13	13	13	13
Major oxides												
SiO_2	69.72	72.73	73.26	74.66	75.63	73.38	71.00	73.79	75.06	73.83	73.55	72.74
TiO_2	0.27	0.25	0.17	0.18	0.22	0.21	0.29	0.15	0.06	0.02	0.32	0.09
Al_2O_3	14.67	15.17	15.73	14.43	13.76	15.13	15.50	15.50	15.04	14.46	14.45	16.07
Fe_2O_3	-	0.32	0.23	0.24	0.15	0.26	0.39	0.19	0.14	0.10	0.30	0.11
FeO	-	1.16	0.85	0.86	0.02	0.95	1.30	0.70	0.51	0.38	1.08	0.41
MnO	0.07	0.04	0.03	0.03	0.30	0.02	0.04	0.03	0.03	0.02	0.60	0.02
MgO	0.56	0.34	0.32	0.38	0.30	0.46	0.62	0.23	0.08	0.09	0.04	0.11
CaO	1.46	0.95	0.52	0.77	0.40	0.73	0.66	0.54	0.41	0.38	0.60	0.60
Na_2O	3.47	3.14	3.41	2.82	3.40	2.98	3.45	3.71	4.12	4.98	3.19	3.61
K_2O	4.04	4.90	4.65	5.06	4.32	4.93	4.52	4.82	3.96	3.67	4.40	5.94
P_2O_5	0.07	0.26	0.24	0.21	0.10	0.22	0.27	0.25	0.31	0.32	0.12	0.20
H_2O+	1.00	-	-	-	-	-	-	-	-	-	-	-
H_2O-	0.14	-	-	-	-	-	-	-	-	-	-	-
CO_2	-	-	-	-	-	-	-	-	-	-	-	-
Cl	-	-	-	-	-	-	-	-	-	-	-	-
F	0.03	-	-	-	-	-	-	-	-	-	-	-
LOI	1.17	0.80	1.05	0.72	0.96	0.82	1.15	0.82	0.85	0.64	1.20	0.71
TOTAL	97.17	100.21	100.42	100.32	99.54	100.04	98.95	100.73	100.55	98.87	99.80	100.60
Fe_2O_3T	1.88	1.61	1.17	1.19	0.17	1.31	1.63	0.97	0.71	0.52	1.50	0.57
FeOT	1.67	1.43	1.04	1.06	0.15	1.16	1.45	0.86	0.63	0.46	1.33	0.51
A/CNK	1.11	1.13	1.23	1.12	1.14	1.17	1.21	1.15	1.20	1.09	1.19	1.06
Trace els												
Ba	293	376	111	342	91	430	240	227	31	-	206	667
Rb	163	237	243	235	236	230	248	256	374	415	241	249
Sr	140	102	48	86	34	96	67	61	24	30	60	105
Y	18	-	-	-	-	-	-	-	-	-	-	-
Zr	79	100	75	77	59	100	102	83	66	29	74	83
Nb	8	19	21	21	7	3	7	10	1	6	10	-
Th	9	-	-	-	-	-	3	5	9	4	21	2
Pb	30	9	8	2	17	2	55	37	31	40	48	39
Ga	17	30	29	33	53	39	-	-	-	-	-	-
Zn	42	-	-	-	-	-	15	14	17	15	72	16
Cu	-	53	51	39	41	26	-	-	-	-	2	-
Ni	3	-	-	-	2	-	-	38	20	34	3	66
V	-	5	-	-	2	-	4	-	-	-	2	-
Cr	19	244	13	179	4	5	404	9	-	18	8	6
Hf	-	-	-	-	-	-	-	-	-	-	-	-
Cs	-	-	-	-	-	-	-	-	-		-	-
Sc	-	-	7	-	7	6	-	5	5	1	5	3
Ta	-	-	-	-	-	-	-	-	-	-	-	-
Co	-	-	-	-	-	-	-	-	-	-	-	-
Li	72	-	-	-	-	-	-	-	-	-	-	-
Be	4.5	-	-	-	-	-	-	-	-	-	-	-
B	15	-	-	-	-	-	-	-	-	-	-	-
U	3.4	12	15	19	-	22	25	23	26	35	-	17
W	3	-	-	-	-	-	-	-	-	-	-	-
Sn	2	-	-	-	-	-	-	-	-	-	-	-
Mo	1	-	-	-	-	-	-	-	-	-	-	-
Rare-earths												
La	-	46	69	65	54	30	22	57	68	37	29	60
Ce	37.84	44	27	6	12	-	35	4	-	15	43	-
Pr	-	-	-	-	-	-	-	-	-	-	-	-
Nd	18.27	-	-	-	-	-	-	-	-	-	-	-
Sm	4.76	-	-	-	-	-	-	-	-	-	-	-
Eu	0.7	-	-	-	-	-	-	-	-	-	-	-
Gd	-	-	-	-	-	-	-	-	-	-	-	-
Tb	0.46	-	-	-	-	-	-	-	-	-	-	-
Dy	-	-	-	-	-	-	-	-	-	-	-	-
Ho	-	-	-	-	-	-	-	-	-	-	-	-
Er	-	-	-	-	-	-	-	-	-	-	-	-
Tm	-	-	-	-	-	-	-	-	-	-	-	
Yb	1.79	-	-	-		-	-	-	-	-	-	-
Lu	0.23	-	-	-		-	-	-	-	-	-	-

Table E1 1 (Continued) Compilation of Meguma Zone granitoid lithogeochemistry

Sample	NKA065	NKA069	NKA069A	NKA083	NPS122	NPS124	NPS126	NPS200	NPS205	NS1749	NSI751	NSI753
Batholith	-	-	-	-	-	-	-	-	-	-	-	-
Pluton	ShP	ShP	ShP	ShP	ShP	ShP	ShP	ShP	ShP	SIP	SIP	SIP
Lithology	Mzg	Mzg	Mzg	Mzg	Mzg	Mzg	Mzg	Mzg	Mzg	Mzg	Mzg	Mzg
Source	13	13	13	13	23	23	23	23	23	5	5	5
Major oxides												
SiO_2	74 56	75 82	74 50	75 55	72 21	73 86	75 00	72 65	73 35	72 66	73 98	73 54
TiO_2	0 24	0 18	0 27	0 03	0 20	0 14	0 11	0 05	0 13	0 35	0 23	0 17
Al_2O_3	14 35	13 33	14 08	14 84	14 30	15 11	14 53	15 26	14 48	14 30	13 98	14 40
Fe_2O_3	0 32	0 25	0 34	0 07	0 26	0 22	0 16	0 24	0 17	-	-	-
FeO	1 15	0 89	1 24	0 23	1 17	1 01	0 59	0 61	0 83	-	-	-
MnO	0 03	0 02	0 46	0 01	0 02	0 03	0 02	0 02	0 02	0 05	0 03	0 04
MgO	0 48	0 31	0 03	0 04	0 51	0 08	0 27	0 16	0 27	0 42	0 26	0 31
CaO	0 76	0 50	0 40	0 42	0 66	0 53	0 62	0 49	0 64	0 68	0 74	0 57
Na_2O	3 06	2 57	3 44	5 02	3 66	3 68	3 81	4 07	3 88	3 41	3 69	3 26
K_2O	4 47	4 83	4 83	3 77	4 53	4 23	5 11	4 17	4 55	4 48	4 24	4 53
P_2O_5	0 23	0 18	0 10	0 03	0 22	0 22	0 16	0 31	0 25	0 12	0 21	0 22
H_20+	-	-	-	-	0 81	0 81	0 43	0 70	0 71	-	-	-
H_2O-	-	-	-	-	0 07	0 01	0 01	0 01	0 01	-	-	-
CO_2	-	-	-	-	0 16	0 04	0 11	0 28	0 22	-	-	-
Cl	-	-	-	-	-	-	-	-	-	-	-	-
F	-	-	-	-	0 05	0 05	0 03	0 07	0 05	0 04	0 06	0 09
LOI	0 79	0 69	0 98	0 30	1 09	0 91	0 58	1 06	0 99	0 52	0 75	0 76
TOTAL	100 39	99 53	100 62	100 30	98 79	99 98	100 93	99 06	99 53	99 52	99 67	99 56
Fe_2O_3T	1 60	1 24	1 72	0 33	1 56	1 34	0 81	0 92	1 09	2 85	1 76	1 98
FeOT	1 42	1 10	1 53	0 29	1 39	1 19	0 72	0 82	0 97	2 53	1 56	1 76
A/CNK	1 16	1 12	1 09	1 10	1 09	1 21	1 02	1 18	1 08	1 12	1 09	1 16
Trace els												
Ba	312	294	271	-	390	110	430	12	10	712	565	672
Rb	216	232	229	228	242	216	199	305	210	132	165	186
Sr	90	75	64	38	75	54	97	11	36	195	85	99
Y	-	-	-	-	-	-	-	-	-	17	20	27
Zr	109	97	74	46	-	-	-	-	-	201	156	149
Nb	12	31	6	10	-	-	-	-	-	17	20	18
Th	8	6	25	2	5	4	2	2	4	1 8	5 4	5 1
Pb	34	31	74	50	17	16	30	7	16	19	16	22
Ga	-	-	-	-	-	-	-	-	-	19	25	24
Zn	51	29	49	-	54	49	26	40	38	42	67	52
Cu	-	-	2	-	5	7	6	5	5	-	-	-
Ni	34	21	2	-	-	-	-	-	-	6	7	13
V	-	1	2	-	-	-	-	-	-	27	12	8
Cr	10	17	2	240	-	-	-	-	-	33	41	32
Hf	-	-	-	-	-	-	-	-	-	-	-	-
Cs	-	-	-	-	-	-	-	-	-	-	-	-
Sc	7	6	6	-	-	-	-	-	-	-	-	-
Ta	-	-	-	-	-	-	-	-	-	-	-	-
Co	-	-	-	-	-	-	-	-	-	-	-	-
Li	-	-	-	-	187	104	61	263	103	45	31	92
Be	-	-	-	-	6	11	8 3	7 5	9	-	4 6	-
B	-	-	-	-	12	8	5	8	9	-	-	-
U	18	16	-	11	3 6	3 2	1 6	9 4	2 9	3 5	3	8 8
W	-	-	-	-	4	4	4	4	4	-	-	-
Sn	-	-	-	-	14	9	6 5	35	8	11	11	10
Mo	-	-	-	-	2 1	1 5	1 5	2 2	1 3	-	-	-
Rare-earths												
La	62	55	27	41	-	-	-	-	-	-	-	-
Ce	40	16	23	42	-	-	-	-	-	-	-	-
Pr	-	-	-	-	-	-	-	-	-	-	-	-
Nd	-	-	-	-	-	-	-	-	-	-	-	-
Sm	-	-	-	-	-	-	-	-	-	-	-	-
Eu *	-	-	-	-	-	-	-	-	-	-	-	-
Gd	-	-	-	-	-	-	-	-	-	-	-	-
Tb	-	-	-	-	-	-	-	-	-	-	-	-
Dy	-	-	-	-	-	-	-	-	-	-	-	-
Ho	-	-	-	-	-	-	-	-	-	-	-	-
Er	-	-	-	-	-	-	-	-	-	-	-	-
Tm	-	-	-	-	-	-	-	-	-	-	-	-
Yb	-	-	-	-	-	-	-	-	-	-	-	-
Lu	-	-	-	-	-	-	-	-	-	-	-	-

Table E1 1 (Continued) Compilation of Meguma Zone granitoid lithogeochemistry

Sample	NSI758	NSI761	NSL00I	NSL003	NSL004	NSL005	NSL006	NSL007	NSLOO8	NSLOO9	NSL010	NSL011
Batholith	-	-	-	-	-	-	-	-	-	-	-	-
Pluton	SIP	SIP	SLP	SLP	SLP	SLP	SLP	SLP	SLP	SLP	SLP	SLP
Lithology	Mzg	Mzg	Mzg	Mzg	Mzg	Mzg	Mzg	Mzg	Mzg	Mzg	Mzg	Mzg
Source	5	5	16	16	16	16	16	16	16	16	16	16
Major oxides												
SiO_2	74 35	72 11	72 62	72.30	72 41	72 86	72 99	75 07	73 25	73 55	73 06	72 19
TiO_2	0 25	0 29	0 11	0 11	0 16	0 12	0 17	0 17	0 03	0 07	0 15	0 29
Al_2O_3	14 32	14 47	15 05	15 31	15 09	14 92	14 99	13 87	15 05	15 27	15 36	15 43
Fe_2O_3	-	-	0 10	0 11	0 44	0 11	0 11	0 05	-	0 09	0 14	0 41
FeO	-	-	1 02	1 03	1 05	1 02	1 33	0 91	-	0 37	1 26	1 60
MnO	0 30	0 06	0 05	0 05	0 05	0 05	0 04	0 03	0 03	0 04	0 06	0 05
MgO	0 21	0 56	0 24	0 25	0 34	0 25	0 35	0 29	0 05	0 06	0 29	0 49
CaO	0 50	1 45	0 61	0 44	0 47	0 50	0 43	0 62	0 47	0 63	0 48	0 47
Na_2O	3 16	3 57	4 14	4 06	3 91	4 03	3 89	4 55	4 58	4 89	4 03	3 59
K_2O	4 42	4 12	3 76	3 84	3 97	3 69	3 94	3 31	3 58	3 38	3 95	4 13
P_2O_5	0 19	0 12	0 62	0 48	0 47	0 51	0 50	0 28	0 62	0 75	0 60	0 34
H_2O+	-	-	1 23	1 15	0 95	1 02	0 92	0 60	0 60	0 52	0 93	0 79
H_2O-	-	-	0 12	0 20	0 11	0 09	0 14	0 10	0 17	0 12	0 14	0 19
CO_2	-	-	0 19	0 15	0 19	0 19	0 09	0 15	0 19	0 10	0 17	0 13
Cl	-	-	-	-	-	-	-	-	-	-	-	-
F	0 06	0 04	0 08	0 07	0 05	0 06	0 06	0 02	0 02	0 03	0 07	0 06
LOI	0 77	0 48	1 62	1 57	1 30	1 36	1 21	0 87	0 98	0 77	1 31	1 17
TOTAL	99 97	97 65	99 91	99 52	99 60	99 39	99 92	100 00	99 08	99 85	100 56	100 00
Fe_2O_3T	1 69	0 47	1 23	1 25	1 61	1 24	1 59	1 06	0 60	0 50	1 64	2 08
FeOT	1 50	0 42	1 09	1 11	1 43	1 10	1 41	0 94	0 44	0 44	1 37	1 85
A/CNK	1 19	1 08	1 20	1 24	1 22	1 23	1 23	1 12	1 19	1 17	1 23	1 27
Trace els												
Ba	516	496	26	17	24	21	26	261	14	38	72	62
Rb	185	163	432	391	347	375	293	191	423	506	385	267
Sr	73	160	72	32	33	29	17	79	95	53	57	22
Y	16	25	-	-	-	-	-	-	-	-	-	-
Zr	114	182	42	40	57	48	57	61	20	18	100	78
Nb	19	19	-	-	-	-	-	-	-	-	-	-
Th	5 7	4 3	3	3	5	4	4	5	1	2	3	7
Pb	18	22	14	16	19	17	17	26	13	11	8	20
Ga	26	20	-	-	-	-	-	-	-	-	-	-
Zn	48	47	43	52	69	57	59	33	16	25	75	80
Cu	-	-	-	-	-	-	-	-	-	-	-	-
Ni	5	8	-	-	-	-	-	-	-	-	-	-
V	3	22	-	-	-	-	-	-	-	-	-	-
Cr	40	34	-	-	-	-	-	-	-	-	-	-
Hf	-	-	-	-	-	-	-	-	-	-	-	-
Cs	-	-	-	-	-	-	-	-	-	-	-	-
Sc	-	-	-	-	-	-	-	-	-	-	-	-
Ta	-	-	-	-	-	-	-	-	-	-	-	-
Co	-	-	-	-	-	-	-	-	-	-	-	-
Li	69	77	248	246	252	228	217	95	64	60	271	135
Be	3 7	3 4	12.5	9	14	13	7 5	3	29 5	50	23	4 5
B	-	-	20	30	30	20	25	25	25	9	15	20
U	5 2	4 5	16	13 9	13 4	13 8	10	3 9	23	16 4	15 4	12 2
W	-	-	4	10	5	3	4	4	1	4	4	4
Sn	11	17	19	21	22	20	12	1	25	15	19	9
Mo	-	-	2	2	1	1	1	1	1	0 7	1	1
Rare-earths												
La	-	-	-	-	-	-	-	-	-	-	-	-
Ce	-	-	-	-	-	-	-	-	-	-	-	-
Pr	-	-	-	-	-	-	-	-	-	-	-	-
Nd	-	-	-	-	-	-	-	-	-	-	-	-
Sm	-	-	-	-	-	-	-	-	-		-	-
Eu	-	-	-	-	-	-	-	-	-	-	-	-
Gd	-	-	-	-	-	-	-	-	-	-	-	-
Tb	-	-	-	-	-	-	-	-	-	-	-	-
Dy	-	-	-	-	-	-	-	-	-	-	-	-
Ho	-	-	-	-	-	-	-	-	-	-	-	-
Er	-	-	-	-	-	-	-	-	-	-	-	-
Tm	-	-	-	-	-	-	-	-	-	-	-	-
Yb	-	-	-	-	-	-	-	-	-	-	-	-
Lu	-	-	-	-	-	-	-	-	-	-	-	-

Table E1.1 (Continued) Compilation of Meguma Zone granitoid lithogeochemistry

Sample	NSL012	NSL013	NSL014	NSL015	NSL018	NSL022	NSL024	NMK102	NMK114	NMK119	NMK121	NMK124
Batholith	-	-	-	-	-	-	-	SMB	SMB	SMB	SMB	SMB
Pluton	SLP	SLP	SLP	SLP	SLP	SLP	SLP	-	-	-	-	-
Lithology	Mzg	Mzg	Mzg	Mzg	Mzg	Mzg	Mzg	Mzg	Mzg	Mzg	Mzg	Grd
Source	16	16	16	16	16	16	16	2, 3	2, 3	2, 3	2, 3	2, 3
Major oxides												
SiO_2	72.21	72.68	71.82	73.00	73.41	73.19	74.38	73.70	74.50	74.30	73.50	68.80
TiO_2	0.23	0.21	0.24	0.17	0.10	0.02	0.03	0.26	0.12	0.22	0.18	0.68
Al_2O_3	15.34	15.27	15.83	15.11	14.95	14.81	14.60	13.42	13.40	13.08	13.87	14.52
Fe_2O_3	0.31	0.19	0.69	-	0.09	-	-	0.17	0.16	0.05	0.22	0.45
FeO	1.39	1.39	1.35	-	0.92	-	-	1.69	1.51	1.77	1.55	3.88
MnO	0.07	0.06	0.07	0.05	0.03	0.06	0.05	0.04	0.05	0.05	0.03	0.10
MgO	0.40	0.39	0.48	0.28	0.28	0.10	0.06	0.28	0.12	0.24	0.24	1.18
CaO	0.46	0.46	0.42	0.48	0.56	0.50	0.77	0.58	0.45	0.66	0.60	2.21
Na_2O	3.89	3.82	3.80	4.08	3.51	4.67	4.65	3.32	3.46	3.60	3.54	3.18
K_2O	3.98	4.03	4.33	3.81	5.23	3.61	3.15	4.91	4.59	4.34	4.72	3.46
P_2O_5	0.43	0.39	0.32	0.49	0.27	0.33	0.87	0.07	0.14	0.07	0.15	0.10
H_2O+	0.97	0.73	0.80	0.63	0.48	0.56	0.56	0.82	0.58	0.77	0.69	0.91
H_2O-	0.20	0.10	0.13	0.16	0.25	0.18	0.17	-	-	-	-	-
CO_2	0.08	0.13	0.01	0.07	0.11	0.19	0.10	-	-	-	-	-
Cl	-	-	-	-	-	-	-	-	-	-	-	-
F	0.06	0.06	0.07	0.07	0.03	0.04	0.08	0.13	0.28	0.10	0.18	0.05
LOI	1.31	1.02	1.01	0.93	0.87	0.97	0.91	0.95	0.86	0.87	0.87	0.96
TOTAL	99.96	99.87	100.27	99.60	100.20	98.78	100.04	99.35	99.33	99.22	99.42	99.42
Fe_2O_3T	1.85	1.73	2.19	1.35	1.11	0.58	0.64	2.05	1.84	2.01	1.94	4.76
FeOT	1.64	1.54	1.95	1.20	0.99	0.52	0.57	1.82	1.64	1.79	1.72	4.23
A/CNK	1.25	1.24	1.25	1.22	1.08	1.15	1.17	1.02	1.06	1.03	1.05	1.13
Trace els												
Ba	26	34	28	20	371	11	8	230	66	200	164	668
Rb	339	294	357	367	208	315	441	330	532	299	441	143
Sr	19	17	17	51	99	12	88	-	-	-	-	156
Y	-	-		-	-	-	-	-	-	-	-	-
Zr	61	62	94	45	57	19	15	91	51	76	64	210
Nb	-	-	-	-	-	-	-	-	-	-	-	-
Th	5	4	6	6	4	1	1	-	10.9	11	-	-
Pb	19	18	18	17	30	15	14	-	-	-	-	-
Ga	-	-	-	-	-	-	-	-	-	-	-	-
Zn	81	72	94	63	44	12	15	72	64	56	64	71
Cu	-	-	-	-	-	-	-	-	-	-	-	-
Ni	-	-	-	-	-	-	-	8	8	10	9	16
V	-	-	-	-	-	-	-	-	-	-	-	-
Cr	-	-	-	-	-	-	-	43	45	47	47	50
Hf	-	-	-	-	-	-	-	-	-	-	-	-
Cs	-	-	-	-	-	-	-	-	-	-	-	-
Sc	-	-	-	-	-	-	-	-	-	-	-	-
Ta	-	-	-	-	-	-	-	-	-	-	-	-
Co	-	-	-	-	-	-	-	-	-	-	-	-
Li	234	210	263	246	92	69	47	-	-	-	-	-
Be	5	4.5	4.5	7.5	5.5	5.5	12.5	-	-	-	-	-
B	25	40	20	65	15	20	20	-	-	-	-	-
U	17.6	10.9	20.1	15.5	4.6	9.9	15.5	-	-	-	-	-
W	4	5	5	5	4	2	1	-	-	-	-	-
Sn	14	11	15	20	2	30	27	19	30	15	20	7
Mo	1	1	1	1	2	2	2	-	-	-	-	-
Rare-earths												
La	-	-	-	-	-	-	-	-	-	-	-	-
Ce	-	-	-	-	-	-	-	-	-	-	-	-
Pr	-	-	-	-	-	-	-	-	-	-	-	-
Nd	-	-	-	-	-	-	-	-	-	-	-	-
Sm	-	-	-	-	-	-	-	-	-	-	-	-
Eu	-	-	-	-	-	-	-	-	-	-	-	-
Gd	-	-	-	-	-	-		-	-	-	-	-
Tb	-	-	-	-	-	-	-	-	-	-	-	-
Dy	-	-	-	-	-	-	-	-	-	-	-	-
Ho	-	-	-	-	-	-	-	-	-	-	-	-
Er	-	-	-	-	-	-	-	-	-	-	-	-
Tm	-	-	-	-	-	-	-	-	-	-	-	-
Yb	-	-	-	-	-	-	-	-	-	-	-	-
Lu	-	-	-	-	-	-	-	-	-	-	-	-

Table E1 1 (Continued) Compilation of Meguma Zone granitoid lithogeochemistry

Sample	NMK127	NFE1	NFE11	NFE2	NMK102	NMK114	NMK119	NMK121	NMK124	NMK127	NMK137	NMK161
Batholith	SMB	SMB	SMB	SMB	SMB	SMB	SMB	SMB	SMB	SMB	SMB	SMB
Pluton	-	-	-	-	-	-	-	-	-	-	-	-
Lithology	Grd	Mzg	Mzg	Mzg	Mzg	Mzg	Mzg	Mzg	Grd	Grd	Grd	Mzg
Source	2, 3	11	11	11	2, 3	2, 3	2, 3	2, 3	2, 3	2, 3	2, 3	2, 3
Major oxides												
SiO_2	72 20	75 83	-	74 70	73 70	74 50	74 30	73 50	68 80	72 20	68 20	72 40
TiO_2	0 42	0 06	-	0 12	0 26	0 12	0 22	0 18	0 58	0 42	0 68	0 29
Al_2O_3	14 26	13 82	-	14 02	13 42	13 40	13 08	13 87	14 52	14 26	14 52	14 10
Fe_2O_3	0 26	0 13	-	0 29	0 17	0 16	0 05	0 22	0 45	0 26	0 45	0 18
FeO	2.52	0 79	-	1 42	1 69	1 51	1 77	1 55	3 88	2 52	3 88	1 87
MnO	0 09	0 02	-	0 05	0 04	0 05	0 05	0 03	0 10	0 09	0 10	0 05
MgO	0 75	0 09	-	0 25	0 28	0 12	0 24	0 24	1 18	0 75	1 18	0 50
CaO	1 44	0 59	-	0 57	0 58	0 45	0 68	0 60	2.21	1 44	2 21	0 71
Na_2O	3 31	3 68	-	3 31	3 32	3 46	3 60	3 54	3 18	3 31	3 18	3 23
K_2O	4 04	4 30	-	4 27	4 91	4 59	4 34	4 72	3 46	4 04	3 46	4 83
P_2O_5	0 16	0 36	-	0 26	0 07	0 14	0 07	0 15	0 10	0 16	0 10	0 10
H_2O+	0 88	0 84	-	1 23	0 82	0 58	0 77	0 69	0 91	0 88	0 94	0 74
H_2O-	-	-	-	-	-	-	-	-	-	-	-	-
CO_2	-	-	-	-	-	-	-	-	-	-	-	-
Cl	-	-	-	-	-	-	-	-	-	-	-	-
F	0 06	-	-	-	0 13	0 28	0 10	0 18	0 05	0 06	0 07	0 16
LOI	0 94	0 84	-	1 23	0 95	0 86	0 87	0 87	0 96	0 94	1 01	0 90
TOTAL	100 33	100 49	-	100 44	99 35	99 33	99 22	99 42	99 42	100 33	98 87	99 12
Fe_2O_3T	3 06	1 01	-	1 87	2 05	1 84	2 01	1 94	4 76	3 06	4 76	2 26
FeOT	2.72	0 90	-	1 66	1 82	1 64	1 79	1 72	4 23	2 72	4 23	2 01
A/CNK	1 10	1 09	-	1 16	1 02	1 06	1 03	1 05	1 13	1 10	1 13	1 08
Trace els												
Ba	429	31	67	118	230	66	200	164	668	429	738	341
Rb	174	616	359	357	330	532	299	441	143	174	132	324
Sr	112	14	2	25	-	-	-	-	166	112	174	2
Y	-	-	-	-	-	-	-	-	-	-	-	-
Zr	168	37	56	87	91	51	76	64	210	168	260	118
Nb	-	19	11	10	-	-	-	-		-	-	-
Th	8 33	-	-	-	-	10 9	11	-	-	8 33	-	19 6
Pb	-	-	-	-	-	-	-	-	-	-	-	-
Ga	~	-	-	-	-	-	-	-	-	-	-	-
Zn	60	-	-	-	72	64	56	64	71	60	68	62
Cu		-	-	-	-		-	-	-	-	-	-
Ni	12	-	-	-	8	8	10	9	16	12	20	11
V	-	-	-	-	-	-	-	-	-	-	-	-
Cr	42	-	-	-	43	45	47	47	50	42	59	40
Hf	-	-	-	-	-	-	-	-	-	-	-	-
Cs	-	-	-	-	-	-	-	-	-	-	-	-
Sc	-	-	-	-	-	-	-	-	-	-	-	-
Ta	-	-	-	-	-	-	-	-	-	-	-	-
Co	-	-	-	-	-	-	-	-	-	-	-	-
Li	-	-	-	-	-	-	-	-	-	-	-	-
Be	-	-	-	-	-	-	-	-	-	-	-	-
B	-	-	-	-	-	-	-	-	-	-	-	-
U	-	-	-	-	-	-	-	-	-	-	-	-
W	-	-	-	-	-	-	-	-	-	-	-	-
Sn	18	-	-	-	19	30	15	20	7	18	8	15
Mo	-	-	-	-	-	-	-	-	-	-	-	-
Rare-earths												
La	-	8	6	10	-	-	-	-	-	-	-	-
Ce	-	17	17	27	-	-	-	-	-	-	-	-
Pr	-	-	-	-	-	-	-	-	-	-	-	-
Nd	-	-	-	-	-	-	-	-	-	-	-	-
Sm	-	-	-	-	-	-	-	-	-	-	-	-
Eu	-	-	-	-	-	-	-	-	-	-	-	-
Gd	-	-	-	-	-	-	-	-	-	-	-	-
Tb	-	-	-	-	-	-	-	-	-	-	-	-
Dy	-	-	-	-	-	-	-	-	-	-	-	-
Ho	-	-	-	-	-	-	-	-	-	-	-	-
Er	-	-	-	-	-	-	-	-	-	-	-	-
Tm	-	-	-	-	-	-	-	-	-	-	-	-
Yb	-	-	-	-	-	-	-	-	-	-	-	-
Lu	-	-	-	-	-	-	-	-	-	-	-	-

Table E1 1 (Continued) Compilation of Meguma Zone granitoid lithogeochemistry

Sample	NMK166	NMK172	NMK176	NMK189	NMK192	NMK39	NMK50	NMK53	NMK54E	NMK60	NMK72	NMK82
Batholith	SMB	SMB	SMB	SMB	SMB	SMB	SMB	SMB	SMB	SMB	SMB	SMB
Pluton	-	-	-	-	-	-	-	-	-	-	-	-
Lithology	Mzg	Grd	Mzg	Mzg	Grd	Grd	Mzg	Grd	Grd	Grd	Grd	Mzg
Source	2, 3	2, 3	2, 3	2, 3	2, 3	2, 3	2, 3	2, 3	2, 3	2, 3	2, 3	2, 3
Major oxides												
SiO_2	74 30	70 90	72 00	75 20	69 60	70 30	73 20	67 40	66 80	70 40	68 60	71 10
TiO_2	0 14	0 44	0 32	0 17	0 61	0 61	0 29	0 72	0 81	0 54	0 61	0 42
Al_2O_3	13 58	14 08	13 86	13 7*	14 14	13 63	13 93	14 65	14 41	14 42	14 66	14 50
Fe_2O_3	0 12	0 29	0 08	0 08	0 43	0 50	0 20	0 33	0 87	0 47	0 23	0 29
FeO	1 22	2.48	2.16	1 40	3 78	3 47	1 80	4 20	4 71	2 62	3 78	2 13
MnO	0 06	0 10	0 06	0 04	0 10	0 09	0 04	0 10	0 13	0 09	0 10	0 06
MgO	0 18	1 03	0 54	0 27	0 99	0 89	0 49	1 24	1 41	0 74	0 98	0 63
CaO	0 52	1 84	0 78	0 51	1 82	1 72	0 80	2.28	2 28	1 72	1 93	1 10
Na_2O	3 29	3 08	3 36	3 32	3 13	3 14	3 24	3 29	3 32	3 47	3 34	3 30
K_2O	4 90	3 73	4 43	4 76	4 08	3 85	5 12	3 90	3 57	4 16	4 10	4 90
P_2O_5	0 06	0 02	0 31	0 16	0 14	0 05	0 04	0 14	0 10	0 12	0 08	0 08
H_2O+	0 65	0 93	1 05	0 67	0 76	1 08	0 96	0 84	0 98	0 56	0 89	0 66
H_2O-	-	-	-	-	-	-	-	-	-	-	-	-
CO_2	-	-	-	-	-	-	-	-	-	-	-	-
Cl	-	-	-	-	-	-	-	-	-	-	-	-
F	0 06	0 05	0 08	0 09	0 06	0 06	0 06	0 06	0 08	0 07	0 07	0 08
LOI	0 71	0 98	1 13	0 76	0 82	1 14	1 02	0 90	1 06	0 63	0 96	0 74
TOTAL	99 05	98 90	98 99	100 35	95 99	95 73	100 13	95 50	99 31	99 29	99 30	99 19
Fe_2O_3T	1 47	3 04	2 48	1 63	0 63	0 35	2 20	0 99	6 10	3 38	4 43	2 65
FeOT	1 31	2.70	2 20	1 45	0 56	0 31	1 96	0 88	5 42	3 00	3 94	2 36
A/CNK	1 04	1 11	1 09	1 07	1 07	1 07	1 02	1 06	1 08	1 05	1 07	1 05
Trace els												
Ba	124	618	312	193	616	619	418	856	760	632	732	491
Rb	295	136	264	362	144	156	272	130	123	162	148	221
Sr	-	154	22	-	111	118	47	176	144	114	146	40
Y	-	-	-	-	-	-		-	-	-	-	-
Zr	40	120	125	44	198	196	118	253	267	175	204	125
Nb	-	-	-	-	-	-	-	-	-	-	-	-
Th	-	9 85	-	-	11 3	-	15 1	-	-	-	12	-
Pb	-	-	-	-	-	-	-	-	-	-	-	-
Ga	-	-	-	-	-	-	-	-	-	-	-	-
Zn	38	53	60	52	68	72	62	74	82	-	-	-
Cu	-	-	-	-	-	-	-	-	-	-	-	-
Ni	8	14	12	8	16	16	12	18	22	12	16	14
V	-	-	-	-	-	-	-	-	-	-	-	-
Cr	35	52	41	28	56	54	42	56	58	42	52	44
Hf	-	-	-	-	-	-	-	-	-	-	-	-
Cs	-	-	-	-	-	-	-	-	-	-	-	-
Sc	-	-	-	-	-	-	-	-	-	-	-	-
Ta	-	-	-	-	-	-	-	-	-	-	-	-
Co	-	-	-	-	-	-	-	-	-	-	-	-
Li	-	-	-	-	-	-	-	-	-	-	-	-
Be	-	-	-	-	-	-	-	-	-	-	-	-
B	-	-	-	-	-	-	-	-	-	-	-	-
U	-	-	-	-	-	-	-	-	-	-	-	-
W	-	-	-	-	-	-	-	-	-	-	-	-
Sn	10	15	18	20	16	10	10	8	15	10	10	7
Mo	-	-	-	-	-	-	-	-	-	-	-	-
Rare-earths												
La	-	-	-	-	-	-	-	-	-	-	-	-
Ce	-	-	-	-	-	-	-	-	-	-	-	-
Pr	-	-	-	-	-	-	-	-	-	-	-	-
Nd	-	-	-	-	-	-	-	-	-	-	-	-
Sm	-	-	-	-	-	-	-	-	-	-	-	-
Eu	-	-	-	-	-	-	-	-	-	-	-	-
Gd	-	-	-	-	-	-	-	-	-	-	-	-
Tb	-	-	-	-	-	-	-	-	-	-	-	-
Dy	-	-	-	-	-	-	-	-	-	-	-	-
Ho	-	-	-	-	-	-	-	-	-			-
Er	-	-	-	-	-	-	-	-	-	-	-	-
Tm	-	-	-	-	-	-	-	-	-	-	-	-
Yb	-	-	-	-	-	-	-	-	-	-	-	-
Lu	-	-	-	-	-	-	-	-	-	-	-	-

Table E1 1 (Continued) Compilation of Meguma Zone granitoid lithogeochemistry

Sample	NMK86	NAL10	NSH205	NSH213	NSH230	NSH252	NSH255	NSH263	NSH269	NSH270	NSH331	NSH422
Batholith	SMB	-	-	-	-	-	-	-	-	-	-	-
Pluton	-	SP	SP	SP	SP	SP	SP	SP	SP	SP	SP	SP
Lithology	Grd	Mzg	Grd	Grd	Grd	Grd	Ton	Grd	Grd	Grd	Grd	Grd
Source	2, 3	1	5	5	5	5	5	5	5	5	5	5
Major oxides												
SiO_2	70 00	72 74	70 65	74 78	74 45	73 82	67 74	73 61	74 43	73 10	74 26	73 61
TiO_2	0 55	0 19	0 54	0 11	0 10	0 24	0 55	0 25	0 14	0 17	0 25	0 30
Al_2O_3	14 71	15 35	14 81	14 44	14 35	14 27	16 51	14 40	14 47	14 35	13 83	14 47
Fe_2O_3	0 59	0 23	-	-	-	-	-	-	-	-	-	-
FeO	3 45	0 97	-	-	-	-	-	-	-	-	-	-
MnO	0 10	0 04	0 05	0 04	0 04	0 03	0 05	0 06	0 04	0 03	0 03	0 06
MgO	0 85	0 28	0 86	0 20	0 17	0 28	1 41	0 43	0 18	0 24	0 24	0 47
CaO	1 78	0 82	0 94	0 63	0 59	0 44	3 32	1 25	0 36	1 98	0 48	1 71
Na_2O	3 72	3 65	3 23	3 36	3 35	3 22	4 47	3 87	3 81	3 44	3 21	4 22
K_2O	4 13	3 97	4 28	4 39	4 47	5 07	1 81	3 47	4 39	4 17	4 83	2 47
P_2O_5	0 08	0 07	0 22	0 19	0 33	0 27	0 10	0 25	0 36	0 14	0 20	0 10
H_2O+	0 94	0 77	-	-	-	-	-	-	-	-	-	-
H_2O-	-	0 04	-	-	-	-	-	-	-	-	-	-
CO_2	-	-	-	-	-	-	-	-	-	-	-	-
Cl	-	-	-	-	-	-	-	-	-	-	-	-
F	0 08	-	0 05	0 02	0 02	0 04	0 04	0 03	0 02	0 02	0 03	0 03
LOI	1 02	0 81	0 92	0 76	0 93	0 92	0 70	0 69	0 73	0 67	0 79	0 73
TOTAL	100 87	99 08	98 75	99 93	99 81	99 57	99 41	99 71	99 65	99 59	99 05	99 51
Fe_2O_3T	4 42	1 31	2 52	1 16	1 16	1 14	3 09	1 61	0 83	1 46	1 05	1 54
FeOT	3 93	1 16	2 24	1 03	1 03	1 01	2.75	1 43	0 74	1 30	0 93	1 37
A/CNK	1 04	1 23	1 18	1 16	1 15	1 09	1 22	1 15	1 14	1 02	1 09	1 20
Trace els												
Ba	672	-	782	592	475	640	457	351	427	562	728	437
Rb	172	-	116	82	127	195	53	147	160	85	161	89
Sr	117	-	356	308	63	125	484	85	48	106	81	167
Y	-	-	10	20	14	13	10	16	12	1	19	14
Zr	218	-	239	183	50	190	120	111	34	70	96	111
Nb	-	-	-	-	9	6	5	9	10	8	8	7
Th	13 2	-	2.6	5 1	5 4	5	1 5	6 3	6 5	3 7	4 6	3 8
Pb	-	-	15	17	27	20	13	22	23	28	29	22
Ga	-	-	19	21	17	21	19	17	16	16	16	18
Zn	-	-	66	74	42	91	55	56	38	33	42	41
Cu	-	-	-	-	-	-	-	-	-	-	-	-
Ni	15	-	16	20	2	9	3	4	4	1	2	2
V	-	-	121	93	1	38	65	10	2	3	5	17
Cr	51	-	102	111	36	63	44	43	50	31	22	32
Hf	-	-	-	-	-	-	-	-	-	-	-	-
Cs	-	-	-	-	-	-	-	-	-	-	-	-
Sc	-	-	-	-	-	-		-	-	-	-	-
Ta	-	-	-	-	-	-	-	-	-	-	-	-
Co	-	-	-	-	-	-	-	-	-	-	-	
Li	-	-	85	72	60	62	42	262	105	53	57	67
Be	-	-	4 9	3 2	4 9	3 2	2 8	2 8	5 1	2	1 5	3 7
B	-	-	-		-	-	-	-	-	-	-	-
U	-	-	6 3	3 1	4 1	5 8	1 8	9 9	4 7	3 5	5 9	3 9
W	-	-	-	-	-	-	-	-	-	-	-	-
Sn	12	-	10	6	3	31	3	9	2	8	16	9
Mo	-	-	-	-	-	-	-	-	-	-	-	-
Rare-earths												
La	-	-	-	-	-	-	-	-	-	-	-	-
Ce	-	-	-	-	-	-	-	-	-	-	-	-
Pr	-	-	-	-	-	-	-	-	-	-	-	-
Nd	-	-	-	-	-	-	-	-	-	-	-	-
Sm	-	-	-	-	-	-	-	-	-	-	-	-
Eu	-	-	-	-	-	-	-	-	-	-	-	-
Gd	-	-	-	-	-	-	-	-	-	-	-	-
Tb	-	-	-	-	-	-	-	-	-	-	-	-
Dy	-	-	-	-	-	-	-	-	-	-	-	-
Ho	-	-	-	-	-	-	-	-	-	-	-	-
Er	-	-	-	-	-	-	-	-	-	-	-	-
Tm	-	-	-	-	-	-	-	-	-	-	-	-
Yb	-	-	-	-	-	-	-	-	-	-	-	-
Lu	-	-	-	-	-	-	-	-	-	-	-	-

Table E1 1 (Continued) Compilat Table E1 1 (Continued) Compilation of Meguma Zone granitoid lithogeochemistry

Sample	NSH423	NSH427	NSH428	NSH430	NSH501	NSH508	NSH519	NSHS21	NSH522	NSH583	NSH729	NSH794
Batholith	-	-	-	-	-	-	-	-	-	-	-	-
Pluton	SP	SP	SP	SP	SP	SP	SP	SP	SP	SP	SP	SP
Lithology	Grd	Grd	Grd	Ton	Grd	Grd	Ton	Grd	Ton	Grd	Grd	Grd
Source	5	5	5	5	5	5	5	5	5	5	5	5
Major oxides												
SiO_2	72 03	73 09	72 54	67 17	73 52	73 35	67 41	74 31	65 99	74 30	72 90	73 64
TiO_2	0 27	0 32	0 21	0 35	0 17	0 06	0 55	0 24	0 60	0 17	0 26	0 11
Al_2O_3	15 37	14 08	13 71	20 18	14 36	15 11	16 41	13 81	17 09	13 94	14 88	15 32
Fe_2O_3	-	-	-	-	-	-	-	-	-	-	-	-
FeO	-	-	-	-	-	-	-	-	-	-	-	-
MnO	0 06	0 05	0 06	0 07	0 05	0 06	0 06	0 04	0 05	0 04	0 05	0 05
MgO	0 56	0 45	0 66	1 02	0 17	0 24	1 19	0 28	1 46	0 17	0 54	0 53
CaO	1 95	1 24	0 74	5 19	0 65	0 66	3 25	0 64	3 56	0 61	0 85	1 50
Na_2O	4 19	3 42	3 20	4 69	3 38	3 94	4 62	2.65	4 47	3 17	3 59	4 43
K_2O	2 21	4 30	5 11	1 19	4 83	3 92	1 55	5 29	1 69	4 68	4 24	2 52
P_2O_5	0 16	0 18	0 23	0 18	0 33	0 15	0 15	0 12	0 14	0 17	0 22	0 22
H_2O+	-	-	-	-	-	-	-	-	-	-	-	-
H_2O-	-	-	-	-	-	-	-	-	-	-	-	-
CO_2	-	-	-	-	-	-	-	-	-	-	-	-
Cl	-	-	-	-	-	-	-	-	-	-	-	-
F	0 02	0 04	0 03	0 03	0 03	0 02	0 04	0 03	0 04	0 02	0 01	0 02
LOI	0 75	0 58	0 88	0 53	0 68	0 81	0 69	0 82	0 67	0 79	0 91	0 47
TOTAL	99 55	99 31	98 89	102 64	99 39	99 10	99 32	99 89	99 20	99 36	100 09	100 22
Fe_2O_3T	2 25	1 80	1 74	2 33	1 41	0 90	3 87	1 90	3 91	1 49	1 86	1 61
FeOT	2 00	1 60	1 55	2 07	1 25	0 80	3 44	1 69	3 48	1 32	1 65	1 43
A/CNK	1 28	1 07	1 02	1 31	1 09	1 20	1 23	1 07	1 25	1 11	1 16	1 26
Trace els												
Ba	467	783	776	245	500	287	399	767	456	589	388	659
Rb	88	176	204	49	210	138	61	161	56	181	277	78
Sr	158	116	74	274	55	58	556	126	565	74	82	249
Y	16	18	22	13	22	12	8	25	11	15	11	21
Zr	127	176	105	159	72	38	124	80	142	76	132	127
Nb	8	9	9	7	9	8	6	8	6	10	7	7
Th	3 8	4 7	6	1 8	6	5 3	3 1	4	2 1	4 8	4 4	0 7
Pb	17	23	34	11	25	25	9	31	14	29	18	26
Ga	18	16	17	23	15	16	21	15	20	18	23	12
Zn	54	57	75	52	50	28	57	45	51	46	74	29
Cu	-	-	-	-	-	-	-	-	-	-	-	-
Ni	-	5	11	2	6	3	9	5	9	3	7	8
V	16	19	11	37	-	84	54	8	75	5	15	14
Cr	19	40	40	37	29	74	57	50	77	40	26	26
Hf	-	-	-	-	-	-	-	-	-	-	-	-
Cs	-	-	-	-	-	-	-	-	-	-	-	-
Sc	-	-	-	-	-	-	-	-	-	-	-	-
Ta	-	-	-	-	-	-	-	-	-	-	-	-
Co	-	-	-	-	-	-	-	-	-	-	-	-
Li	91	96	38	93	155	68	81	30	68	73	118	43
Be	5 5	3 9	2 8	-	4 1	-	0 9	3 5	2 3	3 4	-	-
B	-	-	-	-	-	-	-	-	-	-	-	-
U	3 9	6 2	5 7	3 1	8 5	2.9	1 5	7 7	1 1	2 8	5 6	3 9
W	-	-	-	-	-	-	-	-	-	-	-	-
Sn	8	23	12	1	11	4	1	13	2	14	24	9
Mo	-	-	-	-	-	-	-	-	-	-	-	-
Rare-earths												
La	-	-	-	-	-	-	-	-	-	-	-	-
Ce	-	-	-	-	-	-	-	-	-	-	-	-
Pr	-	-	-	-	-	-	-	-	-	-	-	-
Nd	-	-	-	-	-	-	-	-	-	-	-	-
Sm	-	-	-	-	-	-	-	-	-	-	-	-
Eu	-	-	-	-	-	-	-	-	-	-	-	-
Gd	-	-	-	-	-	-	-	-	-	-	-	-
Tb	-	-	-	-	-	-	-	-	-	-	-	-
Dy	-	-	-	-	-	-	-	-	-	-	-	-
Ho	-	-	-	-	-	-	-	-	-	-	-	-
Er	-	-	-	-	-	-	-	-	-	-	-	-
Tm	-	-	-	-	-	-	-	-	-	-	-	-
Yb	-	-	-	-	-	-	-	-	-	-	-	-
Lu	-	-	-	-	-	-	-	-	-	-	-	-

Table E1 1 (Continued) Compilation of Meguma Zone granitoid lithogeochemistry

Sample	NSH796	NSHA26	NSHA27	NSHA34	NSHA35	NSHA84	NIW002	NIW003	NIW004	NIW005	NIW006	NIW008
Batholith	-	-	-	-	-	-	-	-	-	-	-	-
Pluton	SP	SP	SP	SP	SP	SP	WP	WP	WP	WP	WP	WP
Lithology	Grd	Grd	Grd	Grd	Grd	Grd	Mzg	Mzg	Mzg	Mzg	Mzg	Mzg
Source	5	5	5	5	5	5	12	12	12	12	12	12
Major oxides												
SiO_2	74 50	72 30	72 74	73 10	72 70	74 50	76 70	75 40	76 70	75 00	74 60	74 60
TiO_2	0 09	0 16	0 37	0 21	0 17	0 05	0 12	0 20	0 09	0 20	0 22	0 23
Al_2O_3	14 90	15 10	14 64	14 40	15 10	14 30	12.30	12 40	12 80	13 40	13 20	12 90
Fe_2O_3	-	-	-	-	-	-	0 54	0 95	0 38	0 75	0 76	0 84
FeO	-	-	-	-	-	-	0 80	1 00	0 80	0 90	1 30	1 30
MnO	0 04	0 04	0 04	0 05	0 03	-	0 02	0 04	0 03	0 03	0 03	0 03
MgO	0 31	0 56	0 54	0 54	0 39	0 23	0 09	0 36	0 14	0 29	0 23	0 27
CaO	0 57	1 59	0 70	1 64	1 80	0 40	0 67	0 93	0 52	1 21	0 93	0 90
Na_2O	3 48	5 11	3 27	4 30	4 80	4 43	3 49	3 73	4 16	4 28	3 60	3 59
K_2O	4 75	2 05	4 53	3 05	2 69	4 05	4 98	5 07	4 51	4 51	4 99	4 69
P_2O_5	0 27	0 21	0 26	0 16	0 13	0 17	0 03	0 06	0 03	0 07	0 09	0 07
H_2O+	-	-	-	-	-	-	-	-	-	-	-	-
H_2O-	-	-	-	-	-	-	-	-	-	-	-	-
CO_2	-	-	-	-	-	-	-	-	-	-	-	-
Cl	-	-	-	-	-	-	-	-	-	-	-	-
F	0 02	0 03	-	0 04	0 03	0 03	0 13	0 10	0 03	0 05	0 12	0 09
LOI	0 57	0 54	0 98	1 16	0 77	1 16	0 93	0 70	0 62	0 23	0 77	1 23
TOTAL	100 70	98 98	99 54	100 01	99 80	#VALUE!	100 60	100 72	100 73	100 78	100 62	100 74
Fe_2O_3T	1 37	1 48	1 65	1 58	1 37	0 74	1 43	2 06	1 27	1 75	2 20	2 28
FeOT	1 22	1 32	1 47	1 40	1 22	0 66	1 27	1 83	1 13	1 56	1 96	2 03
A/CNK	1 14	1 21	1 16	1 11	1 13	1 09	0 90	0 86	0 94	0 91	0 93	0 95
Trace els												
Ba	405	250	-	360	560	190	-	-	-	-	-	-
Rb	159	80	-	130	90	200	300	330	320	220	360	300
Sr	58	120	-	190	260	40	20	110	-	60	70	80
Y	15	-	-	-	-	-	-	-	-	-	-	-
Zr	82	-	-	100	80	-	150	160	90	130	160	160
Nb	9	-	-	-	-	-	-	-	-	-	-	-
Th	4 1	-	-	-	-	2	-	-	-	-	-	-
Pb	29	-	-	-	6	6	16	6	-	-	-	-
Ga	16	-	-	-	-	-	-	-	10	10	16	4
Zn	38	-	-	36	36	5	30	39	-	-	-	-
Cu	-	-	-	-	-	-	10	12	21	25	38	21
Ni	-	-	-	-	0 5	3	-	-	-	-	4	4
V	3	-	-	-	-	-	-	-	-	-	-	-
Cr	27	-	-	-	-	110	40	30	40	50	30	40
Hf	-	-	-	-	-	-	-	-	-	-	-	-
Cs	-	-	-	-	-	-	-	-	-	-	-	-
Sc	-	-	-	-	-	-	-	-	-	-	-	-
Ta	-	-	-	-	-	-	-	-	-	-	-	-
Co	-	-	-	-	-	-	-	-	-	-	-	-
Li	54	110	-	72 0	89	99	37	53	49	92	76	57
Be	-	-	-	-	-	-	-	-	-	-	-	-
B	-	-	-	-	-	-	25	25	-	25	50	25
U	5 1	-	-	-	3 8	3 6	-	-	-	-	-	-
W	-	-	-	-	-	-	24	20	4	4	34	18
Sn	12	-	-	-	5	7	10	30	3	7	10	25
Mo	-	-	-	-	-	-	5 5	3	-	-	10	6 5
Rare-earths												
La	-	-	-	-	-	-	-	-	-	-	-	-
Ce	-	-	-	-	-	-	-	-	-	-	-	-
Pr	-	-	-	-	-	-	-	-	-	-	-	-
Nd	-	-	-	-	-	-	-	-	-	-	-	-
Sm	-	-	-	-	-	-	-	-	-	-	-	-
Eu	-	-	-	-	-	-	-	-	-	-	-	-
Gd	-	-	-	-	-	-	-	-	-	-	-	-
Tb	-	-	-	-	-	-	-	-	-	-	-	-
Dy	-	-	-	-	-	-	-	-	-	-	-	-
Ho	-	-	-	-	-	-	-	-	-	-	-	-
Er	-	-	-	-	-	-	-	-	-	-	-	-
Tm	-	-	-	-	-	-	-	-	-	-	-	-
Yb	-	-	-	-	-	-	-	-	-	-	-	-
Lu	-	-	-	-	-	-	-	-	-	-	-	-

Table E1 1 (Continued) Compilation of Meguma Zone granitoid lithogeochemistry

Sample	L9	L10	L11	L12	AI410	AI411A	AI449	AI467A	AI582	BB654	BB830	BB831
Batholith	-	-	-	-	-	-	-	-	-	-	-	-
Pluton	LC	LC	LC	LC	CP	CP	CP	CP	CP	CP	CP	CP
Lithology	Grd	Mzg	Lmzg	Lmzg	Mzg	Mzg	Mzg	Mzg	Mzg	Mzg	Mzg	Mzg
Source	26	26	26	26	25	25	25	25	25	25	25	25
Major oxides												
SiO_2	68 76	72 34	72 61	72 21	70 90	71 50	70 00	71 10	72 20	72 30	72 10	69 20
TiO_2	0 51	0 30	0 19	0 25	0 26	0 28	0 32	0 26	0 28	0 19	0 16	0 16
Al_2O_3	15 77	14 81	15 15	14 96	14 90	15 20	15 30	15 20	14 20	15 10	15 70	17 20
Fe_2O_3	-	-	-	-	0 09	0 16	0 17	0 23	0 03	0 10	0 56	-
FeO	-	-	-	-	1 74	1 86	1 99	1 58	2 00	0 97	0 40	-
MnO	0 09	0 04	0 03	0 03	0 07	0 08	0 07	0 08	0 07	0 04	0 02	0 04
MgO	1 09	0 57	0 34	0 47	0 65	0 75	0 75	0 66	0 62	0 34	0 35	0 28
CaO	1 71	0 96	0 65	0 68	1 62	1 91	1 69	1 63	1 60	0 70	0 54	0 72
Na_2O	3 42	3 46	3 74	3 51	3 94	4 03	4 03	4 04	3 72	3 81	4 12	4 50
K_2O	4 17	4 31	4 70	4 68	3 97	3 37	3 90	4 29	3 83	5 01	5 19	5 78
P_2O_5	0 17	0 23	0 25	0 27	0 11	0 12	0 12	0 11	0 09	0 28	0 18	0 38
H_2O+	-	0 86	-	-	-	-	-	-	-	-	-	-
H_2O-	-	0 13	-	-	-	-	-	-	-	-	-	
CO_2	-	0 09	-	-	-	-	-	-	-	-	-	
Cl	-	-	-	-	-	-	-	-	-	-	-	-
F	0 05	0 04	0 05	0 05	0 04	0 04	0 05	0 06	0 07	0 06	0 04	-
LOI	0 82	0 83	0 83	0 90	0 93	0 70	0 70	0 54	0 62	0 93	1 08	0 93
TOTAL	99 97	99 94	99 80	99 63	99 10	99 87	98 94	99 64	99 17	99 72	100 35	100 23
Fe_2O_3T	3 85	2 32	1 46	1 86	1 95	2 15	2.29	1 92	2 16	1 14	1 01	1 16
FeOT	3 46	2.09	1 31	1 67	1 75	1 93	2 06	1 73	1 94	1 02	0 91	1 04
A/CNK	1 16	1 15	1 12	1 14	1 07	1 12	1 09	1 04	1 06	1 07	1 07	1 05
Trace els												
Ba	762	414	434	354	610	570	620	550	560	380	430	440
Rb	164	187	213	232	220	230	240	230	220	320	340	450
Sr	169	106	72	66	200	200	210	190	190	90	70	90
Y	24	17	12	14	20	30	30	20	40	10	10	10
Zr	169	97	88	98	100	110	100	80	100	60	30	40
Nb	10 8	9	8	9 2	10	10	20	10	20	10	20	10
Th	13 8	7 8	7 4	9 2	-	-	-	8	-	-	4	-
Pb	39	26	30	24	37	33	32	35	28	27	34	-
Ga	20 2	22	20 4	21 3	-	-	-	-	-	-	-	-
Zn	84	62	52	65	47	47	-	-	-	-	-	-
Cu	6 9	5 8	6	5 5	-	-	-	-	-	-	-	-
Ni	20	16	14	20	-	-	-	-	-	-	-	-
V	34	18	6	12	-	-	-	-	-	-	-	-
Cr	46	30	30	32	-	-	-	-	-	-	-	-
Hf	-	-	-	-	-	-	-	-	-	-	-	-
Cs	7 6	16 2	12 5	10 4	-	-	-	-	-	-	-	-
Sc	8 7	3 7	2 3	3 1	-	-	-	-	-	-	-	-
Ta	-	-	-	-	-	-	-	-	-	-	-	-
Co	6 8	4 2	5	5	-	-	-	-	-	-	-	-
Li	56 5	82 7	79 5	75 9	95	123	109	124	113	190	-	-
Be	-	-	-	-	5	4	5	5	3	7	-	-
B	-	-	-	-	-	-	-	-	-	-	-	-
U	3 42	4	5 31	4 87	3	1	2	2	2	4	2	-
W	-	-	-	-	-	-	-	-	-	-	-	-
Sn	3 3	5 2	9 2	8 3	4	7	7	3	3	10	10	11
Mo	-	-	-	-	-	-	-	-	-	-	-	-
Rare-earths												
La	34 96	21 38	15 05	16 65	-	-	-	24	-	-	-	-
Ce	55 23	40 15	27 96	43 19	-	-	-	41	-	-	-	-
Pr	6 79	5 13	3 72	5 71	-	-	-	-	-	-	-	-
Nd	28 41	19 15	19 39	21 89	-	-	-	15	-	-	-	-
Sm	6 21	4 43	4 7	5 28	-	-	-	4 12	-	-	-	-
Eu	0 89	0 58	0 41	0 37	-	-	-	0 49	-	-	-	-
Gd	4 23	2.93	2 67	3 35	-	-	-	-	-	-	-	-
Tb	0 72	0 42	0 38	0 47	-	-	-	0 7	-	-	-	-
Dy	4 05	1 98	1 6	2.01	-	-	-	-	-	-	-	-
Ho	0 8	0 34	0 25	0 3	-	-	-	-	-	-	-	-
Er	2 27	0 97	0 66	0 81	-	-	-	-	-	-	-	-
Tm	0 33	0 14	0 09	0 11	-	-	-	-	-	-	-	-
Yb	2 05	0 89	0 53	0 64	-	-	-	1 67	-	-	-	-
Lu	0 32	0 13	0 07	0 09	-	-	-	0 31	-	-	-	-

Table E1.1 (Continued) Compilation of Meguma Zone granitoid lithogeochemistry

Sample	CH480	CL147	CL149	CL152A	CL580	CL603	CL616B	CL676	CL814	DH167B	DH525A	DH556A
Batholith	-	-	-	-	-	-	-	-	-	-	-	-
Pluton	CP	CP	CP	CP	CP	CP	CP	CP	ˉP	CP	CP	CP
Lithology	Lmzg	Mzg	Lmzg	Lmzg	Mzg	Lmzg	Lmzg	Lmzg	Mzg	Mzg	Mzg	Grd
Source	25	25	25	25	25	25	25	25	25	25	25	25
Major oxides												
SiO_2	74.80	72.00	75.70	74.10	72.90	74.60	75.40	74.00	73.90	71.70	71.60	68.70
TiO_2	0.17	0.21	0.26	0.19	0.35	0.18	0.25	0.25	0.31	0.34	0.26	0.25
Al_2O_3	14.00	15.00	12.50	13.70	14.00	13.90	12.80	13.50	13.00	14.70	14.50	16.40
Fe_2O_3	0.10	0.17	0.31	0.11	0.02	0.01	0.06	0.26	-	0.50	0.42	0.22
FeO	0.97	1.17	1.23	0.96	1.45	1.08	1.33	1.22	-	1.22	1.01	1.03
MnO	0.04	0.05	0.05	0.03	0.04	0.03	0.05	0.04	0.04	0.04	0.05	0.04
MgO	0.33	0.42	0.43	0.29	0.48	0.35	0.46	0.39	0.49	0.55	0.48	0.45
CaO	0.52	0.76	0.51	0.56	0.59	0.66	0.49	0.57	0.48	0.71	0.66	0.73
Na_2O	3.63	3.65	3.11	3.37	2.95	3.34	3.01	3.17	2.83	3.41	3.09	3.58
K_2O	4.21	4.98	4.25	4.86	5.28	4.92	4.57	5.05	5.36	5.62	5.41	6.53
P_2O_5	0.31	0.30	0.23	0.27	0.27	0.29	0.28	0.30	0.30	0.31	0.25	0.26
H_2O+	-	-	-	-	-	-	-	-	-	-	-	-
H_2O-	-	-	-	-	-	-	-	-	-	-	-	-
CO_2	-	-	-	-	-	-	-	-	-	-	-	-
Cl	-	-		-	-	-	-	-	-	-	-	-
F	0.05	0.05	0.06	0.04	0.07	0.03	0.06	0.05	-	0.04	0.04	0.04
LOI	0.93	1.00	0.85	0.77	0.93	0.93	1.16	0.93	0.54	0.77	1.08	1.00
TOTAL	99.96	99.65	99.36	99.16	99.20	100.24	99.80	99.61	99.09	99.78	98.74	99.13
Fe_2O_3T	1.14	1.42	1.63	1.14	1.56	1.16	1.48	1.57	2.04	1.82	1.51	1.32
FeOT	1.02	1.28	1.47	1.02	1.41	1.04	1.33	1.41	1.84	1.63	1.36	1.19
A/CNK	1.13	1.08	1.07	1.05	1.06	1.05	1.06	1.03	1.00	1.01	1.06	1.01
Trace els												
Ba	260	460	260	220	330	300	300	180	260	490	460	610
Rb	320	290	310	250	370	230	310	300	280	330	310	330
Sr	40	100	50	30	60	100	40	30	50	100	110	140
Y	10	10	10	10	10	10	10	10	10	20	10	10
Zr	30	60	60	50	140	40	90	60	60	110	90	80
Nb	30	10	20	20	10	20	10	20	20	20	10	10
Th	-	-	8	-	-	-	-	-	-	25	-	-
Pb	23	185	26	26	28	30	27	32	-	35	37	44
Ga	-	-	-	-	-	-	-	-	-	-	-	-
Zn	-	-	-	-	-	-	-	-	-	72	51	40
Cu	-	-	-	-	-	-	-	-	-	-	-	-
Ni	-	-	-	-	-	-	-	-	-	-	-	-
V	-	-	-	-	-	-	-	-	-	-	-	-
Cr	-	-	-	-	-	-	-	-	-	-	-	-
Hf	-	-	-	-	-	-	-	-	-	-	-	-
Cs	-	-	-	-	-	-	-	-	-	-	-	-
Sc	-	-	-	-	-	-	-	-	-	-	-	-
Ta	-	-	-	-	-	-	-	-	-	-	-	-
Co	-	-	-	-	-	-	-	-	-	-	-	-
Li	51	78	127	70	103	51	121	62	-	90	72	68
Be	-	5	5	6	4	5	9	4	-	7	9	8
B	-	-	-	-	-	-	-	-	-	-	-	-
U	9	1	6	7	7	5	7	5	-	5	6	1
W	-	-	-	-	-	-	-	-	-	-	-	-
Sn	6	12	11	9	7	7	9	-	-	8	3	5
Mo	-	-	-	-	-	-	-	-	-	-	-	-
Rare-earths												
La	-	-	17	-	-	-	-	-	-	30.3	-	-
Ce	-	-	32	-	-	-	-	-	-	62	-	-
Pr	-	-	-	-	-	-	-	-	-	-	-	-
Nd	-	-	15	-	-	-	-	-	-	32	-	-
Sm	-	-	4.23	-	-	-	-	-	-	7.5	-	-
Eu	-	-	0.48	-	-	-	-	-	-	0.66	-	-
Gd	-	-	-	-	-	-	-	-	-	-	-	-
Tb	-	-	0.6	-	-	-	-	-	-	0.9	-	-
Dy	-	-	-	-	-	-		-	-	-	-	-
Ho	-	-	-	-	-	-	-	-	-	-	-	-
Er	-	-	-	-	-	-	-	-	-	-	-	-
Tm	-	-	-	-	-	-	-	-	-	-	-	-
Yb	-	-	0.48	-	-	-	-	-	-	0.68	-	-
Lu	-	-	0.08	-	-	-	-	-	-	0.1		-

Table E1.1 (Continued) Compilation of Meguma Zone granitoid lithogeochemistry

Sample	DH680	DH709	DI126	DI131	DI348A	DI352	DI373A	DIa348B	DIa350	FC167A	FC411B	FC488
Batholith	-	-	-	-	-	-	-	-	-	-	-	-
Pluton	CP	CP	CP	CP	CP	CP	CP	CP	CP	CP	CP	CP
Lithology	Grd	Mzg	Mzg	Mzg	Mzg	Mzg	Mzg	Mzg	Mzg	Mzg	Mzg	Mzg
Source	25	25	25	25	25	25	25	25	25	25	25	25
Major oxides												
SiO_2	68.00	72.00	74.10	72.40	71.40	73.10	72.40	72.40	72.50	72.20	72.10	71.90
TiO_2	0.29	0.27	0.18	0.14	0.19	0.23	0.14	0.13	0.13	0.23	0.19	0.20
Al_2O_3	17.40	16.10	14.10	15.00	15.30	14.20	15.40	14.90	14.90	15.10	15.10	14.80
Fe_2O_3	0.34	0.31	0.47	0.25	0.29	0.02	0.06	0.25	0.21	0.17	0.04	0.18
FeO	1.10	1.00	0.71	0.78	0.72	1.19	0.96	0.77	0.66	1.10	0.92	0.95
MnO	0.05	0.05	0.03	0.04	0.03	0.03	0.05	0.03	0.04	0.03	0.03	0.03
MgO	0.62	0.55	0.46	0.34	0.40	0.47	0.40	0.30	0.27	0.49	0.34	0.36
CaO	0.96	0.72	0.63	0.81	0.82	0.74	0.65	0.78	0.77	0.72	0.98	0.63
Na_2O	3.81	3.27	3.60	3.53	3.88	3.37	3.97	3.56	3.60	3.42	3.53	3.80
K_2O	6.03	5.53	4.65	4.84	5.31	4.98	5.02	5.14	5.04	5.08	5.11	5.15
P_2O_5	0.33	0.26	0.25	0.31	0.30	0.25	0.21	0.30	0.30	0.35	0.23	0.37
H_2O+	-	-	-	-	-	-	-	-	-	-	-	-
H_2O-	-	-	-	-	-	-	-	-	-	-	-	-
CO_2	-	-	-	-	-	-	-	-	-	-	-	-
Cl	-	-	-	-	-	-	-	-	-	-	-	-
F	0.05	0.03	0.03	0.04	0.03	0.04	0.02	0.03	0.04	0.04	0.04	0.04
LOI	1.00	1.08	0.93	1.08	0.93	0.93	0.77	1.31	1.08	1.00	1.00	1.23
TOTAL	99.86	100.08	100.05	99.47	99.52	99.46	99.99	99.82	99.46	99.83	99.53	99.55
Fe_2O_3T	1.52	1.39	1.24	1.09	1.07	1.29	1.08	1.08	0.92	1.35	1.02	1.20
FeOT	1.37	1.25	1.12	0.98	0.96	1.16	0.98	0.97	0.83	1.21	0.92	1.08
A/CNK	1.08	1.06	1.07	1.10	1.03	1.05	1.08	1.06	1.07	1.10	1.06	1.04
Trace ele												
Ba	740	640	510	410	570	470	650	410	360	580	520	470
Rb	300	290	220	240	240	250	190	240	270	250	260	320
Sr	150	110	90	100	150	110	190	110	90	80	120	60
Y	20	10	10	10	10	10	10	20	10	10	10	10
Zr	100	90	50	40	60	70	30	40	40	90	90	60
Nb	-	-	20	10	20	20	10	10	10	20	10	10
Th	12	10	-	3	-	-	-	-	-	-	-	-
Pb	40	32	31	39	34	35	41	37	34	33	34	27
Ga	-	-	-	-	-	-	-	-	-	-	-	-
Zn	56	50	28	39	55	48	18	30	35	63	45	67
Cu	-	-	-	-	-	-	-	-	-	-	-	-
Ni	-	-	-	-	-	-	-	-	-	-	-	-
V	-	-	-	-	-	-	-	-	-	-	-	-
Cr	-	-	-	-	-	-	-	-	-	-	-	-
Hf	-	-	-	-	-	-	-	-	-	-	-	-
Cs	-	-	-	-	-	-	-	-	-	-	-	-
Sc	-	-	-	-	-	-	-	-	-	-	-	-
Ta	-	-	-	-	-	-	-	-	-	-	-	-
Co	-	-	-	-	-	-	-	-	-	-	-	-
Li	-	-	34	35	59	103	24	38	66	105	69	97
Be	-	-	5	7	6	4	3	7	9	9	9	8
B	-	-	-	-	-	-	-	-	-	-	-	-
U	6	2	1	5	4	3	2	6	3	3	4	4
W	-	-	-	-	-	-	-	-	-	-	-	-
Sn	10	4	4	9	6	7	5	6	12	7	8	12
Mo	-	-	-	-	-	-	-	-	-	-	-	-
Rare-earths												
La	-		-	11.3	-	-	-	-	-	-	-	-
Ce	-	-	-	20	-	-	-	-	-	-	-	-
Pr	-	-	-	-	-	-	-	-	-	-	-	-
Nd	-	-	-	8	-	-	-	-	-	-	-	-
Sm	-	-	-	2.37	-	-	-	-	-	-	-	-
Eu	-	-	-	0.63	-	-	-	-	-	-	-	-
Gd	-	-	-	-	-	-	-	-	-	-	-	-
Tb	-	-	-	0.6	-	-	-	-	-	-	-	-
Dy	-	-	-	-	-	-	-	-	-	-	-	-
Ho	-	-	-	-	-	-	-	-	-	-	-	-
Er	-	-	-	-	-	-	-	-	-	-	-	-
Tm	-	-	-	-	-	-	-	-	-	-	-	-
Yb	-	-	-	0.62	-	-	-	-	-	-	-	-
Lu	-	-	-	0.09	-	-	-	-	-	-	-	-

Table E1 1 (Continued) Compilation of Meguma Zone granitoid lithogeochemistry

Sample	FH289	FH293	FH647	FH651	FH714	FH724	FH725	FL067A	FL069C	FL074	FL080	FL081A
Batholith	-	-	-	-	-	-	-	-	-	-	-	-
Pluton	CP	CP	CP	CP	CP	CP	CP	CP	CP	CP	CP	CP
Lithology	Mzg	Mzg	Mzg	Mzg	Mzg	Mzg	Mzg	Mzg	Mzg	Lmzg	Mzg	Mzg
Source	25	25	25	25	25	25	25	25	25	25	25	25
Major oxides												
SiO_2	73 90	72 60	71 50	73 60	72 50	72 40	73 60	71 10	72 00	74 40	73 20	73 40
TiO_2	0.13	0 15	0 17	0 14	0 17	0 11	0 15	0 19	0 20	0 10	0 17	0 16
Al_2O_3	14 70	14 80	15 10	14 50	14 60	15 00	14 90	14 70	14 90	14 70	14 90	14 70
Fe_2O_3	0 17	0 16	0 48	0 20	0 17	0 06	0 16	0 21	0 13	0 37	0 22	0 43
FeO	0 69	0 89	0 71	0 76	0 91	0 54	0 80	0 96	0 89	0 31	0 88	0 57
MnO	0 05	0 06	0 06	0 04	0 04	0 04	0 06	0 03	0 03	0 03	0 03	0 04
MgO	0 28	0 29	0 36	0 20	0 31	0 24	0 28	0 43	0 32	0 21	0 36	0 33
CaO	0 54	0 56	0 60	0 51	0 64	0 51	0 51	0 63	0 59	0 50	0 60	0 59
Na_2O	4 01	4 02	4 27	3 90	3 81	4 61	3 81	3 59	3 77	4 20	3 94	3 80
K_2O	4 48	4 72	4 82	4 59	4 71	5 05	4 57	4 93	5 12	3 89	4 54	4 62
P_2O_5	0 32	0 34	0 35	0 36	0 36	0 32	0 30	0 31	0 32	0 30	0 31	0 29
H_20+	-	-	-	-	-		-	-	-	-	-	
H_2O-	-	-	-	-	-	-	-	-	-	-	-	-
CO_2	-	-	-	-	-	-	-	-	-	-	-	-
Cl	-	-	-	-	-	-	-	-	-	-	-	-
F	0 04	0 05	0 06	0 06	0 06	0 05	0 05	0 05	0 06	0 05	0 06	0 07
LOI	0 77	1 00	0 93	0 93	1 00	0 85	1 16	1 47	1 08	1 00	0 93	0 93
TOTAL	100 00	99 54	99 29	99 68	99 17	99 70	100 26	98 50	99 30	99 97	100 01	99 81
Fe_2O_3T	0 91	1 11	1 25	1 02	1 14	0 64	1 02	1 24	1 08	0 71	1 14	1 05
FeOT	0 82	1 00	1 13	0 91	1 03	0 57	0 92	1 12	0 97	0 64	1 03	0 95
A/CNK	1 10	1 07	1 05	1 09	1 07	1 00	1 13	1 08	1 06	1 16	1 11	1 10
Trace els												
Ba	310	290	360	100	290	390	230	410	330	110	300	340
Rb	360	350	360	420	350	350	350	360	360	360	370	360
Sr	60	80	50	10	80	90	40	50	60	20	30	60
Y	10	10	10	10	10	10	10	10	10	10	10	10
Zr	30	40	60	30	50	30	20	60	60	10	60	50
Nb	10	10	10	20	20	10	10	30	10	20	10	20
Th	-	-	-	-	-	-	3	-	-	-	-	-
Pb	29	30	20	18	26	27	22	23	23	11	24	24
Ga	-	-	-	-	-	-	-	-	-	-	-	-
Zn	38	69	34	42	51	17	44	33	37	23	33	35
Cu	-	-	-	-	-	-	-	-	-	-		-
Ni	-	-	-	-	-	-	-	-	-	-	-	-
V	-	-	-	-	-	-	-	-	-	-	-	-
Cr	-	-	-	-	-	-	-	-	-	-	-	-
Hf	-	-	-	-	-	-	-	-	-	-	-	-
Cs	-	-	-	-	-	-	-	-	-	-	-	-
Sc	-	-	-	-	-	-	-	-	-	-	-	-
Ta	-	-	-	-	-	-	-	-	-	-	-	-
Co	-	-	-	-	-	-	-	-	-	-	-	-
Li	92	163	109	136	106	73	154	42	36	18	97	93
Be	6	5	12	5	7	9	6	4	6	2	4	8
B	-	-	-	-	-	-	-	-	-	-	-	-
U	2	4	3	4	3	5	3	7	3	14	8	7
W	-	-	-	-	-	-	-	-	-	-	-	-
Sn	12	10	11	12	6	10	10	14	17	13	11	13
Mo	-	-	-	-	-	-	-	-	-	-	-	-
Rare-earths												
La	-	-	-	-	-	-	7 3	-	-	-	-	-
Ce	-	-	-	-	-	-	13	-	-	-	-	-
Pr	-	-	-	-	-	-	-	-	-	-	-	-
Nd	-	-	-	-	-	-	6	-	-	-	-	-
Sm	-	-	-	-	-	-	1 77	-	-	-	-	-
Eu	-	-	-	-	-	-	0 37	-	-	-		-
Gd	-	-	-	-	-	-	-	-	-	-	-	-
Tb	-	-	-	-	-	-	-	-	-	-	-	-
Dy	-	-	-	-	-	-	-	-	-	-	-	-
Ho	-	-	-	-	-	-	-	-	-	-	-	-
Er	-	-	-	-	-	-	-	-	-	-	-	-
Tm	-	-	-	-	-	-	-	-	-	-	-	-
Yb	-	-	-	-	-	-	0 34	-	-	-	-	-
Lu	-	-	-	-	-	-	0 05	-	-	-	-	-

Table E1.1 (Continued) Compilation of Meguma Zone granitoid lithogeochemistry

Sample	FL742	FLs55A	FLs55B	GH358	GH392	GH407	GH408	GH416B	GH424B	GH448	GH737	GI502
Batholith	-	-	-	-	-	-	-	-	-	-	-	-
Pluton	CP	CP	CP	CP	CP	CP	CP	CP	CP	CP	CP	CP
Lithology	Mzg	Ton	Ton	Lmzg	Grd	Mzg	Mzg	Mzg	Mzg	Mzg	Mzg	Mzg
Source	25	25	25	25	25	25	25	25	25	25	25	25
Major oxides												
SiO_2	72.60	60.80	61.90	73.20	71.60	72.80	73.50	71.90	72.40	72.90	72.30	72.50
TiO_2	0.19	0.20	0.22	0.19	0.29	0.16	0.15	0.19	0.16	0.17	0.19	0.07
Al_2O_3	14.60	21.30	20.70	14.60	14.80	14.80	14.50	15.00	14.70	15.10	14.80	15.40
Fe_2O_3	0.27	-	-	0.25	0.18	0.07	0.08	0.10	0.25	0.06	0.10	0.16
FeO	0.77	-	-	0.95	1.31	0.93	0.77	0.95	0.67	0.89	0.99	0.59
MnO	0.03	0.03	0.03	0.04	0.04	0.03	0.02	0.03	0.03	0.04	0.04	0.04
MgO	0.29	0.46	0.38	0.36	0.50	0.35	0.26	0.31	0.29	0.29	0.35	0.10
CaO	0.57	0.88	0.79	0.56	0.51	0.58	0.65	0.64	0.56	0.57	0.58	0.72
Na_2O	3.83	5.30	5.58	3.69	3.30	3.93	3.82	4.05	3.69	3.57	3.79	4.41
K_2O	5.11	7.48	7.59	4.64	5.50	4.72	5.26	5.19	5.51	5.35	4.95	3.90
P_2O_5	0.33	0.49	0.43	0.31	0.23	0.32	0.32	0.32	0.38	0.31	0.35	0.63
H_2O+	-	-	-	-	-	-	-	-	-	-	-	-
H_2O-	-	-	-	-	-	-	-	-	-	-	-	-
CO_2	-	-	-	-	-	-	-	-	-	-	-	-
Cl	-	-	-	-	-	-	-	-	-	-	-	-
F	0.06	0.07	0.05	0.05	0.03	0.04	0.03	0.04	0.04	0.05	0.07	0.18
LOI	0.77	1.31	0.93	1.00	1.08	1.23	0.77	0.77	0.85	0.85	1.00	1.31
TOTAL	99.31	99.84	100.01	99.73	99.27	99.88	100.06	99.40	99.34	100.06	99.39	99.79
Fe_2O_3T	1.10	1.77	1.62	1.27	1.58	1.06	0.90	1.11	0.97	1.01	1.16	0.79
FeOT	0.99	1.59	1.46	1.14	1.42	0.96	0.81	1.00	0.87	0.91	1.04	0.71
A/CNK	1.03	1.05	1.00	1.11	1.06	1.08	1.00	1.02	1.02	1.07	1.07	1.16
Trace els												
Ba	320	440	420	270	540	360	390	350	320	340	310	110
Rb	400	380	360	350	320	330	300	320	350	340	380	810
Sr	60	110	90	50	100	60	70	70	50	60	60	8
Y	10	-	-	20	10	10	10	20	10	10	10	30
Zr	50	90	70	50	110	50	50	60	40	50	50	20
Nb	10	16	12	20	10	20	10	20	20	10	20	20
Th	-	15	15	-	-	-	-	-	-	4	-	-
Pb	28	15	12	25	28	24	28	33	28	26	30	12
Ga	-	-	-	-	-	-	-	-	-	-	-	-
Zn	50	20	12	57	39	38	36	50	35	41	44	69
Cu	-	-	-	-	-	-	-	-	-	-	-	-
Ni	-	-	-	-	-	-	-	-	-	-	-	-
V	-	-	-	-	-	-	-	-	-	-	-	-
Cr	-	-	-	-	-	-	-	-	-	-	-	-
Hf	-	-	-	-	-	-	-	-	-	-	-	-
Cs	-	-	-	-	-	-	-	-	-	-	-	-
Sc	-	-	-	-	-	-	-	-	-	-	-	-
Ta	-	-	-	-	-	-	-	-	-	-	-	-
Co	-	-	-	-	-	-	-	-	-	-	-	-
Li	111	52	40	105	32	115	80	119	105	98	148	189
Be	8	3	4	7	2	11	5	7	9	9	7	21
B	-	-	-	-	-	-	-	-	-	-	-	-
U	10	7	6	5	7	7	6	3	2	6	5	10
W	-	-	-	-	-	-	-	-	-	-	-	-
Sn	11	5	14	10	5	12	8	11	13	13	14	23
Mo	-	-	-	-	-	-	-	-	-	-	-	-
Rare-earths												
La	-	-	-	-	-	-	-	-	-	10.6	-	-
Ce	-	-	-	-	-	-	-	-	-	20	-	-
Pr	-	-	-	-	-	-	-	-	-	-	-	-
Nd	-	-	-	-	-	-	-	-	-	10	-	-
Sm	-	-	-	-	-	-	-	-	-	2.92	-	-
Eu	-	-	-	-	-	-	-	-	-	0.65	-	-
Gd	-	-	-	-	-	-	-	-	-	-	-	-
Tb	-	-	-	-	-	-	-	-	-	0.6	-	-
Dy	-	-	-	-	-	-	-	-	-	-	-	-
Ho	-	-	-	-	-	-	-	-	-	-	-	-
Er	-	-	-	-	-	-	-	-	-	-	-	-
Tm	-	-	-	-	-	-	-	-	-	-	-	-
Yb	-	-	-	-	-	-	-	-	-	0.35	-	-
Lu	-	-	-	-	-	-	-	-	-	0.07	-	-

Table E1 1 (Continued) Compilation of Meguma Zone granitoid lithogeochemistry

Sample	GI505	GI506	KH415B	Kh433A	KH477	KH489B	KH492	LH751	LH818	LL046A	LL047B	LL118
Batholith	-	-	-	-	-	-	-	-	-	-	-	-
Pluton	CP	CP	CP	CP	CP	CP	CP	CP	CP	CP	CP	CP
Lithology	Mzg	Mzg	Grd	Mzg	Mzg	Mzg	Mzg	Grd	Grd	Mzg	Mzg	Mzg
Source	25	25	25	25	25	25	25	25	25	25	25	25
Major oxides												
SiO_2	73 20	73 30	70 50	72 00	71 50	71 30	70 50	69 50	69 50	73 10	73 00	73 90
TiO_2	0 08	0 08	0 32	0 36	0 39	0 37	0 35	0 36	0 38	0 11	0 16	0 18
Al_2O_3	14 90	14 90	15 20	14 10	14 60	14 70	15 10	16 60	16 10	14 90	14 90	14 20
Fe_2O_3	0 31	0 41	0 07	0 26	0 21	0 23	0 18	0 73	-	0 39	0 44	0 36
FeO	0 60	0 60	1 21	1 35	1 50	1 35	1 28	1 30	-	0 51	0 53	0 72
MnO	0 04	0 03	0 05	0 04	0 05	0 05	0 05	0 05	0 05	0 04	0 04	0 07
MgO	0 13	0 13	0 49	0 57	0 62	0 57	0 55	0 78	0 76	0 21	0 35	0 36
CaO	0 41	0 45	0 63	0 69	0 69	0 62	0 65	0 71	0 72	0 52	0 59	0 62
Na_2O	4 22	4 43	3 31	3 08	3 07	3 05	3 34	3 49	3 24	4 42	3 80	3 97
K_2O	4 41	4 52	5 88	5 54	5 79	5 81	5 96	4 82	5 10	4 16	4 64	4 48
P_2O_5	0 35	0 37	0 42	0 28	0 29	0 31	0 28	0 24	0 24	0 37	0 34	0 30
H_2O+	-	-	-	-		-	-	-	-	-	-	-
H_2O-	-	-	-	-	-	-	-	-	-	-	-	-
CO_2	-	-	-	-	-	-	-	-	-	-	-	-
Cl	-	-	-	-	-	-	-	-	-	-	-	-
F	0 13	0 12	0 09	0 06	0 06	0 06	0 06	0 07	-	0 05	0 08	0 04
LOI	0 50	0 50	0 93	0 77	0 77	1 08	0 93	1 31	1 47	1 16	1 00	0 70
TOTAL	99 10	99 67	98 95	98 97	99 40	99 37	99 10	99 79	99 53	99 84	99 74	99 81
Fe_2O_3T	0 96	1 06	1 36	1 71	1 81	1 68	1 55	2 14	2 19	0 95	1 02	1 14
FeOT	0 86	0 96	1 22	1 54	1 63	1 51	1 39	1 93	1 97	0 85	0 92	1 03
A/CNK	1 11	1 07	1 03	1 01	1 02	1 03	1 01	1 24	1 19	1 11	1 11	1 06
Trace els												
Ba	140	140	500	400	490	520	620	690	670	120	280	310
Rb	650	630	500	340	330	330	340	330	330	430	450	330
Sr	10	10	100	80	80	110	110	130	130	10	50	70
Y	20	20	10	10	20	20	10	10	10	10	10	10
Zr	20	20	110	130	140	150	150	100	100	20	30	50
Nb	20	10	20	20	10	20	10	10	20	10	10	10
Th	3	2	-	-	-	-	26	8	-	-	-	-
Pb	20	22	32	39	40	41	36	26	-	19	23	25
Ga	-	-	-	-	-	-	-	-	-	-	-	-
Zn	64	100	72	80	79	77	67	44	-	27	62	31
Cu	-	-	-	-	-	-	-	-	-	-	-	-
Ni	-	-	-	-	-	-	-	-	-	-	-	-
V	-	-	-	-	-	-	-	-	-	-	-	-
Cr	-	-	-	-	-	-	-	-	-	-	-	-
Hf	-	-	-	-	-	-	-	-	-	-	-	-
Cs	-	-	-	-	-	-	-	-	-	-	-	-
Sc	-	-	-	-	-	-	-	-	-	-	-	-
Ta	-	-	-	-	-	-	-	-	-	-	-	-
Co	-	-	-	-	-	-	-	-	-	-	-	-
Li	180	170	120	68	75	66	97	-	-	34	110	35
Be	-	-	11	3	8	10	8	-	-	3	8	4
B	-	-	-	-	-	-	-	-	-	-	-	-
U	9	14	5	5	3	9	5	8	-	7	4	5
W	-	-	-	-	-	-	-	-	-	-	-	-
Sn	20	16	13	8	8	7	4	10	-	17	16	11
Mo	-	-	-	-	-	-	-	-	-	-	-	-
Rare-earths												
La	3 8	-	-	-	-	-	35 5	-	-	-	-	-
Ce	8	-	-	-	-	-	72	-	-	-	-	-
Pr	-	-	-	-	-	-	-	-	-	-	-	-
Nd	5	-	-	-	-	-	33	-	-	-	-	-
Sm	1 32	-	-	-	-	-	8 86	-	-	-	-	-
Eu	0 05	-	-	-	-	-	0 58	-	-	-	-	-
Gd	-	-	-	-	-	-	-	-	-	-	-	-
Tb	0 3	-	-	-	-	-	1 1	-	-	-	-	-
Dy	-	-	-	-	-	-	-	-	-	-	-	-
Ho	-	-	-	-	-	-	-	-	-	-	-	-
Er	-	-	-	-	-	-	-	-	-	-	-	-
Tm	-	-	-	-	-	-	-	-	-	-	-	-
Yb	0 41	-	-	-	-	-	0 58	-	-	-	-	-
Lu	0 06	-	-	-	-	-	0 16	-	-	-	-	-

Table E1.1 (Continued) Compilation of Meguma Zone granitoid lithogeochemistry

Sample	LL157	LL668	LL670	LLF68A1	LLF68A2	LLF68B	LLF68C	LLs015B	ML577	MP415A	MP432B	MP433B
Batholith	-	-	-	-	-	-	-	-	-	-	-	-
Pluton	CP	CP	CP	CP	CP	CP	CP	CP	CP	CP	CP	CP
Lithology	Mzg	Mzg	Mzg	Mzg	Lmzg	Lmzg	Lmzg	Ton	Mzg	Grd	Mzg	Grd
Source	25	25	25	25	25	25	25	25	25	25	25	25
Major oxides												
SiO_2	72.20	72.80	73.50	73.20	74.90	74.10	73.60	62.10	73.50	69.50	70.40	68.50
TiO_2	0.18	0.19	0.17	0.13	0.07	0.12	0.17	0.14	0.11	0.25	0.31	0.20
Al_2O_3	14.70	14.80	14.30	15.00	14.30	14.50	14.40	20.30	14.80	16.50	15.50	16.80
Fe_2O_3	0.17	0.14	0.20	-	-	-	-	0.27	0.01	0.08	0.47	0.09
FeO	0.78	0.90	0.77	-	-	-	-	1.04	0.65	1.17	1.10	0.88
MnO	0.03	0.03	0.03	0.05	0.02	0.02	0.02	0.05	0.03	0.04	0.05	0.03
MgO	0.34	0.31	0.29	0.29	0.12	0.19	0.31	0.44	0.20	0.47	0.61	0.39
CaO	0.55	0.60	0.60	0.61	0.40	0.49	0.55	0.83	0.53	0.64	0.80	0.75
Na_2O	3.62	3.87	3.85	4.48	3.91	4.00	3.77	5.89	4.02	3.79	3.41	3.71
K_2O	5.30	5.04	4.75	4.18	4.35	4.47	4.73	6.86	4.87	6.18	5.48	6.82
P_2O_5	0.30	0.31	0.31	0.40	0.34	0.35	0.31	0.43	0.30	0.25	0.33	0.27
H_2O+	-	-	-	-	-	-	-	-	-	-	-	-
H_2O-	-	-	-	-	-	-	-	-	-	-	-	-
CO_2	-	-	-	-	-	-	-	-	-	-	-	-
Cl	-	-	-	-	-	-	-	-	-	-	-	-
F	0.05	0.07	0.05	0.05	0.05	0.08	0.04	0.05	0.03	0.04	0.05	0.03
LOI	1.08	1.00	0.70	0.93	1.00	1.00	1.00	1.08	0.85	0.93	1.08	0.70
TOTAL	99.21	99.94	99.42	100.36	100.11	100.00	99.83	99.37	99.84	99.75	99.46	99.10
Fe_2O_3T	1.01	1.10	1.03	1.21	0.78	0.84	1.08	1.39	0.70	1.33	1.66	1.03
FeOT	0.91	0.99	0.92	1.09	0.70	0.76	0.97	1.25	0.63	1.20	1.49	0.93
A/CNK	1.04	1.05	1.05	1.10	1.11	1.09	1.07	1.01	1.06	1.04	1.07	0.99
Trace els												
Ba	360	320	290	170	70	170	200	500	140	600	580	710
Rb	320	400	380	300	370	300	230	480	310	410	320	330
Sr	50	40	40	30	10	20	40	130	20	120	120	140
Y	10	10	30	-	-	-	-	10	10	10	20	10
Zr	60	60	50	30	-	40	60	70	10	90	130	50
Nb	10	10	10	19	13	11	14	10	10	10	10	10
Th	-	-	8	6	2	6	9	-	-	12	16	-
Pb	25	24	31	14	25	22	19	25	27	38	34	42
Ga	-	-	-	-	-	-	-	-	-	-	-	-
Zn	33	50	54	15	13	24	24	194	36	45	62	40
Cu	-	-	-	-	-	-	-	-	-	-	-	-
Ni	-	-	-	-	-	-	-	-	-	-	-	-
V	-	-	-	-	-	-	-	-	-	-	-	-
Cr	-	-	-	-	-	-	-	-	-	-	-	-
Hf	-	-	-	-	-	-	-	-	-	-	-	-
Cs	-	-	-	-	-	-	-	-	-	-	-	-
Sc	-	-	-	-	-	-	-	-	-	-	-	-
Ta	-	-	-	-	-	-	-	-	-	-	-	-
Co	-	-	-	-	-	-	-	-	-	-	-	-
Li	34	99	66	36	31	40	37	38	63	120	-	50
Be	5	6	4	2	2	2	2	7	5	10	-	2
B	-	-	-	-	-	-	-	-	-	-	-	-
U	4	10	8	6	7	5	11	5	3	8	6	3
W	-	-	-	-	-	-	-	-	-	-	-	-
Sn	11	14	7	15	8	12	7	17	5	9	6	5
Mo	-	-	-	-	-	-	-	-	-	-	-	-
Rare-earths												
La	-	-	12.2	-	-	-	-	-	-	20.1	-	-
Ce	-	-	24	-	-	-	-	-	-	39	-	-
Pr	-	-	-	-	-	-	-	-	-	-	-	-
Nd	-	-	14	-	-	-	-	-	-	17	-	-
Sm	-	-	3.4	-	-	-	-	-	-	4.6	-	-
Eu	-	-	0.37	-	-	-	-	-	-	0.72	-	-
Gd	-	-	-	-	-	-	-	-	-	-	-	-
Tb	-	-	0.3	-	-	-	-	-	-	0.4	-	-
Dy	-	-	-	-	-	-	-	-	-	-	-	-
Ho	-	-	-	-	-	-	-	-	-	-	-	-
Er	-	-	-	-	-	-	-	-	-	-	-	-
Tm	-	-	-	-	-	-	-	-	-	-	-	-
Yb	-	-	0.3	-	-	-	-	-	-	0.3	-	-
Lu	-	-	0.06	-	-	-	-	-	-	0.06	-	-

Table E1 1 (Continued) Compilation of Meguma Zone granitoid lithogeochemistry

Sample	MP472A	MP489A	OI346B	OI346C	OI346D	OI384B	PC416A	PC424A	PC441B	PC445	PC467B	PC625
Batholith	-	-	-	-	-	-	-	-	-	-	-	-
Pluton	CP	CP	CP	CP	CP	CP	CP	CP	CP	CP	CP	CP
Lithology	Mzg	Grd	Mzg	Mzg	Lmzg	Lmzg	Mzg	Mzg	Mzg	Mzg	Lmzg	Mzg
Source	25	25	25	25	25	25	25	25	25	25	25	25
Major oxides												
SiO_2	71 60	68 00	73 90	72 80	75 60	74 10	73 60	74 60	74 00	72 10	75 00	72 20
TiO_2	0 28	0 19	0 29	0 41	0 40	0 41	0 38	0 26	0 20	0 41	0 29	0 34
Al_2O_3	14 90	17 40	13 70	13 20	12 00	12.70	13 00	13 30	13 80	14 10	12 60	14 00
Fe_2O_3	0 40	0 11	1 10	0 95	1 14	0 51	0 27	0 17	0 04	0 09	0 09	0 03
FeO	1 06	0 83	1 09	2 66	1 53	2 40	1 74	1 23	1 25	1 66	1 35	1 34
MnO	0 05	0 03	0 07	0 10	0 06	0 08	0 05	0 04	0 03	0 05	0 03	0 04
MgO	0 51	0 37	0 85	1 12	1 09	1 14	0 53	0 40	0 34	0 66	0 44	0 51
CaO	0 72	0 77	1 10	1 09	0 78	1 23	0 48	0 52	0 72	0 71	0 63	0 62
Na_2O	3 30	3 87	4 36	2 75	3 37	3 40	2 77	3 26	2 65	2 93	2 55	2 98
K_2O	5 40	7 07	2.46	2 59	2 38	2 66	5 34	5 10	5 08	5 42	5 16	5 83
P_2O_5	0 26	0 25	0 12	0 08	0 13	0 23	0 31	0 31	0 35	0 28	0 30	0 29
H_2O+	-	-	-	-	-	-	-	-	-	-	-	-
H_2O-	-	-	-	-	-	-	-	-	-	-	-	-
CO_2	-	-	-	-	-	-	-	-	-	-	-	-
Cl	-	-	-	-	-	-	-	-	-	-	-	-
F	0 05	0 03	0 02	0 03	0 04	0 03	0 07	0 06	0 05	0 08	0 04	0 06
LOI	0 85	0 70	1 08	1 39	1 39	0 50	0 77	0 70	0 77	0 77	0 62	0 70
TOTAL	99 26	99 55	100 00	98 96	99 73	99 22	99 15	99 83	99 17	99 10	98 99	98 82
Fe_2O_3T	1 54	1 00	2 30	3 82	2 81	3 08	2 13	1 49	1 37	1 86	1 53	1 46
FeOT	1 39	0 90	2.07	3 43	2 53	2.77	1 92	1 34	1 23	1 67	1 38	1 31
A/CNK	1 06	0 99	1 20	1 41	1 26	1 20	1 01	1 00	1 09	1 04	1 01	0 99
Trace els												
Ba	450	720	430	280	400	580	170	230	260	480	290	500
Rb	310	340	130	150	140	140	380	350	320	340	300	350
Sr	100	150	240	130	190	240	30	50	50	80	70	90
Y	10	10	10	40	20	30	10	10	10	10	20	20
Zr	90	60	90	170	250	180	110	40	50	150	70	140
Nb	20	10	20	20	20	20	30	20	10	10	10	20
Th	-	-	-	-	-	6	-	-	-	-	-	-
Pb	33	42	29	23	17	30	29	28	32	33	35	48
Ga	-	-	-	-	-	-	-	-	-	-	-	-
Zn	60	41	56	79	45	56	85	55	55	93	80	47
Cu	-	-	-	-	-	-	-		-	-	-	-
Ni	-	-	-	-	-	-	-	-	-	-	-	-
V	-	-	-	-	-	-	-	-	-	-	-	-
Cr	-	-	-	-	-	-	-	-	-	-	-	-
Hf	-	-	-	-	-	-	-	-	-	-	-	-
Cs	-	-	-	-	-	-	-	-	-	-	-	-
Sc	-	-	-	-	-	-	-	-	-	-	-	-
Ta	-	-	-	-	-	-	-	-	-	-	-	-
Co	-	-	-	-	-	-	-	-	-	-	-	-
Li	75	46	27	73	29	55	155	124	108	71	75	51
Be	10	8	4	2	2	-	7	3	8	8	3	4
B	-	-	-	-	-	-	-	-	-	-	-	-
U	7	4	1	4	1	2	6	5	6	5	3	3
W	-	-	-	-	-	-	-	-	-	-	-	-
Sn	7	3	3	6	3	2	9	11	6	10	5	2
Mo	-	-	-	-	-	-	-	-	-	-	-	-
Rare-earths												
La	-	-	-	-	-	0 3	-	-	-	-	-	-
Ce	-	-	-	-	-	43	-	-	-	-	-	-
Pr	-	-	-	-	-	-	-	-	-	-	-	-
Nd	-	-	-	-	-	16	-	-	-	-	-	-
Sm	-	-	-	-	-	3 83	-	-	-	-	-	-
Eu	-	-	-	-	-	0 56	-	-	-	-	-	-
Gd	-	-	-	-	-	-	-	-		-	-	-
Tb	-	-	-	-	-	0 6	-	-	-	-	-	-
Dy	-	-	-	-	-	-	-	-	-	-	-	-
Ho	-	-	-	-	-	-	-	-	-	-	-	-
Er	-	-	-	-	-	-	-	-	-	-	-	-
Tm	-	-	-	-	-	-	-	-	-	-	-	-
Yb	-	-	-	-	-	1 76	-	-	-	-	-	-
Lu	-	-	-	-	-	0 35	-	-	-	-	-	-

Table E1 1 (Continued) Compilation of Meguma Zone granitoid lithogeochemistry

Sample	PH175	PH269	PH275	PH278	PH512	PH514	PH525B	PH532	PH555	PH556B	PH731	PI262A
Batholith	-	-	-	-	-	-	-	-	-	-	-	-
Pluton	CP	CP	CP	CP	CP	CP	CP	CP	CP	CP	CP	CP
Lithology	Mzg	Mzg	Mzg	Mzg	Mzg	Mzg	Mzg	Mzg	Mzg	Mzg	Mzg	Mzg
Source	25	25	25	25	25	25	25	25	25	25	25	25
Major oxides												
SiO_2	70 90	72 20	72 80	73 80	71 80	72.80	71 20	71 70	71 00	70 60	73 10	73 40
TiO_2	0 36	0 34	0 34	0 28	0 30	0 31	0 35	0 37	0 39	0 38	0 21	0 25
Al_2O_3	15 00	14 10	14 50	13 90	14 70	14 30	14 70	14 30	14 50	14 50	14 30	14 50
Fe_2O_3	0 12	1.13	0 84	0 73	0 42	0 01	0 48	0 60	0 29	0 20	0 33	0 53
FeO	1 53	0 52	0 87	0 86	1 03	1.17	1 19	1 16	1 50	1 54	0 82	0 98
MnO	0 05	0 05	0 04	0 04	0 04	0 03	0 05	0 04	0 05	0 05	0 04	0 06
MgO	0 57	0 51	0 51	0 45	0 46	0 28	0 55	0 55	0 63	0 60	0 29	0 44
CaO	0 70	0 70	0 74	0 63	0 62	0 57	0 69	0 70	0 71	0 69	0 45	0 59
Na_2O	3 12	3 14	3 26	3 15	3 33	3 59	3 37	3 15	2 96	3 06	3 53	3 22
K_2O	5 65	5 47	5 41	4 82	5 92	5 40	5 50	5 56	5 71	5 68	5 26	4 75
P_2O_5	0 28	0 29	0 29	0 26	0 27	0 25	0 30	0 30	0 30	0 29	0 31	0 29
H_20+	-	-	-	-	-	-	-	-	-	-	-	-
H_2O-	-	-	-	-	-	-	-	-	-	-	-	-
CO_2	-	-	-	-	-	-	-	-	-	-	-	-
Cl	-	-	-	-	-	-	-	-	-	-	-	-
F	0 07	0 06	0 41	0 06	0 07	0 07	0 07	0 07	0 07	0 07	0 08	0 06
LOI	0 77	0 62	0 54	0 77	0 70	0 47	0 93	0 93	1 08	1 16	1 00	0 93
TOTAL	98 98	98 97	100 05	99 60	99 52	99 13	99 23	99 27	99 04	98 67	99 58	99 86
Fe_2O_3T	1 75	1 72	1 80	1 67	1 53	1 26	1 76	1 86	1 90	1 85	1 21	1 59
FeOT	1 58	1 55	1 62	1 50	1 38	1 13	1 59	1 67	1 71	1 66	1 09	1 43
A/CNK	1 06	1 01	1 03	1 08	0 99	1 00	1 03	1 02	1 03	1 03	1 04	1 14
Trace els												
Ba	520	350	470	260	400	170	480	450	530	470	190	360
Rb	380	350	380	370	370	420	370	370	370	350	440	340
Sr	80	60	90	40	70	30	110	90	120	100	30	60
Y	10	10	10	20	20	10	20	10	10	10	10	20
Zr	140	120	110	80	100	50	130	130	160	140	50	70
Nb	10	10	20	10	10	20	20	10	10	10	10	20
Th	-	-	21	-	-	-	-	-	-	-	-	-
Pb	66	31	32	26	37	28	33	36	32	42	26	41
Ga	-	-	-	-	-	-	-	-	-	-	-	-
Zn	72	66	80	84	74	100	72	73	83	77	63	65
Cu	-	-	-	-	-	-	-	-	-	-	-	-
Ni	-	-	-	-	-	-	-	-	-	-	-	-
V	-	-	-	-	-	-	-	-	-	-	-	-
Cr	-	-	-	-	-	-	-	-	-	-	-	-
Hf	-	-	-	-	-	-	-	-	-	-	-	-
Cs	-	-	-	-	-	-	-	-	-	-	-	-
Sc	-	-	-	-	-	-	-	-	-	-	-	-
Ta	-	-	-	-	-	-	-	-	-	-	-	-
Co	-	-	-	-	-	-	-	-	-	-	-	-
Li	112	84	85	106	75	77	74	75	66	76	106	109
Be	5	5	6	6	9	3	8	7	8	8	6	7
B	-	-	-	-	-	-	-	-	-	-	-	-
U	2	6	3	6	10	6	10	9	3	7	4	5
W	-	-	-	-	-	-	-	-	-	-	-	-
Sn	13	7	12	7	6	7	7	6	7	8	12	10
Mo	-	-	-	-	-	-	-	-	-	-	-	-
Rare-earths												
La	-	-	28 9	-	-	-	-	-	-	-	-	-
Ce	-	-	57	-	-	-	-	-	-	-	-	-
Pr	-	-	-	-	-	-	-	-	-	-	-	-
Nd	-	-	24	-	-	-	-	-	-	-	-	-
Sm	-	-	7 18	-	-	-	-	-	-	-	-	-
Eu	-	-	0 6	-	-	-	-	-	-	-	-	-
Gd	-	-	-	-	-	-	-	-	-	-	-	-
Tb	-	-	1 1	-	-	-	-	-	-	-	-	-
Dy	-	-	-	-	-	-	-	-	-	-	-	-
Ho	-	-	-	-	-	-	-	-	-	-	-	-
Er	-	-	-	-	-	-	-		-	-	-	-
Tm	-	-	-	-	-	-	-	-	-	-	-	-
Yb	-	-	0 44	-	-	-	-	-	-	-	-	-
Lu	-	-	0 1	-	-	-	-	-	-	-	-	-

Table E1.1 (Continued) Compilation of Meguma Zone granitoid lithogeochemistry

Sample	PI297A	PI303A	PI315	PI326	SC442	SC469	SC571	SC587A	SI496	SI565	SI605	SI606
Batholith	-	-	-	-	-	-	-	-	-	-	-	-
Pluton	CP	CP	CP	CP	CP	CP	CP	CP	CP	CP	CP	CP
Lithology	Mzg	Mzg	Lmzg	Mzg	Ton	Ton	Grd	Ton	Mzg	Mzg	Mzg	Mzg
Source	25	25	25	25	25	25	25	25	25	25	25	25
Major oxides												
SiO_2	72.60	71.80	74.50	72.10	64.70	59.60	67.10	65.00	72.90	73.30	72.20	72.20
TiO_2	0.30	0.31	0.27	0.25	0.75	0.96	0.60	0.72	0.13	0.12	0.19	0.20
Al_2O_3	14.10	14.40	13.60	14.60	16.30	17.70	15.80	15.90	14.70	14.70	14.70	14.80
Fe_2O_3	0.43	0.30	0.28	0.22	0.25	0.67	0.23	0.43	0.17	0.01	0.09	0.31
FeO	1.07	1.41	1.29	1.16	3.98	4.49	3.10	3.77	0.68	1.02	0.99	0.96
MnO	0.06	0.06	0.06	0.05	0.17	0.16	0.12	0.16	0.04	0.05	0.04	0.04
MgO	0.52	0.49	0.53	0.45	2.03	2.22	1.51	1.94	0.19	0.18	0.33	0.36
CaO	0.73	0.58	0.69	0.67	2.81	4.04	2.46	3.19	0.52	0.52	0.58	0.56
Na_2O	3.13	3.40	3.19	3.62	3.22	3.44	3.83	3.40	4.04	4.18	3.68	3.71
K_2O	4.92	4.96	4.00	5.02	3.34	3.26	3.23	3.25	5.08	4.62	5.06	5.09
P_2O_5	0.26	0.30	0.28	0.28	0.19	0.26	0.18	0.19	0.36	0.38	0.35	0.34
H_2O+	-	-	-	-	-	-	-	-	-	-	-	-
H_2O-	-	-	-	-	-	-	-	-	-	-	-	-
CO_2	-	-	-	-	-	-	-	-	-	-	-	-
Cl	-	-	-	-	-	-	-	-	-	-	-	-
F	0.05	0.07	0.05	0.05	0.07	0.08	0.09	0.08	0.09	0.11	0.07	0.07
LOI	1.08	1.08	1.08	1.00	1.00	1.23	0.85	0.93	1.00	1.08	1.16	1.39
TOTAL	99.13	99.01	99.70	99.36	98.56	97.80	98.86	98.69	99.75	100.2	99.32	99.90
Fe_2O_3T	1.58	1.81	1.66	1.46	4.50	5.47	3.54	4.46	0.88	1.10	1.15	1.34
FeOT	1.43	1.63	1.50	1.32	4.05	4.93	3.18	4.01	0.79	0.99	1.03	1.21
A/CNK	1.08	1.08	1.16	1.05	1.20	1.15	1.15	1.12	1.03	1.06	1.06	1.06
Trace els												
Ba	490	290	370	530	680	990	520	710	270	150	320	330
Rb	310	410	300	320	220	180	260	220	510	540	390	380
Sr	80	60	70	100	270	390	200	290	30	10	60	50
Y	20	10	10	10	40	20	10	10	10	10	10	10
Zr	90	70	90	100	190	270	170	210	50	10	50	60
Nb	10	10	10	10	20	20	20	10	20	10	10	20
Th	-	-	-	-	-	12	-	12	-	-	-	7
Pb	35	30	28	29	31	36	33	25	22	18	22	26
Ga	-	-	-	-	-	-	-	-	-	-	-	-
Zn	86	87	61	55	119	109	92	72	66	54	63	60
Cu	-	-	-	-	-	-	-	-	-	-	-	-
Ni	-	-	-	-	-	-	-	-	-	-	-	-
V	-	-	-	-	-	-	-	-	-	-	-	-
Cr	-	-	-	-	-	-	-	-	-	-	-	-
Hf	-	-	-	-	-	-	-	-	-	-	-	-
Cs	-	-	-	-	-	-	-	-	-	-	-	-
Sc	-	-	-	-	-	-	-	-	-	-	-	-
Ta	-	-	-	-	-	-	-	-	-	-	-	-
Co	-	-	-	-	-	-	-	-	-	-	-	-
Li	75	169	96	87	104	61	102	80	132	145	112	133
Be	8	5	8	8	3	12	4	2	6	4	5	6
B	-	-	-	-	-	-	-	-	-	-	-	-
U	7	7	8	5	6	2	1	4	7	12	7	5
W	-	-	-	-	-	-	-	-	-	-	-	-
Sn	8	14	7	6	7	1	5	7	11	16	14	12
Mo	-	-	-	-	-	-	-	-	-	-	-	-
Rare-earths												
La	-	-	-	-	-	28	39.4	-	-	-	14.6	-
Ce	-	-	-	-	-	48	68	-	-	-	29	-
Pr	-	-	-	-	-	-	-	-	-	-	-	-
Nd	-	-	-	-	-	21	24	-	-	-	12	-
Sm	-	-	-	-	-	4.7	6.27	-	-	-	3.8	-
Eu	-	-	-	-	-	1.53	0.99	-	-	-	0.5	-
Gd	-	-	-	-	-	-	-	-	-	-	-	-
Tb	-	-	-	-	-	0.6	0.9	-	-	-	0.4	-
Dy	-	-	-	-	-	-	-	-	-	-	-	-
Ho	-	-	-	-	-	-	-	-	-	-	-	-
Er	-	-	-	-	-	-	-	-	-	-	-	-
Tm	-	-	-	-	-	-	-	-	-	-	-	-
Yb	-	-	-	-	-	1.4	1.51	-	-	-	0.43	-
Lu	-	-	-	-	-	0.23	0.3	-	-	-	0.08	-

Table E1.1 (Continued) Compilation of Meguma Zone granitoid lithogeochemistry

Sample	SI616A	SI618	SI755	SL562A	SL562B	SL562C	SL757	WH029	WH181	WH196
Batholith	-	-	-	-	-	-	-	-	-	-
Pluton	CP	CP	CP	CP	CP	CP	CP	CP	CP	CP
Lithology	Mzg	Mzg	Mzg	Mzg	Mzg	Mzg	Mzg	Mzg	Mzg	Mzg
Source	25	25	25	25	25	25	25	25	25	25
Major oxides										
SiO_2	72.90	72.50	73.10	72.30	73.10	72.30	74.70	74.10	73.90	74.30
TiO_2	0.14	0.18	0.18	0.09	0.12	0.08	0.12	0.15	0.10	0.11
Al_2O_3	14.80	14.60	14.70	15.20	14.60	15.60	14.70	14.20	15.00	14.50
Fe_2O_3	0.10	0.06	0.45	0.12	0.01	0.08	0.36	0.29	0.08	0.31
FeO	0.74	1.02	0.70	0.63	0.94	0.56	0.50	0.72	0.85	0.63
MnO	0.04	0.04	0.04	0.04	0.05	0.04	0.03	0.03	0.04	0.04
MgO	0.26	0.29	0.36	0.13	0.15	0.10	0.24	0.21	0.15	0.21
CaO	0.55	0.56	0.58	0.44	0.49	0.48	0.41	0.48	0.47	0.50
Na_2O	4.09	3.80	3.78	4.08	3.76	4.34	3.62	3.80	4.26	4.11
K_2O	4.95	4.96	4.93	4.21	4.68	4.00	4.05	4.98	4.26	4.07
P_2O_5	0.34	0.35	0.38	0.38	0.41	0.39	0.30	0.28	0.34	0.32
H_2O+	-	-	-	-	-	-	-	-	-	-
H_2O-	-	-	-	-	-	-	-	-	-	-
CO_2	-	-	-	-	-	-	-	-	-	-
Cl	-	-	-	-	-	-	-	-	-	-
F	0.05	0.07	0.09	0.18	0.17	0.16	0.11	0.07	0.09	0.07
LOI	0.93	1.16	1.00	1.39	1.31	1.31	1.00	0.75	0.93	0.85
TOTAL	99.80	99.47	100.14	98.98	99.58	99.25	99.98	99.94	100.34	99.90
Fe_2O_3T	0.89	1.15	1.21	0.80	1.01	0.68	0.91	1.07	0.99	0.99
FeOT	0.80	1.03	1.09	0.72	0.91	0.61	0.81	0.96	0.89	0.89
A/CNK	1.04	1.05	1.06	1.18	1.10	1.20	1.23	1.03	1.13	1.13
Trace els										
Ba	320	320	250	110	180	100	100	170	120	130
Rb	330	400	480	680	770	760	560	460	550	490
Sr	50	60	30	5	30	10	10	10	10	10
Y	10	10	10	20	10	10	10	10	10	20
Zr	40	60	60	40	30	30	10	30	20	20
Nb	10	20	20	30	20	10	20	10	10	20
Th	-	-	8	4	-	-	2	-	-	-
Pb	23	24	24	17	20	9	16	30	14	24
Ga	-	-	-	-	-	-	-	-	-	-
Zn	36	52	66	87	100	58	64	40	72	54
Cu	-	-	-	-	-	-	-	-	-	-
Ni	-	-	-	-	-	-	-	-	-	-
V	-	-	-	-	-	-	-	-	-	-
Cr	-	-	-	-	-	-	-	-	-	-
Hf	-	-	-	-	-	-	-	-	-	-
Cs	-	-	-	-	-	-	-	-	-	-
Sc	-	-	-	-	-	-	-	-	-	-
Ta	-	-	-	-	-	-	-	-	-	-
Co	-	-	-	-	-	-	-	-	-	-
Li	86	134	-	232	237	188	-	85	161	146
Be	7	7	-	4	5	4	-	3	3	5
B	-	-	-	-	-	-	-	-	-	-
U	5	5	8	23	8	21	6	7	2	11
W	-	-	-	-	-	-	-	-	-	-
Sn	13	10	16	24	23	25	20	9	14	14
Mo	-	-	-	-	-	-	-	-	-	-
Rare-earths										
La	-	-	-	7	-	-	-	-	-	-
Ce	-	-	-	12	-	-	-	-	-	-
Pr	-	-	-	-	-	-	-	-	-	-
Nd	-	-	-	9	-	-	-	-	-	-
Sm	-	-	-	2.25	-	-	-	-	-	-
Eu	-	-	-	0.17	-	-	-	-	-	-
Gd	-	-	-	-	-	-	-	-	-	-
Tb	-	-	-	0.5	-	-	-	-	-	-
Dy	-	-	-	-	-	-	-	-	-	-
Ho	-	-	-	-	-	-	-	-	-	-
Er	-	-	-	-	-	-	-	-	-	-
Tm	-	-	-	-	-	-	-	-	-	-
Yb	-	-	-	0.54	-	-	-	-	-	-
Lu	-	-	-	0.09	-	-	-	-	-	-

Table E1 1 (Continued) Compilation of Meguma Zone granitoid lithogeochemistry

Sample	WH197	WH198	WH204	WH263	WH266	WH317	WH329	WH330	WH331	WH333	WH338	WH340
Batholith	-	-	-	-	-	-	-	-	-	-	-	-
Pluton	CP	CP	CP	CP	CP	CP	CP	CP	CP	CP	CP	CP
Lithology	Lmzg	Lmzg	Lmzg	Lmzg	Mzg	Mzg	Mzg	Mzg	Mzg	Lmzg	Lmzg	Lmzg
Source	25	25	25	25	25	25	25	25	25	25	25	25
Major oxides												
SiO_2	74.60	74.60	74.30	75.30	73.90	73.40	74.60	74.60	74.00	74.60	74.20	74.50
TiO_2	0.09	0.14	0.09	0.16	0.09	0.13	0.12	0.13	0.14	0.11	0.10	0.11
Al_2O_3	14.40	13.90	14.50	13.20	14.10	14.00	13.90	14.20	14.00	13.90	14.10	14.40
Fe_2O_3	0.20	0.01	0.13	0.44	0.28	0.09	0.17	0.43	0.10	0.32	0.44	0.65
FeO	0.72	0.95	0.84	0.65	0.57	0.80	0.71	0.60	0.86	0.50	0.39	0.25
MnO	0.04	0.03	0.04	0.04	0.04	0.03	0.03	0.03	0.04	0.03	0.03	0.03
MgO	0.13	0.20	0.16	0.20	0.12	0.18	0.18	0.19	0.20	0.15	0.14	0.15
CaO	0.46	0.56	0.45	0.35	0.42	0.46	0.53	0.53	0.47	0.46	0.47	0.49
Na_2O	4.16	3.84	3.96	3.13	3.97	3.71	4.01	3.74	3.85	3.82	4.04	4.08
K_2O	4.28	4.65	4.44	4.81	4.53	5.02	4.51	4.71	4.77	5.24	4.60	4.03
P_2O_5	0.32	0.24	0.35	0.26	0.35	0.28	0.33	0.28	0.28	0.28	0.28	0.27
H_2O+	-	-	-	-	-	-	-	-	-	0.40	-	-
H_2O-	-	-	-	-	-	-	-	-	-	0.05	-	-
CO_2	-	-	-	-	-	-	-	-	-	-	-	-
Cl	-	-	-	-	-	-	-	-	-	-	-	-
F	0.07	0.06	0.11	0.06	0.11	0.05	0.05	0.06	0.05	0.05	0.07	0.07
LOI	0.62	0.70	0.77	0.85	0.93	0.85	0.77	0.70	0.86	0.50	0.62	1.00
TOTAL	99.98	99.78	99.99	99.33	99.26	98.91	99.82	100.09	99.52	99.87	99.36	99.91
Fe_2O_3T	0.97	1.02	1.03	1.15	0.90	0.94	0.93	1.08	1.02	0.86	0.87	0.94
FeOT	0.88	0.92	0.93	1.03	0.81	0.85	0.84	0.98	0.92	0.78	0.78	0.85
A/CNK	1.09	1.03	1.11	1.06	1.07	1.02	1.04	1.06	1.04	0.98	1.04	1.13
Trace els												
Ba	110	110	140	130	110	120	120	150	140	120	150	100
Rb	520	400	610	450	600	430	430	380	420	430	460	430
Sr	10	10	10	10	10	10	10	10	20	10	10	10
Y	20	10	10	20	10	10	10	10	10	10	10	10
Zr	10	20	30	30	10	30	20	20	20	20	10	30
Nb	20	10	20	10	20	10	30	10	10	10	10	10
Th	3	-	-	-	-	-	-	2	-	-	-	-
Pb	15	108	15	23	14	24	19	24	23	28	20	17
Ga	-	-	-	-	-	-	-	-	-	-	-	-
Zn	68	59	80	43	54	62	26	64	76	56	60	55
Cu	-	-	-	-	-	-	-	-	-	-	-	-
Ni	-	-	-	-	-	-	-	-	-	-	-	-
V	-	-	-	-	-	-	-	-	-	-	-	-
Cr	-	-	-	-	-	-	-	-	-	-	-	-
Hf	-	-	-	-	-	-	-	-	-	-	-	-
Cs	-	-	-	-	-	-	-	-	-	-	-	-
Sc	-	-	-	-	-	-	-	-	-	-	-	-
Ta	-	-	-	-	-	-	-	-	-	-	-	-
Co	-	-	-	-	-	-	-	-	-	-	-	-
Li	159	98	176	81	143	72	40	85	[illegible]	71	95	91
Be	2	2	3	3	3	2	3	-	2	-	2	2
B	-	-	-	-	-	-	-	-	-	-	-	-
U	6	6	3	1	3	6	7	4	4	2	5	7
W	-	-	-	-	-	-	-	-	-	-	-	-
Sn	14	11	16	10	18	12	8	6	6	8	12	13
Mo	-	-	-	-	-	-	-	-	-	-	-	-
Rare-earths												
La	3.1	-	-	-	-	-	-	-	-	-	-	-
Ce	8	-	-	-	-	-	-	-	-	-	-	-
Pr	-	-	-	-	-	-	-	-	-	-	-	-
Nd	4	-	-	-	-	-	-	-	-	-	-	-
Sm	1.16	-	-	-	-	-	-	-	-	-	-	-
Eu	0.19	-	-	-	-	-	-	-	-	-	-	-
Gd	-	-	-	-	-	-	-	-	-	-	-	-
Tb	0.1	-	-	-	-	-	-	-	-	-	-	-
Dy	-	-	-	-	-	-	-	-	-	-	-	-
Ho	-	-	-	-	-	-	-	-	-	-	-	-
Er	-	-	-	-	-	-	-	-	-	-	-	-
Tm	-	-	-	-	-	-	-	-	-	-	-	-
Yb	0.31	-	-	-	-	-	-	-	-	-	-	-
Lu	0.06	-	-	-	-	-	-	-	-	-	-	-

Table E1 1 (Continued) Compilation of Meguma Zone granitoid lithogeochemistry

Sample	WH519	WH826	WHF36	WHF38A	WHF38B	BM040	BR059	BR060	BR123	BR139	BR141	BR145
Batholith	-	-	-	-	-	-	-	-	-	-	-	-
Pluton	CP	CP	CP	CP	CP	CP	CP	CP	CP	CP	CP	CP
Lithology	Lmzg	Lmzg	Lmzg	Lmzg	Lmzg	Mzg	Mzg	Grd	Grd	Mzg	Mzg	Mzg
Source	25	25	25	25	25	25	25	25	25	25	25	25
Major oxides												
SiO_2	74 50	73 70	74 20	74 50	75 80	74 10	71 00	70 60	70 60	71 70	72 40	71 70
TiO_2	0 10	0 13	0 16	0 08	0.07	0 08	0 20	0 26	0 32	0 23	0 22	0 24
Al_2O_3	14 10	14 20	14 00	14 20	13 90	15 00	15 60	15 40	14 90	14 90	15 20	15 40
Fe_2O_3	0 11	-	-	-	-	0 31	0 35	0 34	0 36	0 37	0 27	0 30
FeO	0 71	-	-	-	-	0 20	0 60	0 90	1 50	0 90	1 10	0 90
MnO	0 04	0 03	0 04	0 02	0 02	0 04	0 02	0 03	0 04	0 04	0 04	0 03
MgO	0 15	0 17	0 20	0 09	0 11	0 15	0 38	0 61	0 64	0 36	0 51	0 53
CaO	0 48	0 47	0 45	0 42	0 39	0 37	0 67	0 86	1 42	0 68	1 11	0 79
Na_2O	4 04	3 76	3 85	4 21	3 76	5 18	3 93	3 99	4 05	3 38	4 84	3 96
K_2O	4 56	4 81	4 71	3 82	4 14	3 78	5 65	4 91	4 37	5 13	3 43	5 19
P_2O_5	0 31	0 29	0 34	0 33	0 30	0 20	0 28	0 29	0 17	0 37	0 22	0 26
H_2O+	-	-	-	-	-	0 30	0 40	0 40	0 50	0 60	0 40	0 30
H_2O-	-	-	-	-	-	0 10	0 10	0 10	0 10	0 10	0 10	0 10
CO_2	-	-	-	-	-	-	-	-	-	-	-	-
Cl	-	-	-	-	-	-	-	-	-	-	-	-
F	0 06	-	0 10	0 10	0 10	0 09	0 04	0 07	0 03	0 06	0 05	0 07
LOI	0 54	0 93	1 00	1 08	1 00	0 49	0 54	0 57	0 63	0 76	0 55	0 47
TOTAL	99 60	99 36	100 26	99 59	100 24	99 87	99 17	98 70	98 91	98 76	99 83	99 71
Fe_2O_3T	0 87	0 97	1 46	0 93	0 83	0 53	1 00	1 31	1 97	1 34	1 45	1 27
FeOT	0 78	0 87	1 31	0 84	0 75	0 48	0 90	1 18	1 77	1 21	1 31	1 14
A/CNK	1 05	1 06	1 05	1 14	1 13	1 10	1 02	1 07	1 03	1 09	1 11	1 04
Trace els												
Ba	130	130	160	60	60	70	740	550	780	320	310	550
Rb	450	420	410	410	380	500	280	330	200	350	260	330
Sr	10	10	-	-	-	14	100	86	200	72	100	82
Y	10	10	-	-	-	2	6	4	12	12	8	6
Zr	20	20	40	-	-	27	72	90	120	90	57	78
Nb	10	10	14	9	12	8	8	8	10	16	10	6
Th	-	-	9	2	1	2	6	6	10	6	4	6
Pb	21	-	13	11	13	24	32	28	34	32	28	30
Ga	-	-	-	-	-	-	-	-	-	-	-	-
Zn	87	-	40	22	46	20	40	96	42	66	64	74
Cu	-	-	-	-	-	-	-	-	-	-	-	-
Ni	-	-	-	-	-	-	-	-	-	-	-	-
V	-	-	-	-	-	-	-	-	-	-	-	-
Cr	-	-	-	-	-	-	-	-	-	-	-	-
Hf	-	-	-	-	-	-	-	-	-	-	-	-
Cs	-	-	-	-	-	-	-	-	-	-	-	-
Sc	-	-	-	-	-	-	-	-	-	-	-	-
Ta	-	-	-	-	-	-	-	-	-	-	-	-
Co	-	-	-	-	-	-	-	-	-	-	-	-
Li	98	-	117	127	167	160	60	140	54	150	64	95
Be	3	-	2	2	1	-	-	-	-	-	-	-
B	-	-	-	-	-	-	-	-	-	-	-	-
U	4	-	5	4	3	12	4	2	4	6	6	6
W	-	-	-	-	-	-	-	-	-	-	-	-
Sn	10	-	11	7	15	35	6	8	6	14	12	10
Mo	-	-	-	-	-	-	-	-	-	-	-	-
Rare-earths												
La	-	6 1	-	-	-	5 6	-	23 3	-	-	-	-
Ce	-	10	-	-	-	10	-	44	-	-	-	-
Pr	-	-	-	-	-	-	-	-	-	-	-	-
Nd	-	5	-	-	-	4	-	19	-	-	-	-
Sm	-	1 5	-	-	-	1 07	-	5 73	-	-	-	-
Eu	-	0 11	-	-	-	0 18	-	0 62	-	-	-	-
Gd	-	-	-	-	-	-	-	-	-	-	-	-
Tb	-	0 3	-	-	-	0 1	-	0 4	-	-	-	-
Dy	-	-	-	-	-	-	-	-	-	-	-	-
Ho	-	-	-	-	-	-	-	-	-	-	-	-
Er	-	-	-	-	-	-	-	-	-	-	-	-
Tm	-	-	-	-	-	-	-	-	-	-	-	-
Yb	-	0 42	-	-	-	0 22	-	0 39	-	-	-	-
Lu	-	0 11	-	-	-	0 01	-	0 06	-	-	-	-

Table E1 1 (Continued) Compilation of Meguma Zone granitoid lithogeochemistry

Sample	CR143A	CR159	CR211	CR236	DB191	DB195	DB215	DB218	EB250	EB253	GL014	GL114B
Batholith	-	-	-	-	-	-	-	-	-	-	-	-
Pluton	CP	CP	CP	CP	CP	CP	CP	CP	CP	CP	CP	CP
Lithology	Mzg	Mzg	Mzg	Mzg	Mzg	Mzg	Mzg	Mzg	Mzg	Mzg	Ton	Ton
Source	25	25	25	25	25	25	25	25	25	25	25	25
Major oxides												
SiO_2	70 50	71 00	71 10	72 20	70 70	71 30	70 60	72 50	72 40	72 30	62 50	58 80
TiO_2	0 28	0 30	0 31	0 19	0 32	0 22	0 29	0 10	0 17	0 19	0 71	0 86
Al_2O_3	15 50	15 20	15 30	15 10	15 60	15 50	15 40	15 70	15 40	15 10	17 30	18 10
Fe_2O_3	0 12	0 53	0 50	0 38	0 29	0 22	0 43	0 31	0 50	0 43	0 50	0 77
FeO	1.10	1 00	1 00	0 70	1 20	0 90	1 00	0 30	0 50	0 60	3 60	4 60
MnO	0 03	0 03	0 03	0 03	0 03	0 03	0 03	0 03	0 03	0 02	0 10	0 12
MgO	0 47	0 48	0 53	0 31	0 74	0 39	0 65	0 17	0 34	0 37	2 24	3 62
CaO	0 73	0 75	0 73	0 62	0 92	0 65	0 89	0 70	0 63	0 70	3 38	5 38
Na_2O	3 52	3 54	3 54	4 06	3 66	3 80	3 90	4 16	3 92	3 88	3 75	3 09
K_2O	6 08	5 52	5 53	4 68	5 21	5 19	5 00	5 47	4 94	4 93	3 61	2 16
P_2O_5	0 23	0 23	0 23	0 24	0 27	0 32	0 30	0 30	0 33	0 35	0 19	0 15
H_2O+	0 50	0 50	0 50	0 40	0 40	0 50	0 40	0 40	0 60	0 70	0 70	0 90
H_2O-	0 10	0 10	0 10	0 10	0 10	0 10	0 10	0 10	0 20	0 20	0 10	0 20
CO_2	-	-	-	-	-	-	-	-	-	-	-	-
Cl	-	-	-	-	-	-	-	-	-	-	-	-
F	0 07	0 08	0 07	0 10	0 06	0 05	0 07	0 03	0 02	0 04	0 03	0 04
LOI	0 67	0 68	0 67	0 60	0 56	0 65	0 57	0 53	0 82	0 94	0 83	1 14
TOTAL	99 18	99 18	99 39	99 05	99 33	99 12	98 99	100 24	99 93	99 76	98 33	98 54
Fe_2O_3T	1 30	1 61	1 58	1 14	1 58	1 19	1 51	0 64	1 05	1 08	4 24	5 70
FeOT	1 17	1 45	1 42	1 02	1 42	1 07	1 36	0 58	0 95	0 98	3 82	5 12
A/CNK	1 00	1 04	1 05	1 09	1 07	1 08	1 06	1 02	1 09	1 07	1 13	1 21
Trace els												
Ba	570	490	470	300	770	550	610	300	420	440	780	600
Rb	350	380	380	410	320	300	340	300	280	270	220	160
Sr	100	88	88	58	110	78	88	72	74	78	300	380
Y	6	6	4	4	6	6	6	6	10	10	12	16
Zr	110	110	110	66	90	63	90	42	57	66	110	66
Nb	6	8	6	8	6	12	8	10	12	14	10	8
Th	14	16	20	12	8	4	[illegible]	2	4	2	10	4
Pb	34	30	30	28	28	32	36	34	32	32	38	24
Ga	-	-	-	-	-	-	-	-	-	-	-	-
Zn	28	120	48	60	86	60	100	24	44	48	140	74
Cu	-	-	-	-	-	-	-	-	-	-	-	-
Ni	-	-	-	-	-	-	-	-	-	-	-	-
V	-	-	-	-	-	-	-	-	-	-	-	-
Cr	-	-	-	-	-	-	-	-	-	-	-	-
Hf	-	-	-	-	-	-	-	-	-	-	-	-
Cs	-	-	-	-	-	-	-	-	-	-	-	-
Sc	-	-	-	-	-	-	-	-	-	-	-	-
Ta	-	-	-	-	-	-	-	-	-	-	-	-
Co	-	-	-	-	-	-	-	-	-	-	-	-
Li	100	110	110	160	110	100	140	60	79	96	160	65
Be	-	-	-	-	-	-	-	-	-	-	-	-
B	-	-	-	-	-	-	-	-	-	-	-	-
U	6	6	2	2	2	2	4	6	4	6	2	2
W	-	-	-	-	-	-	-	-	-	-	-	-
Sn	12	6	4	14	6	12	10	4	8	12	4	4
Mo	-	-	-	-	-	-	-	-	-	-	-	-
Rare-earths												
La	-	-	25	-	-	-	23 4	-	-	-	63 6	22
Ce	-	-	68	-	-	-	45	-	-	-	93	36
Pr	-	-	-	-	-	-	-	-	-	-	-	-
Nd	-	-	32	-	-	-	23	-	-	-	50	22
Sm	-	-	7 75	-	-	-	5 96	-	-	-	10 1	5 05
Eu	-	-	0 72	-	-	-	0 56	-	-	-	1 17	1 15
Gd	-	-	-	-	-	-	-	-	-	-	-	-
Tb	-	-	0 7	-	-	-	0 4	-	-	-	0 7	0 7
Dy	-	-	-	-	-	-	-	-	-	-	-	-
Ho	-	-	-	-	-	-	-	-	-	-	-	-
Er	-	-	-	-	-	-	-	-	-	-	-	-
Tm	-	-	-	-	-	-	-	-	-	-	-	-
Yb	-	-	0 34	-	-	-	0 4	-	-	-	0 95	1 08
Lu	-	-	0 05	-	-	-	0 1	-	-	-	0 2	0 2

Table E1 1 (Continued) Compilation of Meguma Zone granitoid lithogeochemistry

Sample	GL133	RL026	SP015	SP018	A09-2132	A09-2146-2	A09-2152-1	A09-2152-2	A09-2153-3	A09-2154	A09-2155	A09-2161
Batholith	-	-	-	-	SMB	SMB	SMB	SMB	SMB	SMB	SMB	SMB
Pluton	CP	CP	CP	CP	SaLP	BBP	BBP	BBP	PLP	PLP	PLP	PLP
Lithology	Ton	Mzg	Mzg	Mzg	Mzg	Lg	Lg	Lg	Lmzg	Lmzg	Lmzg	Lmzg
Source	25	25	25	25	27	27	27	27	27	27	27	27
Major oxides												
SiO_2	54 90	73 50	70 10	71 40	67 33	74 77	74 90	74 27	73 44	75 10	73 80	73 97
TiO_2	0 81	0 12	0 34	0 21	0 60	0 08	0 08	0 13	0 13	0 07	0 15	0 14
Al_2O_3	19 70	15 30	15 00	14 80	15 34	14 22	14 16	13 88	14 70	14 07	14 02	13 33
Fe_2O_3	0 59	0 61	0 43	0 46	-	-	-	-	-	-	-	-
FeO	5 00	0 30	1 70	0 90	-	-	-	-	-	-	-	-
MnO	0 13	0 03	0 05	0 04	0 09	0 03	0 03	0 04	0 04	0 02	0 04	0 02
MgO	4 84	0 30	0 76	0 44	2 63	0 09	0 66	0 84	0 88	0 74	0 77	0 78
CaO	7 01	0 84	1 51	1 10	1 98	0 21	0 26	0 31	0 36	0 31	0 41	1 31
Na_2O	3 23	3 89	3 94	4 25	3 58	3 72	3 49	3 21	3 83	3 40	2 97	3 57
K_2O	1 02	3 27	4 53	4 59	3 88	4 37	4 23	4 38	4 57	4 27	4 84	4 70
P_2O_5	0 14	0 25	0 18	0 16	0 21	0 29	0 34	0 33	0 30	0 36	0 31	0 21
H_20+	1 00	0 60	0 50	0 50	-	-	-	-	-	-	-	-
H_2O-	0 20	0 10	0 20	0 20	-	-	-	-	-	-	-	-
CO_2	-	-	-	-	-	-	-	-	-	-	-	-
Cl	-	-	-	-	-	-	-	-	-	-	-	-
F	0 04	0 03	0 05	0 05	0 06	0 42	0 42	0 40	0 06	0 18	0 18	0 77
LOI	1 24	0 73	0 75	0 75	0 57	0 71	0 82	0 70	0 53	0 49	0 67	1 30
TOTAL	98 36	99 09	99 19	99 03	100 02	100 33	100 17	99 70	99 90	99 72	99 53	100 04
Fe_2O_3T	5 93	0 95	2 26	1 43	4 23	1 38	1 33	1 79	1 24	0 99	1 72	0 79
FeOT	5 34	0 86	2.03	1 29	3 81	1 24	1 20	1 61	1 12	0 89	1 55	0 71
A/CNK	1 26	1 31	1 02	1 01	1 11	1 15	1 19	1 18	1 13	1 18	1 14	0 94
Trace els												
Ba	350	390	710	450	602	27	34	80	210	19	150	591
Rb	44	190	260	310	154	754	677	691	277	521	487	246
Sr	520	130	170	110	172	11	16	23	43	10	28	63
Y	10	10	12	10	36	38	37	41	19	26	32	32
Zr	51	21	130	72	183	44	42	76	53	32	78	73
Nb	8	12	10	10	11	27	22	22	12	15	14	7
Th	2	2	12	6	12	6 2	6 9	13	4	3 4	12	8 4
Pb	16	26	32	34	20	22	15	22	-	13	24	42
Ga	-	-	-	-	18	28	24	24	17	23	22	15
Zn	70	16	64	44	60	69	55	69	32	48	59	12
Cu	-	-	-	-	-	-	-	-	-	-	-	8
Ni	-	-	-	-	-	-	-	-	-	-	-	-
V	-	-	-	-	48	-	-	5	-	-	5	-
Cr	-	-	-	-	-	-	-	-	-	-	-	-
Hf	-	-	-	-	6	2	2	3	2	1	3	3
Cs	-	-	-	-	-	-	-	-	-	-	-	-
Sc	-	-	-	-	11	2 2	2 4	2 7	2 9	2 2	2 5	2 1
Ta	-	-	-	-	1 2	7	6 6	5 7	2	3 6	3 1	1 6
Co	-	-	-	-	-	-	-	-	-	-	-	-
Li	52	28	160	100	64	324	375	419	90	182	129	12
Be	-	-	-	-	-	-	-	-	-	-	-	-
B	-	-	-	-	15	17	38	18	44	20	13	16
U	2	4	2	2	4	4	3 6	4 4	2 1	14	13	6 2
W	-	-	-	-	-	11	9	7	4	6	6	3
Sn	2	10	8	12	3	39	26	30	16	16	12	5
Mo	-	-	-	-	-	-	-	-	-	-	-	-
Rare-earths												
La	-	6 3	-	-	33	5	6	12	7	3	14	40
Ce	-	11	-	-	-	-	-	-	-	-	-	-
Pr	-	-	-	-	-	-	-	-	-	-	-	-
Nd	-	1	-	-	-	-	-	-	-	-	-	-
Sm	-	1 26	-	-	-	-	-	-	-	-	-	-
Eu	-	0 38	-	-	-	-	-	-	-	-	-	-
Gd	-	-	-	-	-	-	-	-	-	-	-	-
Tb	-	0 3	-	-	-	-	-	-	-	-	-	-
Dy	-	-	-	-	-	-	-	-	-	-	-	-
Ho	-	-	-	-	-	-	-	-	-	-	-	-
Er	-	-	-	-	-	-	-	-	-	-	-	-
Tm	-	-	-	-	-	-	-	-	-	-	-	-
Yb	-	0 53	-	-	-	-	-	-	-	-	-	-
Lu	-	0 08	-	-	-	-	-	-	-	-	-	-

Table E1 1 (Continued) Compilation of Meguma Zone granitoid lithogeochemistry

Sample	A09-2177-1	A09-2181	A09-2185	A09-2186	A09-2190	A09-2192	A09-2193	A09-2196	A09-2205-B	A09-2206	A09-2207	A09-2208
Batholith	SMB	SMB	SMB	SMB	SMB	SMB	SMB	SMB	SMB	SMB	SMB	SMB
Pluton	PLP	PLP	SaLP	SaLP	PLP	PLP	PLP	PLP	SaLP	SpLP	NRP	SwP
Lithology	Lmzg	Lmzg	Mzg	Mzg	Lmzg	Lmzg	Lmzg	Lmzg	Mzg	Lmzg	Lmzg	Mzg
Source	27	27	27	27	27	27	27	27	27	27	27	27
Major oxides												
SiO_2	75 87	74 12	72 03	71 05	69 74	74 64	74 56	74 09	71 78	73 84	74 46	71 96
TiO_2	0 12	0 11	0 30	0 38	0 38	0 04	0 07	0 18	0 31	0 19	0 11	0 25
Al_2O_3	13 09	14 21	14 63	• 14 69	15 37	13 98	14 14	14 06	14 56	13 88	13 82	14 70
Fe_2O_3	-	-	-	-	-	-	-	-	-	-	-	-
FeO	-	-	-	-	-	-	-	-	-	-	-	-
MnO	0 03	0 03	0 06	0 07	0 06	0 05	0 07	0 03	0 06	0 03	0 03	0 03
MgO	0 81	0 84	1 27	1 39	1 32	0 80	0 76	0 82	1 51	0 92	0 76	1 31
CaO	0 31	0 35	0 61	0 60	0 95	0 25	0 35	0 46	0 67	0 70	0 38	0 48
Na_2O	3 01	4 56	2 95	2 95	3 03	3 41	3 35	3 43	2.98	2 98	3 45	3 55
K_2O	4 27	4 33	4 75	4 68	4 89	4 36	4 60	4 81	4 82	4 73	4 32	4 82
P_2O_5	0 27	0 36	0 19	0 22	0 12	0 24	0 24	0 31	0 12	0 27	0 33	0 29
H_2O+	-	-	-	-	-	-	-	-	-	-	-	-
H_2O-	-	-	-	-	-	-	-	-	-	-	-	-
CO_2	-	-	-	-	-	-	-	-	-	-	-	-
Cl	-	-	-	-	-	-	-	-	-	-	-	-
F	0 25	0 32	0 05	0 06	0 06	0 04	0 05	0 24	0 07	0 13	0 46	0 22
LOI	0 62	0 40	0 68	0 69	0 77	0 49	0 58	0 54	0 80	0 40	0 70	0 90
TOTAL	99 82	100 58	99 50	99 28	99 30	99 10	99 74	100 21	99 77	99 47	99 68	99 89
Fe_2O_3T	1 58	1 41	2 26	2 84	2 97	0 93	1,13	1 65	2 40	1 70	1 47	1 78
FeOT	1 42	1 27	2 03	2.56	2.67	0 84	1 02	1 48	2 16	1 53	1 32	1 60
A/CNK	1 15	1 04	1 18	1 20	1 16	1 17	1 14	1 08	1 15	1 11	1 14	1 12
Trace els												
Ba	44	29	369	415	467	32	66	139	526	271	52	254
Rb	499	572	235	262	208	321	314	416	190	294	676	331
Sr	10	15	86	95	97	9	18	31	106	52	17	56
Y	32	20	26	29	33	22	21	29	35	20	26	17
Zr	69	53	107	124	135	29	36	81	98	94	58	99
Nb	17	21	8	10	10	7	8	14	7	14	24	15
Th	11	6 3	10	12	12	2 7	3 2	11	9 3	12	8 1	15
Pb	15	27	26	13	30	11	17	15	10	21	23	20
Ga	21	25	18	17	17	17	19	23	15	22	25	21
Zn	60	59	51	80	51	13	30	63	40	53	114	78
Cu	-	-	-	-	-	-	-	-	5	-	11	-
Ni	-	-	-	-	-	-	-	-	-	-	-	-
V	-	3	21	32	28	-	-	-	26	11	3	16
Cr	-	-	-	-	-	-	-	-	-	-	-	-
Hf	3	1	4	4	4	1	2	3	4	3	1	1
Cs	-	-	-	-	-	-	-	-	-	-	-	-
Sc	2 1	3 7	5 2	6 6	7 2	2 7	3 2	2 8	6 4	2.3	2 2	2 9
Ta	3 6	5 1	1 6	1 3	0 8	2 7	2 9	3 1	0 8	2	4 6	1 6
Co	-	-	-	-	-	-	-	-	-	-	-	-
Li	96	342	47	81	53	16	46	73	41	97	431	182
Be	-	-	-	-	-	-	-	-	-	-	-	-
B	14	25	22	19	21	13	16	15	13	25	30	30
U	28 6	24 1	5 4	5 6	3 4	10	3 1	15	2 2	2 9	24 8	5 4
W	5	14	2	3	1	4	2	6	-	2	11	26
Sn	22	34	10	22	7	7	11	21	5	12	41	20
Mo	-	-	-	-	-	-	-	-	-	-	-	-
Rare-earths												
La	9	6	18	21	25	2	5	14	21	18	7	9
Ce	-	-	-	-	-	-	-	-	-	-	-	-
Pr	-	-	-	-	-	-	-	-	-	-	-	-
Nd	-	-	-	-	-	-	-	-	-	-	-	-
Sm	-	-	-	-	-	-	-	-	-	-	-	-
Eu	-	-	-	-	-	-	-	-	-	-	-	-
Gd	-	-	-	-	-	-	-	-	-	-	-	-
Tb	-	-	-	-	-	-	-	-	-	-	-	-
Dy	-	-	-	-	-	-	-	-	-	-	-	-
Ho	-	-	-	-	-	-	-	-	-	-	-	-
Er	-	-	-	-	-	-	-	-	-	-	-	-
Tm	-	-	-	-	-	-	-	-	-	-	-	-
Yb	-	-	-	-	-	-	-	-	-	-	-	-
Lu	-	-	-	-	-	-	-	-	-	-	-	-

Table E1.1 (Continued) Compilation of Meguma Zone granitoid lithogeochemistry

Sample	A09-2210	A09-2211-1	A09-2212	A09-2222	A09-2224	A09-2228	A09-2231	A09-2234	A09-2235	A09-2240-A	A09-2242	A09-2243
Batholith	SMB	SMB	SMB	SMB	SMB	SMB	SMB	SMB	SMB	SMB	SMB	SMB
Pluton	SwP	PLP	PLP	PLP	PLP	NRP	NRP	SaLP	SaLP	SaLP	SaLP	SaLP
Lithology	Mzg	Lmzg	Lmzg	Lmzg	Lmzg	Lmzg	Lmzg	Mzg	Mzg	Mzg	Mzg	Mzg
Source	27	27	27	27	27	27	27	27	27	27	27	27
Major oxides												
SiO_2	72.34	74.81	73.35	73.10	73.51	71.44	72.09	70.45	69.19	69.52	69.54	70.46
TiO_2	0.34	0.06	0.15	0.17	0.14	0.31	0.21	0.32	0.49	0.45	0.46	0.39
Al_2O_3	14.22	13.91	14.36	14.97	14.67	14.43	14.95	14.91	15.00	15.06	14.91	14.87
Fe_2O_3	-	-	-	-	-	-	-	-	-	-	-	-
FeO	-	-	-	-	-	-	-	-	-	-	-	-
MnO	0.05	0.07	0.06	0.03	0.04	0.06	0.04	0.07	0.08	0.08	0.07	0.07
MgO	1.14	0.77	0.97	0.89	2.16	1.31	1.04	1.36	1.54	1.48	1.50	1.23
CaO	0.94	0.24	0.39	0.37	0.34	0.39	0.52	0.95	1.18	1.21	1.42	1.08
Na_2O	2.92	3.62	3.32	3.38	3.49	3.26	3.32	3.50	3.22	3.01	3.39	3.58
K_2O	4.60	4.22	4.63	4.80	4.67	4.68	4.76	4.80	4.20	4.77	4.42	4.54
P_2O_5	0.26	0.22	0.19	0.32	0.30	0.23	0.30	0.19	0.19	0.17	0.16	0.19
H_2O+	-	-	-	-	-	-	-	-	-	-	-	-
H_2O-	-	-	-	-	-	-	-	-	-	-	-	-
CO_2	-	-	-	-	-	-	-	-	-	-	-	-
Cl	-	-	-	-	-	-	-	-	-	-	-	-
F	0.12	0.09	0.05	0.14	0.12	0.05	0.05	0.05	0.05	0.05	0.05	0.06
LOI	0.30	0.77	0.63	0.80	0.40	1.00	0.60	1.20	0.62	0.40	0.57	0.66
TOTAL	99.38	99.81	99.61	100.00	100.93	99.49	99.27	99.95	98.86	99.16	99.44	99.66
Fe_2O_3T	2.52	1.24	1.73	1.30	1.34	2.65	1.60	2.45	3.50	3.34	3.33	2.88
FeOT	2.27	1.12	1.56	1.17	1.21	2.38	1.44	2.20	3.15	3.01	3.00	2.59
A/CNK	1.13	1.16	1.15	1.17	1.16	1.16	1.17	1.09	1.18	1.13	1.10	1.09
Trace els												
Ba	288	34	155	292	212	410	311	463	547	479	519	470
Rb	272	390	288	356	321	216	236	195	187	192	184	208
Sr	65	8	34	37	31	64	51	109	145	117	126	96
Y	27	29	28	17	17	23	14	24	32	37	33	27
Zr	146	41	63	66	59	112	77	114	155	139	150	126
Nb	15	10	8	9	14	11	12	10	10	10	9	11
Th	17	4.8	6.7	8.7	6.6	9.1	9	8.9	14	12	13	12
Pb	20	15	15	10	17	18	19	20	21	21	25	24
Ga	20	18	18	21	20	17	20	20	18	18	18	15
Zn	56	36	28	49	46	32	47	75	60	68	69	59
Cu	-	-	-	-	-	-	-	-	-	-	-	-
Ni	-	-	-	-	-	-	-	-	-	-	-	-
V	20	-	-	5	2	22	11	30	46	31	31	27
Cr	-	-	-	-	-	-	-	-	-	-	-	-
Hf	5	2	3	1	1	4	3	4	6	5	6	4
Cs	-	-	-	-	-	-	-	-	-	-	-	-
Sc	4	3.5	3.6	1.9	2.9	5	2.9	4.4	9.2	8.5	8.3	6
Ta	1.6	3.2	1.8	1.6	2.6	1.9	1.1	1.5	1.1	1	0.8	1.3
Co	-	-	-	-	-	-	-	-	-	-	-	-
Li	128	88	68	221	156	68	99	63	93	89	106	75
Be	-	-	-	-	-	-	-	-	-	-	-	-
B	20	19	20	35	25	25	35	30	28	14	16	15
U	3	7.6	4.6	5.1	4.4	4.3	2.9	4.5	4.7	3.1	3.2	6.1
W	1	7	3	3	2	2	3	1	-	-	1	-
Sn	10	23	12	20	14	10	16	8	6	6	7	6
Mo	-	-	-	-	-	-	-	-	-	-	-	-
Rare-earths												
La	25	4	10	11	10	17	14	20	33	29	31	24
Ce	-	-	-	-	-	-	-	-	-	-	-	-
Pr	-	-	-	-	-	-	-	-	-	-	-	-
Nd	-	-	-	-	-	-	-	-	-	-	-	-
Sm	-	-	-	-	-	-	-	-	-	-	-	-
Eu	-	-	-	-	-	-	-	-	-	-	-	-
Gd	-	-	-	-	-	-	-	-	-	-	-	-
Tb	-	-	-	-	-	-	-	-	-	-	-	-
Dy	-	-	-	-	-	-	-	-	-	-	-	-
Ho	-	-	-	-	-	-	-	-	-	-	-	-
Er	-	-	-	-	-	-	-	-	-	-	-	-
Tm	-	-	-	-	-	-	-	-	-	-	-	-
Yb	-	-	-	-	-	-	-	-	-	-	-	-
Lu	-	-	-	-	-	-	-	-	-	-	-	-

Table E1 1 (Continued) Compilation of Meguma Zone granitoid lithogeochemistry

Sample	A09-2350	A09-2351	A09-2352	A09-2353	A09-2354	A09-2356	A09-2357	A09-2360	A09-2361	A09-2365	A09-2366	A09-2368
Batholith	SMB	SMB	SMB	SMB	SMB	SMB	SMB	SMB	SMB	SMB	SMB	SMB
Pluton	PLP	NRP	PLP	PLP	PLP	SaLP	SaLP	NRP	NRP	PLP	PLP	SaLP
Lithology	Lmzg	Lmzg	Lmzg	Lmzg	Lmzg	Mzg	Mzg	Lmzg	Lmzg	Lmzg	Lmzg	Mzg
Source	27	27	27	27	27	27	27	27	27	27	27	27
Major oxides												
SiO_2	74 98	73 65	74 21	75 22	73 18	73 07	72 00	72.30	74 79	74 65	75 42	69 55
TiO_2	0 06	0 21	0 10	0 12	0 19	0 21	0 31	0 24	0 14	0 14	0 06	0 52
Al_2O_3	14 24	14 02	14 08	13 69	14 17	14 45	14 23	14 66	13 99	13 81	13 71	14 85
Fe_2O_3	-	-	-	-	-	-	-	-	-	-	-	-
FeO	-	-	-	-	-	-	-	-	-	-	-	-
MnO	0 04	0 05	0 03	0 04	0 05	0 04	0 06	0 05	0 04	0 04	0 03	0 10
MgO	0 81	1 07	0 83	0 83	0 97	1 06	1 17	1.14	0 82	0 87	0 80	1 89
CaO	0 28	0 75	0 43	0 31	0 68	0 41	0 74	1 21	0 37	0 35	0 30	1 30
Na_2O	3 53	3 13	4 75	3 82	3 61	3 36	3 98	3 93	3 21	3 32	2 91	3 62
K_2O	4 38	4 75	4 46	4 49	4 58	4 87	4 38	3 92	4 65	4 43	5 30	4 04
P_2O_5	0 24	0 18	0 36	0 24	0 21	0 24	0 29	0 22	0 23	0 22	0 15	0 21
H_2O+	-	-	-	-	-	-	-	-	-	-	-	-
H_2O-	-	-	-	-	-	-	-	-	-	-	-	-
CO_2	-	-	-	-	-	-	-	-	-	-	-	-
Cl	-	-	-	-	-	-	-	-	-	-	-	-
F	0 06	0 06	0 06	0 08	0 08	0 04	0 08	0 12	0 08	0 06	0 02	0 06
LOI	0 30	0 40	0 60	0 20	0 40	0 50	0 90	0 40	0 40	0 40	0 48	0 54
TOTAL	100 05	99 94	100 78	100 35	99 67	99 79	100 17	99 91	99 88	99 73	99 82	99 84
Fe_2O_3T	1 32	1 92	1 03	1 55	1 81	1 76	2 34	2.05	1 38	1 67	0 73	3 58
FeOT	1 19	1 73	0 93	1 39	1 63	1 58	2.11	1 84	1 24	1 50	0 66	3 22
A/CNK	1 17	1 09	0 99	1 07	1 08	1 12	1 06	1 10	1 14	1 14	1 07	1 13
Trace els												
Ba	15	224	155	72	158	273	324	412	140	78	100	548
Rb	290	260	296	319	273	259	247	280	348	296	235	172
Sr	-	53	30	23	48	53	56	135	31	26	26	148
Y	20	27	22	26	26	23	25	26	22	27	22	31
Zr	26	84	50	57	81	101	116	113	52	67	24	160
Nb	8	10	9	10	10	13	13	11	10	10	6	10
Th	3 1	11	4 6	7 1	8 2	15	15	12	7 3	7 2	2 2	13
Pb	29	25	-	24	22	14	13	12	13	12	25	16
Ga	18	16	18	20	18	18	20	16	18	19	17	18
Zn	32	40	17	42	44	34	53	53	39	33	41	95
Cu	5	-	-	-	-	-	5	-	-	-	10	14
Ni	-	-	-	-	-	-	-	-	-	-	-	-
V	-	11	-	-	8	7	24	13	-	-	6	41
Cr	-	-	-	-	-	-	-	-	-	-	-	-
Hf	-	3	1	3	3	3	5	5	2	3	-	6
Cs	-	-	-	-	-	-	-	-	-	-	-	-
Sc	2 3	4 2	3 1	2.9	3 7	3 7	5 6	3 8	3 1	3 2	1 9	9 5
Ta	1 7	1 4	2 2	2 5	1 6	2 2	2	2	2.1	1 7	1	1 5
Co	-	-	-	-	-	-	-	-	-	-	-	-
Li	70	86	52	90	76	65	90	162	109	73	6	57
Be	-	-	-	-	-	-	-	-	-	-	-	-
B	13	-	-	-	-	19	29	13	16	18	20	19
U	13	3 5	6 9	7 4	7 8	5 1	7 6	3 2	8 3	5 9	6	2 6
W	41	-	4	5	2	4	4	5	3	2	2	1
Sn	14	6	17	13	10	6	16	11	10	13	9	-
Mo	-	-	-	-	-	-	-	-	-	-	-	-
Rare-earths												
La	2	18	6	10	15	21	24	26	11	10	4	33
Ce	-	-	-	-	-	-	-	-	-	-	-	-
Pr	-	-	-	-	-	-	-	-	-	-	-	-
Nd	-	-	-	-	-	-	-	-	-	-	-	-
Sm	-	-	-	-	-	-	-	-	-	-	-	-
Eu	-	-	-	-	-	-	-	-	-	-	-	-
Gd	-	-	-	-	-	-	-	-	-	-	-	-
Tb	-	-	-	-	-	-	-	-	-	-	-	-
Dy	-	-	-	-	-	-	-	-	-	-	-	-
Ho	-	-	-	-	-	-	-	-	-	-	-	-
Er	-	-	-	-	-	-	-	-	-	-	-	-
Tm	-	-	-	-	-	-	-	-	-	-	-	-
Yb	-	-	-	-	-	-	-	-	-	-	-	-
Lu	-	-	-	-	-	-	-	-	-	-	-	-

Table E1 1 (Continued) Compilation of Meguma Zone granitoid lithogeochemistry

Sample	A09-2369	A09-2370	A09-2371	A09-2372	A09-2373	A09-2374	A09-2375	A09-2376	A09-2377	A09-2378	A09-2380	A09-2381
Batholith	SMB	SMB	SMB	SMB	SMB	SMB	SMB	SMB	SMB	SMB	SMB	SMB
Pluton	NRP	SaLP	SaLP	NRP	PLP	PLP	SwP	SwP	NRP	SpLP	PLP	SaLP
Lithology	Lmzg	Mzg	Mzg	Lmzg	Lmzg	Lmzg	Mzg	Mzg	Lmzg	Lmzg	Lmzg	Mzg
Source	27	27	27	27	27	27	27	27	27	27	27	27
Major oxides												
SiO_2	74.52	73.72	72.42	73.01	75.24	74.78	72.42	72.17	74.09	72.68	75.37	69.84
TiO_2	0.16	0.17	0.31	0.30	0.07	0.06	0.31	0.28	0.16	0.34	0.04	0.46
Al_2O_3	13.99	14.04	14.21	14.13	14.00	14.27	14.23	14.47	13.79	13.76	14.26	14.60
Fe_2O_3	-	-	-	-	-	-	-	-	-	-	-	-
FeO	-	-	-	-	-	-	-	-	-	-	-	-
MnO	0.04	0.04	0.06	0.05	0.04	0.04	0.05	0.05	0.07	0.05	0.03	0.07
MgO	0.92	0.93	1.13	1.03	0.80	0.72	1.12	1.25	0.92	1.13	0.67	1.56
CaO	0.29	0.42	0.35	0.57	0.30	0.30	0.71	0.67	0.50	0.91	0.24	1.28
Na_2O	3.91	3.37	3.49	3.43	3.80	3.93	3.75	4.21	3.65	3.38	3.76	3.68
K_2O	4.27	4.47	4.97	4.68	4.48	4.06	4.66	4.69	4.90	4.70	4.29	4.30
P_2O_5	0.27	0.28	0.13	0.27	0.28	0.32	0.27	0.27	0.17	0.24	0.17	0.18
H_2O+	-	-	-	-	-	-	-	-	-	-	-	-
H_2O-	-	-	-	-	-	-	-	-	-	-	-	-
CO_2	-	-	-	-	-	-	-	-	-	-	-	-
Cl	-	-	-	-	-	-	-	-	-	-	-	-
F	0.04	0.04	0.02	0.12	0.07	0.18	0.11	0.17	0.09	0.12	0.04	0.06
LOI	0.74	0.60	0.78	0.57	0.51	0.60	0.40	0.56	0.39	0.21	0.59	0.43
TOTAL	100.62	99.48	99.88	100.12	100.56	100.18	100.06	100.55	100.32	99.70	99.96	99.37
Fe_2O_3T	1.68	1.71	2.26	2.31	1.16	1.22	2.38	2.14	1.87	2.56	0.60	3.30
FeOT	1.51	1.54	2.03	2.08	1.04	1.10	2.14	1.93	1.68	2.30	0.54	2.97
A/CNK	1.11	1.14	1.08	1.09	1.10	1.16	1.05	1.02	1.02	1.03	1.16	1.07
Trace els												
Ba	161	155	375	275	14	12	240	291	161	292	23	488
Rb	240	254	179	289	409	547	299	347	308	296	234	196
Sr	37	42	112	52	9	-	56	56	37	63	8	128
Y	18	20	22	30	24	32	28	29	38	33	20	33
Zr	69	77	106	118	26	34	116	127	77	134	35	143
Nb	10	10	7	13	11	13	13	13	10	12	10	11
Th	6.1	6.6	9.2	18	3	3.7	17	20.6	9	20.6	3.8	13
Pb	-	12	15	-	20	16	19	24	23	14	22	18
Ga	18	19	13	17	22	22	21	20	17	18	16	17
Zn	19	38	37	55	51	42	58	60	44	55	20	61
Cu	-	-	-	-	-	-	-	-	-	-	37	12
Ni	-	-	-	-	-	-	-	-	-	-	-	-
V	6	5	27	13	-	-	19	13	9	19	-	36
Cr	-	-	-	-	-	-	-	-	-	-	-	-
Hf	3	3	3	4	1	1	4	4	3	5	2	5
Cs	-	-	-	-	-	-	-	-	-	-	-	-
Sc	3.5	3.8	5.6	5	2.2	2.4	4.9	4.2	3.8	5.1	3.9	7.8
Ta	2	2.3	1.1	2	2.8	3.7	2.1	2.3	1.8	1.9	2.7	1.2
Co	-	-	-	-	-	-	-	-	-	-	-	-
Li	21	19	10	61	18	59	41	71	47	39	23	99
Be	-	-	-	-	-	-	-	-	-	-	-	-
B	41	20	21	17	16	15	18	15	17	18	20	20
U	8.4	10	2.7	5.1	16	4.9	3.3	4.1	3.3	4.1	15	3.4
W	3	2	1	2	5	6	1	3	2	-	35	2
Sn	13	9	3	5	18	35	5	8	16	7	21	5
Mo	-	-	-	-	-	-	-	-	-	-	-	-
Rare-earths												
La	7	11	14	26	2	3	25	25	13	30	2	28
Ce	-	-	-	-	-	-	-	-	-	-	-	-
Pr	-	-	-	-	-	-	-	-	-	-	-	-
Nd	-	-	-	-	-	-	-	-	-	-	-	-
Sm	-	-	-	-	-	-	-	-	-	-	-	-
Eu	-	-	-	-	-	-	-	-	-	-	-	-
Gd	-	-	-	-	-	-	-	-	-	-	-	-
Tb	-	-	-	-	-	-	-	-	-	-	-	-
Dy	-	-	-	-	-	-	-	-	-	-	-	-
Ho	-	-	-	-	-	-	-	-	-	-	-	-
Er	-	-	-	-	-	-	-	-	-	-	-	-
Tm	-	-	-	-	-	-	-	-	-	-	-	-
Yb	-	-	-	-	-	-	-	-	-	-	-	-
Lu	-	-	-	-	-	-	-	-	-	-	-	-

Table E1 1 (Continued) Compilation of Meguma Zone granitoid lithogeochemistry

Sample	A09-2382	A09-2383	A09-2384	A09-2386	A09-2388	A09-2389	A09-2390	A09-2391	A09-2392	A09-2398	A09-2399	A10-3001
Batholith	SMB	SMB	SMB	SMB	SMB	SMB	SMB	SMB	SMB	SMB	SMB	SMB
Pluton	NRP	PLP	PLP	NRP	SpLP	NRP	PLP	SaLP	PLP	NRP	PLP	EDP
Lithology	Lmzg	Lmzg	Lmzg	Lmzg	Lmzg	Lmzg	Lmzg	Mzg	Lmzg	Lmzg	Lmzg	Lmzg
Source	27	27	27	27	27	27	27	27	27	27	27	27
Major oxides												
SiO_2	74 14	74 38	74 32	74 93	73 44	75 25	74 84	70 18	75 24	74 25	74 51	74 63
TiO_2	0 22	0 11	0 03	0 14	0 22	0 14	0 05	0 41	0 05	0 20	0 10	0 12
Al_2O_3	13 65	13 71	14 52	13 38	14 20	13 47	14 42	15 06	14 35	13 32	13 96	13 93
Fe_2O_3	-	-	-	-	-	-	-	-	-	-	-	-
FeO	-	-	-	-	-	-	-	-	-	-	-	-
MnO	0 06	0 09	0 04	0 06	0 03	0 04	0 05	0 07	0 05	0 04	0 03	0 04
MgO	1 02	0 96	0 75	0 89	0 96	0 86	0 68	1 35	0 76	0 90	0 74	0 76
CaO	0 67	0 38	0 24	0 52	0 83	0 46	0 31	1 33	0 32	0 51	0 33	0 32
Na_2O	3 04	3 13	4 28	3 16	2 87	3 25	3 75	3 09	3 75	3 44	2 95	3 10
K_2O	4 62	4 46	4 37	4 59	5 10	4 82	3 92	4 46	3 94	4 39	4 14	4 37
P_2O_5	0 17	0 18	0 21	0 15	0 23	0 12	0 29	0 15	0 26	0 29	0 34	0 29
H_2O+	-	-	-	-	-	-	-	-	-	-	-	-
H_2O-	-	-	-	-	-	-	-	-	-	-	-	-
CO_2	-	-	-	-	-	-	-	-	-	-	-	-
Cl	-	-	-	-	-	-	-	-	-	-	-	-
F	0 10	0 08	0 06	0 15	0 06	0 02	0 09	0 05	0 08	0 11	0 19	0 10
LOI	0 20	0 70	0 33	0 10	0 24	0 48	0 54	0 60	0 41	0 50	0 70	0 65
TOTAL	99 69	99 51	99 84	99 57	99 70	99 97	99 48	99 42	99 62	99 50	99 08	99 41
Fe_2O_3T	2 11	1 57	0 83	1 83	1 76	1 20	0 70	3 02	0 54	1 85	1 42	1 44
FeOT	1 90	1 41	0 75	1 65	1 58	1 08	0 63	2 72	0 49	1 66	1 28	1 30
A/CNK	1 10	1 15	1 10	1 09	1 08	1 06	1 22	1 15	1 21	1 07	1 26	1 20
Trace els												
Ba	136	72	17	101	392	249	33	449	28	144	20	82
Rb	278	332	401	304	245	194	457	172	442	336	504	383
Sr	45	22	6	32	70	54	6	125	8	34	5	20
Y	37	31	25	35	27	21	21	33	26	20	20	22
Zr	91	55	35	73	112	60	26	133	23	84	46	54
Nb	10	8	10	10	11	6	13	11	10	15	19	13
Th	11	6 3	4 1	9	18	4 8	1 8	11	1 6	12	5	5 6
Pb	16	16	25	23	18	19	18	12	14	18	14	27
Ga	18	17	21	15	20	15	21	17	19	24	25	21
Zn	51	49	58	59	40	36	24	47	27	61	46	48
Cu	-	5	-	-	-	5	-	-	-	-	-	-
Ni	-	-	-	-	-	-	-	-	-	-	-	-
V	11	-	-	5	7	7	-	28	-	10	1	-
Cr	-	-	-	-	-	-	-	-	-	-	-	-
Hf	3	3	2	3	4	2	2	5	2	3	1	2
Cs	-	-	-	-	-	-	-	-	-	-	-	-
Sc	4 5	3 3	3 3	3 6	2.2	3	3 9	7 7	3 3	2 7	2 5	3 2
Ta	1 7	2.6	2 7	2 2	1 1	1 3	3 8	1 1	3 1	2	4 5	2 7
Co	-	-	-	-	-	-	-	-	-	-	-	-
Li	126	124	67	192	55	47	83	88	127	135	190	172
Be	-	-	-	-	-	-	-	-	-	-	-	-
B	14	14	16	11	-	15	19	14	20	20	25	11
U	3 9	5 3	22 1	5 2	3	5 4	14	6 3	7 1	3 3	13	11
W	1	4	6	2	1	2	9	-	6	3	7	5
Sn	10	21	25	9	9	5	33	4	30	14	22	16
Mo	-	-	-	-	-	-	-	-	-	-	-	-
Rare-earths												
La	16	7	2	11	27	8	-	26	-	17	5	7
Ce	-	-	-	-	-	-	-	-	-	-	-	-
Pr	-	-	-	-	-	-	-	-	-	-	-	-
Nd	-	-	-	-	-	-	-	-	-	-	-	-
Sm	-	-	-	-	-	-	-	-	-	-	-	-
Eu	-	-	-	-	-	-	-	-	-	-	-	-
Gd	-	-	-	-	-	-	-	-	-	-	-	-
Tb	-	-	-	-	-	-	-	-	-	-	-	-
Dy	-	-	-	-	-	-	-	-	-	-	-	-
Ho	-	-	-	-	-	-	-	-	-	-	-	-
Er	-	-	-	-	-	-	-	-	-	-	-	-
Tm	-	-	-	-	-	-	-	-	-	-	-	-
Yb	-	-	-	-	-	-	-	-	-	-	-	-
Lu	-	-	-	-	-	-	-	-	-	-	-	-

Table E1 1 (Continued) Compilation of Meguma Zone granitoid lithogeochemistry

Sample	A10-3004	A10-3005	A10-3006	A10-3008	A10-3008-C	A10-3009-1	A10-3012	A10-3014	A10-3017-2	A10-3020	A10-3021-C	A10-3025
Batholith	SMB	SMB	SMB	SMB	SMB	SMB	SMB	SMB	SMB	SMB	SMB	SMB
Pluton	StLP	StLP	StLP	PLP	PLP	StLP	PLP	StLP	NRP	NRP	WaP	NRP
Lithology	Mzg	Mzg	Mzg	Lmzg	Lmzg	Mzg	Lmzg	Mzg	Lmzg	Lmzg	Lmzg	Lmzg
Source	·27	27	27	27	27	27	27	27	27	27	27	27
Major oxides												
SiO_2	69 04	68 75	68 52	74 69	74 82	68 93	74 00	68 25	74 11	73 12	72 06	72 31
TiO_2	0 59	0 61	0 68	0 11	0 08	0 56	0 09	0 62	0 11	0 19	0 22	0 25
Al_2O_3	14 42	14 74	14 67	13 86	13 87	14 92	14 52	14 98	14 11	14 33	15 11	14 72
Fe_2O_3	-	-	-	-	-	-	-	-	-	-	-	-
FeO	-	-	-	-	-	-	-	-	-	-	-	-
MnO	0 09	0 09	0 10	0 04	0 03	0 08	0 04	0 08	0 02	0 04	0 04	0 06
MgO	1 51	1 52	1 66	0 80	0 68	1 55	0 81	1 53	0 80	0 87	1 09	1 17
CaO	1 40	1 56	1 79	0 30	0 27	1 75	0 40	1 70	0 31	0 36	0 56	0 85
Na_2O	3 45	2 83	3 17	3 54	3 46	2 97	3 67	3 87	2 98	3 46	3 17	3 43
K_2O	3 95	4 19	3 44	4 64	4 45	4 09	4 39	3 98	4 91	4 53	4 83	4 46
P_2O_5	0 22	0 21	0 24	0 26	0 28	0 19	0 30	0 24	0 28	0 27	0 31	0 22
H_2O+	-	-	-	-	-	-	-	-	-	-	-	-
H_2O-	-	-	-	-	-	-	-	-	-	-	-	-
CO_2	-	-	-	-	-	-	-	-	-	-	-	-
Cl	-	-	-	-	-	-	-	-	-	-	-	-
F	0 06	0 06	0 07	0 13	0 10	0 05	0 02	0 06	0 10	0 09	0 05	0 05
LOI	0 70	0 49	0 70	0 60	0 63	0 24	0 40	0 50	0 73	0 63	0 53	0 54
TOTAL	99 06	98 87	99 22	100 17	99 78	98 85	99 61	99 61	99 50	99 40	99 38	99 77
Fe_2O_3T	4 10	4 31	4 72	1 48	1 35	3 97	1 10	4 29	1 27	1 78	1 62	1 96
FeOT	3 69	3 88	4 25	1 33	1 21	3 57	0 99	3 86	1 14	1 60	1 46	1 76
A/CNK	1 12	1 17	1 20	1 10	1 14	1 15	1 16	1 07	1 15	1 15	1 18	1 14
Trace els												
Ba	511	547	496	67	30	552	207	569	140	173	341	254
Rb	157	164	154	347	386	158	187	160	353	303	246	210
Sr	138	127	132	17	8	126	54	141	29	43	61	76
Y	32	35	34	17	23	34	14	29	20	24	18	22
Zr	197	185	216	61	47	165	40	193	54	73	81	86
Nb	13	11	13	12	11	11	10	12	10	12	10	9
Th	12	12	12	5 6	4 2	11	1 2	11	6 1	6 3	10	7 7
Pb	23	13	20	27	14	18	28	21	16	27	23	22
Ga	20	16	26	20	22	16	19	21	20	18	17	17
Zn	72	60	77	43	66	58	78	75	44	49	53	49
Cu	6	8	-	-	57	8	-	-	-	-	-	-
Ni	-	-	-	-	-	-	-	-	-	-	-	-
V	41	16	54	4	-	42	5	45	-	8	12	12
Cr	-	-	-	-	-	-	-	-	-	-	-	-
Hf	6	6	7	1	2	6	1	6	2	3	3	2
Cs	-	-	-	-	-	-	-	-	-	-	-	-
Sc	9 4	11	10	2.5	2.3	10	4 5	9 3	2 2	3 5	3 4	4 5
Ta	12	1 5	0 8	1 2	2.5	1	2.4	1 6	2 2	2 3	1 7	1 4
Co	-	-	-	-	-	-	-	-	-	-	-	-
Li	88	79	94	162	87	40	34	113	35	36	28	48
Be	-	-	-	-	-	-	-	-	-	-	-	-
B	25	29	20	30	12	27	40	30	25	30	30	17
U	3	4 7	3 6	11	7 6	3 7	1 5	2 9	3 5	4 3	4	3
W	1	1	1	4	6	-	5	2	3	8	4	-
Sn	11	5	6	21	22	1	12	9	13	22	11	10
Mn	-	-	-	-	-	-	-	-	-	-	-	-
Rare-earths												
La	32	32	33	8	4	30	5	30	9	11	15	15
Ce	-	-	-	-	-	-	-	-	-	-	-	-
Pr	-	-	-	-	-	-	-	-	-	-	-	-
Nd	-	-	-	-	-	-	-	-	-	-	-	-
Sm	-	-	-	-	-	-	-	-	-	-	-	-
Eu	-	-	-	-	-	-	-	-	-	-	-	-
Gd	-	-	-	-	-	-	-	-	-	-	-	-
Tb	-	-	-	-	-	-	-	-	-	-	-	-
Dy	-	-	-	-	-	-	-	-	-	-	-	-
Ho	-	-	-	-	-	-	-	-	-	-	-	-
Er	-	-	-	-	-	-	-	-	-	-	-	-
Tm	-	-	-	-	-	-	-	-	-	-	-	-
Yb	-	-	-	-	-	-	-	-	-	-	-	-
Lu	-	-	-	-	-	-	-	-	-	-	-	-

Table E1 1 (Continued) Compilation of Meguma Zone granitoid lithogeochemistry

Sample	A10-3033	A10-3037-C	A10-3040	A10-3040-C	A10-3052	A10-3054	A10-3056	A10-3057	A10-3057-C	A10-3060	A10-3071-G	A10-3074
Batholith	SMB	SMB	SMB	SMB	SMB	SMB	SMB	SMB	SMB	SMB	SMB	SMB
Pluton	NRP	WLP	NCP	NCP	-	EDP	EDP	EDP	EDP	EDP	WLP	EDP
Lithology	Lmzg	Mzg	Lmzg	Lmzg	MPOR	Lmzg	Lmzg	Lmzg	Lmzg	Lmzg	Mzg	Lmzg
Source	27	27	27	27	27	27	27	27	27	27	27	27
Major oxides												
SiO_2	72.95	70 56	73 17	73 16	67 22	74 05	74 70	74 46	74 06	73 79	72 47	74 38
TiO_2	0 33	0 38	0 27	0 30	0 87	0 06	0 07	0 09	0 09	0 03	0 18	0 07
Al_2O_3	13 70	15 03	13 83	14 00	15 36	14 51	14 45	14 03	14 30	14 57	14 73	14 36
Fe_2O_3	-	-	-	-	-	-	-	-	-	-	-	-
FeO	-	-	-	-	-	-	-	-	-	-	-	-
MnO	0 05	0 06	0 05	0 05	0 07	0 04	0 04	0 03	0 05	0 02	0 08	0 03
MgO	1 12	1 31	1 18	1 15	1 78	0 73	0 78	0 80	0 85	0 65	0 83	0 69
CaO	0 61	0 93	0 38	0 51	1 26	0 30	0 28	0 24	0 33	0 25	0 63	0 32
Na_2O	2.80	3 39	2 97	3 06	3 21	3 71	3 22	3 65	3 95	3 45	3 74	3 29
K_2O	4 76	4 44	4 91	4 96	4 25	4 20	4 28	4 33	4 17	4 29	4 25	4 57
P_2O_5	0 22	0 26	0 22	0 23	0 21	0 36	0 32	0 29	0 38	0 44	0 31	0 29
H_2O+	-	-	-	-	-	-	-	-	-	-	-	-
H_2O-	-	-	-	-	-	-	-	-	-	-	-	-
CO_2	-	-	-	-	-	-	-	-	-	-	-	-
Cl	-	-	-	-	-	-	-	-	-	-	-	-
F	0 10	0 06	0 02	0 02	0 07	0 18	0 20	0 11	0 32	0 17	0 04	0 05
LOI	0 47	0 55	0 85	0 37	0 67	0 46	0 70	0 23	0 80	0 63	0 43	0 47
TOTAL	99 30	99 33	99 41	99 56	98 83	99 43	99 77	99 19	100 07	99 03	99 12	99 60
Fe_2O_3T	2 54	2 69	1 76	1 97	4 37	1 12	1 03	1 16	1 21	1 01	1 66	1 15
FeOT	2.29	2.42	1 58	1 77	3 93	1 01	0 93	1 04	1 09	0 91	1 49	1 03
A/CNK	1 12	1 16	1 12	1 10	1 19	1 19	1 25	1 15	1 14	1 22	1 15	1 18
Trace els												
Ba	249	443	334	382	888	26	6	41	23	18	215	12
Rb	261	227	200	203	153	567	497	430	506	668	220	304
Sr	61	98	41	49	132	-	3	10	8	11	55	9
Y	26	25	17	19	32	27	18	26	19	29	18	24
Zr	121	124	92	99	222	34	37	41	42	14	63	39
Nb	11	10	6	7	9	15	13	13	15	23	9	12
Th	12	12	15	17	16	2 2	2 5	3 8	3 5	1 1	4 4	3
Pb	16	13	24	15	12	25	20	19	26	-	20	20
Ga	19	18	17	17	19	25	28	21	24	29	16	21
Zn	57	65	24	32	70	51	46	47	65	56	41	29
Cu	-	5	26	22	8	-	-	-	-	-	-	13
Ni	-	-	-	-	-	-	-	-	-	-	-	-
V	16	24	9	10	69	-	2	-	1	-	10	-
Cr	-	-	-	-	-	-	-	-	-	-	-	-
Hf	4	4	3	4	6	2	1	2	1	-	2	2
Cs	-	-	-	-	-	-	-	-	-	-	-	-
Sc	4 8	6 2	3 9	3 9	9 4	2 1	2.6	3 1	2 4	2 6	4 1	2 8
Ta	1 8	1 3	1 1	1 1	1 1	5 1	13	3 3	3 2	3 8	1 9	2
Co	-	-	-	-	-	-	-	-	-	-	-	-
Li	39	38	10	19	31	76	254	73	341	70	91	47
Be	-	-	-	-	-	-	-	-	-	-	-	-
B	15	17	13	10	19	21	30	27	25	19	16	15
U	2 9	5 1	6 1	5 6	4 1	4	2 4	5	4 1	1 9	5 2	7 6
W	1	-	3	-	-	8	8	6	10	6	3	2
Sn	11	4	9	10	2	39	30	26	48	24	21	13
Mo	-	-	-	-	-	-	-	-	-	-	-	-
Rare-earths												
La	20	22	19	22	38	-	3	3	4	-	9	3
Ce	-	-	-	-	-	-	-	-	-	-	-	-
Pr	-	-	-	-	-	-	-	-	-	-	-	-
Nd	-	-	-	-	-	-	-	-	-	-	-	-
Sm	-	-	-	-	-	-	-	-	-	-	-	-
Eu	-	-	-	-	-	-	-	-	-	-	-	-
Gd	-	-	-	-	-	-	-	-	-	-	-	-
Tb	-	-	-	-	-	-	-	-	-	-	-	-
Dy	-	-	-	-	-	-	-	-	-	-	-	-
Ho	-	-	-	-	-	-	-	-	-	-	-	-
Er	-	-	-	-	-	-	-	-	-	-	-	-
Tm	-	-	-	-	-	-	-	-	-	-	-	-
Yb	-	-	-	-	-	-	-	-	-	-	-	-
Lu	-	-	-	-	-	-	-	-	-	-	-	-

Table E1 1 (Continued) Compilation of Meguma Zone granitoid lithogeochemistry

Sample	A10-3077	A10-3078	A10-3079	A10-3082	A10-3085-C	A10-3056	A10-3087	A10-3087-2	A10-3093	A10-3095-C	A10-3098-C	A10-3100
Batholith	SMB	SMB	SMB	SMB	SMB	SMB	SMB	SMB	SMB	SMB	SMB	SMB
Pluton	WLP	WLP	ScLP	EDP	ScLP	ScLP	LGP	LGP	EDP	EDP	ScLP	LGP
Lithology	Mzg	Mzg	Grd	Lmzg	Grd	Grd	Lmzg	Lmzg	Lmzg	Lmzg	Grd	Lmzg
Source	27	27	27	27	27	27	27	27	27	27	27	27
Major oxides												
SiO_2	70 20	69 95	67 15	73 39	66 75	68 39	72 60	72 03	72 56	72 25	66 88	73 01
TiO_2	0 40	0 38	0 73	0 16	0 74	0 64	0 19	0 23	0 19	0 19	0 71	0 20
Al_2O_3	15 21	15 21	14 95	14 64	15 15	15 06	14 78	14 96	14 70	14 91	15 37	14 40
Fe_2O_3	-	-	-	-	-	-	-	-	-	-	-	-
FeO	-	-	-	-	-	-	-	-	-	-	-	-
MnO	0 05	0 06	0 09	0 04	0 10	0 08	0 05	0 05	0 05	0 05	0 10	0 05
MgO	1 41	1 24	1 68	0 92	1 78	1 63	0 97	0 99	1 10	1 01	1 77	0 88
CaO	1 01	1 04	2 08	0 48	2.01	1 71	0 71	0 70	0 40	0 35	2.04	0 60
Na_2O	3 19	3 51	3 14	3 48	3 42	3 07	3 41	3 72	3 04	3 70	3 24	3 18
K_2O	4 34	4 39	3 61	4 51	3 77	4 02	4 69	5 03	4 69	4 87	3 61	4 78
P_2O_5	0 23	0 25	0 22	0 31	0 22	0 16	0 24	0 25	0 24	0 27	0 22	0 22
H_20+	-	-	-	-	-	-	-	-	-	-	-	-
H_2O-	-	-	-	-	-	-	-	-	-	-	-	-
CO_2	-	-	-	-	-	-	-	-	-	-	-	-
Cl	-	-	-	-	-	-	-	-	-	-	-	-
F	0 06	0 06	0 07	0 11	0 06	0 05	0 11	0 10	0 05	0 06	0 05	0 09
LOI	0 49	0 48	0 47	0 34	0 33	0 69	0 35	0 24	0 73	0 80	0 65	0 25
TOTAL	99 06	98 92	98 59	99 66	98 86	99 27	99 65	99 94	99 05	99 79	99 04	99 28
Fe_2O_3T	2 81	2 68	4 97	1 57	5 10	4 24	1 85	1 93	1 50	1 55	4 94	1 90
FeOT	2 53	2.41	4 47	1 41	4 59	3 82	1 66	1 74	1 35	1 39	4 45	1 71
A/CNK	1 20	1 15	1 16	1 16	1 13	1 17	1 13	1 06	1 21	1 12	1 19	1 13
Trace els												
Ba	450	476	625	174	634	702	185	285	233	249	630	239
Rb	210	219	145	353	149	134	287	272	247	273	144	256
Sr	98	98	156	37	152	153	45	54	50	46	162	44
Y	25	25	36	24	35	31	27	24	20	18	35	25
Zr	127	126	229	67	213	197	87	83	79	75	211	84
Nb	11	9	12	11	13	11	10	10	11	11	12	9
Th	13	13	14	10	13	15	7 8	17	10	10	14	12
Pb	13	18	10	24	14	16	15	13	11	18	10	-
Ga	19	18	20	23	19	19	19	19	17	18	20	18
Zn	59	59	70	52	68	66	52	50	44	46	72	51
Cu	7	-	9	-	9	10	-	-	-	-	15	-
Ni	-	-	-	-	-	-	-	-	-	-	-	-
V	27	29	68	-	61	45	5	11	7	9	74	8
Cr	-	-	-	-	-	-	-	-	-	-	-	-
Hf	5	4	7	2	7	7	3	2	2	2	7	3
Cs	-	-	-	-	-	-	-	-	-	-	-	-
Sc	6 5	5 9	13	3	13	11	3 2	2 8	2.6	3 1	13	3 1
Ta	1 1	1 5	1 4	2 6	1 3	1 2	1 8	2	1 4	1 6	1 1	1 6
Co	-	-	-	-	-	-	-	-	-	-	-	-
Li	83	89	67	161	66	56	85	58	75	89	50	91
Be	-	-	-	-	-	-	-	-	-	-	-	-
B	16	15	12	15	-	12	14	12	19	19	12	12
U	3 3	5 5	3 2	11	3 8	3 4	5 1	4 1	3 4	4 5	2 8	6 2
W	-	-	1	5	-	-	-	-	1	3	-	-
Sn	11	12	6	18	3	9	14	10	10	13	2	7
Mo	-	-		-	-	-	-	-	-	-	-	-
Rare-earths												
La	23	23	38	11	38	37	13	19	13	16	39	16
Ce	-	-	-	-	-	-	-	-	-	-	-	-
Pr	-	-	-	-	-	-	-	-	-	-	-	-
Nd	-	-	-	-	-	-	-	-	-	-	-	-
Sm	-	-	-	-	-	-	-	-	-	-	-	-
Eu	-	-	-	-	-	-	-	-	-	-	-	-
Gd	-	-	-	-	-	-	-	-	-	-	-	-
Tb	-	-	-	-	-	-	-	-	-	-	-	-
Dy	-	-	-	-	-	-	-	-	-	-	-	-
Ho	-	-	-	-	-	-	-	-	-	-	-	-
Er	-	-	-	-	-	-	-	-	-	-	-	-
Tm	-	-	-	-	-	-	-	-	-	-	-	-
Yb	-	-	-	-	-	-	-	-	-	-	-	-
Lu	-	-	-	-	-	-	-	-	-	-	-	-

Table E1.1 (Continued) Compilation of Meguma Zone granitoid lithogeochemistry

Sample	A10-3100-1	A10-3105	A10-3106	A10-3107	A10-3107-G	A10-3108-C	A10-3109-G	A10-3120-C	A10-3121	A10-3121-1	A10-3122	A10-3129-1
Batholith	SMB	SMB	SMB	SMB	SMB	SMB	SMB	SMB	SMB	SMB	SMB	SMB
Pluton	LGP	ScLP	ScLP	JSP	JSP	LRoP	LRoP	LGP	LRoP	EDP	LRoP	EDP
Lithology	Lmzg	Grd	Grd	Mzg	Mzg	Mzg	Mzg	Lmzg	Mzg	Lmzg	Mzg	Lmzg
Source	27	27	27	27	27	27	27	27	27	27	27	27
Major oxides												
SiO_2	72.74	66.47	65.76	72.64	73.21	68.88	71.23	71.90	71.36	74.32	73.09	73.52
TiO_2	0.21	0.77	0.80	0.21	0.20	0.50	0.42	0.23	0.36	0.12	0.27	0.12
Al_2O_3	14.68	15.23	15.49	14.21	14.12	15.18	14.15	14.82	14.39	14.10	13.97	14.54
Fe_2O_3	-	-	-	-	-	-	-	-	-	-	-	-
FeO	-	-	-	-	-	-	-	-	-	-	-	-
MnO	0.05	0.10	0.10	0.04	0.03	0.08	0.08	0.04	0.07	0.04	0.07	0.06
MgO	0.86	1.79	1.84	0.90	0.98	1.36	1.23	1.02	1.11	0.63	1.06	0.78
CaO	0.59	2.11	2.35	0.58	0.53	1.56	1.14	0.55	0.59	0.37	0.52	0.47
Na_2O	3.08	3.44	3.34	3.01	3.01	3.26	2.93	3.34	2.84	3.33	2.93	3.78
K_2O	4.91	3.62	3.72	5.36	5.39	4.19	4.02	4.90	4.63	4.34	4.54	4.36
P_2O_5	0.22	0.22	0.24	0.17	0.18	0.22	0.18	0.29	0.22	0.34	0.22	0.30
H_2O+	-	-	-	-	-	-	-	-	-	-	-	
H_2O-	-	-	-	-	-	-	-	-	-	-	-	-
CO_2	-	-	-	-	-	-	-	-	-	-	-	-
Cl	-	-	-	-	-	-	-	-	-	-	-	-
F	0.10	0.07	0.08	0.05	0.04	0.08	0.06	0.12	0.09	0.14	0.04	0.03
LOI	0.35	0.23	0.42	0.44	0.51	0.40	0.59	0.76	0.83	0.74	0.97	0.52
TOTAL	99.46	98.61	98.88	99.25	99.85	98.86	98.86	99.38	98.94	99.50	99.68	99.66
Fe_2O_3T	1.97	5.15	5.36	1.88	1.88	3.59	3.21	1.70	2.82	1.30	2.27	1.34
FeOT	1.77	4.63	4.82	1.69	1.69	3.23	2.89	1.53	2.54	1.17	2.04	1.21
A/CNK	1.15	1.14	1.13	1.06	1.05	1.15	1.18	1.13	1.20	1.18	1.17	1.14
Trace els												
Ba	252	623	795	462	426	521	394	323	389	124	263	174
Rb	262	143	149	210	215	176	177	306	263	393	226	228
Sr	45	160	171	76	64	123	102	52	78	15	59	39
Y	24	41	41	20	19	35	34	21	32	22	26	17
Zr	87	228	239	112	117	160	145	91	126	48	93	48
Nb	10	13	13	11	11	10	9	13	11	16	10	9
Th	13	14	15	12	11	12	10	14	12	5.2	7.1	2.6
Pb	20	12	13	18	19	22	17	16	17	21	20	18
Ga	18	21	19	17	17	20	16	19	18	21	16	16
Zn	50	72	69	38	43	59	51	48	85	40	55	23
Cu	-	8	12	-	5	5	-	-	31	7	10	-
Ni	-	-	-	-	-	-	-	-	-	-	-	-
V	10	68	72	-	10	34	34	7	24	5	19	-
Cr	-	-	-	-	-	-	-	-	-	-	-	-
Hf	3	8	8	4	4	5	4	3	4	-	3	-
Cs	-	-	-	-	-	-	-	-	-	-	-	-
Sc	3.5	14	14	2.9	3.7	9	7.9	3.3	6.3	2.7	4.8	2.6
Ta	1.6	1.4	1.4	1.4	1	1.2	1.1	2.1	1.6	3.2	1.5	1.6
Co	-	-	-	-	-	-	-	-	-	-	-	-
Li	99	66	50	18	30	73	66	93	84	63	67	120
Be	-	-	-	-	-	-	-	-	-	-	-	-
B	11	-	-	17	13	10	15	25	23	19	24	35
U	6.5	2.5	2.3	5.1	4.3	2.9	2.6	4.6	6.1	7.3	4.5	4.1
W	2	-	1	1	2	2	-	4	6	7	3	1
Sn	6	4	4	7	4	9	7	17	15	29	10	10
Mo	-	-	-	-	-	-	-	-	-	-	-	-
Rare-earths												
La	17	41	44	21	19	28	25	19	24	6	14	6
Ce	-	-	-	-	-	-	-	-	-	-	-	-
Pr	-	-	-	-	-	-	-	-	-	-	-	-
Nd	-	-	-	-	-	-	-	-	-	-	-	-
Sm	-	-	-	-	-	-	-	-	-	-	-	-
Eu	-	-	-	-	-	-	-	-	-	-	-	-
Gd	-	-	-	-	-	-	-	-	-	-	-	-
Tb	-	-	-	-	-	-	-	-	-	-	-	-
Dy	-	-	-	-	-	-	-	-	-	-	-	-
Ho	-	-	-	-	-	-	-	-	-	-	-	-
Er	-	-	-	-	-	-	-	-	-	-	-	-
Tm	-	-	-	-	-	-	-	-	-	-	-	-
Yb	-	-	-	-	-	-	-	-	-	-	-	-
Lu	-	-	-	-	-	-	-	-	-	-	-	-

Table E1 1 (Continued) Compilation of Meguma Zone granitoid lithogeochemistry

Sample	A10-3136-1	A10-3140	A10-3144	A10-3147	A10-3149	A10-3158	A15-0002	A15-0003	A15-0007	\15-0007-2	.\15-0007-2-I	A15-0008
Batholith	SMB	SMB	SMB	SMB	SMB	SMB	SMB	SMB	SMB	SMB	SMB	SMB
Pluton	LRoP	LRoP	LRoP	LRoP	ScLP	LRoP	LGP	LGP	GLP	GLP	GLP	MuLP
Lithology	Mzg	Mzg	Mzg	Mzg	Grd	Mzg	Lmzg	Lmzg	Grd	Grd	Grd	Lg
Source	27	27	27	27	27	27	27	27	27	27	27	27
Major oxides												
SiO_2	70 31	71 37	70 59	74 30	68 23	69 03	72 95	71 49	66 71	65 36	68 33	72 20
TiO_2	0 45	0 34	0 41	0 24	0 53	0 60	0 17	0 24	0 76	0 84	0 66	0 01
Al_2O_3	14 50	14 46	14 51	13 34	14 62	15 10	14 55	15 12	15 40	15 44	14 83	15 43
Fe_2O_3	-	-	-	-	-	-	-	-	-	-	-	-
FeO	-	-	-	-	-	-	-	-	-	-	-	-
MnO	0 08	0 09	0 08	0 07	0 07	0 09	0 04	0 04	0 09	0 10	0 08	0 03
MgO	1 32	1 24	1 27	1 00	1 51	1 39	0 91	0 90	1 87	1 95	1 64	0 72
CaO	1 36	0 78	1 15	0 49	1 75	1 12	0 51	0 46	1 90	2 28	1 96	0 43
Na_2O	3 43	3 41	3 48	2 79	3 64	2.96	3 31	3 15	3 06	3 21	2 96	3 58
K_2O	4 19	4 48	4 09	4 58	3 96	4 38	4 96	5 41	3 85	3 76	3 59	4 33
P_2O_5	0 18	0 21	0 25	0 18	0 18	0 22	0 26	0 28	0 21	0 25	0 19	0 67
H_20+	-	-	-	-	-	-	-	-	-	-	-	-
H_2O-	-	-	-	-	-	-	-	-	-	-	-	-
CO_2	-	-	-	-	-	-	-	-	-	-	-	-
Cl	-	-	-	-	-	-	-	-	-	-	-	-
F	0 05	0 08	0 06	0 03	0 06	0 05	0 12	0 16	0 07	0 05	0 08	0 23
LOI	0 60	0 74	0 55	0 40	0 57	0 55	0 80	0 70	0 70	0 55	0 42	0 80
TOTAL	99 51	99 57	99 17	99 13	98 51	98 71	99 96	99 62	98 91	98 72	98 66	99 13
Fe_2O_3T	3 43	2.72	3 10	1 93	3 83	3 74	1 67	2 03	4 84	5 54	4 45	1 03
FeOT	3 09	2 45	2.79	1 74	3 45	3 37	1 50	1 83	4 36	4 98	4 00	0 93
A/CNK	1 10	1 12	1 13	1 13	1 07	1 21	1 11	1 12	1 19	1 15	1 19	1 25
Trace els												
Ba	489	297	388	193	505	502	172	230	781	775	[illegible]	37
Rb	171	231	194	176	158	182	310	361	145	143	138	843
Sr	109	65	96	52	[illegible]	116	37	40	151	177	158	14
Y	34	29	31	24	35	41	19	21	31	36	35	22
Zr	150	111	133	88	170	155	83	104	234	227	212	23
Nb	12	11	11	7	11	11	13	16	14	13	12	30
Th	10	11	8 7	5 6	11	9 4	12	15	15	12	13	12
Pb	18	13	16	17	12	17	23	30	28	12	-	17
Ga	17	18	18	13	16	18	26	26	20	18	16	33
Zn	57	52	50	23	61	64	53	66	87	76	67	72
Cu	-	10	-	15	5	5	-	-	2	10	10	-
Ni	-	-	-	-	-	-	-	-	-	-	-	-
V	34	19	23	15	39	35	7	6	62	70	64	1
Cr	-	-	-	-	-	-	-	-	-	-	-	-
Hf	6	5	4	3	6	4	3	3	8	8	6	4
Cs	-	-	-	-	-	-	-	-	-	-	-	-
Sc	8 3	6 9	7 6	4 7	9 3	10	2.1	2.6	12	14	11	5 8
Ta	1 2	1 6	2	1 1	1 2	1 1	4 8	2 1	1 9	0 9	1 2	0 9
Co	-	-	-	-	-	-	-	-	-	-	-	-
Li	66	92	78	29	53	85	138	164	116	55	76	205
Be	-	-	-	-	-	-	-	-	-	-	-	-
B	-	15	12	15	-	17	25	30	20	15	12	30
U	3 5	3 1	2 9	4 8	3 3	3 7	4 2	6 6	3 5	2.1	2	2 6
W	-	2	2	5	-	2	3	3	3	-	-	2
Sn	9	4	6	11	6	12	15	18	7	-	2	28
Mo	-	-	-	-	-	-	-	-	-	-	-	-
Rare-earths												
La	26	22	22	11	30	26	16	21	43	38	39	25
Ce	-	-	-	-	-	-	-	-	-	-	-	-
Pr	-	-	-	-	-	-	-	-	-	-	-	-
Nd	-	-	-	-	-	-	-	-	-	-	-	-
Sm	-	-	-	-	-	-	-	-	-	-	-	-
Eu	-	-	-	-	-	-	-	-	-	-	-	-
Gd	-	-	-	-	-	-	-	-	-	-	-	-
Tb	-	-	-	-	-	-	-	-	-	-	-	-
Dy	-	-	-	-	-	-	-	-	-	-	-	-
Ho	-	-	-	-	-	-	-	-	-	-	-	-
Er	-	-	-	-	-	-	-	-	-	-	-	-
Tm	-	-	-	-	-	-	-	-	-	-	-	-
Yb	-	-	-	-	-	-	-	-	-	-	-	-
Lu	-	-	-	-	-	-	-	-	-	-	-	-

Table E1.1 (Continued) Compilation of Meguma Zone granitoid lithogeochemistry

Sample	A15-0008-3	A15-0008-4	A15-0014-2	A15-0014-3	A15-0014-4	A15-0014-5	A15-0015	A15-0016	A15-0018	A15-0019	A15-0020	A15-0020-2
Batholith	SMB	SMB	SMB	SMB	SMB	SMB	SMB	SMB	SMB	SMB	SMB	SMB
Pluton	MuLP	MuLP	MuLP	MuLP	MuLP	GLP	GLP	GLP	MuLP	StLP	MuLP	MuLP
Lithology	Lg	Lg	Lg	Lg	Lg	Grd	Grd	Grd	Lg	Mzg	Lg	Lg
Source	27	27	27	27	27	27	27	27	27	27	27	27
Major oxides												
SiO_2	72.56	72.20	73.30	73.44	73.95	67.62	67.72	67.30	74.05	69.48	74.21	72.97
TiO_2	0.02	0.02	0.07	0.08	0.05	0.62	0.72	0.67	0.09	0.17	0.08	0.02
Al_2O_3	15.29	15.50	14.99	14.24	14.43	15.38	15.03	15.55	13.79	[illegible]	14.13	15.01
Fe_2O_3	-	-	-	-	-	-	-	-	-		-	-
FeO	-	-	-	-	-	-	-	-	-		-	-
MnO	0.04	0.04	0.04	0.03	0.03	0.09	0.08	0.08	0.03	0.09	0.04	0.05
MgO	0.66	0.63	0.84	0.77	0.71	1.72	1.77	1.72	0.87	1.51	0.79	0.82
CaO	0.57	0.60	0.50	0.30	0.35	1.37	2.07	2.05	0.38	1.35	0.38	0.73
Na_2O	3.97	4.20	3.69	4.02	3.29	3.10	3.37	3.02	3.19	3.40	3.41	4.69
K_2O	3.46	3.48	3.82	4.35	4.30	4.18	3.53	3.92	4.35	4.10	4.40	3.16
P_2O_5	0.69	0.71	0.48	0.36	0.35	0.24	0.18	0.20	0.29	0.21	0.36	0.72
H_2O+	-	-	-	-	-	-	-	-	-	-	-	-
H_2O-	-	-	-	-	-	-	-	-	-	-	-	-
CO_2	-	-	-	-	-	-	-	-	-	-	-	-
Cl	-	-	-	-	-	-	-	-	-	-	-	-
F	0.26	0.27	0.21	0.15	0.16	0.22	0.09	0.07	0.15	0.07	0.19	0.21
LOI	0.91	0.81	1.11	0.87	0.77	0.58	0.52	0.30	0.80	0.60	0.84	0.90
TOTAL	99.30	99.22	99.96	99.43	99.18	98.85	99.39	98.97	99.09	99.36	100.05	100.13
Fe_2O_3T	1.26	1.15	1.25	1.08	1.06	4.39	4.89	4.62	1.39	3.53	1.57	1.18
FeOT	1.13	1.03	1.12	0.97	0.95	3.95	4.40	4.16	1.25	3.18	1.41	1.06
A/CNK	1.30	1.28	1.27	1.11	1.22	1.21	1.15	1.18	1.17	1.15	1.16	1.20
Trace els												
Ba	14	24	15	54	33	752	643	770	47	472	42	25
Rb	745	737	650	497	539	303	144	144	396	183	473	613
Sr	21	24	10	10	7	146	151	166	16	131	17	12
Y	34	36	34	27	25	47	43	28	19	26	27	28
Zr	42	16	34	33	23	182	237	220	51	158	40	18
Nb	29	28	30	16	18	13	14	14	13	11	16	34
Th	1.7	1.1	2.1	4.4	1.9	12	16	14	5	10	3.6	1.5
Pb	14	-	12	13	-	15	20	23	14	27	11	-
Ga	34	32	31	24	24	19	16	25	23	22	20	33
Zn	75	77	51	36	27	103	69	79	39	72	63	44
Cu	-	-	8	-	-	13	11	6	-	-	-	-
Ni	-	-	-	-	-	-	-	-	-	-	-	-
V	-	7	-	-	-	53	58	56	1	36	-	-
Cr	-	-	-	-	-	-	-	-	-	-	-	-
Hf	4	-	-	1	-	5	7	8	1	6	1	1
Cs	-	-	-	-	-	-	-	-	-	-	-	-
Sc	1.7	1.4	5.4	2.1	2.2	9.3	11	11	1.9	7.9	1.6	1.8
Ta	5	4.1	5.9	3	4.2	1.7	1.5	2.6	1.1	1.2	3.3	8.2
Co	-	-	-	-	-	-	-	-	-	-	-	-
Li	205	205	173	134	97	220	54	65	122	100	153	92
Be	-	-	-	-	-	-	-	-	-	-	-	-
B	12	12	15	13	12	16	26	20	30	35	14	16
U	3.8	2.6	2.5	2.2	1.7	3.1	2.8	2.7	4	3.5	2.2	1.9
W	8	8	8	5	6	2	2	1	4	2	4	8
Sn	26	27	29	25	23	11	-	4	21	6	20	28
Mo	-	-	-	-	-	-	-	-	-	-	-	-
Rare-earths												
La	-	-	-	6	2	30	38	39	5	26	5	-
Ce	-	-	-	-	-	-	-	-	-	-	-	-
Pr	-	-	-	-	-	-	-	-	-	-	-	-
Nd	-	-	-	-	-	-	-	-	-	-	-	-
Sm	-	-	-	-	-	-	-	-	-	-	-	-
Eu	-	-	-	-	-	-	-	-	-	-	-	-
Gd	-	-	-	-	-	-	-	-	-	-	-	-
Tb	-	-	-	-	-	-	-	-	-	-	-	-
Dy	-	-	-	-	-	-	-	-	-	-	-	-
Ho	-	-	-	-	-	-	-	-	-	-	-	-
Er	-	-	-	-	-	-	-	-	-	-	-	-
Tm	-	-	-	-	-	-	-	-	-	-	-	-
Yb	-	-	-	-	-	-	-	-	-	-	-	-
Lu	-	-	-	-	-	-	-	-	-	-	-	-

Table E1 1 (Continued) Compilation of Meguma Zone granitoid lithogeochemistry

Sample	A15-0027	A15-0035	A15-0041	A15-0044-2	A15-0044-3	A15-0046	A15-0046-2	A15-0046-3	A15-0049	A15-0050	A15-0050-2	A15-0054
Batholith	SMB	SMB	SMB	SMB	SMB	SMB	SMB	SMB	SMB	SMB	SMB	SMB
Pluton	MuLP	GLP	MuLP	EDP	EDP	EDP	EDP	EDP	ScLP	ScLP	ScLP	LGP
Lithology	Lg	Grd	Lg	Lmzg	Lmzg	Lmzg	Lmzg	Lmzg	Grd	Grd	Grd	Lmzg
Source	27	27	27	27	27	27	27	27	27	27	27	27
Major oxides												
SiO_2	74 99	66 27	73 55	74 37	73 35	74 40	75 12	73 03	66 87	68 09	66 20	74 18
TiO_2	0 04	0 75	0 04	0 10	0 08	0 07	0 10	0 13	0 75	0 79	0 83	0 11
Al_2O_3	14 18	15 39	14 66	14 40	14 02	14 15	14 16	14 11	14 96	14 07	15 19	14 03
Fe_2O_3	-	-	-	-	-	-	-	-	-	-	-	-
FeO	-	-	-	-	-	-	-	-	-	-	-	-
MnO	0 03	0 08	0 04	0 03	0 04	0 04	0 05	0 03	0 10	0 13	0 12	0 03
MgO	0 74	1 88	0 61	0 74	0 81	0 84	0 85	0 84	1 77	1 86	1 83	0 78
CaO	0 37	2 14	0 45	0 30	0 28	0 31	0 31	0 34	1 83	1 86	2 32	0 27
Na_2O	3 87	3 17	3 38	3 61	3 25	3 18	3 14	3 68	3 25	2 98	2 93	3 58
K_2O	4 19	3 77	4 14	4 31	4 44	4 41	4 64	4 30	3 80	3 82	3 69	4 77
P_2O_5	0 37	0 23	0 46	0 33	0 29	0 28	0 27	0 31	0 21	0 23	0 23	0 26
H_20+	-	-	-	-	-	-	-	-	-	-	-	-
H_2O-	-	-	-	-	-	-	-	-	-	-	-	-
CO_2	-	-	-	-	-	-	-	-	-	-	-	-
Cl	-	-	-	-	-	-	-	-	-	-	-	-
F	0 20	0 11	0 29	0 11	0 12	0 15	0 18	0 14	0 07	0 06	0 07	0 17
LOI	0 75	0 53	0 70	0 40	0 80	0 90	0 60	0 70	0 48	0 69	0 51	0 40
TOTAL	100 47	98 78	99 09	99 74	98 56	99 87	100 54	98 65	98 58	99 28	98 78	99 67
Fe_2O_3T	1 04	5 08	1 18	1 28	1 33	1 43	1 45	1 31	5 07	5 29	5 49	1 40
FeOT	0 94	4 57	1 06	1 15	1 20	1 29	1 30	1 18	4 56	4 76	4 94	1 26
A/CNK	1 13	1 16	1 24	1 18	1 18	1 20	1 17	1 14	1 15	1 11	1 17	1 09
Trace els												
Ba	16	730	8	32	22	20	59	82	610	631	685	60
Rb	537	167	601	442	426	411	463	406	160	153	144	443
Sr	6	173	5	8	8	6	16	28	147	158	161	21
Y	26	42	20	18	20	20	20	19	40	46	35	21
Zr	26	230	36	49	47	48	61	54	211	205	218	56
Nb	16	13	20	14	14	11	12	13	12	11	13	13
Th	2 4	13	3 1	3 7	3 7	4 2	5 4	5 1	14	10	13	6 1
Pb	-	13	15	16	24	25	25	17	-	17	-	21
Ga	24	18	26	23	24	25	20	24	18	17	21	23
Zn	32	79	68	45	57	66	53	54	79	70	73	77
Cu	-	17	-	-	-	1	-	-	11	8	11	-
Ni	-	-	-	-	-	-	-	-	-	-	-	-
V	-	65	3	3	1	1	4	5	58	60	63	5
Cr	-	-	-	-	-	-	-	-	-	-	-	-
Hf	-	7	1	1	1	1	1	1	6	6	7	2
Cs	-	-	-	-	-	-	-	-	-	-	-	-
Sc	2.1	12	2.2	2 7	2 3	2 3	2 8	2.9	13	14	15	2 2
Ta	3 3	1 3	0 9	5 5	2 8	2 7	2 5	2 8	1 4	1 1	1 4	2 7
Co	-	-	-	-	-	-	-	-	-	-	-	-
Li	140	96	329	235	212	256	386	213	72	65	66	209
Be	-	-	-	-	-	-	-	-	-	-	-	-
B	19	28	25	30	45	30	28	20	17	15	13	25
U	2.1	2 3	2 9	3 8	3 6	3 4	2 3	5 9	3 8	2 8	3 2	2 2
W	7	1	9	5	8	10	6	5	-	1	-	3
Sn	23	5	43	26	26	35	36	22	4	6	5	20
Mo	-	-	-	-	-	-	-	-	-	-	-	-
Rare-earths												
La	-	37	2	5	5	5	7	7	37	32	39	7
Ce	-	-	-	-	-	-	-	-	-	-	-	-
Pr	-	-	-	-	-	-	-	-	-	-	-	-
Nd	-	-		-	-	-	-	-	-	-	-	-
Sm	-	-	-	-	-	-	-	-	-	-	-	-
Eu	-	-	-	-	-	-	-	-	-	-	-	-
Gd	-	-	-	-	-	-	-	-	-	-	-	-
Tb	-	-	-	-	-	-	-	-	-	-	-	-
Dy	-	-	-	-	-	-	-	-	-	-	-	-
Ho	-	-	-	-	-	-	-	-	-	-	-	-
Er	-	-	-	-	-	-	-	-	-	-	-	-
Tm	-	-	-	-	-	-	-	-	-	-	-	-
Yb	-	-	-	-	-	-	-	-	-	-	-	-
Lu	-	-	-	-	-	-	-	-	-	-	-	-

Table E1 1 (Continued) Compilation of Meguma Zone granitoid lithogeochemistry

Sample	A15-0055	A15-0055-2	A15-0055-212	A15-0055-3	A15-0057	A15-0060	A15-0060-2	A15-0062	A15-0067	A15-0067-2	A15-0068	A15-0068-2
Batholith	SMB	SMB	SMB	SMB	SMB	SMB	SMB	SMB	SMB	SMB	SMB	SMB
Pluton	KLP	KLP	KLP	KLP	KLP	LGP	LGP	LGP	MuLP	LGP	MuLP	MuLP
Lithology	Mzg	Mzg	Mzg	Mzg	Mzg	Lmzg	Lmzg	Lmzg	Lg	Lmzg	Lg	Lg
Source	27	27	27	27	27	27	27	27	27	27	27	27
Major oxides												
SiO_2	72 87	71 85	72 89	72 17	66 66	74 04	74 13	76 36	74 31	72 86	73 93	75 17
TiO_2	0 21	0 21	0 18	0 22	0 75	0 13	0 15	0 07	0 10	0 11	0 04	0 03
Al_2O_3	14 31	14 65	14 50	14 80	15 05	14 30	13 98	12 89	14 05	14 52	14 66	14 16
Fe_2O_3	-	-	-	-	-	-	-	-	-	-	-	-
FeO	-	-	-	-	-	-	-	-	-	-	-	-
MnO	0 04	0 04	0 04	0 04	0 10	0 04	0 04	0 03	0 03	0 05	0 03	0 02
MgO	1 05	0 92	0 97	1 04	1 88	0 80	0 79	0 73	0 81	0 80	0 75	0 70
CaO	0 50	0 54	0 56	0 56	2 02	0 31	0 38	0 34	0 30	0 41	0 28	0 37
Na_2O	3 55	3 70	3 63	3 09	2 87	3 12	3 30	3 41	3 25	3 76	4 68	4 75
K_2O	5 28	5 05	4 98	5 06	3 92	4 70	4 79	4 30	4 57	4 96	3 88	3 02
P_2O_5	0 23	0 27	0 25	0 25	0 23	0 30	0 25	0 27	0 28	0 23	0 41	0 38
H_2O+	-	-	-	-	-	-	-	-	-	-	-	-
H_2O-	-	-	-	-	-	-	-	-	-	-	-	-
CO_2	-	-	-	-	-	-	-	-	-	-	-	-
Cl	-	-	-	-	-	-	-	-	-	-	-	-
F	0 11	0 10	0 10	0 10	0 09	0 15	0 14	0 13	0 12	0 11	0 17	0 15
LOI	0 29	0 51	0 74	0 64	0 48	0 83	0 72	0 44	0 70	0 35	0 80	0 68
TOTAL	99 96	99 30	100 22	99 41	98 63	99 87	100 00	99 84	99 75	99 53	100 45	100 16
Fe_2O_3T	1 81	1 73	1 64	1 71	5 19	1 44	1 63	1 11	1 50	1 64	1 10	0 97
FeOT	1 63	1 56	1 48	1 54	4 67	1 30	1 47	1 00	1 35	1 48	0 99	0 87
A/CNK	1 03	1 06	1 06	1 14	1 17	1 18	1 11	1 08	1 16	1 07	1 13	1 19
Trace els												
Ba	336	288	322	296	681	97	99	50	77	97	11	11
Rb	294	290	297	277	155	408	334	323	373	317	498	437
Sr	51	53	58	55	156	20	29	10	17	22	5	6
Y	26	19	24	22	41	26	26	18	23	25	25	19
Zr	103	94	96	99	216	53	68	51	60	46	23	17
Nb	14	13	14	13	13	13	13	11	12	9	22	18
Th	15	15	12	15	13	5 2	7 1	3 9	5 2	6 9	1 8	1 3
Pb	14	19	11	13	-	11	11	18	20	-	-	-
Ga	19	20	19	18	20	19	20	18	22	18	28	28
Zn	48	53	48	50	76	52	53	47	54	52	49	39
Cu	-	-	-	6	16	-	-	-	-	-	-	-
Ni	-	-	-	-	-	-	-	-	-	-	-	-
V	5	7	7	7	64	-	-	6	-	-	-	-
Cr	-	-	-	-	-	-	-	-	-	-	-	-
Hf	3	4	3	3	7	2	3	1	2	2	1	1
Cs	-	-	-	-	-	-	-	-	-	-	-	-
Sc	2 9	2.8	2.9	2.8	14	1 6	1 6	1 2	2 3	1 9	2 8	2 2
Ta	1 9	2	2	1 7	1 1	2 3	1 4	2 1	2 1	1	3 4	3 6
Co	-	-	-	-	-	-	-	-	-	-	-	-
Li	85	93	94	79	82	135	116	95	105	79	98	92
Be	-	-	-	-	-	-	-	-	-	-	-	-
B	25	23	28	23	14	22	23	19	18	17	20	19
U	4 1	3 5	4	3 1	2 4	2	3 3	10	3 8	3 8	5 8	1 8
W	2	2	4	2	1	3	2	2	4	2	5	5
Sn	13	13	8	5	4	16	12	18	18	11	22	20
Mo	-	-	-	-	-	-	-	-	-	-	-	-
Rare-earths												
La	23	20	18	19	38	8	10	6	6	6	-	-
Ce	-	-	-	-	-	-	-	-	-	-	-	-
Pr	-	-	-	-	-	-	-	-	-	-	-	-
Nd	-	-	-	-	-	-	-	-	-	-	-	-
Sm	-	-	-	-	-	-	-	-	-	-	-	-
Eu	-	-	-	-	-	-	-	-	-	-	-	-
Gd	-	-	-	-	-	-	-	-	-	-	-	-
Tb	-	-	-	-	-	-	-	-	-	-	-	-
Dy	-	-	-	-	-	-	-	-	-	-	-	-
Ho	-	-	-	-	-	-	-	-	-	-	-	-
Er	-	-	-	-	-	-	-	-	-	-	-	-
Tm	-	-	-	-	-	-	-	-	-	-	-	-
Yb	-	-	-	-	-	-	-	-	-	-	-	-
Lu	-	-	-	-	-	-	-	-	-	-	-	-

Table E1 1 (Continued) Compilation of Meguma Zone granitoid lithogeochemistry

Sample	A15-0068-3	A15-0072	A15-0072-2	A15-0072-3	A15-0074	A15-0075	A15-0075-2	A15-0075-2	A15-0075-A	A15-0080	A15-0080-2	A15-0081
Batholith	SMB	SMB	SMB	SMB	SMB	SMB	SMB	SMB	SMB	SMB	SMB	SMB
Pluton	MuLP	ScLP	ScLP	ScLP	StLP	KLP	KLP	MuLP	StLP	BLP	BLP	BLP
Lithology	Lg	Mzg	Mzg	Mzg	Mzg	Mzg	Mzg	Lg	Mzg	Grd	Grd	Grd
Source	27	27	27	27	27	27	27	27	27	27	27	27
Major oxides												
SiO_2	72 78	66 25	66 73	67 42	67 10	72 73	72 50	73 68	65 23	64 72	70 58	65 36
TiO_2	0 03	0 77	0 71	0 72	0 71	0 20	0 22	0 11	0 85	0 77	0 31	0 82
Al_2O_3	15 04	15 45	15 11	14 91	14 84	14 48	14 43	14 33	15 29	16 63	15 30	15 33
Fe_2O_3	-	-	-	-	-	-	-	-	-	-	-	-
FeO	-	-	-	-	-	-	-	-	-	-	-	-
MnO	0 04	0 10	0 10	0 10	0 10	0 05	0 05	0 04	0 07	0 08	0 06	0 11
MgO	0 60	1 91	1 83	1 66	1 69	0 96	0 93	0 80	1 98	2 13	1 37	1 80
CaO	0 79	2 24	2.06	1 90	1 90	0 59	0 60	0 35	2 09	3 07	1 33	2 38
Na_2O	4 35	3 64	3 47	3 32	3 08	3 54	3 45	3 60	3 39	3 98	3 99	3 33
K_2O	3 60	3 78	3 66	3 98	3 88	4 87	5 17	4 37	3 76	2 64	3 95	3 46
P_2O_5	0 70	0 22	0 23	0 24	0 21	0 26	0 25	0 34	0 37	0 28	0 17	0 24
H_2O+	-	-	-	-	-	-	-	-	-	-	-	-
H_2O-	-	-	-	-	-	-	-	-	-	-	-	-
CO_2	-	-	-	-	-	-	-	-	-	-	-	-
Cl	-	-	-	-	-	-	-	-	-	-	-	-
F	0 25	0 06	0 07	0 08	0 07	0 11	0 11	0 12	0 07	0 06	0 03	0 07
LOI	0 81	0 29	0 49	0 47	0 41	0 72	0 37	0 60	0 60	0 40	0 50	0 41
TOTAL	99 56	99 25	98 68	99 04	98 32	99 99	99 74	99 44	98 61	99 10	99 58	98 62
Fe_2O_3T	0 91	5 11	4 77	4 80	4 89	1 77	1 97	1 36	5 54	4 89	2 25	5 98
FeOT	0 82	4 60	4 29	4 32	4 40	1 59	1 77	1 22	4 98	4 40	2.02	5 38
A/CNK	1 17	1 10	1 13	1 11	1 14	1 08	1 05	1 16	1 14	1 20	1 13	1 15
Trace els												
Ba	41	745	654	498	610	282	315	70	616	562	551	819
Rb	564	141	150	162	157	309	315	406	165	141	141	130
Sr	18	170	167	140	149	51	55	17	159	209	150	179
Y	26	39	33	50	39	23	25	26	39	27	16	48
Zr	27	205	206	186	210	98	104	50	247	162	97	286
Nb	29	13	12	12	12	14	15	18	18	12	8	15
Th	1 5	2.5	14	10	13	12	14	6 2	14	8 4	10	15
Pb	11	15	-	17	17	24	32	12	-	-	21	12
Ga	33	20	16	20	15	17	23	23	24	22	17	21
Zn	40	75	75	70	67	53	54	40	101	83	45	84
Cu	7	15	12	11	10	-	-	-	9	28	-	13
Ni	-	-	-	-	-	-	-	-	-	-	-	-
V	7	69	61	57	57	6	5	9	65	61	27	65
Cr	-	-	-	-	-	-	-	-	-	-	-	-
Hf	2	8	7	7	7	3	3	3	8	5	3	10
Cs	-	-	-	-	-	-	-	-	-	-	-	-
Sc	3 2	14	14	13	13	3 2	3 2	2.9	14	13	5 7	16
Ta	11	1 5	1 2	1 2	1 4	2 4	2 4	4 4	1 6	1	0 6	1 4
Co	-	-	-	-	-	-	-	-	-	-	-	-
Li	115	58	66	65	66	99	126	111	65	65	49	51
Be	-	-	-	-	-	-	-	-	-	-	-	-
B	19	15	15	17	13	19	19	23	18	13	13	15
U	2 3	3 5	3 5	2.5	3	4 8	8 5	7	3 2	4 2	2 7	3 4
W	9	-	-	-	-	4	4	6	-	-	-	-
Sn	34	6	2	2	2	16	13	18	5	-	3	2
Mo	-	-	-	-	-	-	-	-	-	-	-	-
Rare-earths												
La	-	15	39	29	38	20	20	9	41	25	21	48
Ce	-	-	-	-	-	-	-	-	-	-	-	-
Pr	-	-	-	-	-	-	-	-	-	-	-	-
Nd	-	-	-	-	-	-	-	-	-	-	-	-
Sm	-	-	-	-	-	-	-	-	-	-	-	-
Eu	-	-	-	-	-	-	-	-	-	-	-	-
Gd	-	-	-	-	-	-	-	-	-	-	-	-
Tb	-	-	-	-	-	-	-	-	-	-	-	-
Dy	-	-	-	-	-	-	-	-	-	-	-	-
Ho	-	-	-	-	-	-	-	-	-	-	-	-
Er	-	-	-	-	-	-	-	-	-	-	-	-
Tm	-	-	-	-	-	-	-	-	-	-	-	-
Yb	-	-	-	-	-	-	-	-	-	-	-	-
Lu	-	-	-	-	-	-	-	-		-	-	-

Table E1 1 (Continued) Compilation of Meguma Zone granitoid lithogeochemistry

Sample	A15-0083	A15-0087	A15-0101	A15-0102	A15-0103	A15-0104	A15-0111	A15-0111-2	A15-0114	A15-0115	A15-0115-4	A15 0115-5
Batholith	SMB	SMB	SMB	SMB	SMB	SMB	SMB	SMB	SMB	SMB	SMB	SMB
Pluton	ScLP	BLP	LGP	JSP	JSP	ScLP	JSP	JSP	JSP	ScLP	WDP	WDP
Lithology	Mzg	Grd	Lmzg	Lmzg	Lmzg	Grd	Lmzg	Lmzg	Lmzg	Mzg	Mzg	Mzg
Source	27	27	27	27	27	27	27	27	27	27	27	27
Major oxides												
SiO_2	66 89	60 85	73 34	71 76	69 77	68 60	72 51	72 55	72 89	69 28	71 32	70 87
TiO_2	0 65	0 88	0 19	0 37	0 42	0 80	0 20	0 20	0 18	0 52	0 31	0 30
Al_2O_3	15 32	18 70	13 90	14 52	15 25	14 13	14 86	15 03	14 62	14 73	14 63	15 09
Fe_2O_3	-	-	-	-	-	-	-	-	-	-	-	-
FeO	-	-	-	-	-	-	-	-	-	-	-	-
MnO	0 09	0 18	0 05	0 08	0 04	0 09	0 03	0 04	0 07	0 07	0 05	0 05
MgO	1 76	2 04	0 97	1 22	1 30	1 84	0 94	0 92	1 04	1 49	1 04	1 06
CaO	1 95	0 96	0 57	0 86	0 80	2 15	0 44	0 48	0 62	1 64	0 74	0 69
Na_2O	3 33	2 13	3 27	3 36	3 10	2 87	3 29	3 07	3 18	3 24	3 46	3 57
K_2O	4 13	4 48	4 52	4 19	5 16	3 13	5 23	5 22	4 84	3 95	4 88	5 09
P_2O_5	0 20	0 16	0 22	0 12	0 24	0 22	0 23	0 23	0 20	0 20	0 21	0 21
H_2O+	-	-	-	-	-	-	-	-	-	-	-	-
H_2O-	-	-	-	-	-	-	-	-	-	-	-	-
CO_2	-	-	-	-	-	-	-	-	-	-	-	-
Cl	-	-	-	-	-	-	-	-	-	-	-	-
F	0 06	0 05	0 09	0 05	0 08	0 08	0 05	0 05	0 02	0 06	0 07	0 10
LOI	0 51	2.48	0 60	0 68	0 73	0 41	0 95	0 74	0 74	0 61	0 48	0 49
TOTAL	98 85	98 58	99 40	99 62	99 20	98 71	100 04	99 75	99 91	98 89	99 12	99 34
Fe_2O_3T	4 47	6 36	1 97	2 73	2 66	4 97	1 51	1 41	1 70	3 62	2 22	2 13
FeOT	4 02	5 72	1 77	2 46	2 39	4 47	1 36	1 27	1 53	3 26	2 00	1 92
A/CNK	1 11	1 65	1 12	1 17	1 13	1 19	1 11	1 14	1 13	1 14	1 08	1 08
Trace els												
Ba	692	1101	124	438	558	603	283	288	294	481	377	379
Rb	155	164	303	180	232	133	289	286	194	148	253	278
Sr	150	166	45	97	111	159	78	87	94	131	73	72
Y	35	43	26	31	22	35	21	20	23	30	24	24
Zr	194	220	86	119	154	208	81	80	77	166	124	119
Nb	10	15	11	11	13	13	13	13	10	12	13	14
Th	13	15	8 7	11	23 8	14	12	12	5 9	12	20	18
Pb	-	-	15	16	25	-	24	20	36	10	19	18
Ga	21	25	20	17	21	18	19	18	15	18	19	20
Zn	66	98	52	58	88	69	52	60	44	59	55	59
Cu	11	35	-	-	8	10	-	6	13	5	-	-
Ni	-	-	-	-	-	-	-	-	-	-	-	-
V	54	106	9	23	31	70	7	-	6	45	15	14
Cr	-	-	-	-	-	-	-	-	-	-	-	-
Hf	7	7	4	4	5	8	3	3	3	6	4	4
Cs	-	-	-	-	-	-	-	-	-	-	-	-
Sc	12	15	3 4	6 4	4 7	13	2.1	2	3 1	10	4 2	3 9
Ta	1 1	1 3	1 8	0 7	1 3	1 1	1 5	1 6	1 5	1 3	1 6	1 7
Co	-	-	-	-	-	-	-	-	-	-	-	-
Li	52	69	109	78	82	77	84	114	49	53	91	86
Be	-	-	-	-	-	-	-	-	-	-	-	-
B	13	31	16	20	19	19	30	44	21	26	20	50
U	4	4 2	3 1	2.9	5	3 2	5 4	8 1	3 8	3	6	8 2
W	-	-	2	-	2	-	2	3	4	-	2	-
Sn	4	-	8	1	6	-	13	10	7	-	-	9
Mo	-	-	-	-	-	-	-	-	-	-	-	-
Rare-earths												
La	37	51	15	21	39	4J	23	24	14	33	34	32
Ce	-	-	-	-	-	-	-	-	-	-	-	-
Pr	-	-	-	-	-	-	-	-	-	-	-	-
Nd	-	-	-	-	-	-	-	-	-	-	-	-
Sm	-	-	-	-	-	-	-	-	-	-	-	-
Eu	-	-	-	-	-	-	-	-	-	-	-	-
Gd	-	-	-	-	-	-	-	-	-	-	-	-
Tb	-	-	-	-	-	-	-	-	-	-	-	-
Dy	-	-	-	-	-	-	-	-	-	-	-	-
Ho	-	-	-	-	-	-	-	-	-	-	-	-
Er	-	-	-	-	-	-	-	-	-	-	-	-
Tm	-	-	-	-	-	-	-	-	-	-	-	-
Yb	-	-	-	-	-	-	-	-	-	-	-	-
Lu	-	-	-	-	-	-	-	-	-	-	-	-

Table E1 1 (Continued) Compilation of Meguma Zone granitoid lithogeochemistry

Sample	A15-0116	A15-0116-2	A15-0116-3	A15-0118	A15-0120-2	A15-0141-2	A15-0142	A15-0147	A15-0147-2	A15-0148	A15-1307	A15-1318
Batholith	SMB	SMB	SMB	SMB	SMB	SMB	SMB	SMB	SMB	SMB	SMB	SMB
Pluton	CLP	CLP	CLP	CLP	CLP	CLP	EDP	EDP	EDP	StLP	StLP	StLP
Lithology	Mzg	Mzg	Mzg	Mzg	Mzg	Mzg	Lmzg	Lmzg	Lmzg	Mzg	Mzg	Mzg
Source	27	27	27	27	27	27	27	27	27	27	27	27
Major oxides												
SiO_2	68 30	68 77	69 05	67 82	67 23	67 46	75 27	71 26	71 82	67 39	69 73	68 28
TiO_2	0 56	0 53	0 56	0 59	0 62	0 55	0 06	0 28	0 26	0 63	0 49	0 57
Al_2O_3	14 80	14 73	14 39	15 06	15 13	15 02	13 36	14 97	15 03	15 54	14 44	14 81
Fe_2O_3	-	-	-	-	-	-	-	-	-	-	-	-
FeO	-	-	-	-	-	-	-	-	-	-	-	-
MnO	0 09	0 09	0 09	0 09	0 09	0 10	0 07	0 06	0 03	0 10	0 09	0 09
MgO	1 45	1 43	1 40	1 80	1 46	1 59	0 75	0 97	1 07	1 47	1 15	1 49
CaO	1 73	1 63	1 59	1 44	1 94	1 63	0 28	0 95	0 44	1 72	0 44	1 51
Na_2O	3 24	3 45	3 36	3 73	3 70	3 88	3 67	3 32	3 51	3 07	4 49	3 97
K_2O	3 97	4 24	4 23	3 85	3 88	4 09	4 71	4 11	5 13	4 18	3 61	3 86
P_2O_5	0 20	0 19	0 18	0 20	0 19	0 18	0 13	0 27	0 28	0 23	0 22	0 22
H_20+	-	-	-	-	-	-	-	-	-	-	-	-
H_2O-	-	-	-	-	-	-	-	-	-	-	-	-
CO_2	-	-	-	-	-	-	-	-	-	-	-	-
Cl	-	-	-	-	-	-	-	-	-	-	-	-
F	0 07	0 07	0 07	0 07	0 07	0 07	0 03	0 07	0 04	0 07	0 03	0 06
LOI	0 40	0 11	0 12	0 52	0 20	0 38	0 13	0 80	0 70	0 50	1 11	0 76
TOTAL	98 60	98 81	98 82	99 01	98 68	98 75	99 75	98 91	99 77	98 73	98 90	99 27
Fe_2O_3T	4 29	4 05	4 28	4 35	4 71	4 30	1 47	2 13	1 67	4 33	3 48	4 12
FeOT	3 86	3 64	3 85	3 91	4 24	3 87	1 32	1 92	1 50	3 90	3 13	3 71
A/CNK	1 13	1 08	1 07	1 14	1 09	1 07	1 03	1 21	1 11	1 18	1 15	1 08
Trace els												
Ba	581	599	625	546	642	643	91	505	399	623	444	437
Rb	151	172	164	158	151	174	259	194	213	167	132	160
Sr	133	124	119	127	143	126	16	121	60	137	99	136
Y	45	43	46	45	48	43	32	18	18	30	31	40
Zr	214	200	211	208	219	207	58	135	89	195	160	193
Nb	13	12	12	13	12	13	7	14	11	12	11	12
Th	12	13	12	13	13	13	5 3	7 8	13	12	10	11
Pb	-	15	20	18	14	17	14	18	27	29	19	10
Ga	18	19	20	17	21	21	16	19	20	25	18	19
Zn	60	59	68	59	70	67	28	66	54	78	65	65
Cu	8	9	10	11	9	6	-	2	-	-	10	11
Ni	-	-	-	-	-	-	-	-	-	-	-	-
V	36	41	40	47	51	39	-	14	11	44	39	51
Cr	-	-	-	-	-	-	-	-	-	-	-	-
Hf	7	7	6	7	8	7	2	4	3	6	5	6
Cs	-	-	-	-	-	-	-	-	-	-	-	-
Sc	11	10	10	12	12	11	3 1	5 1	3 4	11	9 2	11
Ta	1 2	1 3	1	1 4	1 3	1 3	1 7	2 2	1 9	1 6	1 2	1 2
Co	-	-	-	-	-	-	-	-	-	-	-	-
Li	57	66	62	62	59	63	65	137	87	99	44	90
Be	-	-	-	-	-	-	-	-	-	-	-	-
B	30	17	24	25	18	35	29	30	30	20	21	27
U	3 7	4 7	2 8	3 1	4 5	3 4	3 5	6	4	3 7	6 4	2 7
W	2	3	-	-	-	-	3	2	1	1	-	-
Sn	-	3	9	5	1	-	9	10	11	8	8	1
Mo	-	-	-	-	-	-	-	-	-	-	-	-
Rare-earths												
La	34	35	34	35	38	35	6	28	17	34	25	31
Ce	-	-	-	-	-	-	-	-	-	-	-	-
Pr	-	-	-	-	-	-	-	-	-	-	-	-
Nd	-	-	-	-	-	-	-	-	-	-	-	-
Sm	-	-	-	-	-	-	-	-	-	-	-	-
Eu	-	-	-	-	-	-	-	-	-	-	-	-
Gd	-	-	-	-	-	-	-	-	-	-	-	-
Tb	-	-	-	-	-	-	-	-	-	-	-	-
Dy	-	-	-	-	-	-	-	-	-	-	-	-
Ho	-	-	-	-	-	-	-	-	-	-	-	-
Er	-	-	-	-	-	-	-	-	-	-	-	-
Tm	-	-	-	-	-	-	-	-	-	-	-	-
Yb	-	-	-	-		-	-	-	-	-	-	-
Lu	-	-	-	-		-	-	-	-	-		-

Table E1 1 (Continued) Compilation of Meguma Zone granitoid lithogeochemistry

Sample	A15-1320	A15-1327	A15-1328	A16-1102	A16-1102-C	A16-1103	A16-1103-C	A16-1137	A16-1159	A16-1166
Batholith	SMB	SMB	SMB	SMB	SMB	SMB	SMB	SMB	SMB	SMB
Pluton	StLP	StLP	StLP	MG	MG	MG	MG	MG	BIP	SwP
Lithology	Mzg	Mzg	Mzg	Grd	Grd	Grd	Grd	Grd	Mzg	Mzg
Source	27	27	27	27	27	27	27	27	27	27
Major oxides										
SiO_2	70 36	70 37	69 80	68 94	65 94	69 65	69 34	66 35	74 89	72 47
TiO_2	0 39	0 49	0 61	0 61	0 72	0 42	0 38	0 61	0 09	0 31
Al_2O_3	14 65	14 37	14 12	14 93	15 81	15 26	15 61	16 35	13 08	14 61
Fe_2O_3	-	-	-	-	-	-	-	-	-	-
FeO	-	-	-	-	-	-	-	-	-	-
MnO	0 08	0 09	0 08	0 07	0 08	0 07	0 07	0 08	0 05	0 05
MgO	1 26	1 41	1 68	1 96	2.22	1 64	1 44	1 89	0 86	1 08
CaO	1 01	1 12	1 72	2 15	2 42	1 39	1 32	2 75	0 45	0 71
Na_2O	3 66	3 21	3 22	3 31	3 75	3 86	4 13	3 91	3 66	3 58
K_2O	4 24	4 05	3 40	3 16	3 45	4 22	4 55	3 31	4 72	4 67
P_2O_5	0 25	0 24	0 20	0 19	0 24	0 15	0 15	0 19	0 09	0 28
H_2O+	-	-	-	-	-	-	-	-	-	-
H_2O-	-	-	-	-	-	-	-	-	-	-
CO_2	-	-	-	-	-	-	-	-	-	-
Cl	-	-	-	-	-	-	-	-	-	-
F	0 06	0 05	0 07	0 06	0 07	0 05	0 06	0 06	0 03	0 13
LOI	0 65	0 60	0 60	0 60	0 60	0 60	0 70	0 50	1 30	0 60
TOTAL	99 23	98 92	99 07	99 53	99 42	100 09	100 26	99 61	100 18	100 29
Fe_2O_3T	2 98	3 30	4 04	4 01	4 66	3 14	2 86	4 08	1 10	2 26
FeOT	2 68	2 97	3 64	3 61	4 19	2.83	2 57	3 67	0 99	2 03
A/CNK	1 11	1 16	1 16	1 19	1 13	1 10	1 06	1 14	1 00	1 09
Trace els										
Ba	381	419	538	830	905	586	565	755	76	292
Rb	196	173	139	105	121	152	153	126	182	310
Sr	93	102	133	203	214	123	124	225	22	57
Y	27	28	28	21	25	31	29	28	19	20
Zr	135	166	210	174	201	130	119	169	40	140
Nb	11	11	15	10	12	10	10	11	6	14
Th	8 6	11	13	11	14	10	12	12	4	20
Pb	20	37	20	22	25	19	18	20	25	22
Ga	18	18	20	19	22	19	21	22	19	20
Zn	47	55	85	324	278	47	44	60	27	56
Cu	-	-	-	4	6	1	-	11	-	-
Ni	-	-	-	-	-	-	-	-	-	-
V	25	31	48	54	63	33	35	53	4	11
Cr	-	-	-	-	-	-	-	-	-	-
Hf	4	6	8	5	7	5	4	5	2	3
Cs	-	-	-	-	-	-	-	-	-	-
Sc	7 7	8 4	8 6	9	12	6 8	7 4	10	2 4	3 7
Ta	1 5	1 3	1	0 8	0 9	1 1	0 8	0 9	0 9	2 1
Co	-	-	-	-	-	-	-	-	-	-
Li	94	105	83	33	36	50	53	41	76	104
Be	-	-	-	-	-	-	-	-	-	-
B	23	30	20	20	20	25	25	20	20	20
U	2 8	4 3	3	3	3 4	2	2	2 7	2 3	3 2
W	3	1	1	1	1	1	1	1	1	2
Sn	4	10	10	4	4	9	8	8	5	13
Mo	-	-	-	-	-	-	-	-	-	-
Rare-earths										
La	22	30	36	29	37	25	28	37	6	26
Ce	-	-	-	-	-	-	-	-	-	-
Pr	-	-	-	-	-	-	-	-	-	-
Nd	-	-	-	-	-	-	-	-	-	-
Sm	-	-	-	-	-	-	-	-	-	-
Eu	-	-	-	-	-	-	-	-	-	-
Gd	-	-	-	-	-	-	-	-	-	-
Tb	-	-	-	-	-	-	-	-	-	-
Dy	-	-	-	-	-	-	-	-	-	-
Ho	-	-	-	-	-	-	-	-	-	-
Er	-	-	-	-	-	-	-	-	-	-
Tm	-	-	-	-	-	-	-	-	-	-
Yb	-	-	-	-	-	-	-	-	-	-
Lu	-	-	-	-	-	-	-	-	-	-

Table E1 1 (Continued) Compilation of Meguma Zone granitoid lithogeochemistry

Sample	A16-1167	A16-1169	A16-1170	A16-1171	A16-1172	A16-1172-C	A16-1174	A16-1202-C	A16-1202-C	A16-1206	A16-1207-7	A16-1208-A	A16-1213
Batholith	SMB	SMB	SMB	SMB	SMB	SMB	SMB	SMB	SMB	SMB	SMB	SMB	SMB
Pluton	NRP	MG	NRP	SaLP	MG	MG	NRP	StLP	StLP	StLP	StLP	StLP	NRP
Lithology	Lmzg	Grd	Lmzg	Mzg	Grd	Grd	Lmzg	Mzg	Mzg	Mzg	Mzg	Mzg	Lmzg
Source	27	27	27	27	27	27	27	27	27	27	27	27	27
Major oxides													
SiO_2	74.38	67.25	72.98	69.83	66.89	66.91	74.80	69.76	70.14	68.97	69.05	68.29	73.49
TiO_2	0.12	0.90	0.18	0.20	0.63	0.67	0.15	0.49	0.45	0.48	0.52	0.54	0.11
Al_2O_3	14.20	14.79	14.58	15.07	15.86	15.61	13.00	14.76	14.56	15.08	14.56	15.41	14.54
Fe_2O_3	-	-	-	-	-	-	-	-	-	-	-	-	-
FeO	-	-	-	-	-	-	-	-	-	-	-	-	-
MnO	0.05	0.10	0.06	0.50	0.08	0.10	0.05	0.08	0.07	0.09	0.08	0.08	0.03
MgO	0.84	1.98	0.90	0.91	2.03	1.83	0.82	1.42	1.41	1.41	1.45	1.55	0.77
CaO	0.48	2.12	0.62	0.83	2.63	1.77	0.34	1.47	1.29	1.23	1.08	1.28	0.38
Na_2O	3.62	3.04	3.83	3.50	3.62	3.84	3.48	3.52	3.35	3.50	3.63	3.10	3.49
K_2O	4.52	3.06	4.58	5.32	3.42	3.85	4.81	3.90	4.12	4.30	4.22	4.15	4.93
P_2O_5	0.23	0.22	0.18	0.16	0.19	0.21	0.19	0.20	0.21	0.22	0.22	0.22	0.30
H_2O+	-	-	-	-	-	-	-	-	-	-	-	-	-
H_2O-	-	-	-	-	-	-	-	-	-	-	-	-	-
CO_2	-	-	-	-	-	-	-	-	-	-	-	-	-
Cl	-	-	-	-	-	-	-	-	-	-	-	-	-
F	0.07	0.07	0.07	0.07	0.07	0.08	0.06	0.05	0.06	0.06	0.07	0.06	0.18
LOI	0.60	0.50	0.60	0.50	0.30	0.60	0.50	0.70	0.60	0.70	0.75	0.80	0.40
TOTAL	100.49	99.20	100.35	98.71	99.38	99.52	99.90	99.34	99.13	98.96	99.04	98.82	99.70
Fe_2O_3T	1.61	5.82	2.16	2.10	4.14	4.59	1.96	3.38	3.26	3.31	3.87	3.78	1.40
FeOT	1.45	5.24	1.94	1.89	3.73	4.13	1.76	3.04	2.93	2.98	3.48	3.40	1.26
A/CNK	1.11	1.24	1.09	1.05	1.13	1.13	1.01	1.13	1.13	1.13	1.11	1.22	1.11
Trace els													
Ba	83	594	230	310	803	673	120	504	459	445	468	486	86
Rb	275	133	275	261	126	166	274	173	169	185	183	174	374
Sr	22	172	53	64	224	183	33	106	104	104	96	103	25
Y	17	36	26	27	26	33	25	28	27	27	35	30	20
Zr	55	250	84	94	171	198	77	155	148	161	177	175	62
Nb	11	15	11	10	11	13	10	12	12	14	11	14	14
Th	6.2	14	8.8	10	13	12	7.5	10	10	11	12	11	5.5
Pb	24	14	20	21	17	16	24	33	22	27	41	18	14
Ga	23	23	20	24	24	23	22	18	19	23	18	19	19
Zn	40	80	49	47	56	67	60	82	72	88	95	63	71
Cu	-	10	-	-	6	1	-	5	-	-	15	-	-
Ni	-	-	-	-	-	-	-	-	-	-	-	-	-
V	2	68	11	9	53	52	6	36	36	32	35	35	4
Cr	-	-	-	-	-	-	-	-	-	-	-	-	-
Hf	1	8	3	3	6	7	3	5	5	5	6	6	2
Cs	-	-	-	-	-	-	-	-	-	-	-	-	-
Sc	2	14	3.8	3.5	11	11	2.5	7.8	7.5	8.2	10	8.7	1.7
Ta	1.7	1.1	1.4	1.1	0.9	1.1	1.3	0.9	1.2	0.8	1.2	0.8	0.9
Co	-	-	-	-	-	-	-	-	-	-	-	-	-
Li	74	43	99	73	41	82	67	95	98	110	88	118	209
Be	-	-	-	-	-	-	-	-	-	-	-	-	-
B	20	15	30	20	15	20	25	35	25	30	19	30	25
U	3.6	3.2	3.8	2.3	2	2.4	3.8	3	4.7	5.4	3.2	4.2	7.1
W	3	1	1	1	1	1	4	1	1	2	-	1	3
Sn	12	8	13	15	9	10	16	4	9	10	6	11	24
Mo	-	-	-	-	-	-	-	-	-	-	-	-	-
Rare-earths													
La	9	44	16	17	38	38	11	28	25	27	29	32	8
Ce	-	-	-	-	-	-	-	-	-	-	-	-	-
Pr	-	-	-	-	-	-	-	-	-	-	-	-	-
Nd	-	-	-	-	-	-	-	-	-	-	-	-	-
Sm	-	-	-	-	-	-	-	-	-	-	-	-	-
Eu	-	-	-	-	-	-	-	-	-	-	-	-	-
Gd	-	-	-	-	-	-	-	-	-	-	-	-	-
Tb	-	-	-	-	-	-	-	-	-	-	-	-	-
Dy	-	-	-	-	-	-	-	-	-	-	-	-	-
Ho	-	-	-	-	-	-	-	-	-	-	-	-	-
Er	-	-	-	-	-	-	-	-	-	-	-	-	-
Tm	-	-	-	-	-	-	-	-	-	-	-	-	-
Yb	-	-	-	-	-	-	-	-	-	-	-	-	-
Lu	-	-	-	-	-	-	-	-	-	-	-	-	-

Table E1.1. (Continued) Compilation of Meguma Zone granitoid lithogeochemistry

Sample	A16-1216-4	A16-1217-1	A16-1221	A16-1222	A16-1224	A16-1232	A16-1238-A	A16-1245-2	A16-1251-2	A16-1252	A16-1255-2	A16-1256	A16-1260-1
Batholith	SMB	SMB	SMB	SMB	SMB	SMB	SMB	SMB	SMB	SMB	SMB	SMB	SMB
Pluton	LLP	NRP	NRP	PLP	PLP	StLP	PLP	GRP	GRP	GRP	GRP	LLP	BBP
Lithology	Lg	Lmzg	Lmzg	Lmzg	Lmzg	Mzg	Lmzg	Lmzg	Lmzg	Lmzg	Lmzg	Lg	Lg
Source	27	27	27	27	27	27	27	27	27	27	27	27	27
Major oxides													
SiO_2	73 82	73.70	73.50	74 33	72.71	69 89	73 90	71 63	68 16	69 07	66 49	73 81	72 05
TiO_2	0.06	0.09	0.18	0 06	0.05	0.40	0 06	0 17	0 55	0.59	0 67	0 06	0 04
Al_2O_3	14.48	14.33	14.33	14 20	14.59	14.69	14.97	14 58	15 53	14 44	15 34	14 72	15 38
Fe_2O_3	-	-	-	-	-	-	-	-	-	-	-	-	-
FeO	-	-	-	-	-	-	-	-	-	-	-	-	-
MnO	0.04	0.04	0.03	0 03	0.03	0.08	0.02	0 04	0.08	0 09	0.08	0 03	0 03
MgO	0.70	0.73	0.86	0 74	0.73	1.41	0.80	0 95	1 48	1 71	1 74	0 71	0 72
CaO	0.31	0.36	0.43	0 32	0.43	1.07	0 34	0 42	1 60	1 27	1 54	0 32	0 40
Na_2O	3.55	4.39	3 23	3 74	4 08	3.52	3 83	3 59	3 16	3 53	3 67	3 97	4 86
K_2O	4.30	4.18	4.63	4.16	3.38	4.25	3 64	4.56	4 19	3 72	3 83	4 09	3 50
P_2O_5	0.41	0.38	0.31	0 34	0.50	0.23	0.46	0.31	0 23	0 21	0 21	0 48	0 54
H_2O+	-	-	-	-	-	-	-	-	-	-	-		-
H_2O-	-	-	-	-	-	-	-	-	-	-	-	-	-
CO_2	-	-	-	-	-	-	-	-	-	-	-	-	-
Cl	-	-	-	-	-	-	-	-	-	-	-	-	-
F	0.33	0.39	0.17	0.12	0.12	0.05	0.12	0 04	0.06	0 05	0 05	0 37	0 41
LOI	0.60	0 89	0 60	0 60	0 80	0.70	0 80	0 80	0 50	0 98	0 47	0 20	0 67
TOTAL	99 31	100 28	99 59	99 55	98 11	98 82	99 59	98 28	98 82	99 39	98 17	99 41	99 04
Fe_2O_3T	1.18	1.32	1.66	1.15	0.90	2 87	0 86	1 37	3 71	4 20	4 59	1 13	0 95
FeOT	1.06	1.19	1.49	1 03	0.81	2.58	0.77	1 23	3 34	3 78	4 13	1 02	0 85
A/CNK	1.19	1.09	1.16	1.16	1.26	1.13	1 30	1 14	1 18	1 16	1 16	1 19	1 20
Trace els.													
Ba	19	48	164	26	14	469	17	330	524	469	709	15	77
Rb	765	692	347	409	485	177	550	202	169	162	149	896	845
Sr	14	32	30	6	15	88	6	44	120	124	140	16	26
Y	26	35	19	16	16	24	17	18	30	36	35	25	39
Zr	39	44	79	33	28	129	20	64	175	183	226	39	20
Nb	28	24	16	13	25	12	34	8	12	11	13	28	34
Th	4.5	5.7	11	2.2	1 3	8.3	1	4 4	12	13	15	5	2
Pb	17	24	20	13	12	19	15	25	27	23	24	17	11
Ga	30	26	25	23	29	19	34	22	24	18	21	32	30
Zn	77	67	48	56	58	55	69	35	65	86	85	87	64
Cu	-	-	-	-	-	3	-	-	-	12	6	-	-
Ni	-	-	-	-	-	-	-	-	-	-	-	-	-
V	3	10	6	2	-	25	-	10	50	44	54	4	-
Cr	-	-	-	-	-	-	-	-	-	-	-	-	-
Hf	1	1	3	1	1	5	1	1	6	7	8	1	2
Cs	-	-	-	-	-	-	-	-	-	-	-	-	-
Sc	1.7	2.5	2.5	1.4	4 2	6.7	7.6	4 3	8 2	11	12	1 8	2 2
Ta	1.1	5.6	6.8	2.2	0 8	2 9	1.2	1 2	1 3	1	1 2	1 1	14
Co	-	-	-	-	-	-	-	-	-	-	-	-	-
Li	417	312	123	143	89	133	109	160	98	80	84	502	336
Be	-	-	-	-	-	-	-	-	-	-	-	-	-
B	20	19	30	30	30	60	30	80	30	29	22	25	14
U	5 2	5.8	16	10	21 4	3.1	8 8	5 9	2.5	2 9	2 6	4 6	4 3
W	19	13	5	5	8	1	10	3	1	2	-	8	8
Sn	38	40	16	19	20	12	31	13	8	4	2	41	31
Mo	-	-	-	-	-	-	-	-	-	-	-	-	-
Rare-earths													
La	3	6	13	2	2	21	2	8	30	32	39	2	-
Ce	-	-	-	-	-	-	-	-	-	-	-	-	-
Pr	-	-	-	-	-	-	-	-	-	-	-	-	-
Nd	-	-	-	-	-	-	-	-	-	-	-	-	-
Sm	-	-	-	-	-	-	-	-	-	-	-	-	-
Eu	-	-	-	-	-	-	-	-	-	-	-	-	-
Gd	-	-	-	-	-	-	-	-	-	-	-	-	-
Tb	-	-	-	-	-	-	-	-	-	-	-	-	-
Dy	-	-	-	-	-	-	-	-	-	-	-	-	-
Ho	-	-	-	-	-	-	-	-	-	-	-	-	-
Er	-	-	-	-	-	-	-	-	-	-	-	-	-
Tm	-	-	-	-	-	-	-	-	-	-	-	-	-
Yb	-	-	-	-	-	-	-	-	-	-	-	-	-
Lu	-	-	-	-	-	-	-	-	-	-	-	-	-

Table E1 1 (Continued) Compilation of Meguma Zone granitoid lithogeochemistry

Sample	A16-1265	A16-1268-1	A16-1269-1	A16-1276	A16-1277-1	A16-1278	A16-1279-3	A16-1281	A16-1287-1	A16-1290-1	A16-1299	A16-1302	A16-1333
Batholith	SMB	SMB	SMB	SMB	SMB	SMB	SMB	SMB	SMB	SMB	SMB	SMB	SMB
Pluton	LLP	StLP	StLP	StLP	GRP	StLP	StLP	MG	StLP	PLP	GRP	GRP	StLP
Lithology	Lg	Mzg	Mzg	Mzg	Lmzg	Mzg	Mzg	Grd	Mzg	Lmzg	Lmzg	Lmzg	Mzg
Source	27	27	27	27	27	27	27	27	27	27	27	27	27
Major oxides													
SiO_2	72 74	67 45	68 95	69 12	72 45	67 37	68 54	68 94	68 72	73 91	73 18	72 01	71 08
TiO_2	0 06	0 69	0 57	0 53	0 21	0 53	0 41	0 61	0 54	0 11	0 17	0 16	0 40
Al_2O_3	14 66	14 74	14 53	14 84	14 57	15 38	15 37	14 62	14 85	13 74	14 95	15 02	14 51
Fe_2O_3	-	-	-	-	-	-	-	-	-	-	-	-	-
FeO	-	-	-	-	-	-	-	-	-	-	-	-	-
MnO	0 03	0 10	0 09	0 09	0 03	0 07	0 07	0 07	0 09	0 05	0 03	0 04	0 06
MgO	0 70	1 56	1 47	1 49	1 05	1 52	1 22	1 82	1 38	0 78	1 06	0 78	1 31
CaO	0 22	1 83	1 49	1 34	0 65	1 62	1 36	1 75	1 22	0 31	0 36	0 36	1 42
Na_2O	3 57	3 47	3 77	3 09	3 31	3 73	3 90	3 35	3 63	4 11	3 31	4 15	3 30
K_2O	4 17	3 89	3 88	4 05	5 06	4 22	4 84	3 52	4 27	4 41	4 69	4 88	4 03
P_2O_5	0 41	0 23	0 21	0 22	0 14	0 21	0 18	0 19	0 22	0 28	0 30	0 34	0 16
H_2O+	-	-		-	-	-	-	-	-	-	-	-	-
H_2O-	-	-	-	-	-	-	-	-	-	-	-	-	-
CO_2	-	-	-	-	-	-	-	-	-	-	-	-	-
Cl	-	-	-	-	-	-	-	-	-	-	-	-	-
F	0 37	0 06	0 05	0 07	0 03	0 05	0 03	0 07	0 05	0 10	0 04	0 01	0 04
LOI	0 70	0 32	0 51	0 50	0 53	0 44	0 57	0 80	0 82	0 45	0 50	0 75	0 80
TOTAL	98 33	98 72	99 21	98 57	99 36	98 45	99 13	99 22	99 21	99 46	99 71	99 56	99 57
Fe_2O_3T	1 19	4 93	4 16	3 67	1 51	3 73	2 97	3 94	3 86	1 46	1 29	1 19	2 78
FeOT	1 07	4 44	3 74	3 30	1 36	3 36	2 67	3 55	3 47	1 31	1 16	1 07	2 50
A/CNK	1 24	1 10	1 09	1 19	1 08	1 10	1 03	1 16	1 11	1 05	1 20	1 08	1 13
Trace els													
Ba	23	616	533	397	537	651	606	525	476	63	435	503	504
Rb	866	156	160	175	248	162	157	143	179	364	191	199	142
Sr	20	148	125	106	71	135	112	127	127	17	44	48	122
Y	27	41	38	29	33	35	31	30	36	23	17	21	24
Zr	43	226	194	176	122	163	129	182	181	56	64	63	128
Nb	29	12	11	12	10	11	8	15	10	12	9	10	10
Th	5 5	15	14	11	20 7	12	10	12	12	4 8	4 8	5 2	8 8
Pb	23	14	-	28	24	-	31	26	22	11	28	23	27
Ga	26	17	18	23	17	21	19	21	17	19	21	16	19
Zn	74	70	64	101	39	68	81	88	63	49	38	23	51
Cu	-	19	7	-	-	7	-	1	8	13	-	-	3
Ni	-	-	-	-	-	-	-	-	-	-	-	-	-
V	1	56	43	41	7	42	43	53	37	-	5	-	31
Cr	-	-	-	-	-	-	-	-	-	-	-	-	-
Hf	1	8	7	5	4	5	4	7	6	2	2	3	4
Cs	-	-	-	-	-	-	-	-	-	-	-	-	-
Sc	1 7	14	12	8 3	4 2	9	6 6	8 9	10	3	3 4	4	6 1
Ta	8 7	1 2	1 5	8 3	1 5	1	0 9	1 2	1 2	2 7	1 2	1 6	0 9
Co	-	-	-	-	-	-	-	-	-	-	-	-	-
Li	497	65	70	102	96	80	52	74	73	132	68	49	65
Be	-	-	-	-	-	-	-	-	-	-	-	-	-
B	25	15	24	60	38	23	33	30	24	22	45	36	65
U	5 7	5 3	3 9	3 1	6 4	4 2	3 8	2 2	2.9	5	5 7	7 9	1 9
W	9	-	-	1	2	-	-	1	2	5	3	6	2
Sn	36	4	8	10	13	2	2	2	3	22	16	11	7
Mo	-	-	-	-	-	-	-	-	-	-	-	-	-
Rare-earths													
La	3	41	36	30	36	30	21	34	28	7	9	9	24
Ce	-	-	-	-	-	-	-	-	-	-	-	-	-
Pr	-	-	-	-	-	-	-	-	-	-	-	-	-
Nd	-	-	-	-	-	-	-	-	-	-	-	-	-
Sm	-	-	-	-	-	-	-	-	-	-	-	-	-
Eu	-	-	-	-	-	-	-	-	-	-	-	-	-
Gd	-	-	-	-	-	-	-	-	-	-	-	-	-
Tb	-	-	-	-	-	-	-	-	-	-	-	-	-
Dy	-	-	-	-	-	-	-	-	-	-	-	-	-
Ho	-	-	-	-	-	-	-	-	-	-	-	-	-
Er	-	-	-	-	-	-	-	-	-	-	-	-	-
Tm	-	-	-	-	-	-	-	-	-	-	-	-	-
Yb	-	-	-	-	-	-	-	-	-	-	-	-	-
Lu	-	-	-	-	-	-	-	-	-	-	-	-	-

Table E1 1 (Continued) Compilation of Meguma Zone granitoid lithogeochemistry

Sample	A16-3016	A16-3024	A16-3027	A16-3036	A16-3046	A16-3047	A16-3048	A16-3049	A16-3051	A16-3052	A16-3053	A16-3054	A16-3056
Batholith	SMB	SMB	SMB	SMB	SMB	SMB	SMB	SMB	SMB	SMB	SMB	SMB	SMB
Pluton	BIP	PLP	SaLP	BIP	-	-	PLP	NRP	MG	MG	MG	PLP	PLP
Lithology	Mzg	Lmzg	Mzg	Mzg	MPOR	MPOR	Lmzg	Lmzg	Grd	Grd	Grd	Lmzg	Lmzg
Source	27	27	27	27	27	27	27	27	27	27	27	27	27
Major oxides													
SiO_2	75 85	73 19	69 15	73 63	69 50	70 01	73 00	72 09	67 86	66 06	67 80	73 58	71 88
TiO_2	0 02	0 22	0 46	0 09	0 51	0 47	0 12	0 21	0 61	0 73	0 68	0 28	0 25
Al_2O_3	13 83	14 11	15 28	13 54	14 47	14 28	14 61	14 08	14 57	15 99	15 35	14 88	14 44
Fe_2O_3	-	-	-	-	-	-	-	-	-	-	-	-	-
FeO	-	-	-	-	-	-	-	-	-	-	-	-	-
MnO	0 04	0 05	0 06	0 08	0 06	0 07	0 04	0 05	0 08	0 09	0 07	0 03	0 05
MgO	0 64	1 24	2.18	0 84	1 64	1 50	0 90	1 00	1 78	2 14	1 92	0 99	0 97
CaO	0 32	0 32	1 59	0 43	0 87	0 97	0 36	0 71	2 16	2 41	2 61	0 83	0 60
Na_2O	3 53	3 03	3 62	3 44	3 43	3 93	3 82	3 47	3 34	3 32	3 32	3 33	3 69
K_2O	4 89	5 20	4 57	5 60	4 12	4 35	4 62	5 01	3 52	3 39	2 99	4 97	4 97
P_2O_5	0 12	0 18	0 19	0 13	0 21	0 21	0 34	0 17	0 21	0 22	0 19	0 19	0 27
H_20+	-	-	-	-	-	-	-	-	-	-	-	-	-
H_2O-	-	-	-	-	-	-	-	-	-	-	-	-	-
CO_2	-	-	-	-	-	-	-	-	-	-	-	-	-
Cl	-	-	-	-	-	-	-	-	-	-	-	-	-
F	0 01	0 06	0 09	0 01	0 06	0 07	0 05	0 06	0 06	0 07	0 06	0 07	0 10
LOI	0 40	0 60	0 20	0 50	0 80	0 70	0 60	0 40	0 80	0 70	0 60	0 30	0 50
TOTAL	100 31	100 04	100 42	99 30	98 9?	99 60	99 71	98 99	98 76	99 23	99 39	100 95	99 56
Fe_2O_3T	0 75	2 11	3 47	1 13	3 68	3 46	1 44	2 00	4 26	4 64	4 29	1 75	2 16
FeOT	0 67	1 90	3 12	1 02	3 31	3 11	1 30	1 80	3 83	4 18	3 86	1 57	1 94
A/CNK	1 06	1 10	1 06	0 95	1 16	1 05	1 12	1 03	1 11	1 21	1 19	1 10	1 05
Trace els													
Ba	5	312	484	126	483	467	183	277	644	825	830	396	222
Rb	175	243	201	166	210	217	248	233	129	130	105	250	334
Sr	5	53	125	33	118	99	37	66	191	227	235	74	48
Y	11	26	32	16	25	25	15	25	41	30	25	18	23
Zr	26	101	160	46	160	152	54	92	182	196	185	132	112
Nb	4	11	13	6	12	12	11	11	11	14	11	9	17
Th	0 8	10	16	3 9	11	11	2 9	10	15	12	12	17	15
Pb	22	23	20	27	25	20	22	25	19	17	14	21	23
Ga	18	23	27	20	26	22	20	20	22	22	24	25	25
Zn	17	30	53	24	73	57	29	42	59	69	60	46	59
Cu	-	-	-	-	5	-	-	-	7	-	7	-	-
Ni	-	-	-	-	-	-	-	-	-	-	-	-	-
V	-	10	28	4	40	36	6	10	56	64	61	16	9
Cr	-	-	-	-	-	-	-	-	-	-	-	-	-
Hf	1	3	5	2	4	4	2	3	6	6	6	4	4
Cs	-	-	-	-	-	-	-	-	-	-	-	-	-
Sc	0 5	4 1	7 4	2 9	8 5	7 9	3 8	3 7	11	11	10	3 4	3 8
Ta	0 5	1 6	1 3	0 7	1 5	1 5	2 4	1 2	0 9	1	0 7	1 1	2 5
Co	-	-	-	-	-	-	-	-	-	-	-	-	-
Li	25	60	56	29	73	73	46	75	49	44	48	68	114
Be	-	-	-	-	-	-	-	-	-	-	-	-	-
B	25	25	20	20	30	25	35	25	20	20	20	20	25
U	1 6	3 2	3 6	2 9	4 3	2 9	2 6	3 3	3 1	2 2	1 3	4	5 4
W	1	2	1	2	1	1	5	1	1	1	1	1	2
Sn	6	15	8	7	11	10	22	17	8	9	8	10	20
Mo	-	-	-	-	-	-	-	-	-	-	-	-	-
Rare-earths													
La	2	19	36	7	31	29	7	19	41	39	37	32	25
Ce	-	-	-	-	-	-	-	-	-	-	-	-	-
Pr	-	-	-	-	-	-	-	-	-	-	-	-	-
Nd	-	-	-	-	-	-	-	-	-	-	-	-	-
Sm	-	-	-	-	-	-	-	-	-	-	-	-	-
Eu	-	-	-	-	-	-	-	-	-	-	-	-	-
Gd	-	-	-	-	-	-	-	-	-	-	-	-	-
Tb	-	-	-	-	-	-	-	-	-	-	-	-	-
Dy	-	-	-	-	-	-	-	-	-	-	-	-	-
Ho	-	-	-	-	-	-	-	-	-	-	-	-	-
Er	-	-	-	-	-	-	-	-	-	-	-	-	-
Tm	-	-	-	-	-	-	-	-	-	-	-	-	-
Yb	-	-	-	-	-	-	-	-	-	-	-	-	-
Lu	-	-	-	-	-	-	-	-	-	-	-	-	-

Table E1 1 (Continued) Compilation of Meguma Zone granitoid lithogeochemistry

Sample	A16-3057	D05-0002	D05-0003	D05-0005	D05-0015	D05-0015-2	D05-0016-1	D05-0016-2	D05-0018	D05-3043-1	D05-3051	D05-3052	D05-3059
Batholith	SMB	SMB	SMB	SMB	SMB	SMB	SMB	SMB	SMB	SMB	SMB	SMB	SMB
Pluton	PLP	HFP	HP	HFP	HP	HP	PCP	PCP	PCP	HFP	HP	HFP	-
Lithology	Lmzg	Mzg	Lmzg	Mzg	Lmzg	Lmzg	Mzg	Mzg	Mzg	Mzg	Lmzg	Mzg	MPOR
Source	27	27	27	27	27	27	27	27	27	27	27	27	27
Major oxides													
SiO_2	73 68	71 90	73 23	69 11	72 14	72 09	72 57	70 66	69 50	69 95	73 41	68 74	70 13
TiO_2	0 16	0 32	0 21	0 44	0 23	0 29	0 31	0 41	0 44	0 40	0 21	0 49	0 29
Al_2O_3	13 92	14 33	14 01	15 25	14 40	14 45	14 03	14 63	14 96	15 10	13 92	15 42	14 65
Fe_2O_3	-	-	-	-	-	-	-	-	-	-	-	-	-
FeO	-	-	-	-	-	-	-	-	-	-	-	-	-
MnO	0 04	0 07	0 07	0 07	0 05	0 05	0 06	0 06	0 07	0 07	0 06	0 07	0 07
MgO	0 80	0 98	0 85	1 14	1 21	1 21	1 25	1 52	1 25	1 41	1 03	1 50	3 60
CaO	0 37	1 08	0 73	1 32	0 92	0 87	1 06	1 37	1 44	1 54	0 84	1 73	1 21
Na_2O	3 65	3 31	3 39	3 23	3 93	3 44	3 59	3 56	3 13	3 62	3 64	3 46	3 63
K_2O	4 75	4 34	4 35	4 60	4 29	4 68	4 57	4 18	4 64	4 13	4 43	4 31	4 14
P_2O_5	0 24	0 21	0 21	0 27	0 18	0 25	0 17	0 19	0 18	0 20	0 19	0 17	0 20
H_2O+	-	-	-	-	-	-	-	-	-	-		-	-
H_2O-	-	-	-	-	-	-	-	-	-	-	-		-
CO_2	-	-	-	-	-	-	-	-	-	-	-	-	-
Cl	-	-	-	-	-	-	-	-	-	-	-	-	-
F	0 08	0 06	0 05	0 09	0 06	0 09	0 06	0 06	0 06	0 07	0 06	0 07	0 07
LOI	0 70	0 60	0 60	0 70	0 50	0 40	0 40	0 40	0 60	0 70	0 30	0 40	0 50
TOTAL	99 90	99 42	99 67	99 11	99 74	99 84	100 29	99 65	99 07	99 78	99 86	99 44	100 67
Fe_2O_3T	1 77	2.53	2 24	3 31	2 10	2.34	2 53	2 97	3 18	2 96	2 03	3 50	2 50
FeOT	1 59	2 28	2 02	2.98	1 89	2.11	2.28	2 67	2 86	2 66	1 83	3 15	2 25
A/CNK	1 07	1 11	1 12	1 13	1 07	1 08	1 03	1 09	1 10	1 11	1 06	1 11	1 11
Trace els													
Ba	139	320	178	393	234	321	327	412	640	472	272	552	262
Rb	298	223	253	253	226	258	192	190	176	194	237	178	220
Sr	31	97	59	93	84	78	88	122	151	132	67	161	89
Y	20	23	24	26	26	22	28	24	27	27	23	30	22
Zr	73	107	81	143	90	116	118	135	142	147	91	161	90
Nb	12	10	11	14	10	12	10	10	11	13	11	11	10
Th	7 7	10	7 7	11	8 7	11	11	13	12	13	8 5	12	12
Pb	21	19	21	19	19	26	27	25	20	29	23	21	18
Ga	24	25	21	20	23	24	19	21	18	24	21	26	19
Zn	46	52	44	58	43	47	53	53	54	62	40	57	43
Cu	-	-	-	-	-	-	-	-	5	-	-	6	-
Ni	-	-	-	-	-	-	-	-	-	-	-	-	-
V	3	23	12	30	18	16	22	29	31	28	14	38	20
Cr	-	-	-	-	-	-	-	-	-	-	-	-	-
Hf	2	3	2	5	3	4	4	5	4	4	3	5	3
Cs	-	-	-	-	-	-	-	-	-	-	-	-	-
Sc	2.8	5 3	4 3	8	4 7	4 5	5 2	6 8	7 2	6 8	4 3	8 6	8 8
Ta	1 9	1 6	1 8	2 4	1 3	1 4	1 2	1 3	1 1	1	1 4	1	1 1
Co	-	-	-	-	-	-	-	-	-	-	-	-	-
Li	80	97	82	78	95	95	79	81	65	91	99	82	95
Be	-	-	-	-	-	-	-	-	-	-	-	-	-
B	30	25	30	30	30	40	25	30	25	30	35	25	20
U	4	5 4	5 9	8	3 3	7 8	4 2	3 1	2 2	5 9	3	3 1	3 6
W	1	1	1	1	1	1	1	1	1	1	2	1	1
Sn	16	13	12	12	3	8	8	9	8	7	6	5	15
Mo	-	-	-	-	-	-	-	-	-	-	-	-	-
Rare-earths													
La	12	21	14	31	16	22	21	27	30	28	16	32	27
Ce	-	-	-	-	-	-	-	-	-	-	-	-	-
Pr	-	-	-	-	-	-	-	-	-	-	-	-	-
Nd	-	-	-	-	-	-	-	-	-	-	-	-	-
Sm	-	-	-	-	-	-	-	-	-	-	-	-	-
Eu	-	-	-	-	-	-	-	-	-	-	-	-	-
Gd	-	-	-	-	-	-	-	-	-	-	-	-	-
Tb	-	-	-	-	-	-	-	-	-	-	-	-	-
Dy	-	-	-	-	-	-	-	-	-	-	-	-	-
Ho	-	-	-	-	-	-	-	-	-	-	-	-	-
Er	-	-	-	-	-	-	-	-	-	-	-	-	-
Tm	-	-	-	-	-	-	-	-	-	-	-	-	-
Yb	-	-	-	-	-	-	-	-	-	-	-	-	-
Lu	-	-	-	-	-	-	-	-	-	-	-	-	-

Table E1 1 (Continued) Compilation of Meguma Zone granitoid lithogeochemistry

Sample	D05-3060	D05-3098-3	D05-3099	D05-3105	D12-0001	D12 0004	D12-0004-2	D12 0021-1	D12-0021-2	D12 0021-3	D12-0022-2	D12-0023-1	D12 0028
Batholith	SMB	SMB	SMB	SMB	SMB	SMB	SMB	SMB	SMB	SMB	SMB	SMB	SMB
Pluton	-	PCP	HFP	HFP	TP	TP	TP	HFP	HFP	HFP	HFP	HFP	SaLP
Lithology	MPOR	Mzg	Mzg	Mzg	Lmzg	Lmzg	Lmzg	Mzg	Mzg	Mzg	Mzg	Mzg	Mzg
Source	27	27	27	27	27	27	27	27	27	27	27	27	27
Major oxides													
SiO_2	67 94	69 75	71 01	70 37	76 08	74 31	73 68	71 11	71 44	72 34	70 77	70 05	69 28
TiO_2	0 56	0 46	0 37	0 32	0 10	0 22	0 22	0 45	0 42	0 36	0 45	0 44	0 51
Al_2O_3	14 84	14 93	14 87	15 18	12.94	14 36	14 87	14 27	14 16	14 09	14 72	14 96	15 10
Fe_2O_3	-	-	-	-	-	-	-	-	-	-	-	-	-
FeO	-	-	-	-	-	-	-	-	-	-	-	-	-
MnO	0 08	[illegible]	0 06	0 05	0 05	0 06	0 06	0 06	0 06	0 06	0 06	0 06	0 07
MgO	2 12	1 32	1 19	1 24	0 63	0 75	0 83	1 47	1 01	0 99	1 08	1 36	1 34
CaO	2.32	1 40	1 16	0 91	0 28	0 48	0 59	1 16	1 17	1 11	1 16	1 13	1 68
Na_2O	4 56	3 13	3 66	3 11	2 70	3 20	3 53	3 85	3 30	3 10	3 21	3 41	3 40
K_2O	3 49	4 22	4 67	5 17	4 34	4 68	4 43	4 12	4 18	4 24	4 43	4 64	4 13
P_2O_5	0 20	0 19	0 25	0 25	0 18	0 19	0 26	0 26	0 25	0 27	0 28	0 26	0 18
H_20+	-	-	-	-	-	-	-	-	-	-	-	-	-
H_2O-	-	-	-	-	-	-	-	-	-	-	-	-	-
CO_2	-	-	-	-	-	-	-	-	-	-	-	-	-
Cl	-	-	-	-	-	-	-	-	-	-	-	-	-
F	0 06	0 07	0 09	0 07	0 06	0 06	0 06	0 08	0 08	0 07	0 07	0 08	0 06
LOI	0 70	0 90	0 40	0 70	1 00	0 60	0 80	0 50	0 70	0 60	0 80	0 60	0 60
TOTAL	100 39	99 51	100 09	99 56	99 78	100 83	100 89	100 11	99 51	99 69	99 82	99 66	99 63
Fe_2O_3T	3 98	3 48	2 72	2 51	1 64	2 20	2 02	3 18	3 13	2 81	3 18	2 94	3 71
FeOT	3 58	3 13	2 45	2.26	1 48	1 98	1 82	2 86	2 82	2 53	2 86	2 65	3 34
A/CNK	0 99	1 16	1 06	1 11	1 18	1 15	1 16	1 06	1 11	1 13	1 13	1 10	1 12
Trace els													
Ba	446	484	415	501	78	170	240	325	304	303	363	466	584
Rb	182	184	245	258	248	273	286	236	235	226	238	249	173
Sr	151	125	89	99	18	44	62	89	91	79	92	106	145
Y	22	30	22	22	19	26	24	28	25	24	24	24	31
Zr	148	153	123	116	63	89	79	152	139	123	140	139	166
Nb	12	11	14	13	8	12	11	16	13	13	16	14	12
Th	8	12	11	11	5 1	7 6	5 9	13	5 7	10	12	11	12
Pb	14	19	33	29	20	19	16	24	18	21	22	30	20
Ga	20	19	22	26	19	21	20	22	20	17	18	23	22
Zn	74	64	56	58	37	136	41	84	54	17	60	57	59
Cu	4	2	-	-	2	2	2	-	-	55	3	10	3
Ni	-	-	-	-	-	-	-	-	-	-	-	-	-
V	50	33	23	18	3	13	12	36	30	20	28	32	33
Cr	-	-	-	-	-	-	-	-	-	-	-	-	-
Hf	3	5	4	4	2	2	2	6	3	3	4	4	4
Cs	-	-	-	-	-	-	-	-	-	-	-	-	-
Sc	5 5	7 7	5 8	4 8	1 8	4 3	3 7	7 2	4 9	5 2	5 9	6 7	7 7
Ta	1 6	1 2	1 6	1 4	1 7	1 8	1 8	1 9	0 7	1 4	1 6	1 7	1 1
Co	-	-	-	-	-	-	-	-	-	-	-	-	-
Li	94	88	97	89	62	112	134	113	110	122	126	90	96
Be	-	-	-	-	-	-	-	-	-	-	-	-	-
B	30	25	35	30	40	25	30	30	20	35	30	30	25
U	4 4	2 9	4 1	4	3 4	3 9	4 5	8 5	1 9	5 6	2 7	3 9	3 4
W	1	1	1	1	5	3	2	1	1	1	1	1	1
Sn	12	1	9	4	13	10	12	9	3	11	9	7	5
Mo	-	-	-	-	-	-	-	-	-	-	-	-	-
Rare-earths													
La	16	31	23	22	8	15	13	30	17	22	26	24	31
Ce	-	-	-	-	-	-	-	-	-	-	-	-	-
Pr	-	-	-	-	-	-	-	-	-	-	-	-	-
Nd	-	-	-	-	-	-	-	-	-	-	-	-	-
Sm	-	-	-	-	-	-	-	-	-	-	-	-	-
Eu	-	-	-	-	-	-	-	-	-	-	-	-	-
Gd	-	-	-	-	-		-	-	-	-	-	-	-
Tb	-	-	-	-	-	-	-	-	-	-	-	-	-
Dy	-	-	-	-	-	-	-	-	-	-	-	-	-
Ho	-	-	-	-	-	-	-	-	-	-	-	-	-
Er	-	-	-	-	-	-	-	-	-	-	-	-	-
Tm	-	-	-	-	-	-	-	-	-	-	-	-	-
Yb	-	-	-	-	-	-	-	-	-	-	-	-	-
Lu	-	-	-	-	-	-	-	-	-	-	-	-	-

Table E1 1 (Continued) Compilation of Meguma Zone granitoid lithogeochemistry

Sample	D12-0030-3	D12-0030-C	D12-0033	D12-0033-3	D12-0035	D12-0037	D12-0039	D12 0040-1	D12-0042	D12-0043	D12-0044	D12-0045-C	D12-0048-3
Batholith	SMB	SMB	SMB	SMB	SMB	SMB	SMB	SMB	SMB	SMB	SMB	SMB	SMB
Pluton	HP	HP	HFP	HFP	HFP	HFP	HFP	HFP	HFP	HP	TP	HFP	PCP
Lithology	Lmzg	Lmzg	Mzg	Mzg	Mzg	Mzg	Mzg	Mzg	Mzg	Lmzg	Lmzg	Mzg	Mzg
Source	27	27	27	27	27	27	27	27	27	27	27	27	27
Major oxides													
SiO_2	72 53	70 31	70 40	71 06	70 78	71 72	71 39	71 98	71 77	71 65	74 42	71 83	70 83
TiO_2	0 28	0 24	0 46	0 42	0 38	0 37	0 37	0 31	0 35	0 37	0 05	0 27	0 38
Al_2O_3	14 43	15 57	14 83	14 37	14 80	14 46	14 57	14 64	14 28	14 27	14 48	14 76	14 64
Fe_2O_3	-	-	-	-	-	-	-	-	-	-	-	-	-
FeO	-	-	-	-	-	-	-	-	-	-	-	-	-
MnO	0 04	0 04	0 08	0 07	0 06	0 06	0 05	0 05	0 04	0 06	0 04	0 06	0 06
MgO	0 86	1 12	1 08	1 52	1 19	1 26	1 26	1 30	1 37	1 05	0 40	1 12	1 31
CaO	0 90	0 96	1 05	0 66	0 86	1 03	0 90	0 70	0 52	1 00	0 34	0 71	1 32
Na_2O	3 [illegible]6	4 18	3 36	3 61	3 82	3 96	3 53	3 84	3 85	3 01	3 99	4 89	3 64
K_2O	4 02	5 02	4 41	4 19	4 83	4 31	4 58	4 79	4 62	4 72	4 10	4 49	4 61
P_2O_5	0 24	0 23	0 26	0 23	0 26	0 22	0 26	0 28	0 27	0 23	0 33	0 30	0 14
H_20+	-	-	-	-	-	-	-	-	-	-	-	-	-
H_2O-	-	-	-	-	-	-				-			
CO_2	-	-	-	-	-	-	-	-	-	-	-	-	-
Cl	-	-	-	-	-	-	-	-	-	-	-	-	-
F	0 06	0 07	0 07	0 05	0 08	0 07	0 07	0 07	0 06	0 09	0 14	0 08	0 05
LOI	0 70	0 40	0 90	1 00	0 60	0 40	0 60	0 60	0 80	0 70	0 70	0 60	0 60
TOTAL	100 19	99 93	99 73	100 00	99 96	100 14	99 82	100 51	99 97	99 65	99 88	100 94	100 13
Fe_2O_3T	2 26	2 07	3 22	3 19	2 65	2 61	2 57	2 25	2 33	2 88	1 14	2 12	2 89
FeOT	2 03	1 86	2.90	2.87	2 38	2.35	2.31	2 02	2.10	2 59	1 03	1 91	2 60
A/CNK	1 07	1 04	1 14	1 15	1 05	1 06	1 09	1 06	1 07	1 10	1 16	0 99	1 04
Trace els													
Ba	319	283	390	247	366	264	369	305	369	374	33	279	477
Rb	261	246	237	235	278	240	246	275	270	220	499	264	178
Sr	78	89	106	80	89	80	89	70	75	105	7	65	124
Y	22	26	24	27	23	24	23	23	24	25	14	20	34
Zr	103	102	141	135	122	119	133	124	131	127	34	107	137
Nb	11	11	14	15	15	14	13	14	14	13	14	14	10
Th	8 8	10	11	10	11	11	13	12	14	11	1 6	9 3	11
Pb	21	25	21	83	25	22	21	25	22	19	16	21	30
Ga	18	25	20	24	22	20	24	23	23	21	24	24	24
Zn	44	46	85	234	60	55	60	50	57	65	44	55	53
Cu	-	1	-	-	-	-	-	3	-	3	-	-	-
Ni	-	-	-	-	-	-	-	-	-	-	-	-	-
V	21	14	35	32	27	23	22	20	15	21	3	13	27
Cr	-	-	-	-	-	-	-	-	-	-	-	-	-
Hf	3	3	5	4	4	4	3	3	3	3	1	3	5
Cs	-	-	-	-	-	-	-	-	-	-	-	-	-
Sc	4 3	4 2	6 2	6 3	5 6	5 5	5 2	4 9	4 8	5 8	2 3	4 2	6 6
Ta	1 5	1 3	1 8	1 5	1 9	1 8	1 4	1 8	2	1 3	3 8	1 9	1
Co	-	-	-	-	-	-	-	-	-	-	-	-	-
Li	106	63	89	63	96	95	94	83	90	80	230	95	75
Be	-	-	-	-	-	-	-	-	-	-	-	-	-
B	30	50	20	35	40	30	35	30	30	15	25	40	25
U	6 9	6 1	3	4 1	2 4	3 4	5 9	5 2	4 1	3 4	19	4 9	3 4
W	1	1	1	5	1	1	2	2	2	1	8	2	1
Sn	7	5	12	12	8	6	10	10	13	4	27	12	5
Mo	-	-	-	-	-	-	-	-	-	-	-	-	-
Rare-earths													
La	17	20	25	23	23	22	23	22	25	23	2	17	24
Ce	-	-	-	-	-	-	-	-	-	-	-	-	-
Pr	-	-	-	-	-	-	-	-	-	-	-	-	-
Nd	-	-	-	-	-	-	-	-	-	-	-	-	-
Sm	-	-	-	-	-	-	-	-	-	-	-	-	-
Eu	-	-	-	-	-	-	-	-	-	-	-	-	-
Gd	-	-	-	-	-	-	-	-	-	-	-	-	-
Tb	-	-	-	-	-	-	-	-	-	-	-	-	-
Dy	-	-	-	-	-	-	-	-	-	-	-	-	-
Ho	-	-	-	-	-	-	-	-	-	-	-	-	-
Er	-	-	-	-	-	-	-	-	-	-	-	-	-
Tm	-	-	-	-	-	-	-	-	-	-	-	-	-
Yb	-	-	-	-	-	-	-	-	-	-	-	-	-
Lu	-	-	-	-	-	-	-	-	-	-	-	-	-

Table E1 1 (Continued) Compilation of Meguma Zone granitoid lithogeochemistry

Sample	D12-0049	D12-0050	D12-0051	D12-0052	D12-0058-1	D12-0066	D12-0069	D12-0077-2	)12-0077-2-ı	D12-0081	D12 0082	D12-0085-2	D12-0095
Batholith	SMB	SMB	SMB	SMB	SMB	SMB	SMB	SMB	SMB	SMB	SMB	SMB	SMB
Pluton	PCP	HP	HP	HP	HFP	TP	HP	MG	MG	HP	MG	SaLP	SaLP
Lithology	Mzg	Lmzg	Lmzg	Lmzg	Mzg	Lmzg	Lmzg	Grd	Grd	Lmzg	Grd	Mzg	Mzg
Source	27	27	27	27	27	27	27	27	27	27	27	27	27
Major oxides													
SiO_2	69 30	72.97	73 55	73 55	70 80	75 14	72 65	68 16	69 19	72 59	66 89	70 19	68 71
TiO_2	0 33	0 21	0 13	0 14	0 46	0 08	0 17	0 62	0 48	0 28	0 66	0 38	0 53
Al_2O_3	15 88	14 35	14 56	14 45	14 66	14 11	14 95	15 45	15 23	14 15	15 50	14 99	15 43
Fe_2O_3	-	-	-	-	-	-	-	-	-	-	-	-	-
FeO	-	-	-	-	-	-	-	-	-	-	-	-	-
MnO	0 07	0 07	0 08	0 06	0 06	0 04	0 05	0 10	0 08	0 06	0 09	0 07	0 08
MgO	1 04	0 77	0 58	0 64	1 31	0 52	0 66	1 50	1 63	0 85	1 72	1 17	1 68
CaO	1 25	0 59	0 51	0 53	1 17	0 36	0 50	1 81	0 96	0 63	1 89	1 18	1 08
Na_2O	3 50	3 14	3 30	3 38	3 49	3 66	3 30	3 51	3 66	3 29	3 81	3 41	3 55
K_2O	5 20	4 89	4 63	4 83	4 45	4 31	4 84	3 64	4 69	4 37	3 99	4 64	4 45
P_2O_5	0 16	0 19	0 21	0 23	0 27	0 26	0 28	0 21	0 18	0 18	0 22	0 19	0 20
H_20+	-	-	-	-	-	-	-	-	-	-	-	-	-
H_2O-	-	-	-	-	-	-	-	-	-	-	-	-	-
CO_2	-	-	-	-	-	-	-	-	-	-	-	-	-
Cl	-	-	-	-	-	-	-	-	-	-	-	-	-
F	0 06	0 08	0 10	0 09	0 07	0 11	0 11	0 07	0 07	0 06	0 06	0 07	0 09
LOI	0 60	0 70	0 70	0 50	0 50	0 70	0 70	0 60	0 70	0 70	0 70	0 50	0 80
TOTAL	99 72	99 81	99 94	99 93	99 93	100 39	99 83	99 57	99 99	99 63	99 43	99 35	99 91
Fe_2O_3T	2 66	2 14	1 88	1 80	3 07	1 34	1 92	4 41	3 55	2 81	4 40	2 92	3 78
FeOT	2 39	1 93	1 69	1 62	2.76	1 21	1.73	3 97	3 19	2 53	3 96	2 63	3 40
A/CNK	1 08	1 12	1 16	1 11	1 09	1 14	1 16	1 18	1 11	1 15	1 10	1 10	1 15
Trace els													
Ba	470	216	127	104	399	50	173	588	556	222	648	446	726
Rb	199	287	339	330	253	427	340	169	195	225	157	201	249
Sr	124	60	28	27	94	19	37	179	140	58	160	112	150
Y	28	24	23	21	25	16	19	30	38	34	32	28	33
Zr	110	80	64	59	141	37	74	181	163	117	179	123	173
Nb	10	11	11	11	14	13	14	13	11	11	11	11	13
Th	10	8 2	7	6 5	12	3 5	6 7	12	12	12	13	11	12
Pb	23	23	19	20	24	14	18	14	25	17	24	21	27
Ga	20	21	23	19	21	20	22	22	27	20	19	18	21
Zn	48	48	54	50	61	32	51	64	69	33	93	57	100
Cu	-	-	-	-	-	-	-	-	-	-	2	4	8
Ni	-	-	-	-	-	-	-	-	-	-	-	-	-
V	23	10	8	5	33	3	8	50	37	17	41	23	40
Cr	-	-	-	-	-	-	-	-	-	-	-	-	-
Hf	3	3	2	1	4	1	2	6	5	4	5	3	5
Cs	-	-	-	-	-	-	-	-	-	-	-	-	-
Sc	5 3	4 3	3 5	3 6	6 2	4 1	3 7	11	7 9	5 6	8 9	6 8	8 2
Ta	1 2	1 9	2 3	2 6	1 6	3 5	2 6	1 3	1	1 7	1 2	1 4	1 1
Co	-	-	-	-	-	-	-	-	-	-	-	-	-
Li	84	101	136	137	94	157	157	103	87	63	78	90	106
Be	-	-	-	-	-	-	-	-	-	-	-	-	-
B	20	20	20	25	20	25	15	20	30	20	10	15	30
U	3	4 6	3 2	2 9	2 6	5 2	8 1	3 9	2 5	3 3	3	4 8	3
W	1	3	6	2	1	6	1	1	1	1	2	2	3
Sn	8	14	21	16	6	24	18	5	3	16	8	12	9
Mo	-	-	-	-	-	-	-	-	-	-	-	-	-
Rare-earths													
La	23	14	9	10	26	5	12	37	34	23	36	26	34
Ce	-	-	-	-	-	-	-	-	-	-	-	-	-
Pr	-	-	-	-	-	-	-	-	-	-	-	-	-
Nd	-	-	-	-	-	-	-	-	-	-	-	-	-
Sm	-	-	-	-	-	-	-	-	-	-	-	-	-
Eu	-	-	-	-	-	-	-	-	-	-	-	-	-
Gd	-	-	-	-	-	-	-	-	-	-	-	-	-
Tb	-	-	-	-	-	-	-	-	-	-	-	-	-
Dy	-	-	-	-	-	-	-	-	-	-	-	-	-
Ho	-	-	-	-	-	-	-	-	-	-	-	-	-
Er	-	-	-	-	-	-	-	-	-	-	-	-	-
Tm	-	-	-	-	-	-	-	-	-	-	-	-	-
Yb	-	-	-	-	-	-	-	-	-	-	-	-	-
Lu	-	-	-	-	-	-	-	-	-	-	-	-	-

Table E1 1 (Continued) Compilation of Meguma Zone granitoid lithogeochemistry

Sample	D12-0098	D12-0099	D12-0103-1	D12-0103-2	D12-0103-3	D12-0104	D12-0105	D12-0106	D12-0122-C	D12-0130-4	D12-0130-6	D12-0130-8	D12-0134
Batholith	SMB	SMB	SMB	SMB	SMB	SMB	SMB	SMB	SMB	SMB	SMB	SMB	SMB
Pluton	SaLP	SaLP	HP	HP	HP	SaLP	MG	SaLP	SaLP	MG	MG	MG	MG
Lithology	Mzg	Mzg	Lmzg	Lmzg	Lmzg	Mzg	Grd	Mzg	Mzg	Grd	Grd	Grd	Grd
Source	27	27	27	27	27	27	27	27	27	27	27	27	27
Major oxides													
SiO_2	70 13	67 29	71 81	72 12	73 10	71 99	69 17	69 63	72 85	67 09	66 47	67 55	67 63
TiO_2	0 42	0 66	0 27	0 24	0 14	0 27	0 51	0 45	0 35	0 59	0 67	0 59	0 59
Al_2O_3	15 12	15 43	14 57	14 50	14 53	14 74	14 88	14 92	13 84	15 90	15 86	15 90	15 70
Fe_2O_3	-	-	-	-	-	-	-	-	-	-	-	-	-
FeO	-	-	-	-	-	-	-	-	-	-	-	-	-
MnO	0 09	0 10	0 05	0 05	0 06	0 06	0 09	0 07	0 07	0 09	0 08	0 09	0 08
MgO	1 34	1 63	0 90	0 77	0 69	1 16	1 59	1 19	1 56	1 88	1 96	1 57	1 56
CaO	0 96	1 72	0 88	0 76	0 43	0 79	1 53	1 47	0 85	1 93	2 33	1 93	1 77
Na_2O	3 41	3 49	2 99	3 39	3 14	3 40	4 13	3 04	3 52	3 87	3 56	3 55	3 42
K_2O	4 52	3 86	4 89	4 77	4 74	5 07	3 90	4 33	4 01	3 99	3 64	3 94	3 77
P_2O_5	0 19	0 21	0 21	0 24	0 27	0 15	0 14	0 18	0 17	0 20	0 21	0 19	0 18
H_2O+	-	-	-	-	-	-	-	-	-	-	-	-	-
H_2O-	-	-	-	-	-	-	-	-	-	-	-	-	-
CO_2	-	-	-	-	-	-	-	-	-	-	-	-	-
Cl	-	-	-	-	-	-	-	-	-	-	-	-	-
F	0 08	0 07	0 07	0 06	0 11	0 06	0 05	0 07	0 06	0 06	0 07	0 06	0 05
LOI	0 70	0 80	0 50	0 60	0 60	0 50	1 10	0 50	0 70	0 60	0 50	0 70	0 80
TOTAL	99 81	99 39	99 18	99 39	99 27	100 31	100 30	98 86	100 47	99 78	99 36	99 83	99 24
Fe_2O_3T	3 26	4 67	2 35	2 17	1 74	2 42	3 62	3 42	2 83	4 04	4 53	4 24	4 16
FeOT	2.93	4 20	2.11	1 95	1 57	2.18	3 26	3 08	2.55	3 64	4 08	3 82	3 74
A/CNK	1 15	1 16	1 12	1 09	1 17	1 07	1 07	1 14	1 12	1 11	1 15	1 16	1 20
Trace els													
Ba	500	614	242	245	123	304	507	474	295	794	624	550	534
Rb	222	165	234	266	350	242	154	177	198	161	148	144	152
Sr	129	182	69	68	27	67	165	126	85	210	190	181	178
Y	32	32	25	22	18	29	34	31	29	27	32	29	29
Zr	149	194	102	93	64	107	157	148	134	197	202	170	174
Nb	11	13	11	11	13	12	12	10	11	11	13	12	11
Th	11	12	10	8 2	7	10	10	12	12	13	12	13	12
Pb	25	21	20	18	20	27	22	21	24	35	23	20	18
Ga	17	20	20	20	24	24	23	21	21	24	21	18	19
Zn	75	71	43	44	54	51	82	59	52	80	69	54	57
Cu	14	6	-	3	-	-	-	-	-	-	7	-	-
Ni	-	-	-	-	-	-	-	-	-	-	-	-	-
V	29	49	13	13	4	17	45	33	26	48	50	45	43
Cr	-	-	-	-	-	-	-	-	-	-	-	-	-
Hf	4	6	4	3	1	4	5	4	4	7	6	6	6
Cs	-	-	-	-	-	-	-	-	-	-	-	-	-
Sc	6 9	10	4 3	3 9	3 3	4 9	7 5	7 2	5 5	9 3	10	10	10
Ta	1 1	1 2	1 2	1 7	2 8	1 3	0 8	1 1	1 2	1	1 1	1 1	1 2
Co	-	-	-	-	-	-	-	-	-	-	-	-	-
Li	128	102	58	76	123	82	63	96	108	70	64	86	69
Be	-	-	-	-	-	-	-	-	-	-	-	-	-
B	20	20	20	30	30	25	30	15	35	40	30	20	25
U	2 8	2.8	6 1	5 8	5	3 8	2 3	2 6	5 4	2 4	3 2	2 5	3 4
W	1	2	1	2	6	1	1	1	1	1	1	1	1
Sn	10	5	12	13	24	10	1	9	6	2	1	10	7
Mo	-	-	-	-	-	-	-	-	-	-	-	-	-
Rare-earths													
La	27	37	19	16	11	19	27	30	23	36	34	34	34
Ce	-	-	-	-	-	-	-	-	-	-	-	-	-
Pr	-	-	-	-	-	-	-	-	-	-	-	-	-
Nd	-	-	-	-	-	-	-	-	-	-	-	-	-
Sm	-	-	-	-	-	-	-	-	-	-	-	-	-
Eu	-	-	-	-	-	-	-	-	-	-	-	-	-
Gd	-	-	-	-	-	-	-	-	-	-	-	-	-
Tb	-	-	-	-	-	-	-	-	-	-	-	-	-
Dy	-	-	-	-		-	-	-	-	-	-	-	-
Ho	-	-	-	-	-	-	-	-	-	-	-	-	-
Er	-	-	-	-	-	-	-	-	-	-	-	-	-
Tm	-	-	-	-	-	-	-	-	-	-	-	-	-
Yb	-	-	-	-	-	-	-	-	-	-	-	-	-
Lu	-	-	-	-	-	-	-	-	-	-	-	-	-

Table E1.1 (Continued) Compilation of Meguma Zone granitoid lithogeochemistry

Sample	D12-0134-C	D12-0142	D12-3008	D12-3015	D12-3036	D12-3036-5	D12-3037-C	D12-3072	D12-3077-3	D12-3082	D12-3083	D12-3084-2	D12-3088
Batholith	SMB	SMB	SMB	SMB	SMB	SMB	SMB	SMB	SMB	SMB	SMB	SMB	SMB
Pluton	MG	SaLP	HP	HFP	HFP	HFP	HFP	HFP	HP	HP	HP	PCP	PCP
Lithology	Grd	Mzg	Lmzg	Mzg	Mzg	Mzg	Mzg	Mzg	Lmzg	Lmzg	Lmzg	Mzg	Mzg
Source	27	27	27	27	27	27	27	27	27	27	27	27	27
Major oxides													
SiO_2	67 71	70.77	73.51	71.57	73.88	70 60	71 39	70 80	74 41	73.15	73 46	71 40	70 10
TiO_2	0.60	0.37	0.18	0.46	0.21	0.45	0 46	0 38	0 16	0 18	0.17	0 38	0 36
Al_2O_3	15 46	14.54	14.06	14.32	13.99	14.75	14 21	14 87	13 86	14.01	14 13	14 24	14 96
Fe_2O_3	-	-	-	-	-	-	-	-	-	-	-	-	-
FeO	-	-	-	-	-	-	-	-	-	-	-	-	-
MnO	0.10	0.07	0.05	0.06	0.05	0.07	0.07	0.05	0 04	0.06	0.07	0 07	0 08
MgO	1 65	1.52	0.74	1.13	0.85	1.14	1 52	1 40	0.78	0 99	1 03	2 30	1 09
CaO	1.97	0.79	0.65	1.10	0.45	1.23	1.11	0.74	0 52	0 66	0.68	0 92	1 14
Na_2O	3.36	3.58	3.11	3.11	3.40	2.99	3.49	4 34	3 27	3 72	4 13	4 05	3 17
K_2O	4.00	4.30	4.47	4.27	4.54	4.61	4.22	4 67	4 51	4 38	4 63	4 62	4 75
P_2O_5	0 21	0.18	0.26	0.25	0 25	0 26	0.26	0 28	0 25	0 19	0 16	0 16	0 14
H_2O+	-	-	-	-	-	-	-	-	-	-	-	-	
H_2O-	-	-	-	-	-	-	-	-	-	-	-	-	
CO_2	-	-	-	-	-	-	-	-	-	-	-	-	-
Cl	-	-	-	-	-	-	-	-	-	-	-	-	-
F	0.09	0.08	0.09	0 07	0.05	0.06	0.08	0.08	0 08	0 08	0 09	0 05	0 06
LOI	0.50	1.00	0.50	0 60	0 80	0.70	0 80	0 60	0 40	0 60	0 50	0 30	0 60
TOTAL	99 35	99 82	99 33	99 80	100 10	99 68	100 32	100 49	99 77	99 63	100 66	100 99	99 05
Fe_2O_3T	4.21	3.00	2.00	3.26	1.87	3.20	3.10	2.62	1 74	1.99	1 89	2.95	2 97
FeOT	3.79	2.70	1.80	2.93	1.68	2.88	2.79	2.36	1 57	1 79	1 70	2 65	2 67
A/CNK	1.13	1.13	1.15	1.14	1.12	1.13	1 09	1 03	1.12	1 08	1 01	1 02	1 11
Trace els.													
Ba	541	325	155	376	105	442	308	363	147	163	146	441	428
Rb	174	204	299	219	278	220	230	269	282	261	278	197	207
Sr	166	99	45	100	33	100	92	92	39	52	46	130	109
Y	32	30	21	25	20	25	26	24	18	28	28	29	31
Zr	177	139	78	138	83	140	147	137	72	82	76	136	132
Nb	12	12	12	14	13	14	14	16	12	10	10	12	11
Th	11	12	7.4	12	7 6	11	12	13	9 3	7.4	7 2	12	12
Pb	21	22	16	18	17	19	21	23	19	32	25	25	24
Ga	24	25	24	20	22	19	23	23	21	24	20	24	21
Zn	65	69	43	56	44	61	58	63	63	80	80	73	65
Cu	5	-	-	1	1	-	-	-	-	-	-	-	-
Ni	-	-	-	-	-	-	-	-	-	-	-	-	-
V	43	30	10	35	12	29	31	21	8	13	9	25	23
Cr	-	-	-	-	-	-	-	-	-	-	-	-	-
Hf	6	5	3	5	2	4	4	3	3	2	3	5	4
Cs	-	-	-	-	-	-	-	-	-	-	-	-	-
Sc	11	6.8	3.9	6.7	3 7	5.7	6.1	5.4	3 6	3.7	3 4	5 4	6 7
Ta	1.1	1.5	1.9	1.4	2 4	1.7	2	2	2 1	1 6	1 5	1 1	1 1
Co	-	-	-	-	-	-	-	-	-	-	-	-	-
Li	59	60	127	87	88	73	97	84	89	88	105	80	72
Be	-	-	-	-	-	-	-	-	-	-	-	-	-
B	30	35	30	30	30	25	30	35	30	45	35	30	25
U	3	2.5	5.8	5	3.8	4.2	3.5	3 5	12	4 2	4.1	6 9	4 4
W	1	1	2	1	2	1	1	3	3	1	1	1	1
Sn	4	2	13	9	15	10	13	10	14	10	12	4	15
Mo	-	-	-	-	-	-	-	-	-	-	-	-	-
Rare-earths													
La	33	24	14	28	15	25	26	25	16	12	11	22	27
Ce	-	-	-	-	-	-	-	-	-	-	-	-	-
Pr	-	-	-	-	-	-	-	-	-	-	-	-	-
Nd	-	-	-	-	-	-	-	-	-	-	-	-	-
Sm	-	-	-	-	-	-	-	-	-	-	-	-	-
Eu	-	-	-	-	-	-	-	-	-	-	-	-	-
Gd	-	-	-	-	-	-	-	-	-	-	-	-	-
Tb	-	-	-	-	-	-	-	-	-	-	-	-	-
Dy	-	-	-	-	-	-	-	-	-	-	-	-	-
Ho	-	-	-	-	-	-	-	-	-	-	-	-	-
Er	-	-	-	-	-	-	-	-	-	-	-	-	-
Tm	-	-	-	-	-	-	-	-	-	-	-	-	-
Yb	-	-	-	-	-	-	-	-	-	-	-	-	-
Lu	-	-	-	-	-	-	-	-	-	-	-	-	-

Table E1 1 (Continued) Compilation of Meguma Zone granitoid lithogeochemistry

Sample	D12-3097	D12-3111	D12-3114	D12-3128-C	D12-3133	D12-3136	D12-3136-2	D13-2001	D13-2003	D13-2004	D13-2026	D13-2027	D13-2030
Batholith	SMB	SMB	SMB	SMB	SMB	SMB	SMB	SMB	SMB	SMB	SMB	SMB	SMB
Pluton	PCP	HP	HP	HP	MG	HP	HP	MG	MG	MG	WBP	WBP	MG
Lithology	Mzg	Lmzg	Lmzg	Lmzg	Grd	Lmzg	Lmzg	Grd	Grd	Grd	Lg	Lg	Grd
Source	27	27	27	27	27	27	27	27	27	27	27	27	27
Major oxides													
SiO_2	69 31	71 77	72.52	72 98	68 01	74 17	74 68	68 75	68 79	67 26	72 81	73 01	68 10
TiO_2	0 36	0 22	0 19	0 13	0 53	0 09	0 09	0 59	0 51	0 83	0 19	0 15	0 59
Al_2O_3	15 46	14 70	14 55	14 67	15 65	13 64	13 83	15 19	15 42	15 10	15 07	14 70	15 22
Fe_2O_3	-	-	-	-	-	-	-	-	-	-	-	-	-
FeO	-	-	-	-	-	-	-	-	-	-	-	-	-
MnO	0 06	0 04	0 07	0 04	0 08	0 06	0 06	0 08	0 07	0 08	0 03	0 03	0 08
MgO	1 38	1 08	0 79	0 92	1 67	0 68	0 95	1 61	1 59	1 74	0 85	0 77	1 69
CaO	1 13	0 67	0 79	0 65	1 41	0 32	0 31	1 43	1 60	2 37	0 38	0 37	2 14
Na_2O	3 41	4 13	2 96	4 06	3 81	3 28	3 61	3 38	3 14	2 99	3 14	3 41	3 31
K_2O	5 16	4 84	4 60	4 67	4 27	4 48	4 50	3 62	3 87	3 18	4 69	4 36	3 71
P_2O_5	0 17	0 26	0 18	0 25	0 19	0 19	0 20	0 23	0 24	0 21	0 31	0 32	0 19
H_2O+	-	-	-	-	-	-	-	-	-	-	-	-	-
H_2O-	-	-	-	-	-	-	-	-	-	-	-	-	-
CO_2	-	-	-	-	-	-	-	-	-	-	-	-	-
Cl	-	-	-	-	-	-	-	-	-	-	-	-	-
F	0 06	0 08	0 07	0 09	0 08	0 05	0 04	0 05	0 06	0 07	0 02	0 03	0 06
LOI	0 60	0 60	0 80	0 40	0 50	0 70	0 60	0 90	0 90	0 60	0 90	1 00	0 50
TOTAL	99 54	100 06	99 28	100 00	99 61	98 98	100 13	99 21	99 12	98 91	99 68	99 41	99 01
Fe_2O_3T	2 78	1 94	2 03	1 59	3 88	1 52	1 44	3 81	3 32	5 06	1 46	1 43	3 87
FeOT	2.50	1 75	1 83	1 43	3 49	1 37	1 30	3 43	2 99	4 55	1 31	1 29	3 48
A/CNK	1 07	1 03	1 17	1 06	1 12	1 13	1 10	1 23	1 22	1 22	1 23	1 21	1 14
Trace els													
Ba	503	249	176	152	537	74	68	537	479	670	226	216	708
Rb	215	294	253	323	188	303	303	150	158	121	188	194	130
Sr	127	58	53	38	138	23	20	137	126	191	49	43	192
Y	28	20	24	18	33	19	22	22	23	31	14	12	29
Zr	129	94	84	61	173	48	52	157	135	226	70	60	164
Nb	10	13	11	11	13	7	9	12	10	13	9	10	11
Th	11	10	8 7	5 2	15	5 3	5	12	11	13	5 5	4 8	12
Pb	50	21	19	19	28	22	20	17	18	18	19	36	19
Ga	26	24	22	23	18	20	24	21	22	20	18	21	21
Zn	138	77	50	38	72	34	34	58	61	72	58	190	55
Cu	-	-	-	-	-	-	-	-	4	13	-	2	1
Ni	-	-	-	-	-	-	-	-	-	-	-	-	-
V	24	12	12	4	36	8	3	46	40	70	8	11	45
Cr	-	-	-	-	-	-	-	-	-	-	-	-	-
Hf	4	3	3	2	6	2	2	5	4	7	2	1	6
Cs	-	-	-	-	-	-	-	-	-	-	-	-	-
Sc	5 6	3 5	4 8	2 6	8 8	2 7	3	9 4	8 3	12	2 5	2 9	10
Ta	0 9	2	1 7	2 2	1 4	2 3	2 5	1 1	1	1	1 4	1 4	1
Co	-	-	-	-	-	-	-	-	-	-	-	-	-
Li	90	88	73	103	77	62	84	52	68	39	23	22	38
Be	-	-	-	-	-	-	-	-	-	-	-	-	-
B	35	40	30	140	30	30	35	20	20	20	100	50	20
U	2 7	5 9	3 1	6 9	3 4	10	11	3 2	4 2	2 8	2 5	3 6	2 1
W	1	8	2	5	1	2	2	1	1	1	4	5	1
Sn	3	9	13	17	5	9	10	7	6	6	4	14	11
Mo	-	-	-	-	-	-	-	-	-	-	-	-	-
Rare-earths													
La	24	17	17	10	36	8	7	31	24	42	11	9	34
Ce	-	-	-	-	-	-	-	-	-	-	-	-	-
Pr	-	-	-	-	-	-	-	-	-	-	-	-	-
Nd	-	-	-	-	-	-	-	-	-	-	-	-	-
Sm	-	-	-	-	-	-	-	-	-	-	-	-	-
Eu	-	-	-	-	-	-	-	-	-	-	-	-	-
Gd	-	-	-	-	-	-	-	-	-	-	-	-	-
Tb	-	-	-	-	-	-	-	-	-	-	-	-	-
Dy	-	-	-	-	-	-	-	-	-	-	-	-	-
Ho	-	-	-	-	-	-	-	-	-	-	-	-	-
Er	-	-	-	-	-	-	-	-	-	-	-	-	-
Tm	-	-	-	-	-	-	-	-	-	-	-	-	-
Yb	-	-	-	-	-	-	-	-	-	-	-	-	-
Lu	-	-	-	-	-	-	-	-	-	-	-	-	-

Table E1.1 (Continued) Compilation of Meguma Zone granitoid lithogeochemistry

Sample	D13-2048	D13-2048-1	D13-2049	D13-2057	D13-2058	D13-2058-C	D13-2060-1	D13-2060-2	D13-2065	D13-2066	D13-2069-2	D13-2072	D13-2072-C
Batholith	SMB	SMB	SMB	SMB	SMB	SMB	SMB	SMB	SMB	SMB	SMB	SMB	SMB
Pluton	BIP	BIP	BIP	BIP	MG	MG	BIP	BIP	PLP	SaLP	PLP	SaLP	SaLP
Lithology	Mzg	Mzg	Mzg	Mzg	Grd	Grd	Mzg	Mzg	Lmzg	Mzg	Lmzg	Mzg	Mzg
Source	27	27	27	27	27	27	27	27	27	27	27	27	27
Major oxides													
SiO_2	73.20	73.53	73.38	74.66	69.17	69.30	73.70	74.85	73.00	72.95	74.56	70.97	71.47
TiO_2	0.18	0.05	0.22	0.11	0.50	0.52	0.14	0.04	0.19	0.28	0.04	0.35	0.33
Al_2O_3	14.38	14.75	14.18	14.02	15.35	15.23	14.47	14.35	14.46	14.00	13.50	14.49	14.64
Fe_2O_3	-	-	-	-	-	-	-	-	-	-	-	-	-
FeO	-	-	-	-	-	-	-	-	-	-	-	-	-
MnO	0.08	0.19	0.08	0.05	0.07	0.06	0.08	0.13	0.07	0.06	0.03	0.07	0.07
MgO	0.95	0.55	0.94	0.75	1.49	1.70	0.84	0.55	1.14	1.27	0.90	1.26	1.33
CaO	0.41	0.05	0.38	0.24	1.05	1.17	0.40	0.20	0.66	0.78	0.34	1.02	1.13
Na_2O	3.05	2.37	3.35	3.12	3.70	3.82	4.05	3.97	3.65	3.45	3.98	3.24	3.48
K_2O	4.65	7.84	4.41	5.27	4.28	4.16	3.85	4.15	4.52	4.34	4.17	4.70	4.49
P_2O_5	0.32	0.19	0.27	0.14	0.24	0.24	0.27	0.20	0.19	0.22	0.19	0.23	0.22
H_2O+	-	-	-	-	-	-		-	-	-	-	-	-
H_2O	-	-	-	-	-	-	-	-	-	-	-	-	-
CO_2	-	-	-	-	-	-	-	-	-	-	-	-	-
Cl	-	-	-	-	-	-	-	-	-	-	-	-	-
F	0.04	0.01	0.04	0.01	0.05	0.05	0.05	0.01	0.07	0.06	0.02	0.06	0.07
LOI	1.00	0.20	0.90	0.60	0.90	0.60	0.60	0.30	0.80	0.70	0.50	0.70	0.80
TOTAL	99.91	100.54	99.90	100.08	99.82	99.90	99.80	99.60	100.38	100.25	98.99	99.71	100.55
Fe_2O_3T	1.88	0.91	1.99	1.24	3.41	3.45	1.56	0.96	1.89	2.45	0.87	2.98	2.88
FeOT	1.69	0.82	1.79	1.12	3.07	3.10	1.40	0.86	1.70	2.20	0.78	2.68	2.59
A/CNK	1.19	0.94	1.17	1.08	1.15	1.13	1.18	1.16	1.10	1.10	1.07	1.09	1.09
Trace els													
Ba	236	144	230	130	489	487	133	6	230	203	89	390	324
Rb	243	261	241	186	191	173	260	235	262	239	168	228	217
Sr	40	21	41	29	124	114	26	2	62	61	27	85	88
Y	17	21	15	17	21	20	18	12	23	26	10	27	28
Zr	70	27	71	47	140	135	52	25	77	110	24	121	129
Nb	12	3	12	6	10	11	12	7	11	12	5	12	14
Th	5.3	2.1	7.2	4.3	14	14	5	2.2	7.3	10	1.2	11	11
Pb	42	42	22	27	19	19	16	14	15	17	38	22	24
Ga	19	17	18	17	20	20	18	20	20	20	19	21	18
Zn	64	32	60	45	66	63	34	24	44	51	20	57	58
Cu	-	-	-	2	6	7	-	-	-	-	4	29	28
Ni	-	-	-	-	-	-	-	-	-	-	-	-	-
V	12	3	16	4	38	38	10	-	9	14	-	19	17
Cr	-	-	-	-	-	-	-	-	-	-	-	-	-
Hf	2	1	3	1	4	5	2	1	2	3	1	3	3
Cs	-	-	-	-	-	-	-	-	-	-	-	-	-
Sc	3.9	4.8	4.3	2.3	7.2	8.3	4.6	4.4	4	5	0.6	5.7	5.4
Ta	3	0.8	3.3	1.2	1.1	1.4	3.1	1.2	1.6	1.6	1	1.5	1.3
Co	-	-	-	-	-	-	-	-	-	-	-	-	-
Li	59	8	57	30	50	56	68	26	95	91	28	94	91
Be	-	-	-	-	-	-	-	-	-	-	-	-	-
B	40	20	35	20	20	25	25	20	30	20	25	20	20
U	4.9	3.5	5	3.7	3	4.2	10	10	2.8	3.5	5.1	6.8	6.9
W	1	2	2	2	2	2	1	1	1	2	3	3	2
Sn	12	6	15	9	10	14	12	12	12	11	9	11	12
Mo	-	-	-	-	-	-	-	-	-	-	-	-	-
Rare-earths													
La	12	4	14	5	28	31	10	2	14	20	3	25	25
Ce	-	-	-	-	-	-	-	-	-	-	-	-	-
Pr	-	-	-	-	-	-	-	-	-	-	-	-	-
Nd	-	-	-	-	-	-	-	-	-	-	-	-	-
Sm	-	-	-	-	-	-	-	-	-	-	-	-	-
Eu	-	-	-	-	-	-	-	-	-	-	-	-	-
Gd	-	-	-	-	-	-	-	-	-	-	-	-	-
Tb	-	-	-	-	-	-	-	-	-	-	-	-	-
Dy	-	-	-	-	-	-	-	-	-	-	-	-	-
Ho	-	-	-	-	-	-	-	-	-	-	-	-	-
Er	-	-	-	-	-	-	-	-	-	-	-	-	-
Tm	-	-	-	-	-	-	-	-	-	-	-	-	-
Yb	-	-	-	-	-	-	-	-	-	-	-	-	-
Lu	-	-	-	-	-	-	-	-	-	-	-	-	-

Table E1 1 (Continued) Compilation of Meguma Zone granitoid lithogeochemistry

Sample	D13-2078	D13-2086	D13-2086-1	D13-2090-1	D13-2090-2	D13-2090-4	D13-2091-1	D13-2093-2	D13-2093-3	D13-2095	D13-2095-1	D13-2095-C	D13-2118
Batholith	SMB	SMB	SMB	SMB	SMB	SMB	SMB	SMB	SMB	SMB	SMB	SMB	SMB
Pluton	MG	WBP	WBP	MG	BIP	BIP	MG	BIP	BIP	BIP	MG	BIP	MG
Lithology	Grd	Lg	Lg	Grd	Mzg	Mzg	Grd	Mzg	Mzg	Mzg	Grd	Mzg	Grd
Source	27	27	27	27	27	27	27	27	27	27	27	27	27
Major oxides													
SiO_2	66 23	73 93	73 19	63 86	73 91	71 06	65 14	74 04	73 91	74 55	63 88	73 25	64 04
TiO_2	0 66	0 18	0 14	0 81	0 17	0 39	0 81	0 04	0 08	0 20	0 94	0 19	0 77
Al_2O_3	16 55	14 98	14 69	16 78	13 79	14 82	15 93	13 70	14 02	13 33	16 28	14 34	16 87
Fe_2O_3	-	-	-	-	-	-	-	-	-	-	-	-	-
FeO	-	-	-	-	-	-	-	-	-	-	-	-	-
MnO	0 08	0 03	0 03	0 13	0 05	0 09	0 07	0 05	0 06	0 06	0 16	0 05	0 09
MgO	1 99	1 10	0 98	2 51	1 10	1 44	2 48	0 87	0 97	1 24	2 56	1 28	2 25
CaO	2 17	0 39	0 33	0 88	0 64	0 76	1 67	0 41	0 42	0 39	1 48	0 38	2 55
Na_2O	3 46	3 74	3 60	5 29	3 27	3 31	4 31	3 05	4 00	3 43	4 07	3 38	3 79
K_2O	4 02	4 64	4 93	3 22	4 51	4 71	2 86	5 80	4 36	4 78	3 20	5 07	3 10
P_2O_5	0 20	0 30	0 30	0 28	0 14	0 17	0 24	0 14	0 17	0 11	0 35	0 11	0 25
H_20+	-	-	-	-	-	-	-	-	-	-	-	-	-
H_2O-	-	-	-	-	-	-	-	-	-	-	-	-	-
CO_2	-	-	-	-	-	-	-	-	-	-	-	-	-
Cl	-	-	-	-	-	-	-	-	-	-	-	-	-
F	0 05	0 03	0 03	0 06	0 02	0 05	0 05	0 01	0 02	0 03	0 09	0 03	0 06
LOI	0 40	0 60	1 10	1 20	0 60	1 00	1 70	0 50	0 80	0 40	1 00	0 60	1 10
TOTAL	99 67	101 31	100 41	99 84	99 66	100 26	100 01	99 23	99 83	100 09	99 57	100 16	99 44
Fe_2O_3T	4 34	1 68	1 25	5 42	1 65	2 79	5 34	0 70	1 16	1 79	6 27	1 68	5 15
FeOT	3 91	1 42	1 12	4 88	1 48	2 51	4 80	0 63	1 04	1 61	5 64	1 51	4 63
A/CNK	1 18	1 15	1 11	1 23	1 10	1 14	1 25	0 98	1 08	1 04	1 28	1 09	1 24
Trace els													
Ba	790	280	218	621	189	502	681	107	56	384	489	383	756
Rb	148	207	207	177	160	201	91	169	213	164	191	172	127
Sr	204	55	40	230	55	119	178	25	17	70	174	81	236
Y	30	15	15	25	16	25	32	18	14	16	34	17	31
Zr	201	66	57	228	66	137	220	44	41	74	250	72	238
Nb	12	10	10	14	8	10	14	4	8	7	15	7	14
Th	14	4 7	3 5	11	5 4	15	15	3 1	3 1	5 3	13	5 6	15
Pb	20	20	9	15	22	22	10	23	20	21	24	25	18
Ga	22	20	19	22	16	23	23	20	20	20	31	22	21
Zn	62	26	22	78	34	56	43	26	32	40	121	36	90
Cu	12	-	-	8	-	-	1	9	6	-	6	-	11
Ni	-	-	-	-	-	-	-	-	-	-	-	-	-
V	53	8	7	76	9	22	74	2	3	11	83	14	57
Cr	-	-	-	-	-	-	-	-	-	-	-	-	-
Hf	6	2	2	6	2	5	8	2	2	2	8	2	8
Cs	-	-	-	-	-	-	-	-	-	-	-	-	-
Sc	11	3 2	3	12	3 6	6 3	13	2 1	3 1	3 4	14	3 5	13
Ta	1 2	1 3	1 4	1 3	0 8	1	1 1	-	1	0 8	1 2	0 5	0 8
Co	-	-	-	-	-	-	-	-	-	-	-	-	-
Li	54	36	19	62	39	53	53	13	37	37	126	35	56
Be	-	-	-	-	-	-	-	-	-	-	-	-	-
B	20	50	40	50	20	30	30	15	20	25	35	20	30
U	2.8	2.5	7 3	4	3 1	4 1	2.4	2.8	4 4	2.5	3 5	2 7	2 6
W	2	3	4	1	1	3	2	1	1	2	1	2	1
Sn	2	14	12	12	8	8	7	7	13	9	2	8	2
Mo	-	-	-	-	-	-	-	-	-	-	-	-	-
Rare-earths													
La	42	10	9	31	9	30	44	5	5	11	41	11	45
Ce	-	-	-	-	-	-	-	-	-	-	-	-	-
Pr	-	-	-	-	-	-	-	-	-	-	-	-	-
Nd	-	-	-	-	-	-	-	-	-	-	-	-	-
Sm	-	-	-	-	-	-	-	-	-	-	-	-	-
Eu	-	-	-	-	-	-	-	-	-	-	-	-	-
Gd	-	-	-	-	-	-	-	-	-	-	-	-	-
Tb	-	-	-	-	-	-	-	-	-	-	-	-	-
Dy	-	-	-	-	-	-	-	-	-	-	-	-	-
Ho	-	-	-	-	-	-	-	-	-	-	-	-	-
Er	-	-	-	-	-	-	-	-	-	-	-	-	-
Tm	-	-	-	-	-	-	-	-	-	-	-	-	-
Yb	-	-	-	-	-	-	-	-	-	-	-	-	-
Lu	-	-	-	-	-	-	-	-	-	-	-	-	-

Table E1.1. (Continued) Compilation of Meguma Zone granitoid lithogeochemistry

Sample	D13-2119	D13-2120	D13-2122	D13-2123	D13-2124	D13-2124-2	D13-2125-2	D13-2176	D13-2127	D13-2128	A11-2283	A11-3015	A11-3005
Batholith	SMB	SMB	SMB	SMB	SMB	SMB	SMB	SMB	SMB	SMB	SMB	SMB	SMB
Pluton	BIP	BIP	BIP	MG	BIP	BIP	BIP	BIP	BIP	MG	WDP	WDP	WDP
Lithology	Mzg	Mzg	Mzg	Grd	Mzg	Mzg	Mzg	Mzg	Mzg	Grd	Mzg	Mzg	Mzg
Source	27	27	27	27	27	27	27	27	27	27	27	27	27
Major oxides													
SiO_2	73 17	72 91	74 93	63 85	63 37	73 84	72 72	73 25	76 37	66 51	71 16	73 31	74 19
TiO_2	0 18	0 12	0 05	0 83	0 18	0 14	0 05	0 32	0 07	0 65	0 36	0 32	0 24
Al_2O_3	14 18	13 52	13 71	16 57	20 87	13 62	13 59	13 86	13 98	16 08	14 98	13 94	13 87
Fe_2O_3	-	-	-	-	-	-	-	-	-	-	-	-	-
FeO	-	-	-	-	-	-	-	-	-	-	-	-	-
MnO	0 06	0 04	0 07	0 09	0 07	0 07	0 04	0 08	0 08	0 08	0 08	0 04	0 04
MgO	1,10	1 04	0 99	2 17	1 18	0 98	0 87	1 35	0 91	2,14	1 24	0 94	1 02
CaO	0 60	0 58	0 43	2.55	3 38	0 40	0 25	0 69	0 27	? 58	0 96	0 70	0 60
Na_2O	3 29	3 79	3 88	3 79	5 64	3 51	3 39	3 60	3 67	3 09	3 42	3 00	3 11
K_2O	5 00	4 62	4 31	3 32	2 48	4 60	5 11	4 50	4 75	3 59	4 38	4 64	4 72
P_2O_5	0 14	0 09	0 12	0 24	0 17	0 13	0 17	0 12	0 09	0 22	0 21	0 24	0 23
H_2O+	-	-	-	-	-	-	-	-	-	-	-	-	-
H_2O-	-	-	-	-	-	-	-	-	-	-	-		
CO_2	-	-	-	-	-	-	-	-	-	-	-	-	-
Cl	-	-	-	-	-	-	-	-	-	-	-	-	-
F	0 03	0 03	0 01	0 06	0 04	0 03	0 01	0 05	0 01	0 06	0 06	0 10	0 08
LOI	0 30	0 60	0 40	0 90	1 10	0 40	0 90	0 50	0 30	0 20	0 70	0 40	0 70
TOTAL	99 52	98 46	100 06	99 34	99 86	99 10	97 90	100 54	101 41	99 05	100 05	99 45	99 96
Fe_2O_3T	1 67	1 28	1 30	5 59	1 58	1 57	0 90	2 63	1 02	4 34	2 86	2 13	1 60
FeOT	1 50	1 15	1.17	5 03	1 42	1 41	0 81	2 37	0 92	3 91	2.58	1 92	1 44
A/CNK	1 07	1 01	1 07	1 19	1 28	1 07	1 04	1 07	1 08	1 20	1 16	1 12	1 09
Trace els													
Ba	188	113	233	868	216	137	43	304	58	842	459	355	260
Rb	166	192	148	123	135	205	136	178	114	126	208	267	256
Sr	46	33	37	108	294	29	11	72	14	222	82	61	47
Y	19	21	14	24	15	22	11	29	14	33	30	20	18
Zr	68	53	41	140	101	61	26	113	35	193	113	122	90
Nb	8	6	5	9	10	7	3	9	5	12	12	13	12
Th	5 6	6 1	2	15	4 4	4 9	0 9	8 9	2.9	14	7 5	24 9	17
Pb	19	24	31	23	23	27	16	24	14	16	-	-	-
Ga	17	19	20	18	30	19	19	19	15	19	17	18	17
Zn	28	19	39	66	42	31	23	42	20	62	56	63	55
Cu	-	-	16	2	-	-	-	-	-	9	-	-	-
Ni	-	-	-	-	-	-	-	-	-	-	-	-	-
V	11	8	3	29	15	5	-	21	4	55	27	14	9
Cr	-	-	-	-	-	-	-	-	-	-	-	-	-
Hf	2	2	2	7	3	2	1	4	1	6	3	3	3
Cs	-	-	-	-	-	-	-	-	-	-	-	-	-
Sc	3 9	3 2	2.1	12	3 7	3 4	0 9	6 4	1 5	10	6	2 6	2
Ta	1 4	1	0 5	0 9	1 8	1 4	0 5	1	0 5	1	1 7	2	2
Co	-	-	-	-	-	-	-	-	-	-	-	-	-
Li	31	33	28	47	41	45	20	41	25	41	79	119	90
Be	-	-	-	-	-	-	-	-	-	-	-	-	-
B	20	20	25	25	30	25	20	20	25	20	-	-	-
U	2.5	4 6	3 1	2 1	1 4	4 1	2.7	3 6	1 8	2 9	5 8	4 6	3 7
W	1	2	3	2	5	1	1	1	1	1	2	1	2
Sn	6	10	5	6	10	12	7	10	6	9	3	10	2
Mo	-	-	-	-	-	-	-	-	-	-	-	-	-
Rare-earths													
La	11	8	5	46	19	9	3	20	6	38	19	33	23
Ce	-	-	-	-	-	-	-	-	-	-	-	-	-
Pr	-	-	-	-	-	-	-	-	-	-	-	-	-
Nd	-	-	-	-	-	-	-	-	-	-	-	-	-
Sm	-	-	-	-	-	-	-	-	-	-	-	-	-
Eu	-	-	-	-	-	-	-	-	-	-	-	-	-
Gd	-	-	-	-	-	-	-	-	-	-	-	-	-
Tb	-	-	-	-	-	-	-	-	-	-	-	-	-
Dy	-	-	-	-	-	-	-	-	-	-	-	-	-
Ho	-	-	-	-	-	-	-	-	-	-	-	-	-
Er	-	-	-	-	-	-	-	-	-	-	-	-	-
Tm	-	-	-	-	-	-	-	-	-	-	-	-	-
Yb	-	-	-	-	-	-	-	-	-	-	-	-	-
Lu	-	-	-	-	-	-	-	-	-	-	-	-	-

Table E1.1 (Continued) Compilation of Meguma Zone granitoid lithogeochemistry

Sample	A11-2239	A14-0007	A11-2293	A11-2259	A14-0007-1	A11-2249	A11-3013	A04-1214	A04-1218	A04-1217	A04-1216	A04-1206	A12-1020-1
Batholith	SMB	SMB	SMB	SMB	SMB	SMB	SMB	SMB	SMB	SMB	SMB	SMB	SMB
Pluton	WDP	WDP	WDP	WDP	WDP	WDP	WDP	SoLP	SoLP	SoLP	SoLP	SoLP	ScLP
Lithology	Mzg	Mzg	Mzg	Mzg	Mzg	Mzg	Mzg	Mzg	Mzg	Mzg	Mzg	Mzg	Mzg
Source	27	27	27	27	27	27	28	28	28	28	28	28	27
Major oxides													
SiO_2	73.01	70.32	74.28	73.34	71.55	72.62	72.06	72.18	74.70	74.64	73.97	72.57	67.03
TiO_2	0.29	0.34	0.16	0.21	0.35	0.23	0.23	0.26	0.12	0.12	0.12	0.33	0.65
Al_2O_3	14.02	15.69	13.97	14.13	14.89	14.55	14.94	13.68	12.97	12.74	12.97	13.50	15.68
Fe_2O_3	-	-	-	-	-	-	-	-	-	-	-	-	-
FeO	-	-	-	-	-	-	-	-	-	-	-	-	-
MnO	0.04	0.05	0.05	0.04	0.04	0.04	0.04	0.07	0.06	0.04	0.05	0.07	0.08
MgO	0.93	1.28	0.97	1.05	1.27	1.17	1.00	1.16	0.77	0.90	1.05	1.25	1.64
CaO	0.63	0.88	0.47	0.45	0.79	0.54	0.69	0.68	0.41	0.29	0.36	1.26	2.23
Na_2O	2.94	3.09	3.25	3.09	2.89	3.30	2.95	3.62	3.50	3.38	3.63	3.59	3.66
K_2O	4.97	5.49	4.76	4.97	5.10	5.00	5.07	4.64	4.58	4.56	4.57	3.99	4.04
P_2O_5	0.25	0.21	0.17	0.14	0.20	0.18	0.23	0.17	0.10	0.10	0.10	0.13	0.20
H_2O+	-	-	-	-	-	-	-	-	-	-	-	-	-
H_2O-	-	-	-	-	-	-	-	-	-	-	-	-	-
CO_2	-	-	-	-	-	-	-	-	-	-	-	-	-
Cl	-	-	-	-	-	-	-	-	-	-	-	-	-
F	0.07	0.04	0.04	0.04	0.06	0.03	0.08	0.31	0.31	0.19	0.24	0.30	0.06
LOI	0.50	0.70	0.60	0.60	0.70	1.10	0.50	1.10	0.80	0.70	0.70	0.60	0.60
TOTAL	99.27	100.08	100.06	99.72	99.98	100.41	99.40	99.79	99.68	99.22	99.23	99.58	99.65
Fe_2O_3T	1.86	2.37	1.55	1.89	2.44	1.87	1.88	2.48	1.74	1.94	1.90	2.54	4.27
FeOT	1.69	2.13	1.39	1.70	2.20	1.68	1.69	2.23	1.57	1.75	1.71	2.29	3.84
A/CNK	1.10	1.10	1.11	1.11	1.14	1.10	1.15	1.03	1.03	1.04	1.02	1.04	1.08
Trace els													
Ba	355	497	202	438	467	391	288	318	61	97	68	210	980
Rb	239	258	258	221	245	216	266	431	558	528	515	441	132
Sr	58	94	43	73	87	72	62	58	9	17	19	60	176
Y	19	23	23	23	20	20	22	54	60	61	58	62	31
Zr	120	132	61	86	143	95	90	115	83	76	75	127	218
Nb	14	14	8	10	14	10	13	14	14	14	14	15	13
Th	22.2	19	5.7	10	23.2	12	15	18	18	18	18	18	12
Pb	-	23		-	34			-		-		-	-
Ga	17	21	15	15	19	16	18	20	20	21	20	18	18
Zn	52	59	30	36	60	40	58	57	33	33	35	42	62
Cu	-	-	-	-	-	-	-	30	10	10	7	8	-
Ni	-	-	-	-	-	-	-	-	-	-	-	-	-
V	6	17	11	15	15	12	8	28	-	7	7	22	55
Cr	-	-	-	-	-	-	-	-	-	-	-	-	-
Hf	3	5	2	2	6	3	2	2	2	3	2	3	6
Cs	-	-	-	-	-	-	-	-	-	-	-	-	-
Sc	2.7	4	3.2	3.4	4.3	2.8	2.1	4.8	3.5	3.7	3.2	4.5	10
Ta	1.6	1.3	1.8	1.7	1.4	1.5	1.9	2.7	4.2	4	4.1	3.1	1.1
Co	-	-	-	-	-	-	-	-	-	-	-	-	-
Li	89	70	54	71	65	36	107	142	136	122	107	171	37
Be	-	-	-	-	-	-	-	-	-	-	-	-	-
B	-	13	-	-	27	-	-	-	-	-	-	-	-
U	4.5	4.2	4.2	5.1	4.5	4.4	5.8	14	23.7	23.7	24.8	15	3.2
W	-	-	4	3	2	-	1	5	7	6	8	102	-
Sn	6	4	11	9	3		7	22	25	25	15	9	3
Mo	-	-	-	-	-	-	-	-	-	-	-	-	-
Rare-earths													
La	32	34	10	20	40	20	24	19	13	15	13	22	34
Ce	-	-	-	-	-	-	-	-	-	-	-	-	-
Pr	-	-	-	-	-	-	-	-	-	-	-	-	-
Nd	-	-	-	-	-	-	-	-	-	-	-	-	-
Sm	-	-	-	-	-	-	-	-	-	-	-	-	-
Eu	-	-	-	-	-	-	-	-	-	-	-	-	-
Gd	-	-	-	-	-	-	-	-	-	-	-	-	-
Tb	-	-	-	-	-	-	-	-	-	-	-	-	-
Dy	-	-	-	-	-	-	-	-	-	-	-	-	-
Ho	-	-	-	-	-	-	-	-	-	-	-	-	-
Er	-	-	-	-	-	-	-	-	-	-	-	-	-
Tm	-	-	-	-	-	-	-	-	-	-	-	-	-
Yb	-	-	-	-	-	-	-	-	-	-	-	-	-
Lu	-	-	-	-	-	-	-	-	-	-	-	-	-

Table E1 1 (Continued) Compilation of Meguma Zone granitoid lithogeochemistry

Sample	A12-8008	A11-2296	A06-3016	A06-3016-1	A06-3017	A11-2276-1	A12-8017	A06-3030	A12-1010	A12-8002-1	A11-2280-1	A14-1032	A11-2316
Batholith	SMB	SMB	SMB	SMB	SMB	SMB	SMB	SMB	SMB	SMB	SMB	SMB	SMB
Pluton	ScLP	ScLP	ScLP	ScLP	ScLP	ScLP	ScLP	ScLP	ScLP	ScLP	ScLP	ScLP	ScLP
Lithology	Mzg	Mzg	Mzg	Mzg	Mzg	Mzg	Mzg	Mzg	Mzg	Mzg	Mzg	Mzg	Mzg
Source	27	27	27	27	27	27	27	27	27	27	27	27	27
Major oxides													
SiO_2	66 85	70 02	68 23	69 77	68 41	72 74	69 23	70 07	68 04	65 79	68 30	69 24	68 65
TiO_2	0 73	0 44	0 43	0 50	0 51	0 32	0 60	0 55	0 62	0 82	0 62	0 62	0 53
Al_2O_3	15 42	14 55	16 08	14 27	14 97	13 65	14 76	14 62	15 47	15 43	14 85	14 56	14 96
Fe_2O_3	-	-	-	-	-	-	-	-	-	-	-	-	-
FeO	-	-	-	-	-	-	-	-	-	-	-	-	-
MnO	0 09	0 08	0 05	0 08	0 08	0 08	0 08	0 07	0 09	0 10	0 10	0 08	0 08
MgO	1 73	1 44	1 13	1 49	1 48	1 24	1 62	1 47	1 65	1 97	1 68	1 67	1 63
CaO	2 00	1 40	1 84	1 57	1 45	1 05	1 47	1 62	1 62	2 27	1 80	1 71	1 71
Na_2O	3 48	3 50	3 67	3 22	3 28	2 98	2 94	3 31	3 46	3 60	3 31	2 77	3 25
K_2O	3 90	4 03	4 21	3 79	4 39	4 18	4 05	4 06	4 04	3 70	3 94	3 69	4 25
P_2O_5	0 23	0 19	0 19	0 18	0 20	0 16	0 18	0 20	0 21	0 23	0 22	0 24	0 19
H_20+	-	-	-	-	-	-	-	-	-	-	-	-	-
H_2O-	-	-	-	-	-	-	-	-	-	-	-	-	-
CO_2	-	-	-	-	-	-	-	-	-	-	-	-	-
Cl	-	-	-	-	-	-	-	-	-	-	-	-	-
F	0 06	0 05	0 06	0 05	0 06	0 05	0 05	0 05	0 05	0 07	0 07	0 03	0 08
LOI	0 40	0 50	0 80	0 70	0 60	0 30	0 80	0 50	0 70	0 40	0 80	0 30	0 60
TOTAL	99 19	99 16	98 99	98 90	98 85	99 10	99 45	99 99	99 78	99 48	99 61	98 79	99 15
Fe_2O_3T	4 85	3 35	2 62	3 70	3 87	2 67	4 13	3 91	4 31	5 75	4 43	4 37	3 78
FeOT	4 36	3 01	2.36	3 33	3 48	2 40	3 72	3 52	3 88	5 17	3 99	3 93	3 40
A/CNK	1 13	1 11	1 13	1 13	1 11	1 12	1 18	1 11	1 16	1 11	1 12	1 22	1 11
Trace ele													
Ba	819	385	655	372	610	300	591	567	614	830	541	561	602
Rb	137	178	142	147	172	189	162	149	164	144	152	163	159
Sr	159	98	157	109	116	74	126	119	134	163	136	128	124
Y	39	31	35	38	36	31	33	34	33	38	32	38	33
Zr	230	137	193	170	174	101	192	173	205	258	197	190	180
Nb	13	11	10	11	11	7	13	11	12	14	12	16	11
Th	13	8 9	14	10	11	7 3	12	11	12	14	12	14	11
Pb	22	-	-	-	-	-	37	-	-	-	-	12	-
Ga	21	16	19	17	16	15	20	17	18	19	16	18	17
Zn	71	62	52	55	57	43	59	57	61	85	80	70	63
Cu	-	-	-	-	-	-	-	-	-	-	-	-	-
Ni	-	-	-	-	-	-	-	-	-	-	-	-	-
V	61	40	30	39	33	21	50	45	53	80	54	50	50
Cr	-	-	-	-	-	-	-	-	-	-	-	-	-
Hf	7	4	5	4	5	3	5	5	6	7	6	8	6
Cs	-	-	-	-	-	-	-	-	-	-	-	-	-
Sc	10	7 7	4 3	7 5	7 7	5 6	9 2	9	9 2	14	9 3	9 4	8 9
Ta	1 3	1 7	0 9	1 7	1 2	1 4	1 4	1 4	1 6	1 6	1 4	1 4	1
Co	-	-	-	-	-	-	-	-	-	-	-	-	-
Li	38	86	41	60	62	68	50	49	51	66	65	58	57
Be	-	-	-	-	-	-	-	-	-	-	-	-	-
B	-	-	-	-	-	-	-	-	-	-	-	18	-
U	2.2	3 7	2 3	4	4 5	2 9	2 8	3 3	2 5	4 1	3 7	4 6	4 1
W	-	1	-	-	-	-	-	1	4	-	-	1	-
Sn	-	2	4	3	2	6	1	-	7	-	6	6	2
Mo	-	-	-	-	-	-	-	-	-	-	-	-	-
Rare-earths													
La	34	23	32	27	27	18	29	29	32	44	29	35	29
Ce	-	-	-	-	-	-	-	-	-	-	-	-	-
Pr	-	-	-	-	-	-	-	-	-	-	-	-	-
Nd	-	-	-	-	-	-	-	-	-	-	-	-	-
Sm	-	-	-	-	-	-	-	-	-	-	-	-	-
Eu	-	-	-	-	-	-	-	-	-	-	-	-	-
Gd	-	-	-	-	-	-	-	-	-	-	-	-	-
Tb	-	-	-	-	-	-	-	-	-	-	-	-	-
Dy	-	-	-	-	-	-	-	-	-	-	-	-	-
Ho	-	-	-	-	-	-	-	-	-	-	-	-	-
Er	-	-	-	-	-	-	-	-	-	-	-	-	-
Tm	-	-	-	-	-	-	-	-	-	-	-	-	-
Yb	-	-	-	-	-	-	-	-	-	-	-	-	-
Lu	-	-	-	-	-	-	-	-	-	-	-	-	-

Table E1 1 (Continued) Compilation of Meguma Zone granitoid lithogeochemistry

Sample	A12-1008	A14-1021	A11-2286	A11-2270-C	A11-2300	A06-3007	A06-3021	A06-3010-1	A14-0008	A14-1030	A14-0003	A14-0002	A14-0002-1
Batholith	SMB	SMB	SMB	SMB	SMB	SMB	SMB	SMB	SMB	SMB	SMB	SMB	SMB
Pluton	ScLP	ScLP	ScLP	-	LRoP	KP	KP	KP	CLP	CLP	CLP	CLP	CLP
Lithology	Mzg	Mzg	Mzg	MPOR	Mzg	Mzg	Mzg	Mzg	Mzg	Mzg	Mzg	Mzg	Mzg
Source	27	27	27	27	27	28	28	28	27	27	27	27	27
Major oxides													
SiO_2	67 11	71,13	67 67	63 82	70 32	69 56	70 59	69 54	69 58	70 22	69 44	68 97	69 28
TiO_2	0 61	0 40	0 60	0 85	0 50	0 48	0 44	0 46	0 50	0 43	0 58	0 51	0 51
Al_2O_3	15 45	14 65	15 44	16 09	13 97	15 22	15 07	15 17	14 83	14 66	14 71	15 31	14 95
Fe_2O_3	-	-	-	-	-	-	-	-	-	-	-	-	-
FeO	-	-	-	-	-	-	-	-	-	-	-	-	-
MnO	0 08	0 06	0 08	0 17	0 08	0 10	0 09	0 09	0 10	0 08	0 09	0 09	0 09
MgO	1 64	1 38	2.01	2.12	1 52	1 55	1 45	1 46	1 36	1 21	1 68	1 51	1 33
CaO	1.75	1 30	1 25	1 74	1 38	1,12	0 67	1 04	1 46	1,50	1,72	1.66	1 59
Na_2O	3 53	2 62	2 44	3 14	2 85	2 95	3 05	3 27	3 52	3 48	2 65	2 57	3 24
K_2O	4 47	4 74	4 08	3 47	3 91	4 08	4 29	4 49	4 05	4 27	3 98	4 02	4 20
P_2O_5	0 22	0 15	0 18	0 23	0 20	0 24	0 24	0 23	0 18	0 18	0 19	0 20	0 20
H_2O+	-	-	-	-	-	-	-	-	-	-	-	-	-
H_2O-	-	-	-	-	-	-	-	-	-	-	-	-	-
CO_2	-	-	-	-	-	-	-	-	-	-	-	-	-
Cl	-	-	-	-	-	-	-	-	-	-	-	-	-
F	0 05	0 04	0 08	0 07	0 05	0 06	0 05	0 05	0 06	0 06	0 07	0 06	0 06
LOI	0 50	0 50	1 10	1 20	0 60	0 80	1 10	0 60	0 40	0 20	0 10	0 60	0 40
TOTAL	99 18	99 67	98 72	98 65	98 64	99 47	100 00	99 36	99 64	99 42	99 16	99 04	99 41
Fe_2O_3T	4 25	3 04	4 30	6 36	3 68	3 74	3 35	3 34	4 07	3 55	4 47	4 00	4 02
FeOT	3 82	2 74	3 87	5 72	3 31	3 37	3 01	3 01	3 66	3 19	4 02	3 60	3 62
A/CNK	1 08	1 14	1 34	1 32	1 17	1 26	1 27	1 16	1 12	1 08	1 20	1 26	1 13
Trace els													
Ba	818	526	564	744	412	509	531	629	595	519	604	565	606
Rb	154	162	168	135	164	191	204	192	175	182	173	172	169
Sr	145	117	133	181	108	109	96	118	127	112	134	123	127
Y	38	33	25	46	31	28	26	28	37	41	39	38	42
Zr	198	137	169	294	160	159	139	147	194	186	211	196	202
Nb	13	10	11	14	11	10	10	10	14	11	15	11	13
Th	13	11	16	15	11	11	11	11	12	12	12	13	14
Pb	-	14	-	267	-	-	-	-	16	-	23	12	16
Ga	19	14	19	17	16	18	18	18	16	19	18	16	17
Zn	65	46	73	790	57	69	48	58	54	56	61	61	66
Cu	-	-	-	7	-	-	-	-	-	-	-	-	-
Ni	-	-	-	-	-	-	-	-	-	-	-	-	-
V	50	29	74	97	41	43	39	41	30	29	39	33	33
Cr	-	-	-	-	-	-	-	-	-	-	-	-	-
Hf	6	5	4	8	5	4	4	4	7	6	8	8	9
Cs	-	-	-	-	-	-	-	-	-	-	-	-	-
Sc	8 3	6 6	9 3	14	8 4	6 5	6	6 4	9	7 2	9 3	9 1	10
Ta	1 5	1	1 4	1 4	1 5	1 4	2 2	1 4	1 2	1	1 1	1 2	1 2
Co	-	-	-	-	-	-	-	-	-	-	-	-	-
Li	40	52	82	66	66	77	81	69	58	62	62	59	53
Be	-	-	-	-	-	-	-	-	-	-	-	-	-
B	-	18	-	-	-	-	-	-	15	-	32	29	15
U	2 7	3 2	4	3 6	3 8	2 7	7 4	4 3	3 7	3 5	3 3	3 5	3 2
W	1	-	1	-	1	-	3	-	3	1	1	3	1
Sn	3	9	4	-	1	-	6	3	10	5	11	7	2
Mo	-	-	-	-	-	-	-	-	-	-	-	-	-
Rare-earths													
La	30	26	33	45	27	28	26	28	34	31	34	35	38
Ce	-	-	-	-	-	-	-	-	-	-	-	-	-
Pr	-	-	-	-	-	-	-	-	-	-	-	-	-
Nd	-	-	-	-	-	-	-	-	-	-	-	-	-
Sm	-	-	-	-	-	-	-	-	-	-	-	-	-
Eu	-	-	-	-	-	-	-	-	-	-	-	-	-
Gd	-	-	-		-	-	-	-	-	-	-	-	-
Tb	-	-	-	-	-	-	-	-	-	-	-	-	-
Dy	-	-	-	-	-	-	-	-	-	-	-	-	-
Ho	-	-	-	-	-	-	-	-	-	-	-	-	-
Er	-	-	-	-	-	-	-	-	-	-	-	-	-
Tm	-	-	-	-	-	-	-	-	-	-	-	-	-
Yb	-	-	-	-	-	-	-	-	-	-	-	-	-
Lu	-	-	-	-	-	-	-	-	-	-	-	-	-

Table E1 1 (Continued) Compilation of Meguma Zone granitoid lithogeochemistry

Sample	A14-0001	A14-1018	A14-1019	A14-1018-1	A11-2268	A11-2301-2	A11-2301-1	A04-1210	A04-1211	A03-2350	A04-1212	A04-1209	A03-3000
Batholith	SMB	SMB	SMB	SMB	SMB	SMB	SMB	SMB	SMB	SMB	SMB	SMB	SMB
Pluton	CLP	MRP	MRP	MRP	MHP	EDP	EDP	DoLP	DoLP	DLP	DLP	DLP	DLP
Lithology	Mzg	Lmzg	Lmzg	Lmzg	Lmzg	Lmzg	Lmzg	Lmzg	Lmzg	Lmzg	Lmzg	Lmzg	Lmzg
Source	27	28	28	28	28	27	27	28	28	28	28	28	28
Major oxides													
SiO_2	69 74	72 11	72 12	71 62	74 26	74 01	73 33	75 21	73 43	72 26	74 62	75 68	72 25
TiO_2	0 45	0 23	0 33	0 27	0 16	0 14	0 12	0 05	0 04	0 30	0 11	0 10	0 19
Al_2O_3	14 79	14 99	14 76	15 50	13 48	14 27	14 52	13 36	14 00	15 03	13 09	12 57	15 09
Fe_2O_3	-	-	-	-	-	-	-	-	-	-	-	-	-
FeO	-	-	-	-	-	-	-	-	-	-	-	-	-
MnO	0 09	0 04	0 05	0 04	0 06	0 05	0 05	0 06	0 09	0 05	0 04	0 05	0 05
MgO	1 39	1 02	1 12	1 12	0 97	0 91	0 90	0 78	0 83	1 04	0 85	0 86	0 98
CaO	1 35	0 63	0 68	0 68	0 30	0 41	0 45	0 38	0 40	1 11	0 35	0 39	0 59
Na_2O	3 38	3 29	3 17	2 98	3 24	3 36	3 77	3 28	3 47	3 35	3 12	3 70	3 39
K_2O	4 15	5 23	4 86	5 56	4 77	4 56	4 50	4 29	3 83	4 57	5 02	4 51	5 21
P_2O_5	0 18	0 20	0 22	0 21	0 13	0 27	0 32	0 16	0 18	0 24	0 18	0 07	0 21
H_2O+	-	-	-	-	-	-	-	-	-	-	-	-	-
H_2O-	-	-	-	-	-	-	-	-	-	-	-	-	-
CO_2	-	-	-	-	-	-	-	-	-	-	-	-	-
Cl	-	-	-	-	-	-	-	-	-	-	-	-	-
F	0 07	0 05	0 07	0 05	0 03	0 04	0 05	0 30	0 51	0 05	0 16	0 15	0 04
LOI	0 70	0 60	0 60	0 50	0 60	0 80	0 60	0 90	1 50	0 40	0 60	0 70	0 40
TOTAL	99 55	100 02	99 91	100 21	99 78	100 09	99 77	99 90	99 41	100 43	99 64	100 02	100 05
Fe_2O_3T	3 70	1 87	2 22	1 92	2 01	1 46	1 34	1 59	1 82	2 31	1 85	1 48	1 88
FeOT	3 33	1 68	2 00	1 73	1 81	1 31	1 21	1 43	1 64	2 08	1 66	1 33	1 69
A/CNK	1 13	1 10	1 14	1 12	1 08	1 15	1 12	1 13	1 23	1 12	1 03	0 98	1 10
Trace els													
Ba	487	368	361	445	228	147	275	27	21	409	78	63	313
Rb	187	279	262	262	211	252	253	670	817	208	478	499	321
Sr	119	74	75	88	33	33	40	5	5	82	11	10	52
Y	42	22	24	23	34	21	19	56	63	26	[illegible]	62	29
Zr	173	99	138	114	79	52	45	39	29	134	79	74	102
Nb	12	14	15	12	5	8	7	24	17	10	14	11	13
Th	13	14	19	16	6 1	4 8	3 7	13	12	12	14	18	12
Pb	12	37	25	17	-	-	-	-	-	-	-	-	-
Ga	16	19	19	18	14	17	15	23	24	18	22	18	19
Zn	56	55	56	53	33	28	28	49	56	45	54	26	56
Cu	-	-		-	-	-	-	6	8	-	6	6	-
Ni	-	-	-	-	-	-	-	-	-	-	-	-	-
V	30	8	12	12	9	-	6	-	-	17	-	-	7
Cr	-	-	-	-	-	-	-	-	-	-	-	-	-
Hf	7	4	4	4	3	2	-	-	-	4	2	2	3
Cs	-	-	-	-	-	-	-	-	-	-	-	-	-
Sc	7 5	3	3 8	3 5	4 1	3 2	2 3	2 3	2 6	3 7	1 9	3 7	2 7
Ta	1 5	1 9	1 7	1 2	1 3	2	2	7 8	8 7	1 5	2 9	2 7	2 2
Co	-	-	-	-	-	-	-	-	-	-	-	-	-
Li	59	83	93	57	38	73	75	120	354	71	137	144	81
Be	-	-	-	-	-	-	-	-	-	-	-	-	-
B	17	17	13	22	-	-	-	-	-	-	-	-	-
U	3 8	4 1	7	4 3	3 7	6 6	1 7	11	25 5	2 5	12	20	8 5
W	-	-	-	-	3	4	5	7	118	-	4	4	1
Sn	13	2	11	9	7	12	14	36	18	8	13	12	16
Mo	-	-	-	-	-	-	-	-	-	-	-	-	-
Rare-earths													
La	31	24	31	27	10	8	7	6	5	22	10	14	18
Ce	-	-	-	-	-	-	-	-	-	-	-	-	-
Pr	-	-	-	-	-	-	-	-	-	-	-	-	-
Nd	-	-	-	-	-	-	-	-	-	-	-	-	-
Sm	-	-	-	-	-	-	-	-	-	-	-	-	-
Eu	-	-	-	-	-	-	-	-	-	-	-	-	-
Gd	-	-	-	-	-	-	-	-	-	-	-	-	-
Tb	-	-	-	-	-	-	-	-	-	-	-	-	-
Dy	-	-	-	-	-	-	-	-	-	-	-	-	-
Ho	-	-	-	-	-	-	-	-	-	-	-	-	-
Er	-	-	-	-	-	-	-	-	-	-	-	-	-
Tm	-	-	-	-	-	-	-	-	-	-	-	-	-
Yb	-	-	-	-	-	-	-	-	-	-	-	-	-
Lu	-	-	-	-	-	-	-	-	-	-	-	-	-

Table E1 1 (Continued) Compilation of Meguma Zone granitoid lithogeochemistry

Sample	A04-1208	A06-2328	A04-1207	A05-1018	A04-1205	A05-0039	A04-1204	A04-3005	A04-1200	A04-3000	A04-1215	A04-1213	A04-1053
Batholith	SMB	SMB	SMB	SMB	SMB	SMB	SMB	SMB	SMB	SMB	SMB	SMB	SMB
Pluton	DLP	DLP	DLP	DLP	DLP	DLP	DLP	DLP	DLP	DLP	DLP	DLP	DLP
Lithology	Lmzg	Lmzg	Lmzg	Lmzg	Lmzg	Lmzg	Lmzg	Lmzg	Lmzg	Lmzg	Lmzg	Lmzg	Lmzg
Source	28	28	28	28	28	28	28	28	28	28	28	28	28
Major oxides													
SiO_2	73 21	71 65	75 99	70 13	71 03	68 66	74 85	74 12	74 33	71 25	74 23	73 56	73 72
TiO_2	0 19	0 27	0 14	0 34	0 16	0 42	0 12	0 12	0 08	0 28	0 15	0 17	0 22
Al_2O_3	13 60	15 03	12.24	15 72	15 23	16 28	12 77	14 18	13 83	15 02	12 90	13 79	13 74
Fe_2O_3	-	-	-	-	-	-	-	-	-	-	-	-	-
FeO	-	-	-	-	-	-	-	-	-	-	-	-	-
MnO	0 07	0 05	0 05	0 04	0 03	0 05	0 05	0 04	0 05	0 05	0 06	0 05	0 04
MgO	1 05	1 07	0 89	1 09	1 06	1 15	0 93	0 81	0 86	1 00	0 90	1 06	1 00
CaO	0 75	0 99	0 51	1 47	0 18	1 85	0 34	0 40	0 12	1 05	0 33	0 42	0 50
Na_2O	4 17	3 34	3 63	3 13	8 03	3 31	4 27	3 22	2 85	3 62	3 75	2 80	3 18
K_2O	4 33	4 91	4 50	4 94	0 84	4 24	5 05	4 43	4 82	4 92	4 12	4 64	4 66
P_2O_5	0 07	0 24	0 07	0 23	0 15	0 19	0 08	0 33	0 12	0 29	0 27	0 26	0 25
H_2O+	-	-	-	-	-	-	-	-	-	-	-	-	-
H_2O-	-	-	-	-	-	-	-	-	-	-	-	-	-
CO_2	-	-	-	-	-	-	-	-	-	-	-	-	-
Cl	-	-	-	-	-	-	-	-	-	-	-	-	-
F	0 16	0 08	0 11	0 08	0 03	0 05	0 22	0 11	0 36	0 06	0 17	0 05	0 07
LOI	0 40	0 40	0 40	0 40	0 60	0 70	0 60	0 60	1 20	0 50	0 80	0 70	0 50
TOTAL	99 73	99 94	99 96	99 68	98 94	99 25	100 63	99 60	99 83	99 93	99 15	99 03	99 64
Fe_2O_3T	2 10	2 21	1 71	2 43	1 81	2 67	1 74	1 50	1 75	2 17	1 82	1 76	2 03
FeOT	1 89	1 99	1 54	2.19	1 63	2.40	1 57	1 35	1 57	1 95	1 64	1 58	1 83
A/CNK	1 00	1 10	0 95	1 11	1 19	1 18	0 89	1 18	1 18	1 06	1 06	1 17	1 10
Trace els													
Ba	219	374	65	528	23	662	71	98	53	432	61	203	166
Rb	420	260	400	192	103	144	562	409	867	234	484	306	341
Sr	30	71	29	117	43	156	21	24	6	93	15	50	32
Y	66	28	64	34	26	31	70	27	68	33	41	34	32
Zr	101	113	92	172	132	192	72	46	56	132	73	84	90
Nb	12	12	10	10	16	11	11	14	23	10	20	11	13
Th	21 4	11	18	13	22 1	14	20 2	5 8	18	10	11	9 1	10
Pb	-	-	-	-	-	-	-	-	-	-	-	-	-
Ga	20	18	19	17	20	19	18	19	26	18	21	20	18
Zn	35	46	28	50	21	49	29	45	45	47	39	56	52
Cu	5	-	7	-	-	-	6	-	-	-	7	7	-
Ni	-	-	-	-	-	-	-	-	-	-	-	-	-
V	13	19	5	18	-	24	6	-	-	12	5	7	14
Cr	-	-	-	-	-	-	-	-	-	-	-	-	-
Hf	3	3	2	5	4	6	2	-	-	4	-	3	2
Cs	-	-	-	-	-	-	-	-	-	-	-	-	-
Sc	4 4	3 4	3 6	3 7	3	4 5	3 7	2.9	3 4	3 2	2 5	2.6	2 9
Ta	3	1 6	2.2	1 4	2.9	1	3 2	3 3	8 3	1	3 8	2 2	2 1
Co	-	-	-	-	-	-	-	-	-	-	-	-	-
Li	118	100	82	56	32	43	130	126	335	63	143	59	74
Be	-	-	-	-	-	-	-	-	-	-	-	-	-
B	-	-	-	-	-	-	-	-	-	-	-	-	-
U	13	4 4	18	2.4	7 4	2.4	23	7 1	27 2	4 1	21 2	6 4	6 2
W	4	1	4	-	1	-	13	5	11	-	6	-	13
Sn	7	9	5	6	17	7	4	15	117	4	11	4	12
Mo	-	-	-	-	-	-	-	-	-	-	-	-	-
Rare-earths													
La	21	19	15	27	19	33	14	6	6	22	7	13	14
Ce	-	-	-	-	-	-	-	-	-	-	-	-	-
Pr	-	-	-	-	-	-	-	-	-	-	-	-	-
Nd	-	-	-	-	-	-	-	-	-	-	-	-	-
Sm	-	-	-	-	-	-	-	-	-	-	-	-	-
Eu	-	-	-	-	-	-	-	-	-	-	-	-	-
Gd	-	-	-	-	-	-	-	-	-	-	-	-	-
Tb	-	-	-	-	-	-	-	-	-	-	-	-	-
Dy	-	-	-	-	-	-	-	-	-	-	-	-	-
Ho	-	-	-	-	-	-	-	-	-	-	-	-	-
Er	-	-	-	-	-	-	-	-	-	-	-	-	-
Tm	-	-	-	-	-	-	-	-	-	-	-	-	-
Yb	-	-	-	-	-	-	-	-	-	-	-	-	-
Lu	-	-	-	-	-	-	-	-	-	-	-	-	-

Table E1 1 (Continued) Compilation of Meguma Zone granitoid lithogeochemistry

Sample	A04-1050	A05-0014	A03-3024-A	A03-3007	A03-3024	A05-1006	A06-3025	A03-3009	A03-3012	A14-1020-1	A14-1020	A11-2292
Batholith	SMB	SMB	SMB	SMB	SMB	SMB	SMB	SMB	SMB	SMB	SMB	SMB
Pluton	DLP	DLP	DLP	DLP	DLP	DLP	DLP	DLP	DLP	BuBP	BuBP	-
Lithology	Lmzg	Lmzg	Lmzg	Lmzg	Lmzg	Lmzg	Lmzg	Lmzg	Lmzg	Lmzg	Lmzg	Lmzg
Source	28	28	28	28	28	28	28	28	28	28	28	28
Major oxides												
SiO_2	75 97	70 30	72 82	74 07	73 53	67 99	71 33	73 29	73 62	72 83	73 04	73 33
TiO_2	0 11	0 31	0 16	0 20	0 17	0 62	0 24	0 21	0 12	0 26	0 24	0 22
Al_2O_3	13.30	15 21	14 01	14 03	13 71	15 77	14 27	14 00	13 78	14 52	14 27	14 05
Fe_2O_3	-	-	-	-	-	-	-	-	-	-	-	-
FeO	-	-	-	-	-	-	-	-	-	-	-	-
MnO	0 04	0 05	0 04	0 04	0 04	0 06	0 04	0 04	0 03	0 05	0 04	0 04
MgO	0 76	1 09	0 85	0 89	0 96	1 38	1 13	1 01	0 92	1 37	1 08	0 99
CaO	0 28	1 38	0 43	0 71	0 50	2 00	1 04	0 70	0 41	0 80	0 60	0 47
Na_2O	3 32	3 08	3 68	3 20	3 54	3 47	4 06	3 05	3 23	3 14	3 35	3 48
K_2O	4 16	4 50	4 61	4 48	4 44	4 18	4 90	4 99	4 96	4 89	5 04	4 63
P_2O_5	0 30	0 22	0 27	0 20	0 27	0 22	0 21	0 22	0 21	0 15	0 19	0 24
H_2O+	-	-	-	-	-	-	-	-	-	-	-	
H_2O-	-	-	-	-	-	-	-	-	-	-	-	-
CO_2	-	-	-	-	-	-	-	-	-	-	-	-
Cl	-	-	-	-	-	-	-	-	-	-	-	-
F	0 24	0 08	0 09	0 04	0 14	0 07	0 06	0 06	0 07	0 06	0 04	0 08
LOI	0 40	0 70	0 80	0 60	0 60	0 30	0 30	0 70	0 50	0 60	0 60	0 70
TOTAL	99 97	98 94	99 33	99 88	99 47	99 42	99 21	99 92	99 18	100 45	99 92	99 67
Fe_2O_3T	1 44	2.33	1 85	1 62	1 90	3 81	1 88	1 90	1 56	2 04	1 75	1 69
FeOT	1 30	2 10	1 66	1 46	1 71	3 43	1 69	1 71	1 40	1 84	1 57	1 52
A/CNK	1 15	1 15	1 08	1 13	1 09	1 12	0 97	1 07	1 07	1 10	1 06	1 10
Trace els												
Ba	25	447	168	237	134	740	339	275	122	351	400	128
Rb	579	204	385	213	388	144	220	240	346	204	230	290
Sr	6	104	28	54	24	161	77	54	22	78	82	26
Y	40	31	35	19	37	37	30	29	31	24	23	22
Zr	47	144	90	78	86	242	111	106	67	103	107	84
Nb	19	9	17	8	15	12	6	9	12	10	12	14
Th	7 5	12	12	9 5	12	18	12	12	10	11	15	16
Pb	-	-	-	-	-	-	-	-	-	25	21	-
Ga	21	19	21	16	21	19	16	17	18	17	15	18
Zn	53	43	53	33	55	56	37	40	38	43	42	55
Cu	-	-	5	-	-	-	6	-	-	-	-	-
Ni	-	-	-	-	-	-	-	-	-	-	-	-
V	-	13	6	6	7	41	15	10	-	18	12	11
Cr	-	-	-	-	-	-	-	-	-	-	-	-
Hf	-	4	2	2	2	7	4	3	3	4	4	2
Cs	-	-	-	-	-	-	-	-	-	-	-	-
Sc	2.4	3 9	2 4	2 1	2.3	6 6	2 8	2 7	1 7	3 8	2 9	2 5
Ta	4 9	1 5	2 8	1 4	2 6	0 9	1 1	1 8	2 2	1 2	1 4	1 9
Co	-	-	-	-	-	-	-	-	-	-	-	-
Li	269	56	129	65	137	56	82	70	88	84	74	117
Be	-	-	-	-	-	-	-	-	-	-	-	-
B	-	-	-	-	-	-	-	-	-	19	16	-
U	16	2.6	12	16	13	2 8	2 9	11	13	4 3	6 3	4 6
W	8	-	3	-	3	-	-	1	2	-	-	-
Sn	26	10	12	7	15	-	4	8	10	2	5	7
Mo	-	-	-	-	-	-	-	-	-	-	-	-
Rare-earths												
La	5	25	12	14	12	41	20	17	10	22	26	21
Ce	-	-	-	-	-	-	-	-	-	-	-	-
Pr	-	-	-	-	-	-	-	-	-	-	-	-
Nd	-	-	-	-	-	-	-	-	-	-	-	-
Sm	-	-	-	-	-	-	-	-	-	-	-	-
Eu	-	-	-	-	-	-	-	-	-	-	-	-
Gd	-	-	-	-	-	-	-	-	-	-	-	-
Tb	-	-	-	-	-	-	-	-	-	-	-	-
Dy	-	-	-	-	-	-	-	-	-	-	-	-
Ho	-	-	-	-	-	-	-	-	-	-	-	-
Er	-	-	-	-	-	-	-	-	-	-	-	-
Tm	-	-	-	-	-	-	-	-	-	-	-	-
Yb	-	-	-	-	-	-	-	-	-	-	-	-
Lu	-	-		-	-	-	-	-	-	-	-	-

Table E1 1 (Continued) Compilation of Meguma Zone granitoid lithogeochemistry

Sample	A11-2290	A11-2272-1	A12-1019-2	A12-1019	A03-2440	A12-1016-5	A12-1016-4	A12-1016-6	A12-1016	A12-1016-1	A03-2348	A12-1010-2
Batholith	SMB	SMB	SMB	SMB	SMB	SMB	SMB	SMB	SMB	SMB	SMB	SMB
Pluton	-	-	-	-	-	-	-	-	-	-	-	-
Lithology	Lmzg	Lmzg	Lmzg	Lmzg	Lmzg	Lmzg	Lmzg	Lmzg	Lmzg	Lmzg	Lmzg	Lmzg
Source	28	28	28	28	28	28	28	28	28	28	28	28
Major oxides												
SiO_2	76 50	76 29	73 60	74 23	73 03	73 59	74 82	74 57	74 66	76 05	73 24	74 36
TiO_2	0 05	0 05	0 10	0 07	0 22	0 19	0 15	0 18	0 18	0 05	0 22	0 06
Al_2O_3	13 29	13 54	14 18	14 38	14 71	13 99	13 70	13 61	13 61	13 53	14 22	14 49
Fe_2O_3	-	-	-	-	-	-	-	-	-	-	-	-
FeO	-	-	-	-	-	-	-	-	-	-	-	-
MnO	0 03	0 02	0 05	0 04	0 03	0 08	0 07	0 07	0 07	0 05	0 05	0 03
MgO	0 70	0 68	0 92	0 86	1 02	0 89	0 82	0 95	0 90	0 80	1 01	0 78
CaO	0 46	0 40	0 48	0 50	0 48	0 81	0 47	0 50	0 55	0 29	0 52	0 35
Na_2O	3 41	3 80	4 12	3 70	3 46	3 61	3 88	3 16	3 16	3 68	3 09	3 94
K_2O	4 51	4 37	[illegible]	5 28	4 70	4 46	4 54	4 70	4 61	4 81	4 32	4 85
P_2O_5	0 13	0 33	0 25	0 24	0 38	0 14	0 15	0 12	0 13	0 12	0 38	0 19
H_20+	-	-	-	-	-	-	-	-	-	-	-	-
H_2O-	-	-	-	-	-	-	-	-	-	-	-	-
CO_2	-	-	-	-	-	-	-	-	-	-	-	-
Cl	-	-	-	-	-	-	-	-	-	-	-	-
F	0 01	0 03	0 02	0 02	0 05	0 05	0 03	0 03	0 04	0 03	0 05	0 01
LOI	0 10	0 40	0 30	0 40	0 90	0 20	0 50	0 70	0 40	0 30	0 50	0 40
TOTAL	99 80	100 33	100 21	100 58	100 13	99 81	100 73	100 37	100 11	100 80	99 03	100 10
Fe_2O_3T	0 69	0 50	1 28	0 98	1 33	2 06	1 81	2 01	2 05	1 25	1 65	0 72
FeOT	0 62	0 45	1 15	0 88	1 20	1 85	1 63	1 81	1 84	1 12	1 48	0 65
A/CNK	1 07	1 06	0 99	1 02	1 14	1 06	1 04	1 09	1 10	1 03	1 20	1 07
Trace els												
Ba	71	39	292	306	424	268	218	273	269	25	405	144
Rb	159	239	152	153	245	230	235	220	248	258	193	173
Sr	32	11	111	97	55	53	39	39	40	9	52	37
Y	20	15	21	16	20	31	31	29	35	2'	17	16
Zr	19	12	58	45	71	94	83	88	89	32	75	38
Nb	-	7	6	5	7	9	10	8	8	6	8	7
Th	1 9	-	1 8	1	10	5 9	5 2	5 9	5 9	2.4	8 8	1 8
Pb	-	-	29	30	-	31	24	15	26	-	-	30
Ga	11	16	12	13	18	17	18	17	18	16	16	16
Zn	18	43	27	21	33	34	30	33	39	27	60	24
Cu	-	-	-	-	-	-	-	-	-	-	-	-
Ni	-	-	-	-	-	-	-	-	-	-	-	-
V	-	-	-	-	13	10	6	8	10	-	11	-
Cr	-	-	-	-	-	-	-	-	-	-	-	-
Hf	2	-	-	-	-	3	2	3	2	-	1	1
Cs	-	-	-	-	-	-	-	-	-	-	-	-
Sc	1 9	2 1	3	1 8	3 1	4 5	4 1	4 4	4 6	3 2	3 7	1 8
Ta	1 1	3 9	0 8	0 9	1 6	1 8	1 8	1 3	1 5	1 5	1 2	2 1
Co	-	-	-	-	-	-	-	-	-	-	-	-
Li	8	10	13	12	25	94	52	65	77	38	35	11
Be	-	-	-	-	-	-	-	-	-	-	-	-
B	-	-	-	-	-	-	-	-	-	-	-	-
U	5 7	3 9	1 7	1 5	8 3	2 9	7 6	4 4	3 3	3 4	7 1	8 7
W	2	4	10	3	4	2	3	7	3	4	4	4
Sn	1	16		2	27	6	5	1	5	8	16	6
Mo	-	-	-	-	-	-	-	-	-	-	-	-
Rare-earths												
La	3	-	8	4	10	13	11	11	13	3	12	3
Ce	-	-	-	-	-	-	-	-	-	-	-	-
Pr	-	-	-	-	-	-	-	-	-	-	-	-
Nd	-	-	-	-	-	-	-	-	-	-	-	-
Sm	-	-	-	-	-	-	-	-	-	-	-	-
Eu	-	-	-	-	-	-	-	-	-	-	-	-
Gd	-	-	-	-	-	-	-	-	-	-	-	-
Tb	-	-	-	-	-	-	-	-	-	-	-	-
Dy	-	-	-	-	-	-	-	-	-	-	-	-
Ho	-	-	-	-	-	-	-	-	-	-	-	-
Er	-	-	-	-	-	-	-	-	-	-	-	-
Tm	-	-	-	-	-	-	-	-	-	-	-	-
Yb	-	-	-	-	-	-	-	-	-	-	-	-
Lu	-	-	-	-	-	-	-	-	-	-	-	-

Table E1 1 (Continued) Compilation of Meguma Zone granitoid lithogeochemistry

Sample	A12-1010-4	A11-2291	A11-2262-1	A11-2262-2	A04-1201	A04-1054	A04-1202	A04-1061	A04-1203	A11-2267	A11-3002	A11-3019
Batholith	SMB	SMB	SMB	SMB	SMB	SMB	SMB	SMB	SMB	SMB	SMB	SMB
Pluton	-	-	-	-	EKP	EKP	EKP	EKP	EKP	ScLP	ScLP	ScLP
Lithology	Lmzg	Lmzg	Lmzg	Lmzg	Lg	Lg	Lg	Lg	Lg	Mzg	Mzg	Mzg
Source	28	28	28	28	28	28	28	28	28	27	27	27
Major oxides												
SiO_2	74 92	74 75	72 89	74 14	74 19	73 92	73 72	75 40	74 06	68 37	69 58	68 83
TiO_2	0 05	0 11	0 16	0 09	0 06	0 03	0 06	0 05	0 06	0 67	0 51	0 65
Al_2O_3	14 29	14 47	14 82	14 60	13 93	14 73	14 25	13 05	14 00	14 95	14 34	14 18
Fe_2O_3	-	-	-	-	-	-	-	-	-	-	-	-
FeO	-	-	-	-	-	-	-	-	-	-	-	-
MnO	0 03	0 03	0 03	0 04	0 04	0 08	0 12	0 10	0 07	0 08	0 07	0 08
MgO	0 78	0 86	0 96	0 82	0 80	0 65	0 90	0 82	0 80	1 68	1 57	1 69
CaO	0 39	0 33	0 47	0 40	0 43	0 28	0 30	0 13	0 31	2 02	1 71	1 83
Na_2O	4 09	2 92	3 12	3 48	4 37	4 22	2 99	0 81	3 24	2 96	3 14	2 88
K_2O	4 61	4 26	4 90	4 37	4 28	3 97	3 79	4 30	4 15	3 75	4 06	3 63
P_2O_5	0 19	0 27	0 28	0 30	0 36	0 15	0 19	0 15	0 33	0 21	0 18	0 19
H 0+	-	-	-	-	-	-	-	-	-	-	-	-
H_2O-	-	-	-	-	-	-	-	-	-	-	-	-
CO_2	-	-	-	-	-	-	-	-	-	-	-	-
Cl	-	-	-	-	-	-	-	-	-	-	-	-
F	0 01	0 06	0 03	0 03	0 28	0 53	0 56	0 31	0 27	0 07	0 07	0 06
LOI	0 40	0 50	0 80	0 70	0 70	0 80	1 10	1 70	1 10	0 40	0 60	0 60
TOTAL	100 36	99 47	99 58	100 00	100 33	99 94	99 10	100 17	99 43	99 20	99 04	98 57
Fe_2O_3T	0 68	1 08	1 28	1 18	1 30	1 23	1 87	4 07	1 46	4 57	3 65	4 46
FeOT	0 61	0 97	1 15	1 06	1 17	1 11	1 68	3 66	1 31	4 11	3 28	4 01
A/CNK	1 06	1 29	1 17	1 19	1 04	1 18	1 35	1 62	1 22	1 17	1 10	1 16
Trace els												
Ba	82	74	271	172	19	19	14	50	23	628	561	546
Rb	157	329	258	178	717	1109	958	1227	719	142	148	154
Sr	22	17	63	38	19	5	17	7	24	143	130	136
Y	13	20	19	18	50	68	70	81	53	33	32	28
Zr	31	27	56	31	38	19	33	36	41	212	171	200
Nb	5	16	11	8	25	26	24	21	26	13	10	13
Th	1 4	5 1	5 3	1 2	7 9	13	14	16	8 1	14	11	13
Pb	18	-	-	-	-	-	-	158	13		-	-
Ga	17	21	17	15	24	32	27	28	26	17	18	17
Zn	16	31	52	30	75	50	162	115	120	70	61	77
Cu	-	-	-	-	12	-	37	543	125	-	-	-
Ni	-	-	-	-	-	-	-	-	-	-	-	-
V	-	5	-	-	-	-	-	-	-	59	51	63
Cr	-	-	-	-	-	-	-	-	-	-	-	-
Hf	1	-	-	-	-	-	-	-	-	6	4	6
Cs	-	-	-		-	-	-	-	-	-	-	-
Sc	1 6	1 8	1 9	2 6	1 7	2 7	3 5	2 7	1 7	10	8 2	9 3
Ta	1 8	5 4	2	1 7	6 1	13	13	10	6 8	1 1	1	1 4
Co	-	-	-	-	-	-	-	-	-	-	-	-
Li	8	51	125	27	221	371	309	368	376	46	81	45
Be	-	-	-	-	-	-	-	-	-	-	-	-
B	-	-	-	-	-	-	-	-	-		-	-
U	17	14	7 7	2	30 2	20 3	27 7	29 2	30 2	3 4	2	4 7
W	3	6	2	2	10	41	19	11	12	-	1	-
Sn	5	16	11	12	66	16	165	683	89	4	8	7
Mo	-	-	-	-	-	-	-	-	-	-	-	-
Rare-earths												
La	2	7	11	4	3	3	4	4	3	36	29	32
Ce	-	-	-	-	-	-	-	-	-	-	-	-
Pr	-	-		-	-	-	-	-	-		-	-
Nd	-	-	-	-	-	-	-	-	-	-	-	-
Sm	-	-	-	-	-	-	-	-	-	-	-	-
Eu	-	-	-	-	-	-	-	-	-	-	-	-
Gd	-	-	-	-	-	-	-	-	-	-	-	-
Tb	-	-	-	-	-	-	-	-	-	-	-	-
Dy	-	-	-	-	-	-	-	-	-		-	-
Ho	-	-	-	-	-	-	-	-	-	-	-	-
Er	-	-	-	-	-	-	-	-	-	-	-	-
Tm	-	-	-	-	-	-	-	-	-		-	-
Yb	-	-	-	-	-	-	-	-	-		-	-
Lu	-	-	-	-	-	-	-	-	-	-	-	-

Table E1 1 (Continued) Compilation of Meguma Zone granitoid lithogeochemistry

Sample	A03-3029	A03-3030	A11-2270-B	A12-8007	A12-1015	A03-2345-G	A03-2348	A03-2350	A03-2440	A03-3000	A03-3007	A03-3009
Batholith	SMB	SMB	SMB	SMB	SMB	SMB	SMB	SMB	SMB	SMB	SMB	SMB
Pluton	RLP	RLP	LP	LP	LP	DLP	-	DLP	-	DLP	DLP	DLP
Lithology	Grd	Grd	Grd	Grd	Grd	Lmzg	Lmzg	Lmzg	Lmzg	Lmzg	Lmzg	Lmzg
Source	28	28	28	28	28	28	28	28	28	28	28	28
Major oxides												
SiO_2	67 74	67 99	64 72	65 04	65 55	72 58	73 24	72 26	73 03	72 25	74 07	73 29
TiO_2	0 74	0 67	0 81	0 80	0 80	0 24	0 22	0 30	0 22	0 19	0 20	0 21
Al_2O_3	15 40	15 03	15 92	15 58	15 52	14 44	14 22	15 03	14 71	15 09	14 03	14 00
Fe_2O_3	-	-	-	-	-	-	-	-	-	-	-	-
FeO	-	-	-	-	-	-	-	-	-	-	-	-
MnO	0 10	0 09	0 13	0 12	0 10	0 04	0 05	0 05	0 03	0 05	0 04	0 04
MgO	1 92	1 74	1 96	1 95	1 96	0 96	1 01	1 04	1 02	0 98	0 89	1 01
CaO	1 65	1 52	2.07	2 41	2.36	1 07	0 52	1 11	0 48	0 59	0 71	0 70
Na_2O	3 00	3 63	3 33	3 55	3 34	3 31	3 09	3 35	3 46	3 39	3 20	3 05
K_2O	3 90	3 91	3 61	3 51	3 60	4 57	4 32	4 57	4 70	5 21	4 48	4 99
P_2O_5	0 23	0 22	0 24	0 24	0 23	0 20	0 38	0 24	0 38	0 21	0 20	0 22
H_20+	-	-	-	-	-	-	-	-	-	-	-	-
H_2O-	-	-	-	-	-	-	-	-	-	-	-	-
CO_2	-	-	-	-	-	-	-	-	-	-	-	-
Cl	-	-	-	-	-	-	-	-	-	-	-	-
F	0 06	0 06	0 08	0 07	0 06	0 05	0 05	0 05	0 05	0 04	0 04	0 06
LOI	0 60	0 90	0 70	0 40	0 55	0 60	0 50	0 40	0 90	0 40	0 60	0 70
TOTAL	99 44	99 55	98 62	98 85	98 90	99 84	99 03	100 43	100 13	100 05	99 88	99 92
Fe_2O_3T	4 62	4 28	5 70	5 84	5 44	2 03	1 65	2 31	1 33	1 88	1 62	1 90
FeOT	4 16	3 85	5 13	5 25	4 89	1 83	1 48	2 08	1 20	1 69	1 46	1 71
A/CNK	1 23	1 13	1 21	1 13	1 15	1 09	1 20	1 12	1 14	1 10	1 13	1 07
Trace els												
Ba	601	557	913	737	809	262	405	409	424	313	237	275
Rb	159	174	139	143	142	172	193	208	245	321	213	240
Sr	161	134	183	175	169	72	52	82	55	52	54	54
Y	30	32	43	43	38	27	17	26	20	29	19	29
Zr	187	189	281	283	254	112	75	134	71	102	78	106
Nb	11	11	14	16	14	7	8	10	7	13	8	9
Th	12	12	13	14	14	10	8 8	12	10	12	9 5	12
Pb	-	-	-	-	-	-	-	-	-	-	-	-
Ga	17	19	20	21	20	17	16	18	18	19	16	17
Zn	65	69	96	84	82	40	60	45	33	56	33	40
Cu	-	20	-	-	5	-	-	-	-	-	-	-
Ni	-	-	-	-	-	-	-	-	-	-	-	-
V	63	47	74	60	76	10	11	17	13	7	6	10
Cr	-	-	-	-	-	-	-	-	-	-	-	-
Hf	5	5	8	7	6	4	1	4	-	3	2	3
Cs	-	-	-	-	-	-	-	-	-	-	-	
Sc	9 5	8 9	13	14	12	2 8	3 7	3 7	3 1	2 7	2 1	2 7
Ta	1 2	1 1	1 1	1 3	1	0 9	1 2	1 5	1 6	2 2	1 4	1 8
Co	-	-	-	-	-	-	-	-	-	-	-	
Li	69	69	60	60	45	42	35	71	25	81	65	70
Be	-	-	-	-	-	-	-	-	-	-	-	-
B	-	-	-	-	-	-	-	-	-	-	-	-
U	3 8	3	3 3	3 4	2 5	6	7 1	2 5	8 3	8 5	16	11
W	-	-	-	-	-	6	16	8	27	15	7	8
Sn	3	8	6	-	-	-	-	-	-	-	-	-
Mo	-	-	-	-	-	-	-	-	-	-	-	-
Rare-earths												
La	27	28	42	42	39	18	12	22	10	18	14	17
Ce	-	-	-	-	-	-	4	-	4	1	-	1
Pr	-	-	-	-	-	-	-	-	-	-	-	-
Nd	-	-	-	-	-	-	-	-	-	-	-	-
Sm	-	-	-	-	-	-	-	-	-	-	-	-
Eu	-	-	-	-	-	-	-	-	-	-	-	-
Gd	-	-	-	-	-	-	-	-	-	-	-	-
Tb	-	-	-	-	-	-	-	-	-	-	-	-
Dy	-	-	-	-	-	-	-	-	-	-	-	-
Ho	-	-	-	-	-	-	-	-	-	-	-	-
Er	-	-	-	-	-	-	-	-	-	-	-	-
Tm	-	-	-	-	-	-	-	-	-	-	-	-
Yb	-	-	-	-	-	-	-	-	-	-	-	-
Lu	-	-	-	-	-	-	-	-	-	-	-	-

Table E1.1. (Continued) Compilation of Meguma Zone granitoid lithogeochemistry

Sample	A03-3012	A03-3024	A03-3029	A03-3030	A04-1050	A04-1052	A04-1053	A04-1054	A04-1061	A04-1200	A04-1201	A04-1202
Batholith	SMB	SMB	SMB	SMB	SMB	SMB	SMB	SMB	SMB	SMB	SMB	SMB
Pluton	DLP	DLP	RLP	RLP	DLP	DLP	DLP	EKP	EKP	DLP	EKP	EKP
Lithology	Lmzg	Lmzg	Grd	Grd	Lmzg	Lmzg	Lmzg	Lg	Lg	Lmzg	Lg	Lg
Source	28	28	28	28	28	28	28	28	28	28	28	28
Major oxides												
SiO_2	73.62	73.53	67 74	67 99	75 97	74.37	73.72	73 92	75 40	74 33	74 19	73 72
TiO_2	0.12	0.17	0.74	0 67	0.11	0.12	0 22	0 03	0.05	0 08	0 06	0 06
Al_2O_3	13.78	13.71	15 40	15 03	13.30	13 94	13.74	14.73	13 05	13 83	13 93	14 25
Fe_2O_3	-	-	-	-	-	-	-	-	-	-	-	-
FeO	-	-	-	-	-	-	-	-	-	-	-	-
MnO	0.03	0 04	0 10	0 09	0 04	0.05	0.04	0 08	0.10	0.05	0 04	0 12
MgO	0 92	0 96	1.92	1.74	0 76	0 81	1 00	0 65	0 82	0 86	0 80	0 90
CaO	0 41	0 50	1.65	1.52	0 28	0.43	0 50	0.28	0.13	0 12	0 43	0 30
Na_2O	3.23	3 54	3.00	3 63	3.32	3.58	3 18	4 22	0 81	2 85	4 37	2 99
K_2O	4 96	4 44	3 90	3 91	4 16	4 62	4.66	3 97	4 30	4 82	4 28	3 79
P_2O_5	0 21	0 27	0.23	0 22	0 33	0 29	0 25	0 15	0 15	0 12	0 36	0 19
H_2O+	-	-	-	-	-	-	-	-	-	-	-	-
H_2O-	-	-	-	-	-	-	-	-	-	-	-	-
CO_2	-	-	-	-	-	-	-	-	-	-	-	-
Cl	-	-	-	-	-	-	-	-	-	-	-	-
F	0.07	0.14	0 06	0.06	0.24	0.14	0 07	0 53	0 31	0 36	0 28	0 56
LOI	0 50	0 60	0 60	0 90	0 40	0 60	0 50	0 80	1 70	1 20	0 70	1 10
TOTAL	99 18	99 47	99 44	99 55	99 97	100 19	99 64	99 94	100 17	99 83	100 33	99 10
Fe_2O_3T	1 56	1.90	4 62	4 28	1 44	1.53	2 03	1 23	4 07	1 75	1 30	1 87
FeOT	1.40	1.71	4 16	3 85	1.30	1 38	1 83	1.11	3 66	1 57	1 17	1 68
A/CNK	1.07	1 09	1 23	1 13	1 15	1 09	1 10	1 18	1 62	1 18	1 04	1 35
Trace els												
Ba	122	134	601	557	25	87	166	19	50	53	19	14
Rb	346	388	159	174	579	393	341	1109	1227	867	717	958
Sr	22	24	151	134	6	24	32	5	7	6	19	17
Y	31	37	30	32	40	29	32	68	81	68	50	70
Zr	67	86	187	189	47	45	90	19	36	56	38	33
Nb	12	15	11	11	19	13	13	26	21	23	25	24
Th	10	12	12	12	7.5	5 6	10	13	16	18	7 9	14
Pb	-	-	-	-	-	-	-	-	158	-	-	-
Ga	18	21	17	19	21	19	18	32	28	23	24	27
Zn	38	55	65	69	53	50	52	50	115	45	75	162
Cu	-	-	-	20	-	-	-	-	543	-	12	37
Ni	-	-	-	-	-	-	-	-	-	-	-	-
V	-	7	63	47	-	-	14	-	-	-	-	-
Cr	-	-	-	-	-	-	-	-	-	-	-	-
Hf	3	2	5	5	-	-	2	-	-	-	-	-
Cs	-	-	-	-	-	-	-	-	-	-	-	-
Sc	1.7	2.3	9 5	8 9	2.4	2.7	2 9	2.7	2.7	3 4	1 7	3 5
Ta	2 2	2.6	1 2	1.1	4 9	3.2	2.1	13	10	8 3	6 1	13
Co	-	-	-	-	-	-	-	-	-	-	-	-
Li	88	137	69	69	269	120	74	371	368	335	221	309
Be	-	-	-	-	-	-	-	-	-	-	-	-
B	-	-	-	-	-	-	-	-	-	-	-	-
U	13	13	3 8	3	16	6 9	6 2	20 3	29 2	27 2	30 2	27 7
W	10	15	3	8	26	18	12	16	683	117	66	165
Sn	-	-	-	-	-	-	-	-	-	-	-	-
Mo	-	-	-	-	-	-	-	-	-	-	-	-
Rare-earths												
La	10	12	27	28	5	7	14	3	4	6	3	4
Ce	2	3	-	-	8	6	13	41	11	11	10	19
Pr	-	-	-	-	-	-	-	-	-	-	-	-
Nd	-	-	-	-	-	-	-	-	-	-	-	-
Sm	-	-	-	-	-	-	-	-	-	-	-	-
Eu	-	-	-	-	-	-	-	-	-	-	-	-
Gd	-	-	-	-	-	-	-	-	-	-	-	-
Tb	-	-	-	-	-	-	-	-	-	-	-	-
Dy	-	-	-	-	-	-	-	-	-	-	-	-
Ho	-	-	-	-	-	-	-	-	-	-	-	-
Er	-	-	-	-	-	-	-	-	-	-	-	-
Tm	-	-	-	-	-	-	-	-	-	-	-	-
Yb	-	-	-	-	-	-	-	-	-	-	-	-
Lu	-	-	-	-	-	-	-	-	-	-	-	-

Table E1 1 (Continued) Compilation of Meguma Zone granitoid lithogeochemistry

Sample	A04-1203	A04-1204	A04 1205	A04-1206	A04-1207	A04-1208	A04-1209	A04-1210	A04-1211	A04-1212	A04-1213	A04-1214
Batholith	SMB	SMB	SMB	SMB	SMB	SMB	SMB	SMB	SMB	SMB	SMB	SMB
Pluton	EKP	DLP	DLP	SoLP	DLP	DLP	DLP	DoLP	DoLP	DLP	DLP	SoLP
Lithology	Lg	Lmzg	Lmzg	Mzg	Lmzg	Lmzg	Lmzg	Lmzg	Lmzg	Lmzg	Lmzg	Mzg
Source	28	28	28	28	28	28	28	28	28	28	28	28
Major oxides												
SiO_2	74 06	74 85	71 03	72 57	75 99	73 21	75 68	75 21	73 43	74 62	73 56	72 18
TiO_2	0 06	0 12	0 16	0 33	0 14	0 19	0 10	0 05	0 04	0 11	0 17	0 26
Al_2O_3	14 00	12.77	15 23	13 50	12.24	13 60	12 57	13 36	14 00	13 09	13 79	13 68
Fe_2O_3	-	-	-	-	-	-	-	-	-	-	-	-
FeO	-	-	-	-	-	-	-	-	-	-	-	-
MnO	0 07	0 05	0 03	0 07	0 05	0 07	0 05	0 06	0 09	0 04	0 05	0 07
MgO	0 80	0 93	1 06	1 25	0 89	1 05	0 86	0 78	0 83	0 85	1 06	1 16
CaO	0 31	0 34	0 18	1 26	0 51	0 75	0 39	0 38	0 40	0 35	0 42	0 68
Na_2O	3 74	4 27	8 03	3 59	3 63	4 17	3 76	3 28	3 47	3 12	2 80	3 62
K_2O	4 15	5 05	0 84	3 99	4 50	4 33	4 51	4 29	3 83	5 02	4 64	4 64
P_2O_5	0 33	0 08	0 15	0 13	0 07	0 07	0 07	0 16	0 18	0 18	0 26	0 17
H_2O+	-	-	-	-	-	-	-	-	-	-	-	-
H_2O-	-	-	-	-	-	-	-	-	-	-	-	-
CO_2	-	-	-	-	-	-	-	-	-	-	-	-
Cl	-	-	-	-	-	-	-	-	-	-	-	-
F	0 27	0 22	0 03	0 30	0 11	0 16	0 15	0 30	0 51	0 16	0 05	0 31
LOI	1 10	0 60	0 60	0 60	0 40	0 40	0 70	0 90	1 50	0 60	0 70	1 10
TOTAl	99 43	100 63	98 94	99 58	99 96	99 73	100 02	99 90	99 41	99 64	99 03	99 79
Fe_2O_3T	1 46	1 74	1 81	2 54	1 71	2 10	1 48	1 59	1 82	1 85	1 76	2 48
FeOT	1 31	1 57	1 63	2 29	1 54	1 89	1 33	1 43	1 64	1 66	1 58	2 23
A/CNK	1 22	0 89	1 19	1 04	0 95	1 00	0 98	1 13	1 23	1 03	1 17	1 03
Trace els												
Ba	23	71	23	210	65	219	63	27	21	78	203	318
Rb	719	562	103	441	400	420	499	670	817	478	306	431
Sr	24	21	43	60	29	30	10	6	5	11	50	58
Y	53	70	26	62	64	66	62	56	63	49	34	54
Zr	41	72	132	127	92	101	74	39	29	79	84	115
Nb	26	11	16	15	10	12	11	24	17	14	11	14
Th	8 1	20 2	22 1	18	18	21 4	18	13	12	14	9 1	18
Pb	13	-	-	-	-	-	-	-		-	-	-
Ga	26	18	20	18	19	20	18	23	24	22	20	20
Zn	120	29	21	42	28	35	26	49	56	54	56	57
Cu	125	6	-	8	7	5	6	6	8	6	7	30
Ni	-	-	-	-	-	-	-	-	-	-	-	-
V	-	6	-	22	5	13	-	-	-	-	7	28
Cr	-	-	-	-	-	-	-	-	-	-	-	-
Hf	-	2	4	3	2	3	2	-	-	2	3	2
Cs	-	-	-	-	-	-	-	-	-	-	-	-
Sc	1 7	3 7	3	4 5	3 6	4 4	3 7	2 3	2 6	1 9	2.6	4 8
Ta	6 8	3 2	2.9	3 1	2 2	3	2 7	7 8	8 7	2 9	2 2	2 7
Co	-	-	-	-	-	-	-	-	-	-	-	-
Li	376	130	32	171	82	118	144	120	354	137	59	142
Be	-	-	-	-	-	-	-	-	-	-	-	-
B	-	-	-	-	-	-	-	-	-	-	-	-
U	30 2	23	7 4	15	18	13	20	11	25 5	12	6 4	14
W	89	4	17	9	5	7	12	36	18	13	4	22
Sn	-	-	-	-	-	-	-	-	-	-	-	-
Mo	-	-	-	-	-	-	-	-	-	-	-	-
Rare-earths												
La	3	14	19	22	15	21	14	6	5	10	13	19
Ce	12	13	1	102	4	4	4	7	118	4	-	5
Pr	-	-	-	-	-	-	-	-	-	-	-	-
Nd	-	-	-	-	-	-	-	-	-	-	-	-
Sm	-	-	-	-	-	-	-	-	-	-	-	-
Eu	-	-	-	-	-	-	-	-	-	-	-	-
Gd	-	-	-	-	-	-	-	-	-	-	-	-
Tb	-	-	-	-	-	-	-	-	-	-	-	-
Dy	-	-	-	-	-	-	-	-	-	-	-	-
Ho	-	-	-	-	-	-	-	-	-	-	-	-
Er	-	-	-	-	-	-	-	-	-	-	-	-
Tm	-	-	-	-	-	-	-	-	-	-	-	-
Yb	-	-	-	-	-	-	-	-	-	-	-	-
Lu	-	-	-	-	-	-	-	-	-	-	-	-

Table E1.1. (Continued) Compilation of Meguma Zone granitoid lithogeochemistry

Sample	A04-1215	A04-1216	A04-1217	A04-1218	A04-3000	A04-3005	A05-0014	A05-0039	A05-1006	A05-1018	A05-8028	A06-2328
Batholith	SMB	SMB	SMB	SMB	SMB	SMB	SMB	SMB	SMB	SMB	SMB	SMB
Pluton	DLP	SoLP	SoLP	SoLP	DLP	DLP	DLP	DLP	DLP	DLP	DLP	DLP
Lithology	Lmzg	Mzg	Mzg	Mzg	Lmzg	Lmzg	Lmzg	Lmzg	Lmzg	Lmzg	Lmzg	Lmzg
Source	28	28	28	28	28	28	28	28	28	28	28	28
Major oxides												
SiO_2	74 23	73,97	74 64	74,70	71,25	74,12	70 30	68,66	67 99	70 13	71 25	71 65
TiO_2	0,16	0,12	0,12	0,12	0,28	0,12	0,31	0,42	0 62	0 34	0 28	0 27
Al_2O_3	12,90	12,97	12,74	12,97	15,02	14,18	15,21	16,28	15,77	15,72	15 05	15,03
Fe_2O_3	-	-	-	-	-	-	-	-	-	-	-	-
FeO	-	-	-	-	-	-	-	-	-	-	-	-
MnO	0,06	0,05	0,04	0,06	0,05	0 04	0,05	0,05	0,06	0,04	0,04	0 05
MgO	0,90	1,05	0,90	0,77	1,00	0,81	1,09	1,15	1 38	1 09	0,92	1 07
CaO	0,33	0,36	0,29	0,41	1 05	0,40	1,38	1 85	2,00	1,47	1 10	0 99
Na_2O	3,75	3,63	3 38	3,50	3,62	3 22	3 08	3 31	3 47	3 13	3 22	3 34
K_2O	4,12	4,57	4,56	4 58	4 92	4 43	4,60	4 24	4 18	4 94	4 84	4 91
P_2O_5	0,27	0,10	0,10	0,10	0,29	0,33	0 22	0,19	0 22	0 23	0 31	0 24
H_2O+	-	-	-	-	-	-	-	-	-	-	-	-
H_2O-	-	-	-	-	-	-	-	-	-	-	-	-
CO_2	-	-	-	-	-	-	-	-	-	-	-	-
Cl	-	-	-	-	-	-	-	-	-	-	-	-
F	0,17	0 24	0,19	0,31	0,06	0,11	0,08	0,05	0 07	0 08	0 04	0 08
LOI	0,80	0,70	0,70	0,80	0,50	0,60	0,70	0,70	0,30	0,40	0 60	0,40
TOTAL	99 15	99 23	99 22	99 58	99 93	99 60	98 94	99 25	99 42	99 68	99 36	99 94
Fe_2O_3T	1,82	1,90	1,94	1,74	2,17	1,50	2,33	2,67	3 81	2 43	1 95	2 21
FeOT	1,64	1,71	1,75	1,57	1,95	1,35	2,10	2,40	3,43	2,19	1 75	1 99
A/CNK	1,06	1,02	1,04	1,03	1,06	1 18	1 15	1,18	1 12	1 11	1 11	1,10
Trace els.												
Ba	61	68	97	61	432	98	447	662	740	528	431	374
Rb	484	515	528	558	234	409	204	144	144	192	172	260
Sr	15	19	17	9	93	- 24	104	156	161	117	96	71
Y	41	58	61	60	33	27	31	31	37	34	27	28
Zr	73	75	76	83	132	46	144	192	242	172	132	113
Nb	20	14	14	14	10	14	9	11	12	10	9	12
Th	11	18	18	18	10	5,8	12	14	18	13	12	11
Pb	-	-	-	-	-	-	-	-	-	-	-	-
Ga	21	20	21	20	18	19	19	19	19	17	17	18
Zn	39	35	33	33	47	45	43	49	56	50	39	46
Cu	7	7	10	10	-	-	-	-	-	-	-	-
Ni	-	-	-	-	-	-	-	-	-	-	-	-
V	5	7	7	-	12	-	13	24	41	18	14	19
Cr	-	-	-	-	-	-	-	-	-	-	-	-
Hf	-	2	3	2	4	-	4	6	7	5	4	3
Cs	-	-	-	-	-	-	-	-	-	-	-	-
Sc	2.5	3.2	3.7	3,5	3,2	2,9	3 9	4 5	6,6	3,7	2,8	3 4
Ta	3,8	4,1	4	4,2	1	3 3	1,5	1	0 9	1 4	1	1 6
Co	-	-	-	-	-	-	-	-	-	-	-	-
Li	143	107	122	136	63	126	56	43	56	56	65	100
Be	-	-	-	-	-	-	-	-	-	-	-	-
B	-	-	-	-	-	-	-	-	-	-	-	-
U	21,2	24,8	23,7	23,7	4,1	7,1	2,6	2,4	2,8	2,4	4	4 4
W	11	15	25	25	4	15	10	7	-	6	3	9
Sn	-	-	-	-	-	-	-	-	-	-	-	-
Mo	-	-	-	-	-	-	-	-	-	-	-	-
Rare-earths												
La	7	13	15	13	22	6	25	33	41	27	23	19
Ce	6	8	6	7	-	5	-	-	-	-	-	1
Pr	-	-	-	-	-	-	-	-	-	-	-	-
Nd	-	-	-	-	-	-	-	-	-	-	-	-
Sm	-	-	-	-	-	-	-	-	-	-	-	-
Eu	-	-	-	-	-	-	-	-	-	-	-	-
Gd	-	-	-	-	-	-	-	-	-	-	-	-
Tb	-	-	-	-	-	-	-	-	-	-	-	-
Dy	-	-	-	-	-	-	-	-	-	-	-	-
Ho	-	-	-	-	-	-	-	-	-	-	-	-
Er	-	-	-	-	-	-	-	-	-	-	-	-
Tm	-	-	-	-	-	-	-	-	-	-	-	-
Yb	-	-	-	-	-	-	-	-	-	-	-	-
Lu	-	-	-	-	-	-	-	-	-	-	-	-

Table E1.1 (Continued) Compilation of Meguma Zone granitoid lithogeochemistry

Sample	A06-300/	A06-3010-1	A06-3015	A06-3015-1	A06-3017	A06-3021	A06-3025	A06-3030	A11-2239	A11-2249	A11-2259	A11-2262-1
Batholith	SMB	SMB	SMB	SMB	SMB	SMB	SMB	SMB	SMB	SMB	SMB	SMB
Pluton	KP	KP	ScLP	ScLP	ScLP	KP	DLP	ScLP	WDP	WDP	WDP	-
Lithology	Mzg	Mzg	Mzg	Mzg	Mzg	Mzg	Lmzg	Mzg	Mzg	Mzg	Mzg	Lmzg
Source	28	28	28	28	28	28	28	28	28	28	28	28
Major oxides												
SiO_2	69 56	69 54	68 23	69 77	68 41	70 59	71 33	70 07	73 01	72 62	73 34	72 89
TiO_2	0 48	0 46	0 43	0 50	0 51	0 44	0 24	0 55	0 29	0 23	0 21	0 16
Al_2O_3	15 22	15 17	16 08	14 27	14 97	15 07	14 27	14 62	14 02	14 55	14 13	14 82
Fe_2O_3	-	-	-	-	-	-	-	-	-	-	-	-
FeO	-	-	-	-	-	-	-	-	-	-	-	-
MnO	0 10	0 09	0 05	0 08	0 08	0 09	0 04	0 07	0 04	0 04	0 04	0 03
MgO	1 55	1 46	1 13	1 49	1 48	1 45	1 13	1 47	0 93	1 17	1 05	0 96
CaO	1 12	1 04	1 84	1 57	1 45	0 67	1 04	1 62	0 63	0 54	0 45	0 47
Na_2O	2 95	3 27	3 67	3 22	3 28	3 05	4 06	3 31	2 94	3 30	3 09	3 12
K_2O	4 08	4 49	4 21	3,79	4 39	4 29	4 90	4 06	4 97	5 00	4 97	4 90
P_2O_5	0 24	0 23	0 19	0 18	0 20	0 24	0 21	0 20	0 25	0 18	0 14	0 28
H_2O+	-	-	-	-	-	-	-	-	-	-	-	
H_2O-	-	-	-	-	-	-	-	-	-	-	-	-
CO_2	-	-	-	-	-	-	-	-	-	-	-	-
Cl	-	-	-	-	-	-	-	-	-	-	-	-
F	0 06	0 05	0 06	0 05	0 06	0 05	0 06	0 05	0 07	0 03	0 04	0 03
LOI	0 80	0 60	0 80	0 70	0 60	1 10	0 30	0 50	0 50	1 10	0 60	0 80
TOTAL	99 47	99 36	98 99	98 90	98 85	100 00	99 21	99 99	99 27	100 41	99 72	99 58
Fe_2O_3T	3 74	3 34	2 62	3 70	3 87	3 35	1 88	3 91	1 88	1 87	1 89	1 28
FeOT	3 37	3 01	2 36	3 33	3 48	3 01	1 69	3 52	1 69	1 68	1 70	1 15
A/CNK	1 26	1 16	1 13	1 13	1 11	1 27	0 97	1 11	1 10	1 10	1 11	1 17
Trace els												
Ba	509	629	655	372	610	531	339	567	355	391	438	271
Rb	191	192	142	147	172	204	220	149	239	216	221	258
Sr	109	118	157	109	116	96	77	119	58	72	73	63
Y	28	28	35	38	30	26	30	34	19	20	23	19
Zr	159	147	193	170	174	139	111	173	120	95	86	56
Nb	10	10	10	11	11	10	6	11	14	10	10	11
Th	11	11	14	10	11	11	12	11	22 2	12	10	5 3
Pb	-	-	-	-	-	-	-	-	-	-	-	-
Ga	18	16	19	17	16	18	16	17	17	16	15	17
Zn	69	58	52	55	57	48	37	57	52	40	36	52
Cu	-	-	-	-	-	-	6	-	-	-	-	-
Ni	-	-	-	-	-	-	-	-	-	-	-	-
V	43	41	30	39	33	39	15	45	6	12	15	-
Cr	-	-	-	-	-	-	-	-	-	-	-	-
Hf	4	4	5	4	5	4	4	5	3	3	2	-
Cs	-	-	-	-	-	-	-	-	-	-	-	-
Sc	6 5	6 4	4 3	7 5	7 7	6	2 8	9	2 7	2 8	3 4	1 9
Ta	1 4	1 4	0 9	1 7	1 2	2 2	1 1	1 4	1 6	1 5	1 7	2
Co	-	-	-	-	-	-	-	-	-	-	-	-
Li	77	69	41	60	62	81	82	49	89	36	71	125
Be	-	-	-	-	-	-	-	-	-	-	-	-
B	-	-	-	-	-	-	-	-	-	-	-	-
U	2 7	4 3	2 3	4	4 5	7 4	2 9	3 3	4 5	4 4	5 1	7 7
W	-	3	4	3	2	6	4	-	6	-	9	11
Sn	-	-	-	-	-	-	-	-	-	-	-	-
Mo	-	-	-	-	-	-	-	-	-	-	-	-
Rare-earths												
La	28	28	32	27	27	26	20	29	32	20	20	11
Ce	-	-	-	-	-	3	-	1	-	-	3	2
Pr	-	-	-	-	-	-	-	-	-	-	-	-
Nd	-	-	-	-	-	-	-	-	-	-	-	-
Sm	-	-	-	-	-	-	-	-	-	-	-	-
Eu	-	-	-	-	-	-	-	-	-	-	-	-
Gd	-	-	-	-	-	-	-	-	-	-	-	-
Tb	-	-	-	-	-	-	-	-	-	-	-	-
Dy	-	-	-	-	-	-	-	-	-	-	-	-
Ho	-	-	-	-	-	-	-	-	-	-	-	-
Er	-	-	-	-	-	-	-	-	-	-	-	-
Tm	-	-	-	-	-	-	-	-	-	-	-	-
Yb	-	-	-	-	-	-	-	-	-	-	-	-
Lu	-	-	-	-	-	-	-	-	-	-	-	-

Table E1 1 (Continued) Compilation of Meguma Zone granitoid lithogeochemistry

Sample	A11-2262-2	A11-2267	A11-2268	A11-2270-B	A11-2270-C	A11-7272-1	A11-2276-1	A11-2280-1	A11-2283	A11-2286	A11-2290	A11-2291
Batholith	SMB	SMB	SMB	SMB	SMB	SMB	SMB	SMB	SMB	SMB	SMB	SMB
Pluton	-	ScLP	MHP	LP	-	-	ScLP	ScLP	WDP	ScLP	-	-
Lithology	Lmzg	Grd	Lmzg	Grd	MPOR	Lmzg	Mzg	Mzg	Mzg	Mzg	Lmzg	Lmzg
Source	28	28	28	28	28	28	28	28	28	28	28	28
Major oxides												
SiO_2	74 14	68 37	74 28	64 72	63 82	76 29	72 74	68 30	71 16	67 67	76 50	74 75
TiO_2	0 09	0 67	0 10	0 81	0 85	0 05	0 32	0 62	0 36	0 60	0 05	0 11
Al_2O_3	14 60	14 95	13 48	15 92	16 09	13 54	13 65	14 85	14 98	15 44	13 29	14 47
Fe_2O_3	-	-	-	-	-	-	-	-	-	-	-	-
FeO	-	-	-	-	-	-	-	-	-	-	-	-
MnO	0 04	0 08	0 06	0 13	0 17	0 02	0 08	0 10	0 08	0 08	0 03	0 03
MgO	0 82	1 68	0 97	1 98	2 12	0 68	1 24	1 68	1 24	2 01	0 70	0 86
CaO	0 40	2 02	0 30	2.07	1 74	0 40	1 05	1 80	0 96	1 25	0 46	0 33
Na_2O	3 48	2 96	3 24	3 33	3 14	3 80	2 9?	3 31	3 42	2 44	3 41	2 92
K_2O	4 37	3 75	4 77	3 61	3 47	4 37	4 18	3 94	4 38	4 08	4 51	4 26
P_2O_5	0 30	0 21	0 13	0 24	0 23	0 33	0 16	0 22	0 21	0 18	0 13	0 27
H_20+	-	-	-	-	-	-	-	-	-	-		-
H_2O-	-	-	-	-	-	-	-	-	-	-	-	-
CO_2	-	-	-	-	-	-	-	-	-	-	-	-
Cl	-	-	-	-	-	-	-	-	-	-	-	-
F	0 03	0 07	0 03	0 08	0 07	0 03	0 0[illegible]	0 07	0 06	0 08	0 01	0 06
LOI	0 70	0 40	0 60	0 70	1 20	0 40	0 30	0 80	0 70	1 10	0 10	0 60
TOTAL	100 00	99 20	99 78	98 62	98 55	100 33	99 10	99 61	100 05	98 72	99 80	99 47
Fe_2O_3T	1 18	4 57	2 01	5 70	6 36	0 50	2 67	4 43	2 85	4 30	0 69	1 08
FeOT	1 06	4 11	1 81	5 13	5 72	0 45	2.40	3 99	2 56	3 87	0 62	0 97
A/CNK	1 19	1 17	1 08	1 21	1 32	1 06	1 12	1 12	1 16	1 34	1 07	1 29
Trace els												
Ba	172	628	228	913	744	39	300	541	459	564	71	74
Rb	178	142	211	139	135	239	189	152	208	168	159	329
Sr	38	143	33	183	181	11	74	136	82	133	32	17
Y	18	33	34	43	46	15	31	32	30	25	20	20
Zr	31	212	79	281	294	12	101	197	113	169	19	27
Nb	8	13	5	14	14	7	7	12	12	11	-	16
Th	1 2	14	6 1	13	15	-	7 3	12	7 5	16	1 9	5 1
Pb	-	-	-	-	267	-	-	-	-	-	-	-
Ga	15	17	14	20	17	16	15	16	17	19	11	21
Zn	30	70	33	98	790	43	43	80	56	73	18	31
Cu	-	-	-	-	7	-	-	-	-	-	-	-
Ni	-	-	-	-	-	-	-	-	-	-	-	-
V	-	59	9	74	97	-	21	54	27	74	-	5
Cr	-	-	-	-	-	-	-	-	-	-	-	-
Hf	-	6	3	8	8	-	3	6	3	4	2	-
Cs	-	-	-	-	-	-	-	-	-	-	-	-
Sc	2.6	10	4 1	13	14	2.1	5 6	9 3	6	9 3	1 9	1 8
Ta	1 7	1 1	1 3	1 1	1 4	3 9	1 4	1 4	1 7	1 4	1 1	5 4
Co	-	-	-	-	-	-	-	-	-	-	-	-
Li	27	46	38	60	66	10	68	65	79	82	8	51
Be	-	-	-	-	-	-	-	-	-	-	-	-
B	-	-	-	-	-	-	-	-	-	-	-	-
U	2	3 4	3 7	3 3	3 6	3 9	2.9	3 7	5 8	4	5 7	14
W	12	4	7	6	-	16	6	8	3	4	1	16
Sn	-	-	-	-	-	-	-	-	-	-	-	-
Mo	-	-	-	-	-	-	-	-	-	-	-	-
Rare-earths												
La	4	36	10	42	45	-	18	29	19	33	3	7
Ce	2	-	3	-	-	4	-	-	2	1	2	6
Pr	-	-	-	-	-	-	-	-	-	-		-
Nd	-	-	-	-	-	-	-	-	-	-	-	-
Sm	-	-	-	-	-	-	-	-	-	-	-	-
Eu	-	-	-	-	-	-	-	-	-	-	-	-
Gd	-	-	-	-	-	-	-	-	-	-	-	-
Tb	-	-	-	-	-	-	-	-	-	-	-	-
Dy	-	-	-	-	-	-	-	-	-	-	-	-
Ho	-	-	-	-	-	-	-	-	-	-	-	-
Er	-	-	-	-	-	-	-	-	-	-	-	-
Tm	-	-	-	-	-	-	-	-	-	-	-	-
Yb	-	-	-	-	-	-	-	-	-	-	-	-
Lu	-	-	-	-	-	-	-	-	-	-	-	-

Table E1 1 (Continued) Compilation of Meguma Zone granitoid lithogeochemistry

Sample	A11-2292	A11-2293	A11-2296	A11-2300	A11-2301-1	A11-2301-2	A11-2316	A11-3002	A11-3005	A11-3013	A11 3015	A11-3019
Batholith	SMB	SMB	SMB	SMB	SMB	SMB	SMB	SMB	SMB	SMB	SMB	SMB
Pluton	-	WDP	ScLP	LRoP	EDP	EDP	ScLP	ScLP	WDP	WDP	WDP	Scl P
Lithology	Lmzg	Mzg	Mzg	Mzg	Lmzg	Lmzg	Mzg	Mzg	Mzg	Mzg	Mzg	Grd
Source	28	28	28	28	28	28	28	28	28	28	28	28
Major oxides												
SiO_2	73 33	74 28	70 02	70 32	73 33	74 01	68 65	69 58	74 19	72 06	73 31	68 83
TiO_2	0 22	0 16	0 44	0 50	0 12	0 14	0 53	0 51	0 24	0 23	0 32	0 65
Al_2O_3	14 05	13 97	14 55	13 97	14 52	14 27	14 96	14 34	13 67	14 94	13 94	14 18
Fe_2O_3	-	-	-	-	-	-	-	-	-	-	-	-
FeO	-	-	-	-	-	-	-	-	-	-	-	-
MnO	0 04	0 03	0 08	0 08	0 05	0 05	0 08	0 07	0 04	0 04	0 04	0 08
MgO	0 99	0 97	1 44	1 52	0 90	0 91	1 53	1 57	1 02	1 00	0.94	1 69
CaO	0 47	0 47	1 40	1 38	0 45	0 41	1 71	1 71	0 60	0 69	0 70	1 83
Na_2O	3 48	3 25	3 50	2 85	3 77	3 36	3 25	3 14	3 11	2 95	3 00	2 88
K_2O	4 63	4 75	4 03	3 91	4 50	4 56	4 25	4 06	4 72	5 07	4 64	3 63
P_2O_5	0 24	0 17	0 19	0 20	0 32	0 27	0 19	0 18	0 23	0 23	0 24	0 19
H_2O+	-	-	-	-	-	-	-	-	-	-	-	-
H_2O-	-	-	-	-	-	-	-	-	-	-	-	-
CO_2	-	-	-	-	-	-	-	-	-	-	-	-
Cl	-	-	-	-	-	-	-	-	-	-	-	-
F	0 08	0 04	0 05	0 05	0 05	0 04	0 06	0 07	0 08	0 08	0 10	0 06
LOI	0 70	0 60	0 50	0 60	0 60	0 80	0 60	0 60	0 70	0 50	0 40	0 60
TOTAL	99 67	100 06	99 16	98 64	99 77	100 09	99 15	99 04	99 96	99 40	99 45	98 57
Fe_2O_3T	1 69	1 55	3 35	3 68	1 34	1 46	3 78	3 65	1 60	1 88	2 13	4 46
FeOT	1 52	1 39	3 01	3 31	1 21	1 31	3 40	3 28	1 44	1 69	1 92	4 01
A/CNK	1 10	1 11	1 11	1 17	1 12	1 15	1 11	1 10	1 09	1 15	1 12	1 16
Trace els												
Ba	128	202	385	412	275	147	602	561	260	288	355	546
Rb	290	258	178	164	253	252	159	148	256	266	267	154
Sr	26	43	98	108	40	33	124	130	47	62	61	136
Y	22	23	31	31	19	21	33	32	18	22	20	28
Zr	84	61	137	166	45	52	180	171	90	90	122	200
Nb	14	8	11	11	7	8	11	10	12	13	13	13
Th	16	5 7	8 9	11	3 7	4 8	11	11	17	15	24 9	13
Pb	-	-	-	-	-	-	-	-	-	-	-	-
Ga	18	15	16	16	15	17	17	18	17	18	18	17
Zn	55	30	62	57	28	26	63	61	55	58	63	77
Cu	-	-	-	-	-	-	-	-	-	-	-	-
Ni	-	-	-	-	-	-	-	-	-	-	-	-
V	11	11	40	41	6	-	50	51	9	8	14	63
Cr	-	-	-	-	-	-	-	-	-	-	-	-
Hf	2	2	4	5	-	2	5	4	3	2	3	6
Cs	-	-	-	-	-	-	-	-	-	-	-	-
Sc	2.5	3 2	7 7	8 4	2.3	3 2	8 9	8 2	2	2.1	2.6	9 3
Ta	1 9	1 8	1 7	1 5	2	2	1	1	2	1 9	2	1 4
Co	-	-	-	-	-	-	-	-	-	-	-	-
Li	117	54	86	66	75	73	57	81	90	107	119	45
Be	-	-	-	-	-	-	-	-	-	-	-	-
B	-	-	-	-	-	-	-	-	-	-	-	-
U	4 5	4 2	3 7	3 8	1 7	6 6	4 1	2	3 7	5 8	4 6	4 7
W	7	11	2	1	14	12	2	8	2	7	10	7
Sn	-	-	-	-	-	-	-	-	-	-	-	-
Mo	-	-	-	-	-	-	-	-	-	-	-	-
Rare-earths												
La	21	10	23	27	7	8	29	29	23	24	33	32
Ce	-	4	1	1	5	4	-	1	2	1	1	-
Pr	-	-	-	-	-	-	-	-	-	-	-	-
Nd	-	-	-	-	-	-	-	-	-	-	-	-
Sm	-	-	-	-	-	-	-	-	-	-	-	-
Eu	-	-	-	-	-	-	-	-	-	-	-	-
Gd	-	-	-	-	-	-	-	-	-	-	-	-
Tb	-	-	-	-	-	-	-	-	-	-	-	-
Dy	-	-	-	-	-	-	-	-	-	-	-	-
Ho	-	-	-	-	-	-	-	-	-	-	-	-
Er	-	-	-	-	-	-	-	-	-	-	-	-
Tm	-	-	-	-	-	-	-	-	-	-	-	-
Yb	-	-	-	-	-	-	-	-	-	-	-	-
Lu	-	-	-	-	-	-	-	-	-	-	-	-

Table E1 1. (Continued) Compilation of Meguma Zone granitoid lithogeochemistry

Sample	A12-1008	A12-1010	A12-1010-2	A12-1010-4	A12-1015	A12-1016	A12-1016-1	A12-1016-4	A12-1016-5	A12-1016-6	A12-1019	A12-1019-2
Batholith	SMB	SMB	SMB	SMB	SMB	SMB	SMB	SMB	SMB	SMB	SMB	SMB
Pluton	ScLP	ScLP	-	-	LP	-	-	-	-	-	-	-
Lithology	Mzg	Mzg	Lmzg	Lmzg	Grd	Lmzg	Lmzg	Lmzg	Lmzg	Lmzg	Lmzg	Lmzg
Source	28	28	28	28	28	28	28	28	28	28	28	28
Major oxides												
SiO_2	67 11	68 04	74 36	74 92	65 55	74 66	76 05	74 82	73 59	74 57	74 23	73 60
TiO_2	0 61	0 62	0 06	0 05	0 80	0 18	0 05	0 15	0 19	0 18	0 07	0 10
Al_2O_3	15 45	15 47	14 49	14 29	15 52	13 61	13 53	13 70	13 99	13 61	14 38	14 18
Fe_2O_3	-	-	-	-	-	-	-	-	-	-	-	-
FeO	-	-	-	-	-	-	-	-	-	-	-	-
MnO	0 08	0 09	0 03	0 03	0 10	0 07	0 05	0 07	0 08	0 07	0 04	0 05
MgO	1 64	1 65	0 78	0 78	1 96	0 90	0 80	0 82	0 89	0 95	0 86	0 92
CaO	1 75	1 62	0 35	0 39	2 36	0 55	0 29	0 47	0 81	0 50	0 60	0 48
Na_2O	3 53	3 46	3 94	4 09	3 34	3 16	3 68	3 88	3 61	3 16	3 70	4 12
K_2O	4 47	4 04	4 85	4 61	3 60	4 61	4 81	4 54	4 46	4 70	5 28	5 06
P_2O_5	0 22	0 21	0 19	0 19	0 23	0 13	0 12	0 15	0 14	0 12	0 24	0 25
H_20+	-	-	-	-	-	-	-	-	-	-	-	-
H_2O-	-	-	-	-	-	-	-	-	-	-	-	-
CO_2	-	-	-	-	-	-	-	-	-	-	-	-
Cl	-	-	-	-	-	-	-	-	-	-	-	-
F	0 05	0 05	0 01	0 01	0 06	0 04	0 03	0 03	0 05	0 03	0 02	0 02
LOI	0 50	0 70	0 40	0 40	0 55	0 40	0 30	0 50	0 20	0 70	0 40	0 30
TOTAL	99 18	99 78	100 10	100 36	98 90	100 11	100 80	100 73	99 81	100 37	100 58	100 21
Fe_2O_3T	4 25	4 31	0 72	0 68	5 44	2 05	1 25	1 81	2 06	2 01	0 98	1 28
FeOT	3 82	3 88	0 65	0 61	4 89	1 84	1.12	1 63	1 85	1 81	0 88	1 15
A/CNK	1 08	1 16	1 07	1 06	1 15	1 10	1 03	1 04	1 06	1 09	1 02	0 99
Trace els												
Ba	818	614	144	82	809	269	25	218	268	273	306	292
Rb	154	164	173	157	142	248	258	235	230	220	153	152
Sr	145	134	37	22	169	40	9	39	53	39	97	111
Y	38	33	16	13	38	35	21	31	31	29	16	21
Zr	198	205	38	31	254	89	32	83	94	88	45	68
Nb	13	12	7	5	14	8	6	10	9	8	5	6
Th	13	12	1 8	1 4	14	5 9	2 4	5 2	5 9	5 9	1	1 8
Pb	-	-	30	18	-	26	-	24	31	15	30	29
Ga	19	18	16	17	20	18	16	18	17	17	13	12
Zn	65	61	24	16	82	39	27	30	34	33	21	27
Cu	-	-	-	-	5	-	-	-	-	-	-	-
Ni	-	-	-	-	-	-	-	-	-	-	-	-
V	50	53	-	-	76	10	-	6	10	8	-	-
Cr	-	-	-	-	-	-	-	-	-	-	-	-
Hf	6	6	1	1	6	2	-	2	3	3	-	-
Cs	-	-	-	-	-	-	-	-	-	-	-	-
Sc	8 3	9 2	1 8	1 6	12	4 6	3 2	4 1	4 5	4 4	1 8	3
Ta	1 5	1 6	2 1	1 8	1	1 5	1 5	1 8	1 8	1 3	0 9	0 8
Co	-	-	-	-	-	-	-	-	-	-	-	-
Li	40	51	11	8	45	77	38	52	94	65	12	13
Be	-	-	-	-	-	-	-	-	-	-	-	-
B	-	-	-	-	-	-	-	-	-	-	-	-
U	2 7	2 5	8 7	17	2 5	3 3	3 4	7 6	2 9	4 4	1 5	1 7
W	3	7	6	5	-	5	8	5	6	1	2	-
Sn	-	-	-	-	-	-	-	-	-	-	-	-
Mo	-	-	-	-	-	-	-	-	-	-	-	-
Rare-earths												
La	30	32	3	2	39	13	3	11	13	11	4	8
Ce	1	4	4	3	-	3	4	3	2	7	3	10
Pr	-	-	-	-	-	-	-	-	-	-	-	-
Nd	-	-	-	-	-	-	-	-	-	-	-	-
Sm	-	-	-	-	-	-	-	-	-	-	-	-
Eu	-	-	-	-	-	-	-	-	-	-	-	-
Gd	-	-	-	-	-	-	-	-	-	-	-	-
Tb	-	-	-	-	-	-	-	-	-	-	-	-
Dy	-	-	-	-	-	-	-	-	-	-	-	-
Ho	-	-	-	-	-	-	-	-	-	-	-	-
Er	-	-	-	-	-	-	-	-	-	-	-	-
Tm	-	-	-	-	-	-	-	-	-	-	-	-
Yb	-	-	-	-	-	-	-	-	-	-	-	-
Lu	-	-	-	-	-	-	-	-	-	-	-	-

Table E1 1 (Continued) Compilation of Meguma Zone granitoid lithogeochemistry

Sample	A12-1020-1	A12 8002-1	A12 8007	A12-8008	A12-8017	A14-0001	A14-0002	A14-0002-1	A14-0003	A14-0007	A14-0007-1	A14-0008
Batholith	SMB	SMB	SMB	SMB	SMB	SMB	SMB	SMB	SMB	SMB	SMB	SMB
Pluton	ScLP	ScLP	LP	ScLP	ScLP	CLP	CLP	CLP	CLP	WDP	WDP	CLP
Lithology	Mzg	Mzg	Grd	Mzg	Mzg	Mzg	Mzg	Mzg	Mzg	Mzg	Mzg	Mzg
Source	28	28	28	28	28	28	28	28	28	28	28	28
Major oxides												
SiO_2	67 03	65 79	65 04	66 85	69 23	69 74	68 97	69 28	69 44	70 32	71 55	69 58
TiO_2	0 65	0 82	0 80	0 73	0 60	0 45	0 51	0 51	0 58	0 34	0 35	0 50
Al_2O_3	15 68	15 43	15 58	15 42	14 76	14 79	15 31	14 95	14 71	15 59	14 89	14 83
Fe_2O_3	-	-	-	-	-	-	-	-	-	-	-	-
FeO	-	-	-	-	-	-	-	-	-	-	-	-
MnO	0 08	0 10	0 12	0 09	0 08	0 09	0 09	0 09	0 09	0 05	0 04	0 10
MgO	1 64	1 97	1 95	1 73	1 62	1 39	1 51	1 33	1 68	1 28	1 27	1 36
CaO	2.23	2 27	2 41	2 00	1 47	1 35	1 66	1 59	1 72	0 88	0 79	1 46
Na_2O	3 66	3 60	3 55	3 48	2 94	3 38	2.57	3 24	2 65	3 09	2 89	3 52
K_2O	4 04	3 70	3 51	3 90	4 05	4 15	4 02	4 20	3 98	5 49	5 10	4 05
P_2O_5	0 20	0 23	0 24	0 23	0 18	0 18	0 20	0 20	0 19	0 21	0 20	0 18
H_2O+	-	-	-	-	-	-	-	-	-	-	-	-
H_2O-	-	-	-	-	-	-	-	-	-	-	-	-
CO_2	-	-	-	-	-	-	-	-	-	-	-	-
Cl	-	-	-	-	-	-	-	-	-	-	-	-
F	0 06	0 07	0 07	0 06	0 05	0 07	0 06	0 06	0 07	0 04	0 06	0 06
LOI	0 60	0 40	0 40	0 40	0 80	0 70	0 60	0 40	0 10	0 70	0 70	0 40
TOTAL	99 65	99 48	98 85	99 19	99 45	99 55	99 04	99 41	99 16	100 08	99 98	99 64
Fe_2O_3T	4 27	5 75	5 84	4 85	4 13	3 70	4 00	4 02	4 47	2 37	2 44	4 07
FeOT	3 84	5 17	5 25	4 36	3 72	3 33	3 60	3 62	4 02	2 13	2 20	3 66
A/CNK	1 08	1 11	1 13	1 13	1 18	1 13	1 26	1 13	1 20	1 10	1 14	1 12
Trace els												
Ba	980	830	737	819	591	487	565	606	604	497	467	595
Rb	132	144	143	137	162	187	172	169	173	258	245	175
Sr	176	163	175	159	126	119	123	127	134	94	87	127
Y	31	38	43	39	33	42	38	42	39	23	20	37
Zr	218	258	283	230	192	173	196	202	211	132	143	194
Nb	13	14	16	13	13	12	11	13	15	14	14	14
Th	12	14	14	13	12	13	13	14	12	19	23 2	12
Pb	-	-	-	22	37	12	12	16	23	23	34	16
Ga	18	19	21	21	20	16	16	17	18	21	19	16
Zn	62	85	84	71	59	56	61	66	61	59	60	54
Cu	-	-	-	-	-	-	-	-	-	-	-	-
Ni	-	-	-	-	-	-	-	-	-	-	-	-
V	55	80	60	61	50	30	33	33	39	17	15	30
Cr	-	-	-	-	-	-	-	-	-	-	-	-
Hf	6	7	7	7	5	7	8	9	8	5	6	7
Cs	-	-	-	-	-	-	-	-	-	-	-	-
Sc	10	14	14	10	9 2	7 5	9 1	10	9 3	4	4 3	9
Ta	1 1	1 6	1 3	1 3	1 4	1 5	1 2	1 2	1 1	1 3	1 4	1 2
Co	-	-	-	-	-	-	-	-	-	-	-	-
Li	37	66	60	38	50	59	59	53	62	70	65	58
Be	-	-	-	-	-	-	-	-	-	-	-	-
B	-	-	-	-	-	1	2	1	3	1	2	1
U	3 2	4 1	3 4	2.2	2.8	3 8	3 5	3 2	3 3	4 2	4 5	3 7
W	3	-	-	-	1	13	7	2	11	4	3	10
Sn	-	-	-	-	-	-	-	-	-	-	-	-
Mo	-	-	-	-	-	-	-	-	-	-	-	-
Rare-earths												
La	34	44	42	34	29	31	35	38	34	34	40	34
Ce	-	-	-	-	-	-	3	1	1	-	2	3
Pr	-	-	-	-	-	-	-	-	-	-	-	-
Nd	-	-	-	-	-	-	-	-	-	-	-	-
Sm	-	-	-	-	-	-	-	-	-	-	-	-
Eu	-	-	-	-	-	-	-	-	-	-	-	-
Gd	-	-	-	-	-	-	-	-	-	-	-	-
Tb	-	-	-	-	-	-	-	-	-	-	-	-
Dy	-	-	-	-	-	-	-	-	-	-	-	-
Ho	-	-	-	-	-	-	-	-	-	-	-	-
Er	-	-	-	-	-	-	-	-	-	-	-	-
Tm	-	-	-	-	-	-	-	-	-	-	-	-
Yb	-	-	-	-	-	-	-	-	-	-	-	-
Lu	-	-	-	-	-	-	-	-	-	-	-	-

Table E1.1 (Concluded) Compilation of Meguma Zone granitoid lithogeochemistry

Sample	A14-1018	A14-1018-1	A14-1019	A14-1020	A14-1020-1	A14-1021	A14-1030	A14-1032
Batholith	SMB	SMB	SMB	SMB	SMB	SMB	SMB	SMB
Pluton	MRP	MRP	MRP	BuBP	BuBP	ScLP	CLP	ScLP
Lithology	Lmzg	Lmzg	Lmzg	Lmzg	Lmzg	Mzg	Mzg	Mzg
Source	28	28	28	28	28	28	28	28
Major oxides								
SiO_2	72.11	71.62	72.12	73 04	72.83	71 13	70 22	69 24
TiO_2	0 23	0 27	0.33	0 24	0 26	0.40	0 43	0 62
Al_2O_3	14.99	15.50	14.76	14 27	14.52	14 65	14.66	14.56
Fe_2O_3	-	-	-	-	-	-	-	-
FeO	-	-	-	-	-	-	-	-
MnO	0 04	0 04	0.05	0 04	0 05	0 06	0 08	0.06
MgO	1.02	1.12	1.12	1.08	1.37	1.38	1 21	1 67
CaO	0 63	0.68	0 68	0 60	0 80	1 30	1 50	1 71
Na_2O	3 29	2.98	3.17	3 35	3.14	2 62	3 48	2.77
K_2O	5 23	5.56	4 86	5 04	4 89	4 74	4 27	3 69
P_2O_5	0 20	0 21	0 22	0.19	0.15	0 15	0 18	0 24
H_2O+	-	-	-	-	-	-	-	-
H_2O-	-	-	-	-	-	-	-	-
CO_2	-	-	-	-	-	-	-	-
Cl	-	-	-	-	-	-	-	-
F	0.05	0.05	0.07	0 04	0 06	0 04	0 06	0 03
LOI	0 60	0.50	0 60	0 50	0 60	0 50	0 20	0 30
TOTAL	100 02	100 21	99 91	99 92	100 45	99 67	99 42	98 79
Fe_2O_3T	1.87	1.92	2.22	1.75	2.04	3 04	3 55	4 37
FeOT	1 68	1.73	2.00	1 57	1.84	2 74	3 19	3 93
A/CNK	1 10	1 12	1 14	1 06	1 10	1 14	1 08	1 22
Trace els								
Ba	368	445	361	400	351	526	519	561
Rb	279	262	262	230	204	162	182	163
Sr	74	88	75	82	78	117	112	128
Y	22	23	24	23	24	33	41	38
Zr	99	114	138	107	103	137	186	190
Nb	14	12	15	12	10	10	11	16
Th	14	16	19	15	11	11	12	14
Pb	37	17	25	21	25	14	-	12
Ga	19	18	19	15	17	14	19	18
Zn	55	53	56	42	43	46	56	70
Cu	-	-	-	-	-	-	-	-
Ni	-	-	-	-	-	-	-	-
V	8	12	12	12	18	29	29	50
Cr	-	-	-	-	-	-	-	-
Hf	4	4	4	4	4	5	6	8
Cs	-	-	-	-	-	-	-	-
Sc	3	3 5	3 8	2.9	3.8	6 6	7.2	9.4
Ta	1.9	1.2	1.7	1.4	1.2	1	1	1.4
Co	-	-	-	-	-	-	-	-
Li	83	57	93	74	84	52	62	58
Be	-	-	-	-	-	-	-	-
B	1	2	1	1	1	1	-	1
U	4.1	4 3	7	6 3	4.3	3 2	3 5	4 5
W	2	9	11	5	2	9	5	6
Sn	-	-	-	-	-	-	-	-
Mo	-	-	-	-	-	-	-	-
Rare-earths								
La	24	27	31	26	22	26	31	35
Ce	-	-	-	-	-	-	1	1
Pr	-	-	-	-	-	-	-	-
Nd	-	-	-	-	-	-	-	-
Sm	-	-	-	-	-	-	-	-
Eu	-	-	-	-	-	-	-	-
Gd	-	-	-	-	-	-	-	-
Tb	-	-	-	-	-	-	-	-
Dy	-	-	-	-	-	-	-	-
Ho	-	-	-	-	-	-	-	-
Er	-	-	-	-	-	-	-	-
Tm	-	-	-	-	-	-	-	-
Yb	-	-	-	-	-		-	-
Lu	-	-	-	-	-	-	-	-

E-2. The Treatment of Geochemical and Statistical Data

The discriminant function analysis of Richard (1988) used three multivariate models to successfully assign analyses for MZ granitoid rocks into either southern or northern pluton compositional populations: (1) SiO_2-TiO_2-Al_2O_3-FeOT-MgO-CaO-Na_2O-K_2O-P_2O_5-Ba- Rb-Sr; (2) SiO_2-TiO_2-CaO-K_2O-Ba-Rb-Zr-Zn-Th; and (3) SiO_2-TiO_2-CaO-K_2O-Ba-Rb-Sr-Zr-Zn- Th-Pb. All of the models correctly classified 91-96% of a control group containing unknowns extracted from the database, and the eight most statistically significant elements (those having the highest individual discriminant functions) were CaO, FeOT, TiO_2, Rb, Ba, Sr, K_2O, and Pb (Richard, 1988). This study graphically compares the characteristics of the southern and northern plutons with those of the Birchtown hybrid tonalites for all of these statistically discriminant elements, which provide the most complete separation of the northern and southern pluton fields in bivariate plots shown by Figures 5.4 and 5.5 of Chapter 5. Inclusion of new analyses for the CP, LC, PMP, SMB, and SP in this thesis increases the number of geochemical variables available for study (Chapter 5; Section 3.1), of which Al_2O_3, Cr, V, Ga, and Y also provide some graphical separation of the northern and southern plutons. The updated geochemical database does not, however, significantly improve the sample to variable ratio limitation for all of the elements used by Richard and Clarke (1989), and so new discriminant models were not attempted.

Consideration of only the strongest statistical discriminators from Richard's (1988) original study minimizes potential changes to the discriminant function values in the updated database, and use of the term "discriminator" in Chapter 5 refers to "separator of the southern and northern plutons", without implying statistical support for the newly discovered elements. Graphical data are presented as fields that correspond to trends and contain the highest density of data points; less than 10 outlying data points were excluded from the field boundaries to improve graphical separation of the fields. Figure E2.1a and Figure E2.1b show plots of FeOT-CaO for the peripheral plutons and the central intrusions (respectively) that include both the original data points and the estimated field boundaries. Even if the outlying data are included, Figure E2.1c shows that separate least squares linear regressions for the peripheral and central data resemble the qualitative trends estimated from the fields in Figure 5.10 of Chapter 5. Greater variance and a lower correlation coefficient for the peripheral pluton regression results from wider scatter and the much smaller amount of data compared to the central intrusion population. Given that the regression for the peripheral pluton data is colinear with fields for the Birchtown hybrids and Late Devonian mafic intrusions, mafic-granitoid magma mixing in the peripheral plutons can plausibly explain both statistical and graphical geochemical differences among analyses for MZ granitoid rocks.

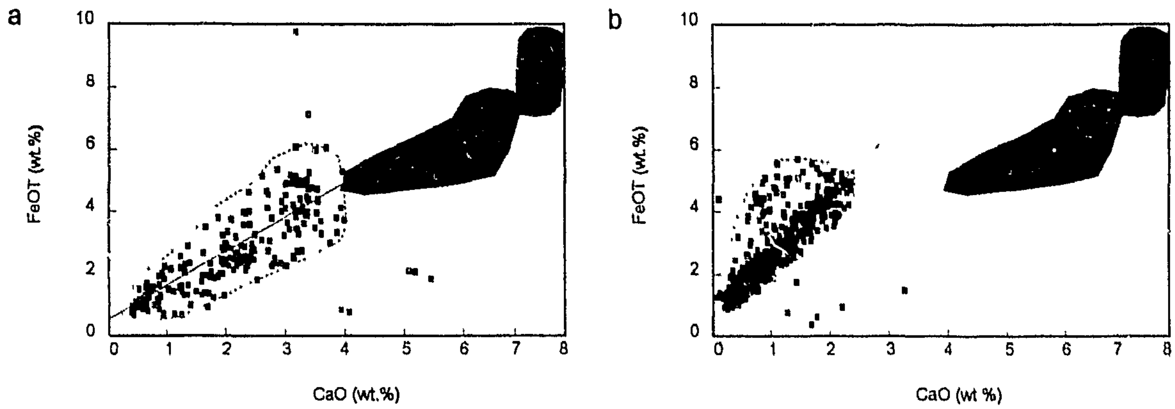

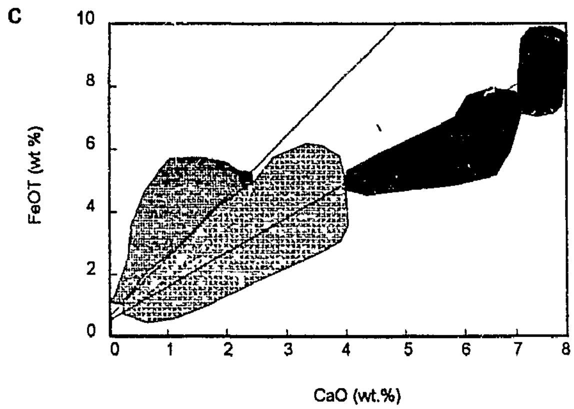

Statistics Peripheral plutons (n = 229):
$r = 0.422 \pm 0.06$
$\Sigma residuals^2 = 70.2 \pm 1.2$
Confidence = 35%
Slope = 1.23

Central intrusions (n = 604):
$r = 0.849 \pm 0.05$
$\Sigma residuals^2 = 64.1 \pm 0.3$
Confidence = 35%
Slope = 2.11

Figure E2.1. Comparative plots of individual data points and field boundaries for the peripheral plutons (shaded in light grey) and the central intrusions (shaded in medium grey). (a) Plot of FeOT-CaO for the peripheral plutons comparing the data points and the estimated field boundaries; (b) Plot of FeOT-CaO for the central intrusions comparing the data points and the estimated field boundaries; (c) comparison of the regressions for the peripheral plutons and the central intrusions. See also the estimated regressions in Figure 5.10 of Chapter 5. Least squares regressions include outlying data points but not data for the Birchtown hybrids (shaded in dark grey) or the Late Devonian mafic intrusions (shaded in black). Data for the mafic intrusions comes from Appendix B-3, and Appendix C-2 contains the hybrid geochemical data.

Appendix F

THEORETICAL HEAT FLOW MODELLING PROCEDURES AND PROGRAMMING FOR CHAPTER 6

F-1. Variables Used by the Models

The one-dimensional thermal model of Huppert and Sparks (1988a, c) relies on the following computed and user-defined variables, which are listed alphabetically. See Appendix F-4 for suggested values and the appropriate units.

Computed

a	thickness of the granitoid melt layer
H	heat required to raise the crust from $T_c(0)$ to T_m
J_b	heat flux out of the basalt
J_g	heat flux into the granite
Ra_b	Rayleigh number of the basalt
Ra_g	Rayleigh number of the granite
x_b	crystal content of the basalt
x_g	crystal content of the granite

Defined

α_b	coefficient of thermal expansion of basalt
α_g	coefficient of thermal expansion of granite
c_b	specific heat capacity of the basalt
c_g	specific heat capacity of the granite
D	thickness of the basalt sill
κ_b	thermal diffusivity of basalt
κ_g	thermal diffusivity of granite
L_c	Latent heat of fusion of solid crust
L_b	Latent heat of crystallization of basalt
L_g	Latent heat of crystallization of granite
ρ_c	density of solid crust
ρ_b	density of basalt magma
ρ_g	density of granite melt
$T_c(0)$	initial regional temperature of the crust
T_c	ambient temperature of the crust
T_m	melting temperature of the crust
T_b	ambient temperature of the basalt
T_g	ambient temperature of the granite

ν_b	kinematic viscosity of the basalt
ν_g	kinematic viscosity of the granite

F-2. Program Listing

The program HTFLOW31.EXE was written entirely by the author and compiled under Borland® Turbo Pascal for Windows™ version 1.5. It runs only under Microsoft® Windows™ 3.1 or higher in either Standard or 386 Enhanced modes. A complete listing of the program appears below; the source code also appears in electronic form on the floppy disk (back pocket), along with a compiled copy of the program.

```
PROGRAM Heatflow;
{------------------------------------------------------------------------------}
{ HTFLOW31.PAS - a program to simulate the dynamic thermal effects of repeated }
{ intrusions of mafic magma into the crust over short periods of geological time. }
{ Based upon the equations of H.E. Huppert and R.S.J Sparks, J. Fluid Mechan.,  }
{ 188: 107-131, and H.E. Huppert and R.S.J. Sparks, J. Petrol., 29: 599-624.   }
{                                                                              }
{ Written by Marcus C. Tate.  Department of Earth Sciences,  Dalhousie University,}
{ Halifax, Nova Scotia, Canada. B3H 3J5. Email: mctate@ac.dal.ca               }
{                                                                              }
{ Current version: Version 3.1. © Copyright Marcus C. Tate 1993-1994.          }
{------------------------------------------------------------------------------}

{$D © Copyright 1993 + 1994 by Marcus C. Tate}

USES HeatCRT, Strings, WinDOS, WinProcs, Wintypes;
LABEL Start, 1;
VAR {global variables}

{Input Constants (read from INCONST.DAT)}

gravaccel : integer;  {Acceleration due to gravity - cm s-2}
thermex_b,            {Ceoff. thermal exp. basalt  - K-1}
thermex_g,            {Ceoff. thermal exp. Granitoid  - K-1}
kinvel_b,            {Kinematic velocity of basalt - cm2 s-1}
kinvel_g,             {Kinematic velocity of Granitoid - cm2 s-1}
thermdiff_b,         {Thermal diffusivity of basalt - cm2 s-1}
thermdiff_g,          {Thermal diffusivity of Granitoid - cm2 s-1}
thermcond_g,         {Thermal conductivity of Granitoid magma - unspecified units}
rho_b,               {Density of basalt magma - g cm-3}
rho_c,               {Density of solid crust - g cm-3}
rho_g,               {Density of granitoid magma - g cm-3}
specheat_b,          {Specific heat of basalt - cal gm-1K-1}
specheat_c,           {Specific heat of solid crust - cal gm-1K-1}
specheat_g,          {Specific heat of granitoid magma      - cal gm-1K-1}
heatfus_b,            {Heat of fusion of basalt      - cal gm-1}
heatfus_c,           {Heat of fusion of solid crust - cal gm-1}
heatfus_g,            {Heat of fusion of granitoid magma - cal gm-1}
J : real;             { J value}

{User Specified variables}
```

```
ModelName: String[20];
Outfilename: String[8];
NoCycles,                {Number of mafic sills intruded}
PercWater : integer;  {% water in the crust - 0,2,6 %}
itemp_b,              {Initial temperature basalt magma       - oC}
irtemp_c,             {Initial regional temp solid crust - oC}
melttemp_c,           {Melting temperature of crust - oC}
Thick_b,              {Thickness of basalt sill - m}
Width_b,              {Width of basalt sill - m}
Length_b: real;        {Length of basalt sill - m}

{miscellaneous variables}

Year, Month, Day, DayOfWeek, Hour, Minute, second, sec100 : Word;

{output files}

OutDatFile,
OutSumFile : Text;

{file names}

OutDatFileName,
OutSumFileName : string[12];

{Calculated variables}

Choice, AnotherModel : char;
temp_b,               {Temperature basalt magma       - oC}
temp_g,               {Temperature of granitoid magma - oC}
temp_c,                {Temperature of solid crust - oC}
ConvTemp_g,            {Temperature at starat of granitoid convection - oC}
CoolingRate_b,         {Cooling rate of the basalt sill}
RaylConv_b,            {Rayleigh number for basalt - ??}
RaylConv_g,            {Rayleigh number for granitoid - ??}
itemp_g,              {Initial temperature of granitoid magma - oC}
InterTemp,             {Temperature of the basalt-granitoid interface - oC}
xtlcont_b,            {Crystal content of basalt}
xtlcont_g,            {Crystal content of granitoid}
FDerivXtlCont,         {First derivative of either basalt or granitoid crystal content}
kinvisc_b,             {kinematic viscosity of basalt - cm2s-1}
kinvisc_g,             {kinematic viscosity of grnanitoid - cm2s-1}
thick_g,              {Thickness of granitoid produced}
heatraisemelt,        {raise crust from T0 to Tm}
htflux_g,              {heat flux through the granitoid magma - ??}
Condflux,              {Conductive heat flux through granitoid melt layer - ??}
RateOfChangeThick_g,   {Rate of change of thickness of granitoid produced - m/yr}
Volume_g,              {volume of granitoid produced - km3}
Volume_b,              {volume of mafic magma intruded - km3}
WorkingThick_g,        {Temporary value of thickness of granitoid in each SM part - m}
RunningTotalThick,     {Existing thickness of granitoid formed by previous SM steps - m}
NewGranite,            {New thickness of granitoid generated in each SM step - m }
VolGranPerc : real;    {volume of granitoid as a % of mafic intruded - %}
ItnNumber : integer;   {number of iterations of the static model}
Melting : boolean;     {Flag to show dynamic model whether melting occurs}

{Mathematical function declarations}

FUNCTION CalcJ (thermex, grav, thermdiffus, kinveloc : real): real;

{Purpose: Calculate the "J" value for the basalt or Granitoid
 H+S Equation (2)}

VAR Temp: real;

BEGIN
  Thermdiffus := thermdiffus*thermdiffus;
  Temp := 0.1*(Exp(0.33333*ln(thermex*grav*thermdiffus/kinveloc)));
  IF Temp <= 0 THEN CalcJ := 0 ELSE CalcJ := Temp;
```

```
END; {CalcJ}

FUNCTION CondfluxNoGranConv (thermcond, int_temp, melttemp, granthick: real): real;

{Purpose: Calculate the conductive heat flux through the granitoid melt
 layer if no convection exists in the granitoid
 H+S Equation (3)}

VAR Temp: real;

BEGIN
  Temp := (thermcond*(int_temp-melttemp))/granthick;
  IF Temp <= 0 THEN CondfluxNoGranConv := 0 ELSE CondfluxNoGranConv := Temp;
END; {CondfluxNoGranConv}

FUNCTION DeltaGraniteThickNoConv (thermcond, heatraise, itemp, melttemp, thick : real):
real;

{Purpose: Calculate the change in granitoid melt thickness with time
 assuming no convection occurs in the granitoid
 H+S Equation (6)}

VAR Temp : real;

BEGIN
  Temp := (thermcond*(1/heatraise)*((itemp-melttemp)/thick));
  IF Temp <= 0 THEN DeltaGraniteThickNoConv := 0 ELSE DeltaGraniteThickNoConv := Temp;
END; {DeltaGraniteThickNoConv}

FUNCTION HeatReqMelt (pcrust, shcrust, irtcrust, mtcrust, hfcrust : real) : real;

{Purpose: Calculate heat required to heat up crust and melt it
 H+S Equation (7)}

VAR Temp : real;

BEGIN
  Temp := (pcrust*(shcrust*(mtcrust-irtcrust)+hfcrust));
  IF Temp <= 0 THEN HeatReqMelt := 0 ELSE HeatReqMelt := Temp;
END; {HeatReqMelt}

FUNCTION GraniteThickness (Hs, Pb, Cb, Tb, D, Tbi, Lb, xb : real) : real;

{Purpose: Calculate a thickness of anatectic Granitoid
 H+S Equation (9)}

VAR Temp : real;

BEGIN
  IF Hs = 0 THEN BEGIN
                   Writeln('Divide by zero encountered in module GRANITETHICKNESS');
                   Close(OutDatFile);
                   Close(OutSumFile);
                   Halt;
                 END
  ELSE
                 BEGIN
                   Temp := ((1/Hs)*(pb*cb*D*(Tbi-Tb)+Pb*Lb*D*xb));
                   IF Temp >= 0 THEN GraniteThickness := Temp ELSE GraniteThickness := 0;
                 END;
END; {GraniteThickness}

FUNCTION CoolingRateBasalt (J, thick, bastemp, heatfus, interftemp, specheat, derivxtls :
real): real;

{Purpose: Calculate the cooling rate of the basalt sill
 H+S Equation (11)}

VAR Temp : real;
```

```
BEGIN
  Temp := (Exp(1.333333*ln(bastemp-interftemp)));
  CoolingRateBasalt := -((J/thick)*temp)/(1-heatfus*(1/specheat)*derivxtls);
END {CoolingRateBasalt}

FUNCTION RayleighConvection (thermex, grav, interftemp, melttemp, thick, thermdiff,
kinvisc : real): real;

{Purpose: Calculate the Rayleigh number of the Granitoid melt layer to
 test for convection
 H+S Equation (12)}

VAR Temp1, Temp2 : real;

BEGIN
  Temp1 := thick*thick*thick;
  Temp2 := (thermex*grav*(interftemp-melttemp)*temp1)/(thermdiff*kinvisc);
  IF Temp2 <= 0 THEN RayleighConvection := 0 ELSE RayleighConvection := Temp2;
END; {RayleighConvection}

FUNCTION CondfluxGranConv (pcrust, specheat, jGran, grantemp, melttemp: real): real;

{Purpose: Calculate the conductive heat flux through the granitoid melt
 layer if convection exists in the granitoid
 H+S Equation (13)}

VAR Temp: real;

BEGIN
  Temp := pcrust*specheat*jgran*Exp(1.333333*ln(grantemp-melttemp));
  IF Temp <= 0 THEN CondfluxGranConv := 0 ELSE CondfluxGranConv := Temp;
END; {CondfluxGranConv}

FUNCTION CalcInterTemp (pcrust, shcrust, pbasalt, shbasalt, J, BasTemp, GranTemp : real):
real;

{Purpose: Calculate the temperature of the interface between the mafic and
 granitic magmas
 H+S Equations (15) and (16)}

VAR Temp1, Temp2 : real;

BEGIN
  Temp1 := Exp(0.75*ln((pcrust*shcrust*J)/(pbasalt*shbasalt*J)));
  Temp2 := (BasTemp+Temp1*GranTemp)/(1+Temp1);
  IF Temp2 <= 0 THEN CalcInterTemp := 0 ELSE CalcInterTemp := Temp2;
END; {CalcInterTemp}

FUNCTION DeltaGraniteThickConv (ConductFlux, HeatMelt : real): real;

{Purpose: Calculate the change in granitoid melt thickness with time
 assuming convection occurs in the granitoid
 H+S Equation (24)}

VAR Temp : real;

BEGIN
  Temp := ConductFlux/HeatMelt;
  IF Temp <= 0 THEN DeltaGraniteThickConv := 0 ELSE DeltaGraniteThickConv := Temp;
END; {DeltaGraniteThickConv}

FUNCTION BasaltCrystalContent (TempBas : real) : real;

{Purpose: Calculate crystal content of the basaltic magma
 H+S Equation (25)}

VAR Temp : real;
BEGIN
  Temp := (7200*(1/TempBas)-6);
  IF Temp > 1 THEN BasaltCrystalContent := 1 ELSE BasaltCrystalContent := Temp;
```

```
  IF Temp < 0 THEN BasaltCrystalContent := 0 ELSE BasaltCrystalContent := Temp;
END; {BasaltCrystalContent}

FUNCTION GraniteCrystalContent (TempGran : real; Water : integer) : real;

{Purpose: Calculate crystal content of the granitic magma
 H+S Equation (26)}

VAR Temp : real;

BEGIN
  IF Water = 0 THEN Temp := ((0.65*(1100-TempGran))/150) ELSE Temp :=
((0.65*(1000-TempGran))/150);

  IF Temp > 1 THEN GraniteCrystalContent := 1 ELSE GraniteCrystalContent := Temp;
  IF Temp < 0 THEN GraniteCrystalContent := 0 ELSE GraniteCrystalContent := Temp;
END; {GraniteCrystalContent}

FUNCTION CalcKinViscBasalt (BasaltXtls : real): real;

{Purpose: Calculate the kinematic viscosity of basalt
 H+S Equation (27)}

VAR Temp1, Temp2 : real;

BEGIN
  Temp1 := (1-(1.67*BasaltXtls));
  IF Temp1 <= 0 THEN Temp1 := 0.02;
  Temp2 := 1000*Exp(-2.5*ln(Temp1));
  IF Temp2 <= 0 THEN CalcKinViscBasalt := 0 ELSE CalcKinViscBasalt := Temp2;
END; {CalcKinViscBasalt}

FUNCTION CalcKinViscGranite (GraniteXtls, Water, TempGran : real): real;

{Purpose: Calculate the kinematic viscosity of grainite
 H+S Equation (28)}

CONST PercWater0 = 62;
      PercWater2 = 0.62;
      PercWater6 = 0.0062;

VAR Temp1, Temp2, Constant : real;

BEGIN
  IF water = 0 THEN Constant := PercWater0; {choose the appropriate constant}
  IF water = 2 THEN Constant := PercWater2; {depending on the water content}
  IF water = 6 THEN Constant := PercWater6; {of the crust}

  IF GraniteXtls >= 0.651 THEN GraniteXtls := 0.651; {prevents crash if xtls = 0.654}

  Temp1 := ((1.85*10000)/(TempGran+273));
  Temp2 := (Constant*(exp(Temp1*(ln(2.718)))*(exp(-2.5*ln(1-1.53*Granitextls)))));
  IF Temp2 <= 0 THEN CalcKinViscGranite := 0 ELSE CalcKinViscGranite := Temp2;
END; {CalcKinViscGranite}

FUNCTION FirstDerivBasXtls (Temp : real): real;

{Purpose: Calculate the first derivative of the basalt crystal content}

BEGIN
  FirstDerivBasXtls := ((-7200/(Temp*Temp))-6);
END; {FirstDerivBasXtls}

FUNCTION FirstDerivGranXtls (Temp : real): real;

{Purpose: Calculate the first derivative of the granite crystal content
 NB. This value is a constant}

BEGIN
  FirstDerivGranXtls := -4.33333333333333;
```

```
END; {FirstDerivGranXtls}

FUNCTION TotalVolume (Thick, Width, Length : real) : real;

{Purpose: Calculate cubic kilometres of Granitoid generated by model
 Assuming Granitoid only forms on top of the sill then, limits of sill size
 then limit size of granitoid melt region produced}

VAR KmVolume : real;

BEGIN

  {convert thickness of granitoid to km}

  Thick := Thick/1000;

  {Multiply thickness by length and width of the basalt sill}

  KmVolume := Thick*Width*Length;
  TotalVolume := KmVolume;

END; {TotalVolume}

FUNCTION PercGranGen (GranVol, BasVol : real) : real;
Var PercentageVol : real;
{Purpose: Calculate the total volume of Granitoid produced as a percentage
of the volume of basalt intruded}

BEGIN
  IF BasVol = 0 THEN BEGIN
                       Writeln('Divide by zero encountered in module PERCGRANGEN');
                       Close(OutDatFile);
                       Close(OutSumFile);
                       Halt;
                     END
                ELSE BEGIN
                       PercentageVol := ((GranVol/BasVol)*100);
                       PercGranGen := PercentageVol;
                     END;
END; {PercGranGen}

{Procedure declarations}

PROCEDURE SetupScrn;
CONST WaitPeriod = 3; {time to pause and show message in seconds}
VAR StartTime : word; {time to start program after above wait}

BEGIN
{Setup console window characteristics}

StrCopy(WindowTitle,'Heatflow Version 3.1');


ScreenSize.X := 65;
ScreenSize.Y := 180;

InitWinCrt;

{DOS screen setup}

Writeln('----------------------------------------------------------------');
Writeln('HTFLOW31.PAS - a program to simulate the dynamic thermal effects');
Writeln('of repeated intrusions of mafic magma into the crust over short');
Writeln('periods of geological time, based upon the equations of H.E.');
Writeln('Huppert and R.S.J Sparks, J. Fluid Mechan., 188: 107-131,'),
Writeln('and H.E. Huppert and R.S.J. Sparks, J. Petrol., 29: 599-624.');
Writeln('----------------------------------------------------------------');
Writeln;
Writeln('                   Written by Marcus C. Tate.');
Writeln('                   Department of Earth Sciences,');
```

```
Writeln('                Dalhousie University,');
Writeln('                Halifax, Nova Scotia,');
Writeln('                Canada. B3H 3J5.');
Writeln('                Email: mctate@ac.dal.ca');
Writeln;
Writeln('                Current version: Version 3.1');
Writeln('                © Copyright Marcus C. Tate 1993-1994.');
Writeln;

{Wait for user to read the nagware message}

GetTime(hour, minute, second, sec100);
StartTime := second + WaitPeriod;
REPEAT
  GetTime(hour, minute, second, sec100);
UNTIL second = StartTime;

ClrScr;    {clear the screen}

gravaccel := 0; thermex_b := 0; thermex_g := 0; kinvel_b := 0; kinvel_g := 0;
thermdiff_b := 0; thermdiff_g := 0; thermcond_g := 0; ; rho_b := 0;
rho_c := 0; rho_g := 0; specheat_b := 0; specheat_c := 0; specheat_g := 0;
heatfus_b := 0; heatfus_c := 0; heatfus_g := 0; itemp_b := 0; temp_b := 0;
irtemp_c := 0; melttemp_c := 0; itemp_g := 0; temp_g := 0; Thick_b := 0;
Width_b := 0; Length_b := 0; thick_g := 0; heatraisemelt := 0; temp_b := 0;
xtlcont_g := 0; xtlcont_b := 0; Volume_g := 0; Volume_b := 0; temp_c := 0;
VolGranPerc :=0; ItnNumber := 0; Choice := 'S'; htflux_g := 0; J := 0;
InterTemp := 0; PercWater := 0; kinvisc_b := 0; kinvisc_g := 0; CondFlux := 0;
RateOfChangeThick_g := 0; FDerivXtlCont := 0; CoolingRate_b := 0;
WorkingThick_g := 0; RunningTotalThick := 0;
NewGranite := 0; RaylConv_b := 0; RaylConv_g := 0; ConvTemp_g := 0;

  END {setupScrn};

PROCEDURE ReadConst; {read contstants from file inconst.dat}
CONST WaitPeriod = 1; {time to pause and show message in seconds}
VAR infile: text;
    tempchar : char; counter : integer;
    StartTime : word; {time to start program after above wait}

  BEGIN
    Assign(infile,'INCONST.DAT');
    {$I-}
    Reset(infile);
    {$I+}

    IF IOResult = 0 THEN {If file opened successfully}
    BEGIN

    Writeln;
    Writeln('Importing constant values from INCONST.DAT...');
    Writeln;

    {skip over the file header}

      For counter := 1 TO 3 DO
      BEGIN
        REPEAT
          read(infile,tempchar)
        UNTIL tempchar = ';';
        readln(infile);
      END; {for counter}

    {read acceleration due to gravity}

      read(infile,gravaccel);
      Write('grav accel = ');
      Write(gravaccel);
      Writeln(' cm sE-1');
      readln(infile);
```

```
{read coeff. thermal expansion of basalt}

  read(infile,thermex_b);
  Write('thermal expansion basalt = ');
  Write(thermex_b:0:5);
  Writeln(' KE-1');
  readln(infile);

{read coeff. thermal expansion of granitoid}

  read(infile,thermex_g);
  Write('thermal expansion granite = ');
  Write(thermex_g:0:5);
  Writeln(' KE-1');
  readln(infile);

{read kinematic velocity of basalt}

  read(infile,kinvel_b);
  Write('kinematic viscosity of basalt = ');
  Write(kinvel_b:0:2);
  Writeln(' cmE2 sE-1');
  readln(infile);

{read kinematic velocity of granite}

  read(infile,kinvel_g);
  Write('kinematic viscosity of granite = ');
  Write(kinvel_g:0:2);
  Writeln(' cmE2 sE-1');
  readln(infile);

{read thermal diffusivity of basalt}

  read(infile,thermdiff_b);
  Write('thermal diffusivity of basalt = ');
  Write(thermdiff_b:0:3);
  Writeln(' cmE2 sE-1');
  readln(infile);

{read thermal diffusivity of granite}

  read(infile,thermdiff_g);
  Write('thermal diffusivity of granite = ');
  Write(thermdiff_g:0:3);
  Writeln(' cmE2 sE-1');
  readln(infile);

{read thermal conductivity of granite ?}

  read(infile,thermcond_g);
  Write('thermal conductivity of granite = ');
  Writeln(thermcond_g:0:2);
  readln(infile);

{read density of basalt}

  read(infile,rho_b);
  Write('density of basalt = ');
  Write(rho_b:0:2);
  Writeln(' g cmE-3');
  readln(infile);

{read density of solid crust}

  read(infile,rho_c);
  Write('density of solid crust = ');
  Write(rho_c:0:2);
  Writeln(' g cmE-3');
```

```
    readln(infile);

  {read density of granite magma}

    read(infile,rho_g);
    Write('density of granite magma = ');
    Write(rho_g:0:2);
    Writeln(' g cmE-3');
    readln(infile);

  {read specific heat of basalt}

    read(infile,specheat_b);
    Write('specific heat of basalt = ');
    Write(specheat_b:0:2);
    Writeln(' cal gmE-1 KE-1');
    readln(infile);

  {read specific heat of solid crust}

    read(infile,specheat_c);
    Write('specific heat of solid crust = ');
    Write(specheat_c:0:2);
    Writeln(' cal gmE-1 KE-1');
    readln(infile);

  {read specific heat of granitic magma}

    read(infile,specheat_g);
    Write('specific heat of granitic magma = ');
    Write(specheat_g:0:2);
    Writeln(' cal gmE-1 KE-1');
    readln(infile);

  {read heat of fusion of basalt}

    read(infile,heatfus_b);
    Write('heat of fusion of basalt = ');
    Write(heatfus_b:0:2);
    Writeln(' cal gmE-1');
    readln(infile);

  {read heat of fusion of solid crust}

    read(infile,heatfus_c);
    Write('heat of fusion of crust = ');
    Write(heatfus_c:0:2);
    Writeln(' cal gmE-1');
    readln(infile);

  {read heat of fusion of granite}

    read(infile,heatfus_g);
    Write('heat of fusion of granitic magma = ');
    Write(heatfus_g:0:2);
    Writeln(' cal gmE-1');
    readln(infile);
  END {IF Ioresult = 0}

  ELSE

  BEGIN
    Writeln('Constant file INCONST.DAT not found. Exiting program...');
    Halt;
  END; {If Ioresult <> 0}

    Writeln;
    Close(infile);
    StartTime := 0;
    GetTime(hour, minute, second, sec100);
```

```
      StartTime := second + WaitPeriod;
      REPEAT
        GetTime(hour, minute, second, sec100);
      UNTIL second = StartTime;
      ClrScr;    {clear the screen}
  END {ReadConst};

PROCEDURE UserParamsStatic; {prompt user for necessary parameters and options}
  LABEL 1,2,3,4,5,6,7;
  CONST DatExtension = '.dat';
        SumExtension = '.Sum';

        MinITB = 1100; MaxITB = 1300;      {miniumum and maximum basalt intrusions temps}
        MinMTC = 850; MaxMTC = 1200;       {minimum and maximum crust melting temperatures}
        MinRTC = 500; MaxRTC = MinMTC;     {minimum and maximum regional crustal temps}
        MinSH = MinMTC + 50; MaxSH = 1100;{minimum and maximum temps for superheated
                                           granitoid}
        MinThB = 10; MaxThB = 20000;      {minimum and maximum thickness of basalt intruded}
        MinWB = 1; MaxWB = 400;           {minimum and maximum basalt sill widths}
        MinLB = 1; MaxLB = 400;           {minimum and maximum basalt sill widths}

  VAR TempString : String[8];
      InputString : String[10];
      Counter, ErrorCode : integer;
  BEGIN

    {prompt for model identifier}

    Write('Enter a unique name for your model (up to 20 chars): ');
    readln(ModelName);

    TempString := ModelName; {shorten string to 8 characters for file name}

    {Prevent the filename being completely empty}

    IF Ord(TempString[0]) = 0 THEN BEGIN
                                     TempString[0] := Chr(3);
                                     TempString[1] := '_';
                                     TempString[2] := '_';
                                     TempString[3] := '_';
                                   END;    {Prevent the filename being completely empty}

    {check the Model Name for characters invalid in DOS filenames}

    counter := 0; {initialize counter}

    FOR counter := 1 TO 8 DO {replace invalid characters with underbars}
    BEGIN
      CASE TempString[counter] OF

          ' ' : TempString[counter] := '_';
          '+' : TempString[counter] := '_';
          ';' : TempString[counter] := '_';
          ',' : TempString[counter] := '_';
          ':' : TempString[counter] := '_';
          '"' : TempString[counter] := '_';
          '''' : TempString[counter] := '_';
          '<' : TempString[counter] := '_';
          '>' : TempString[counter] := '_';
          '.' : TempString[counter] := '_';
          '/' : TempString[counter] := '_';
          '\' : TempString[counter] := '_';
          '|' : TempString[counter] := '_';
          '[' : TempString[counter] := '_';
          ']' : TempString[counter] := '_';
          '*' : TempString[counter] := '_';
          '=' : TempString[counter] := '_';
      END; {case}
    END; {for counter}
```

```
{Setup output file names}

OutDatFileName := TempString + DatExtension;
OutSumFileName := TempString + SumExtension;

Writeln;
Writeln('Your output data file will be called: ', OutDatFileName);
Writeln('Your output summary file will be called: ',OutSumFileName);
Writeln;
Writeln;

{prompt for user input variables}

1:Write('Initial temperature of basalt on intrusion (degrees C): ');
readln(InputString);
Writeln;
Val(InputString,itemp_b, ErrorCode);
IF ErrorCode <> 0 THEN BEGIN {check to see if the value entered is a valid number}
                        Write(InputString,' is not a number.');
                        Write(' Please enter a temperature between ');
                        Writeln(MinITB,' and ', MaxITB, ' degrees.');
                        GOTO 1;
                      END; {IF ErrorCode}

IF (itemp_b < MinITB) OR
   (itemp_b > MaxITB) THEN BEGIN
                            Write(itemp_b:0:2,' degrees C is invalid.');
                            Write(' Please enter a temperature between ');
                            Writeln(MinITB,' and ', MaxITB, ' degrees.');
                            GOTO 1;
                          END;

Writeln(itemp_b:0:2);
Writeln;

2:Write('Initial regional temperature of the crust (degrees C): ');
readln(InputString);
Writeln;
Val(InputString,irtemp_c, ErrorCode);
IF ErrorCode <> 0 THEN BEGIN
                        Write(InputString,' is not a number.');
                        Write(' Please enter a temperature between ');
                        Writeln(MinRTC,' and ', MaxRTC, ' degrees.');
                        GOTO 2;
                      END; {IF ErrorCode}

IF (irtemp_c < MinRTC) OR
   (irtemp_c > MaxRTC) THEN BEGIN
                            Write(irtemp_c:0:2,' degrees C is invalid.');
                            Write(' Please enter a temperature between ');
                            Writeln(MinRTC,' and ', MaxRTC, ' degrees.');
                            GOTO 2;
                          END;

Writeln(irtemp_c:0:2);
Writeln;

3: Write('% water in the crust (0, 2, 6 %): ');
readln(InputString);
Writeln;
Val(InputString,PercWater, ErrorCode);
IF ErrorCode <> 0 THEN BEGIN
                        Write(InputString,' is not a number.');
                        Writeln(' Please enter another water content.');
                        GOTO 3;
                      END; {IF ErrorCode}

CASE PercWater OF
  0 : BEGIN
      Writeln(PercWater);
```

```
        Writeln;
        END;
   2 : BEGIN
        Writeln(PercWater);
        Writeln;
        END;
   6 : BEGIN
        Writeln(PercWater);
        Writeln;
        END;
 ELSE BEGIN
        Write(PercWater,' % is invalid. ');
        Writeln(' Please enter either 0, 2, or 6 %.');
        GOTO 3;
      END;
END; {case}

4:Write('Melting temperature of the crust (degrees C): ');
readln(InputString);
Writeln;
Val(InputString,melttemp_c, ErrorCode);
IF ErrorCode <> 0 THEN BEGIN
                          Write(InputString,' is not a number.');
                          Write(' Please enter a temperature between ');
                          Writeln(MinMTC,' and ', MaxMTC, ' degrees.');
                          GOTO 4;
                        END; {IF ErrorCode}

IF (melttemp_c < MinMTC) OR
   (melttemp_c > MaxMTC) THEN BEGIN
                              Write(melttemp_c:0:2,' degrees C is invalid.');
                              Write(' Please enter a temperature between ');
                              Writeln(MinMTC,' and ', MaxMTC, ' degrees.');
                              GOTO 4;
                            END;

Writeln(melttemp_c:0:2);
Writeln;

5:Write('Thickness of the basalt sill intruded (m): ');
readln(InputString);
Writeln;
Val(InputString,Thick_b, ErrorCode);
IF ErrorCode <> 0 THEN BEGIN
                          Write(InputString,' is not a number.');
                          Write(' Please enter a thickness between ');
                          Writeln(MinThB,' and ', MaxThB, ' metres.');
                          GOTO 5;
                        END; {IF ErrorCode}

IF (Thick_b < MinThB) OR
   (Thick_b > MaxThB) THEN BEGIN
                              Write(Thick_b:0:2,' metres is invalid.');
                              Write(' Please enter a thickness between ');
                              Writeln(MinThB,' and ', MaxThB, ' metres.');
                              GOTO 5;
                            END;

Writeln(Thick_b:0:2);
Writeln;

6:Write('Width of the basalt sill intruded (km): ');
readln(InputString);
Writeln;
Val(InputString,Width_b, ErrorCode);
IF ErrorCode <> 0 THEN BEGIN
                          Write(InputString,' is not a number.');
                          Write(' Please enter a width between ');
                          Writeln(MinWB,' and ', MaxWB, ' kilometres.');
                          GOTO 6;
```

```
                          END; {IF ErrorCode}

IF (Width_b < MinWB) OR
   (Width_b > MaxWB) THEN BEGIN
                            Write(Width_b:0:2,' kilometres is invalid.');
                            Write(' Please enter a width between ');
                            Writeln(MinWB,' and ', MaxWB,' kilometres.');
                            GOTO 6;
                          END;

Writeln(Width_b:0:2);
Writeln;

7:Write('Length of the basalt sill intruded (> thickness, km): ');
readln(InputString);
Writeln;
Val(InputString,Length_b, ErrorCode);
IF ErrorCode <> 0 THEN BEGIN
                          Write(InputString,' is not a number.');
                          Write(' Please enter a length between ');
                          Writeln(MinLB,' and ', MaxLB, ' kilometres.');
                          GOTO 7;
                        END; {IF ErrorCode}

IF (Length_b < MinLB) OR
   (Length_b > MaxLB) THEN BEGIN
                            Write(Length_b:0:2,' kilometres is invalid.');
                            Write(' Please enter a length between ');
                            Writeln(MinLB,' and ', MaxLB, ' kilometres.');
                            GOTO 7;
                          END;

Writeln(Length_b:0:2);
Writeln;

{Open and initialize output data file}

Assign(OutDatFile, OutDatFileName); {create out file in current directory}
Rewrite(OutDatFile); {initialize the empty file}

{Determine the date and time}

GetDate(year, month, day, dayofweek);
GetTime(hour, minute, second, sec100);

Write(OutDatFile,'Output DATA from HTFLOW31.EXE');
Write(OutDatFile,'     ');
Write(OutDatFile, Day);
Write(OutDatFile,'/');
Write(OutDatFile, Month);
Write(OutDatFile,'/');
Write(OutDatFile, Year);
Write(OutDatFile,'     ');
Write(OutDatFile,hour);
Write(OutDatFile,':');
Writeln(OutDatFile,Minute);

Write(OutDatFile,'Type of Model: ');
Case Choice of
   's' : write(OutDatFile,'Static');
   'S' : write(OutDatFile,'Static');
   'd'   write(OutDatFile,'Dynamic');
   'D' : write(OutDatFile,'Dynamic');
End; {case}

Write(OutDatFile,'     ');
Write(OutDatFile,'Name of model: ');
Writeln(OutDatFile,ModelName);
Writeln(OutDatFile);
Writeln(OutDatFile,'-------------------------------------------------------');
```

```
Writeln(OutDatFile,'Initial Parameters: ');
Writeln(OutDatFile);
Write(OutDatFile,'Basalt intrusion temperature: ');
Writeln(OutDatFile,itemp_b:0:2,' degrees C');
Write(OutDatFile,'Initial regional crustal temperature: ');
Writeln(OutDatFile,irtemp_c:0:2,' degrees C');
Write(OutDatFile,'Melting temperature of the crust: ');
Writeln(OutDatFile,melttemp_c:0:2,' degrees C');
Write(OutDatFile,'Percentage of water in the crust: ');
Writeln(OutDatFile,PercWater,' %');
Write(OutDatFile,'Thickness of basalt sill intruded: ');
Writeln(OutDatFile,thick_b:0:2,' metres');
Write(OutDatFile,'Width of basalt sill intruded: ');
Writeln(OutDatFile,width_b:0:2,' km');
Write(OutDatFile,'Length of basalt sill intruded: ');
Writeln(OutDatFile,length_b:0:2,' km');
Writeln(OutDatFile,'-----------------------------------------------------------');
Writeln(OutDatFile,'Model run data: ');
Writeln(OutDatFile);

    {write headers for comma-delimeted file}

Write(OutDatFile,'Increment No.,Cycle,Basalt temp.,Granite temp.,');
Write(OutDatFile,'Crustal temp.,Hs,Basalt crystals,Basalt kinematic viscosity,');
Write(OutDatFile,'Granite crystals,Granite kinematic viscosity,');
Write(OutDatFile,'Ra # basalt,Ra # granite,New granite thickness,');
Write(OutDatFile,'Total granite thickness, Conductive flux through granitoid,');
Write(OutDatFile,'Granite dA/dt,Basalt dT/dt,');
Writeln(OutDatFile,'Granite volume,Granite vol. %');

{Open and initialize output summary file}

Assign(OutSumFile, OutSumFileName); {create out file in current directory}
Rewrite(OutSumFile); {initalize the empty file}

Write(OutSumFile,'Output SUMMARY from HTFLOW31.EXE');
Write(OutSumFile,'     ');
Write(OutSumFile, Day);
Write(OutSumFile,'/');
Write(OutSumFile, Month);
Write(OutSumFile,'/');
Write(OutSumFile, Year);
Write(OutSumFile,'     ');
Write(OutSumFile,hour);
Write(OutSumFile,':');
Writeln(OutSumFile,Minute);

Write(OutSumFile,'Type of Model: ');
Case Choice of
   's' : write(OutSumFile,'Static');
   'S' : write(OutSumFile,'Static');
   'd' : write(OutSumFile,'Dynamic');
   'D' : write(OutSumFile,'Dynamic');
End; {case}

Write(OutSumFile,'     ');
Write(OutSumFile,'Name of model: ');
Writeln(OutSumFile,ModelName);
Writeln(OutSumFile);
Writeln(OutSumFile,'-----------------------------------------------------------');
Writeln(OutSumFile,'Initial Parameters: ');
Writeln(OutSumFile);
Write(OutSumFile,'Basalt intrusion temperature: ');
Writeln(OutSumFile,itemp_b:0:2,' degrees C'),
Write(OutSumFile,'Initial regional crustal temperature: ');
Writeln(OutSumFile,irtemp_c:0:2,' degrees C');
Write(OutSumFile,'Melting temperature of the crust: ');
Writeln(OutSumFile,melttemp_c:0:2,' degrees C');
Write(OutSumFile,'Percentage of water in the crust: ');
Writeln(OutSumFile,PercWater,' %');
```

```
    Write(OutSumFile,'Thickness of basalt sill intruded: ');
    Writeln(OutSumFile,thick_b:0:2,' metres');
    Write(OutSumFile,'Width of basalt sill intruded: ');
    Writeln(OutSumFile,width_b:0:2,' km');
    Write(OutSumFile,'Length of basalt sill intruded: ');
    Writeln(OutSumFile,length_b:0:2,' km');
    Writeln(OutSumFile,'---------------------------------------------------------');
    Writeln(OutSumFile,'Model run data: ');
    Writeln(OutSumFile);

 END; {UserParamsStatic}

PROCEDURE UserParamsDynamic; {prompt user for necessary parameters and options}
  LABEL 1,2,3,4,5,6,7,8;
  CONST DatExtension = '.dat';
        SumExtension = '.sum';

        MinITB = 1100; MaxITB = 1300;      {miniumum and maximum basalt intrusions temps}
        MinMTC = 850; MaxMTC = 1200;       {minimum and maximum crust melting temperatures}
        MinRTC = 500; MaxRTC = MinMTC;     {minimum and maximum regional crustal temps}
        MinSH = MinMTC + 50; MaxSH = 1100;{minimum and maximum temps for superheated
                                           granitoid}
        MinThB = 10; MaxThB = 20000;    {minimum and maximum thickness of basalt intruded}
        MinWB = 1; MaxWB = 400;         {minimum and maximum basalt sill widths}
        MinLB = 1; MaxLB = 400;         {minimum and maximum basalt sill widths}

VAR TempString : String[8];
    InputString : String[10];
    counter, ErrorCode : integer;

  BEGIN

    {prompt for model identifier}

    Write('Enter a unique name for your model (up to 20 chars): ');
    readln(ModelName);

    TempString := ModelName; {shorten string to 8 characters for file name}

    {Prevent the filename being completely empty}

    IF Ord(TempString[0]) = 0 THEN BEGIN
                                     TempString[0] := Chr(3);
                                     TempString[1] := '_';
                                     TempString[2] := '_';
                                     TempString[3] := '_';
                                    END;    {Prevent the filename being completely empty}

    {check the Model Name for characters invalid in DOS filenames}

    counter := 0; {initialize counter}

    FOR counter := 1 TO 8 DO {replace invalid characters with underbars}
    BEGIN
      CASE TempString[counter] OF

         ' ' : TempString[counter] := '_';
         '+' : TempString[counter] := '_';
         ';' : TempString[counter] := '_';
         ',' : TempString[counter] := '_';
         ':' : TempString[counter] := '_';
         '"' : TempString[counter] := '_';
         '''' : TempString[counter] := '_';
         '<' : TempString[counter] := '_';
         '>' : TempString[counter] := '_';
         '.' : TempString[counter] := '_';
         '/' : TempString[counter] := '_';
         '\' : TempString[counter] := '_';
         '|' : TempString[counter] := '_';
         '[' : TempString[counter] := '_';
```

```
      ']' : TempString[counter] := '_';
      '*' : TempString[counter] := '_';
      '=' : TempString[counter] := '_';
    END; {case}
  END; {for counter}

  {Setup output file names}

  OutDatFileName := TempString + DatExtension;
  OutSumFileName := TempString + SumExtension;


  Writeln;
  Writeln('Your output data file will be called: ', OutDatFileName);
  Writeln('Your output summary file will be called: ',OutSumFileName);
  Writeln;
  Writeln;

  {prompt user for number of cycles ( =no. of mafic intrusions)}

  1:Write('How many mafic intrusions for the dynamic model (integer) ?: ');
  readln(InputString);
  Writeln;
  Val(InputString,NoCycles, ErrorCode);
  IF ErrorCode <> 0 THEN BEGIN {check to see if the value entered is a valid number}
                          Write(InputString,' is not a number.');
                          Writeln(' Please re-enter the number of intrusions.');
                         GOTO 1;
                        END; {IF ErrorCode}
  IF (ErrorCode = 0) AND (NoCycles <=1) THEN BEGIN
                                             Write(NoCycles,' is not valid.');
                                             Writeln('Please re-enter an integer
                                                     greater than 1');
                                             GOTO 1;
                                           END; {IF ErrorCode}
  Writeln(NoCycles);
  Writeln;

  {prompt for user input variables}

  2:Write('Initial temperature of basalt on intrusion (degrees C): ');
  readln(InputString);
  Writeln;
  Val(InputString,itemp_b, ErrorCode);
  IF ErrorCode <> 0 THEN BEGIN
                          Write(InputString,' is not a number.');
                          Write(' Please enter a temperature between ');
                          Writeln(MinITB,' and ', MaxITB, ' degrees.');
                          GOTO 2;
                        END; {IF ErrorCode}

  IF (itemp_b < MinITB) OR
     (itemp_b > MaxITB) THEN BEGIN
                              Write(itemp_b:0:2,' degrees C is invalid.');
                              Write(' Please enter a temperature between ');
                              Writeln(MinITB,' and ', MaxITB, ' degrees.');
                              GOTO 2;
                            END;

  Writeln(itemp_b:0:2);
  Writeln;

  3:Write('Initial regional temperature of the crust (degrees C): ');
  readln(InputString);
  Writeln;
  Val(InputString,irtemp_c, ErrorCode);
  IF ErrorCode <> 0 THEN BEGIN
                          Write(InputString,' is not a number.');
                          Write(' Please enter a temperature between ');
                          Writeln(MinRTC,' and ', MaxRTC, ' degrees.');
```

```
                        GOTO 3;
                      END; {IF ErrorCode}

IF (irtemp_c < MinRTC) OR
   (irtemp_c > MaxRTC) THEN BEGIN
                          Write(irtemp_c:0:2,' degrees C is invalid.');
                          Write(' Please enter a temperature between ');
                          Writeln(MinRTC,' and ', MaxRTC, ' degrees.');
                          GOTO 3;
                        END;

Writeln(irtemp_c:0:2);
Writeln;

4: Write('% water in the crust (0, 2, 6 %): ');
readln(InputString);
Writeln;
Val(InputString,PercWater, ErrorCode);
IF ErrorCode <> 0 THEN BEGIN
                        Write(InputString,' is not a number.');
                        Writeln(' Please enter another water content.');
                        GOTO 4;
                      END; {IF ErrorCode}

CASE PercWater OF
  0 : BEGIN
       Writeln(PercWater);
       Writeln;
       END;
  2 : BEGIN
       Writeln(PercWater);
       Writeln;
       END;
  6 : BEGIN
       Writeln(PercWater);
       Writeln;
       END;
 ELSE BEGIN
       Write(PercWater,' % is invalid. ');
       Writeln(' Please enter either 0, 2, or 6 %.');
       GOTO 4;
     END;
END; {case}

5:Write('Melting temperature of the crust (degrees C): ');
readln(InputString);
Writeln;
Val(InputString,melttemp_c, ErrorCode);
IF ErrorCode <> 0 THEN BEGIN
                        Write(InputString,' is not a number.');
                        Write(' Please enter a temperature between ');
                        Writeln(MinMTC,' and ', MaxMTC, ' degrees.');
                        GOTO 5;
                      END; {IF ErrorCode}

IF (melttemp_c < MinMTC) OR
   (melttemp_c > MaxMTC) THEN BEGIN
                          Write(melttemp_c:0:2,' degrees C is invalid.');
                          Write(' Please enter a temperature between ');
                          Writeln(MinMTC,' and ', MaxMTC, ' degrees.');
                          GOTO 5;
                        END;

Writeln(melttemp_c:0:2);
Writeln;

6:Write('Thickness of the basalt sills intruded (m): ');
readln(InputString);
Writeln;
Val(InputString,Thick_b, ErrorCode);
```

```
IF ErrorCode <> 0 THEN BEGIN
                            Write(InputString,' is not a number.');
                            Write(' Please enter a thickness between ');
                            Writeln(MinThB,' and ', MaxThB, ' metres.');
                            GOTO 6;
                          END; {IF ErrorCode}

IF (Thick_b < MinThB) OR
   (Thick_b > MaxThB) THEN BEGIN
                                 Write(Thick_b:0:2,' metres is invalid.');
                                 Write(' Please enter a thickness between ');
                                 Writeln(MinThB,' and ', MaxThB, ' metres.');
                                 GOTO 6;
                               END;

Writeln(Thick_b:0:2);
Writeln;

7:Write('Width of the basalt sills intruded (km): ');
readln(InputString);
Writeln;
Val(InputString,Width_b, ErrorCode);
IF ErrorCode <> 0 THEN BEGIN
                            Write(InputString,' is not a number.');
                            Write(' Please enter a width between ');
                            Writeln(MinWB,' and ', MaxWB, ' kilometres.');
                            GOTO 7;
                          END; {IF ErrorCode}

IF (Width_b < MinWB) OR
   (Width_b > MaxWB) THEN BEGIN
                                 Write(Width_b:0:2,' kilometres is invalid.');
                                 Write(' Please enter a width between ');
                                 Writeln(MinWB,' and ', MaxWB,' kilometres.');
                                 GOTO 7;
                               END;

Writeln(Width_b:0:2);
Writeln;

8:Write('Length of the basalt sills intruded (> thickness, km): ');
readln(InputString);
Writeln;
Val(InputString,Length_b, ErrorCode);
IF ErrorCode <> 0 THEN BEGIN
                            Write(InputString,' is not a number.');
                            Write(' Please enter a length between ');
                            Writeln(MinLB,' and ', MaxLB, ' kilometres.');
                            GOTO 8;
                          END; {IF ErrorCode}

IF (Length_b < MinLB) OR
   (Length_b > MaxLB) THEN BEGIN
                                 Write(Length_b:0:2,' kilometres is invalid.');
                                 Write(' Please enter a length between ');
                                 Writeln(MinLB,' and ', MaxLB, ' kilometres.');
                                 GOTO 8;
                               END;

Writeln(Length_b:0:2);
Writeln;

{Open and initialize output data file}

Assign(OutDatFile, OutDatFileName); {create out file in current directory}
Rewrite(OutDatFile); {initialize the empty file}

{Determine the date and time}

GetDate(year, month, day, dayofweek);
```

```
GetTime(hour, minute, second, sec100);

Write(OutDatFile,'Output DATA from HTFLOW31.EXE');
Write(OutDatFile,'     ');
Write(OutDatFile, Day);
Write(OutDatFile,'/');
Write(OutDatFile, Month);
Write(OutDatFile,'/');
Write(OutDatFile, Year);
Write(OutDatFile,'     ');
Write(OutDatFile,hour);
Write(OutDatFile,':');
Writeln(OutDatFile,Minute);

Write(OutDatFile,'Type of Model: ');
Case Choice of
   's' : write(OutDatFile,'Static');
   'S' : write(OutDatFile,'Static');
   'd' : write(OutDatFile,'Dynamic');
   'D' : write(OutDatFile,'Dynamic');
End; {case}

Write(OutDatFile,'     ');
Write(OutDatFile,'Name of model: ');
Writeln(OutDatFile,ModelName);
Writeln(OutDatFile);
Writeln(OutDatFile,'----------------------------------------------------------');
Writeln(OutDatFile,'Initial Parameters: ');
Writeln(OutDatFile);
Write(OutDatFile,'Basalt intrusion temperature: ');
Writeln(OutDatFile,itemp_b:0:2,' degrees C');
Write(OutDatFile,'Initial regional crustal temperature: ');
Writeln(OutDatFile,irtemp_c:0:2,' degrees C');
Write(OutDatFile,'Melting temperature of the crust: ');
Writeln(OutDatFile,melttemp_c:0:2,' degrees C');
Write(OutDatFile,'Percentage of water in the crust: ');
Writeln(OutDatFile,PercWater,' %');
Write(OutDatFile,'Thickness of basalt sills intruded: ');
Writeln(OutDatFile,thick_b:0:2,' metres');
Write(OutDatFile,'Width of basalt sils intruded: ');
Writeln(OutDatFile,width_b:0:2,' km');
Write(OutDatFile,'Length of basalt sills intruded: ');
Writeln(OutDatFile,length_b:0:2,' km');
Writeln(OutDatFile,'----------------------------------------------------------');
Writeln(OutDatFile,'Model run data: ');
Writeln(OutDatFile);

    {write headers for comma-delimeted file}

Write(OutDatFile,'Increment No.,Cycle,Basalt temp.,Granite temp.,');
Write(OutDatFile,'Crustal temp.,Hs,Basalt crystals,Basalt kinematic viscosity,');
Write(OutDatFile,'Granite crystals,Granite kinematic viscosity,');
Write(OutDatFile,'Ra # basalt,Ra # granite,New granite thickness,');
Write(OutDatFile,'Total granite thickness, Conductive flux through granitoid,');
Write(OutDatFile,'Granite dA/dt,Basalt dT/dt,');
Writeln(OutDatFile,'Granite volume,Granite vol. %');

    {Open and initialize output summary file}

Assign(OutSumFile, OutSumFileName); {create out file in current directory}
Rewrite(OutSumFile); {initalize the empty file}

Write(OutSumFile,'Output SUMMARY from HTFLOW31.EXE');
Write(OutSumFile,'     ');
Write(OutSumFile, Day);
Write(OutSumFile,'/');
Write(OutSumFile, Month);
Write(OutSumFile,'/');
Write(OutSumFile, Year);
Write(OutSumFile,'     ');
```

```
    Write(OutSumFile,hour);
    Write(OutSumFile,':');
    Writeln(OutSumFile,Minute);

    Write(OutSumFile,'Type of Model: ');
    CASE Choice OF
       's' : write(OutSumFile,'Static');
       'S' : write(OutSumFile,'Static');
       'd' : write(OutSumFile,'Dynamic');
       'D' : write(OutSumFile,'Dynamic');
    END; {case}

    Write(OutSumFile,'     ');
    Write(OutSumFile,'Name of model: ');
    Writeln(OutSumFile,ModelName);
    Writeln(OutSumFile);
    Writeln(OutSumFile,'-------------------------------------------------------------');
    Writeln(OutSumFile,'Initial Parameters: ');
    Writeln(OutSumFile);
    Write(OutSumFile,'Basalt intrusion temperature: ');
    Writeln(OutSumFile,itemp_b:0:2,' degrees C');
    Write(OutSumFile,'Initial regional crustal temperature: ');
    Writeln(OutSumFile,irtemp_c:0:2,' degrees C');
    Write(OutSumFile,'Melting temperature of the crust: ');
    Writeln(OutSumFile,melttemp_c:0:2,' degrees C');
    Write(OutSumFile,'Percentage of water in the crust: ');
    Writeln(OutSumFile,PercWater,' %');
    Write(OutSumFile,'Thickness of basalt sills intruded: ');
    Writeln(OutSumFile,thick_b:0:2,' metres');
    Write(OutSumFile,'Width of basalt sills intruded: ');
    Writeln(OutSumFile,width_b:0:2,' km');
    Write(OutSumFile,'Length of basalt sills intruded: ');
    Writeln(OutSumFile,length_b:0:2,' km');
    Writeln(OutSumFile,'-------------------------------------------------------------');
    Writeln(OutSumFile,'Model run data: ');
    Writeln(OutSumFile);

  END; {UserParamsDynamic}

PROCEDURE InitStaticModel; {initialize variables at start of run}
BEGIN

        {Setup the initial conditions}

    Temp_b := (itemp_b-2); {temperature of basalt initially just smaller than the
                            intrusion temperature}
    Itemp_g := melttemp_c; {temperature of granite formed initially same as melting
                            temperature of crust}
    Temp_g := Itemp_g;
    Temp_c := Irtemp_c; {temperature of crust initially same as regional crustal temp.}

END; {InitStaticModel}

PROCEDURE StaticModel; {calculate H+S equations for one mafic intrusion}

CONST WaitPeriod = 2;
VAR BasaltSolid, GraniteConv, Quit : Boolean;
    TempGranThick, AGranThick, ABGranThick, orightf_c : real;
    TempInt : Integer;
    StartTime : word;
  BEGIN

{-----------------------------------------------------------------------
 Begin Part A of static model - Calculate thickness of granite generated
 by the convecting mafic intrusion until either it stops convecting, or
 the granitoid melt layer starts convecting.
-----------------------------------------------------------------------}

         {Increment the number of iterations}
    Melting := False; {set dynamic flag to false}
```

```
Inc(ItnNumber);

{Calculate heat required to heat up crust and melt it}

IF (Temp_c >= melttemp_c) AND (ItnNumber = 1) THEN heatfus_c := (heatfus_c*(60/100));

HeatRaiseMelt := HeatReqMelt(rho_c, specheat_c, Temp_c, melttemp_c, heatfus_c);

     {Calculate existing volume of granite}

RunningTotalThick := Thick_g;

     {cool mafic magma slightly on intrusion to form some crystals}

xtlcont_b := BasaltCrystalContent(Temp_b);
IF xtlcont_b = 0 THEN BEGIN
                         Temp_b := Temp_b-2;
                         xtlcont_b := BasaltCrystalContent(Temp_b)
                       END;

J := CalcJ(thermex_b, gravaccel, thermdiff_b, kinvel_b);
InterTemp := CalcInterTemp(rho_c, specheat_c, rho_b, specheat_b, J, Temp_b, Temp_c);

IF InterTemp > MeltTemp_c THEN

BEGIN {Anatexis occurs}

     Melting := True; {set dynamic flag to true}

     {Initialize flags before entering loop}

     BasaltSolid := False;
     GraniteConv := False;
     Quit := False;

     {Calculate thickness of the granitoid melt layer - m}

  Thick_g := GraniteThickness(HeatRaiseMelt, rho_b, specheat_b, Temp_b, Thick_b,
                              itemp_b, heatfus_b, xtlcont_b);

     {Calculate new thickness of granitoid formed}

  IF Thick_g > RunningTotalThick THEN NewGranite := Thick_g - RunningTotalThick;

     {Calculate the new temperatures for the granitoid and the crust}

  Temp_c := Intertemp;

  InterTemp := CalcInterTemp(rho_c, specheat_c, rho_b, specheat_b, J, Temp_b, Temp_c);
  Temp_g := Intertemp;

     {Calculate volume of basalt intruded - km3}

  Volume_b := TotalVolume(Thick_b, Width_b, Length_b);

     {Calculate volume of granite generated - km3}

  Volume_g := TotalVolume(Thick_g, Width_b, Length_b);

     {Calculate volume of granite generated as a function of the
     volume of mafic magma intruded}

  VolGranPerc := PercGranGen(Volume_g, Volume_b);

     {check for convection in both the granitoid and basaltic melt layers}

          {Calculate crystal contents of granitoid and basalt}

     xtlcont_g := GraniteCrystalContent(Temp_g,PercWater);
```

```
        {Calculate kinematic viscosities of granitoid and basalt}

    Kinvisc_b := CalcKinViscBasalt(xtlcont_b);
    Kinvisc_g := CalcKinViscGranite(xtlcont_g, percwater, temp_g);

  RaylConv_b := RayleighConvection(thermex_b, gravaccel, Temp_b, melttemp_c, thick_b,
                                   thermdiff_b, kinvisc_b);
  RaylConv_g := RayleighConvection(thermex_g, gravaccel, Temp_g, melttemp_c, thick_g,
                                   thermdiff_g, kinvisc_g);

        {Set flags that control loop status}

  IF xtlcont_b > 0.55 THEN BasaltSolid := True;
  IF RaylConv_g > 1000 THEN GraniteConv := True;

        {Calculate other miscellaneous parameters of interest}

  Condflux := CondfluxNoGranConv(thermcond_g,Temp_g,melttemp_c,Thick_g);
  RateOfChangeThick_g := DeltaGraniteThickNoConv(thermcond_g, HeatRaiseMelt,Temp_g,
                                                 melttemp_c, Thick_g);
    FDerivXtlCont := FirstDerivBasXtls(Temp_b);
  CoolingRate_b := CoolingRateBasalt(J,Thick_b, Temp_b, heatfus_b, Temp_c, specheat_b,
                                     FDerivXtlCont);
    FDerivXtlCont := FirstDerivGranXtls(Temp_g);

    {output results to screen}

  Writeln;
  Writeln('---------------------------------------------------------------');
  Writeln('Part A....');
  Writeln('Temperature of basalt: ', Temp_b:0:2);
  Writeln('Temperature of granite: ', Temp_g:0:2);
  Writeln('Temperature of crust: ', Temp_c:0:2);
  Writeln('Hs: ',HeatRaiseMelt:0:2);
  Writeln;
  Writeln('Crystal content of basalt: ',xtlcont_b:0:3);
  Writeln('Kinematic viscosity of basalt: ',kinvisc_b:0:3);
  Writeln('Crystal content of granite: ',xtlcont_g:0:3);
  Writeln('Kinematic viscosity of granite: ',kinvisc_g:0:3);
  Writeln('Rayleigh number of basalt: ',RaylConv_b:0:3);
  Writeln('Rayleigh number of granite: ',RaylConv_g:0:3);
  Writeln;
  Writeln('New thickness of granite: ', NewGranite:0:2);
  Writeln('Total thickness of granite: ', Thick_g:0:2);
  Writeln;
  Writeln('Conductive flux through granitoid: ',Condflux:0:3);
  Writeln('Granite dA/dt: ',RateOfChangeThick_g:0:4);
  Writeln('Basalt dT/dt: ',CoolingRate_b:0:10);
  Writeln('Total volume of granite: ', Volume_g:0:2);
  Writeln('Granite volume/Mafic volume % : ',VolGranPerc:0:2);
  Writeln('---------------------------------------------------------------');
  Writeln;

    {output raw results to output data file}

  Write(OutDatFile,ItnNumber,',');
  Write(OutDatFile,'A,');
  Write(OutDatFile,Temp_b:0:2,',');
  Write(OutDatFile,Temp_g:0:2,',');
  Write(OutDatFile,Temp_c:0:2,',');
  Write(OutDatFile, HeatRaiseMelt:0:2,',');
  Write(OutDatFile,xtlcont_b:0:3,',');
  Write(OutDatFile,kinvisc_b:0:3,',');
  Write(OutDatFile,xtlcont_g:0:3,',');
  Write(OutDatFile,kinvisc_g:0:3,',');
  Write(OutDatFile,RaylConv_b:0:3,',');
  Write(OutDatFile,RaylConv_g:0:3,',');
  Write(OutDatFile,NewGranite:0:2,',');
  Write(OutDatFile,thick_g:0:2,',');
  Write(OutDatFile,Condflux:0:3,',');
```

```
Write(OutDatFile,RateOfChangeThick_g:0:4,',');
Write(OutDatFile,CoolingRate_b:0:10,',');
Write(OutDatFile,Volume_g:0:2,',');
Writeln(OutDatFile,VolGranPerc:0:2,',');

   {output formatted results to output summary file}

Write(OutSumFile,'Increment number: ');
Writeln(OutSumFile,ItnNumber);
Writeln(OutSumFile);

Writeln(OutSumFile,'Part A');
Writeln(OutSumFile,'Basalt temperature: ',Temp_b:0:2,' degrees C');
Writeln(OutSumFile,'Granite temperature: ',Temp_g:0:2,' degrees C');
Writeln(OutSumFile,'Crustal temperature: ',Temp_c:0:2,' degrees C');
Writeln(OutSumFile,'Heat required to melt crust: ',HeatRaiseMelt:0:2);
Writeln(OutSumFile,'Basalt crystal content: ',xtlcont_b:0:3);
Writeln(OutSumFile,'Kinematic viscosity of basalt: ',kinvisc_b:0:3);
Writeln(OutSumFile,'Granite crystal content: ',xtlcont_g:0:3);
Writeln(OutSumFile,'Kinematic viscosity of granite: ',kinvisc_g:0:3);
Writeln(OutSumFile,'Rayleigh # of basalt: ',RaylConv_b:0:3);
Writeln(OutSumFile,'Rayleigh # of granite: ',RaylConv_g:0:3);
Writeln(OutSumFile,'New thickness of granite: ',NewGranite:0:2,' metres');
Writeln(OutSumFile,'Total thickness of granite: ',thick_g:0:2,' metres');
Writeln(OutSumFile,'Conductive flux through granitoid: ',Condflux:0:3);
Writeln(OutSumFile,'dA/dt Granite: ',RateOfChangeThick_g:0:4);
Writeln(OutSumFile,'dT/dt Basalt: ',CoolingRate_b:0:10);
Writeln(OutSumFile,'Volume of granite: ',Volume_g:0:2,' kmE3');
Writeln(OutSumFile,'Volume of granite %: ',VolGranPerc:0:2,' %');
Writeln(OutSumFile);

{Check on status of the loop}

IF BasaltSolid = True THEN Quit := True;
IF GraniteConv = True THEN Quit := True;

{cool the basalt progressively in 1 degree increments}

Temp_b := Temp_b - 1;

IF (BasaltSolid = False) and (GraniteConv = False) THEN
BEGIN
  REPEAT
  RunningTotalThick := Thick_g;

  Thick_g := GraniteThickness(HeatRaiseMelt, rho_b, specheat_b, Temp_b, Thick_b,
                              itemp_b, heatfus_b, xtlcont_b);
  IF Thick_g > RunningTotalThick THEN NewGranite := Thick_g - RunningTotalThick;

  InterTemp := CalcInterTemp(rho_c, specheat_c, rho_b, specheat_b, J, Temp_b,
                             irtemp_c);

  Temp_c := InterTemp;

  InterTemp := CalcInterTemp(rho_c, specheat_c, rho_b, specheat_b, J, Temp_b,
                             Temp_c);
  Temp_g := Intertemp;
  Volume_g := TotalVolume(Thick_g, Width_b, Length_b);
  VolGranPerc := PercGranGen(Volume_g, Volume_b);
  xtlcont_b := BasaltCrystalContent(Temp_b);
  xtlcont_g := GraniteCrystalContent(Temp_g, PercWater);
     Kinvisc_b := CalcKinViscBasalt(xtlcont_b);
     Kinvisc_g := CalcKinViscGranite(xtlcont_g, percwater, temp_g);
  RaylConv_b := RayleighConvection(thermex_b, gravaccel, Temp_b, melttemp_c,
                                   thick_b, thermdiff_b, kinvisc_b);
  RaylConv_g := RayleighConvection(thermex_g, gravaccel, Temp_g, melttemp_c,
                                   thick_g, thermdiff_g, kinvisc_g);

  IF xtlcont_b > 0.55 THEN BasaltSolid := True;
  IF RaylConv_g > 1000 THEN GraniteConv := True;
```

```
Condflux := CondfluxNoGranConv(thermcond_g,Temp_g,melttemp_c,Thick_g);
RateOfChangeThick_g := DeltaGraniteThickNoConv(thermcond_g, HeatRaiseMelt,Temp_g,
                                              melttemp_c, Thick_g);
  FDerivXtlCont := FirstDerivBasXtls(Temp_b);
CoolingRate_b := CoolingRateBasalt(J,Thick_b, Temp_b, heatfus_b, Temp_c,
                                   specheat_b, FDerivXtlCont);
  FDerivXtlCont := FirstDerivGranXtls(Temp_g);

   {output results to screen}

Writeln;
Writeln('-------------------------------------------------------------');
Writeln('Part A....');
Writeln('Temperature of basalt: ', Temp_b:0:2);
Writeln('Temperature of granite: ', Temp_g:0:2);
Writeln('Temperature of crust: ', Temp_c:0:2);
Writeln('Hs: ',HeatRaiseMelt:0:2);
Writeln;
Writeln('Crystal content of basalt: ',xtlcont_b:0:3);
Writeln('Kinematic viscosity of basalt: ',kinvisc_b:0:3);
Writeln('Crystal content of granite: ',xtlcont_g:0:3);
Writeln('Kinematic viscosity of granite: ',kinvisc_g:0:3);
Writeln('Rayleigh number of basalt: ',RaylConv_b:0:3);
Writeln('Rayleigh number of granite: ',RaylConv_g:0:3);
Writeln;
Writeln('New thickness of granite: ', NewGranite:0:2);
Writeln('Total thickness of granite: ', Thick_g:0:2);
Writeln;
Writeln('Conductive flux through granitoid: ',Condflux:0:3);
Writeln('Granite dA/dt: ',RateOfChangeThick_g:0:4);
Writeln('Basalt dT/dt: ',CoolingRate_b:0:10);
Writeln('Total volume of granite: ', Volume_g:0:2);
Writeln('Granite volume/Mafic volume % : ',VolGranPerc:0:2);
Writeln;
Writeln('Completion of Part A');
Writeln('The mafic sill intruded the crust and caused anatexis');
Writeln('-------------------------------------------------------------');
Writeln;

   {output raw results to output data file}

Write(OutDatFile,ItnNumber,',');
Write(OutDatFile,'A,');
Write(OutDatFile,Temp_b:0:2,',');
Write(OutDatFile,Temp_g:0:2,',');
Write(OutDatFile,Temp_c:0:2,',');
Write(OutDatFile, HeatRaiseMelt:0:2,',');
Write(OutDatFile,xtlcont_b:0:3,',');
Write(OutDatFile,kinvisc_b:0:3,',');
Write(OutDatFile,xtlcont_g:0:3,',');
Write(OutDatFile,kinvisc_g:0:3,',');
Write(OutDatFile,RaylConv_b:0:3,',');
Write(OutDatFile,RaylConv_g:0:3,',');
Write(OutDatFile,NewGranite:0:2,',');
Write(OutDatFile,thick_g:0:2,',');
Write(OutDatFile,Condflux:0:3,',');
Write(OutDatFile,RateOfChangeThick_g:0:4,',');
Write(OutDatFile,CoolingRate_b:0:10,',');
Write(OutDatFile,Volume_g:0:2,',');
Writeln(OutDatFile,VolGranPerc:0:2,',');

{Check on status of the loop}

IF BasaltSolid = True THEN Quit := True;
IF GraniteConv = True THEN BEGIN
                             Quit := True;
                             AGranthick := Thick_g;
                             ConvTemp_g := Temp_g;
                           END;
```

```
    {cool the basalt progressively in 1 degree increments}

    IF BasaltSolid = False THEN Temp_b := Temp_b - 1;

    UNTIL Quit = True;

       {output formatted results to output summary file}

    Writeln(OutSumFile);

    Writeln(OutSumFile,'Part A');
    Writeln(OutSumFile,'Basalt temperature: ',Temp_b:0:2,' degrees C');
    Writeln(OutSumFile,'Granite temperature: ',Temp_g:0:2,' degrees C');
    Writeln(OutSumFile,'Crustal temperature: ',Temp_c:0:2,' degrees C');
    Writeln(OutSumFile,'Heat required to melt crust: ',HeatRaiseMelt:0:2);
    Writeln(OutSumFile,'Basalt crystal content: ',xtlcont_b:0:3);
    Writeln(OutSumFile,'Kinematic viscosity of basalt: ',kinvisc_b:0:3);
    Writeln(OutSumFile,'Granite crystal content: ',xtlcont_g:0:3);
    Writeln(OutSumFile,'Kinematic viscosity of granite: ',kinvisc_g:0:3);
    Writeln(OutSumFile,'Rayleigh # of basalt: ',RaylConv_b:0:3);
    Writeln(OutSumFile,'Rayleigh # of granite: ',RaylConv_g:0:3);
    Writeln(OutSumFile,'New thickness of granite: ',NewGranite:0:2,' metres');
    Writeln(OutSumFile,'Total thickness of granite: ',thick_g:0:2,' metres');
    Writeln(OutSumFile,'Conductive flux through granitoid: ',Condflux:0:3);
    Writeln(OutSumFile,'dA/dt Granite: ',RateOfChangeThick_g:0:4);
    Writeln(OutSumFile,'dT/dt Basalt: ',CoolingRate_b:0:10);
    Writeln(OutSumFile,'Volume of granite: ',Volume_g:0:2,' kmE3');
    Writeln(OutSumFile,'Volume of granite %: ',VolGranPerc:0:2,' %');
    Writeln(OutSumFile);

  END; {IF NOT BasaltSolid and GraniteConv}
END

ELSE

BEGIN {No anatexis occurs}
  Writeln('No crustal melting occurs under these conditions.....');
  Writeln(OutSumFile,'Basalt temperature: ',Temp_b:0:2,' degrees C');
  Writeln(OutSumFile,'Granite temperature: ',Temp_g:0:2,' degrees C');
  Writeln(OutSumFile,'Crustal temperature: ',Temp_c:0:2,' degrees C');
  Writeln(OutSumFile,'Heat required to melt crust: ',HeatRaiseMelt:0:2);
  Writeln(OutSumFile,'Basalt crystal content: ',xtlcont_b:0:3);
  Writeln(OutSumFile,'Kinematic viscosity of basalt: ',kinvisc_b:0:3);
  Writeln(OutSumFile,'Granite crystal content: ',xtlcont_g:0:3);
  Writeln(OutSumFile,'Kinematic viscosity of granite: ',kinvisc_g:0:3);
  Writeln(OutSumFile,'Rayleigh # of basalt: ',RaylConv_b:0:3);
  Writeln(OutSumFile,'Rayleigh # of granite: ',RaylConv_g:0:3);
  Writeln(OutSumFile,'New thickness of granite: ',NewGranite:0:2,' metres');
  Writeln(OutSumFile,'Total thickness of granite: ',thick_g:0:2,' metres');
  Writeln(OutSumFile,'Conductive flux through granitoid: ',Condflux:0:3);
  Writeln(OutSumFile,'dA/dt Granite: ',RateOfChangeThick_g:0:4);
  Writeln(OutSumFile,'dT/dt Basalt: ',CoolingRate_b:0:10);
  Writeln(OutSumFile,'Volume of granite: ',Volume_g:0:2,' kmE3');
  Writeln(OutSumFile,'Volume of granite %: ',VolGranPerc:0:2,' %');
  Writeln(OutSumFile);

  Writeln(OutSumFile,'No crustal melting occurs under these conditions.....');
  BasaltSolid := True;
  GraniteConv := False;
  Thick_g := 0;
  Temp_c := intertemp;

  {Wait for user to read the nagware message}

  GetTime(hour, minute, second, sec100);
  StartTime := second + WaitPeriod;
  REPEAT
    GetTime(hour, minute, second, sec100);
  UNTIL second = StartTime;
```

```
    END; {IF InterTemp NOT > MeltTemp_c}

{----------------------------------------------------------------------
 Begin Part B of static model - Calculate thickness of granite generated
 if the mafic sill and granitoid layer convect simultaneously.
----------------------------------------------------------------------}

IF (BasaltSolid = False) AND (GraniteConv = True) THEN
BEGIN

    Quit := False;

  REPEAT
    RunningTotalThick := Thick_g;

    InterTemp := CalcInterTemp(rho_c, specheat_c, rho_b, specheat_b, J, Temp_b, irtemp_c);

    Temp_c := Intertemp;

    InterTemp := CalcInterTemp(rho_c, specheat_c, rho_b, specheat_b, J, Temp_b, Temp_c);
    Temp_g := Intertemp;

    {Calculate thickness of granitoid melt layer generated by the convecting basalt
     - as in Part A}

    Thick_g := GraniteThickness(HeatRaiseMelt, rho_b, specheat_b, Temp_b, Thick_b,
                             itemp_b, heatfus_b, xtlcont_b);

    {Calculate thickness of granitoid melt layer generated by convective self-propogation
     as in Part C below, and add to the thickness calculated above}

    TempGranThick := GraniteThickness(HeatRaiseMelt, rho_g, specheat_g, Temp_g,
                                   AGranThick, ConvTemp_g, heatfus_g, xtlcont_g);
    Thick_g := Thick_g + TempGranThick;

    IF Thick_g > RunningTotalThick THEN NewGranite := Thick_g - RunningTotalThick;
    Volume_b := TotalVolume(Thick_b, Width_b, Length_b);
    Volume_g := TotalVolume(Thick_g, Width_b, Length_b);
    VolGranPerc := PercGranGen(Volume_g, Volume_b);

    xtlcont_b := BasaltCrystalContent(Temp_b);
    xtlcont_g := GraniteCrystalContent(Temp_g,PercWater);
    Kinvisc_b := CalcKinViscBasalt(xtlcont_b);
    Kinvisc_g := CalcKinViscGranite(xtlcont_g, percwater, temp_g);
    RaylConv_b := RayleighConvection(thermex_b, gravaccel, Temp_b, melttemp_c, thick_b,
                                  thermdiff_b, kinvisc_b);
    RaylConv_g := RayleighConvection(thermex_g, gravaccel, Temp_g, melttemp_c, thick_g,
                                  thermdiff_g, kinvisc_g);

    {calculate values for loop flags}

    IF RaylConv_g > 1000 THEN GraniteConv := True ELSE GraniteConv := False;
    IF xtlcont_b > 0.55 THEN BasaltSolid := True;

    Condflux := CondfluxGranConv(rho_g,specheat_g,J,Temp_g,melttemp_c);
    RateOfChangeThick_g := DeltaGraniteThickConv(Condflux,HeatRaiseMelt);
      FDerivXtlCont := FirstDerivBasXtls(Temp_b);
    CoolingRate_b := CoolingRateBasalt(J,Thick_b, Temp_b, heatfus_b, Temp_c, specheat_b,
                                    FDerivXtlCont);
      FDerivXtlCont := FirstDerivGranXtls(Temp_g);

      {output results to screen}

    Writeln;
    Writeln('-------------------------------------------------------------');
    Writeln('Part B....');
    Writeln('Temperature of basalt: ', Temp_b:0:2);
    Writeln('Temperature of granite: ', Temp_g:0:2);
    Writeln('Temperature of crust: ', Temp_c:0:2);
    Writeln('Hs: ',HeatRaiseMelt:0:2);
```

```
  Writeln;
  Writeln('Crystal content of basalt: ',xtlcont_b:0:3);
  Writeln('Kinematic viscosity of basalt: ',kinvisc_b:0:3);
  Writeln('Crystal content of granite: ',xtlcont_g:0:3);
  Writeln('Kinematic viscosity of granite: ',kinvisc_g:0:3);
  Writeln('Rayleigh number of basalt: ',RaylConv_b:0:3);
  Writeln('Rayleigh number of granite: ',RaylConv_g:0:3);
  Writeln;
  Writeln('New thickness of granite: ', NewGranite:0:2);
  Writeln('Total thickness of granite: ', Thick_g:0:2);
  Writeln;
  Writeln('Conductive flux through granitoid: ',Condflux:0:3);
  Writeln('Granite dA/dt: ',RateOfChangeThick_g:0:4);
  Writeln('Basalt dT/dt: ',CoolingRate_b:0:10);
  Writeln('Total volume of granite: ', Volume_g:0:2);
  Writeln('Granite volume/Mafic volume % : ',VolGranPerc:0:2);
  Writeln('--------------------------------------------------------------');
  Writeln;

  {output raw results to output data file}

  Write(OutDatFile,ItnNumber,',');
  Write(OutDatFile,'B,');
  Write(OutDatFile,Temp_b:0:2,',');
  Write(OutDatFile,Temp_g:0:2,',');
  Write(OutDatFile,Temp_c:0:2,',');
  Write(OutDatFile, HeatRaiseMelt:0:2,',');
  Write(OutDatFile,xtlcont_b:0:3,',');
  Write(OutDatFile,kinvisc_b:0:3,',');
  Write(OutDatFile,xtlcont_g:0:3,',');
  Write(OutDatFile,kinvisc_g:0:3,',');
  Write(OutDatFile,RaylConv_b:0:3,',');
  Write(OutDatFile,RaylConv_g:0:3,',');
  Write(OutDatFile,NewGranite:0:2,',');
  Write(OutDatFile,thick_g:0:2,',');
  Write(OutDatFile,Condflux:0:3,',');
  Write(OutDatFile,RateOfChangeThick_g:0:4,',');
  Write(OutDatFile,CoolingRate_b:0:10,',');
  Write(OutDatFile,Volume_g:0:2,',');
  Writeln(OutDatFile,VolGranPerc:0:2,',');

  {Check on status of the loop}

  IF BasaltSolid = True THEN Quit := True;
  IF GraniteConv = False THEN Quit := True;

  {cool the basalt progressively in 1 degree increments}

  IF (GraniteConv = True) THEN Temp_b := Temp_b - 1;
UNTIL Quit = True;

  {output formatted results to output summary file}

  Writeln(OutSumFile);
  Writeln(OutSumFile,'Part B');
  Writeln(OutSumFile,'Basalt temperature: ',Temp_b:0:2,' degrees C');
  Writeln(OutSumFile,'Granite temperature: ',Temp_g:0:2,' degrees C');
  Writeln(OutSumFile,'Crustal temperature: ',Temp_c:0:2,' degrees C');
  Writeln(OutSumFile,'Heat required to melt crust: ',HeatRaiseMelt:0:2);
  Writeln(OutSumFile,'Basalt crystal content: ',xtlcont_b:0:3);
  Writeln(OutSumFile,'Kinematic viscosity of basalt: ',kinvisc_b:0:3);
  Writeln(OutSumFile,'Granite crystal content: ',xtlcont_g:0:3);
  Writeln(OutSumFile,'Kinematic viscosity of granite: ',kinvisc_g:0:3);
  Writeln(OutSumFile,'Rayleigh # of basalt: ',RaylConv_b:0:3);
  Writeln(OutSumFile,'Rayleigh # of granite: ',RaylConv_g:0:3);
  Writeln(OutSumFile,'New thickness of granite: ',NewGranite:0:2,' metres');
  Writeln(OutSumFile,'Total thickness of granite: ',thick_g:0:2,' metres');
  Writeln(OutSumFile,'Conductive flux through granitoid: ',Condflux:0:3);
  Writeln(OutSumFile,'dA/dt Granite: ',RateOfChangeThick_g:0:4);
  Writeln(OutSumFile,'dT/dt Basalt: ',CoolingRate_b:0:10);
```

```
    Writeln(OutSumFile,'Volume of granite: ',Volume_g:0:2,' kmE3');
    Writeln(OutSumFile,'Volume of granite %: ',VolGranPerc:0:2,' %');
    Writeln(OutSumFile);

END; {IF NOT BasaltSolid and GraniteConv}

{-----------------------------------------------------------------------
 Begin Part C of static model - Calculate the thickness of granitoid
 generated by further convection in the granitoid if the mafic layer
 solidified during either Part A or Part B.
-----------------------------------------------------------------------}
 IF (BasaltSolid = True) AND (GraniteConv = False) THEN
BEGIN
  Writeln;
  Writeln('-----------------------------------------------------------------');
  Writeln('Part C....');
  Writeln;
  Writeln('The granitoid does not convect. No further crustal melting occurs.....');
  Writeln;
  Writeln('Completion of Part C');
  Writeln('-----------------------------------------------------------------');
  Writeln;
  Writeln(OutSumFile,'The granitoid does not convect. No further crustal melting
          occurs.....');
END {IF BasaltSolid and NOT GraniteConv}

ELSE

BEGIN {Granitoid still convects}
  Quit := False;
  ABGranThick := Thick_g;
  IF heatfus_c <> 42 THEN HeatRaiseMelt := HeatReqMelt(rho_c, specheat_c, Temp_c,
                                                   melttemp_c, heatfus_c);
  IF HeatRaiseMelt = 0 THEN HeatRaiseMelt := 13.65;

  REPEAT
    RunningTotalThick := Thick_g;

    InterTemp := CalcInterTemp(rho_c, specheat_c, rho_b, specheat_b, J, Temp_b, irtemp_c);

    Temp_c := Intertemp;

    InterTemp := CalcInterTemp(rho_c, specheat_c, rho_b, specheat_b, J, Temp_b, Temp_c);
    Temp_g := Intertemp;

    TempGranThick := GraniteThickness(HeatRaiseMelt, rho_g, specheat_g, temp_g,
                                  AGranThick,ConvTemp_g, heatfus_g, xtlcont_g);
    IF TempGranThick <> 0 THEN Thick_g := (TempGranThick+ABGranThick);
    IF Thick_g > RunningTotalThick THEN NewGranite := Thick_g - RunningTotalThick;

    Volume_b := TotalVolume(Thick_b, Width_b, Length_b);
    Volume_g := TotalVolume(Thick_g, Width_b, Length_b);
    VolGranPerc := PercGranGen(Volume_g, Volume_b);
    xtlcont_b := BasaltCrystalContent(Temp_b);
    xtlcont_g := GraniteCrystalContent(Temp_g,PercWater);
    Kinvisc_g := CalcKinViscGranite(xtlcont_g, percwater, temp_g);
    RaylConv_g := RayleighConvection(thermex_g, gravaccel, Temp_g, melttemp_c, thick_g,
                                 thermdiff_g, kinvisc_g);

    {Test to see when no more self-propogation occurs}
    IF TempGranThick = 0 THEN Quit := True; {thermal conditions in crust produce no more
                                          granite}
    IF RaylConv_g < 1000 THEN GraniteConv := False; {granite stops convecting}
    IF (Temp_g/Temp_c <= 1) THEN Quit := True; {Granite and crust temps become the same -
                                            no temp gradients}
    IF (Temp_b/Temp_c <= 1) THEN Quit := True; {Basalt and crust temps become the same -
                                            no temp gradients}

    Condflux := CondfluxGranConv(rho_g,specheat_g,J,Temp_g,melttemp_c);
    RateOfChangeThick_g := DeltaGraniteThickConv(Condflux,HeatRaiseMelt);
```

```
FDerivXtlCont := FirstDerivGranXtls(Temp_g);

{output results to screen}

Writeln;
Writeln('-------------------------------------------------------------');
Writeln('Part C....');
Writeln('Temperature of basalt: ', Temp_b:0:2);
Writeln('Temperature of granite: ', Temp_g:0:2);
Writeln('Temperature of crust: ', Temp_c:0:2);
Writeln('Hs: ',HeatRaiseMelt:0:2);
Writeln;
Writeln('Crystal content of basalt: ',xtlcont_b:0:3);
Writeln('Crystal content of granite: ',xtlcont_g:0:3);
Writeln('Kinematic viscosity of granite: ',kinvisc_g:0:3);
Writeln('Rayleigh number of granite: ',RaylConv_g:0:3);
Writeln;
Writeln('New thickness of granite: ', NewGranite:0:2);
Writeln('Total thickness of granite: ', Thick_g:0:2);
Writeln;
Writeln('Conductive flux through granitoid: ',Condflux:0:3);
Writeln('Granite dA/dt: ',RateOfChangeThick_g:0:4);
Writeln('Total volume of granite: ', Volume_g:0:2);
Writeln('Granite volume/Mafic volume % : ',VolGranPerc:0:2);
Writeln;
Writeln('Completion of Part C');
Writeln('-------------------------------------------------------------');
Writeln;
{output raw results to output data file}

Write(OutDatFile,ItnNumber,',');
Write(OutDatFile,'C,');
Write(OutDatFile,Temp_b:0:2,',');
Write(OutDatFile,Temp_g:0:2,',');
Write(OutDatFile,Temp_c:0:2,',');
Write(OutDatFile, HeatRaiseMelt:0:2,',');
Write(OutDatFile,xtlcont_b:0:3,',');
Write(OutDatFile,',');
Write(OutDatFile,xtlcont_g:0:3,',');
Write(OutDatFile,kinvisc_g:0:3,',');
Write(OutDatFile,',');
Write(OutDatFile,RaylConv_g:0:3,',');
Write(OutDatFile,NewGranite:0:2,',');
Write(OutDatFile,thick_g:0:2,',');
Write(OutDatFile,Condflux:0:3,',');
Write(OutDatFile,RateOfChangeThick_g:0:4,',');
Write(OutDatFile,',');
Write(OutDatFile,Volume_g:0:2,',');
Writeln(OutDatFile,VolGranPerc:0:2,',');

{Check on status of the loop}

IF GraniteConv = False THEN Quit := True;

{cool the basalt progressively in 1 degree increments}

IF (GraniteConv = True) AND (Temp_b > Temp_c) THEN Temp_b := Temp_b - 1;

UNTIL Quit = True;

{output formatted results to output summary file}

Writeln(OutSumFile);
Writeln(OutSumFile,'Part C');
Writeln(OutSumFile,'Basalt temperature: ',Temp_b:0:2,' degrees C');
Writeln(OutSumFile,'Granite temperature: ',Temp_g:0:2,' degrees C');
Writeln(OutSumFile,'Crustal temperature: ',Temp_c:0:2,' degrees C');
Writeln(OutSumFile,'Heat required to melt crust: ',HeatRaiseMelt:0:2);
Writeln(OutSumFile,'Basalt crystal content: ',xtlcont_b:0:3);
Writeln(OutSumFile,'Granite crystal content: ',xtlcont_g:0:3);
```

```
    Writeln(OutSumFile,'Kinematic viscosity of granite: ',kinvisc_g:0:3);
    Writeln(OutSumFile,'Rayleigh # of granite: ',RaylConv_g:0:3);
    Writeln(OutSumFile,'New thickness of granite: ',NewGranite:0:2,' metres');
    Writeln(OutSumFile,'Total thickness of granite: ',thick_g:0:2,' metres');
    Writeln(OutSumFile,'Conductive flux through granitoid: ',Condflux:0:3);
    Writeln(OutSumFile,'Volume of granite: ',Volume_g:0:2,' kmE3');
    Writeln(OutSumFile,'Volume of granite %: ',VolGranPerc:0:2,' %');
    Writeln(OutSumFile);


    Writeln;
    Writeln('--------------------------------------------------------------');
    Writeln('Part C....');
    Writeln;
    Writeln('The granitoid stopped convecting. No further crustal melting occurs.....');
    Writeln;
    Writeln('Completion of Part C');
    Writeln('--------------------------------------------------------------');
    Writeln;
    Writeln(OutSumFile,'The granitoid stopped convecting. No further crustal melting
            occurs.....');
END; {BasaltSolid and GraniteConv}

  END; {StaticModel}

PROCEDURE DynamicModel; {Loop StaticModel according to user parameters}

CONST WaitPeriod = 2;
VAR CycleCounter : integer;
    DynTotThick_g, DynTotVol_g, DynTotVol_b, DynVolGranPerc : real;
    StartTime : Word;

  BEGIN

    {set all new dynamic variables to zero}

    CycleCounter := 0; DynTotThick_g := 0; DynTotVol_g := 0;
    DynTotVol_b := 0; DynVolGranPerc := 0;

    {Begin dynamic model loop - repeat static model for x number of mafic
    intrusions}

    StaticModel; {Calculate first static model to see if melting occurs}
    DynTotThick_g := DynTotThick_g + Thick_g;
    IF Temp_c > melttemp_c THEN Temp_c := melttemp_c;
    intertemp := Temp_c;
    FOR CycleCounter := 1 TO (NoCycles-1) DO
    BEGIN
      Temp_b := (itemp_b-2);
      IF Temp_c > melttemp_c THEN Temp_c := melttemp_c;
      intertemp := Temp_c;
      StaticModel;
      DynTotThick_g := DynTotThick_g + Thick_g;
    END; {FOR CycleCounter}

      Thick_b := NoCycles*Thick_b;
      DynTotVol_b := TotalVolume(Thick_b, Width_b, Length_b);
      DynTotVol_g := TotalVolume(DynTotThick_g, Width_b, Length_b);
      DynVolGranPerc := PercGranGen(DynTotVol_g, DynTotVol_b);

      {output results to screen}

      Writeln;
      Writeln('--------------------------------------------------------------');
      Writeln('Dynamic model....');
      Writeln('Total thickness of granite formed: ', DynTotThick_g:0:2);
      Writeln;
      Writeln('Total volume of granite formed: ', DynTotVol_g:0:2);
      Writeln('Total Granite volume/Mafic volume % : ',DynVolGranPerc:0:2);
      Writeln;
```

```
      Writeln('Completion of Dynamic model');
      Writeln('--------------------------------------------------------------');

      {output raw results to output data file}

      Write(OutDatFile,',');
      Write(OutDatFile,'D,');
      Write(OutDatFile,',');
      Write(OutDatFile,',');
      Write(OutDatFile,',');
      Write(OutDatFile,',');
      Write(OutDatFile,',');
      Write(OutDatFile,',');
      Write(OutDatFile,',');
      Write(OutDatFile,',');
      Write(OutDatFile,',');
      Write(OutDatFile,',');
      Write(OutDatFile,',');
      Write(OutDatFile,DynTotThick_g:0:2,',');
      Write(OutDatFile,',');
      Write(OutDatFile,',');
      Write(OutDatFile,',');
      Write(OutDatFile,DynTotVol_g:0:2,',');
      Writeln(OutDatFile,DynVolGranPerc:0:2,',');

     {output formatted results to output summary file}

      Writeln(OutSumFile);
      Writeln(OutSumFile,'Part D - Dynamic model results' );
      Writeln(OutSumFile,'Total thickness of granite: ',DynTotThick_g:0:2,' metres');
      Writeln(OutSumFile,'Total volume of granite: ',DynTotVol_g:0:2,' kmE3');
      Writeln(OutSumFile,'Total volume of granite %: ',DynVolGranPerc:0:2,' %');
      Writeln(OutSumFile);

  END; {DynamicModel}


PROCEDURE ChooseModel; {select type of model to run}
LABEL 1;
  BEGIN

    1:Write('Calculate a [S]tatic model or [D]ynamic model ?: ');
    readln(Choice);

    CASE Choice OF
    'S', 's' : BEGIN
                 Writeln;
                 Writeln('Static model....');
                 Writeln;
                 UserParamsStatic;
                 InitStaticModel;
                 StaticModel;
               END;
    'D', 'd' : BEGIN
                 Writeln;
                 Writeln('Dynamic model....');
                 Writeln;
                 UserParamsDynamic;
                 InitStaticModel;
                 DynamicModel;
               END;
    ELSE BEGIN
           Writeln('Invalid response, please try again;');
           Writeln;
           GOTO 1;
         END;
    END; {case}
  END; {ChooseModel}
```

```
PROCEDURE CleanUp; {close output files and clean up}
  BEGIN
    Close(OutDatFile);
    Close(OutSumFile);
  END;


BEGIN {Main Program}
  Start: SetupScrn;
  ReadConst;
  ChooseModel;
  CleanUp;
  1:Writeln;
  ClrScr;
  Write('[R]un another model or [Q]uit ?: ');
  Readln(AnotherModel);
  CASE AnotherModel OF
    'R', 'r' : BEGIN
                 Writeln;
                 Writeln('Running another model....');
                 Writeln;
                 ClrScr;
                 GOTO Start;
                END;
    'Q', 'q' : BEGIN
                  Writeln;
                  Writeln('Quitting....');
                  Writeln;
                  ClrScr;
                  DoneWinCRT;
                END;
    ELSE BEGIN
           ClrScr;
           Writeln('Invalid response, please try again;');
           Writeln;
           GOTO 1;
         END;
  END; {CASE AnotherModel}

END. {Main Program}
```

F-3. Sensitivity Analysis

The HTFLOW31 algorithm decreases the basalt temperature in 1°C increments to ensure stable results, to compute stable Rayleigh numbers at crystal contents close to the critical melt fraction, and to allow the completion of individual model runs in the shortest possible time periods using an IBM-compatible microcomputer. Table F3.1 shows that all cooling increments less than 10°C produce results that differ <2% from the model runs presented in Chapter 6. Models with cooling increments of >3°C do not run significantly faster than those with 1°C increments, whereas models with cooling increments <1°C take much longer times time to complete. The chosen value of 1°C represents the best compromise between convenience and

Table F3.1. Results of a sensitivity analysis used to select the optimum cooling increment for the HTFLOW31 models.

Model	Cooling increment (°C)	$T_b(0)$ (°C)	$T_c(0)$ (°C)	T_m (°C)	% H_2O	D (m)	a (m)
Test1	0.1	1,200	500	850	2	100	49.77
Test2	0.25	1,200	500	850	2	100	49.82
Test3	0.5	1,200	500	850	2	100	49.73
Test4	0.75	1,200	500	850	2	100	49.56
Test5	1	1,200	500	850	2	100	49.56
Test6	2	1,200	500	850	2	100	49.75
Test7	3	1,200	500	850	2	100	48.86
Test8	4	1,200	500	850	2	100	49.07
Test9	5	1,200	500	850	2	100	48.73
Test10	6	1,200	500	850	2	100	49.43
Test11	7	1,200	500	850	2	100	50.66
Test12	8	1,200	500	850	2	100	49.8
Test13	9	1,200	500	850	2	100	46.87
Test14	10	1,200	500	850	2	100	47.05

See Table 6.1 in Chapter 6 and Appendix F-1 for the modelling nomenclature numerical precision, and the results are ±2%.

F-4. Necessary Files

The program HTFLOW31.EXE imports values for the constants required in its calculations from a file called INCONST.DAT. This file allowed the author to change the constants without recompiling the program. Consequently, the INCONST.DAT file must exist and it must reside in the same directory as the executable file; a listing of its format and suggested values for the constants (Huppert and Sparks, 1988a) appears below and in electronic form on the enclosed floppy disk (back pocket). Note that the executable file treats all semicolons (";") as comments and ignores all text after them.

```
            ; INCONST.DAT - Constants for HTFLOW31.EXE
            ; ----------------------------------------
981         ; Acceleration due to gravity - cm s^-2
0.00005     ; Ceoff. thermal exp. basalt  - K^-1
0.00005     ; Ceoff. thermal exp. granite - K^-1
1000        ; Kinematic viscosity of basalt - cm^2s^-1
1000        ; Kinematic viscosity of granite - cm^2s^-1
0.008       ; Thermal diffusivity of basalt - cm^2s^-1
0.008       ; Thermal diffusivity of granite - cm^2s^-1
2.25        ; Thermal conductivity of granite magma
2.7         ; Density of basalt magma - g cm^-3
2.6         ; Density of solid crust - g cm^-3
2.3         ; Density of granitic magma - g cm^-3
0.32        ; Specific heat capacity of basalt - cal g^-1K^-1
0.32        ; Specific heat capacity of solid crust - cal g^-1K^-1
0.32        ; Specific heat capacity of granite magma - cal g^-1K^-1
100         ; Latent heat of crystallization of basalt - cal g^-1
70          ; Latent heat of fusion of solid crust - cal g^-1
45          ; Latent heat of crystallization of granite magma - cal g^-1
```

F-5. Estimating the Volume of Granitoid in the Meguma Zone Crust

This project estimated the volume of peraluminous granitoid in the Meguma crust to constrain the numerical heat flow models. Contacts for the South Mountain Batholith (SMB) were digitized at 1:100,000 scale and AutoCAD™ calculated the area of this complex shape as 7956 km^2 (Table F5.1); replication of this procedure gives an error of ±2% on the calculation. Given that no interpretations of aeromagnetic data exist for Meguma granitoids, detailed gravity surveys represent the best approach for calculating approximate volumes for intrusions. In this

Table F5.1. Estimated onshore geographic areas occupied by granitoids in the Meguma Zone.

Intrusion	Central/Peripheral	km^2	% area of SMB
SMB	Central	7,956	-
BPP	Peripheral	420	5.3
SP	Peripheral	298	3.7
PMP	Peripheral	180	2.3
MB	Central	160	2
LC	Central	154	1.9
CP	Peripheral	126	1.6
HCQP	Central	120	1.5

See Appendix E-1 for the intrusion abbreviations and Figure 5.1 in Chapter 5 for their locations.

study, the 2.5-dimensional gravity models of Douma (1978; Figure F5.1) constrained the thickness of granitoid present in the SMB to between 9 and 17 km, and minimum volume estimates, therefore, range between 101,757 km^3 and 141,458 km^3, depending on the thickness of granitoid adopted. Using the MAGRAV 2.5-dimensional gravity modelling program (Broom, 1986), the maximum depth that a 5 km long slab of monzogranite 500 m thick contributes to the regional gravity field is 16 km, using the density data of O'Reilly (1975) and assuming a maximum detection limit of 0.1 mgal (P. Ryall, pers. comm., 1994). With this approach, the mimimum volume of the SMB is 127,296 km^3, but the order of magnitude remains unchanged at 10^5 $km^3 \pm 30\%$. The lack of detailed gravity data for most other central and peripheral plutons precludes estimation of their volumes directly, and the BPP has no density contrast with the Meguma Group (O'Reilly, 1975). Instead, their collective areas (calculated as for the SMB; Table F4.1) represent only approximately 18% of the area calculated for the SMB and their volumes probably also lie within the error of the minimum volume estimate for the SMB. Volumes for these intrusions were calculated as percentages of the value calculated for the SMB, with the necessary assumption that pluton volumes are directly proportional to their exposed areas.

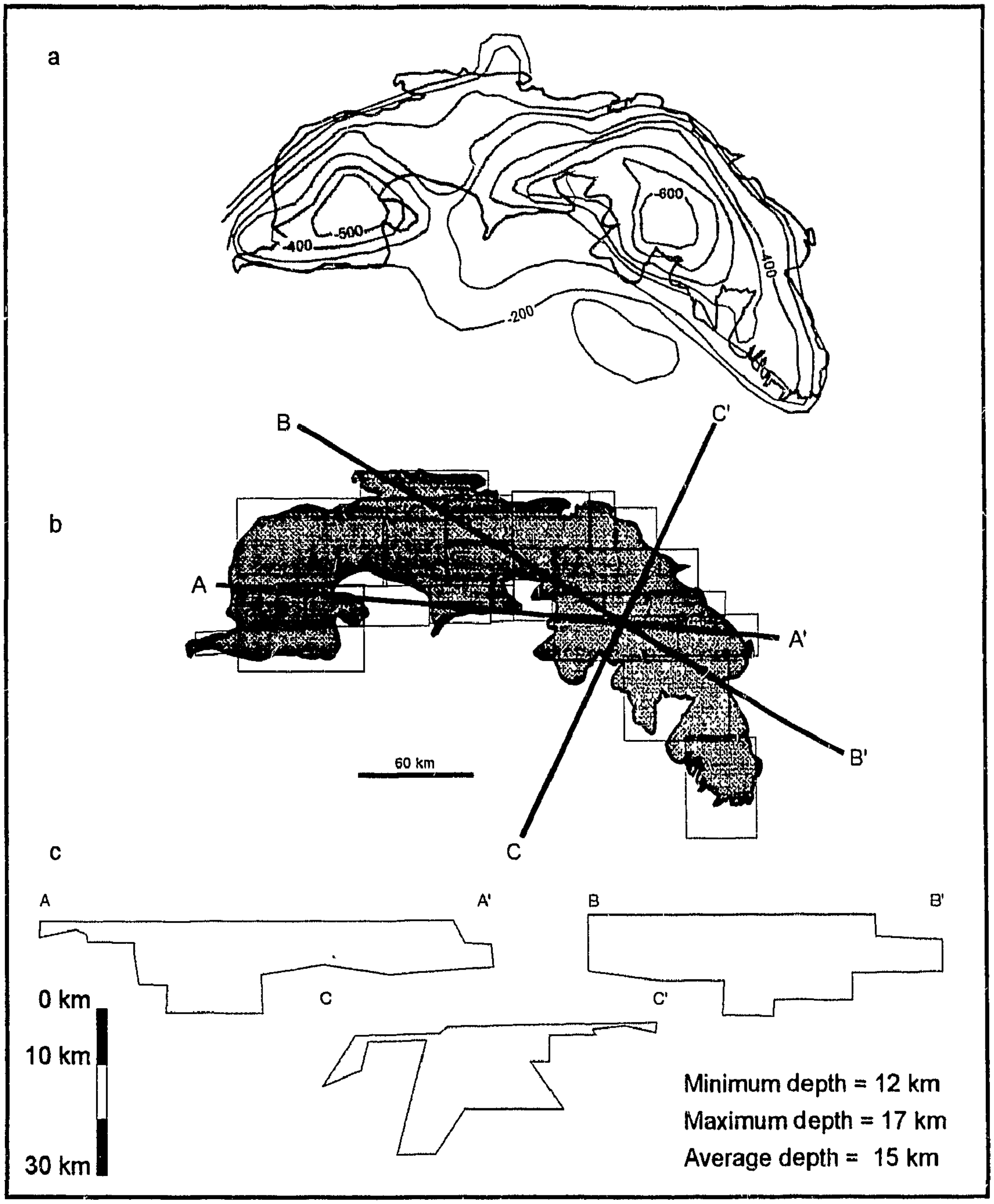

Figure F5.1. Calculation of the total volume of peraluminous granitoid in the South Mountain Batholith. (a); Regional gravity data for the batholith. Modified after Giles and Chatterjee (1986); (b) Division of the batholith into rectangular regions for gravity modelling purposes. After O'Reilly (1975) and Douma (1978); (c) Cross-sections across lines A-A', B-B', and C-C', showing the estimated minimum, maximum and average depths to which granitoid extends (After O'Reilly (1975) and Douma (1978).

Back Pocket

ENCLOSED 3.5" FLOPPY DISK

All of the data tables from Appendices B, C, D, and E, together with the computer program from Appendix F, exist on a 3.5" (High Density) floppy disk formatted with MS-DOS 6.0 (back pocket). The disk is organized into subdirectories for each appendix and a description of the files in each subdirectory appears below Comma-delimited text files represent the simplest and most portable format to transfer data files across platforms.

FILENAME	SIZE (bytes)	DESCRIPTION	FORMAT	TYPE
Directory of \APPEND-B				
TABLE2-1 DAT	427	Appendix B Table 2 1	Comma-delimited	ASCII
TABLE2-2 DAT	1,678	Appendix B Table 2 2	Comma-delimited	ASCII
TABLE2-3 DAT	5,056	Appendix B Table 2 3	Comma-delimited	ASCII
TABLE2-4 DAT	2,765	Appendix B Table 2 4	Comma-delimited	ASCII
TABLE2-5 DAT	3,841	Appendix B Table 2 5	Comma-delimited	ASCII
TABLE3-1 DAT	17,008	Appendix B Table 3 1	Comma-delimited	ASCII
TABLE4-1 DAT	12,466	Appendix B Table 4 1	Comma-delimited	ASCII
Directory of \APPEND-C				
TABLE1-1.DAT	3,038	Appendix C Table 1 1	Comma-delimited	ASCII
TABLE1-2 DAT	3237	Appendix C Table 1 2	Comma-delimited	ASCII
TABLE1-3 DAT	4,307	Appendix C Table 1 3	Comma-delimited	ASCII
TABLE2-1 DAT	4,134	Appendix C Table 2 1	Comma-delimited	ASCII
Directory of \APPEND-D				
TABLE1-1.DAT	11,444	Appendix D Table 1 1	Comma-delimited	ASCII
Directory of \APPEND-E				
TABLE1-1 DAT	222,404	Appendix E Table 1 1	Comma-delimited	ASCII
Directory of \APPEND-F				
INCONST. DAT	1,048	Data file for HTFLOW31 EXE	Free-form	ASCII
HTFLOW31 PAS	83,697	Source code for HTFLOW31 EXE	Free-form	ASCII
HEATCRT.TPU	14,192	Unit needed to compile the source code	-	BINARY
HTFLOW31 EXE	151346	HTFLOW31 executable program	-	BINARY
Total size of files	**542088**			

REFERENCES

Abbott, R.N. 1989. Internal structures in part of the South Mountain Batholith, Nova Scotia, Canada. Bulletin of the Geological Society of America, 101: 1493-1506.

Albarede, F., Dupuis, C., and Taylor, H.P. 1980. $^{18}O/^{16}O$ evidence for non-cogenetic magmas associated in a 300 Ma old concentric pluton at Ploumanac'h (Brittany, France). Journal of the Geological Society of London, 137: 641-647.

Alexander, E.C., Michelson, G.M., and Lanphere, M.A. 1978. MMHb-1: a new $^{40}Ar/^{39}Ar$ dating standard. Fourth International Conference on Geochronology, Cosmology and Isotopic Geology. United States Geological Survey, Open File Report 78-701: 6-8.

Arndt, N.T., and Christensen, V. 1992. The role of the lithospheric mantle in continental flood volcanism: Thermal and geochemical constraints. Journal of Geophysical Research, 97: 10967-10981.

Ayuso, R.A. 1986. Lead-isotopic evidence for distinct sources of granite and for distinct basements in the northern Appalachians, Maine. Geology, 14: 322-325.

Ayuso, R.A., and Arth, J.G. 1992. The Northeast Kingdom batholith, Vermont: magmatic evolution and geochemical constraints on the origin of Acadian granitic rocks. Contributions to Mineralogy and Petrology, 111: 1-23.

Bacon, C.R. 1988. Mafic inclusions in granitic rocks. Eos, 69: 1495.

Bacon, C.R., and Metz, J. 1984. Magmatic inclusions in rhyolites, contaminated basalts, and compositional zonation beneath the Coso volcanic field, California. Contributions to Mineralogy and Petrology, 85: 346-365.

Baird, A.K., and Meisch, A.T. 1984. Batholithic rocks of southern California - A model for the petrochemical nature of source materials. United States Geological Survey Professional Paper 1284: 42pp.

Barbarin, B. 1992. Enclaves of the Mesozoic calc-alkaline granitoids of the Sierra Nevada batholith, California. In: Enclaves and Granite Petrology. Edited by: J. Didier and B. Barbarin. Developments in Petrology 13, Elsevier, Amsterdam: 135-154.

Barbarin, B., and Didier, J. 1992a. Enclaves and granite petrology. In: Enclaves and Granite Petrology. Edited by: J. Didier and B. Barbarin. Developments in Petrology 13, Elsevier, Amsterdam: 545-550.

Barbarin, B., and Didier, J. 1992b. Macroscopic features of mafic microgranular enclaves. In: Enclaves and Granite Petrology. Edited by: J. Didier and B. Barbarin. Developments in Petrology 13, Elsevier, Amsterdam: 253-262.

Barbarin, B., and Didier, J. 1992c. Review of the main hypotheses proposed for the genesis and evolution of mafic microgranular enclaves. In: Enclaves and Granite Petrology. Edited by: J. Didier and B. Barbarin. Developments in Petrology 13, Elsevier, Amsterdam: 267-274.

Barbarin, B., and Didier, J. 1992d. Genesis and evolution of mafic microgranular enclaves through various types of interaction between co-existing felsic and mafic magmas. In: The Second Hutton Symposium on the Origin of Granites and Related Rocks. Edited by: P.E. Brown and B.W. Chappell. Geological Society of America Special Paper 272: 145-154.

Barker, F. 1979. Trondhjemite: definition, environment, and hypotheses of origin. In: Trondhjemites, Dacites, and Related Rocks. Edited by: F. Barker. Developments in Petrology 6, Elsevier Scientific Publishing Company, Amsterdam: 1-12.

Barker, F., Wones, D.R., Sharp, W.N., and Desborough, G.A. 1975. The Pikes Peak Batholith, Colorado Front Range, and a model for the origin of the gabbro-anorthosite-syenite-potassic granite suite. Precambrian Research, 2: 97-160.

Barr, S.M., Doyle, E.M., and Trepasso, L.S. 1983. Geochemistry and tectonic implications of mafic sills in Lower Palaeozoic formations of Nova Scotia. Maritime Sediments and Atlantic Geology, 19: 73-87.

Beard, J.S., and Day, H.W. 1988. Petrology and emplacement of the Smartville Complex, northern California. Journal of Petrology, 29: 965-995.

Bergantz, G.W. 1989. Underplating and partial melting: Implications for melt generation and extraction. Science, 245: 1093-1095.

Biggi, R.J., and Hodge, D.S. 1982. Gravity studies over the Bays-of-Maine Igneous Complex, southeast Maine. Bulletin of Maine Geology, 2: 1-15.

Blake, D.H., Elwell, R.W.D., Gibson, I.L., Skelhorn, R.R., and Walker, G.P.L. 1965. Some relationships resulting from the intimate association of acid and basic magmas. Quarterly Journal of the Geological Society of London, 121: 31-43.

Blundy, J.D., and Sparks, R.S.J. 1992. Petrogenesis of mafic inclusions in granitoids of the Adamello Massif, Italy. Journal of Petrology, 33: 1039-1104.

Bowden, P., Batchelor, R.A., Chappell, B.W., Didier, J., and Lameyre, J. 1984. Petrological, geochemical, and source criteria for the classification of granitic rocks. A discussion. Physics of the Earth and Planetary Interiors, 35: 1-11.

Broom, J. 1986. MAGRAV 2: An interactive magnetics and gravity modelling program for IBM-compatible microcomputers. Geological Survey of Canada Open File 1334: 91pp.

Brown, G.C., Thorpe, R.S., and Webb, P.C. 1984. The geochemical characteristics of granitoids in contrasting arcs and comments on magma sources. Journal of the Geological Society of London, 141: 413-426.

Brown, G.C., and Fyfe, W.S. 1970. The production of granitic melts during ultrametamorphism. Contributions to Mineralogy and Petrology, 28: 310-318.

Brown, P.E., and Chappell, B.W. 1992. The Second Hutton Symposium on the Origin of Granites and Related Rocks. Geological Society of America Special Paper 272: 507pp.

Brown, P.E., Dempster, T.J., Harrison, T.N., and Hutton, D.H.W. 1992. The rapakivi granites of S Greenland - crustal melting in response to extensional tectonics and magmatic underplating. In: The Second Hutton Symposium on the Origin of Granites and Related Rocks. Edited by: P.E. Brown and B.W. Chappell. Geological Society of America Special Paper 272: 173-178.

Bussell, M.A. 1992. Enclaves in the Mesozoic and Cenozoic granitoids of the Peruvian Coastal Batholith. In: Enclaves and Granite Petrology. Edited by: J. Didier and B. Barbarin. Elsevier, Amsterdam: 155-166.

Bussy, F. 1992. Enclaves of the Late Miocene Mote Capanne granite, Elba Island, Italy. In: Enclaves and Granite Petrology. Edited by: J. Didier and B. Barbarin. Elsevier, Amsterdam: 167-178.

Calder, L.M., and Barr, S.M. 1982. Petrology of the Mavillette intrusion, Digby County, Nova Scotia. Maritime Sediments and Atlantic Geology, 18: 29-40.

Cameron, A.E., Smith, D.H., and Walker, R.L. 1969. Mass spectrometry of nanogram-size samples of lead. Analytical Chemistry, 41: 525-526.

Cameron, B. 1985. The contact metamorphic effects of a granitoid pluton on zinc-lead mineralization in the manganiferous metasediments of the Meguma Group, Eastville, Colchester County, Nova Scotia. B.Sc. (honours) thesis, Dalhousie University: 104pp.

Campbell, I.H., and Turner, J.S. 1985. Turbulent mixing between fluids with different viscosities. Nature, 313: 39-42.

Cantagrel, J., Didier, J., and Gourgand, A. 1984. Magma and mixing: origin of intermediate rocks and enclaves from volcanism to plutonism. Physics of the Earth and Planetary Interiors, 35: 63-76.

Castro, A., Moneno-Ventas, I., and De la Rosa, J.D. 1990. Microgranular enclaves as an indicator of hybridization processes in granitoid rocks, Hercynian Belt, Spain. Geological Journal, 25: 391-404.

Cawthorn, R.G., and O'Hara, M.J. 1976. Amphibole fractionation in calc-alkaline magma genesis. American Journal of Science, 276: 309-329.

Chamberlain, C.P., and Rumble, D. 1989. The influence of fluids on the thermal history of a metamorphic terrain: New Hampshire U.S.A. In: Evolution of Metamorphic Belts. Edited by: J.S. Daly, R.A. Cliff, and B.W.D. Yardley. Geological Society Special Publication 43: 203-213.

Chapman, C.A. 1961. Diabase-granite composite dikes with pillow-like structure, Mount Desert Island, Maine. Journal of Geology, 70: 539-564.

Chappell, B.W., White, A.J.R., and Wyborn, D. 1987. The importance of residual source material (restite) in granite petrogenesis. Journal of Petrology, 28: 1111-1138.

Chappell, B.W., and Stephens, W.E. 1988. Origin of infracrustal (I-type) granite magmas. In: The Origin of Granites. Transactions of the Royal Society of Edinburgh, 79: 71-86.

Charest, M.H. 1976. Petrology and mineralization of the New Ross area, Lunenburg County, Nova Scotia. M.Sc. thesis, Dalhousie University: 292pp.

Chatterjee, A.K., Richard, L.R., and Clarke, D.B. 1989. Magmatic and subsolidus amphiboles from the Ten Mile Lake intrusion, Liscomb Complex, Nova Scotia. GAC-MAC Program with Abstracts, 14: 98-99.

Chen, Y.D., Price, R.C., White, A.J.R., and Chappell, B. W. 1990. Mafic inclusions from the Glenbog and Blue Gum granite suites, southeastern Australia. Journal of Geophysical Research, 95: 17757-17774.

Chen, Y., Chappell, B.W., and White, A.J.R. 1992. Mafic enclaves of some I-type granites of the Palaeozoic Lachlan Fold Belt, southeastern Australia. In: Enclaves and Granite Petrology. Edited by: J. Didier and B. Barbarin. Developments in Petrology 13, Elsevier, Amsterdam: 113-124.

Clarke, D.B., and Halliday, A.N. 1980. Strontium isotope geology of the South Mountain Batholith, Nova Scotia. Geochimica et Cosmochimica Acta, 44: 1045-1058.

Clarke, D.B., and Halliday, A.N. 1985. Sm/Nd isotopic investigation of the age and origin of the Meguma Zone metasedimentary rocks. Canadian Journal of Earth Sciences, 22: 102-107.

Clarke, D. B., and Muecke, G. K. 1985. Review of the petrochemistry and origin of the South Mountain Batholith and associated plutons, Nova Scotia, Canada. In: High Heat

Production (HHP) Granites, Hydrothermal Circulation and Ore Genesis. Institute of Mining and Metallurgy, London: 41-55.

Clarke, D.B., Halliday, A.N., and Hamilton, P.S. 1988. Neodymium and strontium isotopic constraints on the origin of the peraluminous granitoids of the South Mountain Batholith, Nova Scotia, Canada. Chemical Geology, 73: 15-24.

Clarke, D.B., and Chatterjee, A.K. 1988. Physical and chemical processes in the South Mountain Batholith. In: Granite-related Mineral Deposits. Edited by: R.P. Taylor and D.F. Strong. Institute of Mining and Metallurgy, Special Volume 39: 223-233.

Clarke, D.B., Chatterjee, A.K., and Giles, P.S. 1993a. Petrochemistry, tectonic history, and Sr-Nd systematics of the Liscomb Complex, Meguma Lithotectonic Zone, Nova Scotia. Canadian Journal of Earth Sciences, 30: 449-464.

Clarke, D.B., MacDonald, M.A., Reynolds, P.H., and Longstaffe, F.J. 1993b. Leucogranites from the eastern part of the South Mountain Batholith, Nova Scotia. Journal of Petrology, 34: 653-679.

Clemens, J.D., and Wall, V.J. 1981. Crystallization and origin of some peraluminous (S-type) granitic magmas. Canadian Mineralogist, 19: 111-132.

Clemens, J.D., Holloway, J.R., and White, A.J.R. 1986. Origin of an A-type granite: Experimental constraints. American Mineralogist, 71: 317-324.

Clemens, J.D., and Vielzeuf, D. 1987. Constraints on melting and magma production in the crust. Earth and Planetary Science Letters, 86: 287-306.

Cook, N.D.J. 1988. Diorites and associated rocks in the Anglem Complex at The Neck, northeastern Stewart Island, New Zealand, an example of magma mingling. Lithos, 21: 247-262.

Cooper, A.F. 1979. Petrology of ocellar lamprophyres from Western Otago, New Zealand. Journal of Petrology, 20: 139-163.

Cullen, J.D. 1983. Metamorphic petrology and geochemistry of the Goldenville Formation metasediments, Yarmouth, Nova Scotia. M.Sc. thesis, Dalhousie University: 241pp.

Dallmeyer, R.D., and Keppie, J.D. 1986. Polyphase Late Palaeozoic tectonothermal evolution of the Meguma Terrane, Nova Scotia. Geological Society of America, Abstracts with Programs, 18: 11.

Davidson, J.P., De Silva, S.L., Holden, P., and Halliday, A.N. 1990. Small-scale disequilibrium in a magmatic inclusion and its more silicic host. Journal of Geophysical Research, 95: 17661-17675.

Davis, D.W. 1982. Optimum linear regression and error estimation applied to U-Pb data. Canadian Journal of Earth Sciences, 19: 2141-2149.

Davy, Ph., and Gillet, Ph. 1986. The stacking of thrust slices in collision zones and its thermal consequences. Tectonics, 5: 913-929.

de Albuquerque, C. A. R. 1977. Geochemistry of the tonalitic and granitic rocks of the Nova Scotian Southern Plutons. Geochimica et Cosmochimica Acta, 44: 1-13.

de Albuquerque, C. A. R. 1979. Origin of the plutonic mafic rocks of southern Nova Scotia. Bulletin of the Geological Society of America, 90: 719-731.

De Yoreo, J.J., Lux, D.R., and Guidotti, C.V. 1989. The role of crustal anatexis and magma migration in the thermal evolution of regions of thickened continental crust. In: Evolution of Metamorphic Belts. Edited by: J.S. Daly, R.A., Cliff, and B.W.D. Yardley. Geological Society Special Publication 43: 187-202.

Denton, R.A., and Woods, I.R. 1979. Turbulent convection between two horizontal plates. International Journal of Heat and Mass Transfer, 22: 1339-1346.

DePaolo, D.J. 1981. A neodymium and strontium isotopic study of the Mesozoic calc-alkaline granitic batholiths of the Sierra Nevada and Peninsular Ranges, California. Journal of Geophysical Research, 86: 10470-10488.

DePaolo, D.J. 1988. Neodymium Isotope Geochemistry. Minerals and Rocks Volume 20. Springer-Verlag, Berlin: 187pp.

DePaolo, D.J., Perry, F.V., and Baldridge, W.S. 1992. Crustal versus mantle sources of granitic magmas: a two-parameter model based on Nd isotopic studies. In: The Second Hutton Symposium on the Origin of Granites and Related Rocks. Edited by: P.E. Brown and B.W. Chappell. Geological Society of America Special Paper 272: 439-446.

Dias, G., and Leterrier, J. 1994. The genesis of mafic-felsic plutonic associations: a Sr and Nd isotope study of the Hercynian Braga Granitoid Massif (Northern Portugal). Lithos, 32: 207-223.

Dickin, A..P., and Exley, R.A. 1981. Isotopic and geochemical evidence for magma mixing in the petrogenesis of the Coire Uaigneich Granophyre, Isle of Skye, northwest Scotland. Contributions to Mineralogy and Petrology, 76: 98-108.

Didier, J. 1973. Granites and their Enclaves: The Bearing of Enclaves on the Origin of Granites. Developments in Petrology 3. Elsevier Scientific Publishing, Amsterdam: 393pp.

Didier, J. 1987. Contribution of enclave studies to the understanding of the origin and evolution of granitic magmas. Geologische Rundschau, 76: 41-50.

Didier, J., Duthou, J.L, and Lameyre, J. 1982. Mantle and crustal granites: genetic classification of orogenic granites and the nature of their enclaves. Journal of Volcanology and Geothermal Research, 14: 125-132.

Dodge, F.C.W., and Kistler, R.W. 1988. Origin of mafic inclusions, Central Sierra Nevada. Eos, 69: 1496.

Donohoe, H.V., and Grantham, R.G. 1989. Geological Highway Map of Nova Scotia. Atlantic Geoscience Society Special Publication 1, second edition. Scale: 1:640,000.

Dorais, M.J., Whitney, J.A., and Roden, M.F. 1989. Origin of mafic enclaves in the Dinkey Creek pluton, central Sierra Nevada, California. Journal of Petrology, 31: 853-881.

Dostal, J., Keppie, J.D., and Dupuy, C. 1983. Petrology and geochemistry of Devono-Carboniferous volcanic rocks in Nova Scotia. Maritime Sediments and Atlantic Geology, 19: 59-71.

Dostal, J., and Greenough, J.D. 1992. Geochemistry and petrogenesis of the early Mesozoic North Mountain basalts of Nova Scotia, Canada. In: Eastern North American Mesozoic Magamatism. Edited by: J.H. Puffer and P.C. Ragland. Geological Society of America Special Paper 268: 149-159.

Douglas, G.V. 1943. Black granite at Shelburne, Nova Scotia. Nova Scotia Department of Mines, Annual Report, 1942: 87-91.

Douma, M. 1978. Gravitational interpretation and modelling of the South Mountain Batholith, southern Nova Scotia. B.Sc. (honours) thesis, Dalhousie Univeristy: 36pp.

Douma, S. 1988. The mineralogy, petrology and geochemistry of the Port Mouton Pluton, Nova Scotia, Canada. M.Sc. thesis, Dalhousie University: 324pp.

Dwyer, G.J. 1975. Petrology of the Mulgrave Lake Adamellite Pluton. B.Sc. (honours) thesis, Dalhousie University: 28pp.

Eberz, G.W., and Nicholls, I.A. 1988. Microgranitoid enclaves from the Swifts Creek Pluton, southeast Australia: Textural and physical constraints on the nature of magma mingling processes in the plutonic environment. Geologische Rundschau, 77: 713-736.

Eberz, G.W., Clarke, D.B., Chatterjee, A.K., and Giles, P.S. 1991. Chemical and isotopic composition of the lower crust beneath the Meguma Lithotectonic Zone, Nova Scotia: evidence from granulite facies xenoliths. Contributions to Mineralogy and Petrology, 109: 69-88.

Eggler, D.H., and Burnham, C.W. 1973. Crystallization and fractionation trends in the system andesite-H_2O-CO_2-O_2 at pressures to 10 Kb. Bulletin of the Geological Society of America, 84: 2517-2532.

Eisbacher, G.H. 1969. Displacement and stress field along part of the Cobequid fault, Nova Scotia. Canadian Journal of Earth Sciences, 6: 1095-1104.

Elias, P. 1986. Thermal history of the Meguma Terrane: A study based on ^{40}Ar-^{39}Ar and fission track dating. Unpublished Ph.D. thesis, Dalhousie University: 408pp.

England, P.C., and Thompson, A.B. 1984. Pressure-temperature-time paths of regional metamorphism I. Heat transfer during the evolution of regions of thickened continental crust. Journal of Petrology, 25: 894-928.

England, P.C., and Thompson, A. 1986. Some thermal and tectonic models for crustal melting in continental collision zones. In: Collision Tectonics. Edited by: M.P. Coward and A.C. Ries. Geological Society Special Publication 19: 83-94.

Eyal, Y. 1980. Synplutonic dykes in the Wadi Um-Mara area, Sinai. Tectonophysics, 67: 35-44.

Farley, E.J. 1979. Mineralization at the Turner and Walker deposits. M.Sc. thesis, Dalhousie University: 252pp.

Feeley, T.C., and Grunder, A.C. 1990. Basalt induced crustal melting during mid-Tertiary magmatism. Evidence from the Egan Range, Nevada. Geological Society of America, Abstracts with Programs, 22: 22.

Fershtater, G.B., and Borodina, N.S. 1976. Petrology of autoliths in granitic rocks. International Geology Reviews, 19: 458-468.

Fleck, R.J. 1990. Neodymium, strontium, and trace-element evidence of crustal anatexis and magma mixing in the Idaho Batholith. In: The Nature and Origin of Cordilleran Magmatism. Edited by J.L. Anderson. Geological Society of America Memoir 174: 355-373.

Flood, R., and Shaw, S. In press. Microgranitoid enclaves in the Looanga Adamellite, New England, Australia: crystal cumulates.

Foster, D.A., and Hyndman, D.W. 1990. Magma mixing and mingling between synplutonic mafic dykes and granite in the Idaho-Bitteroot batholith. In: The Nature and Origin of Cordilleran Magmatism. Edited by: A.J. Lawford. Geological Society of America Memoir 174: 347-358.

Fourcade, S., and Allegre, C.J. 1981. Trace elements behaviour in granite genesis: A case study of the calc-alkaline plutonic association from the Quérigut Complex, Pyrénées, France. Contributions to Mineralogy and Petrology, 76: 177-195.

Fowler, C.M.R. and Nisbett, E.G. 1988. Geotherms in the continental crust. In: Short Course on Heat, Metamorphism, and Tectonics, Volume 14. Edited by: E.G. Nisbet and C.M.R. Fowler. Mineralogical Society of Canada, Ottawa: 32-50.

Fowler, C.M.R., Nisbet, E.G., and Pandit, B.I. 1988. The transfer of heat by conduction in the Earth's crust: Physical constraints. In: Short Course on Heat, Metamorphism, and Tectonics, Volume 14. Edited by: E.G. Nisbet and C.M.R. Fowler. Mineralogical Society of Canada, Ottawa: 1-33.

Fowler, M.B. 1988. Ach 'Uaine hybrid appinite pipe: Evidence for mantle-derived shoshonitic parent magmas in Caledonian granite genesis. Geology, 16: 1026-1030.

Frost, C.D., and O'Nions, R.K. 1985. Caledonian magma genesis and crustal recycling. Journal of Petrology, 26: 515-544.

Frost, T.P., and Mahood, G.A. 1987. Field, chemical, and physical constraints on mafic-felsic magma interaction in the Lamarck Granodiorite, Sierra Nevada, California. Bulletin of the Geological Society of America, 99: 272-291.

Furman, M. T., and Spera, F. J. 1985. Comingling of acid and basic magma with implications for the origin of mafic I-type xenoliths: field and petrochemical relations of an unusual dike complex at Eagle Lake, Sequoia National Park, California, U.S.A. Journal of Volcanology and Geothermal Research, 24: 151-178.

Fyson, W.K. 1966. Structures in the Lower Palaeozoic Meguma Group, Nova Scotia. Bulletin of the Geological Society of America, 77: 931-943.

Gallant, G.K. 1991. Origin of foliation in the Barrington Passage Pluton. B.Sc. (honours) thesis, Dalhousie Univeristy: 121pp.

Gamble, J.A. 1979. Some relationships between coexisting granitic and basaltic magmas and the genesis of hybrid rocks in the Tertiary Central Complex of Slieve Gullion, northeastern Ireland. Journal of Volcanology and Geothermal Research, 5: 297-316.

Geological Survey of Canada. 1986. Geophysics Series Aeromagnetic Total Field Map 21175G, Sheet 21A. Scale 1:25,000.

Gibling, M. In press. Upper Paleozoic Rocks, Nova Scotia. In: Geology of the Appalachian-Caledonian Orogen in Canada and Greenland. Edited by: H.W. Van der Poll, R.S. Hyde, and M.R. Gibling. Geological Survey of Canada, Geology of Canada Volume 6.

Giles, P.S., and Chatterjee, A. K. 1987. Lower crustal xenocrysts and xenoliths in the Tangier Dyke, eastern Meguma Zone, Nova Scotia. In: Nova Scotia Department of Mines and Minerals Branch Report of Activities, 87-5 part A. Edited by: J.L. Bates and D.R. MacDonald: 85-88.

Gill, J. 1981. Orogenic Andesites and Plate Tectonics. Springer-Verlag, Heidelberg: 390pp.

Govindaraju, K. 1989. Compilation of working values and sample description for 272 geostandards. Geostandards Newsletter, 13: 113pp.

Graves, M.C., and Zentilli, M. 1988. The lithogeochemistry of metal-enriched coticules in the Goldenville-Halifax transition zone of the Meguma Group, Nova Scotia. Geological Survey of Canada, Current Research Paper 88-1b: 251-261.

Gray, C.E. 1984. An isotopic mixing model for the origin of granitic rocks in southeast Australia. Earth and Planetary Science Letters, 70: 47-60.

Gray, D.R., and Cull, J.P. 1992. Thermal regimes, anatexis, and orogenesis: relations in the western Lachlan Fold Belt, southeastern Australia. Tectonophysics, 214: 441-461.

Green, T.H., and Ringwood, A.C. 1968a. Origin of garnet phenocrysts in calc-alkaline rocks. Contributions to Mineralogy and Petrology, 18: 163-174.

Green, T.H., and Ringwood, A.E. 1968b. Genesis of the calc-alkaline igneous rock suite. Contributions to Mineralogy and Petrology, 18: 105-162.

Greenough, J.D., Ruffman, A., and Owen, J.V. 1988. Magma injection directions inferred from a fabric study of the Popes Harbour dyke, Eastern Shore, Nova Scotia, Canada. Geology, 16: 547-550.

Gordon, G.E., Randle, K., Coles, G., Corless, J., Beeson, M., and Oxley, S. 1968. Instrumental activation analysis of standard rocks with high resolution gamma ray detectors. Geochimica et Cosmochimica Acta, 32: 359-392.

Grove, T.L., Gerlach, D.C., and Sando, T.W. 1982. Origin of calc-alkaline series lavas at Medicine Lake volcano by fractionation, assimilation, and mixing. Contributions to Mineralogy and Petrology, 80: 160-182.

Grove, T.L., and Baker, M.B. 1984. Phase equilibrium controls on the tholeiitic versus calc-alkaline differentiation trends. Journal of Geophysical Research, 89: 3253-3274.

Gupta, V.K., and Sutcliffe, R.H. 1990. Mafic-ultramafic intrusives and their gravity field; Lac des Iles area, northern Ontario. Bulletin of the Geological Society of America, 102: 1471-1483.

Hall, L.R. 1979. Geology of the LaHave River area, Lunenburg County, Nova Scotia. M.Sc. thesis, Acadia University: 174pp.

Halliday, A.N., Stephens, W.E., and Harmon, R.S. 1981. Isotopic and chemical constraints on the development of peraluminous Caledonian and Acadian granites. Canadian Mineralogist, 19: 205-216.

Ham, L. 1988. The mineralogy, petrology, and geochemistry of the Halfway Cove-Queensport Pluton, Nova Scotia, Canada. M.Sc. thesis, Dalhousie University: 294pp.

Ham, L.J., Marsh, S.W., Corey, M.C., Horne, R.J., and MacDonald, M.A. 1989. Lithogeochemistry of the eastern portion of the South Mountain Batholith, Nova Scotia. Nova Scotia Department of Mines and Energy Open File Report 89-001, 62pp.

Ham, L.J., Corey, M.C., Horne, R.J., and MacDonald, M.A. 1990. Lithogeochemistry of the western portion of the South Mountain Batholith, Nova Scotia. Nova Scotia Department of Mines and Energy Open File Report 90-007: 31pp.

Hanson, G. 1978. The application of trace elements to the petrogenesis of igneous rocks of granitic composition. Earth and Planetary Science Letters, 38: 26-43.

Hanson, R.B., and Barton, M.D. 1989. Thermal development of low-pressure metamorphic belts: results from two-dimensional numerical models. Journal of Geophysical Research, 94: 10,363-10,377.

Hardee, H.C. 1981. Convective heat extraction from molten magma. Journal of Volcanology and Geothermal Research, 10: 175-193.

Harland, W.B., Armstrong, R.L., Cox, A.V., Craig, L.E., Smith, A.G., and Smith, D.G. 1989. A Geologic Time Scale. Cambridge University Press, New York: 263pp.

Harmon, R.S., and Halliday, A.N. 1980. Oxygen and strontium isotope relationships in the British late Caledonian granites. Nature, 283: 21-25.

Harris, N.B.W., Pearce, J.A., and Tindle, A.G. 1986. Geochemical characteristics of collision-zone magmatism. In: Collision Tectonics. Edited by: M.P. Coward and A.C. Ries. Geological Society Special Publication 19: 67-81.

Hart, S.R. 1988. Heterogeneous mantle domains: signatures, genesis, and mixing chronologies. Earth and Planetary Science Letters, 90: 273-296.

Hatcher, R.D. 1988. The third synthesis: Wenlock to mid-Devonian (end of Acadian Orogeny). In: The Caledonian-Appalachian Orogen. Edited by: A.L. Harris and D.J. Fettes. Geological Society Special Publication 38: 499-504.

Hawkesworth, C.J., Kempton, P.D., Rogers, N.W., Ellam, R.M., and Van Calsteren, P.W. 1990. Continental mantle lithosphere and shallow level enrichment processes in the Earth's mantle. Earth and Planetary Science Letters, 96: 256-268.

Hawkesworth, C.J., Gallagher, K., Hergt, J.M., and McDermott, F. 1993. Mantle and slab contributions in arc magmas. Annual Review of Earth and Planetary Sciences, 21: 175-204.

Heaman, L.M., and Parrish, R. 1991. U-Pb geochronology of accessory minerals. In: Short Course Handbook on Applications of Radiogenic Isotope systems to Problems in Geology. Edited by: L.M. Heaman and J.N. Ludden. Mineralogical Association of Canada, Ottawa: 59-102.

Heaman, L.M., and Machado, N. 1992. Timing and origin of midcontinent rift alkaline magmatism, North America: evidence from the Coldwell Complex. Contributions to Mineralogy and Petrology, 110: 289-303.

Hergt, J.M., Chappell, B.W., McCulloch, M.T., MacDougall, I., and Chivas, A.R. 1989. Geochemical and isotopic constraints on the origin of the Jurassic dolerites of Tasmania. Journal of Petrology, 30: 841-883.

Hibbard, M.J. 1981. The magma mixing origin of mantled feldspars. Contributions to Mineralogy and Petrology, 76: 158-170.

Hibbard, M.J., and Watters, L.J. 1985. Fracturing and dyking in incompletely crystallized granitic plutons. Lithos, 18: 1-12.

Hildtreth, W. 1981. Gradients in silicic magma chambers: implications for lithospheric magmatism. Journal of Geophysical Research, 86: 10153-10192.

Hill, J.D. 1986. Granitoid plutons in the Canso area, Nova Scotia. Geological Survey of Canada Paper 86-1A: 185-192.

Hill, J. D. 1988. Late Devonian granitic plutons in the Canso area, eastern Meguma Terrane, Nova Scotia. Maritime Sediments and Atlantic Geology, 24: 11-19.

Hill, J.D. 1991. Petrology, tectonic setting, and economic potential of Devonian peraluminous granitoid plutons in the Canso and Forest Hill areas, Eastern Meguma Terrane, Nova Scotia. Geological Survey of Canada Bulletin 383: 96pp.

Hill, J., and Raeside, P. 1987. Discussion on `Structural study of highly deformed Meguma phyllite, vicinity of Whitehead Village, southeastern Nova Scotia' by C.K. Mawer, and P.F. Williams. Maritime Sediments and Atlantic Geology, 23: 151-154.

Hill, J., Krogh, T. E., and Theriault, R. 1990. Implications of isotopic data from granitoid plutons in the Canso area, eastern Meguma Terrane, Nova Scotia. Atlantic Geology, 26: 173.

Hodge, D.S. 1974. Thermal model for origin of granitic batholiths. Nature, 251: 297-299.

Hogan, J.P., and Sinha, A.K. 1989. Compositional variation of plutonism in the Coastal Maine Magmatic Province: mode of origin and tectonic setting. In: Studies in Maine Geology 4, Edited by: R.D. Tucker and R.G. Marvinny. Maine Geological Survey: 33pp.

Holden, P., Halliday, A.N., and Stephens, W.W. 1987. Nd and Sr isotope content of peridotite enclaves points to mantle input in granitoid production. Nature, 330: 53-56.

Holm, P.E. 1985. The geochemical fingerprints of different tectonomagmatic environments using hygromagmatophile element abundances of tholeiitic basalts and basaltic andesites. Chemical Geology, 51: 303-323.

Holmes, A. 1931. The problem of the association of acid and basic rocks in central complexes. Geological Magazine, 68: 241-255.

Holtz, F. 1989. Importance of melt fraction and source rock composition in crustal genesis - the example of two granitic suites in Portugal. Lithos, 24: 21-35.

Hon, R., and Piqué, A.C. 1989. From the rifting of Paleogondwana to the assembly of Pangea; the tectonic evolution of the eastern margin of the Northern Appalachians. Geological Society of America, Abstracts with Programs, 21: 23.

Horne, R.J., Corey, M.C., Ham, L.J., and MacDonald, M.A. 1988. Emplacement of the South Mountain Batholith; structural and intrusive considerations. Atlantic Geology, 26: 173.

Horne, R.J., Corey, M., Ham, L.J., and MacDonald, M.A. 1989. Lithogeochemical variation in the granodiorite and biotite monzogranite of the South Mountain Batholith, Nova Scotia. Atlantic Geology, 25: 161.

Huppert, H. E., and Sparks, R. S. J. 1988a. The generation of granitic magmas by intrusion of basalts into continental crust. Journal of Petrology, 29: 599-624.

Huppert, H.E., and Sparks, R.S.J. 1988b. The fluid dynamics of crustal melting by injection of basaltic sills. Transactions of the Royal Society of Edinburgh, 79: 237-243.

Huppert, H.E., and Sparks, R.S.J. 1988c. Melting the roof of a chamber containing hot, turbulently convecting fluid. Journal of Fluid Mechanics, 188: 107-131.

Hutton, J. 1795. Theory of the Earth with proofs and illustrations. Second Edition 1972. Bronschweig, New York: 620pp.

Hyndman, D.W., and Foster, D.A. 1988. The role of tonalites and mafic dikes in the generation of the Idaho Batholith. Journal of Geology, 96: 31-46.

Irvine, T.N. 1970. Heat transfer during solidification of layered intrusions; I, sheets and sills. Canadian Journal of Earth Sciences, 7: 1031-1061.

Irvine, T.N., and Baragar, W.R.A. 1971. A guide to the chemical classification of the common volcanic rocks. Canadian Journal of Earth Sciences, 8: 523-548.

Jaeger, J.C. 1957. The temperature in the neighborhood of a cooling intrusive sheet. American Journal of Science, 255: 306-318.

Jamieson, R.A. 1974. The contact of the South Mountain Batholith near Mount Uniacke, Nova Scotia. B.Sc. (honours) thesis, Dalhousie University: 52pp.

Jaupart, C., and Provost, A. 1985. Heat focusing, granite genesis and inverted metamorphic gradients in continent collision zones. Earth and Planetary Science Letters, 73: 385-397.

Jenner, G.A., Longerich, H.P., Jackson, S.E., and Fryer, B.J. 1990. ICP-MS - A powerful tool for high-precision trace-element analysis in Earth Sciences: Evidence from analysis of selected U.S.G.S. reference samples. Chemical Geology, 83: 133-148.

Johnson, R.W. 1987. Delayed partial melting of subduction-modified magma sources in Western Melanesia: New results from the Late Cainozoic. Proceedings of the Pacific Rim Congress: 211-214

Johnston, A.D., and Wyllie, P.J. 1988. Interaction of granitic and basic magmas: experimental observations on contamination processes at 10 kbar with H_2O. Contributions to Mineralogy and Petrology, 98: 352-362.

Keen, C.E., Kay, W.A., Keppie, J.D., Marillier, F., Pe-Piper, G., and Waldron, J.W.F. 1991. Deep seismic reflection data from the Bay of Fundy and Gulf of Maine: tectonic implications for the northern Appalachians. Canadian Journal of Earth Sciences, 28: 1096-1111.

Kempster, R.M.F. 1988. A comparative petrological study of three Nova Scotian intrusions: the Jeddore dyke, the Sober Island dyke, and the Marshdale Intrusive. B.Sc. (honours) thesis, Dalhousie University: 87pp.

Kempster, R.M.F., Clarke, D.B., Reynolds, P.H., and Chatterjee, A.K. 1989. Late Devonian lamprophyric dykes in the Meguma Zone of Nova Scotia. Canadian Journal of Earth Sciences, 26: 611-613.

Kent, D.V., and Keppie, J.D. 1988. Silurian-Permian palaeocontinental reconstructions and circum-Atlantic tectonics. In: The Caledonian-Appalachian Orogen. Edited by: A.L. Harris and D.J. Fettes. Geological Society Special Publication 38: 469-480.

Keppie, J.D. 1977. Paleozoic global tectonics of southern Nova Scotia. In: Nova Scotia Department of Mines Paper 77-1: 34pp.

Keppie, J.D. 1982. The Minas Geofracture. In: Major Structural Zones and Faults of the Northern Appalachians. Edited by: P. St-Julien and J. Béland. Geological Association of Canada Special Paper 24: 263-280.

Keppie, J.D. 1985. The Appalachian Collage. In: The Caledonide Orogen - Scandinavian and Related Areas. Edited by: D.G. Gee and B.A. Sturt. John Wiley and Sons: 1217-1226.

Keppie, J.D. 1989. Northern Appalachian terranes and their accretionary history. Geological Society of America Special Paper 230: 159-191.

Keppie, J.D., and Dallmeyer, R.D. 1986. Late Palaeozoic accretion of the Meguma Terrane with North America. Geological Society of America, Abstracts with Programs, 18: 655.

Keppie, J. D., and Dallmeyer, R. D. 1987. Dating transcurrent terrane accretion; an example from the Meguma and Avalon composite terranes in the Northern Appalachians. Tectonics, 6: 831-847.

Keppie, J.D., and Dostal, J. 1991. Late Proterozoic tectonic model for the Avalon terrane in Maritime Canada. Tectonics, 10: 842-850.

Keppie, J.D., Dallmeyer, R.D., and Krogh, T.E. 1992. U-Pb and $^{40}Ar/^{39}Ar$ mineral ages from Cape North, northern Cape Breton Island: implications for accretion of the Avalon Composite Terrane. Canadian Journal of Earth Sciences, 29: 277-295.

Kleemann, G.J., and Twist, D. 1989. The compositionally-zoned sheet-like granite pluton of the Bushveld Complex; evidence bearing on the nature of A-type magmatism. Journal of Petrology, 30: 1383-1414.

Kontak, D., and Reynolds, P.H. 1994. $^{40}Ar/^{39}Ar$ dating of metamorphic and igneous rocks of the Liscomb Complex, Meguma Terrane, southern Nova Scotia. Canadian Journal of Earth Sciences, 31: 1643-1653.

Kouchi, A., and Sunagawa, I. 1985. A model for mixing basaltic and dacitic magmas as deduced from experimental data. Contributions to Mineralogy and Petrology, 89: 17-23.

Koyagouchi, T. 1992. Enclaves in volcanic rocks from Japan. In: Enclaves and Granite Petrology. Edited by: J. Didier and B. Barbarin. Elsevier, Amsterdam: 235-250.

Kretz, R. 1983. Symbols for the rock-forming minerals. American Mineralogist, 68: 277-279.

Krogh, T.E. 1973. A low-contamination method for hydrothermal decomposition of zircon and extraction of U and Pb for isotopic age determinations. Geochimica et Cosmochimica Acta, 37: 485-494.

Krogh, T.E. 1981a. Improved accuracy of U-Pb zircon dating by selection of more concordant fractions using a high gradient magnetic separation technique. Geochimica et Cosmochimica Acta, 46: 631-635.

Krogh, T.E. 1981b. Improved accuracy of U-Pb zircon ages by the creation of more concordant systems using an air abrasion technique. Geochimica et Cosmochimica Acta, 46: 637-649.

Krogh, T.E., and Davis, G.L. 1975. The production and preparation of ^{205}Pb for use as a tracer in isotope dilution analyses. Yearbook of the Carnegie Institute, Washington, 74: 416-417.

Krogh, T.E., and Keppie, J.D. 1990. Age of detrital zircon and titanite in the Meguma Group, southern Nova Scotia, Canada; clues to the origin of the Meguma Terrane. Tectonophysics, 177: 307-323.

Kubilius, W., and Ohmoto, H. 1984. $\delta^{34}S$ and sulfur contents of granitoids and associated metasediments, southwestern Nova Scotia. Geological Society of America, Abstracts with Programs, 16: 45.

Lane, T.E. 1975a. Stratigraphy of the White Rock Formation. Maritime Sediments, 11: 87-106.

Lane, T.E. 1975b. The Torbrook Formation. Maritime Sediments, 11: 107-118.

Lange, R.A., and Carmichael, I.S.E. 1987. Densities of Na_2O - K_2O - CaO - MgO - FeO - Fe_2O_3 - Al_2O_3 - TiO_2 - SiO_2 liquids: New measurements and derived partial molar properties. Geochimica et Cosmochimica Acta, 51: 2931-2946.

Larsen, L.L., and Smith, E.I. 1990. Mafic igneous enclaves in the Wilson Ridge Pluton, Northwest Arizona: implications for the generation of a calc-alkaline intermediate pluton in an extensional environment. Journal of Geophysical Research, 95: 17693-17723.

Lathrop, A.S., Blum, J.D., and Chamberlain, C.P. 1994. Isotopic evidence for closed-system anatexis at midcrustal levels: An example from the Acadian Appalachians of New England. Journal of Geophysical Research, 99: 9453-9468.

Lee, D.E., and Christiansen, E.H. 1983. The granite problem as exposed in the Southern Snake Creek Range, Nevada. Contributions to Mineralogy and Petrology, 83: 99-116.

Lee, J.K.W. 1993. The argon release mechanisms of hornblende in vacuo. Chemical Geology, 106: 133-170.

Lee, J.K.W., Onstott, T.C., Cashman, K.V., Cumbest, R.J., and Johnson, D. 1991. Incremental heating of hornblende in vacuo; implications for $^{40}Ar/^{39}Ar$ geochronology and the interpretation of thermal histories. Geology, 19: 872-876.

Lesher, C.E. 1990. Decoupling of chemical and isotopic exchange during magma mixing. Nature, 344: 235-237.

Lindberg, B., and Eklund, O. 1988. Interactions between basaltic and granitic magmas in a Svecofennian postorogenic granitoid intrusion, Åland, southwest Finland. Lithos, 22: 13-23.

Litvinovsky, B.A., and Podladchikov, Y.Y. 1993. Crustal anatexis during the influx of mantle volatiles. Lithos, 30: 93-107.

Longerich, H.P., Jenner, G.A., Fryer, B.J., and Jackson, S.E. 1990. Inductively coupled plasma-mass spectrometric analysis of geological samples; a critical evaluation based on case studies. Chemical Geology, 83: 105-118.

Longstaffe, F.J., Smith, T.E., and Muehlenbachs, K. 1980. Oxygen isotope evidence for the genesis of Upper Paleozoic granites from southwest Nova Scotia. Canadian Journal of Earth Sciences, 17: 132-141.

Lorenc, M. 1990. Magmatic mafic enclaves in granitoids of northern Sierra del Paimán, Argentina. Geological Journal, 25: 405-412.

Lynn, H.B., Hale, L.D., and Thompson, G.A. 1981. Seismic reflectors from the basal contacts of batholiths. Journal of Geophysical Research, 86: 10633-10638.

MacDonald, M.A. 1981. The mineralogy, petrology, and geochemistry of the Musquodoboit Batholith. M.Sc. thesis, Dalhousie University: 272pp.

MacDonald, M.A., and Clarke, D.B. 1985. Petrology, geochemistry, and economic potential of the Musquodoboit Batholith, Nova Scotia. Canadian Journal of Earth Sciences, 22: 1633-1642.

MacDonald, M.A., Corey, M.C., Ham, L.J., and Horne, R.J. 1986. South Mountain Batholith project: bedrock mapping. In: Tenth Annual Open House and Review of Activities, Program and Summaries. Edited by: J.L. Bates and D.R. MacDonald. Nova Scotia Department of Mines and Energy, 12: 77-81.

MacDonald, M.A., Corey, M.C., Ham, L.J., and Horne, R.J. 1989. Petrographic and geochemical aspects of the South Mountain Batholith. In: Nova Scotia Department of Mines and Energy Report 89-3. Edited by J.L. Bates and D.R. MacDonald. Nova Scotia Department of Mines and Energy: 75-79.

MacDonald, M.A., Corey, M.C., Ham, L. J., Home, R.J., and Chatterjee, A. K. 1990. Recent advances in the geology of the South Mountain Batholith; anatomy and origin of a batholith. Atlantic Geology, 26: 180.

MacDonald, M.A., Horne, R.J., Corey, M.C., and Ham, L.J. 1992. An overview of recent bedrock mapping and follow-up petrological studies of the South Mountain Batholith, southwestern Nova Scotia, Canada. Atlantic Geology, 28: 7-28.

MacDonald, R., Thorpe, R.S., Gaskarth, J.W., and Grindrod, A.R. 1985. Multi-component origin of Caledonian lamprophyres of northern England. Mineralogical Magazine, 49: 485-494.

Marillier, F., Keen, C.E., Stockmal, G.S., Quinlan, G., Williams, H., Colman-Sadd, S.P., and O'Brien, S.J. 1989. Crustal structure and surface zonation of the Canadian Appalachians: implications of deep seismic reflection data. Canadian Journal of Earth Sciences, 26: 305-321.

Martel, A.T., and Gibling, M.R. 1991. Wave-dominated lacustrine facies and tectonically controlled cyclicity in the Lower Carboniferous Horton Bluff Formation, Nova Scotia, Canada. Special Publication of the International Association of Sedimentologists, 13: 223-243.

Martel, A.T., McGregor, D.C., and Utting, J. 1993. Stratigraphic significance of Upper Devonian and Lower Carboniferous miospores from the type area of the Horton Group, Nova Scotia. Canadian Journal of Earth Sciences, 30: 1091-1098.

Mawer, C.K., and White, J.C. 1987. Sense of displacement on the Cobequid-Chedabucto fault system, Nova Scotia, Canada. Canadian Journal of Earth Sciences, 24: 217-223.

Mawer, C.K., and Williams, P.F. 1986. Structural study of highly deformed Meguma phyllite and granite, vicinity of Whitehead Village, south-eastern Nova Scotia. Maritime Sediments and Atlantic Geology, 22: 51-64.

McBirney, A.R., Taylor, H.P., and Armstrong, R.L. 1987. Paracútin re-examined: a classic example of crustal assimilation in calc-alkaline magma. Contributions Mineralogy and Petrology, 95: 4-20.

McCulloch, M.T., and Gamble, J.A. 1991. Geochemical and geodynamical constraints on subduction zone magmatism. Earth and Planetary Science Letters, 102: 358-374.

McDougall, I., and Harrison, T.M. 1988. Geochronology and Thermochronology by the $^{40}Ar/^{39}Ar$ Method. Oxford Monographs on Geology and Geophysics 9, Oxford University Press, New York: 212pp.

McHone, J.G. 1992. Mafic dyke suites within Mesozoic igneous provinces of New England and Atlantic Canada. In: Eastern North American Mesozoic Magmatism. Edited by J.H. Puffer and P.C. Ragland. Geological Society of America Special Paper 268: 1-12.

McKenzie, C.B. 1974. Petrology of the South Mountain Batholith, Western Nova Scotia. M.Sc. thesis, Dalhousie University: 101pp.

McKenzie, C.B., and Clarke, D.B. 1975. Petrology of the South Mountain Batholith, Nova Scotia. Canadian Journal of Earth Sciences, 12: 1209-1218.

Meschede, M. 1986. A method of discriminating between different types of mid-ocean ridge basalts and continental tholeiites with the Nb-Zr-Y diagram. Chemical Geology, 56: 207-218.

Mezger, K, Attherr, R., Okunsch, M., Henjes-Kunst, F., and Krener, H. 1985. Genesis of acid/basic rock associations: a case study. The Kallithea intrusive complex, Samos, Greece. Contributions to Mineralogy and Petrology, 90: 353-366.

Michael, P.J. 1991. Intrusion of basaltic magma into a crystallizing granitic magma chamber: The Cordillera del Paine pluton in southern Chile. Contributions to Mineralogy and Petrology, 108: 396-418.

Michard, A., Gurriet, P., Soudant, M., and Albarede, F. 1985. Nd isotopes in French Phenerozoic shales: external vs. internal aspects of crustal evolution. Geochimica et Cosmochimica Acta, 49: 601-610.

Miller, C.F. 1985. Are strongly peraluminous magmas derived from pelitic sedimentary sources? Journal of Geology, 93: 673-689.

Mitchell, R.H., Platt, G.R., and Cheadle, S.P. 1983. A gravity study of the Coldwell Complex, northwestern Ontario and its petrological significance. Canadian Journal of Earth Sciences, 20: 1631-1638.

Molnar, P., Chen, W.P., and Padovani, E. 1983. Calculated temperatures in overthrust terrains and possible combinations of heat sources responsible for the Tertiary granites in the Greater Himalaya. Journal of Geophysical Research, 88: 6415-6429.

Muecke, G.K., and Clarke, D.B. 1981. Geochemical evolution of the South Mountain Batholith, Nova Scotia: Rare-earth-element evidence. Canadian Mineralogist, 19: 133-145.

Muecke, G.K., Elias, P., and Reynolds, P.H. 1988. Hercynian/Alleghanian overprinting of an Acadian terrane: $^{40}Ar/^{39}Ar$ studies in the Meguma Zone, Nova Scotia, Canada. Chemical Geology, 73: 153-167.

Mysen, B.O. 1992. Iron and phosphorus in calcium silicate quenched melts. Chemical Geology, 98: 175-202.

Nakada, S. 1991. Magmatic processes in titanite-bearing dacites, central Andes of Chile and Bolivia. American Mineralogist, 76: 548-560.

Nakamura, N. 1974. Determination of REE, Ba, Fe, Mg, Na, and K in carbonaceous and ordinary chondrites. Geochimica et Cosmochimica Acta, 38: 757-773.

Neal, C.R. 1988. The origin and composition of metasomatic fluids and amphiboles beneath Mailaita, Solomon Islands. Journal of Petrology, 29: 149-179.

Nielsen, R.L. 1988. A model for the simulation of combined major and trace element liquid lines of descent. Geochimica et Cosmochimica Acta, 52: 27-38.

Nisbet, E.G., and Pearce, J.A. 1977. Clinopyroxene composition in mafic lavas from different tectonic settings. Contributions to Mineralogy and Petrology, 63: 149-160.

Noblett, J.B., and Staub, M.W. 1990. Mid-Proterozoic lamprophyre commingled with late-stage granitic dikes in the anorogenic San Isabel batholith, Wet Mountains, Colorado. Geology, 18: 120-123.

O'Brien, B.H. 1983. The structure of the Meguma Group between Gegogan Harbour and Country Harbour, Guysborough County. Nova Scotia Department of Mines and Energy Report 83-1: 145-181.

O'Neil, J.R., Shaw, S.E., and Flood, R.H. 1977. Oxygen and hydrogen isotope compositions as indications of granite genesis in the New England Batholith, Australia. Contributions to Mineralogy and Petrology, 62: 313-328.

O'Reilly, C.T. 1975. Gravitational interpretation and modelling of the South Mountain Batholith using two and three dimensional computer programming. B.Sc. (honours) thesis, Dalhousie University: 80pp.

O'Reilly, G.A. 1976. The petrology of the Brenton pluton, Yarmouth County, Nova Scotia. B.Sc. (honours) thesis, Dalhousie University.

O'Reilly, G.A. 1988. Geology and geochemistry of the Sangster Lake and Larrys River Pluton, Guysborough County, Nova Scotia. M.Sc. thesis, Dalhousie University: 290pp.

Oldenburg, C.M., Spera, F.J., Yuen, D.A., and Sewell, G. 1989. Dynamic mixing in magma bodies: Theory, simulations, and implications. Journal of Geophysical Research, 94: 9,215-9,236.

Orisini, J.B.., Cocirta, C., and Zorpi, M.J. 1992. Genesis of mafic microgranular enclaves through differentiation of basic magmas, mingling, and chemical exchange with their host granitoid magmas. In: Enclaves and Granite Petrology. Edited by: J. Didier and B. Barbarin. Developments in Petrology 13, Elsevier, Amsterdam: 445-464.

Owen, J.V., Greenough, J.D., Hy, C., and Ruffman, A. 1988. Xenoliths in a mafic dyke at Popes Harbour, Nova Scotia: implications for the basement of the Meguma Group. Canadian Journal of Earth Sciences, 25: 1464-1471.

Page, N.J., and Zientek, M.L. 1987. Composition of primary postcumulus amphibole and phlogopite within an olivine cumulate in the Stillwater Complex, Montana. United States Geological Survey Bulletin 1674-A: 1-35.

Papezic, V.S., and Barr, S.M. 1981. The Shelburne dike, an early Mesozoic diabase dike in Nova Scotia: mineralogy, chemistry, and regional significance. Canadian Journal of Earth Sciences, 18: 1346-1355.

Pearce, J. A. 1983. Role of the subcontinental lithosphere in magma genesis at active continental margins. In: Continental Basalts and Mantle Xenoliths. Edited by C.J. Hawkesworth and M.J. Norry. Shiva Publishing, Nantwich. 230-249.

Pe-Piper, G. 1988. Calcic amphiboles of mafic rocks of the Jeffers Brook plutonic complex, Nova Scotia, Canada. American Mineralogist, 73: 993-1006.

Pe-Piper, G., and Loncarevic, B.D. 1989. Offshore continuation of the Meguma Terrane, southwestern Nova Scotia. Canadian Journal of Earth Sciences, 26: 176-191.

Perring, C.S., Rock, N.M.S., Golding, S.D., and Roberts, D.E. 1989. Criteria for the recognition of metamorphosed or altered lamprophyres: a case study from the Archean of Kambalda, Western Australia. Precambrian Research, 43: 215-237.

Pin, C., Binon, M., Belin, J.M., Barbarin, B., and Clemens, J.D. 1990. Origin of microgranular enclaves in granitoids: equivocal Sr-Nd evidence from Hercynian rocks in the Massif Central (France). Journal of Geophysical Research, 95: 17821-17828.

Piqué, A., and Skehan, J.W. 1992. Late Palaeozoic orogenies in western Africa and eastern North America: the diachronous closure of the Theic Ocean. Tectonics, 11: 392-404.

Pitcher, W. S. 1979a. Comments on the geological environments of granites. In: Origin of Granite Batholiths. Edited by: M.P. Weaver and J. Tarney. Shiva Publishing, Nantwich: 1-8.

Pitcher, W.S. 1979b. The nature, ascent, and emplacement of granitic magmas. Journal of the Geological Society of London, 136: 627-662.

Pitcher, W.S. 1987. Granites and yet more granites. Geologische Rundschau, 76: 51-79.

Pitcher, W.S. 1992. Synplutonic dykes and mafic enclaves. In: Enclaves and Granite Petrology. Edited by: J. Didier and B. Barbarin. Developments in Petrology 13, Elsevier, Amsterdam: 383-392.

Platevoet, B., and Bonin, B. 1992. Enclaves and mafic-felsic associations in the Permian alkaline province of Corsica, France: Physical and chemical interactions between coeval magmas. In: Enclaves and Granite Petrology. Edited by: J. Didier and B. Barbarin. Elsevier, Amsterdam: 191-204.

Poulson, S., Kubilius, W.P., and Ohmoto, H. 1991. Geochemical behaviour of sulfur in granitoids during intrusion of the South Mountain Batholith, Nova Scotia, Canada. Geochimica et Cosmochimica Acta, 55: 3809-3830.

Powers, M.C. 1953. A new roundness scale for sedimentary particles. Journal of Sedimentary Petrology, 23: 117-119.

Raeside, R.P., Hill, J.D., and Eddy, B.G. 1988. Metamorphism of Meguma Group metasedimentary rocks, Whitehead Harbour area, Guysborough County, Nova Scotia. Maritime Sediments and Atlantic Geology, 24: 1-9.

Rast, N., and Skehan, J.W. 1993. Mid-Paleozoic orogenesis in the North Atlantic: The Acadian Orogeny. In: The Acadian Orogeny: Recent Studies in New England, Maritime Canada, and the Autochthonous Foreland. Edited by: D.C. Roy and J.W. Skehan. Geological Society of America Special Paper 275: 1-25.

Read, H.H. 1948. Granites and granites. In: Origin of granite. Edited by: J. Gilluly. Geological Society of America Memoir, 28: 1-19.

Reid, J.B., Evans, O.C., and Fates, D.G. 1983. Magma mixing in granitic rocks of the central Sierra Nevada, California. Earth and Planetary Science Letters, 66: 243-261.

Reynolds, P.H., Kublich, E.E., and Muecke, G.K. 1973. Potassium-argon dating of slates from the Meguma Group, Nova Scotia. Canadian Journal of Earth Sciences, 10: 1059-1067.

Reynolds, P.H., Elias, P., Muecke, G.K., and Grist, A.M. 1987. Thermal history of the Meguma Zone, Nova Scotia, from an ^{40}Ar-^{39}Ar and fission track dating study of intrusive rocks. Canadian Journal of Earth Sciences, 24: 1952-1965.

Reynolds, R.C. 1972. Rubidium: element and geochemistry. In: The Encyclopedia of Geochemistry and Environmental Sciences IVA. Edited by: R.W. Fairbridge. Van Nostrand Reinhold, New York: 1050-1051.

Richard, L.R. 1988. Geochemical discrimination of the peraluminous Devonian-Carboniferous granitoids of Nova Scotia and Morocco. M.Sc. thesis, Dalhousie University: 344pp.

Richard, L.R., and Clarke, D.B. 1989. Multivariate statistical models for granites in terrane analysis: Nova Scotia, Morocco, and Iberia. Geological Society of America Bulletin, 101: 1157-1162.

Richard, L.R., and Clarke, D.B. 1990. AMPHIBOL: A program for calculating structural formulae and for classifying and plotting chemical analyses of amphiboles. American Mineralogist, 75: 421-423.

Rock, N.M.S. 1987. The nature and origin of lamprophyres; an overview. In: Alkaline Igneous Rocks. Edited by: J.G. Fitton and B.G.J. Upton. Geological Society Special Publication 30, Blackwell, London: 191-226.

Rock, N.M.S. 1990. Lamprophyres. Blackie and Son Ltd., Glasgow: 285pp.

Rock, N.M.S., Gaskarth, J.W., and Rundle, C.C. 1986. Late Caledonian dyke swarms in southern Scotland: A regional zone of primitive, K-rich lamprophyres and associated vents. Journal of Geology, 94: 505-522.

Roddick, J.A., and Armstrong, J.E. 1959. Relict dikes in the coast mountains near Vancouver, British Columbia. Journal of Geology, 67: 603-613.

Roeder, P.L., and Emslie, R.F. 1970. Olivine-liquid equilibrium. Contributions to Mineralogy and Petrology, 29: 275-289.

Rogers, H.D. 1984. Geology and igneous petrology of Shelburne and eastern Yarmouth Counties, Nova Scotia. Geological Survey of Canada Open File Report 840043-1374: 150pp.

Rogers, H.D., and White, C.E. 1984. Geology of the igneous-metamorphic complex of the Shelburne and eastern Yarmouth counties, Nova Scotia. Geological Survey of Canada, Paper 84-1A: 463-465.

Rogers, H.D., and Barr, S.M. 1988. Petrology of the Shelburne and Barrington Passage Plutons, Southern Nova Scotia. Maritime Sediments and Atlantic Geology, 24: 21-31.

Ruffman, A., and Greenough, J.D. 1990. The Weekend Dykes, a newly recognized mafic dyke swarm on the eastern shore of Nova Scotia. Canadian Journal of Earth Sciences, 27: 644-648.

Russell, J.K., and Nicholls, J. 1988. Analysis of petrologic hypotheses with Pearce element ratios. Contributions to Mineralogy and Petrology, 99: 25-35.

Ryall, P.J.C. 1990. A reconnaissance gravity survey of the western part of the Liscomb Complex. Program and Summaries, Fourteenth Annual Open House and Review of Activities. Nova Scotia Department of Mines and Energy Report 90-3: 45.

Sabatier, H. 1991. Vaugnerites: Special lamprophyre-derived mafic enclaves in some Hercynian granites from Western and Central Europe. In: Enclaves and Granite Petrology. Edited by: J. Didier and B. Barbarin. Developments in Petrology 13, Elsevier, Amsterdam: 63-81.

Salters, V.J.M., and Hart, S.R. 1991. The mantle sources of ocean ridges, islands, and arcs: the Hf-isotope connection. Earth and Planetary Science Letters, 104: 364-380.

Sandiford, M., Foden, J., Zhou, S., and Turner, J.S. 1992. Granite genesis and the mechanics of convergent orogenic belts with application to the southern Adelaide Fold Belt. In: The Second Hutton Symposium on the Origin of Granites and Related Rocks. Edited by: P.E. Brown and B.W. Chappell. Geological Society of America Special Paper 272: 83-93.

Sarkar, P.K. 1978. Petrology and geochemistry of the White Rock metavolcanic suite, Yarmouth, Nova Scotia. Unpublished Ph.D. thesis, Dalhousie University: 368pp.

Sass, J.H., Stone, C., and Munroe, R.J. 1984. Thermal conductivity determinations on solid rock - a comparison between a steady-state divided bar apparatus and a commercial transient line-source device. Journal of Volcanology and Geothermal Research, 20: 145-153.

Scarfe, C.M. 1986. Silicate melts: their properties, and structure applied to problems in geochemistry, petrology, economic geology, and planetary geology. Mineralogical Association of Canada Short Course Handbook, 12: 93-129.

Schenk, P.E. 1970. Regional variation of the flysch-like Meguma Group (Lower Palaeozoic) of Nova Scotia compared to recent sedimentation off the Scotian Shelf. In: Flysch sedimentology in North America. Edited by: J. Lajoie. Geological Association of Canada, Special Paper 7: 127-153.

Schenk, P.E. 1975. A regional synthesis (of the Meguma Zone). Maritime Sediments, 11: 9-24.

Schenk, P.E. 1978. Synthesis of the Canadian Appalachians. IGCP Project 27, Canadian contribution 6, Caledonian-Appalachian Orogen of the North Atlantic Region. Geological Survey of Canada, Paper 78-13: 111-136.

Schenk, P.E. 1981. The Meguma Zone of Nova Scotia - a remnant of western Europe, South America, or Africa ? International Geological Congress, Programs with Abstracts, 19: 119-148.

Schenk, P.E. 1983. The Meguma Terrane of Nova Scotia, Canada - an aid in transatlantic correlation. In: Regional trends in the Geology of the

Appalachian-Caledonian-Hercynian-Mauritanide Orogen. Edited by: P.E. Schenk. D. Reidel Publishing: 121-130.

Schenk, P.E. 1991. Events and sea-level changes on Gondwana's margin: The Meguma Zone (Cambrian to Devonian), of Nova Scotia, Canada. Bulletin of the Geological Society of America, 103: 512-521.

Sclater, J.G., Jaupart, C., and Galson, D. 1980. The heat flow through oceanic and continental crust and the heat loss of the Earth. Reviews of Geophysics and Space Physics, 18: 269-311.

Scotese, C.R., Van der Voo, R., Johnson, R.E., and Giles, P.S. 1984. Palaeomagnetic results form the Late Carboniferous of Nova Scotia. In: Plate Reconstruction from Paleozoic Palaeomagnetism. Edited by: R. Van der Voo, C.R. Scotese, and N. Bonhommet. Geodynamics Series Volume 12: 63-81.

Seaman, S.J. 1990. Enclaves in the granites of Cadillac Mountain and Somesville, Mount Desert Island, Maine: Evidence for magma mingling, ionic diffusion, and enclave dispersion. Geological Society of America, Abstracts with Programs, 22: 303.

Seaman, S.J., and Powers, S.L. 1991. Contamination of granitoid magmas by interaction with enclave liquids: Evidence from the granites of Cadillac Mountain and Somesville, Mount Desert Island, Maine. Eos: 72: 303.

Shannon, J.R. 1984. Contemporaneous bimodal mafic-felsic magmatism at Red Mountain, Clear Creek County, and Climax, Colorado. Geological Society of America, Abstracts with Programs, 16: 254.

Shearer, C.K., Papike, J.J., Spilde, M.N., Bickford, M.F., and Van Schmus, W.R. 1988. Proterozoic anorogenic magnetite-sphene granitoids: implications concerning the composition of the lower crust and deep crustal rocks. Geological Society of America, Abstracts with Programs, 20: 128.

Silver, L.T. and Chappell, B.W. 1988. The Peninsular Ranges Batholith: an insight into the evolution of the Cordilleran batholiths of southwestern North America. Transactions of the Royal Society of Edinburgh, 79: 105-121.

Smith, T.E. 1979. The geochemistry and origin of the Devonian granitic rocks of southwest Nova Scotia. Geological Society of America Bulletin, 90: 850-885.

Smith, T.E., Huang, C.H., Walawender, M.J., Cheung, P., and Wheeler, C. 1983. The gabbroic rocks of the Peninsular ranges batholith, southern California: cumulate rocks associated with calc-alkalic basalts and andesites. Journal of Volcanology and Geothermal Research, 18: 249-278.

Smitheringdale, W.G. 1983. Geology of parts of Digby, Bridgetown, and Gaspereau Lake Map Areas, Nova Scotia. Geological Survey of Canada Memoir 375: 78pp.

Sparks, R.S.J., and Marshall, L.A. 1986. Thermal and mechanical constraints on mixing between mafic and silicic magmas. Journal of Volcanology and Geothermal Research, 29: 99-124.

Stacey, J.S., and Kramers, J.D. 1975. Approximation of terrestrial lead isotope evolution by a two-stage model. Earth and Planetary Science Letters, 26: 207-221.

Stanley, C.R., and Russell, J.K. 1989. Pearce.Plot: a Turbo-Pascal program for the analysis of rock compositions with Pearce element ratios. Computers and Geosciences, 15: 905-926.

Stea, R.R., Conley, H., and Brown, Y. 1992. Surficial Geology of the Province of Nova Scotia Map 92-3. Nova Scotia Department of Natural Resources. Scale: 1: 500,000.

Steiger, R.H., and Jäger, E. 1977. Subcommission of geochronology: Convention on the use of decay constants in geo- and cosmochronology. Earth and Planetary Science Letters, 36: 359-362.

Stephens, W.E., Holden, P., and Henney, P.J. 1992. Microdioritic enclaves within the Scottish Caledonian granitoids and their significance for crustal magmatism. In: Enclaves and granite petrology. Edited by: J. Didier and B. Barbarin. Elsevier, Amsterdam: 125-134.

Stern, R. A. and Hanson, G. N. 1991. Archean high-Mg granodiorite: a derivative of light rare earth element-enriched monzodiorite of mantle origin. Journal of Petrology 32: 201-238.

Stockmal, G.S., Colman-Sadd, S.P., and Keen, C.E. 1990. Deep seismic structure and tectonic evolution of the Canadian Appalachians. Tectonics, 9: 45-62.

Streckeisen, A. 1976. To each plutonic rock its proper name. Earth Science Reviews, 12: 1-33.

Streckeisen A. 1979. Classification and nomenclature of volcanic rocks, lamprophyres, carbonatites and melilitic rocks: recommendations and suggestions for the IUGS subcommission on the subdivision of igneous rocks. Geology, 7: 331-335.

Strong, D.F., and Hanmer, S.K. 1981. The leucogranites of southern Brittany: Origin by faulting, frictional heating, fluid flux and fractional melting. Canadian Mineralogist, 19: 163-176.

Sutcliffe, R.H., Smith, A.R., Doherty, W., and Barnett, R.L. 1990. Mantle derivation of Archean amphibole-bearing granitoid and associated mafic rocks: evidence from the southern Superior Province, Canada. Contributions to Mineralogy and Petrology, 105: 225-274.

Tate, M.C., and Clarke, D.B. 1993. Origin of the Late Devonian Weekend lamprophyre dykes, Meguma Zone, Nova Scotia. Canadian Journal of Earth Sciences, 30: 2295-2304.

Taylor, S.R., and McLennan, S.M. 1985. The continental crust: its composition and evolution. Blackwell Scientific Publications, Oxford: 312pp.

Taylor, T.R., Vogel, T.A., and Milband, J.T. 1980. The composite dikes at Mount Desert Island, Maine: An example of coexisting acidic and basic magmas. Journal of Geology, 88: 433-444.

Thompson, A.B., and Tracy, R.J. 1979. Model systems for anatexis of pelitic rocks. II. Facies series melting and reactions in the system $CaO-KAlO_2-NaAlO_2-SiO_2-H_2O$. Contributions to Mineralogy and Petrology, 70: 429-438.

Thompson, R.N., Morrison, M.A., Hendry, G.L., and Parry, S.J. 1984. An assessment of the relative roles of crust and mantle in magma genesis: an elemental approach. Philosophical Transactions of the Royal Society of London, A310: 549-590.

Thompson, R.N., and Fowler, M.B. 1986. Subduction-related shoshonitic and ultrapotassic magmatism: a study of Siluro-Ordovician syenites from the Scottish Caledonides. Contributions to Mineralogy and Petrology, 94: 507-522.

Tilling, R.I. 1973. Boulder Batholith, Montana: A product of two contemporaneous but chemically distinct magma series. Bulletin of the Geological Society of America, 84: 3879-3900.

Todd, V.R., and Shaw, S.E. 1985. S-type granitoids and an I-S line in the Peninsular Ranges batholith, southern California. Geology, 13: 231-233.

Turner, J.S. 1973. Buoyancy effects in fluids. Cambridge Univeristy Press, Cambridge: 367pp.

Ulmer, P. 1988. High-pressure phase equilibria of a calc-alkaline picrobasalt: implications for the genesis of calc-alkaline magmas. Annual Report of the Director of the Geophysical Laboratory, Carnegie Institute 1987-1988: 28-35.

Van der Laan, S.R., and Wyllie, P.J. 1993. Experimental interaction of granitic and basaltic magmas and implications for mafic enclaves. Journal of Petrology, 34: 491-517.

Van der Molen, I., and Paterson, M.S. 1979. Experimental deformation of partially melted granite. Contributions to Mineralogy and Petrology, 70: 299-318.

Van der Plas, L., and Tobi, A.C. 1965. A chart for judging the reliability of point counting results. American Journal of Science, 263: 87-90.

Venturelli, G., Thorpe, R.S., Dal Piaz, G.V., del Moro, A., and Potts, P.J. 1984. Petrogenesis of calc-alkaline, shoshonitic and associated ultrapotassic Oligocene volcanic rocks from the northwestern Alps, Italy. Contributions to Mineralogy and Petrology, 86: 209-220.

Vernon, R.H. 1983. Restite, xenoliths, and microgranitoid enclaves in granites. Journal and Proceedings of the Royal Society of New South Wales, 116: 77-103.

Vernon, R.H. 1984. Microgranitoid enclaves in granites - globules of hybrid magma quenched in a plutonic environment. Nature, 309: 438-439.

Vernon, R.H. 1990. Crystallization and hybridism in microgranitoid enclave magmas: microstructural evidence. Journal of Geophysical Research, 95: 17849-17859.

Vernon, R.H. 1992. Interpretation of microstructures of microgranitoid enclaves. In: Enclaves and Granite Petrology. Edited by: J. Didier and B. Barbarin. Developments in Petrology 13, Elsevier, Amsterdam: 277-292.

Vielzeuf, D., and Holloway, J.R. 1988. Experimental determination of the fluid-absent melting relations in the pelitic system. Contributions to Mineralogy and Petrology, 98: 257-276.

Vogel, T.A. 1982. Magma mixing in the acid-basic complex of Ardnamurchan: implications on the evolution of shallow magma chambers. Contributions to Mineralogy and Petrology, 79: 411-423.

Wager, L.R. and Bailey, E.B. 1955. Basic magma chilled against acid magma. Nature, 172: 68-69.

Wall, V. J., Clemens, J.D., and Clarke, D.B. 1987. Models for granitoid evolution and source compositions. Journal of Geology, 95: 731-749.

Wanless, R.K., Stevens, R.D., Lachance, G.R., and Rimsaite, J.Y.H. 1966. Age determinations and geological studies. K-Ar Isotopic Ages, Report 6. Geological Survey of Canada Paper 65-17: 101pp.

Weagle, M.A. 1983. Study of the Moose Point Pluton, Queens County, Nova Scotia. B.Sc. (honours) thesis, Acadia University.

Whalen, J.B., and Currie, K.L. 1984. The Topsails igneous terrane, western Newfoundland: evidence for magma mixing. Contributions to Mineralogy and Petrology, 87: 319-327.

White, A.J.R., and Chappell, B.W. 1977. Ultrametamorphism and granitoid genesis. Tectonophysics, 43: 7-22.

Wiebe, R.A. 1980. Commingling of contrasted magmas in the plutonic environment: Examples from the Nain anorthositic complex. Journal of Geology, 88: 197-209.

Wiebe, R.A. 1993. The Pleasant Bay layered gabbro-diorite, Coastal Maine: Ponding and crystallization of basaltic injections into a silicic magma chamber. Journal of Petrology, 34: 461-489.

Williams, H., and Hatcher, R.D. 1982. Suspect terranes and the accretionary history of the Appalachian orogen. Geology, 10: 530-536.

Williams, H., and Hatcher, R.D. 1983. Appalachian suspect terranes. In: Contributions to the tectonics and geophysics of mountain chains. Edited by: R.D. Hatcher, H. Williams, and I. Zeitz. Geological Society of America Memoir 158: 33-54.

Williams, H., Colman-Sadd, S.P., and Swinden, H.S. 1988. Tectonic-stratigraphic subdivisions of central Newfoundland. Geological Survey of Canada, Current Research, Paper 88-1A: 91-98.

Williamson, B.J., Downes, H., and Thirlwall, M.F. 1992. The relationship between crustal magmatic underplating and granite genesis: an example from the Velay granite complex, Massif Central, France. In: The Second Hutton Symposium on the Origin of Granites and Related Rocks. Edited by: P.E. Brown and B.W. Chappell. Geological Society of America Special Paper 272: 235-245.

Wolfson, I.K. 1983. A study of the tin mineralization and lithogeochemistry in the area of the Wedgeport pluton, southwestern Nova Scotia. M.Sc. thesis, Dalhousie University: 398pp.

Wones, D.R., and Sinha, A.K. 1988. A brief review of early Ordovician to Devonian plutonism in the North American Caledonides. In: The Caledonian-Appalachian Orogen. Edited by: A.L. Harris and D.J. Fettes. Geological Society Special Publication 38: 381-388.

Wyllie, P.J. 1977. Crustal anatexis: An experimental review. Tectonophysics, 43: 41-71.

Wyllie, P.J. 1984. Sources of granitoid magmas at convergent plate boundaries. Physics of the Earth and Planetary Interiors, 35: 12-18.

Wyman, D.A., and Kerrich, R. 1989. Archean lamprophyre dykes of the Superior Province, Canada: distribution, petrology, and geochemical characteristics. Journal of Geophysical Research, 94: 4667-4696.

Yagi, K., and Takeshita, H. 1987. Impact of hornblende crystallization for the genesis of calc-alkalic andesites. In: Magmatic Processes: Physiochemical Principles. Edited by: R.O. Mysen. The Geochemical Society Publication 1: 183-191.

Younker, L.W., and Vogel, T.A. 1976. Plutonism and plate dynamics: The origin of circum-Pacific batholiths. Canadian Mineralogist, 14: 238-244.

Zeck, H.P. 1992. Restite-melt and mafic-felsic magma mixing and mingling in an S-type dacite, Cerro del Hoyazo, southeastern Spain. In: The Second Hutton Symposium on the Origin of Granites and Related Rocks. Edited by: P.E. Brown and B.W. Chappell. Geological Society of America Special Paper 272: 139-144.

Zen, E-an, and Palmer, A.R. 1981. Did Avalonia form the eastern shore of Iapetus Ocean ? Geological Society of America, Abstracts with Programs, 13: 587.

Zen, E-An. 1986. Aluminum enrichment in silicate melts by fractional crystallization: some mineralogic and petrographic constraints. Journal of Petrology, 27: 1095-1117.

Zen, E-an. 1988. Thermal modelling of stepwise anatexis in a thrust-thickened sialic crust. The Origin of Granites. Transactions of the Royal Society of Edinburgh, 79: 223-235.

Zen, E-an. 1990. 1D modelling of magma genesis by anatexis in a cratonic setting using field-gathered geological constraints: Pioneer Batholith, SW Montana. Geological Society of America, Abstracts with Programs, 22: A301.

Zen, E-an. 1992. Using granite to image the thermal state of the source terrane. In: The Second Hutton Symposium on the Origin of Granites and Related Rocks. Edited by: P.E. Brown and B.W. Chappell. Geological Society of America Special Paper 272: 107-114.

Zorpi, M.J., Coulon, C., Orsini, J.B., and Cocirta, C. 1989. Magma mingling, zoning and emplacement in calc-alkaline granitoid plutons. Tectonophysics: 157: 315-329.